CENTRAL RESEARCH LIBRARY
DOCUMENT COLLECTION

MARTIN MARIETTA ENERGY SYSTEMS LIBRARIES
3 4456 0049755 8

ORNL-2561
Reactors—Power
TID-4500 (14th ed.)

HOMOGENEOUS REACTOR PROJECT

QUARTERLY PROGRESS REPORT

FOR PERIODS ENDING APRIL 30 AND JULY 31, 1958

CENTRAL RESEARCH LIBRARY
DOCUMENT COLLECTION
LIBRARY LOAN COPY
DO NOT TRANSFER TO ANOTHER PERSON
If you wish someone else to see this document, send in name with document and the library will arrange a loan.

OAK RIDGE NATIONAL LABORATORY
operated by
UNION CARBIDE CORPORATION
for the
U.S. ATOMIC ENERGY COMMISSION

LIBRARY
REFERENCE COPY

Printed in USA. Price 500 cents. Available from the

Office of Technical Services
U. S. Department of Commerce
Washington 25, D. C.

LEGAL NOTICE

This report was prepared as an account of Government sponsored work. Neither the United States, nor the Commission, nor any person acting on behalf of the Commission:

A. Makes any warranty or representation, express or implied, with respect to the accuracy, completeness, or usefulness of the information contained in this report, or that the use of any information, apparatus, method, or process disclosed in this report may not infringe privately owned rights; or

B. Assumes any liabilities with respect to the use of, or for damages resulting from the use of any information, apparatus, method, or process disclosed in this report.

As used in the above, "person acting on behalf of the Commission" includes any employee or contractor of the Commission to the extent that such employee or contractor prepares, handles or distributes, or provides access to, any information pursuant to his employment or contract with the Commission.

ORNL-2561
Reactors–Power
TID-4500 (14th ed.)

Contract No. W-7405-eng-26

HOMOGENEOUS REACTOR PROJECT

QUARTERLY PROGRESS REPORT

For Periods Ending April 30 and July 31, 1958

Project Director – R. B. Briggs
Associate Director – C. E. Winters

Homogeneous Reactor Test – S. E. Beall
Reactor Design, Research, and Analysis – R. N. Lyon
Engineering Development – R. N. Lyon
Reactor Materials Research – E. G. Bohlmann
Chemical Engineering Development – D. E. Ferguson
Supporting Chemical Research – E. H. Taylor
Analytical Chemistry – M. T. Kelley

DATE ISSUED

JAN 19 1959

OAK RIDGE NATIONAL LABORATORY
Oak Ridge, Tennessee
operated by
UNION CARBIDE CORPORATION
for the
U. S. ATOMIC ENERGY COMMISSION

3 4456 0049755 8

HRP QUARTERLY PROGRESS REPORT

SUMMARY

PART I. HOMOGENEOUS REACTOR TEST

1. HRT Operations

Following the initial critical tests in January, preparations were completed for operation at power. Leak-testing of the reactor container was completed successfully, with a final leak rate of 4 to 4.3 liters/min at 30 psia. After the north shielding wall was filled with a barytes-colemanite-water mixture, the reactor was made critical on February 7 and was operated for six days at a maximum sustained power of 1.5 Mw. This first power run, with incomplete internal recombination of radiolytic gas, was characterized by a loss of reactivity whenever the power level was increased and by a very high (166 mpy) stainless steel corrosion rate. Shutdown was made on February 13, and a subsequent subcritical run was terminated because of failure of power wiring to the space coolers and fuel circulating pump. A period of electrical repairs and remote viewing of the core and the connecting line to the fuel pressurizer ensued; samples of oxide deposits were removed from both locations.

A new charge of fuel containing copper for internal recombination was added on March 27, and the reactor was again brought to criticality on March 30. By keeping a low level of radiolytic gas in the fuel solution, the reactivity-loss difficulties of run 13 were overcome. Furthermore, the corrosion difficulty of run 13 did not recur. The reactor power was raised in steps to 6.3 Mw on April 4; after operation at this power for 26 min, however, fuel solution leaked into the blanket region. The reactor fuel solution was automatically diluted, and a routine shutdown was made. A total of 390 Mwhr of thermal energy was generated before the leak occurred.

The apparent elevation of the leak was found by a volume calibration to be near the junction of the 30- and 90-deg conical entrance sections toward the bottom of the core; viewing the core surface with periscopes and mirrors failed to reveal the precise location or shape of the leak. However, fluid flow measurements indicated that the opening is a long, narrow horizontal hole with a flow area of about 1.5 in.^{2}. Further attempts were made to view the leak with a 20-ft borescope inserted through the upper core screens, but insufficient illumination was obtainable.

In the meantime, engineering studies were made of several means of continuing operation of the HRT as a two-region or single-region reactor, and a series of tests made to observe hydraulic and intermixing behavior. The goal of these experiments was to determine whether the leakage of fuel to the blanket region could be prevented by supplying the blanket with sufficient heavy water so that the flow would always be from blanket to core. In the first experiment it was found that a maximum flow of 6 lb/min could be provided by transferring condensate from the fuel low-pressure system. Furthermore, by keeping the blanket pressurizer completely filled with water, pressure fluctuations of the high-pressure systems were minimized. Under these circumstances and with fuel being pumped to the core circuit only, it was determined that, although intermixing between the core and blanket could not be prevented, the ratio of core-to-blanket fuel concentration could be controlled. At the 6-lb/min rate of purge into the blanket region, intermixing was at a rate of 3 to 4 lb/min and the core-blanket concentration ratio was 3:1. Calculations indicated that at this ratio more than half the power would still be generated in the core. At lower purge rates the concentration ratio approached 1:1, where 70% of the power would be generated in the blanket. Thus, it appeared that, simply by revising operating procedures, normal operation could be continued and nearly all the original objectives of the experiment realized.

Run 16 was planned to verify these projections; the reactor was brought to criticality on June 4 and was operated continuously at power levels to 5 Mw for 30 days. No significant difficulties developed, and the feasibility of operation with fuel in core and blanket was demonstrated conclusively. When the run was terminated for a scheduled shutdown on June 3, 1600 Mwhr had been accumulated in continuous operation. The corrosion rate was steady at 0.5 to 0.7 mpy throughout the run.

The purpose of the shutdown was to permit further examination of the core and to install corrosion specimens inside the core and blanket. Efforts to view the leak site from the blanket side were again frustrated by inadequate illumination and the extreme difficulty of remotely positioning the viewing mirror at the rear of the core tank; however, the northern half of the core exterior was inspected, as well as the core interior. During the shutdown, control circuitry was modified to provide maximum operating safety during future runs with fuel in both core and blanket regions. Also, the east head of the fuel feed pump was replaced, a crossover was installed between the core and blanket steam systems for increased flexibility in power extraction, a corrosion-specimen array was inserted into the core, and metallurgical specimens were replaced in the blanket.

Operation will be continued to provide long-term corrosion data and further information concerning the fuel stability.

2. HRT Processing Plant

In the HRT processing plant, preparations were completed for radioactive operation. A defective electrically operated weigh cell was replaced, spare power wiring was installed, and the cell air cooler was converted to 220-v operation. Cell leak checks following closure of the cell indicated a leak rate of 9 liters/min at 30 psia pressure, compared with a specification limit of 20 liters/min.

In the first three operating periods, of 120, 310, and 339 hr, the hydroclone system removed 150, 100, and 107 g of corrosion products from the reactor. The first period was during the subcritical mixing experiments of reactor runs 15 and 16 and was followed by two periods of operation during reactor run 16 in which integrated powers totaled 249 and 1235 Mwhr. Solids removed averaged 53% Fe, 5% Cr, and 8% Zr, with the remainder Al and Ni.

Fission-product concentration factors of 390 for Zr, 600 for Ru, and 56 for Te were noted during the second run, the only power run for which data are available.

Modifications completed in the waste system provide for use of the existing waste evaporator for temporary storage of 4 *M* H_2SO_4 waste solutions from chemical plant operations or contaminated fuel from the reactor.

The fission gases were effectively retained on the charcoal beds; as designed, only the 10.3-year Kr^{85} was swept through the bed and discharged up the stack. Maximum bed temperatures were only 10°C above cooling-water temperature.

3. HRT Reactor Analysis

The variation of the inlet and outlet temperatures in the two-region HRT was calculated as a function of power level. The reactor was divided into regions, with the average temperature in each region varying in accordance with the fluid-flow rate and energy-generation rate in that region. Two-dimensional, two-group calculations were used. It was found that the average critical temperature was nearly equal to the arithmetic average of the core inlet and outlet temperatures for powers up to 5 Mw.

The maximum temperature of the stainless steel surface in the HRT dome was estimated to have been no more than 18°C above the core inlet temperature when the reactor was operated at 1.5 Mw as a two-region system. With the dome insulation removed, even at 10 Mw, the maximum bellows-surface temperature will probably be less than 10°C above the core inlet temperature.

An analysis of the stresses which were present in the HRT core vessel indicates that vessel failure could be predicted only if a defect were present which caused serious concentration of stresses.

Pressure and thermal stresses in the wall of the HRT pressure vessel were computed for both one- and two-region reactor operation. The stresses were about the same for the two cases. Based on permissible stresses and a power level of 5 Mw, the maximum permissible temperature difference across the pressure-vessel wall is about 90°F; this temperature difference is limited to 50°F for 10-Mw operation.

The nuclear characteristics of the HRT were calculated for operation with several ratios of blanket-to-core fuel concentrations. With equal fuel concentrations in the core and blanket regions the critical concentration would be 2.5 g of U^{235} per liter in a clean system at 280°C. About 70% of the power would be generated in the blanket region. About 50% of the power would be generated in the blanket when the ratio of blanket-to-core fuel concentrations is 0.5. Under this condition addition of the corrosion samples to the core region would increase the critical concentration of fuel in the core by about 8.5%.

The safety of the present HRT was examined. The blanket pressurizer was assumed to be completely filled, and the core and blanket regions were connected by a small opening. Various blanket fuel concentrations were considered. It appears permissible to operate with blanket fuel concentrations up to about 0.6 of the core fuel concentration insofar as reactor safety is concerned.

4. HRT Component Development

The 400A-1 development pump was installed in the HRT mockup and has circulated 0.04 *m* uranyl sulfate solution for 2623 hr without difficulty. A revised cooling-water configuration used on current Westinghouse production pumps was tested successfully in the 400A-2 pump.

The feed-pump heads and two purge-pump heads have operated well over a year in endurance tests simulating reactor service.

Devices for viewing the outside of the HRT core tank with mirror systems and with a television camera were developed. A hole saw was adapted for cutting specimens from the top diffuser plate of the core tank.

The HRT spare heat exchanger was received, and passed the required thermal-cycle and leak tests.

Tests of a flow model of the HRT core revealed that solids were retained quantitatively in the core, concentrating near the outer edges of the perforated plates and on the diffuser cone. Tests of a flow model with a north polar inlet and concentric outlet showed that solids were removed readily.

The HRT mockup operated for 2623 hr on 0.042 *m* UO_2SO_4 solution containing 0.005 to 0.035 *m* $CuSO_4$ and 0.021 to 0.025 *m* excess acid. The operation was at 1400 psi and 280°C.

The generalized corrosion rate with a titanium letdown heat exchanger has been 0.80 mpy, compared with 1.5 mpy with a stainless steel letdown heat exchanger.

Preliminary inventory measurements indicated a precision of ±3% at the 95% confidence level. However, the variance in the dump-tank volume measurement was controlling and will need to be improved.

A pressurizer purge flow of 10 gph will precipitate from 15 to 30 g of uranium per day. A 3-gph purge rate will redissolve precipitated uranium provided there is at least 60% excess acid.

The only mechanical troubles were packing-gland and suction-check-valve failures in the high-pressure oxygen compressor. However, these did not interrupt the loop operation.

The system was modified to incorporate an all-titanium pressurizer in which fuel solution will be boiled to furnish steam to pressurize the system. The pressurizer is heated by Dowtherm A.

Other modifications include changing the instrumentation to control the pressurizer level by varying the feed rate with a constant letdown, installing an intermediate system on the O_2 compressor to eliminate a troublesome packing gland, and installing a rotometer in the purge-pump suction.

5. HRT Design

Some studies of the operation of the HRT as a single-region machine were completed. An equilibrium concentration between the core and blanket systems can be reached in 4 hr if the transfer rate between systems is about 100 lb/min. The needed transfer rate can be accomplished either by cross-connecting the lines leading to the processing cell or by connecting the core and blanket access ports. A blanket dump-tank pressure of 375 psia was estimated to result from dumping the entire contents of the fuel and blanket systems into this tank. The allowable design pressure is 500 psia. It was recommended that the blanket-system steam flow-control valves be replaced with larger valves. Interconnection of the purge pumps was not recommended.

Based on the data from run 16, the thermal stress in the HRT pressure vessel is estimated to have been 6800 psi at 5 Mw.

The design of a replacement pressure vessel for the HRT has been initiated. Major emphasis is being placed on a vessel with a concentric inlet-outlet core tank. A preliminary investigation of the heat transfer through the core wall is being made.

A special reactor-cell plug was designed to allow leak-tight passage of the new electrical cables to the circulating pumps, the space coolers, and the pressurizer heaters; this plug was installed in place of one of the existing periscope plugs. A study of the feasibility of performing dry maintenance was completed by Vitro Engineering Company. Special sampling stations were designed for drawing samples of boiler

water from the main heat exchangers. Aluminum-can insulation assemblies were designed to replace the insulation that would be removed when flanges are opened for maintenance. A manipulator for handling a 2-in.-dia television camera in the pressure vessel for inspection of the outer surface of the core was designed. To get a metallurgical sample of the core tank, a tool was designed for cutting a piece from the top diffuser plate.

6. HRT Controls and Instrumentation

Because of erosive wear on the shutoff-seating cone of the presently used HRT letdown valve, which has a $\frac{1}{4}$-in.-dia bore seat, a new valve was designed with a $\frac{1}{8}$-in.-dia bore seat. The new valve also features a lower stem guide to avoid plug misalignment.

A 2-in.-dia television camera designed for resistance to radiation is being incorporated in a remotely manipulated mechanism under development for viewing the HRT core vessel. The camera preamplifier is located at the end of a cable 10 ft 6 in. long to permit most of the electronic components to be located out of the high radiation field associated with the core vessel.

The capacity of the capillary pressure-drop system used to measure the flow of oxygen gas into the HRT high-pressure fuel system was increased by installing a shorter length of metering capillary.

The installation of a new power-wiring system inside the reactor containment tank was completed. The new system, consisting of swaged magnesium oxide–insulated wires in copper-tube sheaths with cable ends terminated by hermetic ceramic-to-metal seals, replaces the sealed-conduit Fiberglas-insulated wire system. The Fiberglas-insulated wire was subject to breakdown at operating voltages when moisture was present in the conduit.

To facilitate single-region operation and to provide for the increased heat generation in the blanket system, several revisions were necessary in control-valve sizes and in automatic-control safety functions.

PART II. REACTOR DESIGN, RESEARCH, AND ANALYSIS

7. Reactor Design

Design of HRE-3 as a two-region power breeder reactor has been suspended until the problems which have arisen in operation of the HRT are resolved. The work done on HRE-3 is being summarized in a report. Conceptual layouts were made of the reactor system showing the equipment and compartments. The heat exchangers were studied in some detail. A U-tube heat exchanger was suggested for the fuel solution, and an inverted L-tube heat exchanger was suggested for the blanket slurry.

A small single-region, circulating-slurry reactor to investigate the problems fundamental to slurry fuels in reactor systems is being studied. This reactor, designated as HRE-4, would be in the 1- to 5-Mw range. A flowsheet with a high-pressure dump system is under consideration. Heat exchanger designs with slurry in the tube or slurry in the shell are being considered. ORNL Building 7503 is being considered as a location for the reactor.

8. Research and Analysis

A homogeneous reactor having two concentric blanket regions with different thorium concentrations in each has been examined with respect to its nuclear characteristics. The breeding ratio in this double-blanket reactor was virtually the same as that in a single-blanket reactor. Settling of slurry in the region nearest the core would result in a large reactivity addition, but the reactivity change would be small if settling occurred in the outer region.

The accuracy with which the breeding ratio of HRE-3 could be determined after a period of reactor operation was investigated. Inaccuracies in the core U^{233} inventory and blanket U^{233} and Pa^{233} inventories appear to be the major sources of error. Appreciable errors could result from attempting to determine inventories by sampling the reactor contents.

The influence of the core inlet-outlet line on the flux distribution in HRE-3 was calculated by use of a reactor code which treats two space variables. The ratio of local to average flux

was increased somewhat in the vicinity of the inlet, but the breeding ratio was reduced only 0.3%.

The decrease in HRE-3 breeding ratio associated with an increase in thickness of the Zircaloy core tank and shroud was computed as a function of metal thickness and spacing. For the case of a ½-in.-thick core vessel and ½-in.-thick shroud spaced 5 in. apart, the breeding ratio would be 0.047 less than if there were no Zircaloy present.

The reduction in HRE-3 breeding ratio resulting from neutron absorptions in the core inlet line was examined for spherical and cylindrical cores; it was found to be less than 0.5% if the pipe does not extend more than one fourth of the way to the bottom of the core. The power density at the end of the pipe would be 57 kw/liter if it extended 5 in. into the sphere.

The possibility of criticality occurring in the HRE-3 blanket dump tanks was investigated by estimating the critical concentration for a system having zero neutron leakage. If all the uranium in the HRE-3 were uniformly mixed with all the thorium, the resulting fuel concentration would not cause the system to become critical even at 20°C.

A survey was made of the nuclear characteristics of small, one-region, ThO_2-water reactors fueled with U^{235}. Reactor diameters up to 5 ft were considered. For the D_2O reactors, a minimum in the U^{235}/Th ratio occurred when the thorium concentration was about 200 g/liter. For H_2O reactors, this minimum occurred when the thorium concentration was greater than 600 g/liter.

The standard two-group, two-region Oracle code for spherical reactors was modified to include fissions in the fast group; a first-flight correction was added to an Oracle code which calculates critical concentrations in one-region reactors. A numerical integration procedure for a first-order differential equation was programmed for the IBM-704. Kinetic equations pertaining to two-region reactor operation have been programmed; the two regions can be either separate or connected. A code has been written which calculates the reactivity effects associated with slurry settling in finite, bare cylindrical reactors. A general heat transfer code has been prepared which calculates temperature distributions in three-dimensional geometry.

The accuracy of the Bingham-plastic relation for describing the flow characteristics of thoria slurries was investigated by applying it and a more general equation to data obtained with the horizontal capillary-tube viscometer. The Bingham relation was found to be adequate when the shear-rate range was specified. The spread of yield-stress data for thoria slurries having a specified concentration was reduced from greater than 25- to less than 4-fold by use of a relation involving the mean particle diameter of the thoria.

A vertical capillary-tube viscometer for routine determination of the shear diagrams of thoria slurries has been designed. The viscometer has a length-to-diameter ratio of no less than 1000 and will require about 200 ml of slurry.

A 30-gpm loop has been constructed for use in investigation of the caking of slurries. The loop contains a multidiameter test section in which three different flow velocities exist.

Samples of thoria spheres have been treated with various chemicals in an attempt to make them more resistant to disintegration. Spheres which were dried and calcined at 1200°C after sequential treatment with HNO_3, $Th(NO_3)_4$, and NH_4OH exhibited a marked increase in resistance to degradation.

Dye-retention studies of the flow patterns in two HRE-3 blanket models were completed. The last visible trace of dye was always associated with thin fluid filaments which clung to the outside of the shroud.

Fluid flow in a cylindrical vessel with a concentric inlet and outlet, representing a possible HRE-3 core design, was studied by observing the motion of phosphorescent particles activated by a plane light source. The inlet pipe had to extend to within 3 core diameters of the bottom of the vessel before a well-defined fluid jet that swept the bottom was obtained.

A fluid-flow visualization loop utilizing milling-yellow solution as a working fluid was constructed. Flow patterns in a number of two-dimensional models have been obtained. Results indicate that the stability of flow through a divergent channel is dependent upon the included angle of the channel; at an angle of 60 deg the flow was stable, while at an angle of 30 deg it was unstable.

An analysis of the boundary-layer equations for Bingham plastics showed that these equations

essentially reduce to those for Newtonian fluids if the Hedstrom number is less than the Reynolds number raised to the 1.5 power.

Fluidized-bed studies with thoria spheres indicated a slight decrease in slurry concentration with increasing bed height. The net fluid velocity required for slurry fluidization was found to be nearly the same as the slurry settling velocity.

PART III. ENGINEERING DEVELOPMENT

9. Development of Fuel and Slurry System Components

The high-pressure recombiner loop was repaired, and an Inconel natural-circulation attachment was installed for testing at 1500 psi. The lower explosive limit of $D_2-\frac{1}{2}O_2-D_2O$ steam was observed to be 16 mole % gas compared with 6 mole % in the hydrogen system. The solubility of $H_2-\frac{1}{2}O_2$ in water and UO_2SO_4 solution at 250°C appeared to be 50% greater than that observed for the individual gases. The practicability of boiling uranyl sulfate solution in titanium without excessive corrosive attack was demonstrated in a small system.

The canned-motor blower circulated a steam-nitrogen mixture satisfactorily for 2700 hr. Flowsheets were prepared for conversion of the 4000-gpm Byron Jackson pump loop to slurry operation. The layout of the Reliance 6000-gpm top-maintenance pump was completed, and test programs were started on internal seals and motor irradiation. The 300A slurry loop was fabricated and shakedown runs were completed. Fabrication of a second slurry pump development loop was started. A one-year contract was awarded to Franklin Institute to determine the wear of bearings operating in ThO_2 slurry.

A remote drive was installed on the Pressure Products Industries diaphragm compressor to eliminate plunger-packing failures.

Testing of a 2.7-gpm double diaphragm solution feed-pump head has continued for 2000 hr. Construction of a single-diaphragm head of similar capacity was initiated. A single-stage turbine pump with a 300-psi head has been circulating HRT fuel solution successfully at a 300-psi head. Remote-leg and single-contour slurry feed pumps were developed and are performing satisfactorily in tests.

A gold-ring-seal solution dump valve failed to seal properly after 4000 dumps as a result of mechanical damage to the trim; a valve containing a type 17-4 PH stainless steel plug functioned properly after 4000 dumps.

In slurry valve-trim tests, better wear resistance was observed in materials such as tungsten carbide, boron carbide, and aluminum oxide than in metals. A hole eroded through an 0.063-in.-bore capillary after 1690 hr of continuous slurry letdown service.

Crane Company decided they were unable to fabricate high-pressure titanium-lined $3\frac{1}{2}$-in. and 20-in. pipe. The small titanium-lined heat exchanger was received from Pfaudler Company. The boiling-uranyl-sulfate pressurizer was fabricated successfully from titanium 110AT.

Promising results were obtained with 19-9 DL stainless steel high-strength bolting in contact with UO_2SO_4 solution.

A contract was placed with Griscom-Russell Company for small test steam generators. A loop has been built for flow tests of slurry heat exchangers.

Heat transfer coefficients of 2000 to 5000 $Btu/hr \cdot ft^2 \cdot °F$ were predicted between fluid and HRE-3 core-tank wall on the basis of low-temperature flow model tests. A one-third-scale model of the proposed HRE-3 blanket flow arrangement appeared to behave satisfactorily.

Separation of water from ThO_2 slurries was achieved by filtration and sedimentation.

Slurry was kept in suspension in a 6-in. glass dump tank by boiling around a heating coil. Boiling heat transfer coefficients were the same for water and for slurry containing 950 g of Th per kg of H_2O.

Settled-bed properties of thoria were found to be influenced by particle size, particle shape, additives, and prior history.

10. Development of Reactor Slurry Systems

The 100- and 200-gpm loops were operated for a total of 8389 hr during the last six months. Run 200A-15, to study the degradation characteristics of 1600°C-fired oxide, was started on February 4 and is still continuing. Initially charged to 1500 g of Th per kg of H_2O and operated for 400 hr, the oxide concentration was reduced to 700 g of Th per kg of H_2O to bring down the yield

stress to the selected design maximum of 0.1 lbf/ft^2. At 1544 hr, $UO_3 \cdot H_2O$ was added to ½ wt % to study its effect on the slurry yield stress, and MoO_3 was added at 2149 hr to a concentration of 1.16 mole %. Nitrogen absorption surface area remained constant at 1.5 m^2/g for the first 2032 hr; no later data are available. The average mean particle size decreased from 1.78 ± 0.16 μ to 1.63 ± 0.09 μ by 1350 hr (95% confidence level). The generalized attack rate was 1.5 mpy at the concentration of 1500 g of Th per kg of H_2O and decreased to 0.6 mpy at the concentration of 700 g of Th per kg of H_2O.

Sixteen runs were made in 100-gpm loops. In a slurry of 800°C-fired oxide that otherwise forms spheres, the presence of ½ wt % uranium or 1.16 mole % molybdenum (as the oxides) prevents the formation of spheres or cakes. The presence of 3000 ppm SO_4 (added as H_2SO_4) to 1600°C-fired oxide slurry produced a Newtonian fluid, but the attack rate was more than 10 times that normally experienced. Reducing the sulfate to 300 ppm reduced the attack rate to about 9 mpy in a slurry of at least 1225 g of Th per kg of H_2O, which is not excessive for such concentrated slurry in these loops. Difficulties in loop operation not attributable to the slurries precluded measurement of their rheological properties at the 300 ppm SO_4 level. In circulating a silica-coated 1600°C-fired thoria, the silica concentration in the slurry decreased rapidly to one-tenth of the initial concentration in 48 hr. There was no evidence of caking or sphere formation on circulating an 800°C-fired thoria, the oxalate of which had been digested for 48 hr prior to reduction to the oxide.

Pseudo-shear diagrams were obtained for various slurries being circulated in the 100- and 200-gpm loops. There is evidence that the ratio of yield stress to volume fraction solids cubed is a constant for a wide range of slurry concentrations. This ratio may also be constant for any slurry isotherm at high temperature.

A vertical-capillary-tube viscometer was designed and built for determination of rheological properties of small samples of thoria in water. By proper selection of the capillary tube from the three different sizes which have been calibrated, a wide range of rheological properties may be measured.

Alterations to the 300-SM blanket test facility prior to run SM-5 included replacement of the 1½-in. inlet nozzles with the original 2-in. nozzles, modifications of the blanket exit, installation of a continuously metering density bridge, addition of gamma-transmission survey facilities on the pressurizer, alterations of the pressurizer to permit gas pressurization, and installation of a Zircaloy-2 impeller in the 300A pump.

Run SM-5, of 1097 hr duration (645 hr with slurry in the system), was completed. The system could not be operated stably with gas pressurization, and steam pressurization was used. The Zircaloy-2 impeller showed very slight attack, comparable to that of titanium. The density bridge did not perform satisfactorily, owing to flow disturbances. Studies of the thoria distribution in the blanket showed that uniform distribution could not be obtained in the presently designed HRT blanket system. Substantial improvement can be obtained by using smaller inlet nozzles or by considerably increasing the flow.

An experimental program of gamma-absorption measurements was undertaken to increase confidence in the interpretation of the gamma-survey results obtained on the HRT blanket mockup vessel. A possible explanation of the peculiar shape of the pressure-vessel scans is the fact that the vessel hemispheres were spun from flat stock. Audigage measurements indicate a thickness variation from girth to pole consistent with the gamma transmission patterns.

A contract has been let to Combustion Engineering to fabricate an experimental blanket pressure vessel in conformity with HRE-3 design proposals, for operation at 2000 psi in the 300-SM loop. The new vessel will permit three different flow patterns:

1. entering at the bottom, flowing up between the core and a surrounding flow guide, and down outside the flow guide;
2. entering at the top, flowing down, and out the bottom (in this case, the flow guide is removed);
3. entering through two tangential nozzles 180 deg apart on the equator, and leaving at the top and bottom (flow guide removed).

Because the walls of the new vessel will be heavier than those of the present vessel, a 3-curie gamma source will be required for absorption measurements equivalent to those currently made. A facility capable of handling a 10-curie source

has been designed by Vitro Engineering Corporation.

A new low-pressure dump system for the 300-SM loop has been designed in which the pressure will be allowed to rise to a maximum of 135 psig during dumping by condensing flashing steam from the dump stream. All components are designed for 150-psig operation.

11. Instrument and Valve Development

In further testing of differential-transformer windings at 300°C, it was found that vacuum impregnation of the coil with an insulating medium will markedly reduce the zero and null shifts previously observed.

Heated-thermocouple probes for use as liquid-level sensors incorporating a heating element localized near the thermocouple to increase the speed of response were satisfactory in tests of insulation resistance during operation for 1½ months at 300°C.

Transmitting flowmeters of the variable-area type for measuring pulsating purge and feed flows and incorporating in-line flow connections were received for evaluation testing.

A transistorized electropneumatic converter was developed to provide a more reliable instrument for critical control loops by the elimination of vacuum tubes.

A systems-analysis review was made of the HRT heat exchanger feedwater control system which indicated that the present system is capable of smooth operation in the power range of 1 to 5 Mw.

A new, more compact, reversible, metallic-bellows type of valve actuator with a 40-in.^{2} effective area was received and will be life-tested with a valve load simulated by an opposing spring force. A control-valve actuating system using 500-psi water as the working fluid and a cylinder actuator was placed in preliminary test operation. A stacked-bellows control-valve actuator capable of developing about 20,000 lb of thrust developed a leak in a prime-mover bellows after 18,083 cycles on a test stand.

Three-ply prototype titanium bellows specified for 2500-psi 300°C service were successfully formed for an ORNL order but were not satisfactory upon life-testing. A new design with thicker plies and of double length is now being fabricated. A life-testing program for valve-stem sealing bellows was completed, with very satisfactory life being demonstrated for the type used in the HRT.

A prototype pneumatically actuated slurry sampling valve incorporating a bellows stem seal and replaceable trim was fabricated and will be service-tested in a test loop.

A slurry flow-control valve with a tungsten carbide plug, seal, and plug guide failed after 907 hr of service in the 30-gpm loop because film formation between the plug and close-fitting plug guide caused the valve to freeze.

PART IV. REACTOR MATERIALS RESEARCH

12. Solution Corrosion

Chemical stability studies with a solution similar to that in HRT run No. 13 (0.04 *m* UO_2SO_4, 0.025 *m* D_2SO_4, and 0.03 *m* $CuSO_4$ in D_2O) showed the solution to be stable at 300°C with as much as 750 ppm of nickel; attempts to increase the nickel concentration further resulted in loss of nickel and copper from solution. A solution containing 0.01 *m* UO_2SO_4, 0.02 *m* D_2SO_4, and 0.01 *m* $CuSO_4$ in heavy water was also stable at 300°C with 800 ppm nickel.

Several soluble sulfate salts at the 0.04 *m* concentration were added to 0.04 *m* UO_2SO_4–0.025 *m* D_2SO_4–0.03 *m* $CuSO_4$ solutions in an effort to reduce the corrosiveness of the solutions. Additions of either rubidium or lithium sulfate resulted in unstable solutions at 300°C. Solutions with beryllium and magnesium sulfates were stable, but the corrosion rate was excessive with the beryllium-containing solution. Magnesium sulfate, however, did suppress corrosion appreciably.

Loop runs in which oxygen was excluded from the uranyl sulfate solutions circulated at 250 to 280°C in stainless steel loops showed that uranium was completely reduced and precipitated and that accelerated corrosion occurred. Addition of oxygen resulted in oxidation of the uranium to the soluble hexavalent state and a decrease in the corrosion rate to a low value.

Yorkmesh as used in the entrainment separator of the HRT showed negligible corrosion when exposed in the vapor and solution phases of an iodine-containing uranyl sulfate solution at 100°C.

A final test of the mockup of the Zircaloy-2–stainless steel transition and expansion joint as

used in the HRT reactor vessel has been completed. Corrosion damage or leakage across the gasket was not detected. The apparatus will be disassembled and the components examined.

Corrosion tests in which titanium, Zircaloy-2, and stainless steel were exposed to the heavy phase of a high-temperature uranyl sulfate solution have been completed. Negligible attack of titanium and Zircaloy-2 was observed, but stainless steel corroded at a high rate.

Corrosion tests with carbon and stainless steels have been carried out at 300°C in boiler water containing about 50 ppm chloride ions and various concentrations of oxygen. The chloride had no measurable effect on the corrosion of either steel; however, the corrosion rate of carbon steel and, to a lesser extent stainless steel, was proportional to the oxygen concentration. With oxygen concentrations of <1 and 4 ppm, stressed specimens of stainless steel showed no cracking during 200-hr tests; with 9 ppm oxygen, some cracking was observed.

It has been shown that the presence of low concentrations of ruthenium in uranyl sulfate solutions circulated at 250°C in stainless steel loops causes the rapid oxidation of chromium (from the corroding metal and from previously deposited oxide scale) to the hexavalent state; the chromium(VI) then serves as a corrosion inhibitor. A similar behavior of ruthenium was also found in sulfuric acid solutions.

The stress-corrosion cracking susceptibility of several alloys was investigated by using a technique whereby pipe bends of the alloys were internally heated with steam and externally cooled by a spray of chloride-containing potable water. As-bent type 347 stainless steel pipes developed many cracks, but either shot blasting or cathodically protecting the pipes prevented cracking. Annealing after cold forming did not eliminate cracking in all cases; however, the frequency of cracking was reduced. Titanium, Croloy 16-1 stainless steel, Nionel, and Inconel did not crack during tests of 990 to 4990 hr. Incoloy T developed cracks during a 1990-hr test.

Stress specimens of several alloys have been tested at 300°C in water containing oxygen and 100 ppm of chloride. Generally, at a pH of 10.5, high-nickel alloys such as Nionel and Incoloy were more resistant to cracking than the austenitic stainless steels; but at a pH of 2.8 they were as susceptible to cracking as the austenitic stainless steels. Croloy 16-1 stainless steel cracked at pH 6.5 but did not crack at pH 10.5. No cracking of type 347 stainless steel was experienced when oxygen was completely removed.

The pre-exposure of stress specimens of type 347 stainless steel in boiling, chloride-free uranyl sulfate solution was 100% effective in preventing stress-corrosion cracking in a similar environment containing 50 ppm of chloride. In the absence of the pretreatment, 55% of the specimens cracked in the chloride-containing environment. Prefilming at temperatures of 125, 150, 175, and 200°C has also been completely effective in preventing cracking in the boiling, chloride-containing uranyl sulfate solution.

Niobium was susceptible to mild pitting attack in uranyl sulfate solutions at 100 and 200°C and underwent catastrophic attack at 300°C. The general corrosion resistance of type 17-4 PH stainless steel was excellent in a number of reactor-related environments. However, bolt-type stress specimens partially hardened to 37 Rockwell C cracked during 1000 hr in the vapor and liquid phases of a chloride-free uranyl sulfate solution at 280°C. Additional testing with Croloy 16-1 stainless steel has demonstrated that the alloy is not suitable for use in uranyl sulfate solutions. The corrosion resistance of Nionel was nearly equal to that of type 347 stainless steel in a number of reactor-related environments. Its apparent immunity to cracking in chloride-containing uranyl sulfate solution makes its use especially attractive. Flame-Plate (a hard-facing material) and sensitized type 202 stainless steel were unsatisfactory for service in uranyl sulfate solutions.

13. Slurry Corrosion

The construction and testing of a third slurry corrosion test loop, designated ES, were completed during this report period. The loop performed satisfactorily when circulating thorium oxide slurry at an average concentration of 1154 g of Th per kg of H_2O at 280°C.

Pressure drop measurements of venturi flowmeters in loops BS and CS were correlated with slurry flow rate and density in two slurry runs. These measurements indicate that, in general,

changes in slurry flow and/or density (concentration) can be followed by means of the venturi flowmeter readings.

Hydroclones of 0.4-in. size were used to remove thorium oxide slurry from three loop runs while operating at temperatures to 280°C and circulating thorium oxide slurries at concentrations up to 1580 g of ThO_2 per kg of H_2O; 99% of the thorium oxide was removed from the circulating stream.

Dynamic-corrosion data and operating observations are reported for seven 100A pump-loop tests utilizing oxygenated slurries of high-calcined classified thoria.

Six loop tests were completed at 280°C with oxygenated slurries of thoria (calcined at 1400 to 1600°C) as part of a series of tests to determine the effects of particle size and velocity on the attack on constructional materials. In one test, thoria of 1.2 μ average particle size was circulated at an average concentration of 1010 g of Th per kg of H_2O for 1550 hr. The average attack rate for the entire austenitic stainless steel circulating system was 1 mpy. Average rates of attack on pin-type corrosion specimens which were exposed to slurry having velocities of 20 and 40 fps, respectively, were 2 and 19 mpy for austenitic and martensitic stainless steels, 0.7 and 4 mpy for titanium alloys, and 0.0 and 0.7 mpy for Zircaloy-2. Increased attack at the higher velocity was due principally to erosion.

Approximately the same rates of attack were observed in a similar test of 1003 hr duration in which thoria having an initial mean particle size of 1.7 μ was circulated at a concentration of 1450 g of Th per kg of H_2O. The thoria was degraded to an average size of 1.4 μ during the test. When the degraded thoria was circulated at a concentration of 1210 g of Th per kg of H_2O in a subsequent 579-hr test, the average attack rates were approximately eightfold lower. A Zircaloy-2 impeller used during the run lost only 2.5 g.

Thoria with a mean particle size of 0.9 μ was circulated at concentrations of 800 to 1150 g of Th per kg of H_2O in three tests. Attack rates for austenitic stainless steels and titanium and zirconium alloys were about the same as those obtained in many previous comparable tests with slurries of 1.2 to 1.7 μ thoria. Unlike preparations of larger particle size, the slurry of 0.9 μ thoria formed heavy sludges while being circulated in the test loops.

In loop tests made to study the effect of operating temperature on slurry attack, significantly lower corrosion-erosion rates were observed at 200°C than at 280°C with an oxygenated slurry of 1.7 μ thoria at comparable conditions of slurry pH and concentration. Slurry handling properties were similar at the different operating temperatures.

Corrosion data are reported for in-line coupon and stress specimens of selected alloys which were exposed in run SM-4 of the slurry blanket mockup.

Tests made to study the effect of atmosphere, circulation temperature, and thoria properties on the corrosion-erosion attack by circulating aqueous slurries have been completed. Corrosion rates were greater with hydrogen atmospheres than with oxygen atmospheres, the effect ranging from a factor of 2 for Ti-75A to a factor of 9 for carbon steel. Corrosion rates generally increased about twofold per 35°C increase in temperature. Differences in thoria preparations were noted, possibly associated with particle size.

In toroid tests, coarse sintered aggregates, with a mean diameter of 60 μ, of 1600°C-calcined ThO_2 prepared by jet precipitation were circulated at concentrations of 50 to 1000 g of Th per kg of H_2O at 250°C and velocities of 10 and 26 fps for 300 hr. Attack rates were high, and a pronounced dependence of attack rate on concentration was observed. The large particles were degraded to a mean size of 0.5 to 0.7 μ during circulation and a decrease in crystallite size was observed.

The effect of sodium aluminate additions was examined in a series of toroid tests using two thoria preparations of 800°C-calcined oxides at a concentration of 500 g of Th per kg of H_2O at 26 fps and at an operating temperature of 280°C. Similar tests were made at a concentration of 1000 g of Th per kg of H_2O with one of the preparations. In one test, the sodium ion had been essentially removed by dialysis. In general, the addition of $NaAlO_2$ increased the attack. At the higher $NaAlO_2$ concentrations, the attack of titanium-75A was severe, and was presumably associated with the alkalinity of the slurry. Removal of the sodium ion by dialysis resulted in a greatly reduced general attack.

Tests of the effect of molybdenum trioxide addition were conducted in oxygen and hydrogen atmospheres at a concentration of 1500 g of Th per kg of H_2O at a velocity of 26 fps at 280°C

for 300 hr. The addition of molybdenum trioxide increased the attack of carbon steel and Zircaloy-3A. Attack in a hydrogen atmosphere was greater than that in an oxygen atmosphere, especially for titanium-75A and type 347 stainless steel.

Toroid tests were made to study the corrosion-erosion attack and behavior on circulation of aqueous slurries of thoria spheres by the Houdry Process Corporation. The spheres were of random shape and size, ranging from 3 to 150 μ, and had been calcined at 1000°C. Portions were recalcined for 4 hr at 1200 and 1600°C. At a concentration of 1500 g of Th per kg of H_2O, oxygenated aqueous slurries of the original and recalcined spheres were circulated for 300 hr at 280°C.

The general levels of corrosion by the microspheres appeared to be low, comparing favorably with nonspherical thoria. In none of the tests were the spheres very degraded. No particular effect of size range was noted, except that the smaller size ranges showed a greater relative increase in corrosion rate in response to increased circulation velocity or to increased calcination temperature. In certain of the tests, oxygen depletion occurred, higher pH was found, and quite aggressive corrosion was encountered.

In 100-hr toroid tests at 280°C, at 26 fps, and a concentration of 1500 g of Th per kg of H_2O, the performance of unclassified micropulverized thoria of 1.7 μ mean particle size was compared with that of classified 1.6-μ micropulverized thoria. Both preparations produced moderately high attack rates on type 347 stainless steel, titanium-75A, and Armco iron. Except for type 347 stainless steel, attack of the alloys was less severe with the slurry of the classified thoria.

The stability and corrosion attack of three experimental sol preparations furnished by the Davison Chemical Company were evaluated. These contained ~300 g of thorium and 200 g of SiO_2 per liter, 8000 to 9000 ppm of Na, and up to 800 ppm Cl. Two preparations were circulated at 280°C for 300 hr, and the third at 250°C; all were flocculated after circulation. Corrosion rates were low to moderate.

A generalized corrosion rate of 0.8 mpy based on 1070 hr at 280°C was observed for a Zircaloy-2 autoclave containing an oxygenated thoria-urania slurry in D_2O. The slurry was prepared from thoria containing 0.5% enriched uranium based on thorium and contained 990 g of Th per kg of D_2O with 0.021 m MoO_3 added. It was exposed to 690 hr irradiation in the LITR HB-6 rocking-autoclave facility at an estimated flux of 5×10^{12} neutrons·cm^{-2}·sec^{-1}. The recombination of radiolytic gas was generally consistent with first-order kinetics, having a 280°C catalytic activity at 100 psi radiolytic D_2 of 0.2–0.7 moles D_2/liter·hr and a G value for deuterium production of 0.57–0.71. Correlation of corrosion-rate data indicated that a corrosion rate of several tenths of 1 mpy could be attributed to radiation effects at an estimated maximum fission power density of 0.6 w/ml.

In a Zircaloy-2 autoclave containing a thoria-urania slurry in D_2O with a deuterium atmosphere which was operated for 1230 hr at 280°C, the generalized corrosion rate was 0.4 mpy. The autoclave was exposed to 770 hr irradiation in the LITR HB-6 rocking facility at an estimated flux of 5×10^{12} neutrons·cm^{-2}·sec^{-1}. The thoria used was the same as that used in the above experiment, containing 0.5% uranium based on thorium. No measurable radiolytic gas was observed at 280°C. A maximum of 14 psi radiolytic deuterium was generated at 175°C, giving catalytic activities at 100 psi radiolytic deuterium of 0.004–0.006 mole D_2/liter·hr and G values for deuterium production of 0.010–0.027. Correlation of corrosion-rate data indicated that a corrosion rate of a few tenths of 1 mpy could be attributed to radiation effects at an estimated maximum fission power density of 0.6 w/ml.

Development work on an in-pile slurry toroid rotator was interrupted during this period because of work on the HRT core and blanket corrosion specimen assemblies as well as increased effort on a test model of an in-pile slurry loop. However, a system to maintain and control the toroid temperature during in-pile operation was devised. No operating tests of this system have been made yet.

A test model of a 5-gpm in-pile slurry loop for radiation-corrosion studies with thorium oxide slurries has been assembled. This loop, with a horizontal pressurizer, was designed to operate in the existing in-pile loop facilities of beam hole HB-4 of the LITR and is similar to the loops now used for radiation-corrosion studies with homogeneous reactor fuel solutions.

Test results from an experimental 5-gpm pump loop in which thorium oxide slurry was circulated

were encouraging. This loop was equipped with a vertical pressurizer. In addition, visual observations of slurry flow in transparent plastic models of a suitable loop core section (with corrosion specimens) and horizontal pressurizer, as required to fit into beam hole HB-4, indicated that satisfactory flow patterns could be achieved with these configurations. However, in two test runs in the loop, with the horizontal pressurizer, in which the loop was charged to a slurry concentration of 340 and 500 g of Th per kg of H_2O, thorium oxide accumulated in the pressurizer with a resultant loss from the main circulating stream.

14. Radiation Corrosion

A leak developed in the pump housing of loop L-2-22 after 686 hr of out-of-pile testing. The leak was a result of localized corrosion in the thermal-barrier region of the pump. A new pump has been installed, and the loop is now being operated in beam hole HB-2 at the LITR.

The first ORR test loop, O-1-20, has been assembled, and tests have begun in the mockup facility to demonstrate operating reliability and control under simulated in-pile conditions.

The fourteenth and fifteenth in-pile loop experiments, L-4-18 and L-2-19, were completed. These stainless steel loops were exposed in LITR beam holes HB-4 and HB-2, respectively. The sixteenth loop experiment, L-2-21, also fabricated of stainless steel, was exposed in the LITR beam hole HB-2. Examination of the L-2-21 experiment has not been completed.

The L-4-18 experiment was with a solution 0.17 *m* UO_2SO_4, 0.02 *m* H_2SO_4, and 0.07 *m* $CuSO_4$, in D_2O solvent at main-stream and pressurizer temperatures of 235 and 265°C, respectively. The L-2-19 experiment employed a solution 0.17 *m* UO_2SO_4, 0.02 *m* $CuSO_4$, 0.10 *m* H_2SO_4, and 0.20 *m* Li_2SO_4 (99.9% Li^7), in H_2O solvent at main-stream and pressurizer temperatures of 280 and 295°C, respectively. Termination of the experiments occurred through failure of the solution circulation pumps following 642 and 902 hr, respectively, of radiation with the LITR at 3 Mw. The over-all corrected stainless steel corrosion rates for the experiments, based on oxygen-consumption data, were 0.5 and 1.3 mpy.

Material balances of Fe, Ni, and Zr were attempted for each experiment by employing the results of analyses of scale removed from various portions of the loop outside the core together with the results of oxygen, nickel, and weight measurements. The results of the balance for L-4-18 indicate, qualitatively, a transport of zirconium from the core to the out-of-core locations, and a good balance for the nickel, with more than half in the scale. In contrast to the results from L-4-18 and other previously attempted balances, the L-2-19 balance indicated that only a small part of the zirconium that had oxidized in the core was in the scale. The nickel balance was good, with essentially all the nickel in solution.

The surfaces of Zircaloy-2 and zirconium specimens from the core of L-2-19 were found to be free of all but insignificant amounts of sorbed uranium. This finding is in contrast to that for the previous experiment, L-2-17, which employed a 0.04 *m* UO_2SO_4 solution with low concentrations of solute additives and operated at 300°C. The two specimens which were analyzed from L-2-17 retained sufficient uranium on the surfaces to account for an appreciable fraction of the total intensity of fission-fragment irradiation of the Zircaloy-2 surfaces. With experiment L-4-18, only the type 347 stainless steel core coupon holder was analyzed for sorbed surface uranium. The amount of uranium found, about 6 $\mu g/cm^2$, is comparable with that found on the high-velocity channel specimens in L-2-17.

The corrosion rates of Zircaloy-2 in the 235°C experiment, L-4-18, were lower than those observed at 250°C in previous loop experiments. This decrease in rate with decreasing temperature is in qualitative agreement with the effect noted in autoclave experiments at 250°C and below. Specimens of pickled Zr–15% Nb contained in the core of the experiment exhibited corrosion rates 0.2 to 0.6 of those for Zircaloy-2.

The corrosion rates of types 347 and 430L stainless steel in L-4-18 were in near agreement at fission power densities above about 4 w/ml. At values below 4 w/ml, the 430L specimens, in general, exhibited rates higher than those for type 347 but below 1 mpy. The steel behavior in this experiment was slightly better than that of type 309 SCb and 347 steel in experiment L-4-13, which was operated at 250°C and was the only previous loop to employ D_2O as a solvent.

The corrosion rates of Zircaloy-2 specimens at a given solution power density in L-2-19 appear to be in agreement with those observed in the 280°C experiment, L-2-14 (0.17 *m* UO_2SO_4,

0.4 m H_2SO_4, 0.15 m $CuSO_4$) and are less than those observed for core specimens in 280°C experiments with 0.17 m UO_2SO_4 solutions which were free of appreciable amounts of solution additivies.

The average corrosion rates for type 347 stainless steel core channel specimens in L-2-19 fall between those observed for the other 280°C experiments. A correlation has been observed between the corrosion rate of stainless steel in a given experiment and the estimated steady-state pressure of radiolytic gas in solution during the experiment. The rate is less at the higher pressure. Better corrosion resistance was exhibited by specimens of Incoloy and of types 430L and 304L stainless steel located in the low-velocity core annulus region than by specimens of type 347 stainless steel in the core channel holder.

Seven autoclave solution experiments (six in HB-5 and one in HB-6) were assembled and operated in the LITR. The design of corrosion coupon specimens for use in the HB-5 autoclaves has been changed to increase the fraction of coupon area exposed to the solution. The change may also promote better mixing of solution during rocking.

The data from nine autoclave experiments which were exposed in the three-hole facility in HB-5 are presented and discussed. The data may have been complicated by the thermal gradients and the very gentle stirring prevailing in these axially oriented autoclaves.

Five autoclave experiments in HB-5 comprised a series devoted to the study of four solution additives: lithium sulfate, silicotungstic acid, potassium perrhenate, and beryllium sulfate. The corrosion results are presented as a function of fission power density in solution and of the power density corrected for the amount of uranium in the scale, and the results are compared with a control experiment in the new facility. The data are interpreted as indicating that silicotungstic acid and $KReO_4$ may have a beneficial effect on Zircaloy-2 corrosion. The $BeSO_4$ and Li_2SO_4 additions had no apparent effect in these experiments.

The control experiment employed two specimens of a Zr–5% Sn alloy as well as specimens of Zircaloy-2. The Zr–5% Sn coupons corroded about 85% as much as the Zircaloy-2 at the same solution fission power densities, but the heavy scale from the Zr–5% Sn specimens contained less uranium than that from the Zircaloy-2. However, analyses of samples from the defilmed surfaces of one each of these Zr–5% Sn and Zircaloy-2 coupons indicated the presence of about 10 μg of uranium per square centimeter on each.

Two experiments with 0.17 m UO_2SO_4 depleted of U^{235} were carried out as part of an investigation of the pressure peaking observed with two previously reported experiments with depleted UO_2SO_4 solutions containing $CuSO_4$ in Zircaloy-2. The previous experiments were in vertically oriented autoclaves at 250°C. The present experiments were in the horizontally oriented autoclaves in HB-5, and the solutions were free of $CuSO_4$. The temperature of one test was 250°C; that of the other, 280°C. No pressure peaking was observed in these experiments. Although the exposure conditions were not exactly the same as those in the earlier tests, the results are tentatively regarded as evidence that the peaking observed in the previous tests was associated with a loss of $CuSO_4$ from those solutions during the initial exposures.

The 280°C depleted UO_2SO_4 experiment exhibited a linear corrosion rate of 0.4 mpy. All the Zircaloy-2 specimens exhibited weight gains as-removed. In another experiment in the HB-5 facility, oxygenated D_2O in a Zircaloy-2 autoclave with Zircaloy-2 specimens at 280°C also exhibited a linear rate of 0.4 mpy. Five of the Zircaloy-2 specimens in the D_2O experiment exhibited weight losses as removed from the autoclave. In comparison with data for the out-of-pile corrosion of Zircaloy-2, the results of the oxygen measurements in these two experiments indicate an increase in the rate of corrosion due to radiation, and the same increase for the oxygenated D_2O as for the solutions of depleted UO_2SO_4.

A stainless steel experiment was exposed in HB-5 which used a solution of composition similar to that in HRT run 13 except that uranium depleted of U^{235} was used in the autoclave. The shape of the corrosion-penetration–time curve is similar to that observed with other in-pile stainless steel autoclave experiments with UO_2SO_4 solution containing excess H_2SO_4. In previous experiments (at 250 and 280°C and 2–10 w/ml fission power density) an initial average rate for 100–300 hr of 1–5 mpy was followed by a continuing rate of 0.2–0.5 mpy. The depleted UO_2SO_4 test reported here corroded at an average rate of less than

1 mpy for the first 200–300 hr at 280°C. The temperature was reduced to 250°C after 370 radiation hours, and corrosion occurred at a rate less than 0.1 mpy.

Following HRT runs 13 and 14, several metallic specimens were removed from the high-pressure system and transferred to the Materials Section for examination. Samples of scale were also taken from the high-pressure system after these runs and transferred to the Materials Research Section. Examination and analysis of these several specimens are still in progress, but some of the results are available and are reported.

The assembly of a corrosion specimen holder for installation in the core tank of the HRT was completed during the past quarter with the installation of three thermocouples sheathed with stainless steel–titanium. These thermocouples extend to three different locations in the core vessel and will be used to estimate the temperature of the corrosion test specimens located in the core region. This specimen assembly was installed in the core tank and one without thermocouples was installed in the blanket region during the week of July 21, 1958.

15. Metallurgy

Quench-and-reheat transformation data obtained on the Zr-Nb-*X* alloys showed that the incubation period for hardening at all temperatures below 600°C was delayed in the 15Nb alloys for 1.3 hr by adding 3 wt % V, 2 hr by adding 5Pd, 4 hr by 2Mo, and more than two weeks by 5Mo. The transformation was delayed for more than 2 hr at any temperature below 600°C for the Zr-20Nb alloy and for the Zr-20Nb-*X* alloy with *X* as 2Mo or 2Pd. These times are sufficiently long to permit multipass welding without hardening in the heat-affected zone.

Microstructural examination of the Zr-Nb-*X* alloy specimens exposed in in-pile loop L-2-17 showed that no major changes in structure were caused by the radiation exposure.

A fabrication study of Zircaloy-2 established that the optimum annealing time and temperature to ensure recrystallization after working are ½ hr and 750–800°C. Impact and tensile blanks of nine fabrication schedules were annealed under these conditions. The tensile specimens have been pulled, and the data, including ellipticity along the specimen length from fracture to shoulder, are being analyzed to evaluate the effects of the various fabrication variables on the degree of preferred orientation and mechanical anisotropy.

Zircaloy-2 specimens hydrided at 300°C developed large hydride patches scattered over the surface of the specimens with no detectable hydride between the patches. No successful metallographic technique has been developed for the examination of very thin hydride layers on the surfaces of Zircaloy-2 specimens. The so-called "hydride needles" observed in the interior of Zircaloy-2 grains in a hydride specimen have been identified as deformation twins.

Zirconium, titanium, and type 430 stainless steel specimens exposed in various locations in a recombiner loop were analyzed for hydrogen content. The data do not agree with prior determinations.

Both the energy values and the transition region for Charpy V-notch impact-energy curves for Zircaloy-2 have been shown to vary with fabrication procedure, hydrogen content, specimen orientation, and notch orientation. Improved impact properties were found in plates fabricated by the developed procedure. While anisotropy of Zircaloy-2 plate is not necessarily reflected in the conventional tensile properties, it may be determined by comparing variations in the elliptical axes of the fracture surface.

Impact tests on crystal-bar zirconium and Zircaloy-3a samples which had been exposed in in-pile loops confirmed previous tensile data and showed no significant change in properties. Similar results were obtained with A-55 and A-110AT titanium.

Inert-gas welding procedures have been developed and proved by which Zircaloy-2 may be welded in air with only conventional equipment. Welds of a quality equivalent to those made in dry boxes are possible. Modifications of this procedure have permitted the construction of loop components from the high-strength titanium alloy A-110AT.

Ultrasonic attenuation has been measured in a variety of metals, and the effects of grain size, frequency, orientation, and metallurgical history are being studied. The attenuation in welds in type 347 stainless steel is so great that inspection is very difficult.

In studies of the ignition and combustion of Zircaloy-2 and titanium, it was found that the

oxygen pressures required to sustain the reactions were much lower than those required to start them. Higher oxygen pressures were required for the ignition of Zircaloy-2 than were required for the ignition of titanium. It was not possible to ignite these metals under water, but when the reaction was started in the vapor space, it continued, under some conditions, below the water surface.

Tensile and impact tests were completed on several steels irradiated to various neutron doses and at varying temperatures. For A-212B steel, the shift in impact transition temperature was reduced at irradiation temperatures above 540°F. This reduction cannot, however, be used as a general rule for all steels. It has been shown that in the flux and temperature ranges of interest to the HRP the magnitude of irradiation effects is extremely sensitive to dose and temperature of irradiation. As shown by tensile tests, fast-neutron doses of 2×10^{19} fast neutrons/cm^2 at 575°F were sufficient to cause serious damage to steels. With larger doses, temperatures in excess of 700°F were required to limit these changes to reasonable values.

PART V. CHEMICAL ENGINEERING DEVELOPMENT

16. Uranyl Sulfate Fuel Processing

Exposure of iodate-containing solutions, simulating those of the HRT, to gamma radiation at an intensity of 1.7 w per kg of H_2O did not affect iodate behavior. The silver on silver-coated stainless steel Yorkmesh was rapidly dissolved in simulated HRT fuel solution at 110°C but was not appreciably affected at 98°C.

Measurements of the amount of iodine present in the HRT during power operation indicated an iodine removal rate somewhat faster than the letdown rate from the high- to the low-pressure system. Evaluation of the I^{133}/I^{131} ratios in samples from the high-pressure system indicated a slower removal rate, but in either case the silver bed in the low-pressure system appeared to be trapping fission-produced iodine.

A hydroclone attached to a corrosion loop undergoing daily thermal cycling between 100 and 280°C removed 60% of the solids known to have been loose and circulating in the system. An axial-flow hydroclone of larger capacity but lower efficiency than the conical hydroclone used in the HRT is being tested.

17. Gaseous-Fission-Product Disposal

Evaluation of various inorganic adsorbents and of varieties of charcoal over the temperature range 25 to 300°C showed Columbia G activated charcoal to be the most efficient adsorber for krypton and xenon. The relation between water content and gas adsorption efficiency of charcoal and molecular sieves was evaluated, as were various methods of drying the adsorbents. In studies on the effect of various sweep gases on adsorption of krypton by charcoal, helium had the least effect. The dynamic adsorption coefficient of charcoal for krypton was lowered 51% as the partial pressure of krypton in an oxygen sweep stream was increased from 0.1 to 760 mm. In a dynamic system similar to the inlet section of the HRT charcoal beds, the ignition temperature of charcoal in oxygen was 290°C. With an oxygen flow rate of 250 cc/min in a 0.5-in.-dia pipe, the temperature was 800°C and the flame propagation rate was 0.145 cm/min. Equilibrium adsorption isotherms for xenon on various materials were determined at low pressures by the McBain sorption-balance technique, and similar data for krypton were obtained by tracer-counting techniques.

18. Uranyl Sulfate Blanket Processing

During the final experiment in the P-1 loop, 7.5 g of dissolved plutonium was injected (approximately 1 g every 8 hr) into 1.4 *m* UO_2SO_4 circulating at 250°C under 350 to 400 psi O_2. Although this amount of plutonium was equivalent to 645 mg per kg of H_2O, the amount of plutonium found in solution ranged from 200 mg per kg of H_2O early in the run to 26 mg per kg of H_2O at the end of the run. No solids were collected in the hydroclone underflow pot owing to a plug in the hydroclone feed line. Sufficient plutonium was adsorbed on stainless steel coupons (0.25 to 2.19 mg/cm^2) to account for the plutonium not in solution.

Upon completion of the plutonium runs, the loop was completely descaled and the adsorbed plutonium was removed by treatment with three passes of chromous sulfate descaling solution. The amount of plutonium removed was 4.06, 3.68, and 0.88 g for the three successive passes.

The loop has been transferred to the burial ground, where it will be disassembled and examined.

When dissolved plutonium was added in small increments to 1.4 *m* UO_2SO_4 under 195 psi O_2

at 250°C and contained in titanium, essentially all the plutonium remained in solution until the concentration increased to about 40 mg per kg of H_2O. When more plutonium was added, it hydrolyzed and 12–20% adsorbed on the titanium. The rest formed a loose PuO_2 precipitate. Under similar conditions but with a stoichiometric hydrogen plus oxygen overpressure, hydrolysis occurred at concentrations greater than 5 mg per kg of H_2O. Under these conditions all the plutonium removed from solution was adsorbed on the titanium. No PuO_2 precipitate was formed.

Tetravalent plutonium dissolved in 1.4 *m* UO_2SO_4 was sorbed on Dowex-50 cation exchange resin in the uranyl form. The capacity has not been measured, but it exceeded 1.56 mg of plutonium per gram of 16% cross-linked resin.

19. Thorium Oxide Slurry Development

A slurry of 1300°C-fired thorium–enriched-uranium oxide (0.5% U) containing 750 g of Th per kg of D_2O with 0.05 *m* MoO_3 as a catalyst was irradiated for 322 hr at 300°C in the LITR in the dash-pot-stirred irradiation bomb. Stirring was uninterrupted, and no radiolytic-gas pressure in excess of steam was observed.

Postirradiation examination of the slurries previously irradiated showed essentially all fission products associated with the slurry solids and no change in particle size.

A thoria-urania sol submitted for evaluation by the Davison Chemical Company was irradiated for 145 hr at 280°C without agitation. When examined after irradiation, the sol was found to have broken into a dilute slurry of gray material and a hard yellow cake.

Heat-transfer experiments with an idealized mockup of an ORR slurry autoclave irradiation facility showed that heat inputs up to 5 kw could be controlled with a water jacket (at 100°C) to give a bomb temperature of 300°C by using an air-helium mixture in a narrow annulus surrounding the autoclave as a variable thermal resistance. With a standard dash-pot-bomb autoclave with stirring coils, the rate of heat transfer and the temperature-control range attained by the use of "conductance control" were not significantly better than those obtained by simple air-cooling in the present LITR facility.

Results of out-of-pile tests with slurries at a concentration of 1000 g of Th per kg of H_2O and containing U^{235} at a U/Th ratio of 0.005 indicated that 0.02 *m* MoO_3 would be required to maintain a steady-state radiolytic-gas pressure of $\leq$ 100 psi D_2 at 280°C. This was confirmed in in-pile tests. Heating a slurry of the thorium-uranium oxide (1000 g of Th per kg of H_2O; $U^{235}/Th = 0.005$) containing 0.023 *m* MoO_3 at 200–285°C for 543 hr under O_2 overpressure decreased the catalytic activity for gas recombination (in the absence of H_2 activation) by 20%. With a U^{235}/Th ratio of 0.05, catalytic activity was low at MoO_3 concentrations from 0.013 to 0.3 *m*. After activation by treating with D_2 overpressure, slurries with MoO_3 concentrations from 0.001 to 0.032 *m* MoO_3 showed activities of 2–4 moles D_2/hr·liter, sufficient to be considered for use in in-pile experiments. Experiments on the addition of silver to slurries of this oxide and on "seeding" in catalytically active solids were also made.

The inactivity shown by molybdenum oxide in slurries of low-fired thorium oxide or those containing uranium oxide may result from the reaction of the molybdenum oxide with the thorium and/or uranium oxide to form catalytically inactive species. Data indicate that autoclaving of molybdenum oxide at 280°C in thorium oxide or thorium-uranium oxide slurry converts part of the molybdenum oxide to acid-soluble species; part is either strongly adsorbed on the thoria or converted to a form insoluble in both base and acid. The quantity of nonleachable MoO_3 per square meter of surface area increased with increasing oxide firing temperature and may be associated with the enhanced catalytic activity shown by slurries of the high-fired oxides containing MoO_3.

Thorium oxides with chemically bonded silicated surfaces were prepared by treatment with chlorosilane vapors, washing to remove chloride ion, and refiring to remove organic groups and leave a silicate surface. Thoria so treated showed no crystallite growth on being fired to as high as 1000°C, and as an aqueous slurry the thoria showed complete dispersion in high-temperature settling studies up to 280°C.

The influence of average particle size, uniformity, and shape on the yield stress of aqueous thoria slurries is being investigated. Data indicated that the yield stress is proportional to the reciprocal of the square of the average particle size. The uniformity of the oxide had little or no influence on the yield stress. Both the yield stress and coefficient of rigidity decreased with increasing firing temperature from 650 to 1600°C.

Hard lumps of 1600°C-fired thorium oxide were broken up by a pressure of 20,000 psi, which produced a material suitable for classification in the usual way; a pressure of 50,000 psi broke up even the microscopic agglomerates, dispersing the oxide into the individual particles formed by the oxalate relic structure. Hence, if scale-up of this procedure is possible, it might be used either as a preliminary to the present classification step or as a substitute.

In a high-temperature loop run, BS-22, carried out by the Materials Research Section of REED with a slurry of 1600°C-fired pilot plant oxide containing 1500 g of Th per kg of H_2O, about 40% of the slurry charged settled along the bottom of the loop system and could not be resuspended. No significant differences were found between the settled and the suspended material in chemical content, average particle size, settling rates from room temperature to 300°C (at a concentration of 250 g of Th per kg of H_2O), yield stress, and coefficient of rigidity.

The present concept of the HRE-4 one-region slurry reactor calls for a slurry fuel of thorium-uranium with a mole ratio of uranium to thorium of about 0.08 and a slurry concentration of 200 to 400 g of Th per kg of H_2O. Two methods of preparing the mixed odixe on an engineering scale are under investigation: (1) coprecipitation of the thorium-uranous oxalates and subsequent thermal decomposition and (2) adsorption or precipitation of a uranium compound on the thoria surface followed by a firing step to bind the uranium to the surface and to diffuse it into the thoria particles.

In thorium oxide preparation studies the use of a draft tube around the agitator in the oxalate precipitator permitted particle-size control (from 1 to 5 μ) by control of the recirculation rate of the precipitating system. Oxide products produced with the draft tube were as uniform as those produced without its use and had as small an oversize fraction after firing at 1600°C.

Results of $Th(C_2O_4)_2$ precipitation studies showed that digestion parameters can be changed to give varying products even though the mixing and initial precipitation are completed within seconds. The addition of compounds of the amine type to the precipitating system induced the formation of cubic crystals during the digestion.

Tests indicated that classification of 1600°C-fired thorium oxide in a hydroclone system was practical; a system was therefore designed for use in thorium oxide production. A Sharples P-4 Super-D-Canter gave acceptably small losses and continuously discharged 84% solids cake from a thorium oxide slurry. Rounded particles of oxide were produced by calcination in a zirconia-reflected flame.

Thorium oxide production was discontinued for about six weeks to permit modification to the equipment to improve safety factors in the handling of thorium oxide. About 5560 lb of 650°C-calcined oxide was prepared from the oxalate, and an additional 2535 lb of 650°C-recalcined oxide was prepared from classified product. Totals of 4025 lb of 1600°C-calcined oxide and 190 lb of 1400°C-calcined oxide were prepared in two gas-fired furnaces. Of the 4025 lb of 1600°C-fired oxide, 2915 lb was classified for use in slurry engineering studies.

20. In-Pile Slurry Loop

The in-pile slurry loop experiment has been redesigned to provide additional safeguards against overexposure of personnel to radiation during maintenance. Improved general maintenance of the loop components should also result from the design changes. The use of a hydroclone is being considered for removal of slurry from the irradiated loop. Standard autoclave valves have been modified with gold and 18% nickel–gold alloy seats to improve their performance in slurry service. The present schedule indicates that startup of the first loop in the reactor will be about March 1959. The segmenting facility – a remote-handling facility for segmenting and dismantling the irradiated loops – should be ready for operation by about April 1959.

PART VI. SUPPORTING CHEMICAL RESEARCH

21. Aqueous Systems at Elevated Temperatures

Simplified calculations have been carried out for the solubility of antlerite ($3CuO \cdot SO_3 \cdot 2H_2O$) in the four-component system UO_3-CuO-SO_3-H_2O at 290°C utilizing only data for the independent three-component systems UO_3-SO_3-H_2O and CuO-SO_3-H_2O. The calculated values are compared with experimental values in the four-component system and show some consistent agreement. Plans are to attempt development of a modified

treatment for multicomponent systems pending further solubility studies.

Phase-equilibrium data for the system NiO-SO_3-H_2O have been obtained from 150 to 300°C and from 1 to 10^{-4} m SO_3. These data indicate $NiSO_4 \cdot H_2O$ to be the stable solid phase at high concentration of SO_3 and at the higher temperatures, whereas several basic nickel sulfates appear to exist as stable species in lower concentration ranges. The completed phase-equilibrium data are to be combined with data for other three-component systems such as UO_3-SO_3-H_2O and CuO-SO_3-H_2O in an attempt to correlate solubility interactions in reactor fuel solutions.

The measurement of vapor pressures of aqueous systems at elevated temperature has been resumed. The current goal of this investigation is to attain a method for measuring absolute vapor pressures to a high degree of precision and accuracy to temperatures approaching the critical temperature of water. The use of a differential manometer for measurement at high temperature is being investigated.

An investigation is being made to measure the equilibrium compositions of the light and heavy liquid phases in the systems UO_3-SO_3-H_2O and UO_3-SO_3-D_2O.

22. Reactions in Aqueous Solutions

The decomposition of peroxide in simulated HRT fuel solution was studied at temperatures of 50, 70, and 90°C with solutions prepared from enriched uranium and heavy water. The temperature dependence was found to be not significantly different from that previously reported for light-water solutions at the time of the operation of HRE-1. Decomposition rates in heavy-water solutions were 13% higher than those in analogous light-water solutions, a possible indication of acid catalysis. The addition of copper to catalyze the decomposition did not appear to cause a lowering of the activation energy for the reaction.

23. Thorium Oxide Systems

A method for measuring the pH of suspensions has been tested which is free of the possible error resulting from a calomel electrode in contact with a suspension. It is shown that the method gives reasonable reproducibility when applied to ThO_2 slurries containing HNO_3. Supplementary data show that readings are significantly lower when the calomel electrode is in contact with the slurry and the slurry is contaminated with atmospheric CO_2.

Two samples of ThO_2 slurries are shown to have been strongly peptized by HNO_3. The settled bed of one was found to be a Newtonian fluid after being undisturbed for nearly a year.

24. Heavy-Element and Fission-Product Chemistry

The fate of the neptunyl ion in a nitric acid solution, 7.43×10^{-4} M $RbNp^{237}O_2(NO_3)_3$ in 0.1 M DNO_3–D_2O at 250°C, was followed spectrophotometrically from 0.6 to 1.3 μ for a period of 45 hr and a temperature range from 4.5 to 252°C. Neptunium(VI) was found to be reduced irreversibly and quantitatively to Np(V), the rate of the reduction increasing with rising temperature. The effect of differential-temperature absorbance of the solvent introduced only a minor correction below 1.2 μ, but above 1.2 μ the effect became large enough to complicate seriously the measurements of neptunium spectra.

Samples of HRT fuel solution, withdrawn during runs 13 and 14, were analyzed for radionuclides. The concentration of each fission product determined from the analysis was compared with the concentration calculated on the basis of the fission product being completely soluble in solution. The results are in substantial agreement with earlier results obtained in in-pile loop experiments.

PART VII. ANALYTICAL CHEMISTRY

25. Analytical Chemistry

Improved methods were developed for the determination of thorium, zirconium, titanium, aluminum, fluoride, and chloride in thorium oxide. A rapid high-frequency titration procedure was demonstrated as being satisfactory for the determination of macro amounts of thorium with a coefficient of variation of 0.7%. A method was developed for the separation of microgram quantities of zirconium from thorium and minor components of thorium oxide slurries by an extraction procedure and subsequent determination of the zirconium colorimetrically as a complex with quercetin or, for extremely small amounts of zirconium, fluorometrically as a morin-zirconium complex. Methods were developed for circumventing the interference of chromium(VI), uranium,

and molybdenum(VI) in the spectrophotometric determination of titanium with Tiron as the chromogenic reagent. It has been established that microgram quantities of aluminum can be separated from thorium, fluoride, iron, and other possible interferences by the use of suitable masking agents in conjunction with an extraction procedure, after which the aluminum in the organic extract may be determined either flame photometrically or fluorometrically. Nonleachable fluoride in microgram amounts in high-fired thorium oxide can be removed by a modified form of the fusion-pyrolysis method wherein the flux, $NaBiO_3$, in a silica boat at 1000°C is used. For the removal of nonleachable chloride, $Na_2Mo_3O_{10}$ has been found to be a better flux, in which case the pyrolysis can be carried out at the much lower temperature of 700°C.

A Stanton thermobalance is now being applied to the thermogravimetric analysis of various compounds which are being used in the production of thorium oxide and to study the effect of additives on the change in weight of thorium oxide as a function of temperature. A study has been made of the effect of acetic acid on the extractability of thorium by thenoyltrifluoroacetone in carbon tetrachloride with particular emphasis on the correlation of the predominant complexing reactions as functions of acetate concentration.

Advances in the analytical chemistry of uranyl sulfate solutions, simulated and actual homogeneous reactor fuel solutions, are discussed. These discussions include the application of a polarographic method to the simultaneous determination of mercury and copper; the establishment of an extraction procedure for the separation of iron from interfering elements prior to the colorimetric determination of this element; and the development of coulometric titration methods for determining uranium, copper, and nickel conjointly on a single, relatively small, aliquot of highly radioactive HRT fuel solutions.

A brief description is given of the chemical analyses which have been made incident to the operation of the HRT during runs 12 to 16. This discussion covers the methods used for the determination of uranium, copper, nickel, sulfate, free acid, and pH.

CONTENTS

SUMMARY iii

PART I. HOMOGENEOUS REACTOR TEST

1. HRT OPERATIONS 3
   - 1.1 Reactor Operations 3
     - 1.1.1 Preparations for Power Operation 3
     - 1.1.2 Power Operation – Run 13 3
     - 1.1.3 Shutdown for Maintenance and Corrosion Studies 4
     - 1.1.4 Power Operation – Run 14 5
     - 1.1.5 Remote Viewing, Measurement, and Maintenance Following Run 14 7
     - 1.1.6 Hydraulic and Mixing Studies – Runs 15 and 16 7
     - 1.1.7 Power Operation with Fuel in Blanket – Run 16 9
     - 1.1.8 Maintenance and Inspection Following Run 16 11
   - 1.2 Experimental Analysis 11
     - 1.2.1 Loss of Reactivity During Power Operation 11
     - 1.2.2 Corrosion and Chemistry of the Reactor System 12
     - 1.2.3 Measurements of Radioactivity 15
     - 1.2.4 Power Oscillations and Transients 16
     - 1.2.5 Miscellaneous 17
2. HRT PROCESSING PLANT 19
   - 2.1 Final Cell Maintenance, Closure, and Leak Test 19
     - 2.1.1 Final Cell Maintenance 19
     - 2.1.2 Cell Leak Test 19
   - 2.2 Operation During Runs 15 and 16 19
     - 2.2.1 Data and Conclusions 19
     - 2.2.2 Equipment Performance 21
   - 2.3 Auxiliary Systems 21
     - 2.3.1 Removal of Iodine 21
     - 2.3.2 Charcoal Bed Performance 21
     - 2.3.3 Waste System Revisions 21
3. HRT REACTOR ANALYSIS 23
   - 3.1 Variation of the Inlet and Outlet Temperatures in the Two-Region HRT as a Function of Power 23
   - 3.2 HRT Dome-Wall Temperatures 24
   - 3.3 Stresses in HRT Core Vessel 26
   - 3.4 Stresses in HRT Pressure Vessel for One- and Two-Region Operation 26
   - 3.5 Nuclear Characteristics of the HRT with Various Fuel Concentrations in the Blanket 27
     - 3.5.1 One-Region Operation 27
     - 3.5.2 Effect of HRT Blanket-Fuel Concentration on the Core Critical Concentration 28
     - 3.5.3 Flux Distributions in HRT 30
     - 3.5.4 Effect of Corrosion Samples and Sample Holders on HRT Core Critical Concentration 30
   - 3.6 Safety of the HRT with Blanket Pressurizer Completely Filled 31

4. HRT COMPONENT DEVELOPMENT 34
4.1 Fuel Circulating Equipment 34
4.1.1 400A-1 Pump 34
4.1.2 400A-2 Pump 34
4.2 Feed Pumps 35
4.2.1 Feed-Pump Endurance Testing 35
4.2.2 Purge Pumps 35
4.3 HRT Maintenance Development 35
4.3.1 Core Viewing Development 35
4.3.2 Sample Cutter 36
4.4 HRT Spare Heat Exchanger 36
4.5 HRT Core Studies 36
4.5.1 Behavior of Solids in Reactor Core 36
4.5.2 HRT Replacement Core 36
4.6 HRT Mockup 36
4.6.1 Operation 36
4.6.2 Inventory Determination 38
4.6.3 Fuel-Solution Stability 38
4.6.4 System Modifications 39
5. HRT DESIGN 40
5.1 Single-Region Operation Studies 40
5.1.1 Mixing of the Fuel and Blanket Solutions 40
5.1.2 Blanket Dump-Tank Pressure 40
5.1.3 Steam-System Modifications 40
5.1.4 Interconnection of Purge Pumps 41
5.2 Temperature Distribution in Existing Reactor Vessel 41
5.3 Replacement Pressure Vessel 43
5.4 Piping Layouts for Replacement Pressure Vessel 43
5.5 Cell-Wiring Replacement 43
5.6 Main-Heat-Exchanger Blowdown Sampling Station 45
5.7 Removable Insulation 45
5.8 Inspection of Existing Core Vessel 46
5.9 Dry-Maintenance Studies 47
6. HRT CONTROLS AND INSTRUMENTATION 49
6.1 Component Development 49
6.1.1 Letdown Valves 49
6.1.2 Remote Viewing Equipment 50
6.2 Maintenance and Modifications 52
6.2.1 Oxygen-Injection System 52
6.2.2 Reactor Power-System Rewiring 52
6.2.3 Blanket Dump Valve 53
6.2.4 Instrumentation and Controls Revisions to Facilitate Single-Region Operation 53
6.2.5 Measurement of System Transients 53

PART II. REACTOR DESIGN, RESEARCH, AND ANALYSIS

7. REACTOR DESIGN 57

7.1 Reactor Design Program 57

7.2 HRE-3 Design 57
7.2.1 Conceptual Layouts 57
7.2.2 Fuel and Blanket Heat Exchanger Studies 57
7.2.3 Pressurization 63
7.2.4 Fuel Dump-Tank Concept 63

7.3 HRE-4 Preliminary Design 63
7.3.1 Flowsheet 64
7.3.2 Heat Exchanger 65
7.3.3 Conceptual Layouts 65
7.3.4 Heat Removal System 67

8. RESEARCH AND ANALYSIS 68

8.1 Some Nuclear Characteristics of Spherical Double-Blanket Reactors 68

8.2 Determination of HRE-3 Breeding Ratio 69

8.3 Influence of Core Inlet-Outlet Line on HRE-3 Flux Distribution and Breeding Ratio 72

8.4 Decrease in HRE-3 Breeding Ratio Caused by Absorptions in Core Tank and Shroud 74

8.5 Neutron Absorption in HRE-3 Core-Inlet Pipe and Power Density at Pipe Wall 76

8.6 Criticality in Dump Tanks for HRE-3 Blanket 78

8.7 Nuclear Characteristics of Small One-Region Slurry Reactors 81

8.8 Machine Programing 85

8.9 Rheology of Thorium-Oxide Slurries 86

8.10 Thoria Caking Studies 87

8.11 Model Studies of HRE-3 Blanket Configurations 88

8.12 Model Study of a Cylindrical Core for the HRE-3 89

8.13 Flow-Visualization Studies 90
8.13.1 Flow-Visualization Loop 90
8.13.2 Model Studies 90

8.14 Equations of Motion and Boundary-Layer Equations for Bingham-Plastic Materials 90

8.15 Liquid-Fluidization Studies with Thoria Spheres 92

PART III. ENGINEERING DEVELOPMENT

9. DEVELOPMENT OF FUEL AND SLURRY SYSTEM COMPONENTS 97

9.1 Recombiner and Pressurizer Development 97
9.1.1 High-Pressure Recombiner Loop 97
9.1.2 Syracuse Contract 97
9.1.3 Solubility of Oxygen and Hydrogen in Fuel Solution 98
9.1.4 Titanium Equipment for Boiling UO_2SO_4 Solutions 98
9.1.5 Heating and Cooling of Steam-Oxygen Mixtures 98

9.2 Centrifugal Pumps 98
9.2.1 20-cfm Allis-Chalmers Blower 98
9.2.2 4000-gpm Loop 99
9.2.3 Reliance 6000-gpm Pump 99
9.2.4 300A Slurry Pump and Loop 99
9.2.5 200Z Loop and Pump 99
9.2.6 Byron-Jackson Slurry Pumps 99
9.2.7 Slurry Bearing-Test Program 101
9.3 Oxygen Compressors 101
9.4 Feed Pumps 101
9.4.1 Solution Diaphragm-Pump Development 101
9.4.2 Alternate Feed Pumps 101
9.4.3 Slurry Feed Pumps 102
9.5 Valve Trim 102
9.5.1 Dump-Valve Trim for Solutions 102
9.5.2 Slurry Hand Valves 102
9.5.3 Letdown Valves 104
9.5.4 Slurry Check-Valve Material Test 104
9.6 Titanium Program 104
9.7 Bolting-Material Program 104
9.8 Heat Exchangers 105
9.8.1 Tube-Joint Test 105
9.8.2 Heat Exchanger Test Facility 105
9.8.3 Slurry Heat Exchanger Flow Tests 105
9.9 Hydrodynamics in Cores and Blankets 105
9.9.1 Heat Transfer from HRE-3 Core Wall to Core Solution 105
9.9.2 Low-Pressure Model of HRE-3 Blanket 105
9.9.3 Single-Region Slurry Core 106
9.10 Separation of Water from ThO_2 Slurry 106
9.11 Slurry Dump Tanks and Evaporators 106
9.12 Settled-Bed Properties of Thoria Slurries 106
9.12.1 Low-Speed Centrifuge 106
9.12.2 Effect of Bed Depth 108
9.12.3 Slurry Plug Tester 108

10. DEVELOPMENT OF REACTOR SLURRY SYSTEMS 109
10.1 Circulating-Slurry Behavior 109
10.1.1 200-gpm Loop Operation 109
10.1.2 100-gpm Loop Operation 109
10.1.3 High-Temperature Laminar Flow 116
10.1.4 Low-Temperature Laminar Flow 118
10.2 Blanket System Development 119
10.2.1 Alterations to the 300-SM System 119
10.2.2 Run SM-5 120
10.2.3 Conversion of 300-SM Loop to High-Pressure Operation 126
10.2.4 Gamma-Survey Development 127

11. INSTRUMENT AND VALVE DEVELOPMENT 130
11.1 Instrument Development 130
11.1.1 High-Temperature Radiation-Resistant Differential Transformers 130
11.1.2 Heated-Thermocouple-Probe Liquid-Level Sensor 130
11.1.3 Variable-Area-Type Transmitting Flowmeters 131
11.1.4 Transistorized Electropneumatic Converter 131
11.1.5 Control Analysis of HRT Heat Exchanger Feedwater System 134
11.2 Valve Development 134
11.2.1 Valve Actuators 134
11.2.2 Stem-Sealing Bellows 136
11.2.3 Slurry-Service Valves 138

PART IV. REACTOR MATERIALS RESEARCH

12. SOLUTION CORROSION 147
12.1 Dynamic Solution Corrosion 147
12.1.1 Solution Stability Studies 147
12.1.2 Oxygen Exhaustion Studies 148
12.1.3 Corrosion of York Mesh in Iodine-Containing Uranyl Sulfate Solution at 100°C 150
12.1.4 Sixth Test of the HRT Core–Pressure-Vessel Flange and Transition-Joint Mockup 150
12.1.5 Corrosion of Stainless Steel, Titanium, and Zircaloy-2 in the Heavy Second Liquid Phase of a Uranyl Sulfate Solution 151
12.1.6 Corrosion of Stainless and Carbon Steels at 300°C in Chloride-Containing Boiler Water 151
12.1.7 Effect of Ruthenium Nitroso Sulfate on the Behavior of Dilute Uranyl Sulfate and Sulfuric Acid Solutions 152
12.2 Laboratory Corrosion Studies 153
12.2.1 Stress-Corrosion Cracking 153
12.2.2 Miscellaneous Corrosion Tests 156

13. SLURRY CORROSION 161
13.1 100A Pump Loops 161
13.1.1 Loop Engineering: Corrosion Test Loop ES 161
13.1.2 Loop Engineering: Venturi Performance 161
13.1.3 Loop Engineering: Hydroclone for Slurry Removal 166
13.1.4 Pump Loop Tests: Introduction 169
13.1.5 Circulation of Slurries of 0.9-μ, 1400–1600°C-Calcined Thoria 169
13.1.6 Circulation of 1.7-μ High-Calcined Thoria at 200 and 280°C 173
13.1.7 Corrosion-Erosion Resistance of Miscellaneous Materials 176
13.1.8 Circulation of 1.2-μ Thoria Slurry; Observation of Sludge Dropout 177
13.1.9 Field Corrosion Tests 178
13.2 Toroids 180
13.2.1 Introduction 180
13.2.2 Effect of Atmosphere, Circulation Temperature, and ThO_2 Properties on Attack by Aqueous Slurries 180
13.2.3 Degradation of 1600°C-Calcined ThO_2 Prepared by Jet Precipitation 182
13.2.4 Circulation of Slurries Containing Sodium Aluminate 184
13.2.5 Circulation of Slurries Containing Molybdenum Trioxide 184

13.2.6 Circulation of Thoria Spheres 184
13.2.7 Tests with Micropulverized Thoria 189
13.2.8 Toroid Tests with Thoria Sols 189

13.3 In-Pile Autoclave Slurry Corrosion Tests 191
13.3.1 Introduction to Autoclave Experiments 191
13.3.2 Development, Construction, and Operation 191
13.3.3 Recombination of Radiolytic Gases 193
13.3.4 Effects of Time and Radiation on Generalized Corrosion 195
13.3.5 Examination of Irradiated Thoria and Autoclave Corrosion Specimens 198

13.4 In-Pile Slurry Toroid 199
13.4.1 Engineering Development 199

13.5 In-Pile Slurry Loop 200
13.5.1 Loop Development 200

14. RADIATION CORROSION 202

14.1 In-Pile Loops 202
14.1.1 Development and Construction 202
14.1.2 General Description of In-Pile Loop Experiment L-4-18 203
14.1.3 Qualitative Results of Inspection and Evaluation of Loop L-4-18 206
14.1.4 Quantitative Results of Inspection and Evaluation of Loop L-4-18 208
14.1.5 General Description of In-Pile Loop Experiment L-2-19 214
14.1.6 Qualitative Results of Inspection and Evaluation of Loop L-2-19 216
14.1.7 Quantitative Results of Inspection and Evaluation of Loop L-2-19 219
14.1.8 General Description of In-Pile Loop L-2-21 226

14.2 In-Pile Autoclave Tests – LITR 227
14.2.1 Development, Construction, and Operation 227
14.2.2 Results and Discussion 227

14.3 HRT Service Corrosion 237
14.3.1 HRT Specimen and Scale Examinations 237
14.3.2 HRT Corrosion Specimens 242

15. METALLURGY 245

15.1 Physical Metallurgy 245
15.1.1 Zirconium-Alloy Development 245
15.1.2 Zircaloy-2 Fabrication Study 245
15.1.3 Zirconium Hydride Layer Study 246
15.1.4 Recombiner-Loop Specimens 247

15.2 Mechanical Metallurgy 248
15.2.1 Zirconium Alloys 248
15.2.2 Mechanical Properties of Irradiated Titanium and Zirconium Alloys 250
15.2.3 Creep Testing of Zirconium- and Titanium-Base Alloys 252

15.3 Welding Development 252
15.3.1 Titanium Alloys 252
15.3.2 Zircaloy-2 253
15.3.3 Composite Welds 253

15.4 Nondestructive-Testing Development 253
15.4.1 Ultrasonic Attenuation in Metals 253

15.5 Active-Metal Reactions 256
15.5.1 Titanium 256
15.5.2 Zirconium 256
15.6 Metallurgical Services 257
15.7 Ceramic Developments 257
15.8 Effects of Radiation on Structural Metals and Alloys 257
15.8.1 Equipment and Facilities 257
15.8.2 Impact Tests 258
15.8.3 Tensile Tests 262

PART V. CHEMICAL ENGINEERING DEVELOPMENT

16. URANYL SULFATE FUEL PROCESSING 267
16.1 Iodine Chemistry 267
16.1.1 Laboratory Experiments 267
16.1.2 HRT Operating Experience 267
16.2 Solids Behavior 268
16.3 Alternate Core Processing Development 269
17. GASEOUS-FISSION-PRODUCT DISPOSAL 270
17.1 Dynamic Studies 270
17.2 Equilibrium Studies 273
18. URANYL SULFATE BLANKET PROCESSING 276
18.1 Plutonium Behavior in the P-1 Loop 276
18.1.1 Solids Removed 276
18.1.2 Plutonium Solubility 276
18.1.3 Plutonium Adsorption on Metal 277
18.1.4 Corrosion 277
18.2 Chromous Sulfate Descaling of P-1 Loop 277
18.3 Plutonium Behavior in a Titanium System 277
18.4 Plutonium Sorption on Cation Exchange Resin 278
19. THORIUM OXIDE SLURRY DEVELOPMENT 279
19.1 Slurry Irradiation Studies 279
19.1.1 Slurry Irradiations in the LITR 279
19.1.2 Postirradiation Examination 279
19.1.3 ORNL Graphite Reactor Irradiations 279
19.1.4 Equipment Development 280
19.2 Gas Recombination Studies 281
19.2.1 Studies with Thorium-Uranium Oxide Containing $U^{235}/Th = 0.005$ 281
19.2.2 Studies with Thorium-Uranium Oxide Containing $U^{235}/Th = 0.05$ 282
19.3 Molybdenum Oxide Chemistry in Thorium and Thorium-Uranium Oxide Slurries 283
19.4 Properties of Silica-Coated Thorium Oxide 284
19.4.1 Dri-film Chemistry 285
19.4.2 Preparation and Washing 285
19.4.3 Characteristic Properties 285
19.4.4 Slurry Properties 285
19.4.5 High-Temperature Settling Behavior 285

19.5 Relation of Oxide Particulate Properties to Yield Stress 285
19.6 Particulate Properties of Compressed, High-Fired Thorium Oxide 287
19.7 Evaluation of Pumped High-Fired Oxide 292
19.8 Thorium-Uranium Oxide 292
19.8.1 Coprecipitation 293
19.8.2 Adsorption 293
19.9 Thorium Oxide Preparation Development 293
19.9.1 Laboratory Studies 293
19.9.2 Continuous Thorium Oxalate Precipitation 293
19.9.3 Thorium Oxide Classification 294
19.9.4 Thorium Oxide Slurry Concentration 296
19.9.5 Flame Calcination 297
19.10 Thorium Oxide Production 297

20. IN-PILE SLURRY LOOP 300

PART VI. SUPPORTING CHEMICAL RESEARCH

21. AQUEOUS SYSTEMS AT ELEVATED TEMPERATURES 307
21.1 Calculations of Solubility in Multicomponent Systems from Solubilities in Simpler Systems 307
21.2 Solubility Equilibrium in the System $NiO-SO_3-H_2O$ at High Temperature 308
21.2.1 $NiSO_4 \cdot H_2O$ Solid and Its Region of Stability 309
21.3 Measurement of Aqueous Vapor Pressure at Elevated Temperature and Pressure 311
21.4 Equilibrium Compositions of the Light and Heavy Liquid Phases in the System $UO_3-SO_3-H_2O$ 312

22. REACTIONS IN AQUEOUS SOLUTIONS 313
22.1 Peroxide Decomposition in Uranyl Sulfate Solutions 313
22.1.1 Effect of Solvent Isotopic Composition on Temperature Dependence of Peroxide Decomposition 313
22.1.2 Effect of Solvent Isotopic Composition on Decomposition Rates 314
22.1.3 Effect of Copper and Iron Salts Upon Decomposition Rate and Dependence 314

23. THORIUM OXIDE SYSTEMS 317
23.1 pH of Thorium Oxide Slurries 317
23.2 Effect of pH on Slurry Properties 319

24. HEAVY-ELEMENT AND FISSION-PRODUCT CHEMISTRY 320
24.1 Quantitative Spectrometry of Aqueous Neptunium Ions at Elevated Temperatures and Pressures 320
24.2 Radionuclides Formed in the HRT 321

PART VII. ANALYTICAL CHEMISTRY

25. ANALYTICAL CHEMISTRY 327

25.1 Analysis of Thorium Oxide 327

25.1.1 Determination of Thorium 327

25.1.2 Estimation of Zirconium 327

25.1.3 Determination of Titanium in Thorium Oxide 327

25.1.4 Flame Photometric Determination of Aluminum 328

25.1.5 Separation of Fluoride and Chloride from ThO_2 by Fusion-Pyrolysis 328

25.1.6 Thermogravimetric Analysis of Thorium Compounds 329

25.1.7 The Effect of Acetic Acid on the Extractability of Thorium with Thenoyltrifluoroacetone (TTA) in Carbon Tetrachloride 329

25.2 Analysis of Uranyl Sulfate Solutions 330

25.2.1 Polarographic Determination of Mercury and Copper 330

25.2.2 Determination of Iron 330

25.2.3 Coulometric Determination of Uranium in Synthetic Homogeneous Reactor Fuel 330

25.2.4 Coulometric Determination of Nickel in Homogeneous Reactor Fuel 331

25.3 Chemical Analyses Incident to Reactor Operations 331

ORGANIZATION CHART 333

Part I

HOMOGENEOUS REACTOR TEST

S. E. Beall

1. HRT OPERATIONS

S. E. Beall

H. F. Bauman
N. C. Bradley
D. F. Bruley
J. R. Buchanan
J. R. Engel
J. D. Flynn
D. F. Frech
T. H. Gladney[1]
R. H. Guymon
R. J. Harvey
P. N. Haubenreich
J. Hernandez[2]
J. W. Hill, Jr.
S. I. Kaplan
J. O. Kolb
R. M. Pierce[1]
D. M. Richardson
G. W. Rivenbark
J. A. Russell
D. Scott, Jr.
H. K. Search[3]
J. E. Sutherland
W. Terry
R. Van Winkle
K. W. West

1.1 REACTOR OPERATIONS

1.1.1 Preparations for Power Operation

Upon completion of the low-power critical tests in mid-January, further preparations were carried out for bringing the HRT to full power. After three sets of metallurgical specimens were inserted into the blanket thimble above the source, the reactor container was resealed, pressurized, and charged with helium to 2 vol % to permit external leak-hunting with a helium leak detector. Various leaks ranging from 1 to 100 cc/min were found and repaired. When no further leaks could be located, an odor test was made to ascertain whether undetected leakage was occurring to the control and operating areas. Approximately 2 liters of 10% ethyl mercaptan was vaporized into the container, producing an internal concentration of 40 ppm, about 20 times the concentration employed in natural gas as an odorizer. Several small leaks were located inside the building, and some undetected leakage was presumed to be discharged outside the building. Final leak rates were then determined at 7.5 and 30 psia, by observing container pressure changes over a 12-hr period in each test; the temperature-compensated differential manometer indicated rates of 2.5 liters/min and 4 to 4.3 liters/min, respectively.

The north shield wall, which could not be completed until after it had been examined for leaks, was then filled with a mixture of barytes sand, colemanite, and water and was compacted with vibrators to a density of 195 lb/ft^3.

[1]On loan from TVA.

[2]On loan from Puerto Rico Water Resources Authority.

[3]On loan from Pennsylvania Power and Light Co.

1.1.2 Power Operation – Run 13

By 1200 on February 8, with the reactor pressurized to 1700 psi and heated to 280° C, injection of fuel was started, and the concentration was raised until the reactor was nearly critical at 280° C. Criticality was attained by lowering the temperature very slightly, and then the external steam supply to the fuel heat exchanger was shut off, permitting the nuclear power to rise to about 250 kw.

After less than 2 hr at 250 kw, the reactor temperature began to decrease (see Fig. 1.1). This indicated a loss of reactivity, because there were no apparent changes which could have caused a decrease in core concentration. Increasing the fuel feed rate raised the reactor temperature, but it soon began to fall again.

At 1930, heating steam to the blanket heat exchanger was shut off also, and the nuclear

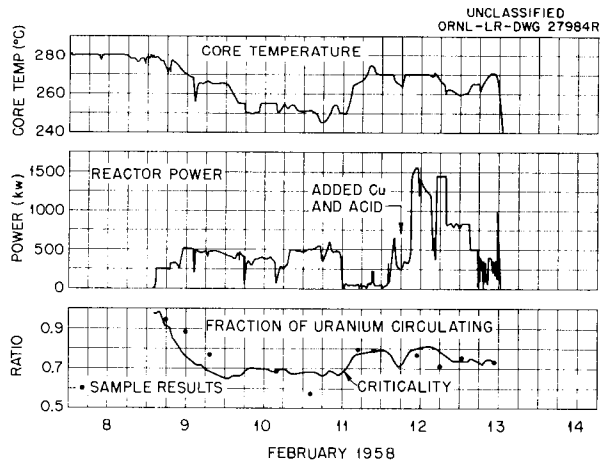

Fig. 1.1. Operating Parameters During Initial Power Run.

power rose to 330 kw as a result and remained at this level until 2215, when sufficient reactor steam was sent to the turbine to raise the power to 500 kw.

During this period, an abnormal condition existed, the significance of which was not immediately recognized. Routine readings of a meter on the off-gas from the charcoal beds indicated no flow between 1800 on February 8, and 0900 on February 9. During this time (as throughout run 13), oxygen had been continuously injected, at 920 cc/min, into the fuel high-pressure system. The off-gas stoppage could not be explained on the basis of temperature or pressure changes elsewhere in the reactor. It was later found that the stoppage coincided with a rapid increase in nickel concentration, indicative of a high stainless steel corrosion rate.

Several experiments were conducted in an attempt to determine the cause of the loss of reactivity during the first 24 hr at power. It was first suspected that there was poor mixing in the dump tanks because of the small liquid inventory there. Improved mixing, however, did not produce an increase in reactivity.

Next, on the basis of HRT mockup experience with precipitation of uranium in the pressurizer connection, an attempt was made to recover reactivity by reducing the flow of condensate to the fuel pressurizer. For a period of 10 hr, beginning at 2200 on February 9, the pressurizer purge rate was kept below 0.2 lb/min, but there was no apparent recovery of uranium.

The core pressure was reduced on February 10, to observe the effects on radiolytic-gas bubbles, which might also affect reactivity. Up to the time that the pressure reduction began, the low-pressure recombiner temperature indicated only the gas dissolved in the liquid letdown stream. As the pressure was lowered to 1300 psig, the recombiner temperature rose sharply, indicating the beginning of gas-bubble letdown. Although there was no sudden change in reactivity, the reactor temperature gradually declined 7°C in the 6 hr at reduced pressure. After the pressure was raised, the reactor temperature recovered. Further manipulation of the reactor power and pressure during the next 24 hr suggested a relation between reactivity loss and radiolytic-gas concentration.

In an effort to correct this objectionable situation by improving the internal recombination of the gases, partial additions of $CuSO_4$ (1.0 mole) and H_2SO_4 (3.4 moles) were made to the fuel. (The experimental procedure specified that the $CuSO_4$ be added in several partial quantities as the power level was increased. Up to this point the fuel solution had contained only 10–20 ppm of Cu.) In the first hour after the addition, the reactor average temperature rose 9°C.

Although the partial copper addition eliminated the loss of reactivity at the lower power levels, the difficulty reappeared as the power was raised to 1500 kw. Before the full interdependence of power, temperature, and reactivity could be determined, chemical analyses indicated a high nickel concentration, >600 ppm, which suggested a very high stainless steel corrosion rate, >166 mpy. Such a high rate had never been experienced before in in-pile corrosion tests, and was all the more surprising because the stainless steel parts of the HRT are outside the reactor core. Power operation was terminated by making a normal shutdown of the reactor until more complete information could be obtained from analyses of fuel solution samples. A total of 48 Mwhr of thermal energy was generated during the run.

1.1.3 Shutdown for Maintenance and Corrosion Studies

After reviewing the information collected during run 13, it was decided to continue reactor operation to seek an explanation for the high stainless steel corrosion rate. During the first period the reactor was to be operated subcritically to establish a corrosion rate in the absence of fission power. However, after only 24 hr, the recurrence of insulation failures in the electrical wiring to the cell coolers and circulating pumps necessitated a shutdown on February 18. The details of these difficulties are described in Sec 6.3.2. It appeared that a satisfactory repair of the wiring could not be achieved, and on February 22 a decision was made to replace all the reactor power wiring.

Such an undertaking would have had little chance of success if the reactor parts could not have been shielded by flooding with water according to the normal maintenance routine. With the water as shielding, it was possible to install ~1000 ft of new wiring in a period of only one month without a single case of personnel overexposure to radiation. To establish the general radiation background of the reactor piping and to detect any

hot spots which might indicate points of fission-product and solids accumulation, an external survey of all accessible portions of the fuel system was made with a waterproofed radiation probe. A fairly uniform gamma activity of 15–30 r/hr along the outside of the piping was found, with two exceptions – the sediment pot below the fuel dump tanks (1100 r/hr) and a point in line 100 between the core thimble and the fuel pressurizer (500 r/hr).

During this time the fuel circulating pump was removed so that the corrosion specimens in its discharge piping could be examined. (The corrosion results are reported in Sec 14.3.) The pump, with new specimens, was replaced, and a new fuel letdown valve was installed in place of the existing valve, which had begun to leak approximately 0.25 gpm at 1700 psig (see Sec 6.1.1). The maintenance techniques previously developed for these two operations worked exceptionally well, and both jobs were accomplished in less than the allocated time. In addition, the core inspection flange was opened and replaced without difficulty.

When the line to the pressurizer was examined with periscopes, a small mound of solids was observed at a location roughly corresponding to that of the hot spot described above. More solids were seen in the core, around the periphery of the topmost diffuser screen; the material appeared similar to the "popcorn oxide" formation frequently observed in corrosion test loops. Samples from both deposits were obtained; the material was found to be preponderantly α-Fe_2O_3, with a uranium content of approximately 1%.

The wall thickness of the pressurizer line was checked with an ultrasonic probe to determine whether significant corrosion had occurred at the point of solids deposition and was found to be unchanged. After removal of the aluminum-foil insulation from the outlet dome (see Sec 3.2), the reactor and shield were restored to operating condition, and the shield was again successfully leak-tested at 15 psig.

1.1.4 Power Operation – Run 14

Because of the large amount of nickel in the fuel solution at the end of run 13, it was decided to replace the fuel solution with a fresh charge. The old solution was boiled down to a small volume and has been isolated in the fuel storage tanks until it can be removed for chemical processing.

Run 14 started on March 24, with a 2500-psi hydrostatic test of the fuel and blanket high-pressure systems. Following the hydrostatic test, oxygenated D_2O was circulated at 270°C for 37 hr. The oxygen injection rate in the fuel system was 2 liters/min, which gave a calculated oxygen concentration of 970 ppm, double that of the previous run, in an effort to avoid oxygen depletion – assuming that it had been the cause of the rapid corrosion. This injection rate into the fuel system was maintained throughout run 14.

On March 27 a fresh batch of fuel was added, bringing the core concentrations to 0.034 *m* UO_2SO_4, 0.027 *m* $CuSO_4$, and 0.024 *m* H_2SO_4. After establishing a corrosion baseline at 270°C in 40 hr of subcritical operation, the reactor was made critical by reducing the heating steam and allowing the temperature to decrease from 270 to 255°C. The reactor reached criticality on March 29, and shortly thereafter the power was raised to 1 Mw. For the next 22 hr the reactor operated smoothly at 1 Mw, 1500 psi, and fuel temperatures between 248 and 257°C. The power and temperature history are presented graphically in Fig. 1.2.

On March 30 the power was raised[4] to 2 Mw. A loss of reactivity again ensued; as had been experienced in run 13, the reactor average temperature fell 10°C in the first 3 hr at 2 Mw. The power was restored to 1 Mw, and the temperature

[4] All power levels referred to in this section are nominal core power; for actual total power, add approximately 20%.

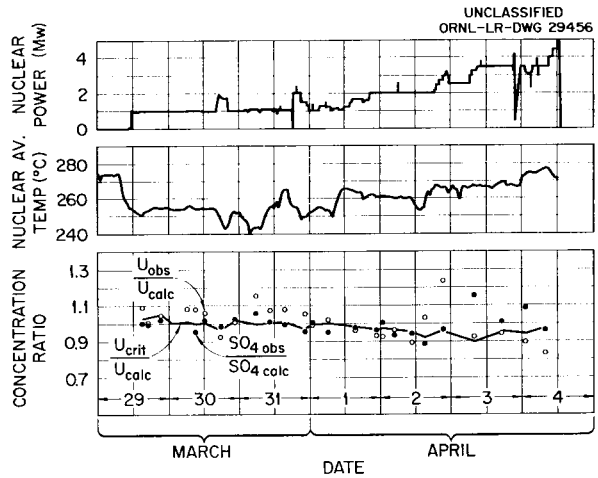

Fig. 1.2. Operating Parameters During Run 14.

came back to the original 257°C. While the reactor was held at 1 Mw, the core temperature was deliberately varied to change the effectiveness of the recombination catalyst, to determine whether any reactivity effects could be observed as the concentration of radiolytic gases was changed. The core average temperature was reduced to 244°C, raised to 268°C, and then reduced to 258°C, all with no apparent change in reactivity.

On the evening of March 31 the power was first briefly reduced to about 100 kw and then was rapidly increased to 2 Mw. It was observed that the core inlet and outlet temperatures diverged uniformly, as would be expected for displacement-type flow in the core.

About 1 hr after the power level had reached 2 Mw, the temperature began to decline; and after a reduction of 7°C, the power was reduced to 1 Mw. At the lower power, the core average returned to the original 258°C. The power was then raised to 1.3 Mw, and the temperature began to fall slowly; when the power was reduced to 1.2 Mw, however, the temperature stabilized. From additional manipulations of the power and average temperature, it was concluded that stability was dependent on maintaining a sufficiently high fuel temperature for efficient recombination by the copper catalyst. With the fuel at 265°C average temperature, the power level was gradually increased to 3 Mw over a period of 4 hr with no significant change in the average temperature.

At about 2200 on April 2 the core pressure was raised to 1700 psi from 1500 psi to give a greater margin of safety against formation of radiolytic-gas bubbles, and later the power was raised to 3.5 Mw without incurring noticeable loss of reactivity.

At 1430 on April 3, 2.6 moles of H_2SO_4 was added to the fuel solution to overcome the reduction in excess acid as a result of increase in nickel concentration. Sample results showed nickel concentrations at this time between 140 and 220 ppm, corresponding to a uniform corrosion rate of 2 to 5 mpy since the beginning of power operation 124 hr before. Before the addition, the reactor had operated for 6 hr at a constant temperature. Within 1 hr after the acid addition, the temperature rose 2°C, then leveled off. The reactor power level was held constant for the next 16 hr, although the core pressure was raised to 1800 psi and the fuel concentration was increased to bring the core outlet to 290°C. Between 0900 and 1200 on April 4 the power was raised in three steps to a nominal 5 Mw. In contrast to the temperature behavior observed earlier, the core outlet temperature did not increase as the power was raised; instead, the core inlet decreased from 262 to 246°C.

The reactor ran very smoothly until 1232, when the fuel pressurizer level suddenly dropped downscale, out of the range of the level instrument. This automatically diluted the core. The pumping rate was quickly increased, but this failed to bring the level on scale. At the same time there were indications that the blanket dump-tank weight was rapidly increasing and that the fuel dump-tank weight was decreasing. In the belief that the level element might have failed, the fuel letdown valve, which had closed automatically, was opened manually to make certain that fuel would not rise into the pressurizer. When the fuel valve was opened, the blanket pressurizer level dropped. Although the blanket letdown valve then closed, it was necessary to start the blanket feed pump to hold the level on the blanket side. In the meantime the steam withdrawal had been stopped. While the core power was decreasing, as indicated by the converging of inlet and outlet temperatures, the blanket temperatures had diverged, indicating increased heat generation in that region. A sample taken from the blanket was highly radioactive (later analysis showed the presence of uranium). The circulating pumps were turned off, and the fuel pressurizer level came on scale. It was then observed that fuel level was affected by the blanket feed-pump operation and that blanket level was affected by the fuel feed-pump operation. Thus there was left no doubt that the core and blanket regions were interconnected. The reactor temperature was held with externally applied heating steam until the core was diluted; then the reactor was allowed to cool down, terminating run 14.

Based on heat-balance data, the highest total power achieved was 6.3 Mw. The total power generated during run 14 was 340 Mwhr.

Following shutdown, the shield was opened above the reactor core, and the core and blanket access flanges were removed to permit remote inspection and measurements (Sec 1.1.5). Study groups were formed to investigate several proposals regarding operating modifications which might be made to allow future operation of the HRT either as a two-region or as a single-region reactor. Preparations were made for a test run

to study the hydraulic and intermixing behavior of the interconnected core and blanket systems.

1.1.5 Remote Viewing, Measurement, and Maintenance Following Run 14

After the reactor piping was rinsed with condensate and the fuel was returned to the fuel dump tanks, measurements were conducted to determine the site and magnitude of the leak in the core tank. On the basis of previously established calibration of liquid level vs system holdup, the break appeared to be in the vicinity of the welded peripheral joint between the 30- and 90-deg cone entrance sections near the bottom of the Zircaloy core vessel (see Fig. 1.3). While pumping from the core to the blanket at 25 lb/min, the water levels in the core and blanket were found to differ by only $\frac{3}{8}$ in., with pneumatic level probes being used for the measurements. A head loss of approximately $\frac{3}{4}$ in. was measured at a flow rate of 65 lb/min. To be consistent with these measurements, the hole must be a long, narrow, horizontal opening; the area is estimated to be 1.5 to 2.0 in.^{2}.

The external core surface was examined with periscopes and a remotely operated mirror (see Fig. 4.2) inserted into the blanket access flange. The precise elevation of the leak was established by observing the level at which liquid stood in the blanket when leakage to the core ceased; however, no evidence of liquid flowing through an identifiable hole was seen when water was pumped into the core and allowed to spill into the blanket. By lowering a light source through the upper diffuser screens, an effort was made to illuminate the leak area so that it could be seen from the blanket side; this method was also unsuccessful. (Later, viewing experiments on a mockup at Y-12 revealed that a sector of the back side of the core had escaped inspection.)

Internal examination of the core was attempted with a 20-ft borescope, the tip of which could pass through the upper diffuser screens. Because of the limited light intensity which could be concentrated at the core wall, however, it was not possible to observe the interior surface of the leak. Observation times were limited by the borescope lenses becoming brown after several hours of exposure to the core activity, measured at 2400 r/hr.

During the shutdown for inspection, the fuel letdown valve was again replaced, using remotely operated tools and a lead-shielded dry-maintenance personnel platform. The steam-generating capacity of the blanket heat exchanger was raised by increasing the size of the feed-water and steam-withdrawal valves.

1.1.6 Hydraulic and Mixing Studies – Runs 15 and 16

During the shutdown period after run 14, engineering study groups proposed several possible modes of operation which would not require repair or replacement of the core. The basis for selection among these lay in the hydraulic and mixing behavior which would exist in the reactor at operating conditions. A run was scheduled to investigate the fluid behavior in the core and blanket and to explore means of continuously supplying condensate to the blanket low-pressure system.

With D_2O in the reactor at 150°C the pressure drops through the core and blanket were found to be sufficiently alike to permit control within the range of the pressurizer level elements. At 280°C, however, the lower fluid density caused the blanket pressurizer level to be above the control region. When it appeared that this mode of operation had undesirable limitations, the experiment was discontinued and a solid disk was installed in the relief line between the two pressurizers so that the blanket pressurizer could be operated completely full of liquid. The system was refilled with D_2O, heated to 150°C, and pressurized to 1800 psig by means of the fuel pressurizer only. In another experiment, conducted in the low-pressure system, continuous transfer of condensate from the fuel condensate tank to the blanket dump tank had been maintained successfully at a rate of 6 lb/min. It was hoped that by keeping the blanket letdown valve closed a condensate flow of 6 lb/min into the blanket would prevent the leakage of uranium from the core. In order to obtain additional evidence, dilute uranyl sulfate solution was introduced into the core, with the circulating pumps operating in both loops. Analyses of the blanket indicated that fuel solution was passing through the leak in spite of the 6-lb/min reverse flow, and it was concluded that pure two-region operation could not be maintained with the present equipment. However, all other aspects of the performance appeared satisfactory.

The mixing experiment was interrupted on May 21 because of a broken valve stem in the blanket

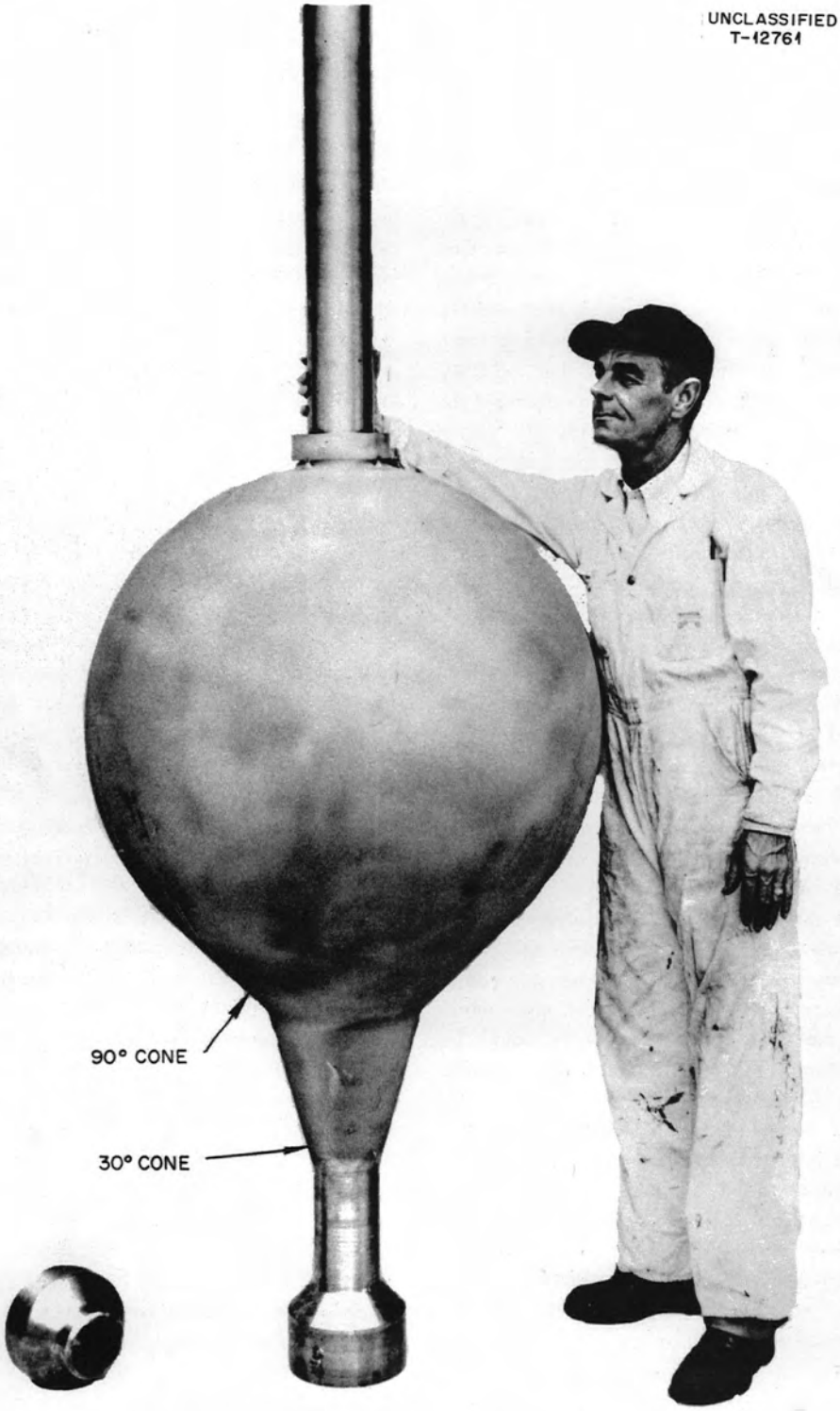

Fig. 1.3. Completed Core Tank Showing Joint Between the 30- and 90-deg Cone Entrance Sections.

high-pressure sampler, which made it impossible to follow the rate of concentration rise in the blanket system. After repair of the sampler and retightening of the bolts on three blanket-system flanges that had indicated slight leakage, the equilibrium mixing experiment was continued. Equilibrium core and blanket concentrations were determined by chemical analyses at a fuel feed rate of 8 lb/min and blanket purge rates of 6, 4, and 2 lb/min. The rate of intermixing was found to be substantially constant at 3 to 4 lb/min, decreasing slightly with increasing blanket purge rate. The ratio of core-to-blanket uranium concentration was very nearly 3:1 at a blanket purge rate of 6 lb/min, approaching 1:1 at the lower purge rates.

Although the mass of uranium in the blanket is approximately 1.7 times that in the core (at the concentration ratio of 3:1), it was calculated that the flux distribution would be such that some 60% of the power would be generated in the core. Furthermore, kinetics calculations indicated that with this power distribution it would be safe to operate with the blanket pressurizer full of liquid. Hence, it was concluded that the reactor could be operated at power in this manner without modification to reactor equipment.

1.1.7 Power Operation with Fuel in Blanket – Run 16

At the conclusion of the mixing experiments the entire U^{235} inventory (5.8 kg) was put into circulation in preparation for operation at power. The purpose of the next run (run 16) was to study the chemical stability of the fuel at the new concentrations (6 g of U^{235} per kg of D_2O in the core, and 2 g of U^{235} per kg of D_2O in the blanket) and the nuclear stability with the new power distribution. First, the reactor was held steady for two days at 260°C with external heating and with a blanket purge rate of 6 lb/min while the core and blanket concentrations were determined by repeated sampling. On June 4 the heating steam was shut off and the temperature was allowed to decrease until the reactor became critical. Criticality was reached at 235°C, and the power rose to match heat losses, about 300 kw (see Fig. 1.4).

After 18 hr at heat-loss power, a sample result was received which indicated very high nickel in the fuel solution. Although oxygen consumption had not indicated an excessive corrosion rate, the reactor was made subcritical by external heating while the nickel concentration was being checked. When further sampling showed the high-nickel result to be erroneous, the reactor was again made critical at heat-loss power and was held at this level for two more days before the level was raised to 750 kw by withdrawal of steam from the heat exchangers. The corrosion rate for this entire period appeared to be satisfactorily low (less than 1 mpy).

On June 8 an additional 1.6 kg of U^{235} was added, together with copper sulfate and sulfuric acid, and the fuel was concentrated to bring the temperature to 260°C. After 30 hr of stable performance at 260°C, the temperature was raised to 275°C with the power level still at ~750 kw. On June 11 the temperature was reduced to 260°C in preparation for increasing the power. In the week which followed, the power was raised to 2.7 Mw in steps of about 0.5 Mw. Each power level was held for about 48 hr to permit scrutiny of sample results before the next step. During this period the average temperature was held around 260°C, with some fluctuations due to variations in the distribution of uranium in the reactor.

On June 12 some activity (about 10 mr/hr at contact) appeared in one of the two intermediate legs of the fuel feed pump, indicating a leaking diaphragm; however, the pump head appeared to be leak-tight when hydrostatically tested. At the same time, contamination (about 350 mr/hr) was found in the fuel sampler cavity, apparently from a leak in the low-pressure sampler. On June 19 gaseous activity issued from the sampler cavity into the operating area, and the reactor was made subcritical by dilution. Investigation showed that the escape of gaseous activity had resulted from a jetting operation which had interrupted the ventilation of the sampler cavity. The tiny leak from the fuel sampler was stopped by filling the isolation chamber with condensate from the fuel low-pressure system and retightening the valves.

While the reactor was subcritical, the temperature was held at 185°C with plant steam. After the sampler leak was stopped, the fuel was concentrated and the reactor was made critical at 185°C. The fuel concentration then was slowly increased, bringing the temperature up with nuclear heat. When the temperature reached 260°C, the power was raised to 3.2 Mw and the run was continued. Again the reactor exhibited good stability, but before the power was raised again, it was planned

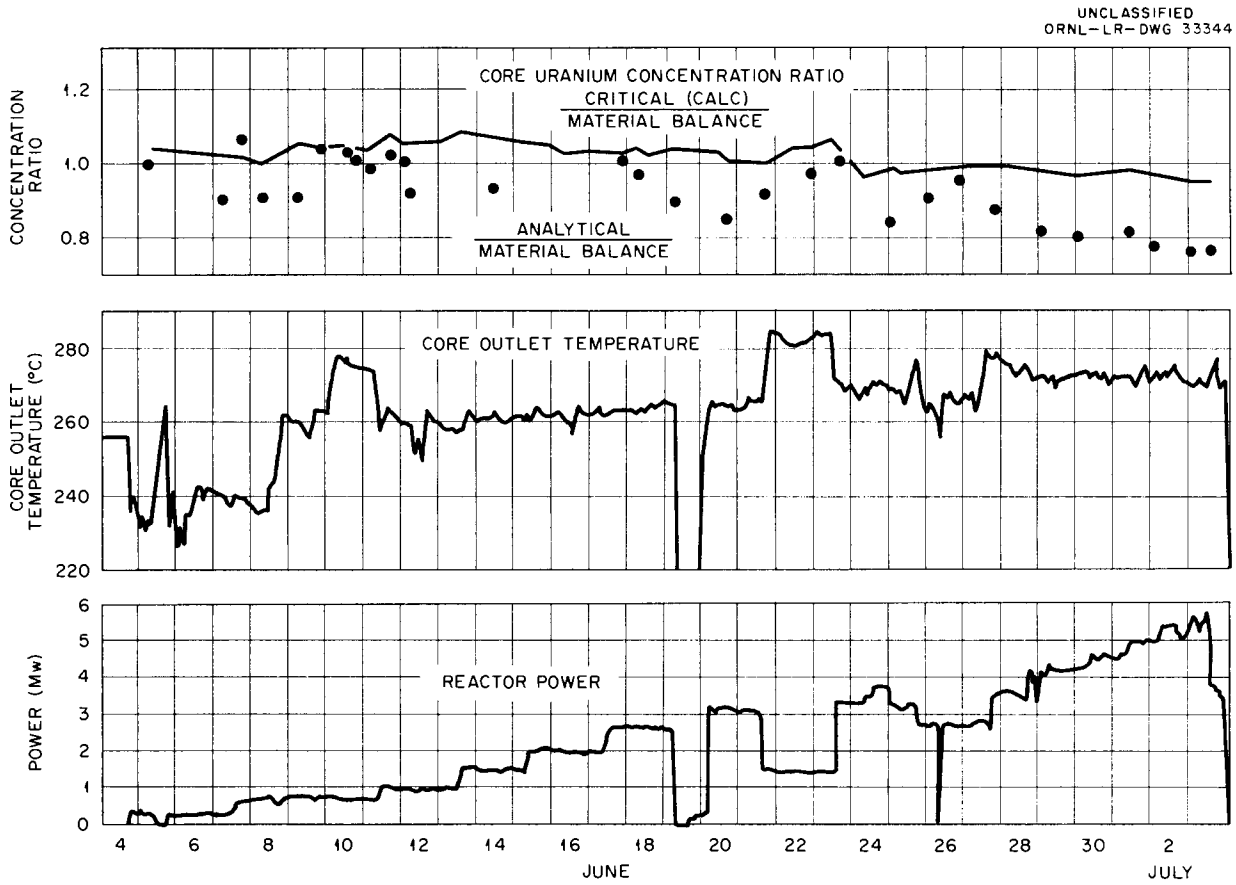

Fig. 1.4. Operating Parameters During Run 16.

to explore the solution behavior at higher temperatures, and at lower power. Accordingly, on June 21 the power was reduced to 1.5 Mw and the temperature was raised to 284°C. Operation at these conditions appeared to be satisfactory; so on the following day the power was raised to 3.3 Mw.

On the afternoon of June 24, after the power had been raised to 3.8 Mw, there was an abrupt, brief surge to about 5.6 Mw. Attention was drawn to the surge when the liquid level in the pressurizer rose off-scale and caused an annunciator to alarm and the fuel feed pump to stop. The level came back in a few seconds, and the power quickly returned to normal without any action on the part of the operators. Numerous excursions, of the same sort but smaller in magnitude, had occurred before during the run. In no case, however, had the pressurizer level gone high enough to cause any upset.

After the large surge, attempts were made to study the events and to establish some correlations. On June 25 the power was lowered to 3.3 Mw and then to 2.8 Mw to observe the effect on the frequency of power surges. The temperature was raised briefly to 278°C for the same purpose. These changes had no observable effect on the frequency (one surge every 1–2 hr).

On June 27, after the temperature had been raised to 275°C to obtain better internal recombination, stepwise increases in power were resumed. No more large power "pips" were observed, but no conclusions have been reached to explain the cause of the pips. The maximum sustained power during the run was about 5.3 Mw, reached early on July 2.

On July 3, after 30 days of continuous operation, the power was reduced and the reactor was diluted for the scheduled shutdown. The high-pressure systems were rinsed for 24 hr with D_2O condensate

in preparation for opening the core and blanket inspection ports.

1.1.8 Maintenance and Inspection Following Run 16

The third inspection of the HRT core was attempted on July 8, by inserting a remotely operated mirror arm and a periscope into the blanket vessel. The mirror arm (see Fig. 4.2) had been tested in a mockup of the core and blanket. The assembly was positioned in the core with much difficulty, although it had performed smoothly in the mockup. Before the core could be examined, failure of the light bulb made it necessary to withdraw the assembly into a plastic bag to minimize particulate contamination of the area; the lower end of the arm had been bent during positioning, however, and the manipulation required to extract the damaged tool caused radioactive dust to spread through the reactor building. Breathing tolerance was not exceeded, and further spread of the activity was prevented by requiring protective clothing inside the building.

A second mirror arm, with a lower extension $1\frac{1}{4}$ in. shorter than the previous one, was readily positioned for core viewing. Although the lamp attached to the arm was more powerful than that employed in the inspection following run 14, the level of illumination was nevertheless too low to permit observation of the leak area. This is attributed to the lower reflectivity of the present, generally brownish, core exterior, as compared with the earlier white surface produced by D_2O-blanket operation.

Although no visual examination of the leak site was possible, detailed observations were made of the core interior and the directly viewable half of the core exterior. Inside the core a moderate deposit of crumbled scale was observed around the outer periphery of the top diffuser screen, extending inward to the first circle of holes from the edge. The wall showed irregular patches of gray-to-brown scale, decreasing in size and surface coverage with elevation. Near the equator the patches appeared as scattered round dots on a granular, light-gray background which resembled etched metal; at higher elevations little or no scale was visible. Numerous bright specks suggestive of bare metal were perceived at all elevations.

The exterior of the core above the 30-deg cone appeared to be a dull, light grayish-brown color, darkening to a rusty appearance in the east and west quadrants. The weld seams were clearly visible and of sound appearance. The 30-deg cone presented a coarser-grained appearance, with a shiny cast as though it were varnished. Two isolated clusters of bright metallic specks were observed on the spherical surface.

Concurrently with the viewing activities, several important items of maintenance were completed. A hydrostatic pressure test conducted on the drive piping of the east fuel-feed pump, which had shown activity during the run, showed no leakage at 2000 psig over a 6-hr period. However, a gamma spectrum scan of a heavy-water sample from the line showed small quantities of fission-gas decay products. As a result, the pump head was removed and replaced. The radiation level above the pump head measured 2000 r/hr in air; after the shield was flooded to a depth of 20 ft, however, the field at the roof plugs was reduced to 1 to 2 mr/hr, allowing the change to be completed by the use of routine remote-maintenance techniques. In addition, a 3-in. bypass line between the fuel and blanket heat exchanger steam lines was installed; new metering orifices and a condensate trap were provided for the steam discharge lines to the air-cooled condenser; the fuel sampling assembly was replaced; and the reactor control circuits were revised to provide additional interlock protection with fuel solution in the blanket. After viewing was terminated, corrosion and metallurgical specimens, respectively, were inserted into the core and blanket, and the vessel flanges were resealed.

1.2 EXPERIMENTAL ANALYSIS

1.2.1 Loss of Reactivity During Power Operation

Although the mechanism for the loss of uranium during power operation in runs 13 and 14 has not been established, there appears to be a definite correlation between the amount of uranium in circulation, the concentration of dissolved radiolytic gas (determined by power level, solution temperature, and internal catalyst activity), and the concentration of excess acid.

Figure 1.1 shows the fraction of the uranium in the fuel system which appeared to be in circulation during run 13, the initial power run. The line is the ratio of the uranium concentration indicated

by the critical temperature[5] to the concentration calculated from a material balance. The points are the ratios of concentrations from fuel-sample results to the concentrations calculated from the material balance. The agreement between the sample results and the concentration estimated from the temperature–critical-concentration relation implies that the core contained few poisons. This is supported by calculations which indicate that the poisoning from fission products and dissolved corrosion products should have been negligible.

Study of gas-recombination data makes it appear very unlikely that gas bubbles were directly responsible for the depression of the reactor temperature, that is, the reactivity loss which attended operation at power. Apparently no bubbles were let down throughout most of run 13, including the period at the beginning when most of the reactivity loss was observed. During the times when bubbles were formed purposely, the effect was slight, as expected. The data do show that during most of the run the concentration of dissolved radiolytic gases was high – often near the limits of solubility. The concentrations were power-dependent, thus indicating the possibility that they were related to the loss of uranium, which was definitely dependent upon power level.

The concentration ratios for run 14 are shown in Fig. 1.2. During this run radiolytic-gas concentrations were much lower than in run 13. The apparent loss of uranium was considerably less than in the first power run.

A similar analysis of run 16 was complicated by the addition of another variable in the criticality relationship, the concentration of uranium in the blanket. Instead of the direct, experimentally verified relation between core concentration and temperature which had existed during two-region operation, the run-16 analysis, presented in Fig. 1.4, was based on a calculated relation between critical temperature, core concentration, and blanket concentration. Verification of the critical calculations was hindered by the imprecision of the analyses of small radioactive samples.

The fact that the line in Fig. 1.4 is above unity at the beginning of the run probably means that the critical calculations were slightly in error and that they indicated slightly higher concentrations than were actually required. Toward the end of the run the dip in the line represents a loss of uranium from circulation. The apparent loss is about 7%, relative to the line at the beginning of the run when all the uranium inventory was presumably in circulation. However, the loss indicated by the points based on analytical results is several times greater than the 7% shown by the critical-temperature data. At the present time there is no explanation for this large disagreement between the two methods.

1.2.2 Corrosion and Chemistry of the Reactor System

(*a*) Corrosion. – As previously mentioned, the first power run (13) was started without copper in solution so that recombination rate constants could be evaluated as the copper was added. During the first 18.5 hr of power operation the stainless steel corrosion rate, based on nickel and sulfate analyses for two samples, was 166 mpy. For the remaining 88.5 hr of power operation the average corrosion rate was 11 mpy. While the average rate for the entire running time at power was thus 38 mpy, the average corrosion rate of a type 347 stainless steel coupon specimen downstream from the fuel circulating pump was only 4.5 mpy, based on the defilmed weight loss. Therefore, localized attack is assumed to have occurred at some part of the system. The run was terminated because the high concentration of nickel (~600 ppm) made it difficult to continue monitoring the corrosion rate by following the nickel analyses and made the stability of the solution questionable.

Run 14 was made with a new charge of fuel solution, which contained copper sulfate and was of a composition previously tested in in-pile loop runs. The stainless steel corrosion rate, based on 29 samples taken over a period of 148 hr prior to and during power operation, was 2 to 4 mpy. Although this rate was a large improvement over the rate seen in run 13, it was still higher than would be anticipated from previous work. Furthermore, the rate was established at zero power and did not appear to increase as the power was increased.

In runs 15 and 16 the stainless steel corrosion rates were still lower, estimated at approximately 1 mpy during the 800 hr covered by these runs.

(*b*) Fuel Chemistry. – In the previous depleted-uranium runs the observed uranium concentrations were consistently 3 to 15% lower than the calculated concentrations, based on temperature,

[5] S. E. Beall *et al.*, *HRP Quar. Prog. Rep. Jan. 31, 1958*, ORNL-2493, p 8.

pressure, volumes, weights, and feed and purge pumping rates. It was further observed that although, on the average, the "book inventory" ratios of the various ionic constituents were confirmed by solution analyses, the analytical ion ratios varied considerably from one sample to another. The relative movements of the ion ratios suggested that a reversible hydrolysis was occurring in the system. Finally, the statistical variance of the analytical ion ratios of samples taken from the reactor system during operation was found to be significantly greater than the variance of samples poured from a large bottle. Thus it appears likely that part of the reactor solute must have been separated from the circulating solution and that it must have been in varying equilibrium with it from time to time. The operating variables which control the apparent reversible phase separation have not yet been identified.

Figure 1.5 is a phase diagram of the three-component system UO_3-CuO-SO_3. The points plotted on this diagram are for 41 high-pressure samples from HRT run 10-B, a depleted-uranium run in light water. The sample volumes were ½ liter, and the uranium analyses were performed gravimetrically in triplicate. The least-squares lines for the two variables defined on the figures are shown. The probability of correlation of these variables was greater than 0.99. The nature of this diagram is such that the mixture of any two compositions of material, represented by points on the diagram, will have a composition lying on the straight line which connects the two points. In this case the reversible separate phase $2UO_3 \cdot SO_3$, or zippeite, is indicated.

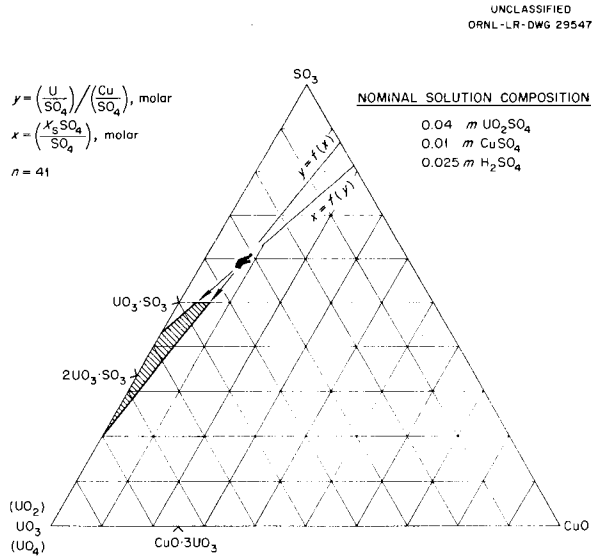

Fig. 1.5. Phase Diagram of Three-Component System UO_3-CuO-SO_3; Data for Run 10-B.

The data for HRT run 14 before and during power are shown in Fig. 1.6. These samples, like all the samples removed since power operation was begun, were approximately 5 ml and were analyzed by the special hot methods developed for the HRT.

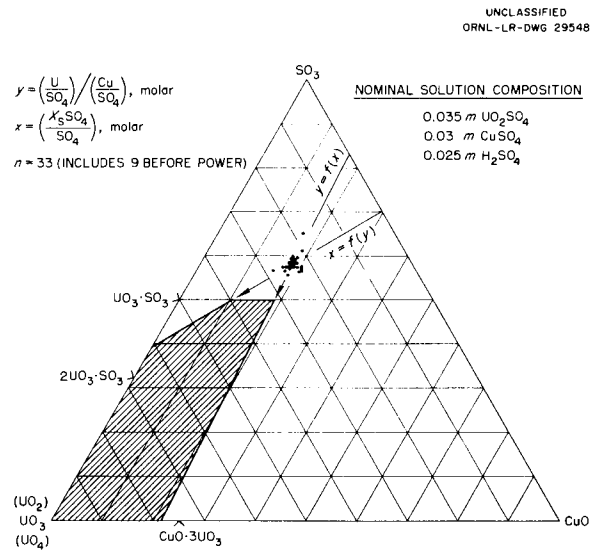

Fig. 1.6. Phase Diagram of Three-Component System UO_3-CuO-SO_3; Data for Run 14 Before and During Power.

The probability of correlation of the least-squares variables was greater than 0.95. Again the reversible second phase, zippeite, is indicated, but in addition the UO_3 point is included. On this diagram UO_2 and UO_4 would also be represented as UO_3. On the basis of this study it appears that the half-hydrolysis compound zippeite might account for the uranium loss in the depleted-uranium runs – assuming, of course, that it was removed from the circulating solution by adsorption or precipitation. It would behave similarly in the power runs and account for part of the loss of reactivity observed. The remainder of the reactivity loss, which appeared whenever the concentration of dissolved radiolytic gas was high, might be explained by the UO_4 (or UO_2 or UO_3) solid indicated by Fig. 1.6.

The results of the next power run, 16, are shown in Table 1.1, which has been divided into portions

Table 1.1. HRT Run 16, Fuel Solution Sample Data Normalized to Total Sulfate

	16-A		16-B			16-C1			16-C2			16-C3		
Reactor power, Mw	Subcritical		0 to 1			1 to 4			4 to 5			Shutdown		
Reactor temperature, °C	150		230 to 260			250 to 290			255 to 290			Shutdown		
Total running time, hr	84		137.5			366.5			240			Shutdown		
Number of samples included	28		41			35			28			2		
Average concentration of U, *m* (core/blanket = ratio)	5.08/2.44 = 2.09		19.5/7.17 = 2.72			21.3/9.00 = 2.37			21.1/8.27 = 2.55			Shutdown		
Book sulfate, moles	~71.52/3		71.52			81.59			81.59			81.59		
	Cation-to-Sulfate Mole Ratios													
	U/SO_4	Cu/SO_4	U/SO_4	Cu/SO_4	Ni/SO_4	U/SO_4	Cu/SO_4	Ni/SO_4	U/SO_4	Cu/SO_4	Ni/SO_4	U/SO_4	Cu/SO_4	Ni/SO_4
Ion ratios, book	0.373	0.318	0.373	0.318		0.400	0.270		0.400	0.270		0.400	0.270	
Ion ratios, sample average	0.402	0.296	0.401	0.294	0.035	0.381	0.229	0.035	0.367	0.221	0.045	0.391	0.234	0.048
Standard deviation, %	±7	±16	±8	±12	±39	±10	±11	±23	±6	±8	±24	±0.6	±1.4	±2.2
Control-chart band limits (95% confidence level), %	±14	±33	±16	±25	±79	±19	±23	±46	±12	±16	±48	±7	±18	±28
Ion ratio, samples/ion ratio, book	1.08	0.93	1.08	0.93		0.95	0.85		0.92	0.82		0.98	0.86	
Estimated cation inventory,* moles	~28.8/3	~21.2/3	28.6	21.0	2.5	31.1	18.7	2.9	29.9	18.0	3.7	31.9	19.1	3.9

*Average (cation/sulfate) × (book sulfate).

A, B, and C. Portion A covers subcritical mixing operations, portion B covers powers to 1 Mw, and portions C1 and C2 cover operation at powers to 5 Mw.

In 16-A, only one-third the run-14 fuel inventory was used in order to keep the reactor subcritical at the 150°C temperature. In run 16-B the remaining fuel-solution inventory (approximately 4 kg of U^{235}) was made available, and operation at low power was started. In both these runs the average sample uranium was 8% higher than the book uranium. At the time, this was considered reasonable since in 16-A there was a significantly lower Cu/SO_4 ratio on the blanket side, and the data indicated loss of a sulfate-containing copper salt. Later, however, in 16-C, it was found that an error was being made in the analytical chemistry, indicating low sulfate, and this may have occurred also in 16-A.

The last 10 days of reactor power operation are designated 16-C2; the data are believed to be especially reliable since U, Cu, and SO_4 standards were run on every laboratory shift and since confirmation of composition was demonstrated by free-acid determinations.

After cooling-down, rinsing, and dumping the reactor, two samples, designated 16-C3, were taken from the dump tanks. From the change in (ion ratio, samples)/(ion ratio, book), it appears that although some uranium and copper were lost as the run progressed nearly all the uranium and part of the copper were recovered by shutting-down.

In analyzing the results of run 16-C2, the samples were plotted as part of the four-component system: UO_3-CuO-NiO-SO_3 (Fig. 1.7). The three corners of the triangles plotted are UO_3-SO_3, CuO-SO_3, and UO_3-CuO. The single point which represents each sample is above each triangle and is the fourth corner of an equilateral tetrahedron. The surprising behavior of both core and blanket samples in 16-C2 was that both uranium and copper were being lost from solution in the same proportion, and therefore the sample points lie on a straight line passing through the SO_3 point.

This loss of uranium and copper from both core and blanket samples in run 16-C2 correlates significantly with both time and reactor power. The two variables could not be distinguished since time and power increased together. After reactor shutdown, however, the solution moved back to the original position along the same straight line shown in Fig. 1.7. Peculiarly, as discussed in Sec 1.2.1, the uranium concentration indicated by the reactor critical temperatures did not agree with the loss indicated by the sample analyses. An explanation of the disagreement is not yet apparent.

(c) Steam and Feedwater Systems. – During all the power runs the reactor steam-generator systems were operated with pH-phosphate control and with continuous hydrazine addition. The oxygen in the reactor steam, at 5 Mw, was kept below 5 ppb. Unfortunately, this low oxygen concentration was accompanied by high chloride concentrations,

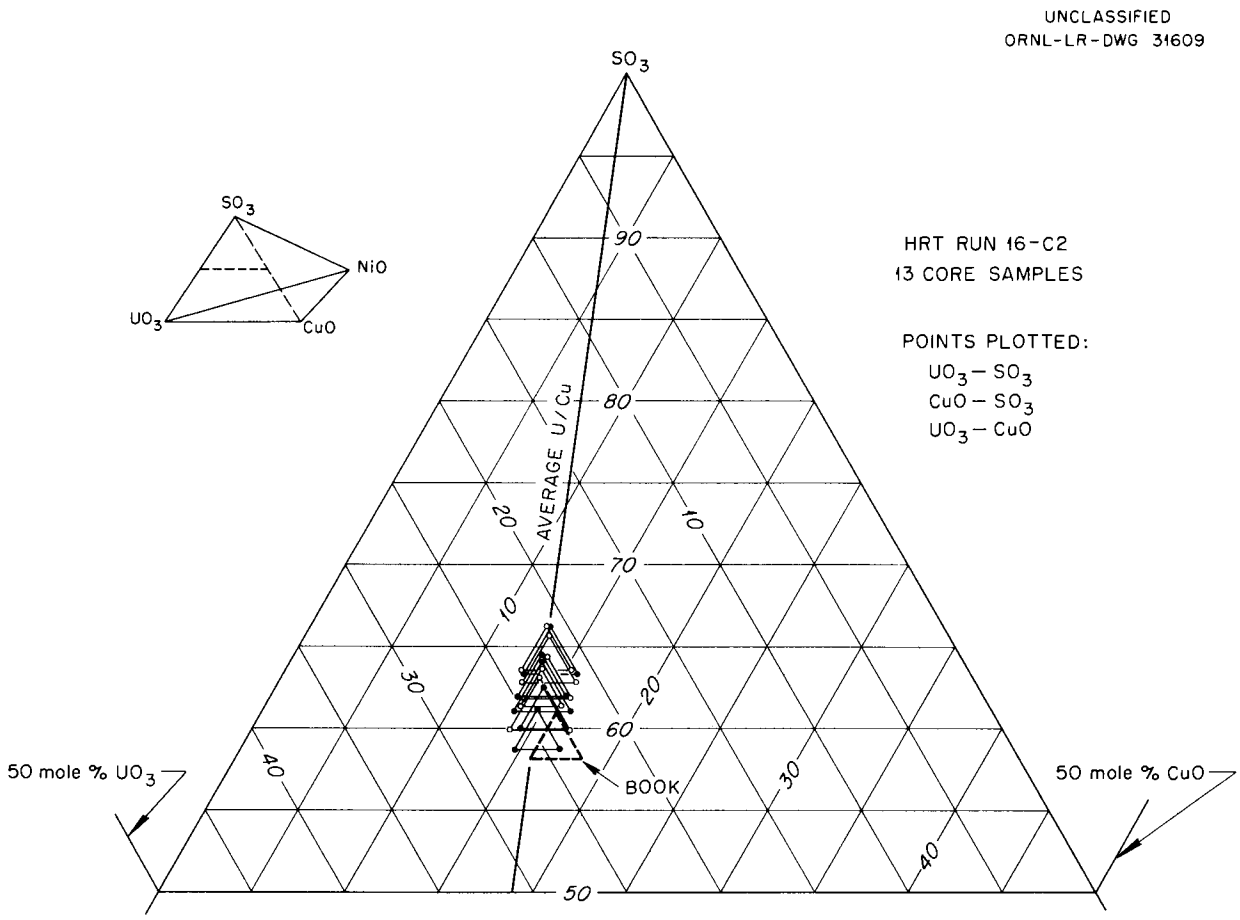

Fig. 1.7. Phase Diagram of Four-Component System UO_3-CuO-NiO-SO_3; Data for Run 16-C2.

about 1 ppm, in the heat exchanger blowdown. This is the result of the high chloride content of commercial hydrazine, and ion exchangers are now being used to remove this contaminant.

Radioactive solids also appeared in the heat exchanger blowdown, but no fission products could be detected. The solids contained iron, copper, and nickel compounds and were probably activated corrosion products.

The fuel steam condensate was found to give off gas bubbles containing hydrogen and nitrogen. At low hydrazine addition rates these bubbles also contained oxygen and could be ignited. The rate of removal of oxygen in the steam condensate, with no hydrazine addition, was essentially identical to the predicted rate of production in these steam generators.

1.2.3 Measurements of Radioactivity

Radiation levels were monitored both inside and outside the shield during operation. Typical values are discussed below.

(*a*) Gamma Radiation Level in Reactor Cell. – Gamma radiation levels at several points in the reactor cell are shown in Table 1.2. The remote gamma monitors generally are located near the top of the cell. RM-4 is partially shielded from the fuel dump tanks by intervening structure. In run 14, essentially all the power was generated in the core, while in run 16 only about 3 Mw was in the core. The shutdown referred to in Table 1.2 is that following run 16.

(*b*) Activity in Auxiliary Process Streams. – Several gamma-sensitive monitors are placed in

Table 1.2. Gamma Radiation Levels in Cell

Location[a]	Monitor No.	Radiation Levels (r/hr)			
		At 5-Mw Operation		After Shutdown	
		Run 14	Run 16	3.6 hr	17 days
Fuel circulating pump	RM-1	68,000	42,000	2,900	350
Blanket circulating pump	RM-2	34,000	22,000	2,000	*b*
Top of thermal shield	RM-3	150,000	65,000	2,200	470
Fuel dump tanks	RM-4	48,000	40,000	17,000	1,000
Blanket dump tanks	RM-5	*c*	1,500	180	34
Fuel feed pump	RM-6	100,000	68,000	30,000	2,400

[a]Exact location is shown on Dwg. F-27939, REED Design Section.
[b]Instrument out of order.
[c]No reading.

shielded locations outside the main cell to detect any possible leakage of radioactive fluid from the fuel piping. They monitor the oxygen supply line, fuel-feed-pump intermediate leg, cell air, condenser cooling-water return, heating-steam condensate return, steam and cooling water leaving cell, heat exchanger sample lines, and stack gas. With the exception of the unit in the steam valve pit which monitors the steam and cooling water, all the monitors remained below 10 mr/hr with the reactor at 5 Mw. The signal from the steam and cooling-water monitor was erratic because of high temperature and humidity, but it was roughly proportional to reactor power, indicating about 100 mr/hr at 5 Mw. The high reading resulted from radiation shining from the reactor cell. The activity of the cooling water itself was found to be very low, and there was no detectable activity in the steam after it had left the pit. Water samples from the fuel and blanket heat exchangers showed no fission-product activity and less than 500 counts/min/ml of other activity (mostly phosphorus).

(c) Radiation Levels Outside the Shield. – The biological shielding proved quite adequate. Except as noted below, the level in the inhabited areas was less than 0.2 mr/hr when the reactor was at 5 Mw. Locally, higher levels existed at the sampler stations, at the top of the nuclear instrument shaft, directly over the core, and at the demineralized-cooling-water pump and heat exchanger. Gamma and neutron dose rates at these locations are given in Table 1.3.

1.2.4 Power Oscillations and Transients

During operation at high power, as mentioned in Sec 1.1.7, there were numerous abrupt, brief surges in the nuclear power, accompanied by disturbances in core pressurizer level. On the logarithmic neutron-level recorder, peak powers were usually

Table 1.3. Radiation Levels Outside the Shield (Reactor at 5 Mw)

Survey Area	Dose Rate	
	Gamma (mr/hr)	Fast Neutrons (mrep/hr)
Shield block C-7 (over core)	33	0.5
Shield block C-8 (over core)	27	0.5
Top of instrument shaft	20	N.D.*
Cooling water pump	10	N.D.
Blanket sampler	7	N.D.
Fuel sampler	0.2	0.1
Chemical plant overflow sampler	2	N.D.

*N.D. = not detectable with Health Physics portable instruments.

10–25% above the average, with one excursion as high as 50%. The shortest positive periods reached during the excursions were around 5 sec. After the peak, the power always dropped rapidly and the disturbances usually were over in a minute or so. These excursions occurred throughout the parts of run 16 in which the nuclear power was 2.0 Mw or above, at intervals which varied from a few minutes to several hours, with an average between 1 and 2 hr. There were no excursions during the low-power parts of run 16, and none at all during run 13. During the last day of run 14, however, there were a few excursions with the same characteristics as those observed during run 16.

During the latter part of run 16 the excursions were examined with the aid of a two-channel fast recorder which monitored the pressurizer level and reactor period. This study disclosed cyclic minor fluctuations in nuclear power, with a fairly uniform period of about 8 to 10 sec and an amplitude of about 1.5%. The large excursions were not simply a divergence of the small oscillations, but began abruptly at any part of the cycle.

The preliminary studies of the oscillations and excursions have produced no conclusive explanation. Although the excursions have not interfered with reactor operation, efforts to determine the mechanism will continue.

1.2.5 Miscellaneous

Throughout power operation the performance of many auxiliary devices was watched with interest. Some of the observations are reported below.

(a) Oxygenation of the Fuel Solution. – The oxygen flow of approximately 1 liter/min in run 13 was monitored with an input flowmeter and an off-gas flow integrator. In addition to the 15-hr stoppage of off-gas flow, which indicated a consumption of 880 ± 100 liters (see Sec 1.1.2), an additional 800 ± 100 liters (STP) of oxygen was consumed during the remainder of the run. Assuming that this quantity of oxygen was consumed in oxidizing stainless steel, the equivalent corrosion rate was about 30 mpy. In run 14 the oxygen flow was studied in much more detail, and in addition to measuring the inlet and outlet flows, a system inventory was also calculated periodically. In spite of the effort to make a good oxygen balance, the oxygen consumption of the 11-day operating period was negative by a small amount (106 liters in a total of 30,000 liters throughput). The error in the measurements is probably as large as 2%. At the run-14 rate of 2900 liters/day throughput, the error could correspond to the oxygen consumption from a corrosion rate of up to 8 mpy.

During run 16, oxygen was injected into the blanket at 1.0 liter/min and into the fuel feed stream at 1.4 liters/min. The oxygen injected into the blanket also passed through the core before being let down. As in run 14, there was some discrepancy in measurements; the indicated outlet gas flow slightly exceeded the oxygen input.

(b) Measurement of Container Leakage. – The reactor cell in-leakage rate is continuously monitored by observing the absolute pressure, with corrections for temperature, and by using a differential manometer which automatically compensates for container temperature changes. The maximum indicated leak during operation was about 1.66 liters/min (STP). During the last 100 hr of run 14, there was no change in the cell pressure after correcting for temperature fluctuations, indicating essentially no leakage. During run 16, after cell temperatures leveled out, the cell leakage measured over a period of 30 days was 0.32 liter/min (STP).

(c) Iodine-Bed Temperatures During Power Operation. – The iodine-reaction bed, located in the fuel low-pressure system directly beneath the catalytic recombiner, is designed to absorb 98–99% of the fission-product iodine in the reactor off-gases. By this means, much of the I^{135} (parent of Xe^{135}), which would otherwise dissolve in the condensate and return to the reactor, is eliminated, and iodine poisoning of the recombiner catalyst is prevented. Because of radiation heating by the iodine decay to xenon and the exothermic iodine-silver reaction

$$Ag + \tfrac{1}{2}I_2 \longrightarrow AgI + 14.9 \text{ kcal}$$

the degree of absorption taking place can be monitored by temperature observations within the bed.

The thermocouple nearest the inlet end of the iodine bed indicated a temperature increase from about 115°C at zero power to 127°C at a nominal power of 4.5 Mw. On the basis of these temperatures it appears that a significant quantity of

iodine was removed by the bed. This was confirmed by analyses of the fuel solution for I_2 (see Sec 2.3.1).

(*d*) Low-Pressure Recombination in Run 16. – During run 16 the pressure in the fuel low-pressure system was observed to follow a regular, sawtooth pattern, that is, a gradual buildup over a period of minutes terminating in an abrupt drop of about 0.4 psi. The period varied with reactor power and temperature, the frequency increasing with power above a threshold power which increased with reactor temperature. This behavior appears to have been caused by successive collection and rapid burning of radiolytic gas in the recombiner condenser. Reactor power and temperature determine the concentration of radiolytic gases in the letdown stream and therefore the concentration of deuterium in the stream to the recombiner. Comparison of the rate of pressure increase with the calculated letdown rate of deuterium indicates a recombiner efficiency of about 99%, which agrees with earlier test results at low concentrations.[6] There appeared to be no significant change in recombiner efficiency during the run. The small after-recombiner downstream of the condenser was effective in removing the remaining 1% on the basis of analyses of off-gas from the charcoal beds which showed no deuterium escaping.

(e) Flange Leak-Detector System. – The degree of tightness of the 182 ring-joint seals throughout the reactor is monitored by a D_2O-filled leak-detector system which is maintained at a pressure several hundred psi above the reactor pressure. Leakage at any flanged joint is indicated by a loss of D_2O from the leak-detector reservoir. During power runs 13, 14, and 16 the total leakage from all the flanges was never greater than 50 cc/day and was normally only 10–15 cc/day. No leakage of fuel solution has been detected at any joint.

---

[6] B. A. Hannaford, *Test of HRT Recombiners*, ORNL CF-57-9-98 (Sept. 20, 1957).

2. HRT PROCESSING PLANT

W. D. Burch P. A. Haas W. E. Unger

L. H. Chase H. O. Weeren
C. S. Lisser R. H. Winget
O. O. Yarbro

The program of the HRT processing plant was integrated with the reactor program in the six months of the report period. Because of the added complexity to the over-all experiment, the hydroclone system was not operated during the first two reactor power runs (13 and 14). In this period final cell maintenance, closure, and leak-testing were completed. The chemical plant was operated continuously during the subcritical run 15 and the third power run (16).

2.1 FINAL CELL MAINTENANCE, CLOSURE, AND LEAK TEST

2.1.1 Final Cell Maintenance

During the final testing period several modifications to cell C components were found necessary. As a result of the reactor power-wiring failures, it appeared advisable to install spare wiring to the pump, heater, and space cooler in cell C. Mineral-insulated wiring similar to the reactor-cell replacement wiring was installed through the cell wall to the vicinity of the power disconnect boards located just under the roof plugs. Existing wiring, which had given no indication of failure, was left intact. While the cell is flooded for shielding, the spare wiring can be connected by removing one seal pan. The space-cooler motor was converted from 400- to 220-v operation to reduce the probability of breakdown of insulation.

The electrically operated weigh cell on the D_2O storage tank was replaced in an attempt to eliminate a troublesome zero shift. The original cell had drifted 5% in 24 hr and up to 15% over extended periods. Performance of the new cell has not been significantly better.

2.1.2 Cell Leak Test

Initial cell C leak tests indicated that the top-closure seal-pan welds were leak-free but that there were major leaks on top of the cell where the two sampler housings are welded to the cell wall. Those leaks were repaired, and all penetrations into the service cells and the top were checked with a helium leak-detector system with the cell at 30 psia pressure.

The permissible leak rate was established by calculating the effects of a postulated accident in which the chemical plant high-pressure system piping ruptured and the isolation valves between the reactor and chemical plant could not be closed. Approximately one-eighth of the reactor fuel would be expelled into cell C before the reactor could be dumped, and cell C pressure would rise from 7.5 psia to 19 psia. For such an accident it was estimated that a leak rate equivalent to 20 liters/min at 25 psia would conform to the standards established for the reactor cell and would be acceptable. Leak rates determined after subsequent maintenance operations in cell C averaged 9 liters/min at a 30-psia test pressure, 4.8 liters/min at 25 psia, and 2.2 liters/min at 7.5 psia (vacuum). During the fourth week in April the cell leak rate increased suddenly to 6 liters/min at 7.5 psia for reasons unknown. This rate, still well within the specifications, has remained constant.

2.2 OPERATION DURING RUNS 15 AND 16

2.2.1 Data and Conclusions

The hydroclone system of the processing plant was operated for 119.7 hr during subcritical mixing experiments in reactor runs 15 and 16 (designated as chemical plant run CP-16-1) and removed 150 g of solids from the reactor fuel system. Operation of the processing plant was continued during the critical portion of reactor run 16, with operating cycles of 310.4 hr (run CP-16-2) and 338.6 hr (run CP-16-3). About 100 g of solids was removed from the reactor fuel system during run CP-16-2 and 107 g was removed during run CP-16-3.

The flow rate through the processing plant was 1.3 gpm, with the hydroclone underflow pot maintained at 2 to 11°C above the reactor core outlet temperature. Reactor power generation amounted to 249 Mwhr during run 16-2 and 1235 Mwhr during run 16-3.

The quantities of material removed from the reactor system during runs 16-1 and 16-2 and the composition of the solids are given in Table 2.1.

Table 2.1. Material Accumulated in Hydroclone Underflow Pot and Composition of Solids Removed by Hydroclone

Element	Material Accumulated (g)		Composition (%) of Solids Removed	
	Run 16-1	Run 16-2	Run 16-1	Run 16-2
U	20.7	47.9		
Cu	4.7	5.9		
Ni*	2.2	3.5	1.4	2.6
Fe	78.0	46.1	52	47
Cr	7.7	4.8	5.1	4.9
Zr	16.3	7.5	10.9	7.6
Al		6.0		4.8
Mn	0.0	0.1		
Total solids removed (g)			150	99

*Since the nickel concentration in the underflow pot was greater than in the fuel, it was assumed that precipitation, probably as $NiSO_4$, had occurred.

The quantity of solids accumulated in the underflow pot was only a small fraction of those estimated to have been formed in the reactor high-pressure system. The remainder was removed from the reactor circulating system by depositing on pipe walls and settling in the reactor vessel, in horizontal runs of pipe, and in the dump tanks. A circulation life of 20 to 30 min for solids produced in the reactor was estimated from activation of iron in solids removed from corrosion specimens.[1,2] With such short circulation time only a small fraction of the solids would reach the hydroclone.

Ratios of underflow-pot concentration to overflow-stream concentration were determined from chemical and radiochemical analyses. These concentration factors for materials that were concentrated significantly in the underflow pot are given in Table 2.2.

Elements not concentrated by the hydroclone included U, Cu, Mn, S, Ba, Sr, and Cs. The concentration of iodine in the underflow pot is believed to have resulted from decay of tellurium which had been concentrated, since no direct method of concentrating iodine can be envisioned.

Since none of the rare-earth fission-product group had reached solubility limits, they could not be concentrated.

Table 2.2. Underflow-Pot Concentration Factors

Element	Concentration Factor
Ru	600
Fe	>500*
Cr	410
Zr**	390
Te	56
I	12
Mo	7
Ce	5
Ni**	5
Al**	4

*Below limit of detection in hydroclone overflow.

**Based on chemical analyses; other factors were determined from radiochemical analyses.

[1] J. C. Suddath, *Rates of Corrosion Product Removal from Circulating System by Film Formation and Settling*, ORNL CF-58-4-119 (April 24, 1958).

[2] J. C. Suddath, *Solids Deposition in the HRT*, ORNL CF-58-6-79 (June 13, 1958).

2.2.2 Equipment Performance

Equipment performance throughout the runs was very satisfactory. Since all reactor fuel samples were taken from the hydroclone overflow sampler, the hydroclone system was kept on-stream as large a fraction of the operating time as feasible. The only unscheduled down-time was a delay of 24 hr after run 16-2 for replacement of three faulty solenoid valves in refrigerant lines. Because of repeated trouble with the type of solenoid valve used, all ten were replaced, following run 16-3, with Alco solenoid valves, which have proved more reliable.

A rupture disk which relieves excessive pressure in the circulating-pump cooling-water line failed four times before it was discovered that improper installation was causing the failures. A relief valve, installed in series with the rupture disk, prevents the accidental loss of the entire cooling-water supply to the cell.

About 85% of the contents of the dissolver were accidentally transferred to the decay tanks during run CP-16-1 dissolution by sudden entrainment at the start of the second dissolution cycle. On two other occasions, during boilup of D_2O from the dissolver, sudden entrainment had been noted. Operating procedures were modified to reduce the allowable boilup rate, and have prevented further difficulties.

2.3 AUXILIARY SYSTEMS

2.3.1 Removal of Iodine

Fission-product iodine is removed from the reactor letdown stream by volatilization from the dump tanks and adsorption on a silver-coated bed of stainless steel mesh in the vapor line preceding the recombiner.

Radiochemical determinations of I^{131} and I^{133} made on fuel samples obtained from the high-pressure system during the three power runs of the reactor showed that most of the long-lived iodine isotopes were being removed from the fuel. Heat generation measurements indicated that iodine was being collected by the absorber. The absence of iodine in condensate taken from the recombiner condenser which is downstream from the absorber is taken as evidence that the silver-plated stainless steel wire is removing all the iodine which is vaporized in the dump tanks.

The ratio of I^{133} to I^{131} decreases with increasing residence time of iodine in the reactor and is used as an indication of iodine behavior. The ratio for freshly formed iodine is 21 if 30-hr Te^{131m} is in equilibrium; that in the reactor should be 19 if iodine is permanently removed at the letdown rate. Activity ratios obtained from the reactor samples decreased to about 12, indicating an average residence time of nearly one day. Results of the analyses were very erratic, and sampling or analytical difficulties may have contributed to the low ratios. Mathematical analysis suggests that only about one-fourth the iodine in the letdown stream is volatile and that the remainder is being returned to the high-pressure system.

2.3.2 Charcoal-Bed Performance

Charcoal-bed temperatures were followed closely during reactor run 16 because the oxygen injection rate was three times the original design rates. Calculations[3] had indicated that bed temperatures might exceed 100°C. Temperatures in the charcoal beds increased at reactor power levels greater than 0.5 Mw; a 10°C increase in the 6-in. sections of beds A and B at 5-Mw operation was the maximum observed. The temperature rise in the smaller diameter beds amounted to only 2–4°C, except for a ten-day period when the 1-in. section of bed A showed a 10°C increase; there was no increase in the 1-in. section of bed B. At this time heating in the 6-in. section of bed B was greater than in the corresponding section of bed A, indicating unsteady operating conditions which are not now understood. The bed temperatures reverted to their original values after this period.

Activity breakthrough occurred after 23 days of operation with a combined off-gas flow of 2.5 liters/min, through beds A and B. The activity leaving the beds was >99% Kr^{85} and a small amount of A^{41} from activation of argon impurities in oxygen. In general, the performance of the charcoal beds exceeded design expectations.

2.3.3 Waste System Revisions

Modifications to the waste system will provide for use of the existing waste evaporator for storage of the 4 *M* H_2SO_4 waste from the chemical processing plant or contaminated UO_2SO_4 solution

[3] R. E. Adams and W. E. Browning, *Estimate of the Probability and Consequences of Ignition of the HRT Charcoal Beds*, ORNL CF-58-6-6 (June 3, 1958).

from the reactor. The overflow line from the evaporator was raised to provide increased storage space, a metering tank was added to permit better control of the unloading operation, and an air purge was installed to dilute radiolytic gas. A schematic flowsheet of the piping modifications is shown in Fig. 2.1. Other modifications include additional shielding, a catch pan on the floor of the waste-evaporator cell, and a revised sampler.

The piping in the processing plant loading pit was revised so that solution can be charged to the waste evaporator from either the reactor or the processing plant decay tanks. Solution from the waste evaporator can be discharged back to the reactor, to the dump tanks, or to a carrier in the loading pit. The 3-gal metering tank installed in the discharge line from the waste evaporator will simplify control of the solution discharged.

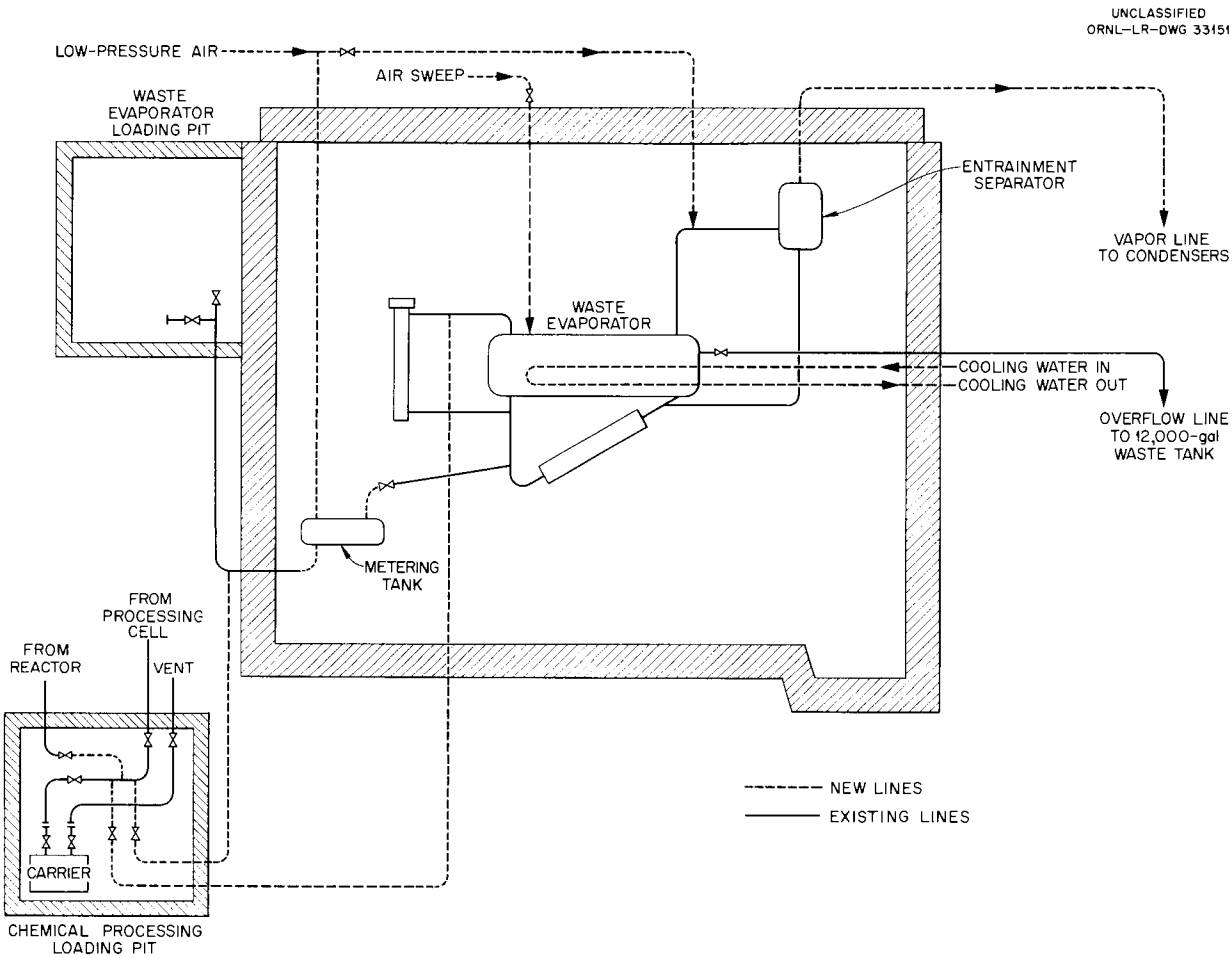

Fig. 2.1. Revisions to HRT Waste System.

3. HRT REACTOR ANALYSIS

P. R. Kasten

R. D. Cheverton
H. C. Claiborne
T. B. Fowler
S. Jaye
M. P. Lietzke
B. E. Prince
M. W. Rosenthal
M. Tobias
E. Volk

3.1 VARIATION OF THE INLET AND OUTLET TEMPERATURES IN THE TWO-REGION HRT AS A FUNCTION OF POWER

While the HRT was being operated as a two-region system, the arithmetic average of the inlet and outlet temperatures of the HRT core fluid appeared to fall with increasing power. For example, on June 19, at a power of 300 kw the inlet- and outlet-fluid temperatures were both close to 263°C. When the power was raised to 3.2 Mw, the outlet temperature rose to 265°C, while the inlet temperature fell to 254°C. This "temperature effect" is often masked or confused by accompanying changes other than simple power increase. However, the failure of the inlet and outlet temperatures to diverge equally about the zero-power critical temperature has been noted frequently enough to assure that the effect is real.

Assuming that there is no mixing in the fuel solution as it passes through the core, there will be a temperature rise from the inlet to the outlet due to heating of the solution by the energy generated. Part of the reactor core will then be below the zero-power critical temperature and the remainder will be at a higher temperature, suggesting that the arithmetic average of the inlet and outlet temperatures may not properly represent the average critical temperature. Analysis of the HRT with the two-dimensional reactor code CURE, however, indicates that the above arithmetic-average temperature does adequately represent the critical temperature for powers up to 5 Mw. For the purposes of the calculation the curved outlines of the reactor were replaced by the jagged cylindrical outline sketched in Fig. 3.1. The core-tank wall was omitted for simplicity. A two-group model was used for criticality calculations. The fuel-to-moderator ratio used corresponded to criticality at 270°C and zero power. Calculations were performed for core powers of 1, 3.5, and 5 Mw. The core was divided into eight regions, and in each one the temperature was assumed to be constant. Nuclear and physical properties were assumed to vary with temperature, and the temperature in each region was computed according to the fraction of power generated in that region. The D_2O reflector temperature was 270°C for all cases. Table 3.1 shows the results of the calculation for 3.5 Mw; the temperature and fraction of power generated in each region are given. The average critical temperature was 270°C.

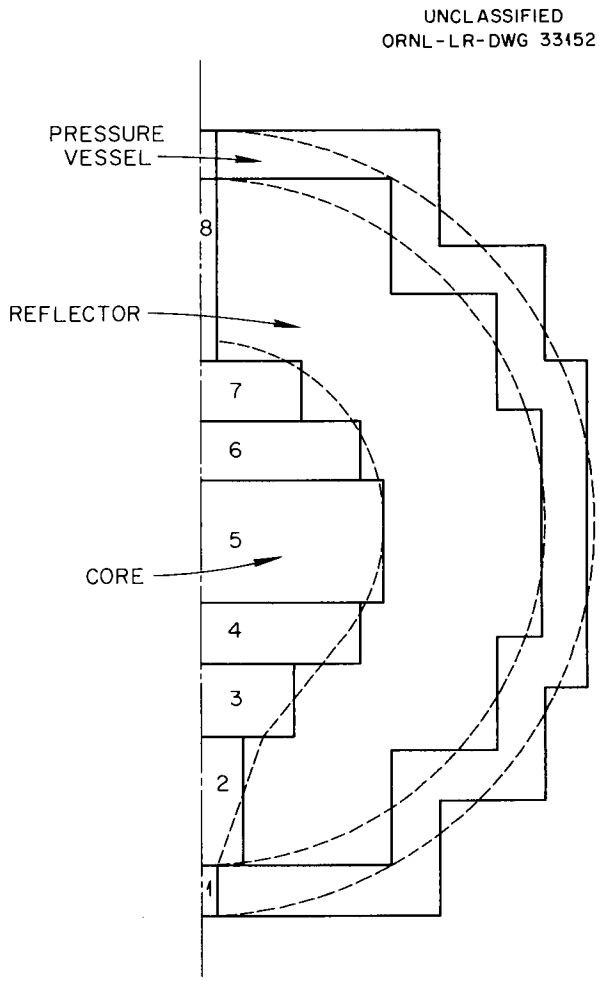

Fig. 3.1. Approximation of HRT Shape Used for CURE Code. Dashed lines represent actual outline; numbers indicate the eight regions into which core was divided.

Table 3.1. Calculated Power and Temperature Distribution in the Core of the HRT at 3.5 Mw (Region Numbers Refer to Those Given in Fig. 3.1)

Region No.	Volume (liters)	Fraction of Total Power Generated in Region	Average Temperature of Region (°C)
1	0.18	3×10^{-5}	253
2	7.06	0.011	253
3	22.4	0.069	254
4	52.0	0.186	259
5	135.2	0.497	269
6	52.0	0.174	280
7	20.8	0.062	283
8	1.38	0.002	284

Based on the results given in Table 3.1, the arithmetic average of the inlet- and outlet-fluid temperatures was 268.5°C. Since the inlet and outlet temperatures differ from 270°C with approximately equal magnitudes, the observed temperature effect cannot be ascribed to non-uniformity in core nuclear properties produced by the power distribution.

A second theory considered here is the possibility that voids produced by subcooled boiling at the core wall cause a reduction in reactivity which could lead to a compensating fall in core temperature. This situation was physically approximated by considering that the spherical core region is separated from the containing core tank by a void region; Fig. 3.2 schematically represents the model used. The core tank is reflected by D_2O contained in a steel pressure vessel. The thickness of the void space required to produce a specified uniform temperature decrease in the fuel was computed with the aid of the multiregion one-dimensional reactor code WANDA. The two-group model was again employed; with zero voids the reactor was critical at 270°C. In order to reduce the critical temperature to 265°C, the required void annulus was computed to be 0.27 cm thick; for a critical temperature of 260°C the required thickness was 0.52 cm. In both cases the fuel-to-moderator ratio was the same as that at 270°C. The required void volume (about 5.6 liters for a 0.27-cm-thick annulus) appears larger than would be associated with reasonable core-wall heat fluxes.

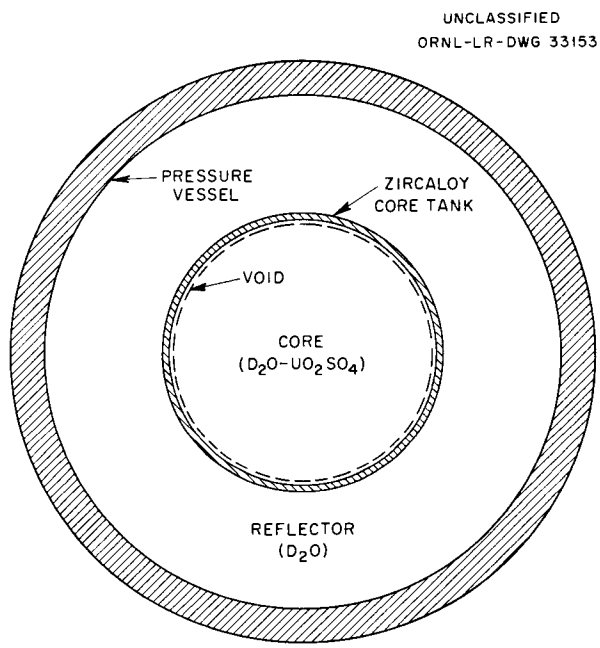

Fig. 3.2. Approximation of HRT Shape Used for Reactor Code WANDA. Used to compute reactivity effect of a spherical annular void.

3.2 HRT DOME-WALL TEMPERATURES

The maximum temperature of the stainless steel surface in the HRT core outlet dome was estimated[1] to determine whether conditions which lead to high corrosion rates might exist at that location.

[1] H. C. Claiborne, *HRT Dome Wall Temperature*, ORNL CF-58-4-53 (April 15, 1958).

Calculations were performed for core powers up to 10 Mw with the outer wall of the dome both insulated and uninsulated.

The HRT dome contains a type 347 stainless steel bellows that is part of the transition joint connecting the Zircaloy-core exit pipe with the external stainless steel piping. The annular space between the bellows and the dome wall is flushed by fuel solution from a bypass line which enters through a drilled hole in the dome flange. On the other side of the bellows, D_2O from the blanket flows through the annular space between the bellows and the core exit pipe. The temperature rise of the fuel solution and the dome-wall temperature are a function of the operating power, the neutron flux, and the flow rate. Heat generation in the dome wall is due to decay and fission gammas from fuel in the core exit pipe and in the dome, and capture gammas originating in the stainless steel. The heat input to the dome fuel solution comes primarily from decay betas, fission, and heat transfer from the dome wall.

The thermal behavior of the dome region has been examined by use of an idealized system to simplify the analysis. The idealized system is based on the following postulates, which are generally conservative in that they result in prediction of higher temperatures than would actually occur:

1. The curvature of the annular region may be neglected, since the average annular spacing is reasonably small compared with the radius.
2. The variable spacing between the bellows and the dome wall may be represented by an equivalent distance.
3. No heat is transferred through the bellows wall.
4. Uniform heat flux (q/A = constant) exists at the heat transfer surface.
5. The physical properties are not a function of temperature.
6. For the case of the uninsulated dome, the varying wall thickness may be represented by an equivalent uniform thickness.
7. Fully developed and stable laminar fluid-velocity profiles always exist.
8. The neutron flux throughout the dome is uniform.
9. Gamma energy sources may be represented by collimated plane sources.

Some pertinent results of the thermal analysis of the insulated HRT dome are shown graphically in Fig. 3.3. The results shown, although for 10 Mw, are proportional to the power and may be adjusted to other power levels. The actual flow rate is uncertain, and so flow values ranging from 45 lb/hr (which appears to be the minimum flow that might exist) to the probable maximum of 1880 lb/hr were considered. The thermal-neutron flux in the dome is difficult to estimate and the value is uncertain. However, it is believed that the flux is probably closer to 10^{10} neutrons·cm^{-2}·sec^{-1} than 10^{11}. Clearly, fluxes below 10^{10} neutrons·cm^{-2}·sec^{-1} have little effect on the maximum surface temperature.

Figure 3.3 shows that even for zero neutron flux and optimum flow rate the maximum surface temperature obtained in the analysis is over 315°C for a 260°C core inlet temperature. Because of corrosion and problems associated with phase stability, temperatures this high in HRT fuel sol· ,on should be avoided. However, these results are for 10 Mw and, in addition, are conservative as a result of the postulations of no entrance effects, stable laminar flow even at high flow rates, complete absorption of gamma energy in the dome wall, and collimated plane source of gamma rays. Hence it is probable that the dome-wall temperature would not exceed 315°C when operating at 5 Mw even with the dome insulated.

During HRT run 13, before the dome insulation was removed, the maximum continuous power was about 1.5 Mw. Even at the minimum estimate of flow rate, the maximum temperature above the core inlet is only 18°C. In view of the conservatism of the analysis, it appears that damagingly high temperatures could not have existed in

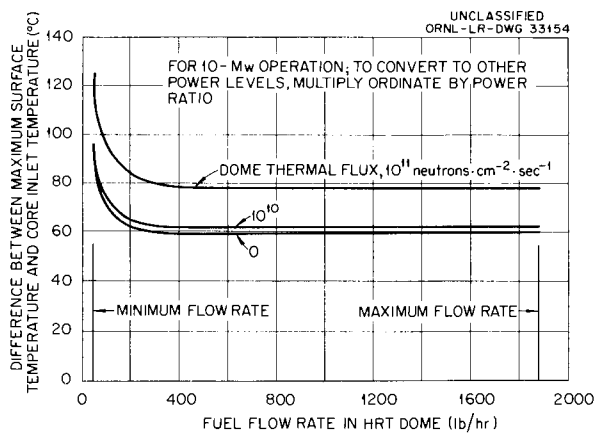

Fig. 3.3. Maximum HRT Dome-Wall Temperature for Insulated Dome.

the dome at this power, provided that there was no extreme condition of channeling of the flow due to poor flow distribution and/or accumulation of uranium-containing solids.

The results of the analysis of the uninsulated HRT dome for a flux of 10^{11} neutrons $cm^{-2} \cdot sec^{-1}$ and a 260°C core inlet temperature are shown in Fig. 3.4. These results are not proportional to power and are not independent of the core inlet temperature as in the insulated case. For relatively small deviations from a 260°C core inlet temperature, the results are still applicable without significant error.

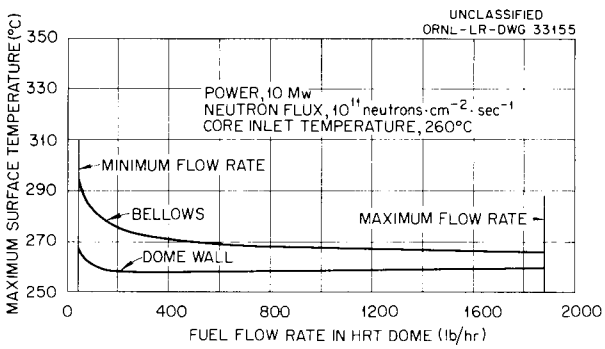

Fig. 3.4. Maximum HRT Dome-Wall Temperature with Insulation Removed.

It is evident from Fig. 3.4 that removal of the insulation will keep the maximum surface temperature of the inner dome wall near the core inlet temperature (slightly above at the low flow rates and slightly below at the higher flow rates). In this case the fuel solution is cooled by heat transfer through the dome wall, and the maximum surface temperature occurs on the bellows surface. Less confidence can be placed on the accuracy of the calculated bellows surface temperature than on the temperature of the dome wall, since a large deviation between the idealized system and the actual system exists at this point. However, in view of the general conservatism of the analysis, the bellows temperatures shown in Fig. 3.4 are a probable upper limit.

3.3 STRESSES IN HRT CORE VESSEL

A detailed investigation of the stresses in the vicinity of the junction between the 90- and 30-deg cones in the HRT core vessel was made to determine whether stresses could be high enough to cause vessel failure.

Experimental data obtained in previous tests were used in the calculations; a brief history of these tests follows. Before the final design and fabrication of the HRT core vessel, an experimental stress analysis was conducted on a full-scale aluminum vessel having a 90-deg cone between the sphere and the inlet cylinder. A final test vessel similar to the present core design, except that screens were used in place of the perforated plates, was used for internal-flow tests to investigate the vibratory characteristics of the entire vessel. During the flow tests no significant vibrations were detected by measurement of vessel deflections or by strain measurements in the wall.

Based on conservative stress-concentration factors taken from the experimental stress analysis and appropriate theoretical considerations, some of the stresses which possibly exist in the region of the transition between the two cones were estimated.[2,3] The particular loading conditions considered the following: pressure, axial loads, temperature difference between the perforated plates and the wall, temperature gradients across and along the wall, pressure differentials across the perforated plates, and wall-temperature distributions unsymmetrical about the core axis. Based on assumptions regarding temperatures and pressures that are believed to be conservative (in that they lead to higher stresses than should actually exist), maximum total stresses of approximately 2000 psi in the wall were calculated. The minimum yield strength for the core-vessel material at 600°F is about 13,500 psi. Therefore, in the absence of some type of defect that would cause a serious concentration of stresses, it is believed that the above stresses could not result in vessel failure.

3.4 STRESSES IN HRT PRESSURE VESSEL FOR ONE- AND TWO-REGION OPERATION

Satisfactory operation of the HRT as a one-region reactor depends to some extent upon the absence of severe stresses in the pressure vessel. Analyses[4] of the steady-state pressure and thermal

[2] R. D. Cheverton, *HRT Core Vessel Stresses at Intersection of 90- and 30-deg Cones*, Intra-Laboratory correspondence to R. B. Briggs, April 10, 1958.

[3] R. D. Cheverton, *HRT Core Vessel Stresses Caused by Transverse Temperature Gradient*, Intra-Laboratory correspondence to P. R. Kasten, April 30, 1958.

[4] R. D. Cheverton and E. R. Volk, *Steady-State Pressure and Thermal Stresses in the HRT Pressure Vessel*, ORNL CF-58-7-43 (July 15, 1958).

stresses in the spherical portion of the vessel show that the stresses for one-region operation are only slightly greater than for two-region operation.

The stresses calculated for the two-region HRT were significantly greater than those originally calculated, owing to a more detailed treatment of the energy generation and deposition. However, based on a special ruling[5] by the ASME Boiler Code's Special Committee on Nuclear Power, the permissible stress is one and one-half times greater than that originally specified. These conditions permit operation of the HRT (either as a single- or two-region reactor) at power levels up to 10 Mw, provided that the outside surface temperature of the pressure-vessel wall is no more than 50°F higher than the inside surface temperature. At 5 Mw the maximum permissible temperature difference is about 90°F. Experimental data from the HRT indicate that the cooling capacity of the blast shield is sufficient to maintain the temperature differences at values below the indicated maximum permissible values.

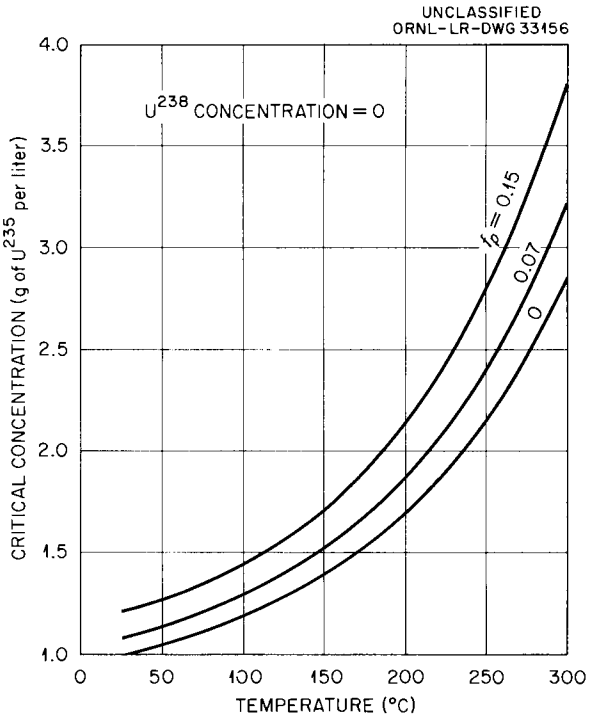

Fig. 3.5. Critical Concentration of One-Region HRT vs Mean Temperature for Various Poison Fractions.

3.5 NUCLEAR CHARACTERISTICS OF THE HRT WITH VARIOUS FUEL CONCENTRATIONS IN THE BLANKET

3.5.1 One-Region Operation

The nuclear characteristics of the HRT have been estimated for operation with the same fuel concentration in the blanket as in the core. A two-group model was used for calculating critical concentrations, but the results were in reasonable agreement with several values computed with the use of a multigroup, multiregion Oracle routine (Corn Pone). Fluxes were obtained from the multigroup results. In all cases concentrations and temperatures were considered to be uniform throughout the reactor.

Critical concentrations are plotted in Figs. 3.5 and 3.6 for various temperatures, poison fractions, and U^{238} concentrations. These results are summarized in Table 3.2*a*, along with the corresponding inventories of the high-pressure system.

Various power densities, fluxes, and related values are given in Table 3.2*b*. The heat release in the blanket is 70% of the total. The fluxes in the pressure vessel given in Table 3.2*b* are space-mean values obtained from the multigroup computations and are broken down by energy levels for use in evaluation of possible radiation damage. For these values, after one year of operation at 10 Mw, the flux time for neutron energies above 0.1 Mev would be 8.2×10^{19} *nvt* and 2.3×10^{19} *nvt* for energies above 1.0 Mev. However, the estimates of the high-energy flux based on multigroup calculations are questionable, and other techniques are being applied to check these results.

The thermal flux in the reactor could be reduced by loading the fuel solution with U^{238}, H_2O, or any other material which would act as a poison and increase the critical concentration. Adding 40 g of U^{238} per liter would lower the thermal flux by about one-third; using H_2O as the moderator would lower it fourfold. The addition of materials which absorb thermal neutrons would cause little change in the flux above 1.0 Mev, although the use of H_2O would reduce it in the range between 0.1 and 1.0 Mev. To appreciably reduce the high-energy flux at the wall, the power distribution in the reactor would have to be shifted so as to reduce the power in the blanket. One way of doing

[5] ASME Pressure Vessel Committee on Nuclear Power, Code Interpretation, Case 1234 (special ruling).

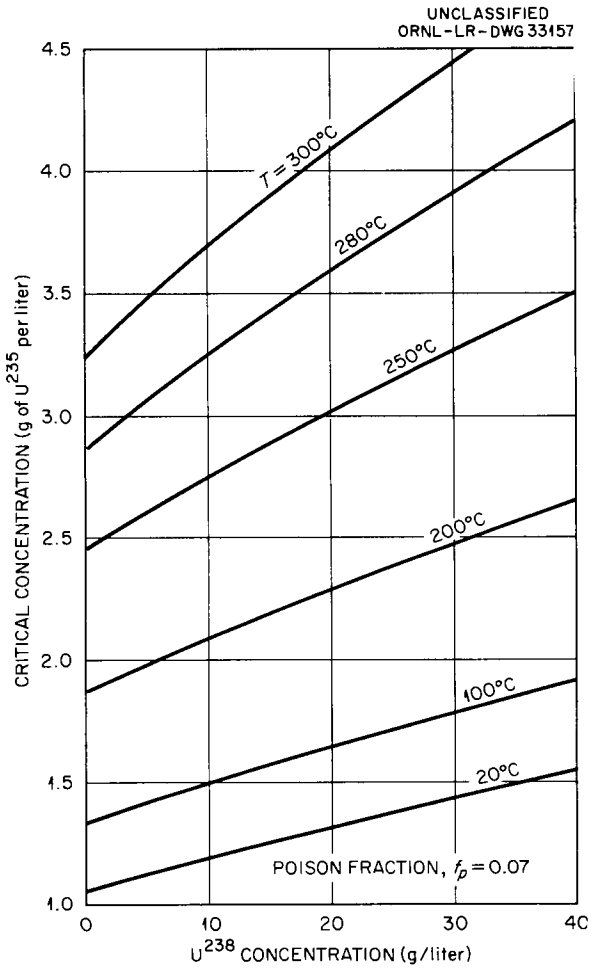

Fig. 3.6. Critical Concentration of One-Region HRT vs U^{238} Concentration for Various Mean Temperatures.

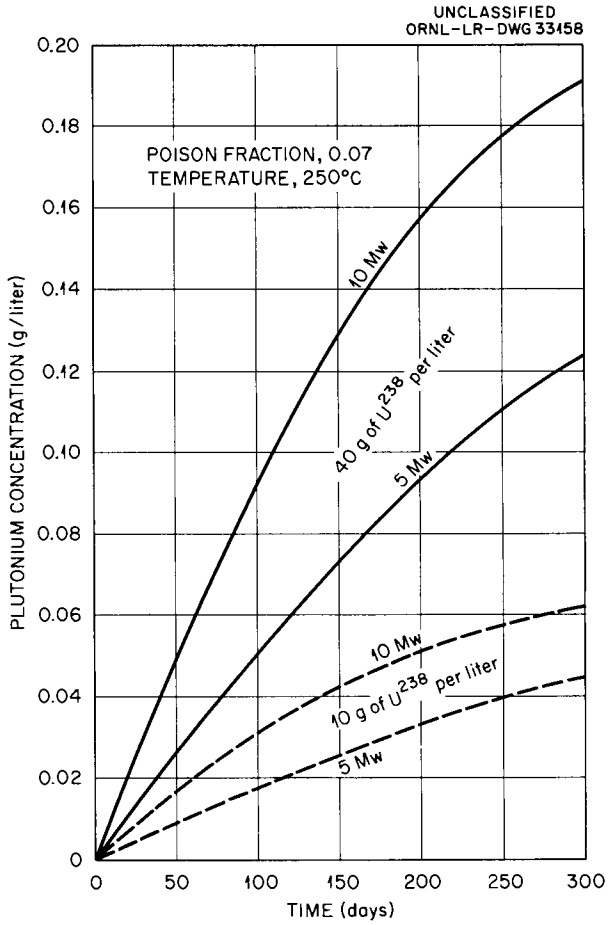

Fig. 3.7. Plutonium Concentration vs Time in One-Region HRT.

this would be to operate in such a manner that the fuel concentration in the blanket remained lower than that in the core.

The daily plutonium production rates for 10 and 40 g of U^{238} per liter are given in Table 3.2*c*, along with the initial conversion ratios. The rate at which the plutonium concentration would build up in the reactor is shown in Fig. 3.7 for different power levels and U^{238} concentrations. The concentrations given are those which would be attained if all the plutonium produced remained in solution.

3.5.2 Effect of HRT Blanket-Fuel Concentration on the Core Critical Concentration

The core U^{235} concentration required for criticality has been calculated for various blanket fuel concentrations and for various reactor temperatures. The results, given in Figs. 3.8 and 3.9, were obtained by using a two-group, four-region, one-dimensional diffusion code (WANDA).

Figure 3.8 gives the ratio of the critical core concentrations obtained with and without fuel in the blanket region as a function of the ratio of fuel concentration in the blanket to that in the core. Figure 3.9 gives the per cent of total reactor power produced in the core as a function of the ratio of fuel concentration in the blanket to that in the core. Since the power distribution is relatively independent of temperature, the results in Fig. 3.9 consider only the limiting temperatures of 20 and 280°C.

Table 3.2. Some Characteristics of the HRT as a One-Region Reactor

a. *Critical Concentrations and U^{235} Inventories at Various Conditions*

	Critical Concentration (g of U^{235} per liter)		Inventory (kg of U^{235})	
	250°C	280°C	250°C	280°C
No U^{238}, $f_p = 0$	2.2	2.5	4.8	5.6
No U^{238}, $f_p = 0.07$	2.5	2.9	5.4	6.3
10 g of U^{238} per liter, $f_p = 0.07$	2.7	3.2	5.9	7.0
40 g of U^{238} per liter, $f_p = 0.07$	3.5	4.2	7.7	9.3

b. *Power Distribution and Flux*

	5 Mw	10 Mw
Core power, kw	1500	3000
Blanket power, kw	3500	7000
Mean power density in reactor, kw/liter	2.7	5.4
Mean power density in core, kw/liter	5.1	10.2
Meon power density in blanket, kw/liter	2.2	4.5
Power density at core-tank wall, kw/liter	4.5	9.0
Power density at inner surface of pressure vessel, kw/liter	0.6	1.2
Temperature rise across core, 400 gpm, °C	13	26
Temperature rise across blanket, 230 gpm, °C	54	108
Fluxes at 280°C, no U^{238}, $f_p = 0$, neutrons·cm^{-2}·sec^{-1}		
Mean thermal flux in reactor	3.6×10^{13}	7.2×10^{13}
Mean fast flux in reactor	2.4×10^{13}	4.7×10^{13}
Mean thermal in pressure vessel	1.3×10^{12}	2.5×10^{12}
Mean fast in pressure vessel (total)	3.6×10^{12}	7.1×10^{12}
Mean fast in pressure vessel (above 0.1 Mev)	1.3×10^{12}	2.6×10^{12}
Mean fast in pressure vessel (above 1.0 Mev)	3.6×10^{11}	7.2×10^{11}

c. *Plutonium Production and Conversion Ratio*

	Initial Conversion Ratio	Plutonium Generation Rate (g/day)	
		5 Mw	10 Mw
10 g of U^{238} per liter, 250°C	0.066	0.44	0.88
40 g of U^{238} per liter, 250°C	0.182	1.22	2.44

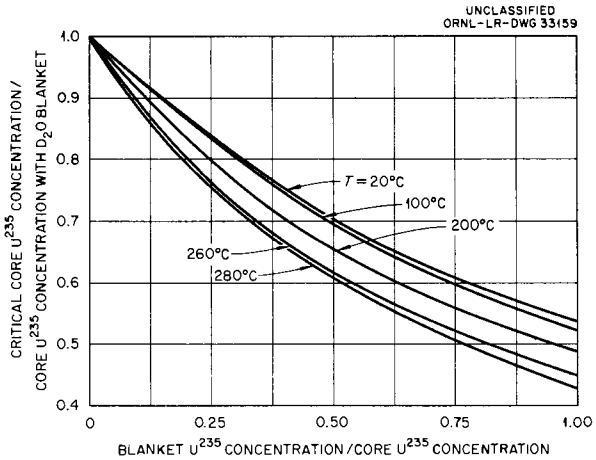

Fig. 3.8. Relative Critical Concentration in HRT Core vs Blanket-to-Core Fuel Concentration Ratio.

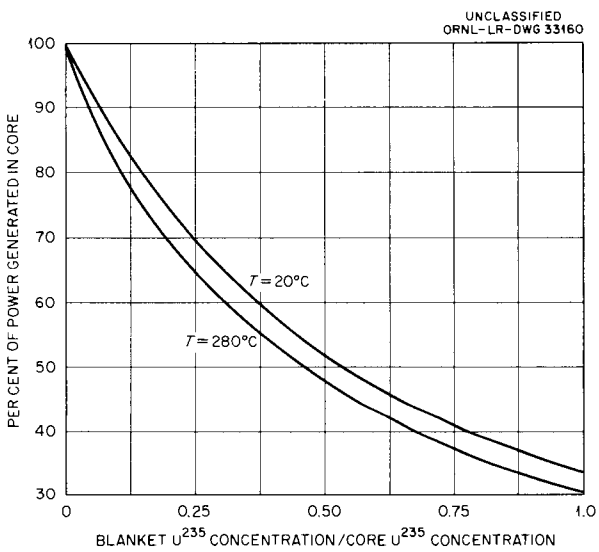

Fig. 3.9. Per Cent of Total Power Generated in HRT Core vs Ratio of Fuel Concentration in Blanket to That in Core.

3.5.3 Flux Distributions in HRT

The flux distributions in the single-region HRT have been calculated for various ratios of blanket-to-core fuel concentrations at a reactor temperature of 280°C. These flux distributions are presented in Fig. 3.10; some pertinent data are given in Table 3.3.

The power densities given in Table 3.3 are those in the fuel solution at the inner surface of the core vessel and are based on a total reactor power of 5 Mw. The flux distributions shown in Fig. 3.10 were calculated by using a two-group, two-region Oracle code.[6]

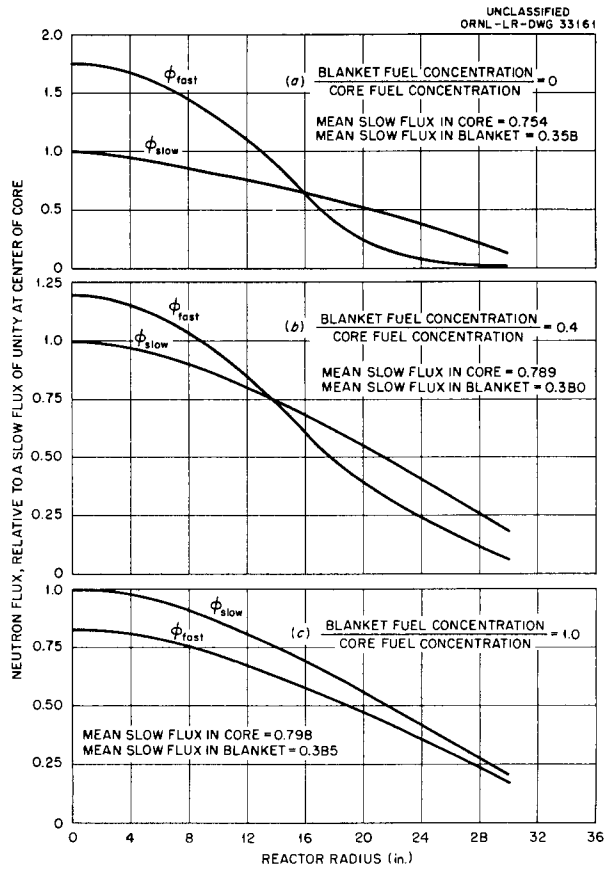

Fig. 3.10. Fast- and Slow-Flux Distributions in HRT.

3.5.4 Effect of Corrosion Samples and Sample Holders on HRT Core Critical Concentration

Estimates have been made of the increase in the core fuel concentration required by the insertion of the corrosion samples and sample holders. The results are given in Table 3.4 in terms of the ratio of the fuel concentrations required with and without these poisons present. Various ratios of fuel concentration in the blanket to that in the core were considered; the reactor temperature was 280°C.

---

[6] T. B. Fowler, *Oracle Code for a General Two-Region, Two-Group Spherical Homogeneous Reactor Calculation*, ORNL CF-55-9-133 (Sept. 22, 1955).

Table 3.3. Average Fluxes and Core-Wall Power Densities in HRT for Various Blanket Fuel Concentrations (Based on 5 Mw Total Power)

Blanket Fuel Concentration / Core Fuel Concentration	Power Density at Core-Tank Wall (kw/liter)	Average Slow Flux	
		In Core*	In Blanket*
0	15	0.754	0.368
0.2	11	0.773	0.368
0.4	8	0.789	0.380
0.7	6	0.796	0.382
1.0	5	0.798	0.385

*Normalized to a slow flux of unity at center of the core.

Table 3.4. Effect of Corrosion Samples on Core Fuel Concentration

Blanket Fuel Concentration / Core Fuel Concentration	U^{235}_{core} (core and blanket samples) / U^{235}_{core} (clean)	U^{235}_{core} (core samples) / U^{235}_{core} (clean)
0	1.097	1.083
0.2	1.090	1.074
0.4	1.085	1.068
0.7	1.082	1.063
1.0	1.079	1.060

The samples and their holders were treated as neutron poisons. The effects were estimated by using a two-group, two-region perturbation calculation in which the fluxes, adjoint fluxes, and critical concentration of the "clean" reactor were obtained from a two-group, two-region Oracle code.[6] To provide a check on the perturbation method, the case with no fuel in the blanket was examined by using the two-group CURE program (for the IBM 704 computer) which treats two space variables. The perturbation calculation resulted in an 8.9% increase in core fuel concentration, while the CURE calculation resulted in an 8.0% increase, based on a reactor temperature of 270°C.

3.6 SAFETY OF THE HRT WITH THE BLANKET PRESSURIZER COMPLETELY FILLED

The HRT presently operates with some fluid transfer between the core and blanket regions, resulting in the presence of fuel in the blanket region. In order to obtain smooth reactor operation and a minimum of fuel transfer into the blanket region, the blanket pressurizer was effectively eliminated as a pressurizer and surge volume by operating it completely filled with liquid. This type of operation is permissible as long as the safety of the reactor is not endangered.

The important quantities influencing reactor safety under these circumstances are the fraction of power generated in the blanket, the possible rates of reactivity addition, and the temperature coefficients of reactivity. Figure 3.11 gives the core and blanket temperature coefficients and also the mean lifetime of prompt neutrons as a function of the blanket fuel concentration; the fraction of power generated in the blanket as a function of blanket fuel concentration is shown in Fig. 3.9. The neutron lifetimes and temperature coefficients are based on a two-group, two-region type of calculation.[6]

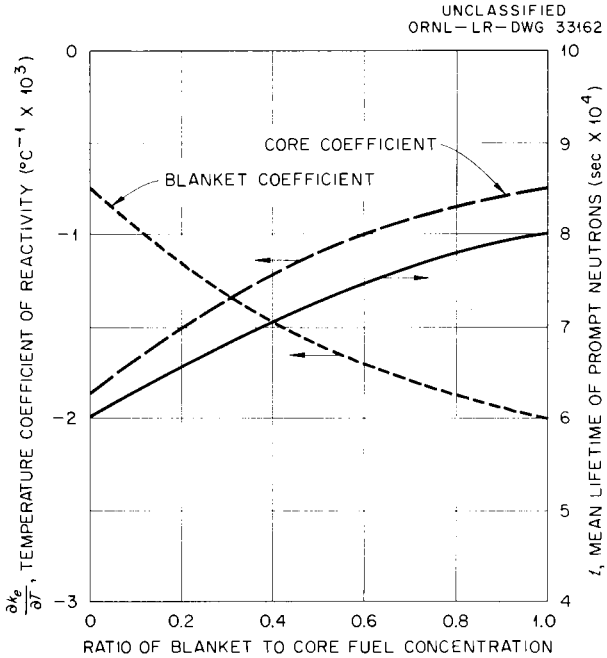

Fig. 3.11. Neutron Lifetime and Temperature Coefficients in HRT as a Function of Blanket Fuel Concentration (260° C).

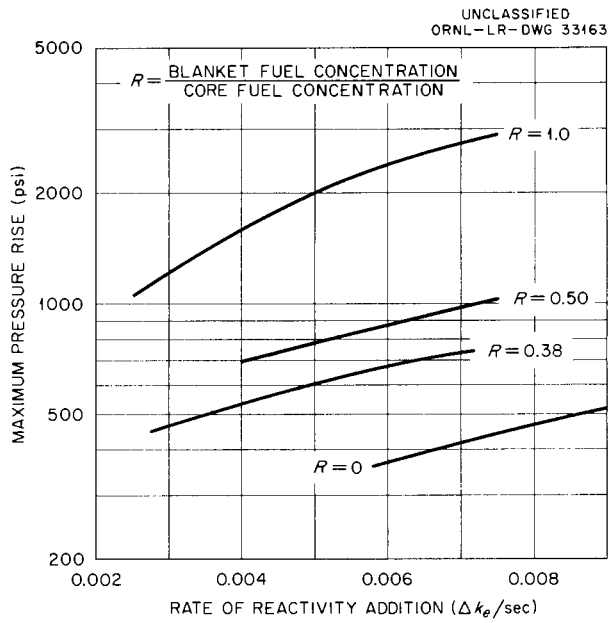

Fig. 3.12. Maximum Reactor Pressure Rise as a Function of Rate of Reactivity Addition and Blanket Fuel Concentration (Initial Reactor Power = 0.04 w).

The pressure rise associated with a specified rate of reactivity addition is given in Fig. 3.12 as a function of fuel concentration in the blanket. In obtaining these results, it was assumed that the core and blanket regions were connected by an opening 1.5 in.^{2} in cross-sectional area. For a given rate of reactivity addition the maximum pressure rise increases with the fraction of power generated in the blanket; however, the possible rate of reactivity addition decreases with increasing blanket power.

It appears that the greatest rate of reactivity addition is associated with the temperature coefficient of reactivity. Under these circumstances the rate of reactivity addition will be determined by the temperature coefficient of reactivity and the rate of temperature fall. For the two-region HRT, the permissible rate of decrease in the effective core temperature was 4.3°C/sec (the reactor design limited the possible rate to values less than 4.3°C/sec). This rate is a function of the fluid flow rate and of the rate of pressure decrease on the steam-generating side of the heat exchangers. The associated fuel temperature decrease is determined by the volume heat capacity of the fluid. In the present HRT, energy removal from the heat exchangers can cause cooling of both the core and the blanket regions. Assuming a rate of pressure decrease in the heat exchangers such that the effective decrease in core temperature is 4.3°C/sec, the associated blanket temperature decrease was calculated. Table 3.5 lists the rate of reactivity addition and maximum pressure rise which would accompany the fall in temperature, as a function of blanket fuel concentration.

Since the permissible reactor pressure is limited by the strength of the pressure vessel, a rise of 1000 psi was assumed as an acceptable maximum. An addition rate of $0.0024\Delta k_e$/sec is sufficient to cause a pressure rise of 1000 psi if there are equal concentrations of fuel in the core and blanket regions. The permissible addition rate is in excess of $0.01\Delta k_e$/sec if the ratio of blanket-to-core fuel concentration is less than 0.38 as it is in the present operation of the HRT.

Table 3.5. Rate of Reactivity Addition and Maximum Pressure Rise Associated with Cooling of Reactor Fluid

Ratio of blanket-to-core fuel concentrations	0.38	0.50	1.0
Cooling of core alone (fluid flow rate = 150 gpm)			
Rate of fluid cooling, °C/sec	4.3	4.3	4.3
Rate of reactivity addition, Δk_e/sec	0.0054	0.0047	0.0032
Maximum pressure rise, psi	630	750	1300
Cooling of blanket alone (fluid flow rate = 230 gpm)			
Rate of fluid cooling, °C/sec	1.2	1.2	1.2
Rate of reactivity addition, Δk_e/sec	0.0017	0.0019	0.0024
Maximum pressure rise, psi	350	420	1000
Cooling of core and blanket			
Rate of reactivity addition, Δk_e/sec	0.0071	0.0066	0.0056
Maximum pressure rise, psi	740	930	2200

4. HRT COMPONENT DEVELOPMENT

I. Spiewak

J. M. Baker
R. Blumberg
J. S. Culver
B. D. Draper
C. H. Gabbard
E. C. Hise
P. P. Holz
C. G. Lawson
J. E. Mott
J. C. Moyers
H. R. Payne
H. C. Roller

4.1 FUEL CIRCULATING EQUIPMENT

4.1.1 400A-1 Pump

The 400A-1 development pump was installed in the HRT mockup and has circulated 0.04 *m* uranyl sulfate solution for 2623 hr without difficulty. The pump contains a special purging circuit (Fig. 4.1) near the root of the thermal-barrier seal weld. It is expected that purge flow in this area will reduce the tendency of the seal weld to crack as a result of corrosion.

4.1.2 400A-2 Pump

An 1100-hr run during which the 400A-2 pump circulated 0.04 *m* uranyl sulfate solution at 250°C was completed. The purpose of the run was to evaluate the cooling-water configuration used on current Westinghouse production pumps.

UNCLASSIFIED
ORNL-LR-DWG 33164

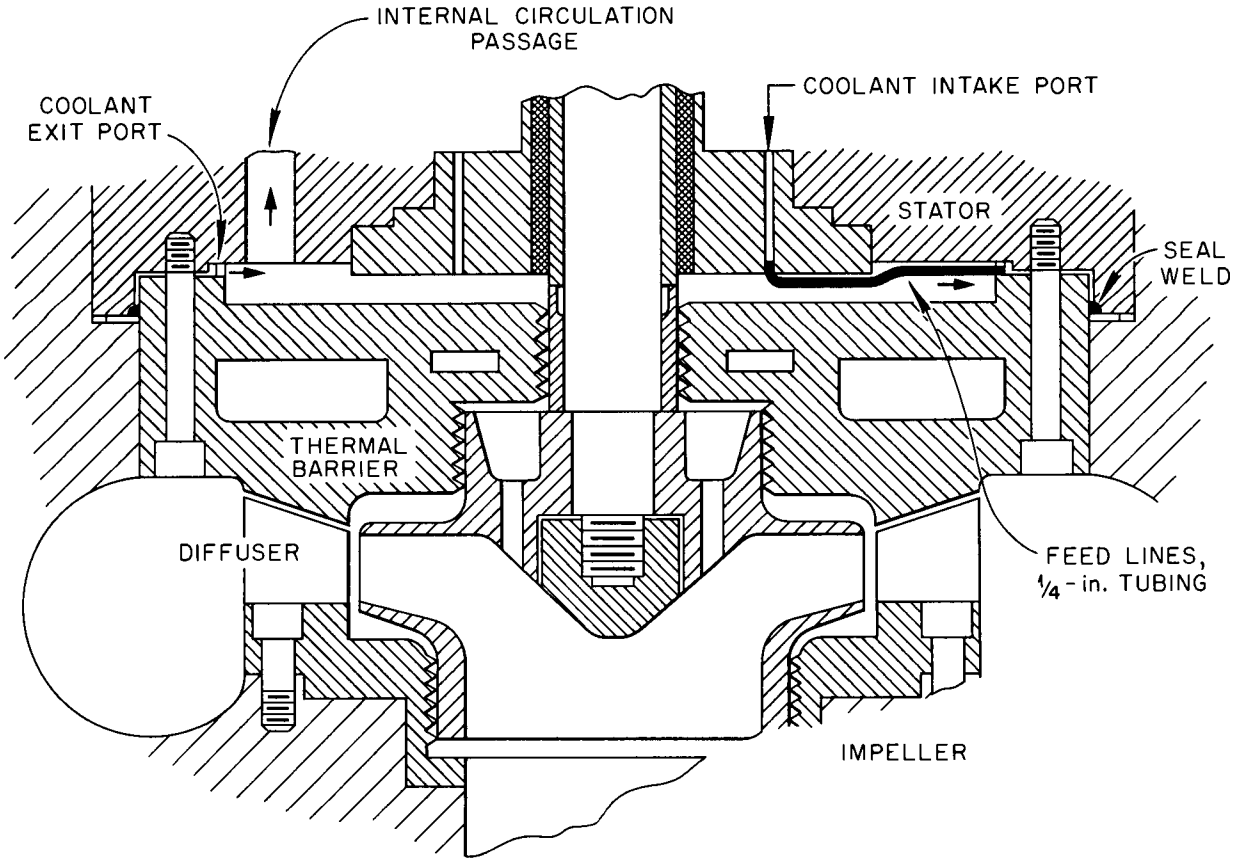

Fig. 4.1. Feed Line To Induce Circulation in Area Behind Thermal-Barrier Seal Weld of 400A-1 Pump.

The configuration, identical to that of the HRT pumps except for omission of the shaft cooling passage, permits the lower bearing to run at a higher temperature. No lower-bearing damage was found at the conclusion of the run, indicating that the revised cooling system is acceptable.

This pump is being converted to a developmental 200-gpm slurry pump and will be designated as the 200Z pump. The pump will incorporate a modified 200A impeller with top and bottom radial shroud vanes, a vaned diffuser, cast Zircaloy hydraulic parts, and aluminum oxide bearings. A test loop for the pump has been designed and is under construction; it is scheduled to be ready for operation in October 1958.

4.2 FEED PUMPS

4.2.1 Feed-Pump Endurance Testing

No failures of feed-pump components occurred in the past six months. Two heads identical to those in the HRT have been operated in fuel solution for 10,500 hr, or more than 14 months. Other test heads have operated for 10,072, 4664, and 2200 hr. Several check valves have operated in excess of 12,000 hr.

4.2.2 Purge Pumps

The HRT mockup purge pump has operated satisfactorily for 5573 hr, and two heads in an accelerated test have operated the equivalent of 11,000 hr each. However, on one of the latter heads the weld between the head and the discharge-check-valve nipple cracked through at 10,500 hr and was repaired. This type of failure is not anticipated in the HRT purge-pump heads, since they contain heavier nipples in this location.

4.3 HRT MAINTENANCE DEVELOPMENT

Existence of the leak in the HRT core vessel created a desire to observe the leak site, and is possible, remove a sample of the Zircaloy. Work on both phases of the problem has been carried out in cooperation with the Operations, Design, and Instrumentation Sections. A full-scale mockup of the reactor core, pressure vessel, and access ports was constructed.

4.3.1 Core Viewing Development

The improvised periscope and movable-mirror equipment used for viewing the outside of the HRT core tank following run 14 was tested and there was a blind spot at the back of the core representing about 20% of the circumference. However, it was demonstrated that holes or cracks would be discernible in the field of vision. An improved version of the viewing device was designed, and two models were built for use in the reactor (Fig. 4.2). The periscopes were enclosed in aluminum boxes in an attempt to reduce spread of contamination. The viewing in the HRT with these devices after run 16 was much poorer than in the mockup because of the dull dark surface of the reactor core tank. Mechanical and lighting failures contributed to the early abandonment of the viewing equipment. Further

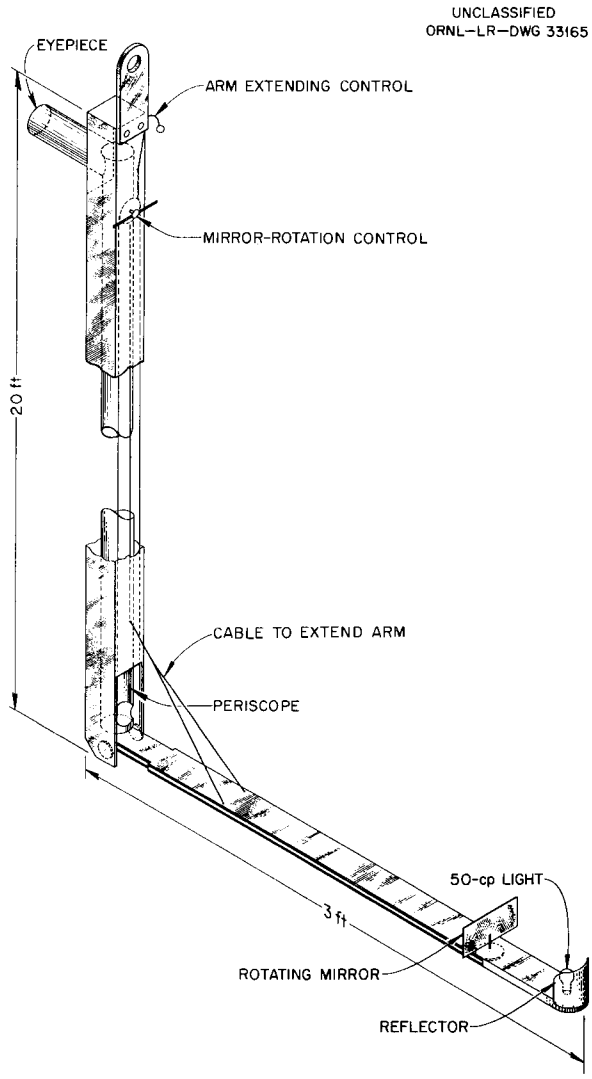

Fig. 4.2. Periscope and Mirror Equipment.

development is under way to increase illumination and mechanical reliability.

A 2-in.-dia television camera was purchased, and a manipulator, for positioning the camera anywhere in the HRT blanket, was designed and fabricated (Fig. 4.3). Hydraulic cylinders position three articulated links, and slide-wire position indicators give continuous indication of the angle of each joint. The mechanical components were tested in the mockup and operated satisfactorily. Present effort is directed toward streamlining the apparatus to facilitate insertion and to permit decontamination after use. (See also Secs 5.8 and 6.1.2.)

4.3.2 Sample Cutter

Preliminary testing demonstrated the feasibility of cutting Zircaloy under water with a commercial hole saw. A device was designed and constructed to cut 1-in.-dia samples from the top diffuser plate near the core wall by this method. Test Zircaloy specimens will be cut in the mockup under simulated reactor conditions.

4.4 HRT SPARE HEAT EXCHANGER

The HRT spare heat exchanger was received from Babcock & Wilcox Company and passed the required thermal-cycle and leak tests. Twenty-five consecutive 2-hr cycles were conducted with the tube temperature varied from 380 to 580°F while 200-psi steam pressure was maintained in the shell. After the thermal cycles, zero leakage was indicated during hydrostatic tests of 4000 and 2500 psi of tubes and shell, respectively, and by a helium leak test.

4.5 HRT CORE STUDIES

4.5.1 Behavior of Solids in Reactor Core

The observation of solids accumulated in the HRT core suggested that flow tests be conducted to study the behavior of sand in a full-scale flow model. Visible particles were retained quantitatively in the model. A thin deposit of sand was observed on top of each perforated plate of the inlet diffuser. Heavier deposits formed near the outer edges of the plates and on the diffuser cone. Where large flakes of rust had separated from the cone, deposits $\frac{1}{8}$ to $\frac{1}{4}$ in. deep accumulated in the stagnant area. It was concluded from these tests that local overheating of the conical diffuser as a result of solids formed in HRT run 13 was possible.

4.5.2 HRT Replacement Core

Experience with the present HRT core vessel indicates that purging of suspended solids and good tank-wall cooling should be requirements in the replacement unit.

Tests were conducted in a 32-in. vessel with a north polar inlet and concentric annular outlet. Gravel in the size range 40μ to $\frac{1}{4}$ in. was injected into the sphere with a water throughput of 300 gpm. It was found that 99% of this material was removed in the outlet in 7 min. The rate of solids removal was doubled by draining a 10% side-stream through a small outlet at the bottom. It was noted that at flows above 150 gpm there was no tendency for particles to settle on any surface. Measurements of the fluid-film heat transfer coefficients at the tank wall are in progress. Earlier investigations of a similar model[1] indicated that its mixing was quite rapid and that no stagnant regions existed.

A 13-in.-dia glass model of a core with annular inlet and polar outlet was constructed and tested at the phosphorescent-particle test facility.[2] A definite tendency for the inlet flow to cling to the wall was observed. However, it was found that the flow symmetry was quite sensitive to inlet concentricity. Further work on this configuration is planned.

4.6 HRT MOCKUP

R. B. Korsmeyer
P. H. Harley D. E. Willis

4.6.1 Operation

The HRT mockup, containing a titanium letdown heat exchanger, operated for 2623 hr during the past six months. Operation was at 1400 psi and 280°C on 0.042 *m* UO_2SO_4 solution containing 0.021 *m* H_2SO_4 and 0.005 *m* $CuSO_4$ for the first 1100 hr. For the last 1523 hr the acid and copper were increased to 0.025 *m* and 0.035 *m*, respectively, to duplicate the HRT fuel concentrations.

During the present run the generalized corrosion rate, based on the increase of nickel in solution, has been 0.80 mpy, compared with 1.5 mpy for

---

[1] I. Spiewak *et al.*, *HRP Quar. Prog. Rep. July 31, 1954*, ORNL-1772, p 34.

[2] F. E. Lynch, L. D. Palmer, and G. M. Winn, *Instantaneous Velocity Profile Measurement by Photography*, ORNL-2257 (in preparation).

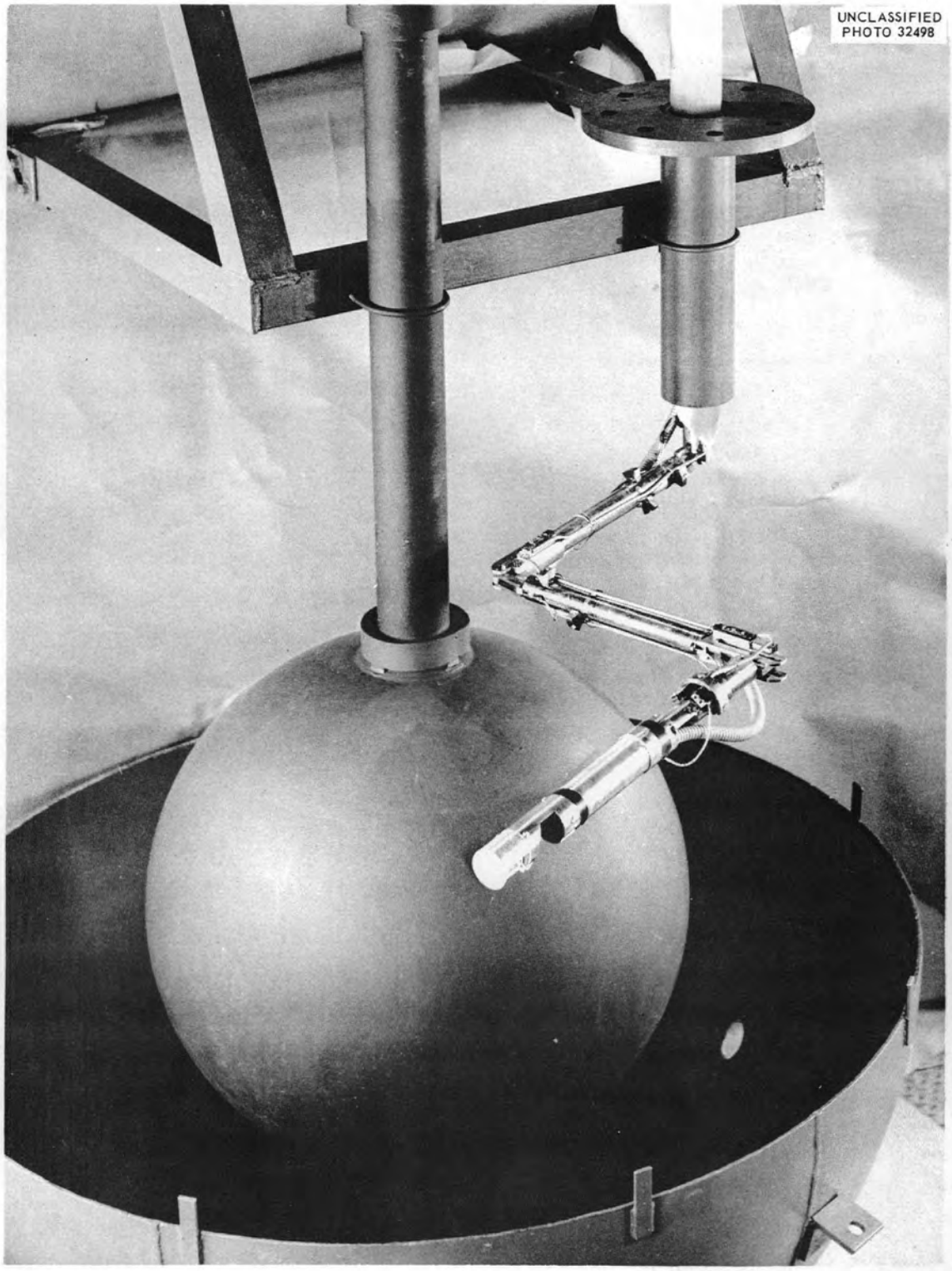

Fig. 4.3. Television Camera and Manipulator.

a similar test with a stainless steel heat exchanger.[3] This indicates that the stainless steel letdown heat exchanger had a generalized corrosion rate of 2.8 mpy.

The only equipment failures involved the compressor which furnishes oxygen for injection into the high-pressure loop. Failures of the packing gland between the drive unit and the water intermediate system occurred; this gland is a leather V-type and has a life of about three weeks. Also, the neoprene O-ring in the water-system suction check valve failed on two occasions. The failures did not interrupt the loop operation.

4.6.2 Inventory Determination

Statistical analysis of the determinations of the uranium inventory from sample analyses, previously determined volumes, and weight measurements indicated a precision of about ±3% at the 95% confidence level.[4] The system was divided into seven sections, as shown in Fig. 4.4, which were determined by the uranium concentration and solution temperature.

The typical variances in the total uranium for the seven sections in one inventory were the following:

Section	σ^2
1	0.54
2	180.41
3	0.001
4	0.0003
5	0.014
6	0.050
7	0.26

From these variances, the standard deviation for the system was 13.42, which resulted in a deviation of ±35 g in an inventory of 1550 g of uranium. However, this inventory had a +10% bias over the actual uranium known to be in the system. Since the variance in the dump-tank liquid volume was 180 times as large as any other variance, a more accurate measurement of the amount of solution in the dump tank will be needed before further experiments are undertaken. A weighing system has been designed which should lower this variance by a factor of at least 100.

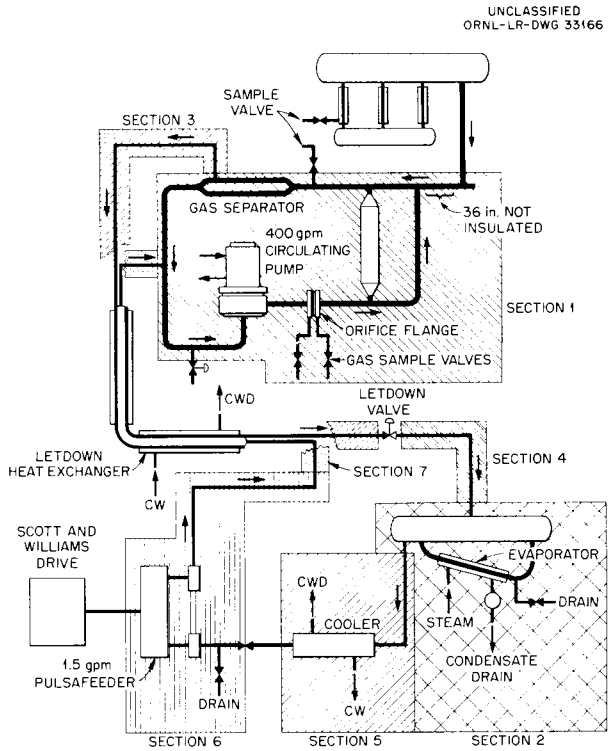

Fig. 4.4. HRT Mockup Fuel-Inventory Sections.

4.6.3 Fuel-Solution Stability

In the last report[5] it was stated that a fuel solution containing sodium and potassium sulfate with low excess acid precipitated uranium between the main loop and the pressurizer with 13 gph of purge flow to the pressurizer. Tests during this period showed that uranium precipitated from 0.042 *m* UO_2SO_4, 0.021 to 0.025 *m* H_2SO_4, and 0.005 to 0.0035 *m* copper solution when the purge rate to the pressurizer was 5 gph or higher. At a 10-gph purge rate, from 15 to 30 g of uranium was precipitated per day over a seven-day test. At a 2-gph purge rate this uranium was completely redissolved in 40 hr or less. A 3-gph purge rate redissolved uranium when the excess acid was

[3] C. B. Graham *et al.*, *HRP Quar. Prog. Rep. July 31, 1956*, ORNL-2148, p 17.

[4] P. H. Harley, *Core Solution System, Run 22*, ORNL CF-58-7-61 (July 21, 1958).

[5] R. B. Korsmeyer *et al.*, *HRP Quar. Prog. Rep. Jan. 31, 1958*, ORNL-2493, p 17.

above 60% and precipitated uranium when the acid was below 60%. A 4-gph purge precipitated uranium when the excess acid was below 72%. These results are shown graphically in Fig. 4.5.

4.6.4 System Modifications

Since the completion of the above tests the system has been down for the modification of several components. These modifications are about 95% complete. The major change was the installation of a titanium pressurizer system. This system consists of a 30-ft jacketed-pipe heat exchanger in which the fuel solution will be boiled by condensing Dowtherm A vapor in the jacket. From the titanium A-40 heat exchanger the fuel-steam mixture passes into a titanium A-110-AT separator, from which the fuel returns to the loop and the steam passes into the existing stainless steel pressurizer.

Several other changes were made in the system. The pressurizer level controller was connected to vary the stroke of the feed pump. Therefore the feed rate will be determined by manually adjusting the letdown valve to pass the desired flow. A smaller letdown valve was installed to to obtain better throttling action. The high-pressure O_2 compressor was changed to incorporate a Scott & Williams drive unit and pulsator to replace the piston drive and packing gland, which was the major source of trouble during the last run. An all-stainless-steel rotometer was installed in the suction line to the purge pump for evaluation for reactor use. This required the use of a head tank to dampen out the pulsating action of the pump.

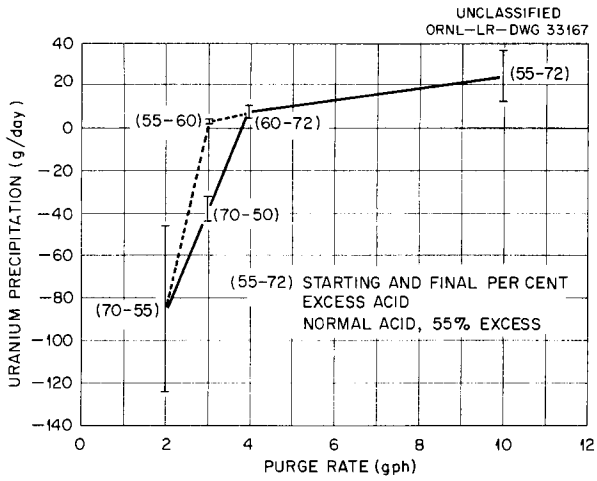

Fig. 4.5. Uranium Precipitation vs Purge Rate in HRT Mockup.

5. HRT DESIGN

W. R. Gall M. I. Lundin J. R. McWherter
R. E. Aven E. H. Gift G. H. Owen
F. C. Bowen E. M. Guglielmo[1] R. C. Robertson
C. A. Burchsted L. A. Haack R. E. Schappel
R. H. Chapman N. Hilvety C. L. Segaser
C. J. Claffey H. A. McLain W. L. Wright
C. W. Collins R. B. Muns F. C. Zapp

5.1 SINGLE-REGION OPERATION STUDIES

As a result of the leak between the fuel and blanket systems that occurred during run 14, a number of studies of the operation of the reactor as a single-region machine were made. Some of these studies are summarized in Secs 5.1.1 through 5.1.4.

5.1.1 Mixing of the Fuel and Blanket Solutions

If it is desired to obtain rapid and uniform mixing between the core and blanket systems, a connection between the systems will be necessary to supplement the transfer that occurs through the existing hole in the core. An equilibrium concentration would be reached within 4 hr if the transfer rate[2] is about 100 lb/min and if

1. the fuel dump tanks supply feed to and receive letdown from the fuel high-pressure system,
2. purge water is fed to both the fuel and blanket high-pressure systems from the fuel-system condensate storage tank,
3. there is no feed to or letdown from the blanket high-pressure system except through the communication with the fuel high-pressure system.

The needed transfer rate can be accomplished either by cross-connecting the lines leading to the chemical processing cell or by connecting the core and blanket access ports.[3] The first arrangement would consist in connecting the chemical processing lines at the inlet of the blanket heat exchanger to the corresponding line at the outlet of the core heat exchanger and connecting the inlet of the core heat exchanger to the outlet of the blanket exchanger in similar fashion. With this arrangement, and assuming equal pressurizer pressures, a transfer rate of about 170 lb/min can be expected. Changing the pressurizer pressures has a marked influence on the individual interconnecting lines between the systems, but the effect on the net mixing rate is negligible. The second arrangement, connection of the core and blanket access ports, would result in a transfer rate of about 140 lb/min when the circulation rate in both the core and blanket is 350 gpm. It is believed that neither of these arrangements would adversely affect operation of the reactor.

5.1.2 Blanket Dump-Tank Pressure

A study was made to determine whether dumping the entire contents of the HRT core and blanket high-pressure systems into the blanket dump tank would result in the dump-tank pressure exceeding the allowable value of 500 psia. The following assumptions were made: a reactor power level of 5 Mw, an average fuel temperature of 280°C in both core and blanket systems, commencement of the dump 2 min after reduction of power, and continued operation of the blanket recombiner-condenser (although with flooded surface during most of the dump). Under these conditions and with allowance taken for the heat capacity of the metal in the system, a blanket dump-tank pressure of 375 psia is estimated.[4]

5.1.3 Steam-System Modifications

If the HRT is operated with complete mixing of the core and blanket solutions, increased heat generation in the blanket will result in a much greater steam flow rate from the blanket heat

[1] On loan from Vitro Engineering Co.

[2] H. A. McLain, *Mixing Rates Between the HRT High Pressure Systems*, ORNL CF-58-5-26 (May 12, 1958).

[3] E. H. Gift *et al.*, *Mixing of the HRT Core and Blanket Systems Through External Connections*, ORNL CF-58-6-111 (June 27, 1958).

[4] N. Hilvety, *HRT Blanket Dump Tank Pressure*, ORNL CF-58-6-42 (June 5, 1958).

exchanger, and the steam system piping will require modification. A study was made[5] of the capacities and pressure drops in the steam piping, and an estimate was made of the steam generation rate and steam pressure as a function of reactor power, as shown in Fig. 5.1. The needed increase in capacity of the blanket-system steam flow-control valves could be achieved either through cross-connecting the blanket- and core-system steam mains ahead of the flow-control valves, permitting part of the blanket-system steam to pass through the core-system control valve, or by replacing the blanket valve with ones of higher capacity. Use of the first method would result in the core and blanket heat exchangers operating at essentially the same steam pressure. With the heat generation in the blanket estimated to be as great as 70% of the total heat generation[6] and with other factors, such as heat transfer coefficients and circulation rates, being essentially equal (i.e., a 360-gpm blanket circulating pump installed), the blanket-system average fuel temperature would be significantly higher than the core fuel temperature. At 5.7-Mw total reactor power and with the ΔT in the blanket limited to 44°C, the average blanket temperature was estimated to be about 270°C as compared with an average core temperature of about 254°C. Use of the second method, in which the blanket-system steam flow-control valves are replaced with larger valves, would permit independent control of the core and blanket steam temperatures and also would allow independent measurement of the steam flow from each of the main heat exchangers to continue without change. The use of the second method was recommended.

[5]N. Hilvety, *Modification of the HRT Blanket System for Operation as a Single-Region Reactor*, memorandum to S. E. Beall (May 5, 1958).

[6]P. R. Kasten *et al.*, *Operation of HRT as a One-Region Reactor*, memorandum (April 11, 1958).

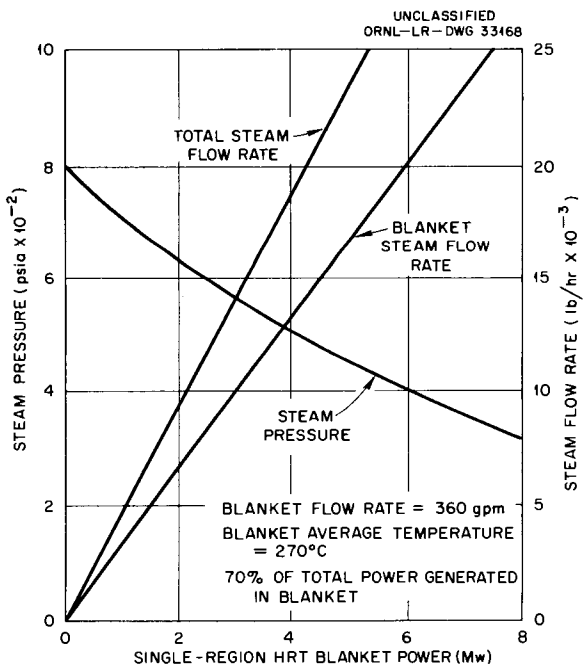

Fig. 5.1. Single-Region HRT Blanket Steam Pressure and Flow Rate vs Blanket Power.

5.1.4 Interconnection of Purge Pumps

A study was made of the manner in which the suctions of the purge pumps in the fuel and blanket systems could be interconnected so that all four pumps could draw purge water from the core-system condensate tank.[7] Since the purge-pump coolers would impose a significant flow restriction in the pump suction line, the maximum rate of flow to the blanket feed pump would be limited to about 4 lb/min. Higher flow rates would lower the purge-pump surge-tank level sufficiently to cause air-binding of the pump. Because of this limitation, it was recommended that this modification not be made.

5.2 TEMPERATURE DISTRIBUTION IN EXISTING REACTOR VESSEL

Data from HRT run 16 are being studied for the following purposes:

1. to determine heat removal from the blast shield and compare the values with the heat losses from the outer surface of the pressure vessel calculated by using average values of measured outside surface temperatures,
2. to estimate the inside surface temperature of the pressure vessel so that the thermal stress may be evaluated,
3. to make recommendations for taking data during future runs.

[7]H. A. McLain, *Flow of D_2O from the Fuel Condensate Tank to Blanket Condensate Tank Through Line Connecting Fuel and Blanket Purge Pumps*, memorandum, HRP 58-310 (July 1, 1958).

The thermal stress is a function of the temperature differences between inside and outside surfaces of the pressure vessel, the stress being a minimum when the temperature difference is zero.[8] Some cooling of the outside surface is therefore desirable, and this is accomplished by the radiation of heat from the pressure vessel to the blast shield. This shield is cooled by water flowing in cooling coils on its outer surface. A heat balance across the blast-shield cooler was made by using the equation

$$q = Wc_p(T_{out} - T_{in}) \ ,$$

where

q = heat transfer rate, Btu/hr,

W = rate of flow of cooling water, lb/hr,

c_p = heat capacity of water (~1.0 Btu/lb·°F),

T_{out} = temperature of cooling water leaving cooler, °F,

T_{in} = temperature of cooling water entering cooler, °F.

Values far heat loss derived from this formula were compared with heat-loss calculations made by using the radiation, convection, and conduction equations used by Aven.[9] The results are shown in Fig. 5.2.

The amount of heat radiated from the pressure vessel is a function of the temperatures of the outside surface of the pressure vessel, T_b, and of the inner surface of the blast shield, T_0. The heat generated in the pressure-vessel wall is a function of reactor power level and has been estimated[9] as

$$\frac{Q}{A} = 2290P \ ,$$

where P = reactor power, Mw, and Q/A = the volume of heat generated in a spherical sector of the pressure vessel of outside surface area of 1 ft^2, Btu/hr·ft^2.

Assuming natural-convection heat transfer between the inner wall of the pressure vessel and the blanket solution, the heat transfer coefficient,

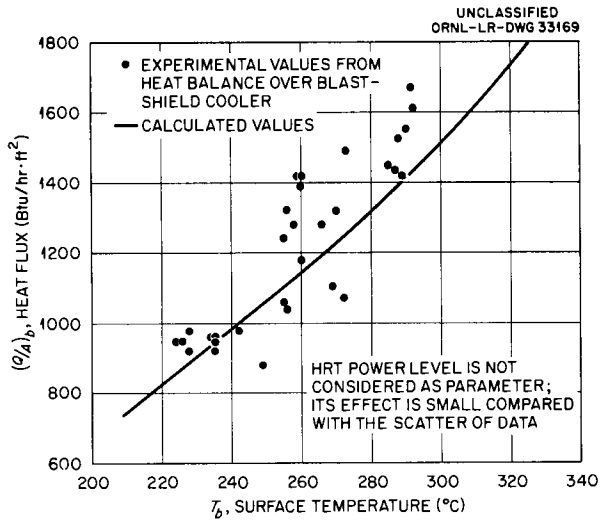

Fig. 5.2. Heat Fluxes from Outer Side of HRT Pressure Vessel.

h_c (Btu/hr·ft^2·°F), has been estimated[10] as

$$h_c = 130(\Delta T_f)^{1/3} \ ,$$

where ΔT_f = temperature drop across the film, °F.

Using the heat generation values estimated by Cheverton,[8] the heat flux into the blanket solution at the inner wall of the pressure vessel can be estimated. Then

$$\left(\frac{q}{A}\right)_{r=R} = h(\Delta T_f) = 130(\Delta T_f)^{4/3}$$

and

$$\Delta T_f = \left[\frac{1}{130}\left(\frac{q}{A}\right)_{r=R}\right]^{3/4} \ ,$$

where R = inside radius of pressure vessel, in. With ΔT_f added to the average measured temperature of the blanket solution, an estimate of the inner wall temperature of the vessel was made. The difference between this temperature, T_R, and the measured temperature of the outer surface of the pressure vessel gives a temperature differential from which the thermal stresses may be estimated.[8] The variation in the temperature

[8] R. D. Cheverton, *Steady-State Pressure and Thermal Stresses in the HRT Pressure Vessel*, ORNL CF-58-7-43 (July 15, 1958).

[9] R. E. Aven, *Heat Removal Systems for the HRT Pressure Vessel*, ORNL CF-55-3-119 (March 14, 1955).

[10] R. E. Aven, *Some Heat Removal Considerations of the HRT Pressure Vessel During Operation*, ORNL CF-55-7-64 (July 15, 1955).

differential across the vessel wall, as a function of power level, is given in Fig. 5.3. On the basis of these values the thermal stress in the pressure-vessel wall appears to vary from about 1800 psi at low power to 6800 psi at 5 Mw.

5.3 REPLACEMENT PRESSURE VESSEL

The design of a replacement pressure vessel for the HRT has been initiated. Vessels with nonremovable core tanks are being considered presently because of the extensive development time and effort required to obtain a pressure-vessel closure capable of satisfying HRT requirements. Major emphasis is being placed on a vessel with a concentric inlet-outlet core tank. Vanes may be used in the core nozzle to impart rotation to the core solution as a means of minimizing boundary-layer separation at the core wall. Cooling of the core wall by use of a shroud to channel the inlet blanket flow around the core is under consideration, as is rotational flow to achieve high flow velocities without the use of a shroud. One version of the replacement vessel is shown in Fig. 5.4. A bottom core drain through which about 5 to 10% of the flow can be bypassed is shown; this would minimize the accumulation of solids.

Calculation of the expected heat transfer from the core wall is difficult because the fuel in the core is a volume heat source. The flow distribution and heat generation must be known before the heat transfer through the core wall can be accurately calculated. In preliminary calculations,[11] assumptions were made regarding the flow distribution and heat generation. If the fuel and blanket heat transfer coefficients at the core wall are 600 and 500 Btu/hr·ft^2·°F, respectively, and the outlet fuel and inlet blanket temperatures are 300 and 260°C, respectively, the core wall temperature at 5 Mw could be as high as 315°C.

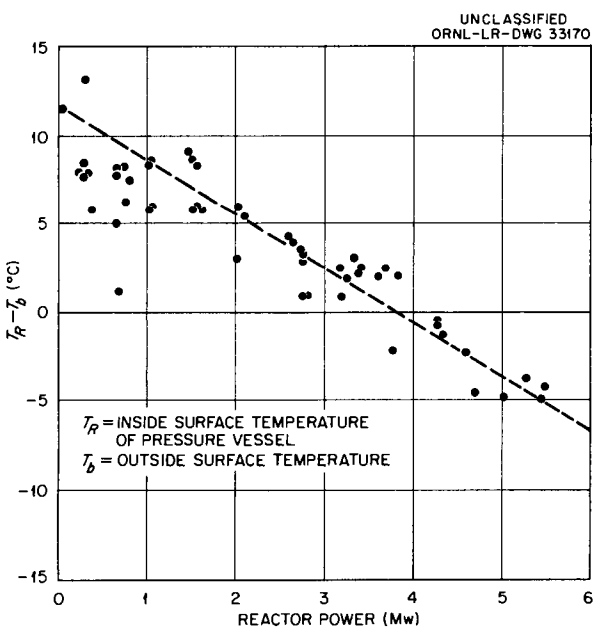

Fig. 5.3. Temperature Drop Across HRT Pressure-Vessel Wall.

5.4 PIPING LAYOUTS FOR REPLACEMENT PRESSURE VESSEL

The lines from the reactor vessel to the fuel and blanket heat exchangers (lines 101 and 201) should require little or no change in either location or configuration on installation of the replacement reactor vessel. The lines from the circulating pumps to the reactor vessel (lines 103 and 203), however, will have to be relocated to permit entry at the top of the vessel. The current layouts show a horizontal surge tank connected to the core outlet and a vertical surge tank connected to the blanket outlet. Separate D_2O boilers will supply steam to these surge tanks for pressurization. The boilers may be located in about the same positions as the present pressurizers, or they may be located in the area immediately east of the removable bulkhead. Core corrosion specimens will be inserted into the fuel solution through the core surge tank.

5.5 CELL-WIRING REPLACEMENT

The original glass-insulated wiring to the circulating pumps, the pressurizer heaters, and the space-cooler motors was replaced with magnesium oxide–insulated cables inside a copper-tubing sheath. In order to maintain a leak-tight seal at the cell wall, the new cables were passed through a modified periscope plug installed in the upper (west) fuel-side periscope as shown in Fig. 5.5. Eighteen cables, four of them spares, were cast into the plug with concrete. Each cable is bent through a 60-deg arc to minimize radiation streaming and is sealed with pressure fittings at each end of the plug. The control-room side of

[11] H. A. McLain, *Preliminary Calculations of Heat Transfer Through the HRT Replacement Core Vessel Wall*, memorandum to W. R. Gall (July 22, 1958).

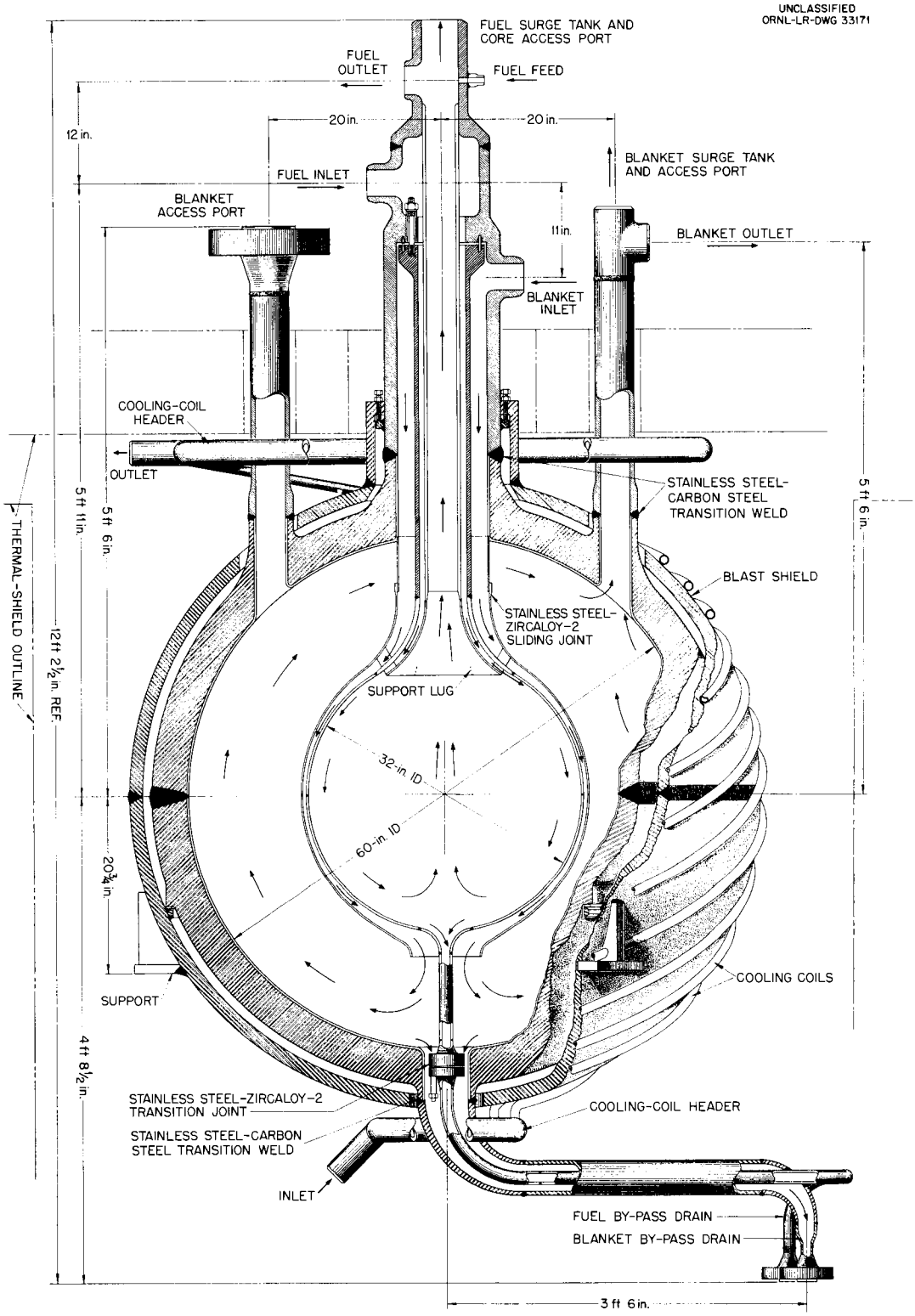

Fig. 5.4. Proposed HRT Replacement Pressure-Vessel Assembly.

UNCLASSIFIED
ORNL-LR-DWG 33538

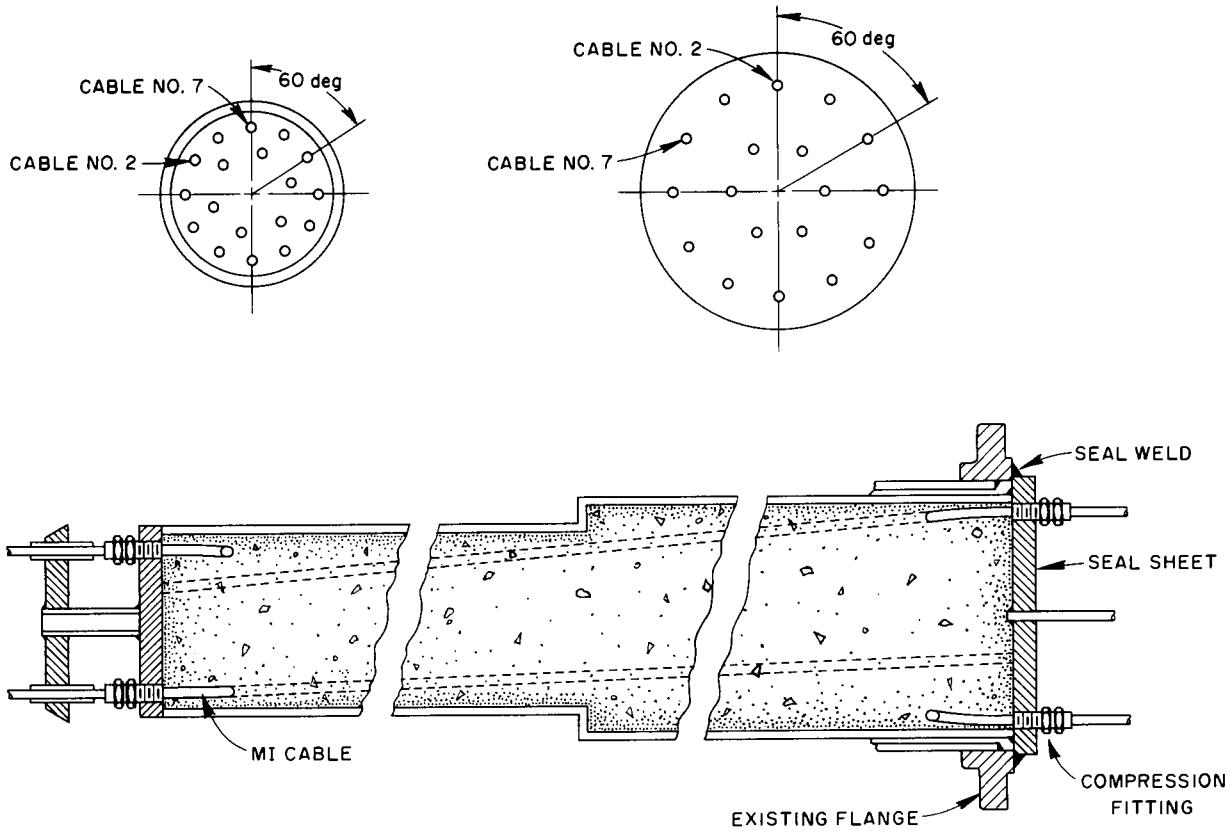

Fig. 5.5. Special Cable Plug for HRT.

the plug was seal-welded to the existing periscope flange. The end of the cable near the equipment is sealed through a special Kovar-type seal and connects through the quick-disconnects to the equipment leads.

5.6 MAIN-HEAT-EXCHANGER BLOWDOWN SAMPLING STATION

Two stations were designed to obtain boiler-water samples from the fuel and blanket heat exchangers. Since the samples may be radioactive, provision was made for adding lead shielding around the sample chamber if necessary. One station will be utilized for taking bottle samples for the usual water analyses; the other station is a continuous dissolved-oxygen analyzer. The sample water flows through two air-operated control valves and a cooler in the east valve pit and then through underground piping to the west wall of the waste-evaporator enclosure where the stations are mounted. Drains from the sample stations are sent to the waste pond (see Fig. 5.6). In addition, an unshielded, continuous dissolved-oxygen and -hydrogen analyzer will be located at the northwest corner of the package-boiler room for sampling steam from the heat exchangers.

5.7 REMOVABLE INSULATION

Remotely attachable and removable insulation cans have been designed for reinsulating HRT pipe and flanges from which the original insulation has been removed to allow access for maintenance. The existing insulation consists of layers of aluminum foil wrapped around the pipes and held in place by aluminum screen and wire.

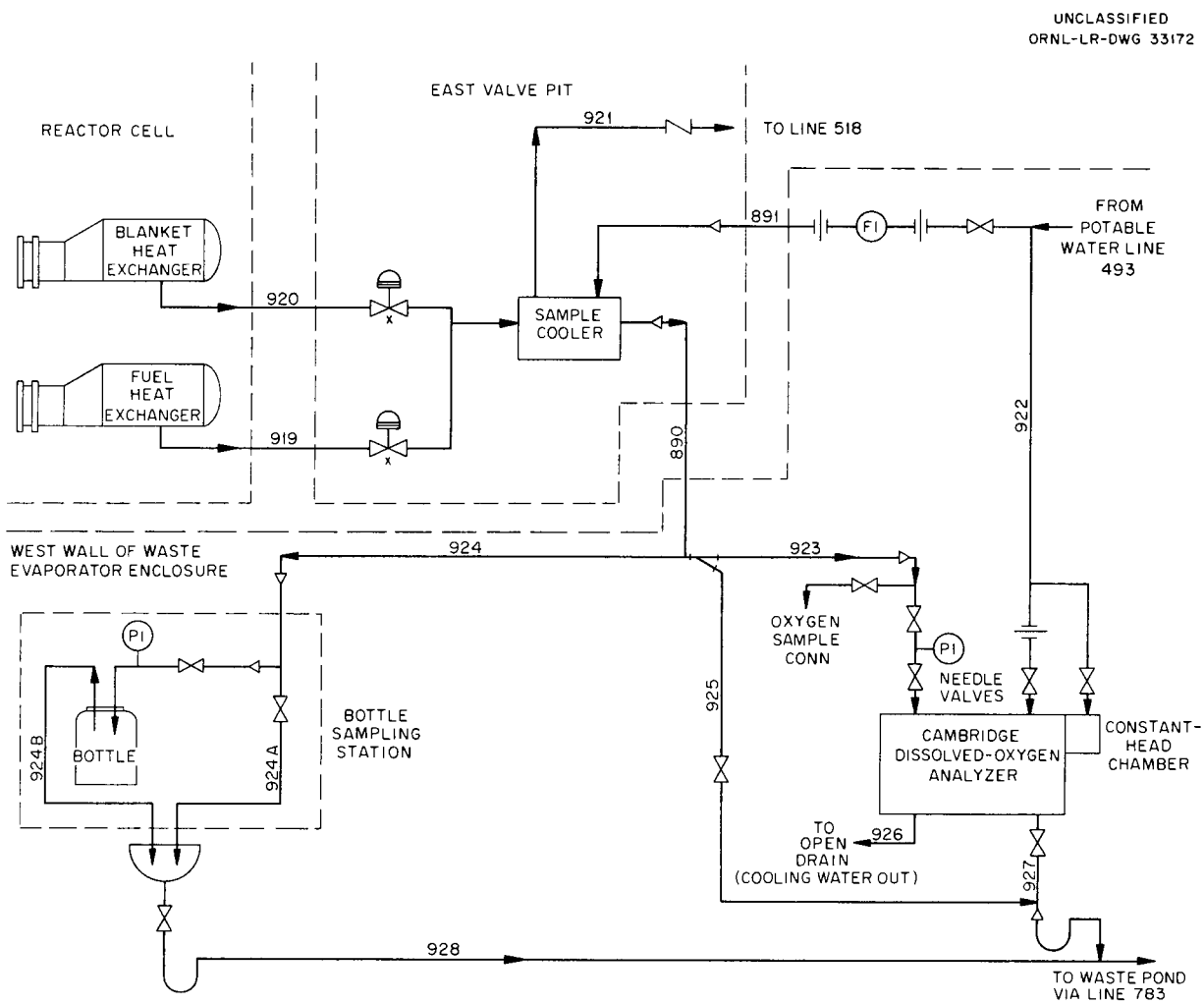

Fig. 5.6. Flowsheet of HRT Heat Exchanger Sample System.

The replacement insulation consists of sheet-aluminum cans, made in halves, containing a blanket of crinkled aluminum foil. The ends of the cans are made of stainless steel to reduce conduction, and self-locking spring-type fasteners are used to hold the halves together. Long-handled rods which screw into each half will be used to install the assemblies (Fig. 5.7).

5.8 INSPECTION OF EXISTING CORE VESSEL

Several special devices have been designed to facilitate the inspection of the existing core vessel. One device is a manipulator for handling a 2-in.-dia television camera in the pressure vessel for inspection of the outer surface of the core.

The camera, which can be rotated by means of a small motor drive, is mounted on the last of a series of hinged arms. Each arm is positioned, relative to adjacent arms, by a hydraulic cylinder. Lighting is provided by several lamps mounted on the camera head. The central operating panel, which contains the controls and indicators for positioning the camera, is mounted at the top of the device and outside the reactor cell. (See also Secs 4.3.1 and 6.1.2.)

A device was designed for cutting a metallurgical specimen from the top screen of the core vessel. The tool is a 1-in. hole saw supported by a shaft and positioned by a linkage with universal joints which permit rotation of the saw. This tool can be inserted into the core

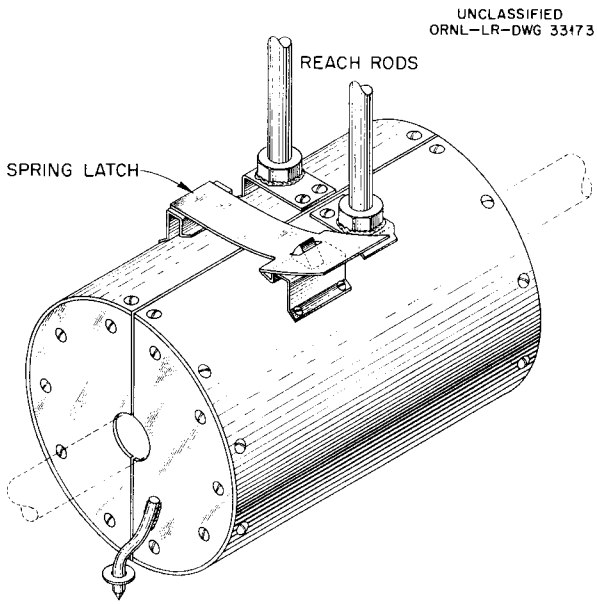

Fig. 5.7. Removable Insulation for HRT.

vessel through the $2\frac{1}{2}$-in. access flange. After the tool support shaft is inserted in the center hole of the screen, the cutting head is extended from the support shaft and inserted in another hole $9\frac{1}{2}$ in. from the center; the cut specimen is retained on a toggle extending from the centering pin of the cutter. The tool is then retracted into the extension handle and withdrawn from the core vessel with the cut specimen.

A viewing window is being designed which will fit into the television camera opening in the existing tool assembly used to remove core and blanket corrosion-specimen holders. This window will provide an alternate visual aid for observing tooling operations within the reactor containment shield.

An optical system was designed to facilitate viewing the outer surface of the core tank with the existing periscope. The system consists of a housing which holds the periscope, with a folding arm which carries a mirror and light source. The assembly is inserted into the blanket through the blanket access flange; then the folding-arm assembly is used as a means of extending the field of vision of the periscope.

Another viewing device, which consists of a series of adjustable mirrors mounted on an arm and which utilizes an external light source, is now being designed. Discouraging results with internal light sources, due to breakage and glass browning initiated this latter design.

5.9 DRY-MAINTENANCE STUDIES

Based on concepts presented in their design study report,[12] the Vitro Engineering Company completed the design of two portable sliding-frame shields. One shield utilizes a cross-slide (Fig. 5.8), and the other does not.

Since a 4 × 4 ft cell opening is adequate for performing the majority of HRT dry-maintenance work, a decision was made to design a shield which would operate over an opening of this size and which would utilize the best features of the sliding-shield and modular-block systems as outlined in the initial study. Merging of the two concepts is accomplished by designing the sliding members as frames into which modular blocks or tool plugs are placed. A tool slide can be added to provide greater motion in a plane perpendicular to the sliding frames. The frames are handled by a crane and are mounted on wheels which rest on portable track sections placed on the shield blocks adjacent to the opening. An electric-motor drive is utilized to position the frames, and provision is made for manual fine adjustment. A preliminary cost estimate indicates that this sliding shield can built for approximately $32,000.

[12] Vitro Engineering Co., *Dry Maintenance Study for the HRT* (March 12, 1958).

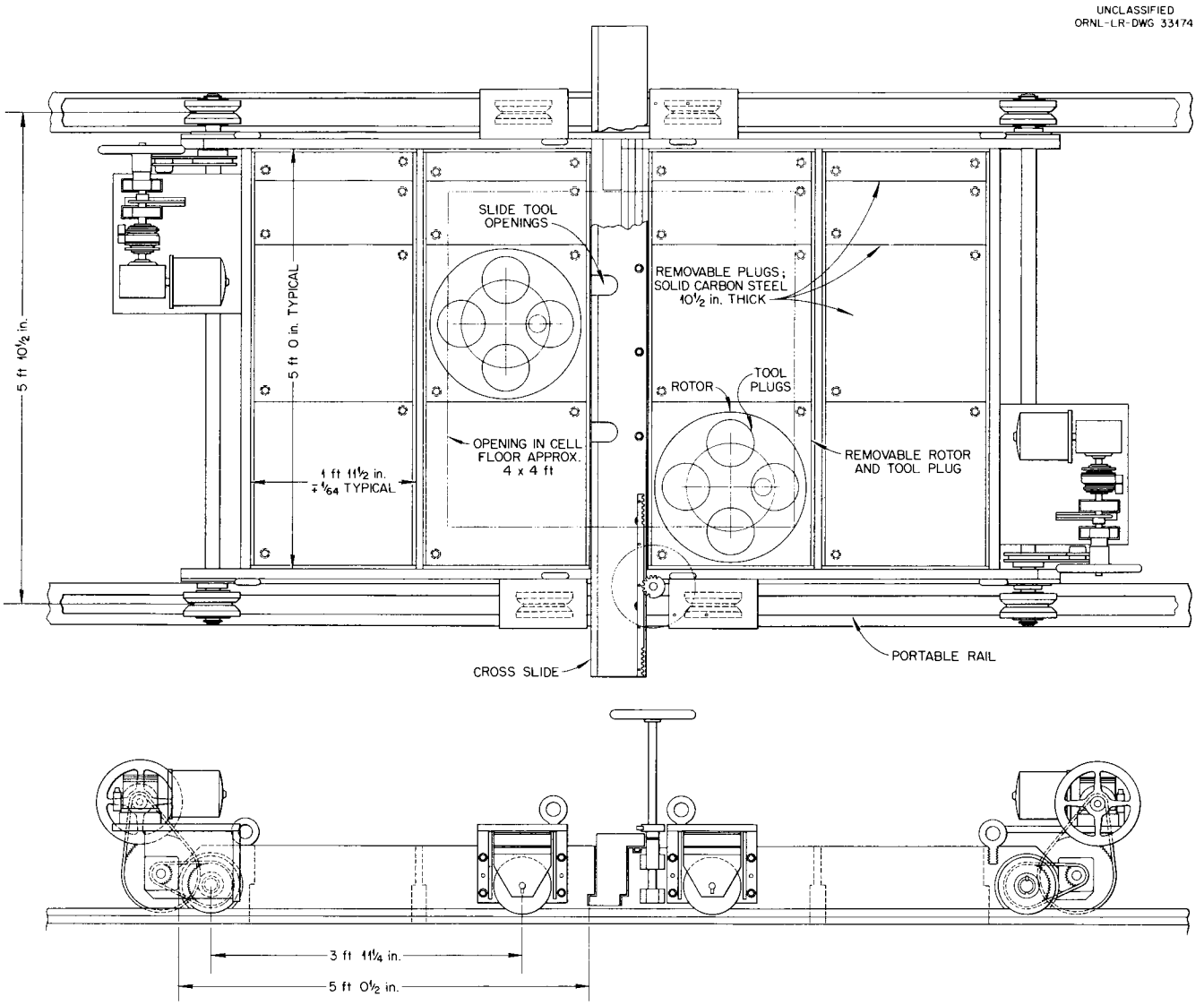

Fig. 5.8. Dry-Maintenance Shield for HRT.

6. HRT CONTROLS AND INSTRUMENTATION

D. S. Toomb

A. M. Billings
J. R. Brown
R. L. Moore
R. M. Pierce[1]
J. A. Russell
K. W. West

6.1 COMPONENT DEVELOPMENT

6.1.1 Letdown Valves

The fuel letdown valve (serial No. K-74), which is throttled to maintain a constant pressurizer liquid level, was removed after the initial reactor power operation because of excessive leakage. This valve was installed in the reactor on November 12, 1957, and it was removed on February 28, 1958. Figure 6.1 indicates the nature of the erosion in the seating cone of the Armco 17-4 PH stainless steel plug. The valve had been sized originally for a mixture of liquid and gas and thus was oversized for the revised operating condition of no gas in the letdown stream. The valve position indicator showed that the valve operated in a nearly closed position, thus intensifying the wear in the seating cone region of the plug. This conical surface mates with the valve seat to effect tight shutoff; wear in a properly sized valve occurs well out on the plug, permitting a reasonable service life before erosion occurs in the seating area.

Valve L-98 replaced valve K-74 on February 28, 1958. Although grossly oversized with a C_v (flow coefficient) of 0.065 at three-fourths stroke and a C_v of 0.12 at full stroke, since this valve was available for service, it was inserted in the HRT to expedite operation. As expected, the valve metered near the seat and had to be removed after nine weeks in the reactor because of excessive seat leakage. Radioactive contamination of the valve is so great that no examination has been possible.

In the meantime, a new valve (serial No. R-21) was fabricated and sized only for liquid flow. The capacity of valve R-21 is 1 gpm of liquid

[1]On loan from TVA.

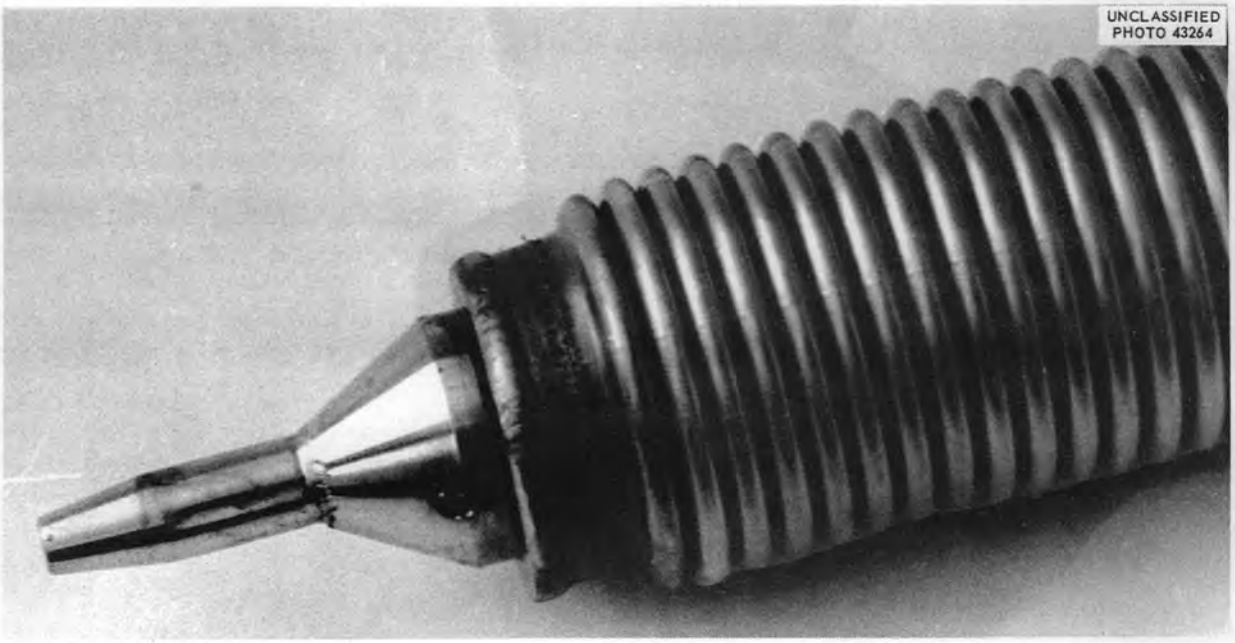

Fig. 6.1. Eroded Fuel Letdown Valve (Serial K-74).

with a differential pressure of 1600 psi at three-fourths stroke. The flow coefficient, C_v, was measured as 0.028 at three-fourths stroke and 0.17 at full stroke. This valve was installed in the HRT on May 1, 1958. Operation to date has been satisfactory.

An experimental letdown valve was designed which incorporates a ⅛-in.-dia body port instead of the presently used ¼-in.-dia. The design, shown in Fig. 6.2, will permit an increase in the close plug-to-seat clearance which is necessary for adequately throttling the letdown flow. The new valve, which will be tested in the HRT mockup loop, should also reduce the possibility of solid particles wedging the plug in the seat because of the increased annular clearance possible with the smaller port diameter. A three-wing type of lower stem guide is provided to achieve better plug-to-seat alignment, to reduce the possibility of the smaller plug being broken, and to avoid fuel-solution stagnation in the stem-sealing bellows compartment.

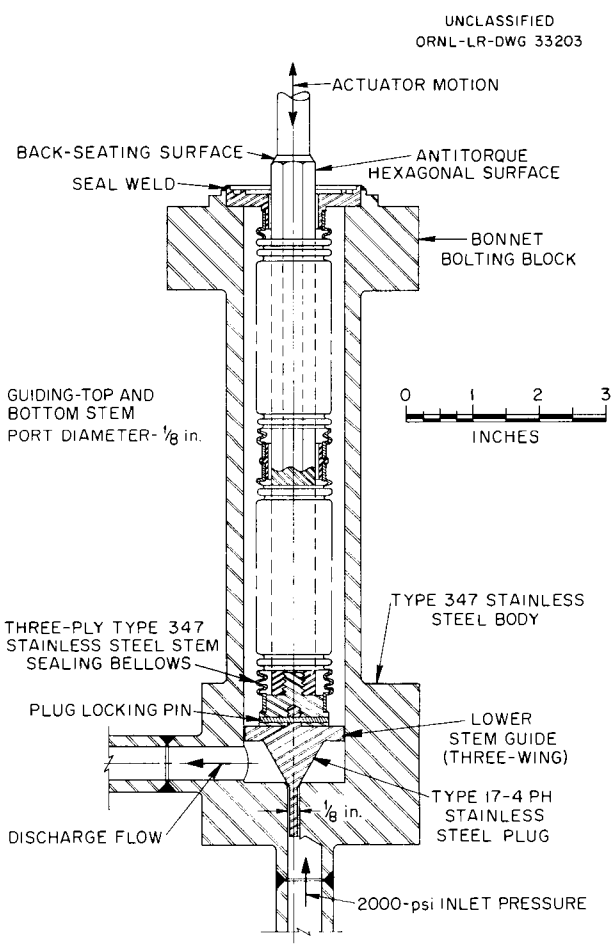

Fig. 6.2. Modified Letdown Valve.

6.1.2 Remote-Viewing Equipment

A 2-in.-dia television camera designed for resistance to radiation was received from the Dage Electronics Division, Thompson Products, Inc. The camera will be installed in a remotely manipulated mechanism under development for viewing the HRT core vessel (see Sec 4.3.1). The camera head, including deflection coils and type 6198A Vidicon and lens, together with the polished Stellite right-angle mirror and G-E type 1183, 50-cp spotlight bulb for illumination, is shown in Fig. 6.3. The preamplifier is located at the end of a cable 10 ft 6 in. long to permit most of the electronic components to be located out of the high radiation field associated with the core vessel. By separating the preamplifier and camera head, a considerable reduction is achieved in the size of the assembly to be inserted in the core. One carbon resistor and one ceramic condenser remain in the camera head; the remainder of the electronic components are located in the preamplifier chassis, shown uncovered in Fig. 6.4.

Available information[2] indicates that the Vidicon sensitivity will decrease about 70% because of lens and Vidicon window browning for a gamma irradiation of 10^7 r. For the gamma flux in the HRT core an expected useful viewing time on this basis should be at least 50 hr. However, the effect on the camera of the beta activity present in the core is unknown, and the light-bulb glass is also expected to brown and thereby further reduce the viewing time.

To provide camera position indication to the operator of the manipulator, the angle of rotation of the three arm-positioning hydraulic cylinders is transmitted to the control console by miniature linear slide-wires manufactured by Bourns Laboratories, Inc.

[2] From WADC-TR-57-361, vol II.

UNCLASSIFIED
PHOTO 31870

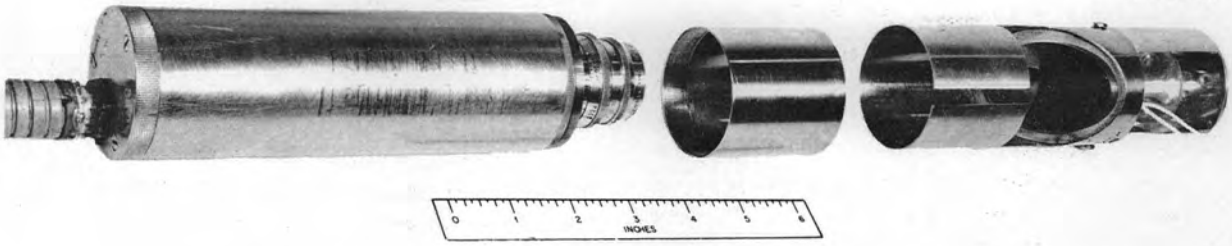

Fig. 6.3. Miniature Television Camera Head, Mirror, and Light Source.

UNCLASSIFIED
PHOTO 31871

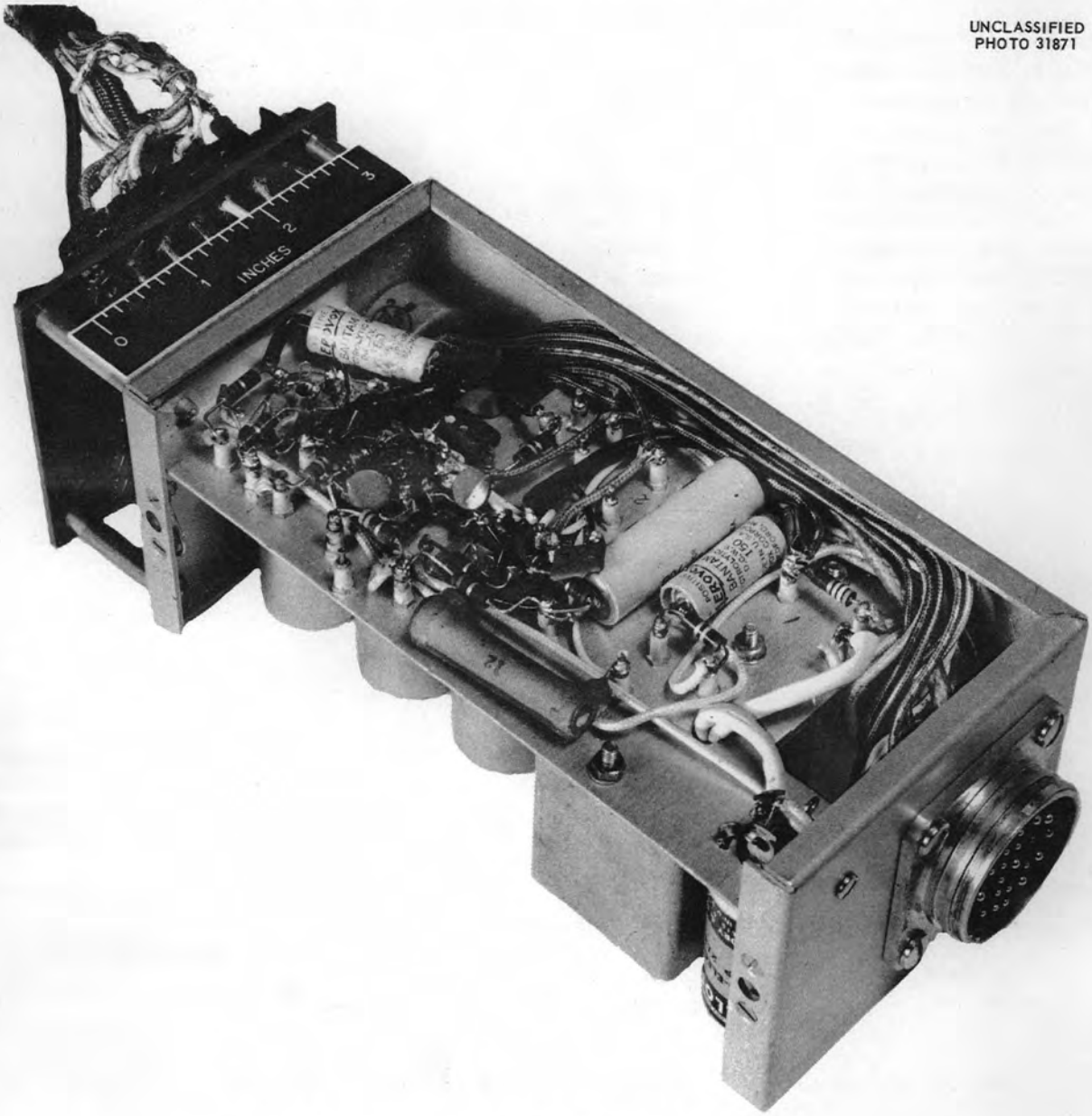

Fig. 6.4. Preamplifier Chassis for Miniature Television Camera.

6.2 MAINTENANCE AND MODIFICATIONS

6.2.1 Oxygen-Injection System

The capacity of the capillary pressure-drop system[3] used to measure the flow of oxygen gas into the HRT high-pressure fuel system was increased by replacing the existing metering capillary with a shorter (2-ft) length of 0.019-in.-ID stainless steel tubing. The capacity of the new system is 2600 std cc/min, with a pressure drop of 300 psi (2100 to 1800 psi) across the thermal valve[4] and capillary. The thermal-valve temperature was 285°C for this flow.

6.2.2 Reactor Power-System Rewiring

The design, procurement, and installation of a new power-wiring system inside the reactor containment tank were completed. This system supplies electric power to the pressurizer heaters, circulating pumps, and space coolers.

The first wiring system consisted of stranded copper wire insulated with a double layer of Fiberglas-woven sleeving lightly impregnated with an oleoresinous varnish. The wiring was routed to the equipment location in sealed conduits. Inside the containment tank the conduits were terminated in boxes containing glass-to-metal seals to which ceramic-beaded wires from the remote-disconnect boards were connected. On the control-room end the conduits and wires were sealed in a box filled with 100% air-blown asphalt.

Much difficulty was experienced from moisture in a conduit causing the Fiberglas insulation to break down at the operating voltage of 460 v ac. The dry-insulation breakdown point in the conduits as measured at 7.2 psia was 1500 v dc.

The new wiring system consists of swaged magnesium oxide–insulated wires in copper-tube sheaths (General Cable Corp. "MI"). The cable ends are terminated inside the containment tank by special hermetic ceramic-to-metal seals and on the control-room side of the shield wall by the standard General Cable sealed terminals. The new cables are terminated at the various remote-disconnect boards by the compression fitting shown in Fig. 6.5, which also illustrates the ceramic-to-metal cable-end seal.

The Fiberglas-insulated wire in sealed conduits is still being used in the containment cell of the chemical plant, and no electrical trouble has been experienced to date. However, mineral-insulated cables were installed near the electrical equipment in this cell and will be connected if necessary.

[3]D. S. Toomb *et al.*, *HRP Quar. Prog. Rep. Oct. 31, 1956*, ORNL-2222, p 22.

[4]D. S. Toomb *et al.*, *HRP Quar. Prog. Rep. Jan. 31, 1958*, ORNL-2493, p 20.

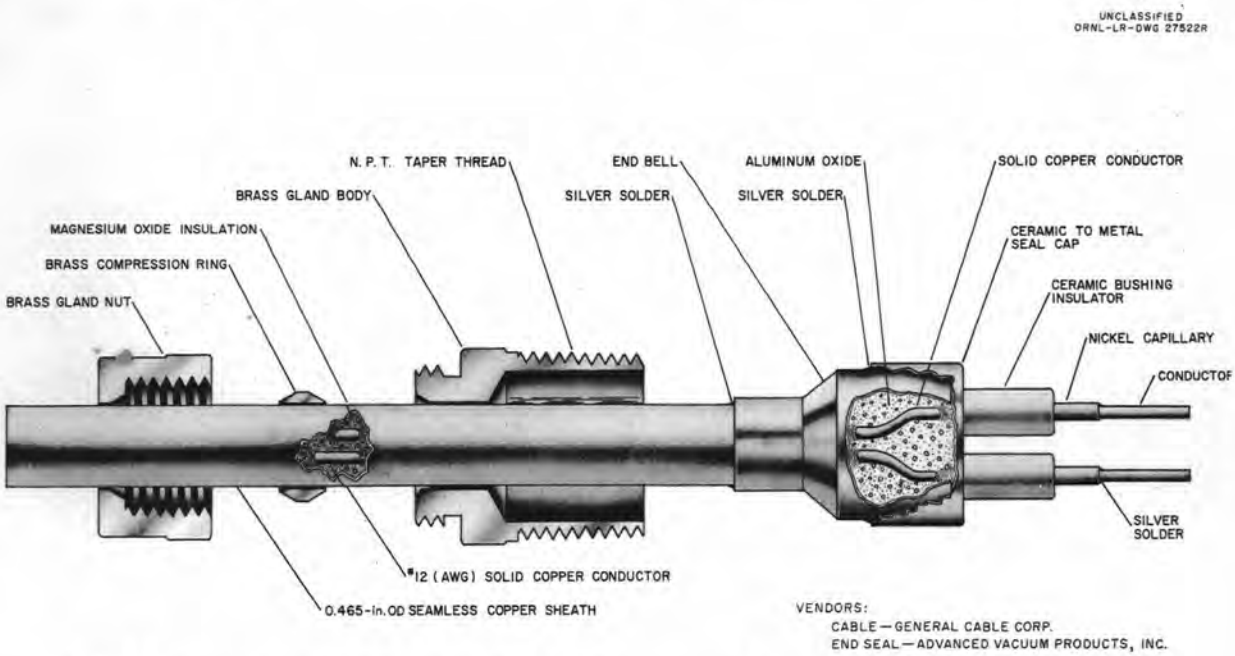

Fig. 6.5. Mineral-Insulated Cable and Associated Compression Attached Fitting and Hermetic End-Seal.

6.2.3 Blanket Dump Valve

The blanket-system dump valve (serial No. K-71) was removed on May 29, 1958, because of excessive leakage. This valve was installed on October 23, 1957, and had given satisfactory service. The leak rate as measured after removal was approximately $1\frac{1}{2}$ gpm with 1500-psi water under the valve seat. The moderate wear of the plug seating region, as shown in Fig. 6.6, indicates that the exorbitant leak rate is probably attributable to misalignment caused by galling of the stem with the inside diameter of the weld spool at the juncture of the tandem bellows.

6.2.4 Instrumentation and Controls Revisions To Facilitate Single-Region Operation

To facilitate reactor operation as a single-region machine and to provide for the increased heat generation in the blanket system, revisions were made to the instrumentation and controls system.

Several changes in size of steam-system valves were necessary to provide for the increased steam generation in the blanket heat exchanger and to permit the interconnection of the core and blanket steam generating systems. The size of the heat exchanger blowdown valves was also decreased to minimize the pressure upset occurring during this operation.

Control-circuit changes include

1. the automatic dilution of the fuel solution if the blanket outlet temperature exceeds 310°C,
2. the elimination of automatic control action for venting the blanket-system pressurizer,
3. the automatic closing of steam-removal valves if either the fuel- or blanket-system circulating pumps are stopped,
4. the automatic stopping of both fuel- and blanket-system circulating pumps if the steam-system pressure drops at a rate exceeding 20 psi/sec,
5. the addition of circuitry to prevent the pumping of fuel solution into the high-pressure system from the blanket-system dump tanks during startup.

6.2.5 Measurement of System Transients

To help in the determination of the cause of the periodic power surges experienced with single-region reactor operation, minor revisions to the instrumentation system were made so that a high-speed recording system could be connected to the neutron-level, period, pressure, and pressurizer-level measurement channels. The equipment used for these measurements was the Sanborn Company "150" direct-writing oscillographic recording system and associated amplifiers.

UNCLASSIFIED
PHOTO 44122

UNCLASSIFIED
PHOTO 44124

Fig. 6.6. Blanket-System Dump Valve (No. K-71) Bellows-Plug and Stem Assemblies.

Part II

REACTOR DESIGN, RESEARCH, AND ANALYSIS

R. N. Lyon

7. REACTOR DESIGN

W. R. Gall M. I. Lundin
J. R. McWherter

R. E. Aven
J. C. Bolger
R. H. Chapman
C. J. Claffey
E. H. Gift
L. A. Haack
N. Hilvety
H. A. McLain
R. C. Robertson
J. N. Robinson
W. Robinson
R. E. Schappel
C. L. Segaser
D. W. Vroom

F. C. Zapp

7.1 REACTOR DESIGN PROGRAM

Design of HRE-3 as a two-region power breeder reactor has been suspended pending resolution of the problems which have arisen in operation of the HRT. A small single-region circulating-slurry reactor for investigating the problems fundamental to slurry fuels in reactor systems is being studied. This reactor, designated as HRE-4, would be in the 1- to 5-Mw range.

7.2 HRE-3 DESIGN

A report describing the work done on HRE-3 is being written.[1] Some of the more recent work is summarized in Secs 7.2.1 through 7.2.4.

7.2.1 Conceptual Layouts

Preliminary conceptual layouts of the HRE-3 reactor system were prepared for use as a basis for detailed study of component compartments with respect to equipment design, shielding requirements, and maintenance philosophy and techniques. The general plan and elevation of the concept chosen for further study are shown in Figs. 7.1 and 7.2. The high- and low-pressure portions of the reactor are housed in separate containment vessels, between which is located a separate sealed and shielded compartment for housing dump and letdown valves, feed pumps, oxygen injection system, and instrumentation. Certain items are readily accessible for maintenance in this concept, and it may be possible to replace some components (such as feed pumps) while the reactor is operating.

Figure 7.3 shows a conceptual design of the reactor core and pressure vessel. This design could be utilized in economic studies to determine whether the vessel should be designed for replacement of the core when necessary or for a nonremovable core. A reactor core compartment with a vessel of the latter type is shown in Fig. 7.4. The vessel, together with a portion of the thermal shield surrounding it, is supported on a dolly. An opening will be made in the containment chamber and biological shield through which the assembly can be withdrawn to a maintenance area.

Figure 7.5 shows a typical concept of the circulating-pump compartment based on the use of a top-maintenance pump. The lower plugs shield the highly radioactive scroll of the pump to permit semidirect maintenance operations at the rotor end of the pump. These plugs are removable so that the scroll can be replaced if necessary.

Possible arrangements of the fuel and blanket heat exchanger compartments are shown in Figs. 7.6 and 7.7. The principal criteria for the layout of the compartments are facility of exchanger removal, protection against radiation from adjacent components during shutdown, and simplicity. The fuel heat exchanger, which is mounted on wheels, is removed by separating the flanges, lifting the unit a few inches, moving it to the rear to clear the support brackets, and lowering it to the track below. The exchanger is then taken through a tunnel to the maintenance area. The layout of the blanket heat exchanger compartment is based on the use of a vertical heat exchanger. In this concept, shown in Fig. 7.7, the exchanger is removed from above with an overhead crane.

7.2.2 Fuel and Blanket Heat Exchanger Studies

A preliminary study[2] has been made of the core and blanket steam generators for the HRE-3 in

[1] R. H. Chapman *et al.*, *HRE-3 Summary and Reference Report* (to be issued).

[2] D. W. Vroom, *Preliminary HRE-3 Core and Blanket Steam Generator Study*, ORNL CF-58-3-106 (March 23, 1958).

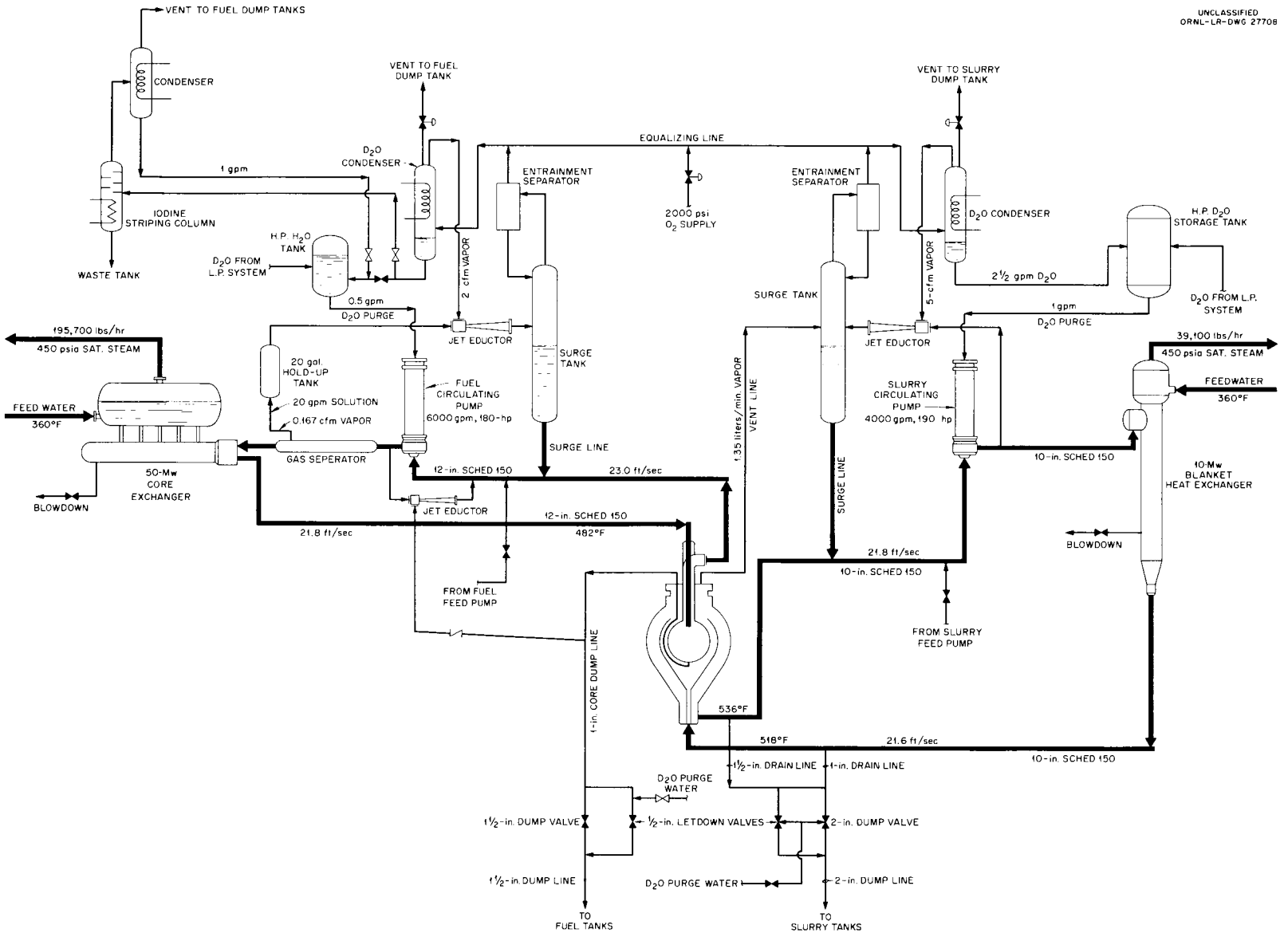

Fig. 7.1. HRE-3 Conceptual Layout – Plan.

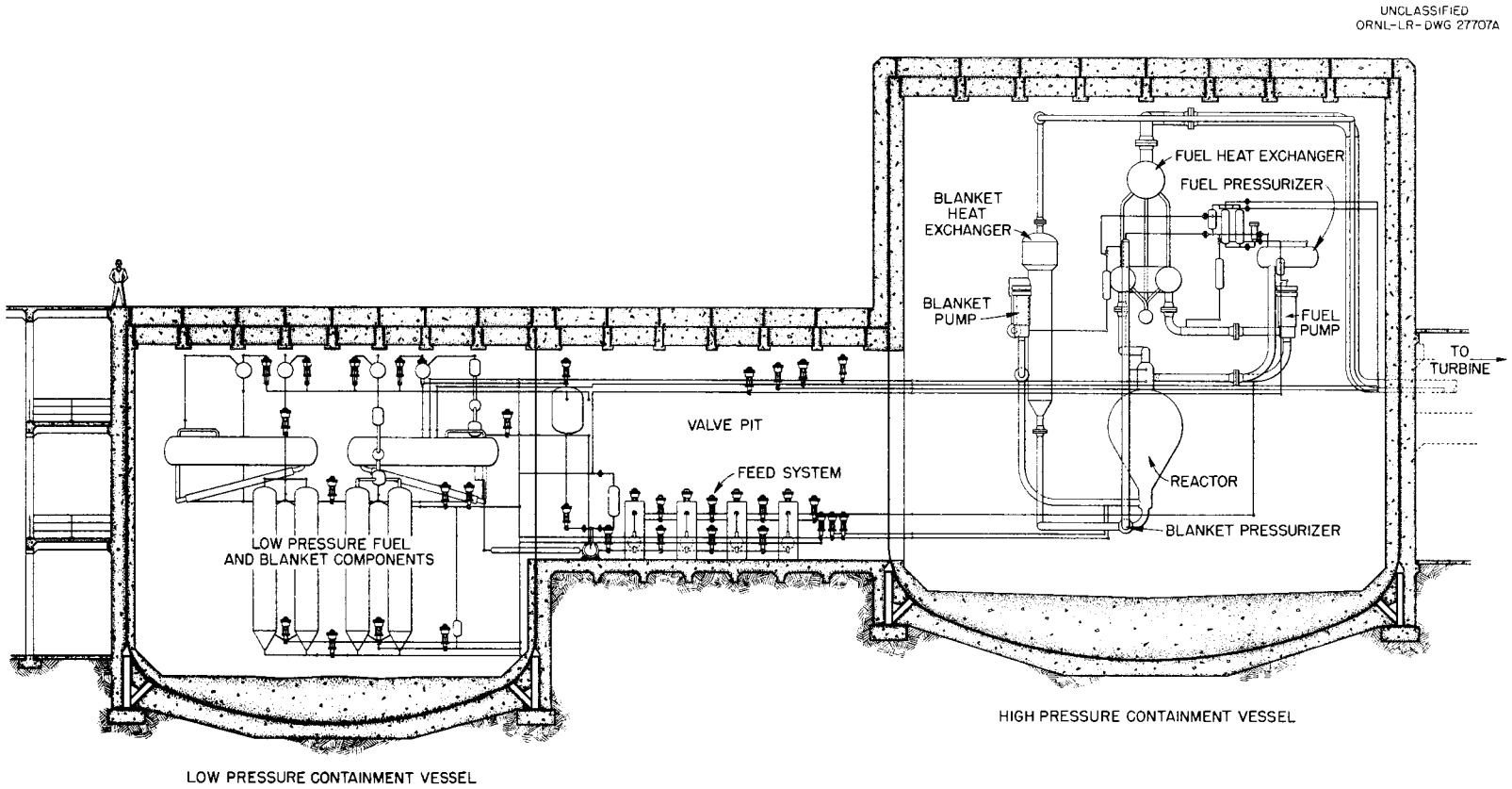

Fig. 7.2. HRE-3 Conceptual Layout – Elevation.

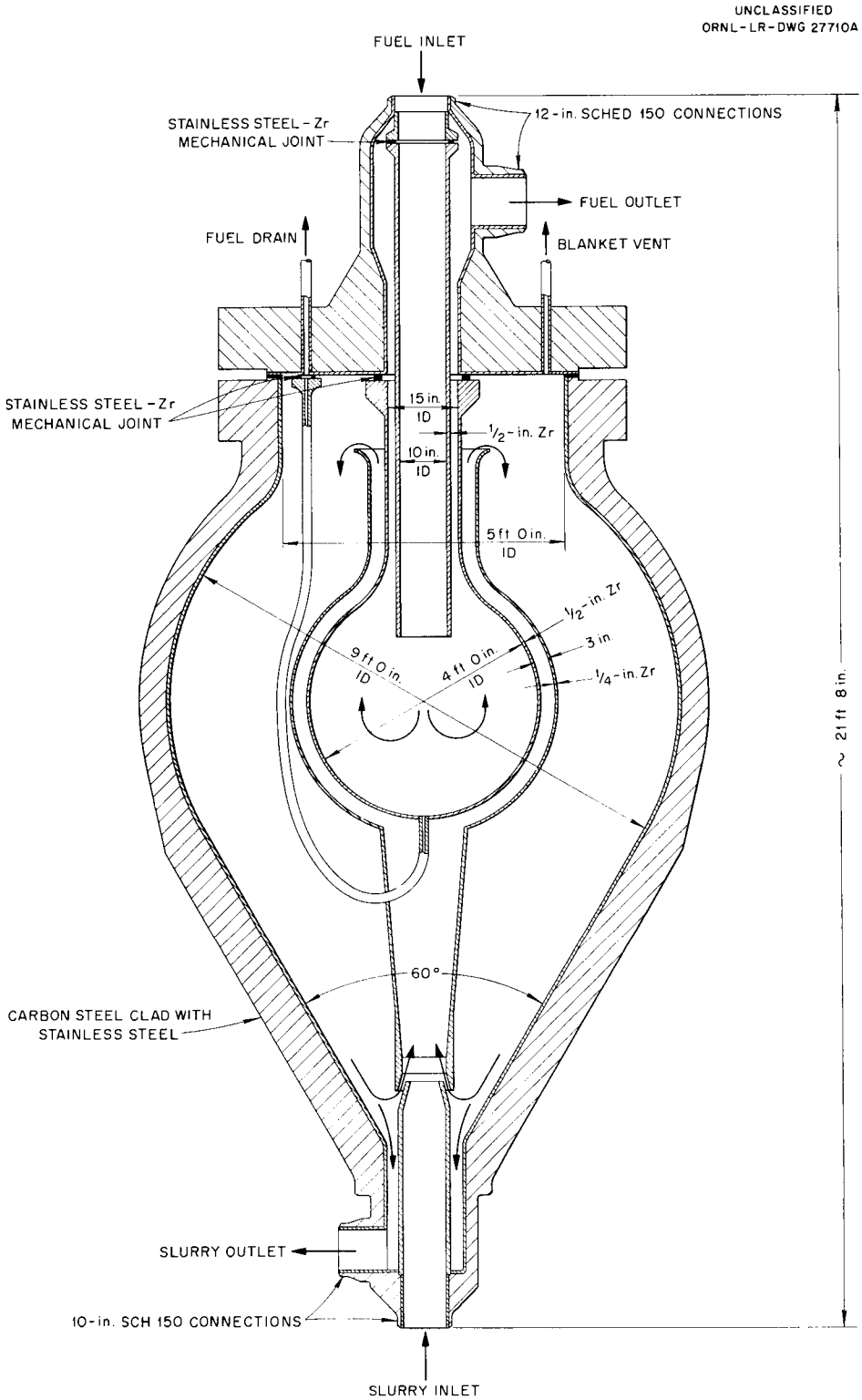

Fig. 7.3. HRE-3 Conceptual Design, Reactor Vessel.

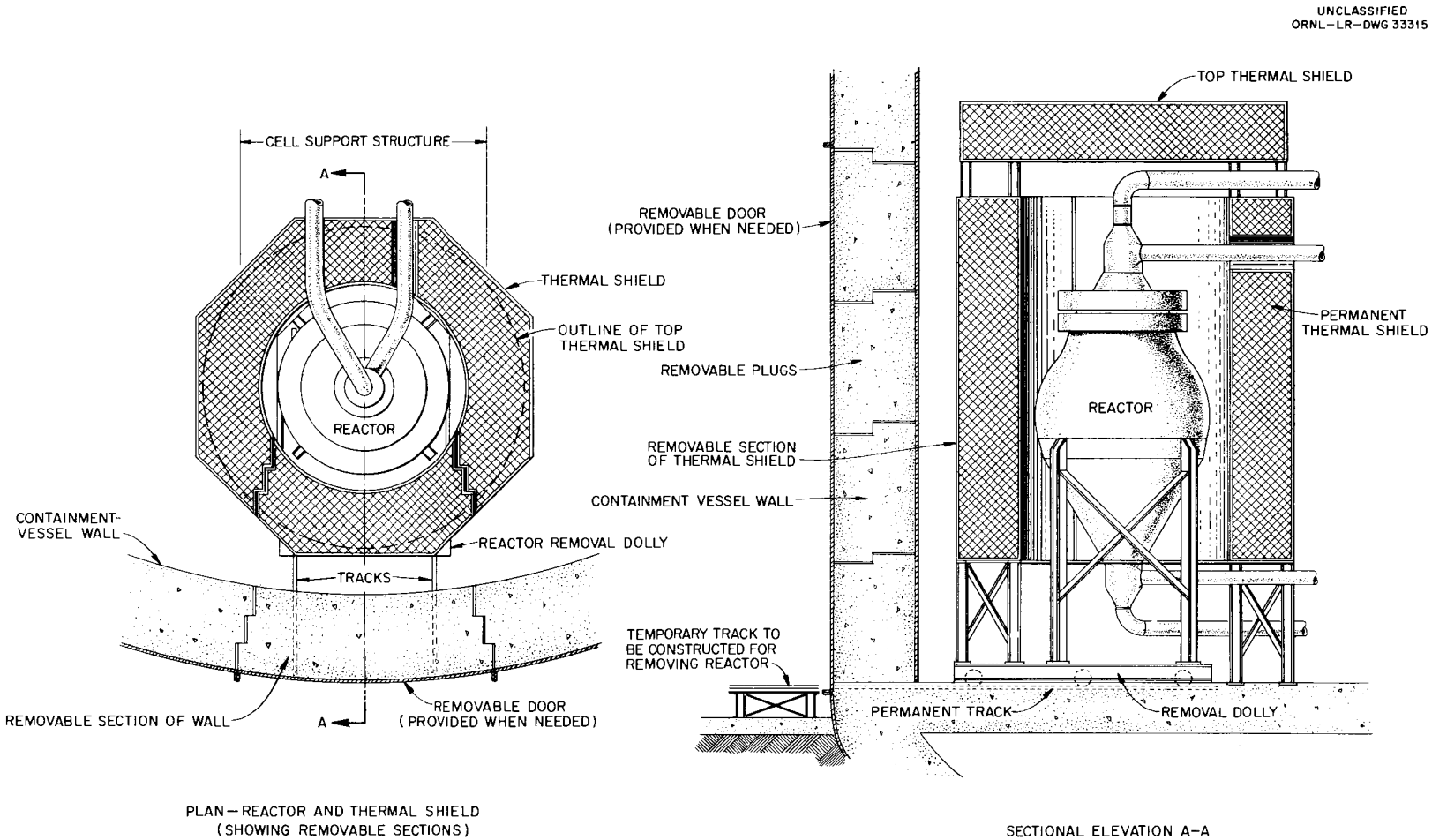

Fig. 7.4. HRE-3 Conceptual Design, Reactor-Vessel Compartment.

order to devise a suitable design concept applicable to a large-scale power plant. This factor has been assumed to limit each steam generator to a single unit capable of fulfilling the design specifications (i.e., a single shell and tube bundle rather than multiple arrangements).

It is believed that the most practical maintenance philosophy for HRE-3 is to make repairs to the heat exchangers in a shielded area external to the reactor shield. The reactor shutdown time would probably be less with this procedure than with making repairs in place.

The effects of tube size and primary-fluid velocity on heat transfer area required, primary-fluid hold-up, pressure drop, and number and length of tubes were determined for units with a single shell and tube bundle and with natural circulation on the shell side. Yearly costs were estimated as a

UNCLASSIFIED
ORNL-LR-DWG 33316

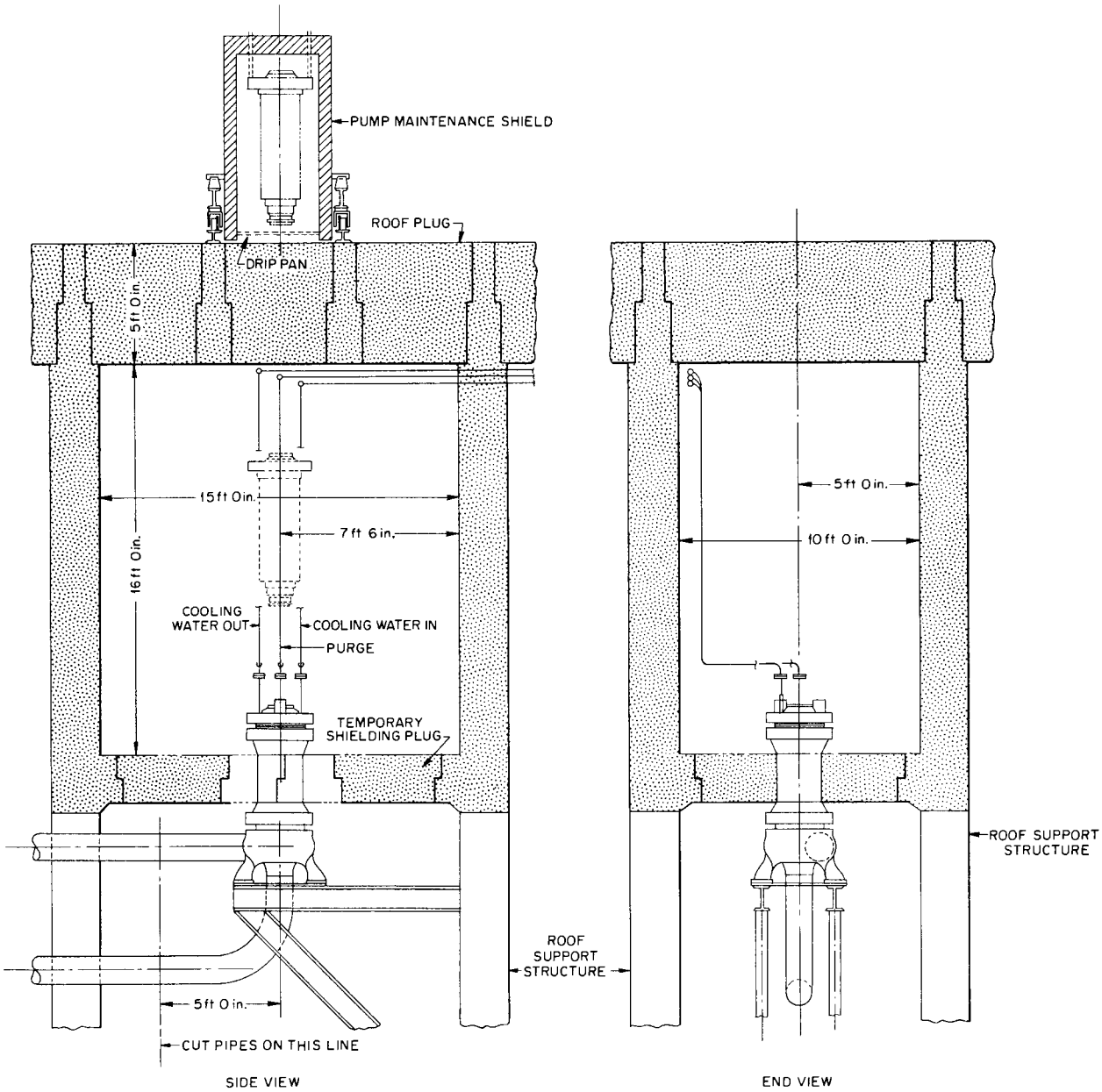

Fig. 7.5. HRE-3 Conceptual Design, Circulating-Pump Compartment.

UNCLASSIFIED
ORNL-LR-DWG 33317

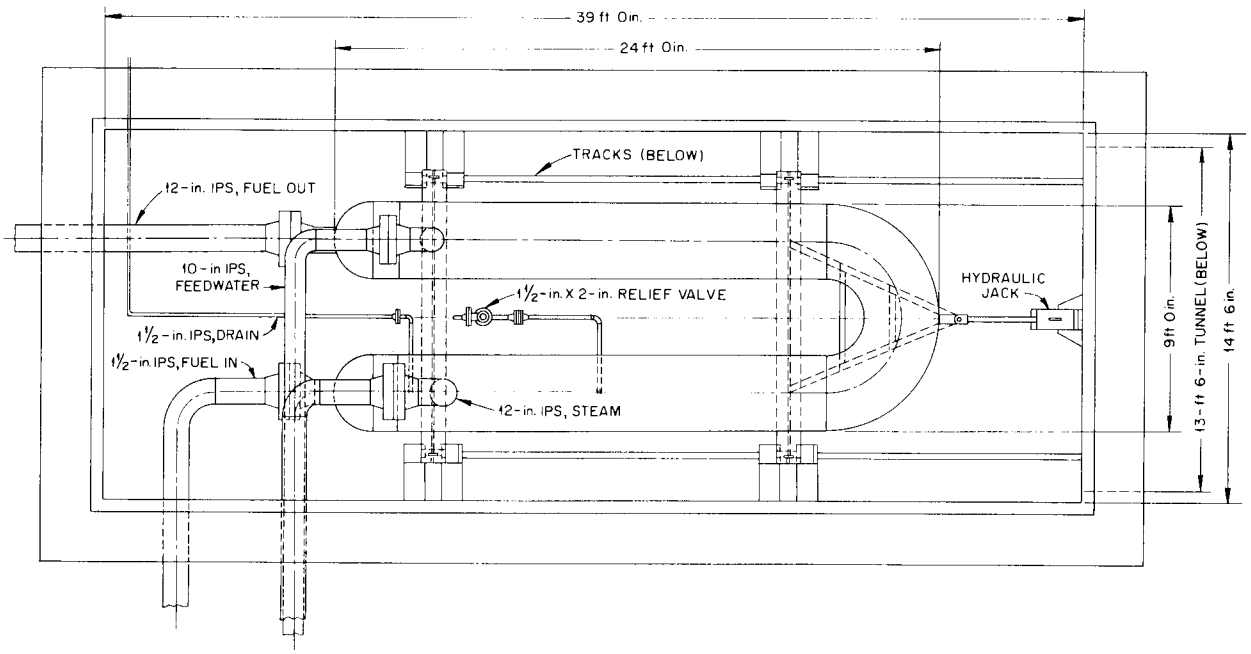

Fig. 7.6. HRE-3 Conceptual Design, Fuel Heat Exchanger Compartment.

function of primary-fluid velocity, with tube size as a parameter.

The design concept suggested for the fuel heat exchanger is a U-tube, U-shell horizontal unit with 950 tubes $\frac{5}{8}$ in. in outside diameter, 14 BWG (0.083-in. wall), and 43 ft average length. The fuel velocity in the tubes is 12 fps, which gives a pressure drop of 15 psi across the unit.

The design concept suggested for the blanket heat exchanger is an inverted L-tube unit with 500 tubes $\frac{5}{8}$ in. in outside diameter, 14 BWG (0.083-in. wall), and 12 ft average length. The slurry velocity in the tubes is 14 fps, which gives a pressure drop of 16 psi across the unit. It is believed that a vertical unit is less likely to become plugged with slurry than a horizontal unit, although this belief has not been substantiated by experiment. The general configurations of the heat exchangers are shown in Figs. 7.6 and 7.7.

7.2.3 Pressurization

Calculations of the effects of pressurizing with oxygen-helium or oxygen-argon mixtures indicate that such a system is feasible but not necessarily more desirable than one utilizing oxygen alone. Figure 7.8 shows the percentage of oxygen in the pressurizing gas vs the mole fraction of oxygen in solution in the pressurizer at various pressurizer temperatures.

7.2.4 Fuel Dump-Tank Concept

A fuel dump-tank concept is shown in Fig. 7.9. This tank, consisting of an array of thirty 5-in. pipes attached to six 10-in. headers, is shown submerged in water to provide shutdown cooling and pressure reduction during a dump.

7.3 HRE-4 PRELIMINARY DESIGN

The HRE-4 is planned as a single-region reactor, with a slurry of the oxides of thorium and U^{235} in heavy water as the circulating fuel. The purpose of this reactor is to study criticality and operational problems, maintenance problems, the effects of radiation on slurry fuels and container materials, the effectiveness of deuterium-oxygen recombination catalysts, and the distribution of fission products. Following operation at practical two-region core concentrations, it is planned to operate the reactor with higher ThO_2 slurry concentrations, approaching those required in the blanket of a two-region breeder reactor.

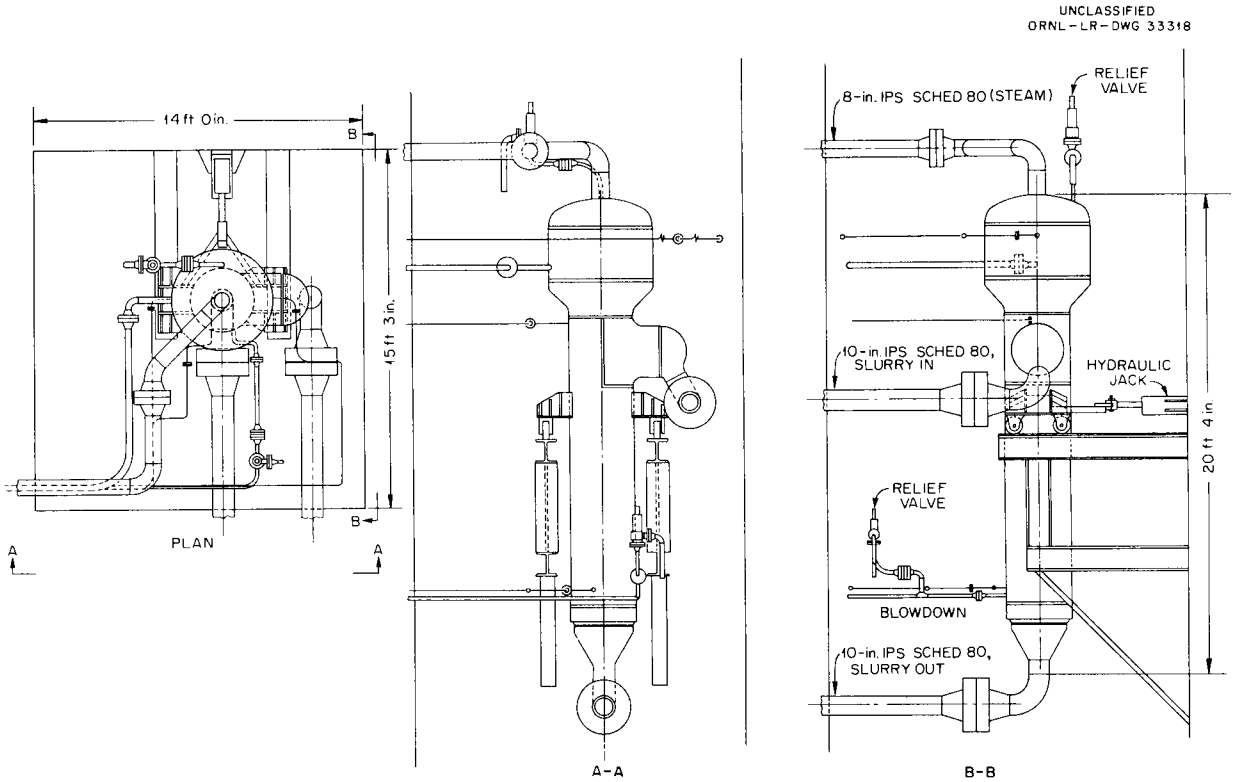

Fig. 7.7. HRE-3 Conceptual Design, Blanket Heat Exchanger Compartment.

The maximum reactor power level attainable will be a function of the pumping performance, of the slurry properties, and of the heat exchanger design, and is expected to be in the range of 1 to 5 Mw. Because it is planned to use D_2O, a reactor vessel of 4.5 ft inside diameter is required, and the slurry concentration to achieve criticality will be about 200 g of Th per liter, with about 8% U to Th. The design core temperature[3] is 280°C.

Preliminary design studies have been completed which outline some of the broad features of the HRE-4 design problem. Some of these are summarized in Secs 7.3.1 through 7.3.4.

[3]B. E. Prince, *Survey of Nuclear Characteristics of Small, One-Region Slurry Reactors*, memorandum, HRP-58-240 (June 4, 1958).

7.3.1 Flowsheet

The main slurry circulating loop of HRE-4 consists of the reactor vessel, heat exchanger, and canned-rotor pump. A full-pressure dump tank is proposed to provide for concentration of the feed slurry and for pressurization of the reactor loop. A small overpressure of oxygen may be desirable to control corrosion. An internal catalyst will be circulated with the slurry for recombination of radiolytic gases, and a supplemental scavenging high-pressure recombiner external to the loop will be provided. Use of a dump tank at system pressure of about 1500 psia removes the design requirements for high-differential-pressure dump valves and feed pumps, or eductors. Level control in the system will be maintained by an overflow to

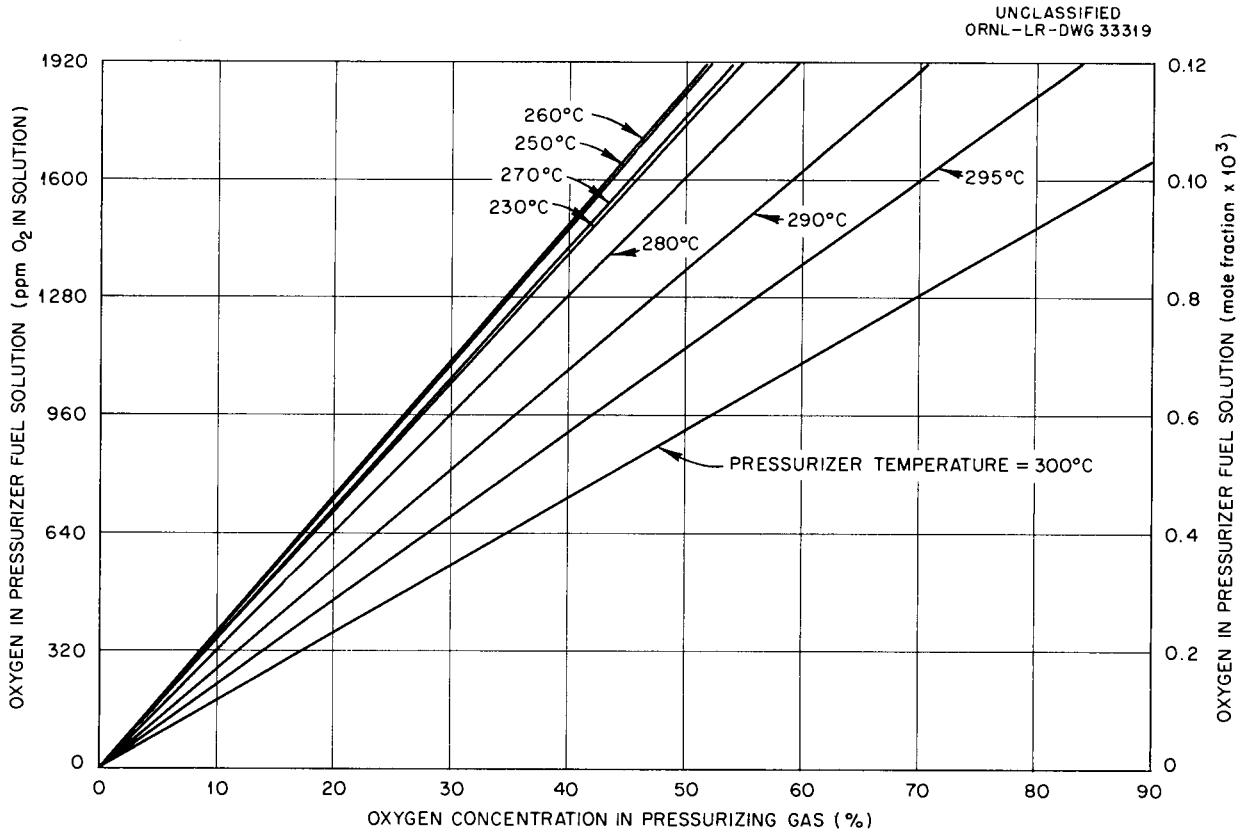

Fig. 7.8. Required Percentage of Oxygen in the Pressurizing Gas Mixture.

the dump tank. The system will avoid horizontal lines and pockets from which slurry would be difficult to drain, purge, or rinse. Purge water for the circulating pump and other points and the rinse-water supply will be obtained as condensate from the pump tank. A tentative flowsheet for the high-pressure system is shown in Fig. 7.10.

7.3.2 Heat Exchanger

Preliminary studies have been made for establishing a 5-Mw heat exchanger design concept based on performance characteristics of an existing 300-gpm canned-rotor circulating pump. Heat exchanger types with slurry in the tube and with slurry in the shell were considered, with boiling water on the secondary side in each case. It was concluded that the requirement of 5 Mw of heat removal with a 300-gpm circulating rate is incompatible with the requirements for compactness, drainage, and system pressure loss due to flow. To obtain a more reasonable design of a heat exchanger for 5 Mw of heat removal, it was judged that the flow rate would have to be several times greater than 300 gpm. Studies are in progress of heat exchangers designed for the greater flow rates obtainable with other canned-rotor pumps that are currently available or that are amenable to short-term development. Parallel operation of pumps will also be considered.

7.3.3 Conceptual Layouts

An attempt is being made to lay out the HRE-4 high-pressure system in the existing ART containment vessel located in Building 7503. This vessel, designed for 200 psig, is a 24-ft-dia vertical cylinder with hemispherical ends and has an over-all height of 36 ft. It is believed that the ART site, presently in disuse, would offer substantial savings in the cost of the physical plant for the HRE-4, since the existing diesel-driven auxiliary a-c power supply, axial blowers and stack system for reactor heat removal, and other service systems can be utilized with little modification. Considerable alterations may be required, however, to the shielding around the containment vessel to provide operating access to

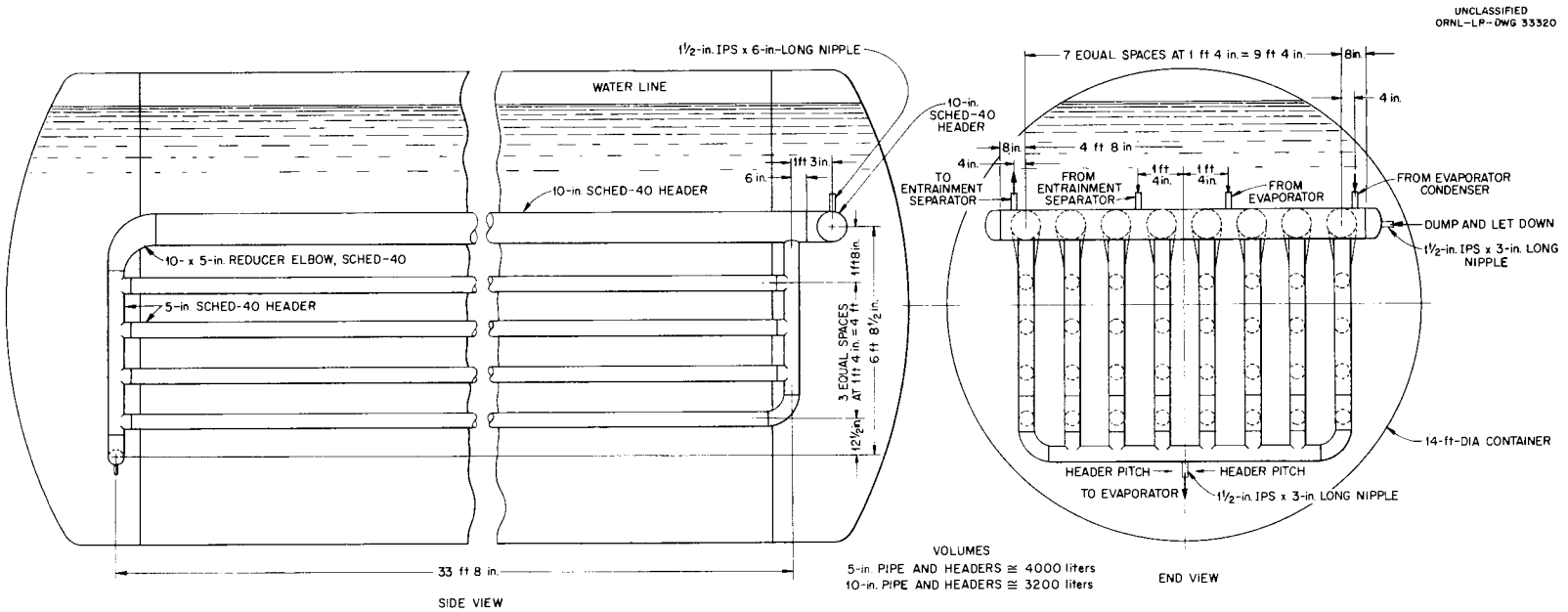

Fig. 7.9. HRE-3 Conceptual Design, Fuel Dump Tank.

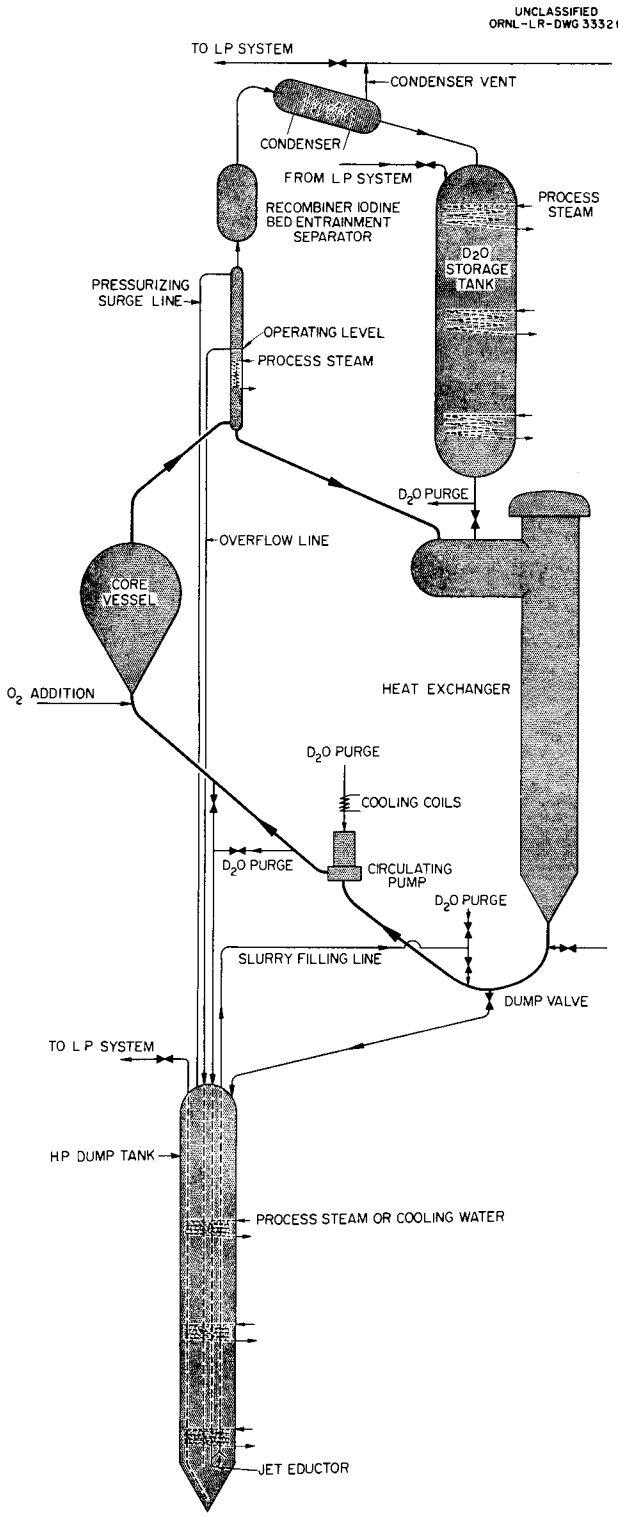

Fig. 7.10. HRE-4 Preliminary High-Pressure Flowsheet.

equipment and controls. Also, the existing shielding will be inadequate to reduce the HRE-4 radiation to an acceptable tolerance, unless additional shielding is provided around the reactor vessel. Space requirements inside the containment vessel may dictate that the extra shielding be provided outside the existing shield, although in this case rather extensive building modifications will be required.

7.3.4 Heat Removal System

Although the HRE-4 at a 5-Mw reactor power level will have an electric generating potential of about 1200 kw, the investment required to recover this energy appears impractical in light of the primary objectives of the experiment. For this reason, it is planned that HRE-4 reactor heat will simply be dissipated to the atmosphere through use of an air-cooled coil. Two 250-hp axial blowers, each of 83,000-cfm capacity at a static pressure of 7 in. H_2O, are in place, together with the necessary ducting, dampers, and discharge stack.

The water for cooling the main slurry heat exchanger may be allowed to boil to generate steam for condensing in the air-cooled coil, or it may be pressurized to provide a single-phase circulating system. The steam-generating type of system would more closely simulate the conditions of possible future application of the reactor type, but the HRE-4 is considered to be a slurry testing reactor rather than a power-reactor prototype. The better heat transfer coefficients obtainable with a boiling film are an important argument for the steam-generating arrangement. Although the full-load steam pressure would be about 325 psia, the steam system would be designed for 2000 psia to permit heating of the reactor system by means of auxiliary steam during startup. If the steam is condensed in a low-pressure air-cooled coil, a high-head feedwater pump of about 25 hp will be required. Use of a pressurized-water circulating system would have the advantage of elimination or reduction of the problems of water-level control, heat exchanger blowdown, chemical treatment of feedwater, and relative elevation of the parts of the system. A low-head circulating pump could be used. An external heater for the water system would have to be provided to permit heating by the water during startup.

8. RESEARCH AND ANALYSIS

P. R. Kasten

L. L. Bennett
R. Benumof[1]
R. Chalkley
R. D. Cheverton
H. C. Claiborne
L. D. Felton[2]
T. B. Fowler
S. Jaye
M. P. Lietzke
T. H. Mauney
W. R. Mixon
C. S. Morgan
R. H. Nimmo
M. W. Rosenthal
P. G. Sexton[2]
D. G. Thomas
M. Tobias
E. H. Volk[3]

8.1 SOME NUCLEAR CHARACTERISTICS OF SPHERICAL DOUBLE-BLANKET REACTORS

It has been suggested that a high-concentration thorium oxide blanket for a breeder reactor might be managed by operation as a fluidized bed rather than as a circulating slurry. Two forms of blanket have been assumed in this study, each of which might be called a double-slurry blanket. The first is associated with fluidizing a high-concentration slurry in a narrow region adjacent to the core and allowing fines to circulate in a larger outer blanket which would have a much lower thorium concentration. The other approach involves fluidization of a low-concentration slurry in the narrow inner blanket, the outer blanket being the region of high thorium concentration. These concepts have been compared with each other and with the single-region blanket system from a nuclear-characteristics viewpoint.

In the calculations for the first concept mentioned above, the double blanket consists of a ½- or 1-ft-thick region (region II) filled with a very high concentration of thorium (4000 g/liter) and surrounded by a 1½- or 2-ft-thick region (region III) containing a lower concentration of thorium (0, 500, or 1000 g/liter). For the other approach the thorium concentrations are reversed. Both fertile regions have been assumed to be ThO_2 slurries in heavy water. The central fuel region (region I) is a 4-ft-dia sphere containing uranyl sulfate–heavy-water solution. The reactor temperature is 280°C. For simplicity, absorptions in sulfur, higher isotopes, and protactinium have been neglected. Regions I, II, and III are separated by ½-in.-thick zirconium tanks; the outer vessel is type 347 stainless steel, 6 in. thick and 9 ft in inside diameter. Figure 8.1 illustrates the arrangement, numbering, and actual dimensions of the various regions.

Twenty-eight cases were selected for examination so that the effects of individual parameters and conditions could be studied. A more detailed discussion of the calculations is given elsewhere.[4] The following observations may be made on the basis of the results:

1. If the region next to the core contains the high-concentration slurry (4000 g of Th per liter) and settling occurs in the outer region, reactivity effects would be negligible. There is practically no change in critical concentration in the core for outer-blanket thorium concentrations between 0 and 1000 g/liter. This behavior appears to be independent of the presence or absence of poison in the core or fuel in the blanket and was noted for both ½- and 1-ft-thick inner blankets.

2. In contrast, if the outer region contains 4000 g of Th per liter and the inner-blanket thorium concentration changes, then the core critical concentration undergoes substantial changes. It is clear that large (about 10%) reactivity additions can accompany settling in the inner blanket.

3. The breeding ratios for reactors with concentrated inner blankets are generally higher than those for reactors with concentrated outer blankets. No double-blanket case showed any important breeding-ratio advantage over a single-blanket-region reactor.

4. The concentrated-outer-region cases showed much the largest inventories of thorium and fuel (for 3 g of U^{233} per kg of Th in the blanket). On the other hand, it may be possible, without loss in breeding ratio, to reduce inventories significantly from those in a single-blanket-region system if a high-concentration inner blanket is used.

[1]Summer research participant.

[2]Summer employee.

[3]On loan from Combustion Engineering, Inc.

[4]M. Tobias and T. B. Fowler, *Some Nuclear Characteristics of Spherical Double-Blanket Reactors*, ORNL CF-58-4-66 (April 18, 1958).

UNCLASSIFIED
ORNL—LR—DWG 33322

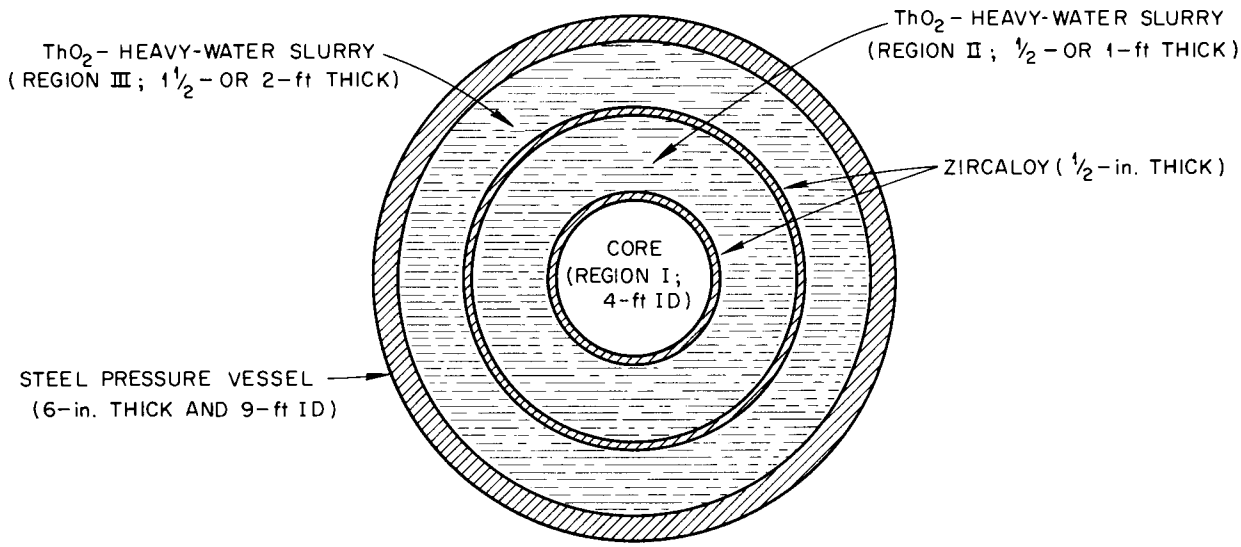

Fig. 8.1. Dimensions and Notation of Double-Blanket Reactors.

5. In all cases where 3 g of U^{233} per kg of Th was assumed to be present in the blankets, between 82 and 85% of the total reactor power was generated in the core. Between 14 and 16% of the power was generated in the inner blanket for the high-concentration cases, and up to 12% was generated when the inner region was low in thorium.

6. The ratio of core-wall thermal flux to core-average thermal flux ranged between 0.35 and 0.61. This ratio depended almost entirely upon the concentration of thorium present in the blanket region adjacent to the core and decreased with increasing thorium concentration. At a given core power the inner wall power density for 4000 g of Th per liter in the inner blanket would be about three-fourths that for 1000 g/liter in the inner blanket.

8.2 DETERMINATION OF HRE-3 BREEDING RATIO

An examination has been made of the accuracy with which the breeding ratio of HRE-3 can be determined after either 100 days or one year of full-power operation. The mean breeding ratio over a period of time, represented by $BR_m(0 \to t)$, is defined as the ratio of the fissionable material produced to that which is destroyed; the amount produced is the algebraic sum of that destroyed, or burnup (BU), and the increase in the inventory of the system, ΔI. Mathematically, this can be expressed by

$$(1) \qquad BR_m(0 \to t) = \frac{BU + \Delta I}{BU} = 1 + \frac{\Delta I}{BU} \ .$$

The burnup is equal to the sum of the amounts of U^{233} and U^{235} destroyed in the core and the blanket:

$$(2) \qquad BU = BU_c^{23} + BU_c^{25} + BU_b^{23} + BU_b^{25} \ ,$$

where the superscripts 23 and 25 refer to U^{233} and U^{235}, respectively, and where the subscripts c and b refer to the core and blanket regions, respectively. The increase in inventory is equal to the system inventory at time t, plus any withdrawals made during the period considered and minus the fuel added to the system (the initial fuel inventory is considered as a fuel addition). This can be expressed by

$$(3) \quad \Delta I = I_c^{23} + I_c^{25} + I_b^{23 + 13} + I_b^{25} + W^{23} + W^{25} - F^{23} - F^{25} \ ,$$

where I is the inventory, W the fuel withdrawal, F the fuel addition, and the superscript 13 refers to Pa^{133}. The quantities in the preceding equations can be determined by the methods discussed below.

Determination of F^{23}, F^{25}. – The amount of uranium added to the system can be measured as accurately as needed. The isotopic composition can be determined by mass-spectrometric means, and equipment giving analyses as accurately as desired will probably be available.

Determination of W^{23}, W^{25}. – The most accurate method of obtaining W^{23} and W^{25} is to dissolve all material withdrawn from the system (to ensure homogeneity) and then determine the uranium content by analysis.

Determination of I_c^{23}, I_c^{25}, I_b^{23+13}, I_b^{25}. – If the fuel inventories are to be ascertained without interrupting the operation of the reactor, the reactor contents must be sampled and analyzed. The danger in this procedure is, of course, that the sample may not be representative. This could easily result from the system not being homogeneous, owing to precipitation of some uranium, or from fuel incorporated in a film of corrosion products. The HRT experience in determining fuel inventory illustrates the difficulties associated with this approach. It may be possible to determine inventory by always adding fuel containing a given percentage of U^{238}; determination of the uranium-isotope ratios based on U^{238} concentration would enable inventory to be calculated. However, use of natural uranium in pretreatment and shakedown would make the U^{238} inventory uncertain. Determination of U^{233} in slurry by the ratio of U^{233} to thorium has the hazard that part of the thorium might accumulate in a stagnant region and not attain the same fuel concentration as the rest. Probably the most dependable way of obtaining the inventories is to drain the blanket and core systems, flush each with reagents that will remove any deposited fuel, and then dissolve the complete inventories. The systems would then be homogeneous, and the contents could be determined accurately by analysis.

Determination of BU_c^{23}. – The core U^{233} burnup could be determined by the net change in U^{233} inventory, given by

$$BU_c^{23} = F_c^{23} - I_c^{23} - W_c^{23} \quad . \tag{4}$$

Determination of BU_c^{25}. – The core U^{235} burnup might be determined by using $\bar{\alpha}_{25}$, the average ratio of neutron capture to fission in U^{235}, and the change in U^{236} inventory. This can be written as

$$BU_c^{25} = \left(I_c^{26} + W_c^{26} - F_c^{26}\right) \frac{1 + \bar{\alpha}_{25}}{\bar{\alpha}_{25}} \quad . \tag{5}$$

The correct average α_{25} would be estimated by multigroup calculations to properly weight the data for energy dependence. This procedure for determining BU_c^{25} ignores the loss of U^{236} by neutron absorption, which would be insignificant for reasonable periods of operation if the feed were essentially free of U^{235} and U^{236}.

Determination of BU_b^{23}. – Two methods of estimating the blanket U^{233} destruction appear feasible, although neither may be very accurate: (1) isolate some long-lived radioactive fission products and determine their concentrations by counting techniques, using a system calibrated for the isotopes used; (2) use multigroup estimates of reactor conditions to compute the blanket burnup from the measured core burnup.

Determination of BU_b^{25}. – The value for BU_b^{25} is so small for reasonable periods of operation that it can be completely neglected ($BU_b^{25}/BU_b^{23} \approx 0.01\%$ for 480 days at 60 Mw).

The maximum fractional error in the breeding ratio, $\delta BR_m/BR_m$, can be obtained from the estimated limits of error in the various quantities that are involved, and can be represented by

$$\frac{\delta BR_m}{BR_m} = \sum_i \left| \left(\frac{\partial BR_m/BR_m}{\partial X/X} \right)_i \left(\frac{\delta X}{X} \right)_i \right| \quad , \tag{6}$$

where $X \equiv I$'s, F's, W's, etc., and the summation over i represents the summation over the various values of X. The equations for the various partial derivatives appearing in Eq. 6 have been formulated and are given in the second column of Table 8.1 divided by $\Delta I/(BU + \Delta I)$, which appears in every term.

The values of the various quantities of interest are given in Table 8.2. An operating period of 100 days and also of one year is considered, assuming a core power of 50 Mw. These values

Table 8.1. Effect of Measurement Errors on Breeding-Ratio Determination in HRE-3

Quantity, X	$\frac{\partial BR_m/BR_m}{\partial X/X} \div \frac{\Delta I}{BU + \Delta I}$	Measurement Error (%)						
		Case I			Case II		Case III	
		$\frac{\delta X}{X}$	$\delta BR_m/BR_m$ for 100 Days	$\delta BR_m/BR_m$ for 1 Year	$\frac{\delta X}{X}$	$\delta BR_m/BR_m$ for 100 Days	$\frac{\delta X}{X}$	$\delta BR_m/BR_m$ for 1 Year
I_c^{23}	$\frac{I_c^{23}}{\Delta I} + \frac{I_c^{23}}{BU}$	±0.5	±1.05	±0.55	±2.7	±5.66	±9.2	±5.04
I_c^{25}	$\frac{I_c^{25}}{\Delta I}$	0.5	0.0011	0.0026	2.7	0.0060	9.2	0.048
I_c^{26}	$\frac{BU_c^{25}}{BU} \times \frac{I_c^{26}}{I_c^{26} + W_c^{26} - F_c^{26}}$	0.5	<0.001	<0.001	2.7	<0.001	9.2	0.0054
I_b^{23+13}	$\frac{I_b^{23+13}}{\Delta I}$	0.5	0.49	0.46				
I_b^{25}	$\frac{I_b^{25}}{\Delta I}$	0.5	<0.001	<0.001				
W_c^{23}	$\frac{W_c^{23}}{\Delta I} + \frac{W_c^{23}}{BU}$	0	0	0				
W_c^{25}	$\frac{W_c^{25}}{\Delta I}$	0	0	0				
W_c^{26}	$-\frac{BU_c^{25}}{BU} \times \frac{W_c^{26}}{I_c^{26} + W_c^{26} - F_c^{26}}$	0	0	0				
F_c^{23}	$-\frac{F_c^{23}}{\Delta I} - \frac{F_c^{23}}{BU}$	0	0	0				
F_c^{25}	$-\frac{F_c^{25}}{\Delta I}$	0	0	0				
F_c^{26}	$\frac{BU_c^{25}}{BU} \times \frac{F_c^{26}}{I_c^{26} + W_c^{26} - F_c^{26}}$	0	0	0				

Table 8.1 (continued)

Quantity, X	$\frac{\partial BR_m/BR_m}{\partial X/X} \doteq \frac{\Delta I}{BU + \Delta I}$	Measurement Error (%)						
		Case I			Case II		Case III	
		$\frac{\delta X}{X}$	$\delta BR_m/BR_m$ for 100 Days	$\delta BR_m/BR_m$ for 1 Year	$\frac{\delta X}{X}$	$\delta BR_m/BR_m$ for 100 Days	$\frac{\delta X}{X}$	$\delta BR_m/BR_m$ for 1 Year
$\bar{\alpha}_{25}$	$-\frac{BU_c^{25}}{BU}$	17	0.0010	0.010				
BU_b^{23}	$\frac{BU_b^{23}}{BU}$	30	0.054	0.26				
BU_b^{25}	$-\frac{BU_b^{25}}{BU}$	0	0	0				
Total			±1.6	±1.3		±5.7		±5.1

were estimated[5] with an Oracle routine which predicts the time-dependent behavior of two-region reactors. It was assumed that the feed was pure U^{233}, that the initial blanket material was free of uranium, and that there were no fuel withdrawals over the operating period.

Table 8.1 gives the errors associated with a determination of BR_m; these values are based on estimated errors in individual measurements of the quantities in Table 8.2. The error in $\bar{\alpha}_{25}$ is taken as ±20% and that in BU_b^{23} as ±30%. The error in BR_m due to different errors is given for three cases. The errors in the inventories are taken as ±0.5% in case I. The consequences of not accounting for uranium in the corrosion film are treated in cases II and III. If generalized attack is at a rate of 1.0 mpy and if the film is 1% uranium, the deposited fuel amounts to 2.7% of the inventory after 100 days of operation (case II) and 9.2% after one year (case III). The errors shown in Table 8.1 are for these conditions, but for other corrosion rates or uranium concentrations the values would be proportionate.

For the assumed conditions of operation, the major sources of error would be the core inventory of U^{233} and the blanket inventory of U^{233} and Pa^{233}, and for a longer period of operation, the burnup of U^{233} in the blanket might be important. Accumulations of uranium in the reactor that are not detected by sampling probably would produce much larger errors than those from other sources. A breeding ratio determined by draining and flushing the system is likely to be much more dependable than one obtained by sampling.

8.3 INFLUENCE OF CORE INLET-OUTLET LINE ON HRE-3 FLUX DISTRIBUTION AND BREEDING RATIO

The CURE code[6] for the IBM-704 has been used to examine the effect of the concentric inlet-outlet line on the breeding ratio, critical mass, and flux distribution of the HRE-3. This code, with the use of two or more neutron groups, solves the two-dimensional neutron-diffusion equations numerically. For the cases considered here, r-z geometry and two energy groups were used (with fissions occurring only in the slow group). About 14 iterations on the flux distribution (at 2 min per iteration) were required to converge to the value of ν which makes the reactor critical for a given fuel concentration.

[5] M. Tobias, M. W. Rosenthal, and T. B. Fowler, *Time-Dependent Studies of the Nuclear Characteristics of HRE-3*, ORNL CF-57-12-1 (Dec. 31, 1957).

[6] E. L. Wachspress, *CURE: A Generalized Two-Space-Dimension Multigroup Coding for the IBM-704*, KAPL-1724 (April 30, 1957).

Table 8.2. Conditions of HRE-3 After 100 Days and After One Year of Operation

Initial core U^{233} inventory: 13.50 kg

No other isotopes present

Quantity	Symbol	After 100 Days	After 1 Year
Inventory (kg)			
Core U^{233}	I_c^{23}	13.60	13.53
Core U^{234}	I_c^{24}	0.62	2.01
Core U^{235}	I_c^{25}	0.017	0.15
Core U^{236}	I_c^{26}	<0.001	0.016
Blanket U^{233}	I_b^{23+13}	7.36	26.13
Blanket U^{234}	I_b^{24}	0.026	0.25
Blanket U^{235}	I_b^{25}	<0.001	0.0019
Blanket U^{236}	I_b^{26}	<0.001	<0.001
Cumulative U^{233} additions (kg)	F_c^{23}	19.94	36.10
$U^{233} + U^{235}$ inventory increase (kg)	ΔI	1.04	3.71
Burnup (kg)			
Core U^{233}	BU_c^{23}	6.34	22.57
Core U^{235}	BU_c^{25}	0.0028	0.11
Blanket U^{233}	BU_b^{23}	0.083	1.61
Blanket U^{235}	BU_b^{25}	<0.001	<0.001
Total $U^{233} + U^{235}$ burnup	BU	6.42	24.29
Integrated core power (Mwd)		5050	18,050
Integrated blanket power (Mwd)		66	1285

While it is possible to mock up curved shapes by using a jagged outline, it was considered sufficient for present purposes to employ two concentric "square" cylinders rather than concentric spheres. The reactor configurations considered are given in Fig. 8.2. The inner cylinder was 43.9 in. in inside height and diameter, while the inner dimensions of the outer cylinder were 103.9 in. A ½-in.-thick Zircaloy tank separated the core solution (UO_2SO_4 in D_2O) from the blanket slurry (1000 g of Th, as ThO_2, per liter in D_2O). The pressure vessel was taken as 6 in. of steel. The "neck" had a length of 36 in. from the inside of the core to the outside of the pressure vessel and was 15 in. in diameter. A total of 575 mesh points were used in the calculation, 143 of which were used for the core without the neck and 191 were for the core with the neck.

No poisons were considered in the core region, and the blanket did not contain any fuel. The reactor temperature was assumed to be 280°C.

The breeding ratio was found to be 1.182 when no neck was present, and 1.178 after addition of the neck; thus the addition of the neck caused a reduction of only 0.3% in the breeding ratio. The critical concentration was about 2% less when the neck region was present. However, the core volume was about 9% greater, so that the critical mass increases owing to the neck.

Figures 8.3, 8.4, and 8.5 show axial and radial ratios of thermal fluxes to core-average thermal fluxes for cases considered. Figure 8.3, which

UNCLASSIFIED
ORNL-LR-DWG 33323

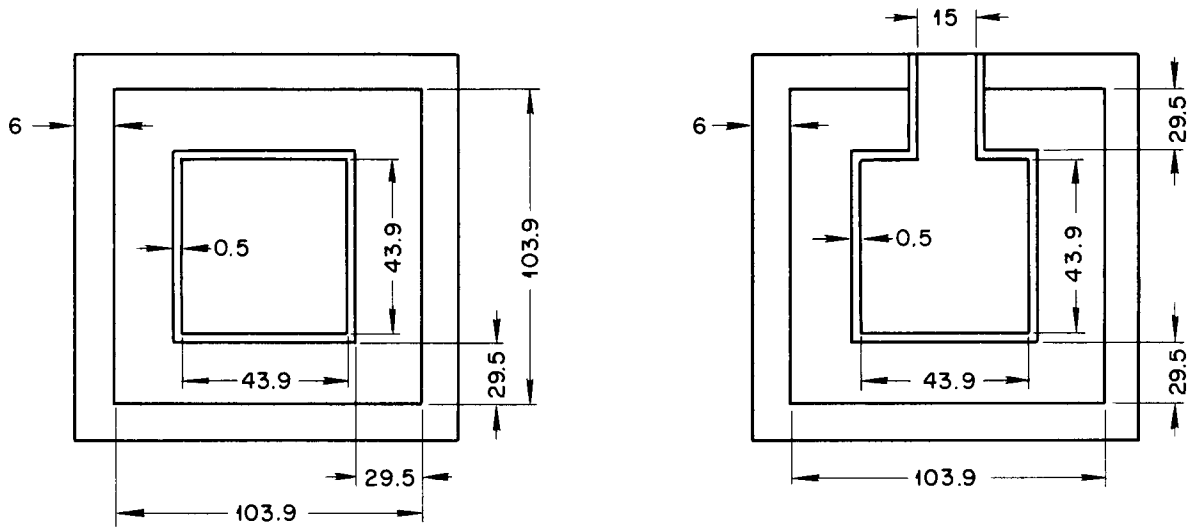

DIMENSIONS ARE IN INCHES

(*a*) WITHOUT NECK (*b*) WITH NECK

Fig. 8.2. Dimensions of the Reactor Configurations Studied with the Use of the CURE Code.

gives the relative flux along a longitudinal traverse down the central axis, shows the axial asymmetry produced by the neck region. It is seen that the flux ratio along this line is higher with the neck added, since the average flux is reduced by inclusion of this low-flux region in the core volume. Figure 8.4 shows that the flux (and therefore the power density) along the core-tank surface in the neck is comparable, for about half its length, to that at the core-tank surface in the main part of the core. The flux distribution on the lower core-tank surface (not shown) appears to be the same both with and without the inlet-outlet line. Figure 8.5, on the other hand, shows that the flux on the upper surface is noticeably higher when the neck is considered. The highest flux ratio at a surface was 0.64 without the neck, while that with the neck was 0.79 (at the lowest point on the neck).

8.4 DECREASE IN HRE-3 BREEDING RATIO CAUSED BY ABSORPTIONS IN CORE TANK AND SHROUD

The HRE-3 breeding-ratio reductions which result from neutron absorptions in the Zircaloy-2 core tank and shroud have been estimated by means of a two-group multiregion code for spherical reactors. In Fig. 8.6 the effect of core-wall thickness on breeding ratio is shown for a spherical 4-ft-ID core in a 9-ft-ID pressure vessel, with a blanket containing 1000 g of Th per liter and 3 g of U^{233} per kg of Th. The additional loss in breeding ratio by absorptions in a concentric, spherical Zircaloy shroud is plotted in Fig. 8.6 as a function of shroud thickness for three spacings of shroud from core tank ("gap" is distance from outside surface of core vessel to inside surface of shroud).

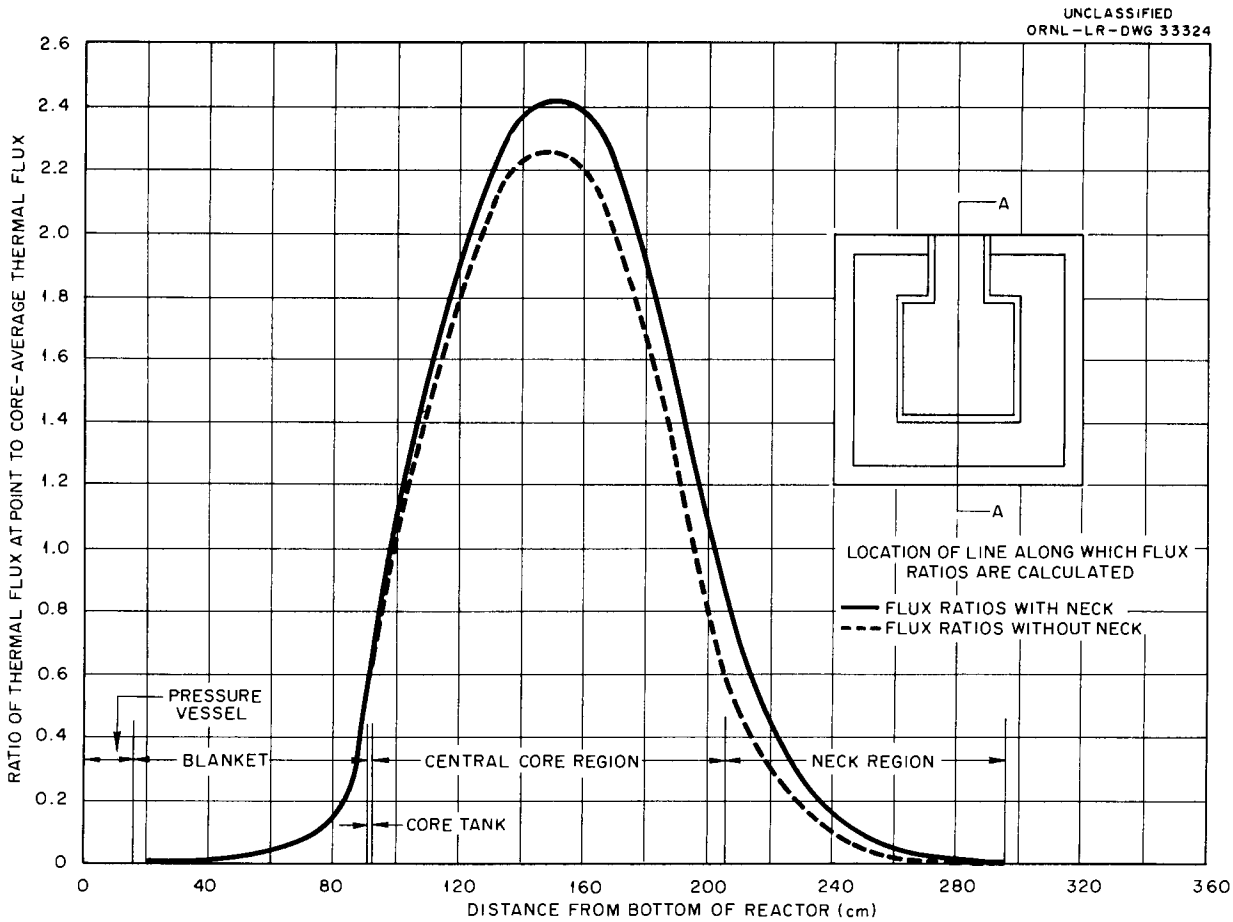

Fig. 8.3. Ratio of Thermal Flux Along Vertical Axis to Core-Average Thermal Flux.

For a reasonable thickness of Zircaloy, the poisoning effect of the core vessel is approximately independent of the shroud thickness and position, and the shroud absorptions are approximately independent of the core thickness. The effects of each can therefore be added. As an example, consider a design with a ½-in. core tank and a ½-in. shroud, 5 in. apart. The breeding ratio would be 0.047 less than if there were no absorptions in the Zircaloy structure.

In obtaining the values shown in Fig. 8.6, the macroscopic absorption cross section of Zircaloy-2 was taken as 0.0059 cm^{-1}, which is 20% above that of pure zirconium. This value is an estimate which includes the effects of various alloying agents and impurities. The results of an analysis[7] of HRT material are shown in Table 8.3, with the ratio of the macroscopic absorption cross section of each constituent to that of the zirconium. The cross section of this sample would be 16% greater than that of pure zirconium.

To check the accuracy of the calculated Zircaloy cross section, the absorption cross section of a specimen of the same material used in the HRT core tank was measured with the X-10 Pile Oscillator. The value obtained was 1.12 times that of pure zirconium; the accuracy was of the order of ±10%, so that the computed value falls within the experimental error. This value is typical of earlier measurements made for similar alloys, and is about 10–20% greater than the result obtained with crystal-bar zirconium.

The values in Fig. 8.6 suffer from (1) the limitations of the two-group technique and (2) the assumption of perfect spherical geometry, whereas

[7] R. E. Morris, *Tests of Special Materials*, Alabama Polytechnic Institute, Auburn, UCNC Contract No. 547 (March 20, 1957).

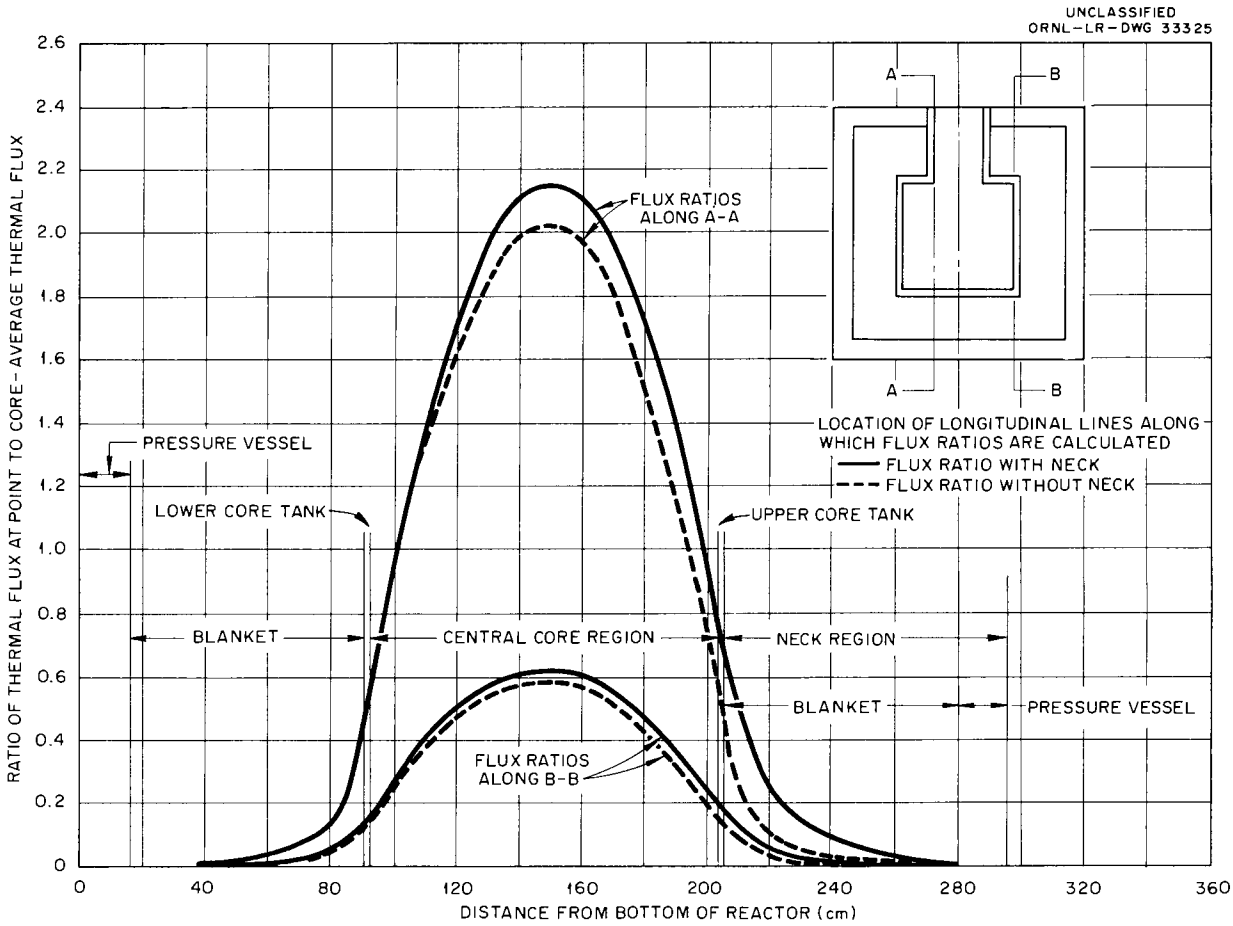

Fig. 8.4. Longitudinal Variation of the Ratio of Thermal Flux at Core-Tank Wall to Core-Average Value.

the HRE-3 will actually have a large inlet-exit line leading from the core. The absorptions in the core tank obtained with the two-group method have been compared with values obtained with the 27-group EYEWASH routine. For the HRE-3 design with a ½-in. core tank and no shroud, the two methods agreed within 4%, and the maximum difference was less than 20% for a variety of core sizes and blanket conditions. The effect of the inlet-exit line on breeding ratio has been found to be quite small (Sec 8.3).

The per cent of total blanket power produced in the gap between the core tank and shroud was obtained from the two-group computations and is plotted in Fig. 8.7 as a function of gap spacing. No core or shroud thicknesses have been specified on the figure, since the fraction of total power generated in the gap is practically independent of these dimensions. With a core power of 50 Mw and a blanket composition of 1000 g of Th per liter and 3 g of U^{233} per kg of Th, the total blanket power is about 10 Mw.

8.5 NEUTRON ABSORPTION IN HRE-3 CORE-INLET PIPE AND POWER DENSITY AT PIPE WALL

Flow studies of re-entrant spherical cores[8] indicate that the HRE-3 core-inlet line should probably extend about ½ pipe ID into the core region to ensure adequate mixing. Only preliminary investigations of cylindrical models have been made, but it is likely that good mixing will necessitate extending the inlet pipe into cylindrical

[8] L. B. Lesem and P. H. Harley, *Scale-up of Alternate HRT Core*, ORNL CF-54-5-47 (May 7, 1954).

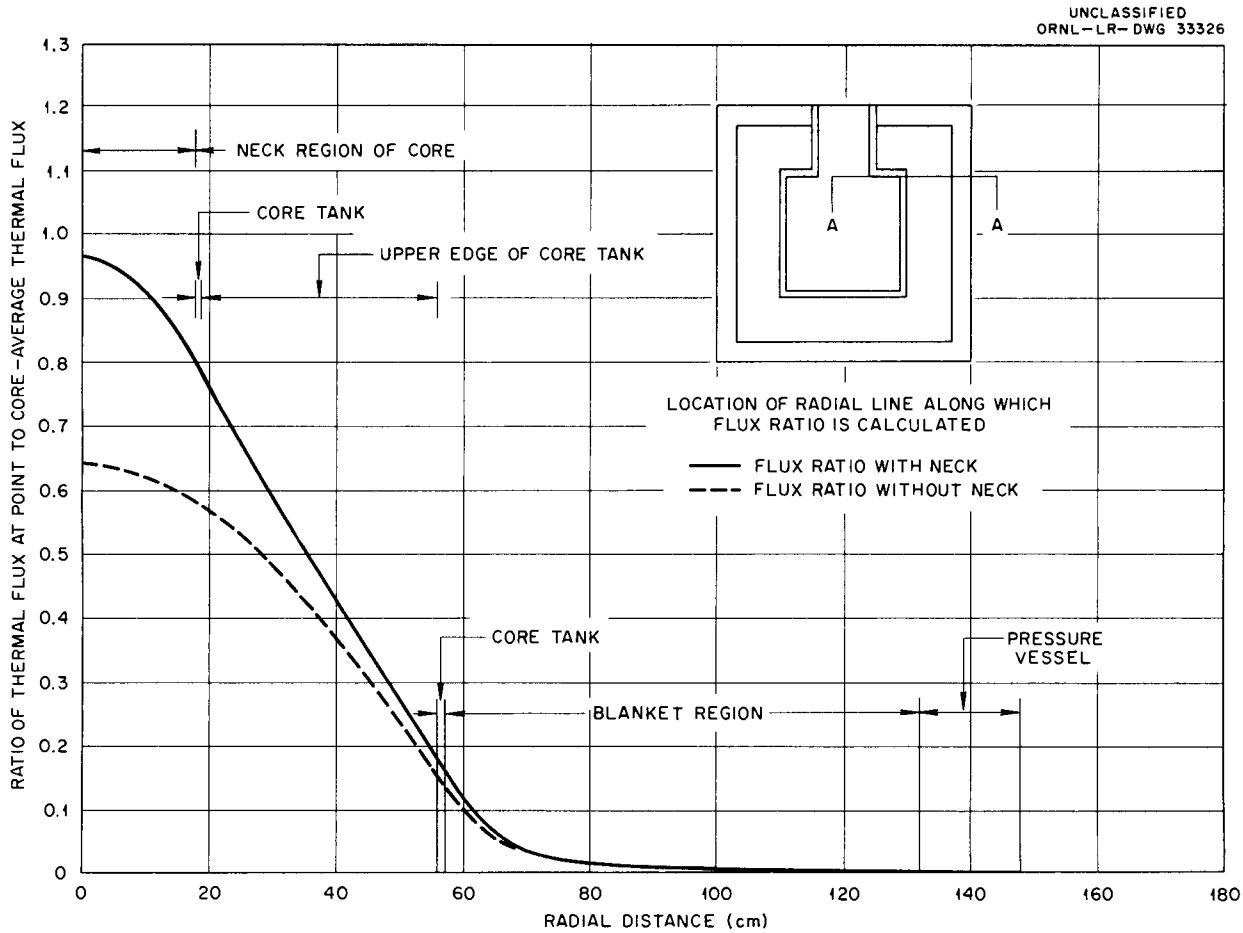

Fig. 8.5. Radial Variation of Ratio of Thermal Flux at Core-Tank Wall to Core-Average Thermal Flux.

cores a minimum of ½ pipe diameter. In order to see what effect the inlet line will have on breeding ratio, estimates of neutron absorptions have been made for two cylindrical cores and one spherical core, with the inlet Zircaloy pipe projecting various distances into the core region. The power density in the fuel solution at the end of the pipe was also computed.

A two-group model for neutron behavior was used; it was assumed that the inlet pipe would have no effect on the flux distribution. The flux distribution in the sphere was computed by means of an Oracle routine for multiregion reactors; the fluxes in the cylinders were obtained by treating the cores as one-region reactors with 6-in. extrapolation distances. Studies of spherical cores have indicated that this method yields results that are in reasonably good agreement with multiregion treatments if the blanket has a high thoria concentration.

Table 8.4 lists the cases studied. The cylinders were treated as if the ends were flat. In all three cases the inlet pipe had a 10-in. diameter and a ½-in. wall thickness.

In Fig. 8.8(*a*) the reduction in breeding ratio is plotted as a function of the fractional penetration (the distance the pipe extends beyond the core wall divided by the length of the vessel). The curves show, for example, that if the line extended 5 in. into the 4-ft sphere, the breeding ratio would be 0.0013 less than if the pipe were not present. The reduction would be 0.006 for a 2-ft penetration into the 7-ft cylinder.

The power density at the exit end of the pipe is shown in Fig. 8.8(*b*) for a core power of 50 Mw. The results for the sphere have been corrected to allow for the effect of the inlet-exit line on the local power densities; flux distributions were obtained from the two-space-variable (CURE)

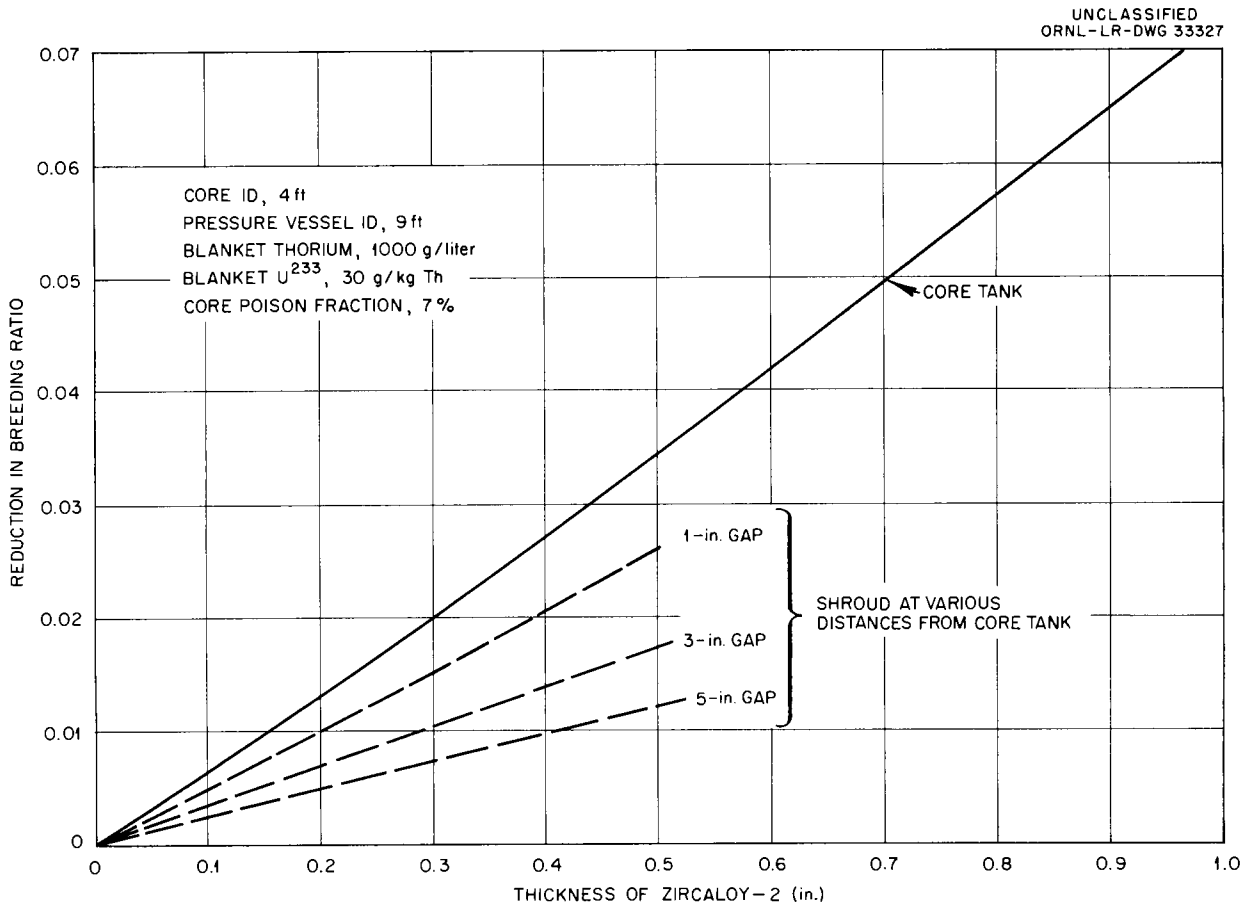

Fig. 8.6. Estimated Reductions in HRE-3 Breeding Ratio from Neutron Capture in Zircaloy-2 Core Tank and Shroud.

computations reported in Sec 8.3. Both the corrected and uncorrected (in which the flux distributions were obtained assuming no inlet pipe) values are plotted in Fig. 8.8(*b*). As shown, the flux distortion resulting from the presence of the "neck" increases the power density near the wall but decreases it at the center. The values for the cylinders have not been corrected in this manner.

If the criterion were established that the maximum power density at the pipe surface should be no greater than the maximum at the core-vessel wall given in Table 8.4, the pipe could extend only 5 in. into the 7-ft cylinder and 10 in. into the 10-ft cylinder. Of course, any penetration beyond the wall of a sphere would lead to higher power densities; at 5 in. the power density would be 57 kw/liter compared with 23 kw/liter at the sphere wall.

8.6 CRITICALITY IN DUMP TANKS FOR HRE-3 BLANKET

The possibility of criticality occurring in the HRE-3 slurry dump tanks has been examined by estimating the critical concentration for an infinite system and comparing it with the concentrations which might conceivably occur if all the core uranium inventory were added to the blanket material. In addition to considering an infinite reactor, the following assumptions were made in obtaining the critical concentration:

1. The fuel is isotopically pure U^{233}.
2. No absorbers are present other than U^{233} and thorium.
3. Nuclear behavior is represented by a Fermi age model with modification to allow for resonance absorptions in fuel. The η of U^{233} is taken to be independent of energy.

Table 8.3. Analysis and Relative Cross Section of HRT Core-Wall Sample*

Element	Analysis (wt %)	Relative Cross Section (%)**
N	0.006	0.4
Fe	0.0959	2.2
Cr	0.0915	2.6
Ni	0.0466	1.9
Sn	1.37	3.5
Al.	0.0045	<0.1
Cu	0.0025	0.1
Pb	0.0045	<0.1
Mg	0.001	<0.1
Co	<0.0020	0.6
Mn	<0.0010	0.1
Si	0.0085	<0.1
Ti	<0.0020	0.1
V	<0.0020	0.1
Mo	<0.0020	<0.1
Cd	<0.000015	0.2
B	0.00002	0.7
Hf	0.0109	3.3
Zr	99.6	100.0
		115.9

*See ref 7.

**Macroscopic cross section of element in sample divided by cross section of zirconium in sample.

Assumptions 1 and 2 are conservative, since an operating reactor would contain protactinium, fission and corrosion products, and higher isotopes of uranium, all of which would increase the critical concentration. Assumption 3 should also be conservative, since η of U^{233} appears to decrease at epithermal energies and since any resonance absorption would tend to decrease the resonance flux. The ratio of U^{233} to thorium required for criticality in an infinite reactor is plotted in Fig. 8.9 for 20 and 280°C as a function of thorium concentration.

The maximum concentration of $U^{233} + U^{235} + Pa^{233}$ in the blanket will be about 3 g per kg of Th. This concentration would be increased to 4.2 g per kg of Th if the equilibrium core inventory of 17.56 kg were *uniformly dispersed* in the blanket thorium. The uranium will probably be associated with the thorium in such a way that this ratio

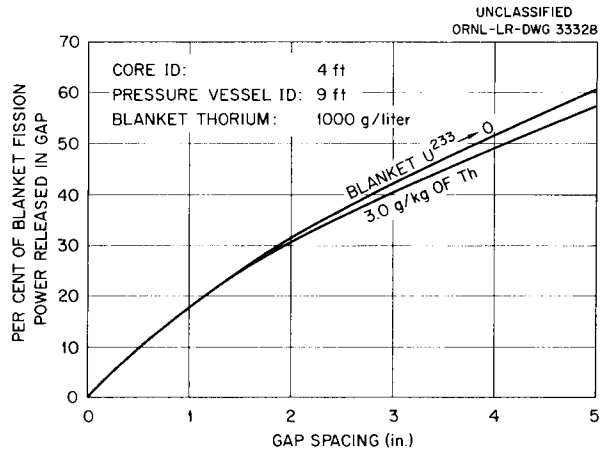

Fig. 8.7. Per Cent of HRE-3 Blanket Fission Power Released in Gap Between Core Tank and Shroud.

Table 8.4. Features of Reactors Analyzed

Core Geometry and Dimensions	Core Volume (liters)	Mean Core Power Density (kw/liter)	Maximum Core-Wall Power Density Without Inlet Line (kw/liter)
4-ft-ID sphere	950	53	23
3-ft-ID × 7-ft cylinder	1400	36	26
3-ft-ID × 10-ft cylinder	2000	25	19

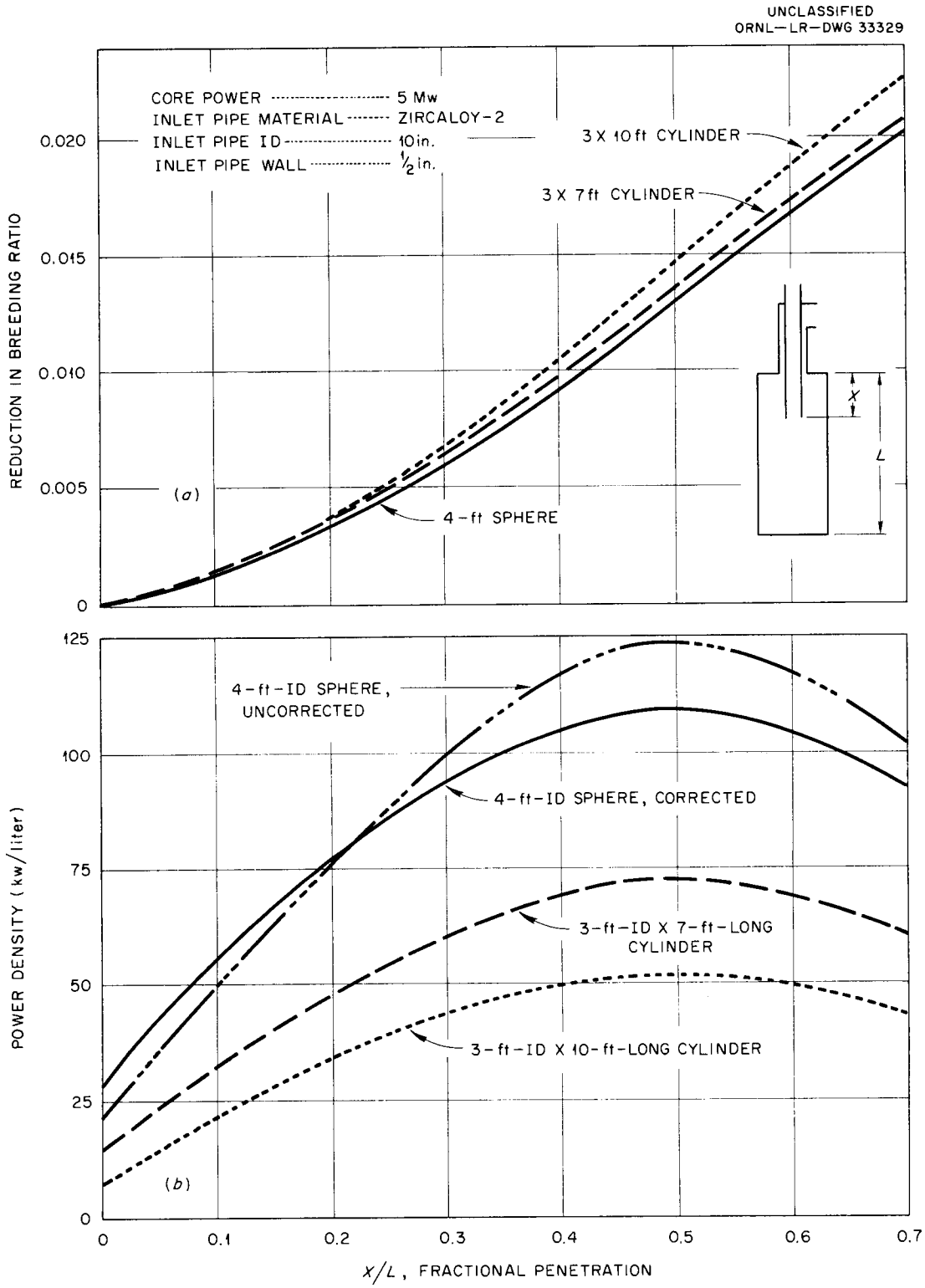

Fig. 8.8. (*a*) Breeding Ratio Reduction Due to Neutron Absorption in Pipe and (*b*) Power Density in Fuel Solution at End of Pipe vs Fractional Distance of Penetration of Inlet Line into HRE-3 Cores of Various Geometry.

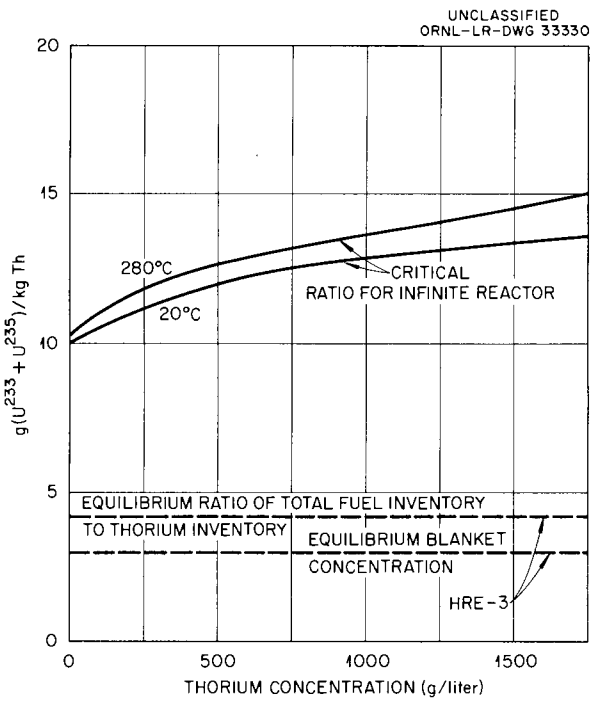

Fig. 8.9. Comparison of Critical Ratio of Fuel to Thorium in Infinite Reactor with Ratio in HRE-3 If Completely Mixed.

would remain constant, even though the ratio of thorium to D_2O changed. Thus the value of 4.2 plotted in Fig. 8.9 represents the maximum fuel-to-thorium ratio which would occur in HRE-3 if the mixture were uniform. Under this circumstance, even an infinitely large dump tank at 20°C could not become critical.

If the core uranium were added to just part of the thorium inventory, higher uranium-to-thorium ratios could occur. However, to attain a ratio of 10 g of U^{233} per kg of Th in a limited part of the system, all the core uranium inventory would have to be added to just one fifth of the thorium.

Since the uranium in the blanket dump tank is not likely to attain the concentration required for criticality in a cold, clean, infinite reactor, there should be no criticality problem in the actual dump tanks for the HRE-3 blanket.

8.7 NUCLEAR CHARACTERISTICS OF SMALL ONE-REGION SLURRY REACTORS

A survey was made[9] of the static nuclear characteristics of some small one-region thorium oxide slurry reactors. Fuels considered were U^{235} and U^{233} (isotopically pure); the moderator was either heavy or light water. In all cases the reactors were assumed to be spherical and to be free of poisons. Neutron absorptions in D_2O were neglected, but absorptions in H_2O were considered. The computations were performed on the Oracle, by using a modified-Fermi-age bare-reactor model, which allowed for resonance absorptions in fuel.

The range of parameters studied is listed in Table 8.5. Computational results for the U^{235}-fueled, D_2O-moderated systems are summarized in Figs. 8.10 to 8.12, which give the critical fuel concentration as a function of reactor diameter, temperature, and thorium concentration. Figures 8.13 to 8.15 give the corresponding results for the U^{235}-H_2O reactors.

Table 8.5. Range of Parameters Studied in Criticality Survey

Fuel	U^{235}, U^{233}
Moderator	D_2O, H_2O
Diameter of bare sphere, ft	3–5½
Temperature, °C	20–300
Thorium concentration, g/liter	0–600

The minima in the critical-mass-ratio curves occurred at about 200 g of Th per liter for the ThO_2-D_2O reactors. However, with H_2O moderator but with the same range in reactor diameters, this ratio continued to decrease up to 600 g of Th per liter because of the absorptions in the moderator.

Figure 8.16 is a cross plot of the critical temperature of a 5-ft-dia U^{235}-D_2O reactor as a function of thorium concentration for various ratios of U^{235} to thorium. These results may be used to examine the effect on criticality produced by *uniform* changes in slurry concentration. For example, if slurry containing a fixed ratio of U^{235} to thorium were slowly added to a low-temperature critical D_2O reactor, the temperature would rise in accordance with the variation of the appropriate curve. Increasing the thorium concentration above

[9] B. E. Prince and M. W. Rosenthal, *Survey of the Static Nuclear Characteristics of Small, One-Region Slurry Reactors*, ORNL CF-58-7-76 (July 28, 1958).

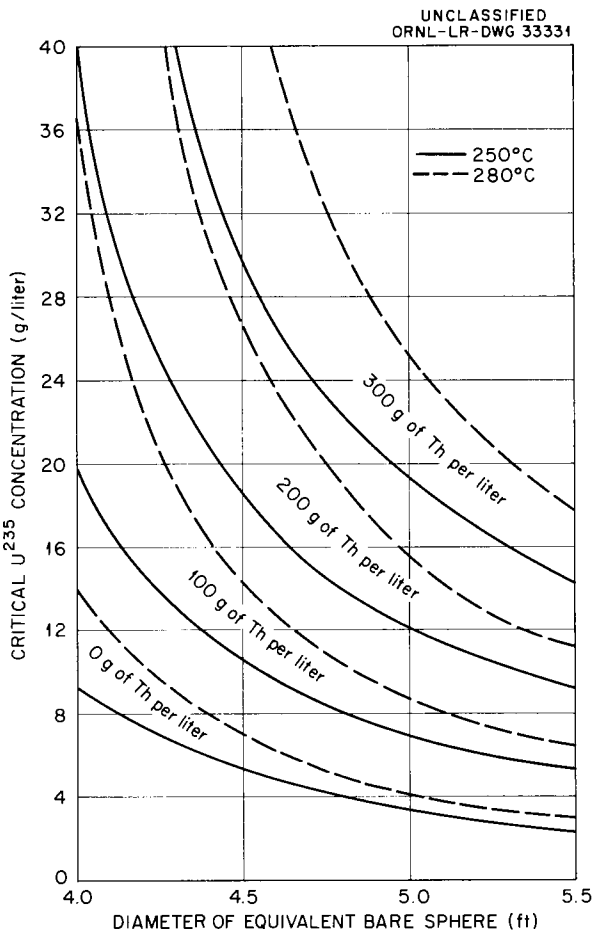

Fig. 8.10. Critical U^{235} Concentration vs Size for One-Region ThO_2-D_2O Reactors.

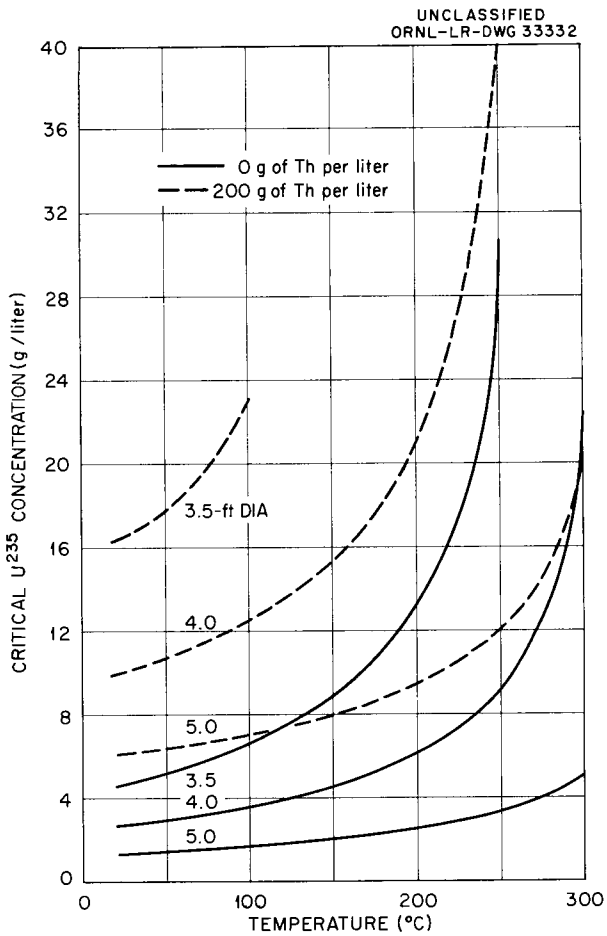

Fig. 8.11. Critical U^{235} Concentration vs Temperature for One-Region ThO_2-D_2O Reactors.

about 200 g/liter would cause the critical temperature to fall owing to the increase in resonance captures in thorium. Figure 8.16 also indicates the fluid temperature required to ensure that a given slurry addition or dilution would not cause the reactor to become supercritical.

In Fig. 8.14, the minima in some of the curves result from the reduction in neutron absorptions by H_2O as the temperature is increased. Although for some reactors the critical concentration decreased with increasing temperature, the temperature coefficient of reactivity is still negative since a temperature increase would result in the removal of fuel along with the moderator.

In these computations the reactor was considered to be a bare sphere; however, the pressure vessel will serve as a neutron reflector. Thus the actual inside diameter of the vessel will be somewhat less than that of a bare reactor having the same critical concentration. In order to estimate this size correction and also to check the validity of some of the assumptions used in the simplified model, criticality in several U^{235}-D_2O reactors was calculated by using a multigroup neutron-diffusion program. These computations were performed on the Oracle, by use of a section of the nuclear code CORNPONE. Twenty fast groups, one thermal group, and two space regions (core and pressure vessel) were employed. Table 8.6 summarizes the CORNPONE critical-mass ratios for the reactors studied; for a thorium concentration of 200 g/liter, as shown, the critical-mass ratio

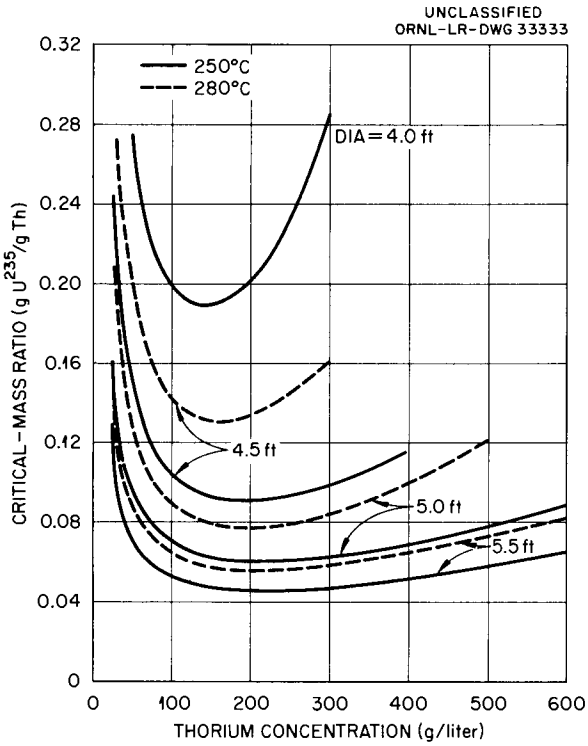

Fig. 8.12. Critical-Mass Ratio vs Thorium Concentration for One-Region ThO_2-D_2O-U^{235} Reactors Fueled with U^{235}.

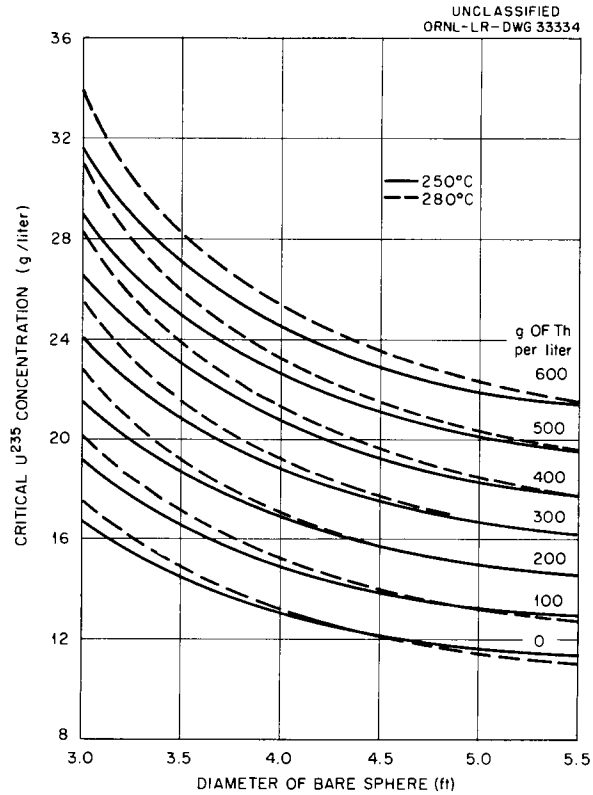

Fig. 8.13. Critical U^{235} Concentration vs Size for One-Region ThO_2-H_2O Reactors.

obtained for the bare 5-ft reactor by using the simple model compares favorably with that obtained from the multigroup calculation. However, the comparison becomes poorer at higher slurry concentrations, owing to the inadequate treatment of resonance fission with the simplified model. As indicated in Table 8.7, increasing the thorium concentration caused a significant upward shift in the neutron-energy spectrum.

The equivalent bare-reactor size corresponding to a $4\frac{1}{2}$-ft-dia reactor having a 4-in.-thick pressure vessel may be estimated from the information in Table 8.6. For example, from Fig. 8.10 it is found that approximately 10 in. should be added to the diameter of the $4\frac{1}{2}$-ft-ID pressure-vessel-enclosed reactor to obtain the diameter of the equivalent bare sphere.

A detailed neutron balance is given in Table 8.7 for two ThO_2-D_2O reactors having a physical diameter of $4\frac{1}{2}$ ft and reflected by a 4-in.-thick

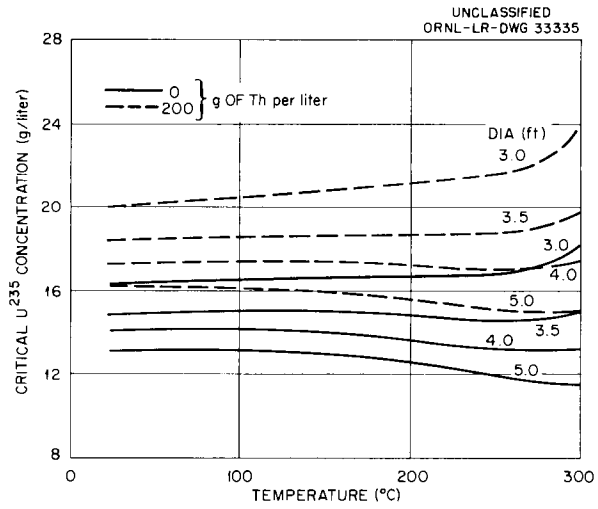

Fig. 8.14. Critical U^{235} Concentration vs Temperature for One-Region ThO_2-H_2O Reactors.

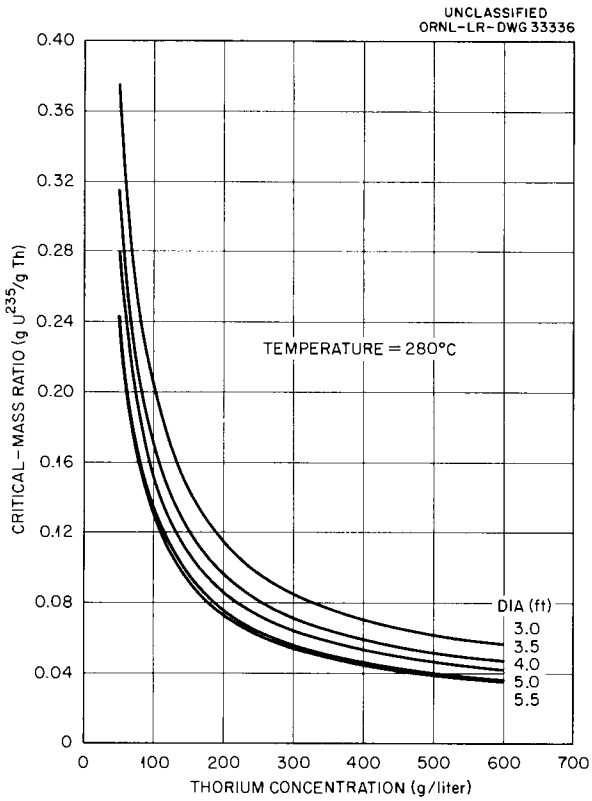

Fig. 8.15. Critical Mass Ratio vs Thorium Concentration for One-Region ThO_2-H_2O-U^{235} Reactors at 280°C.

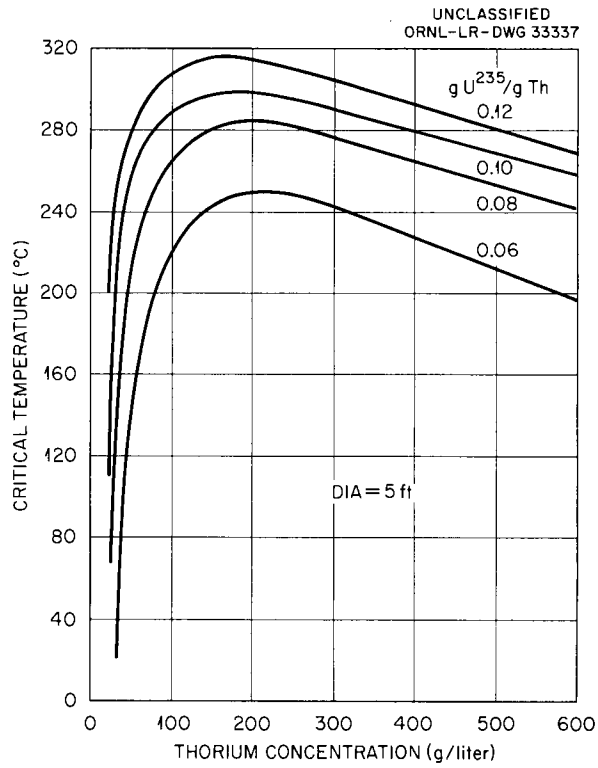

Fig. 8.16. Critical Temperature vs Thorium Concentration for Various Ratios of U^{235} to Thorium in One-Region ThO_2-D_2O Reactors.

Table 8.6. Critical-Mass Ratios for Bare and Pressure-Vessel-Enclosed Reactors at 280°C

Core Diameter (ft)	Conditions	Thorium Concentration (g/liter)	Critical-Mass Ratio	
			Multigroup Calculation (g U^{235}/g Th)	Modified-Age Calculation (g U^{235}/g Th)
5	Bare	200	0.077	0.078
		400	0.141	0.100
4½	4-in. steel shell	200	0.060	
		400	0.105	
4	4-in. steel shell	200	0.082	
		400	0.146	

Table 8.7. Neutron Balance for a U^{235}-Fueled ThO_2-D_2O Slurry Reactor

Core diameter, $4\frac{1}{2}$ ft; pressure-vessel thickness, 4 in.; temperature, 280°C

Neutron Absorptions per 100 Absorptions in U^{235}	200 g of Th per liter	400 g of Th per liter
U^{235}		
Fast	16.38	39.83
Thermal	83.62	60.17
Thorium		
Fast	30.00	49.05
Thermal	16.39	6.77
Pressure shell		
Fast	12.78	9.87
Thermal	19.23	4.85
Leakage from shell		
Fast	26.80	24.90
Thermal	0.22	0.07
	205.42	195.51
Critical-mass ratio (g of U^{235} per g of Th)	0.060	0.105
Initial breeding ratio	0.46	0.56

pressure vessel. In this table, the fast absorptions and leakages listed are the sums of the 20 fast energy groups used in CORNPONE.

8.8 MACHINE PROGRAMMING

The standard two-group, two-region Oracle code for reactor calculations was modified to include fissions in the higher energy group. Addition of this feature requires that the number of different fuel components be restricted to one. Additional input parameters include the infinite resonance integral for the fuel component, the macroscopic scattering cross sections for the core and blanket, and the average fast η for the fuel in the core and blanket regions.

A stress-analysis calculation for transition joints between dissimilar metals has been programmed for the IBM-704. A machine program has been written for the solution of a general first-order differential equation. Numerical integration is performed by the Runge-Kutta method.

A code for one-region spherical reactors has been modified by the addition of a first-flight correction for fission neutrons. Fuel enrichment required for criticality is obtained for a given reactor diameter and fertile-material concentration.

The kinetic equations pertaining to homogeneous reactor safety and behavior have been programmed. Two reactor regions having individual pressurizers are considered in one program; the reactor regions themselves can be directly connected; a constant source of delayed-neutron precursors is assumed. In another program the reactor is treated as one region, but five groups of delayed-neutron precursors are considered.

A code for the IBM-704 has been written which calculates the reactivity effects associated with slurry settling in finite, bare cylindrical reactors. A two-group model is used which includes resonance capture and fission in the fuel material and fission in the fuel material and resonance capture in the fertile material. The reactor is assumed to

consist of two regions, an upper region containing only moderator and a lower region containing fuel, moderator, and fertile material. The critical fuel concentration and ratio of fuel concentration to fertile-material concentration are computed and stored on magnetic tape with other identifying information for off-line printing; average calculation time is about 6 sec. If desired, on-line printer output may also be obtained, but the calculation time is then doubled.

Nuclear-data cards are now available for several fuel-moderator combinations with thorium as fertile material at various temperatures, based on the two-group data given by Fowler and Tobias.[10]

To facilitate the calculation of steady- and unsteady-state temperature distributions in a body that may have internal heat generation, a General Heat Transfer Code (GHTC) has been prepared. The GHTC will calculate temperature distributions in one, two, or three dimensions. The limitations of the code are: (1) all material properties and film coefficients must be a function of position only, (2) the body under consideration must be represented by no more than 999 points, and (3) the transient-solution time step is limited by a convergence criterion depending upon geometry and physical properties. The steady-state solution uses the Liebmann and Extrapolated Liebmann methods with Atkin's δ^2 process to accelerate convergence.

8.9 RHEOLOGY OF THORIUM-OXIDE SLURRIES[11]

A general relation between the shear stress, τ, and the shear rate, dV/dr, for non-Newtonian fluids is

$$\tau = \mu \frac{dV}{dr} + \frac{1}{B} \sinh^{-1}\left(\frac{1}{A}\frac{dV}{dr}\right) , \tag{7}$$

where μ is the viscosity and A and B are constants. Equation 7 has been shown to apply to a wide variety of non-Newtonian fluids.[12–14] Because of the behavior of the $\sinh^{-1}$ function, if the value of A is sufficiently low or if the shear rate dV/dr is sufficiently high, the second term on the right hand of Eq. 7 changes very slowly with variation in dV/dr (ref 15). Hence this nearly constant term corresponds to the yield stress, τ_y, in the Bingham-plastic expression:

$$\tau = \eta \frac{dV}{dr} + \tau_y , \tag{8}$$

where η is the coefficient of rigidity.

Rheological data obtained with the horizontal capillary-tube viscometer (tube ID = 0.124 in., L/D = 1000) are usually associated with slurries having shear rates in the range of 100 to 8000 sec^{-1}; therefore the constants of Eqs. 7 and 8 were calculated for a representative set of data obtained with such slurries; the yield stress varied from 0.01 to 2.0 lb/ft^2. The product $B\tau_y$ obtained by assuming that the $\sinh^{-1}$ term was a constant was found[16] to be 6.4 ± 3.5. The constant μ in Eq. 7 had an almost 1 to 1 correspondence with the constant η of Eq. 8. Thus, over the range of parameters studied, the argument of the $\sinh^{-1}$ term in Eq. 7 appears large enough to permit Eq. 8 to approximate Eq. 7. Consequently, it is believed that, provided the shear-rate range is specified, the Bingham-plastic relation can be used to describe adequately the flow characteristics of ThO_2 slurries in heat-transfer and pressure-drop correlations.

Thorium oxide slurries, when characterized by the Bingham-plastic constants, have a yield stress proportional to the cube of the concentration.[17] The effect of volume fraction solids on the Bingham-plastic constants is given by:[16]

$$k_1 \equiv \frac{\ln \frac{\eta}{\mu}}{\phi} , \tag{9}$$

[10] T. B. Fowler and M. Tobias, *Two-Group Constants for Aqueous Homogeneous Reactor Calculations*, ORNL CF-58-1-79 (Jan. 22, 1958).

[11] See Sec 10.1.3 for additional discussion of viscometer and slurry flow properties.

[12] R. E. Powell and H. Eyring, *Nature* 154, 427–28 (1944).

[13] T. Ree and H. Eyring, *J. Appl. Phys.* 26, 793–809 (1955).

[14] E. B. Christiansen, N. W. Ryan, and W. E. Stevens, *A.I.Ch.E. Journal*, 1, 544–48 (1955).

[15] R. N. Lyon, personal communication, March 1958.

[16] D. G. Thomas, *The Rheology of ThO_2 Slurries. V*, ORNL CF (to be published).

[17] D. G. Thomas, *Solids Dispersed in Liquids*, ORNL CF-56-10-35 (April 25, 1957).

(10) $$k_2 \equiv \frac{\tau_y}{\phi^3} ,$$

where k_1 and k_2 are parameters dependent upon the particular slurry and ϕ is the volume fraction solids. Values for these parameters are given in Table 8.8 for a variety of slurries, together with the past history of the slurries and particle-size data.

A log-log plot of particle diameter against the value of k_2 could be fitted satisfactorily by a line of slope minus 2. Therefore the yield-stress–concentration data are plotted as $\tau_y D_p^2$ vs concentration in Fig. 8.17, where D_p is the mean diameter of the thoria particles. By this procedure the data could be correlated in much better fashion than if the effect of D_p were neglected.

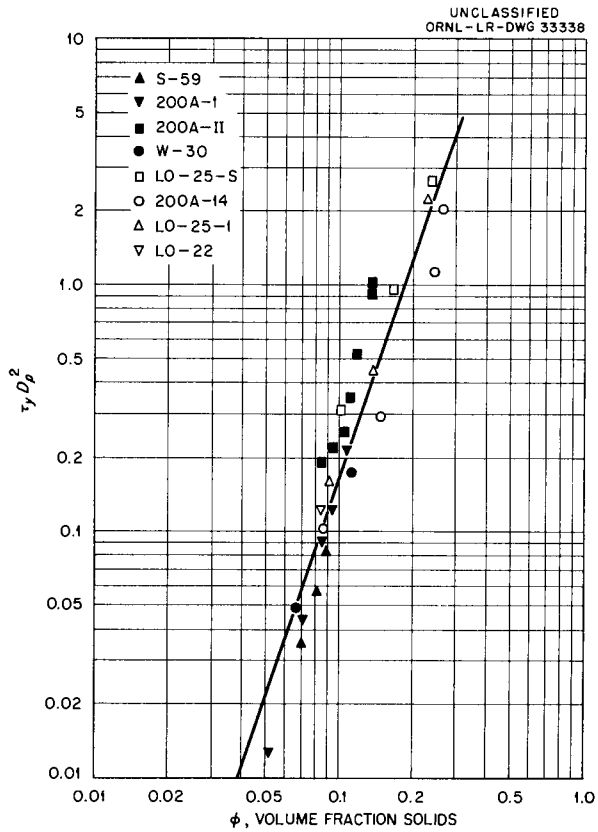

Fig. 8.17. Effect of Particle Diameter and Concentration on ThO_2 Slurry Yield Stress.

8.10 THORIA CAKING STUDIES

A 30-gpm loop for circulating thoria-water slurries at 280°C has been constructed for use in further investigation of the slurry caking problem. The relatively small volume of the 30-gpm loop facilitates testing of special batches of ThO_2. The system contains a multidiameter test section consisting of three pipe sizes in which the nominal fluid velocities are 5, 10, and 20 fps; this multidiameter section permits a study of the effects of slurry velocity upon cake formation.

Table 8.8. Rheologic Properties of Non-Newtonian Thorium Oxide Slurries

Oxide Designation					Particle-Size Distribution			
Sample	Calcination Temperature (°C)	Agitation					$k_1 \equiv \frac{\ln\left(\frac{\eta}{\mu}\right)}{\phi}$	$k_2 \equiv \frac{\tau_y}{\phi^3}$ (lb/ft^2)
		Method	Duration (hr)	Temperature (°C)	σ	D_p (μ)		
S-59	650	Pump	325	290	2.7	0.030	2.4	1100
200A-1	800	Pump	234	300	2.9	0.58	1.8	470
200A-11	800	Pump	900–1800	300	2.8	0.75	1.4	550
W-30	1600	Waring Blendor	0.5	50	1.9	1.0	1.5	145
LO-25-S	1600	None			1.5	1.6	1.2	100
200A-14	1600	Pump	3787	300	1.8	1.4	0.8	60
LO-25-1	1600	None			1.7	2.0	1.0	44
LO-22	1600	Mikro-Pulverizer	4 passes	30	1.7	2.4	1.2	33

The first run in the 30-gpm loop was with slurry containing about 480 g of Th per kg of H_2O at 280°C (ThO_2 from batch LO-20). This slurry formed spheres and cakes, principally in the impeller, duplicating the results obtained previously in 100- and 200-gpm loop runs.

The effect of digestion for 36 hr at 300°C on the caking tendency of slurry prepared from batch LO-20 was also studied. After digestion, circulation of the slurry in the 30-gpm loop was accompanied by the deposit of thick films of oxide on the surfaces of the test section exposed to average fluid velocities of 5 and 10 fps. However, the metal surface of the section exposed to fluid at an average velocity of 20 fps was perfectly clean. As shown in Fig. 8.18, the film in the 10-fps section covered approximately 60% of the surface, while the surface of the 5-fps section was covered completely. Film in the 10-fps section was comparatively difficult to remove; that in the 5-fps section washed away easily. The former film had a glossy appearance, but the latter film was dull. The nature of these films tends to confirm a previously advanced hypothesis[18] that hard ThO_2 cake formation occurs when oxide particles are pushed over each other into positions of minimum energy. Apparently in the 20-fps section the force associated with the high fluid velocity was too great to permit slurry particles to adhere to the pipe wall, while in the 5-fps section the low shear rates did not force particles into very low-energy positions.

[18] R. N. Lyon, *The Choice in Thorium Oxide Slurries for the Prevention of Caking in Circulating Systems*, ORNL CF-57-4-77 (April 22, 1957).

8.11 MODEL STUDIES OF HRE-3 BLANKET CONFIGURATIONS

In the study of fluid-flow patterns in possible HRE-3 blanket configurations by visual and photographic techniques, dye-retention studies with two models were completed. It is hoped that dye-retention studies in small-scale equipment will provide a simple way for evaluating flow patterns in various configurations.

The dye-retention test gave reproducible results. Essentially, the test consisted of filling the blanket-model volume with a bromothymol-blue dye solution, suddenly running water through the model at a preset flow rate, and recording the time required for the last visible trace of dye to be removed from the system. The pressure in the model was always adjusted to 10 psig in order to suppress bubble formation, which had been found to affect seriously the reproducibility of the data.

The two configurations tested were one-sixteenth scale models made of Lucite. The first model (MF-1), basically a cylindrical type, has been described previously.[19] The second model (Fig. 8.19) has a spherical core, with the gap between the shroud and the core having a constant thickness below the equator and a constant cross-sectional area above the equator. This model was tested with both a flat head (MF-2) and a dished head (MF-2D).

The ratio of "sweep-out time" to "retention time" vs Reynolds number (calculated at the equator of the blanket region) is shown in Fig. 8.20. *Sweep-out time* is defined as the ratio of

[19] R. B. Korsmeyer *et al.*, *HRP Quar. Prog. Rep. Oct. 31, 1957*, ORNL-2432, p 62.

UNCLASSIFIED
PHOTO 31904

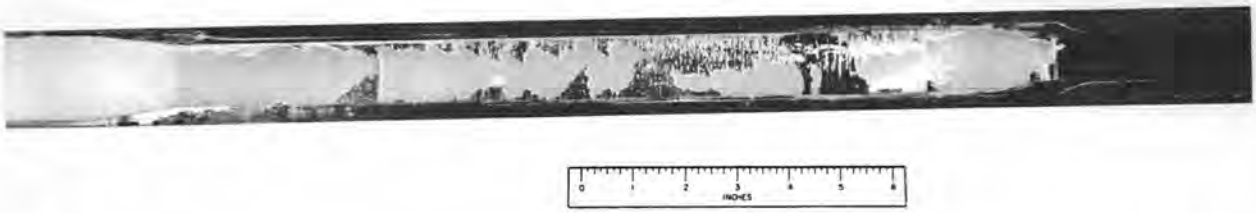

Fig. 8.18. Thoria Film Obtained in Multidiameter Sample Barrel (Nominal Fluid Velocities Were 20, 10, and 5 fps).

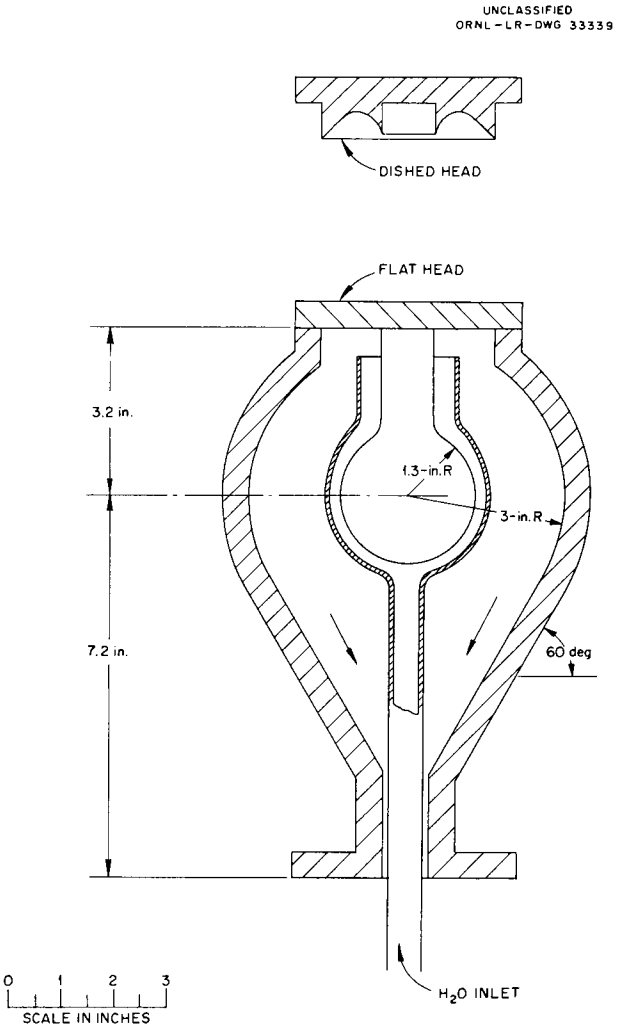

Fig. 8.19. Sketch of Lucite Model (MF-2, Flat Head; MF-2D, Dished Head).

the fluid volume of the model to the water flow rate (i.e., the time required to remove the dye if perfect slug flow existed). *Retention time* is the visually observed dye retention time. Each point represents an average of four to five runs at the same flow rate.

The curves in Fig. 8.20 indicate a change of flow regime at a Reynolds number of 1500 for models MF-1 and MF-2D and somewhere between 900 and 1200 for model MF-2. In all cases the last visible trace of dye was in the form of thin filaments or a film which clung to the outside of the shroud. In model MF-2 dye was last seen on the bottom half of the shroud; its location moved progressively downward with increasing flow rate.

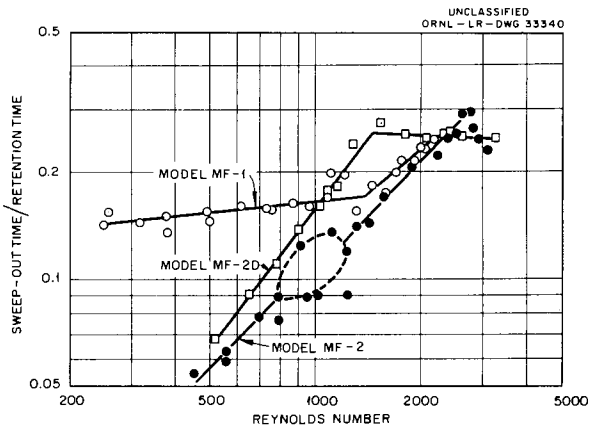

Fig. 8.20. Ratio of Sweep-Out Time (Slug Flow) to Retention Time in Blanket of HRE-3 Models vs Reynolds Number.

In model MF-2D, dye was last seen on the bottom half of the shroud at an angle of approximately 50 deg below the equator and also on the top half of the shroud at an angle of approximately 45 deg above the equator. In model MF-1, the last trace of dye was in the curved portion just below the top of the shroud.

Addition of the dished head to model MF-2 improved the flow distribution for Reynolds numbers less than 2500. Even though comparatively stagnant areas were seen in two places in model MF-2D, the amount of dye held in the stagnant regions and the over-all holdup times were less than those for model MF-2. Above a Reynolds number of 2500 the stagnant area in model MF-2 moved to the lower portion of the shroud, and the holdup times were less than for model MF-2D.

This preliminary information indicates better flow distribution in model MF-1 than in model MF-2. Above the flow transition point (the full-scale HRE-3 would operate above this point), there appears to be little difference between the two models. Using a dished head definitely improves the flow pattern in model MF-2 below the transition point.

8.12 MODEL STUDY OF A CYLINDRICAL CORE FOR HRE-3

One of the conceptual designs for HRE-3 considered a cylindrical core with a concentric inlet-outlet at the top. With this configuration there may be difficulty in obtaining stable flow patterns which cleanly sweep the bottom of the core.

In an effort to get some immediate results on the effect of reactor length-to-diameter ratio (L/D) on flow patterns, a glass model 15 in. long with a diameter of 3 in. was built and tested. This represents a one-twelfth scale model of a 15 × 3 ft cylindrical core with a 10-in.-dia inlet pipe and an annular outlet of the same area as the inlet pipe.

Tests were made by pumping a dilute slurry of phosphorescent particles through the model at various flow rates and at several penetrations of the inlet pipe. On exposure to a strong light source, the phosphorescence of the particles permitted good visual observations of the flow patterns. The general character of the flow patterns appeared to be independent of flow rate in the range of interest and, consequently, should be virtually independent of any characteristic Reynolds number. Tentatively, it may be concluded that relative geometry alone characterizes the flow pattern.

A well-defined and stable jet that cleanly swept the bottom was observed for penetrations of the inlet pipe greater than 8 in. At penetrations between 6 and 8 in., the jet was not clearly defined and pulsated somewhat. There was no question, however, that definite downward transport to the bottom existed. At smaller penetrations, transport to the bottom decreased rapidly, and at penetrations less than 1 in., some phosphor collected at the bottom for all flow rates.

On the basis of this preliminary information, it appears that for small inlet-pipe penetrations a cylindrical core with an L/D of 2.5 will give a well-defined jet that sweeps the bottom, and an L/D up to 3.0 may be permissible. By decreasing the inlet diameter, it may be possible to increase the permissible L/D.

8.13 FLOW-VISUALIZATION STUDIES

8.13.1 Flow-Visualization Loop

A flow-visualization loop was constructed for use in qualitative studies of flow patterns in various models of reactor vessels and components. The loop utilizes a Milling-Yellow solution as the working fluid. Milling Yellow is an organic dye which when dissolved in water exhibits an optical property known as "flow double refraction"; this phenomenon depends on the interference of visible-light frequencies and occurs because of the viscous stresses in the moving liquid (analogous to the photoelastic behavior of some solids). With the solution flowing through a transparent vessel located between two polarizing plates (set at a 90-deg polarizing angle to each other), the light-interference patterns permit clear visual observation of turbulent patterns, regions of flow separation, and in some cases, lines that correspond to constant values of shearing stress.

A photograph of the equipment with a model in place is shown in Fig. 8.21. The constant-temperature bath and the pump, which are necessary components of the loop, are not visible in the photograph.

8.13.2 Model Studies

A number of Plexiglas models have been built that are essentially two-dimensional representations of reactor or other flow configurations. The investigation is directed along lines that will aid in the selection of the HRT replacement vessel and the HRE-4 configuration, as well as the understanding of the hydrodynamic behavior of the preferred types.

Figures 8.22 and 8.23 illustrate the useful information that results from the use of the Milling-Yellow rig. An example of flow separation in a divergent channel (30-deg included angle) is shown in Fig. 8.22; it is evident that flow separation occurs on only one side of the channel. It is possible to cause the separation point to shift from one side to the other by rapidly raising and lowering the flow rate. All this is in agreement with the results of the classic experiments by Nikuradse. However, as shown in Fig. 8.23, a symmetric flow pattern was obtained with a straight-through-flow model of a reactor vessel. In addition to being symmetrical, the flow pattern was very stable and maintained the pattern shown throughout abrupt flow-rate changes. The regions of small turbulence in the vicinity of the two flow separation points in Fig. 8.23 are masses of liquid rotating with a downward direction near the wall.

8.14 EQUATIONS OF MOTION AND BOUNDARY-LAYER EQUATIONS FOR BINGHAM-PLASTIC MATERIALS

The general equations of motion for a Bingham plastic were developed from the appropriate relation between shear rate and stress. The fluid velocity was obtained as a function of position for laminar flow between parallel plates and also for flow in cylindrical pipes.

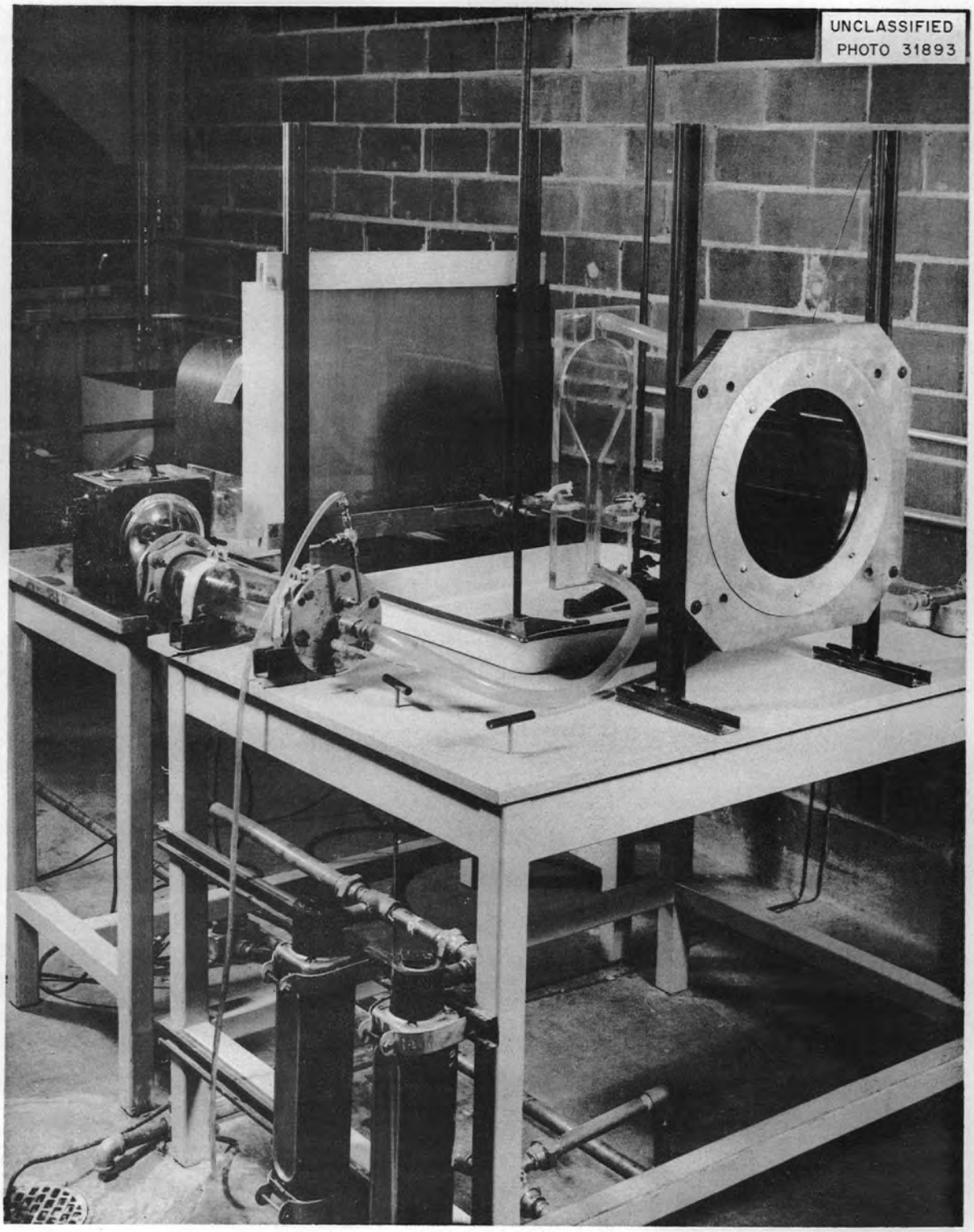

Fig. 8.21. Flow-Visualization Equipment.

The general boundary-layer equations were simplified by eliminating certain terms on the basis of an order-of-magnitude analysis. It was found that the ratio of the Hedstrom number to the square of the Reynolds number determines the final form of the approximate boundary-layer equations. In particular, it was concluded that for a situation in which the Hedstrom number is no larger than the Reynolds number raised to the 1.5 power, the boundary-layer equations for Bingham plastics are essentially the same as those for Newtonian fluids.

Fig. 8.22. Flow Pattern in Diverging Channel.

8.15 LIQUID-FLUIDIZATION STUDIES WITH THORIA SPHERES

Water-fluidization studies with ThO_2 spheres were initiated to determine the agglomeration characteristics of ThO_2 particles as a function of particle size and the concentration range for a stable interface, and to compare fluidization velocities with hindered-settling velocities. Tests were made with ThO_2 spheres formed in the 200A loop and refired at 1200°C. Fluidization and settling tests were made in a 4-in.-ID, 3-ft-long glass column; a porous stainless steel plate was used as a support plate and water flow distributor.

The experimental settling-rate data in Fig. 8.24 are shown in relation to empirical curves which were determined by Steinour[20] and by Richardson and Zaki[21] for various nonflocculated materials. Based on these comparative results, the degree of flocculation was estimated in terms of floc density and floc diameter (based on Stokes' law). Assuming no flocculation (floc density = 10 g/cc), the floc diameter was calculated to be 22 μ; comparison of the settling-rate data obtained for this slurry with data obtained by Steinour for nonflocculated solids indicated that the slurry had a floc density of 8 g/cc and a floc diameter of 25 μ; comparison with the data of Richardson and Zaki indicated a floc density of 6.6 g/cc and a floc diameter of 28 μ. Apparently some flocculation occurred, since the mean diameter of the slurry particles was given initially as approximately 15 μ..

The fluidization velocity for each run is also plotted in Fig. 8.24. As shown, the best straight line through the fluidization data lies quite close to the settling-rate curve. This feature is examined more closely in Fig. 8.25, where the ratio of

[20] H. H. Steinour, *Ind.* and *Eng. Chem.* 36, 618, 840, 901 (July–Dec. 1944).

[21] J. F. Richardson and W. N. Zaki, *Trans. Inst. Chem. Engrs. (London)* 32, suppl, 35 (1954).

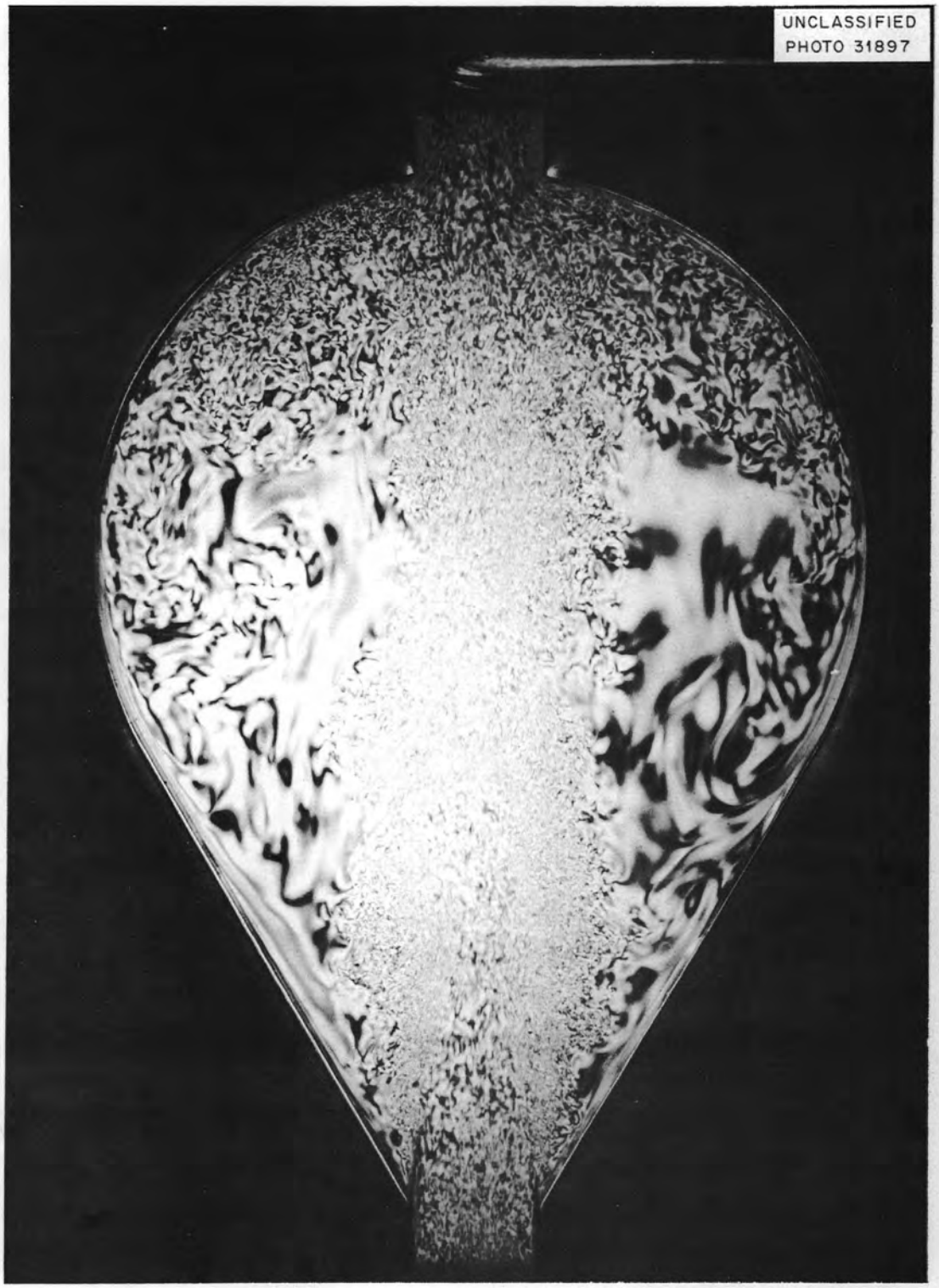

Fig. 8.23. Flow Pattern in Straight-Through-Flow Core Concept with 60-deg Conical Bottom.

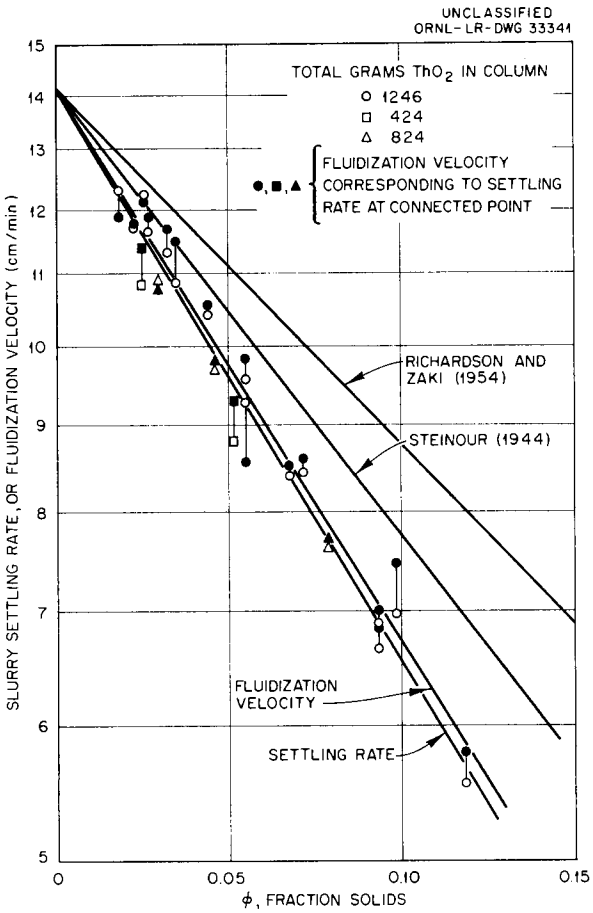

Fig. 8.24. Effect of Thoria Concentration on Settling Rate.

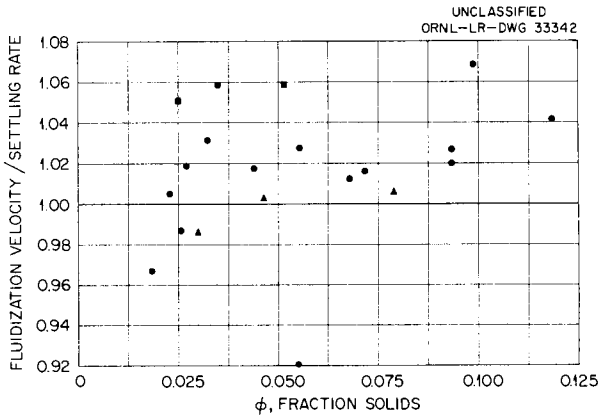

Fig. 8.25. Ratio of Fluidizing Velocity to Settling Rate for Various Slurry Concentrations.

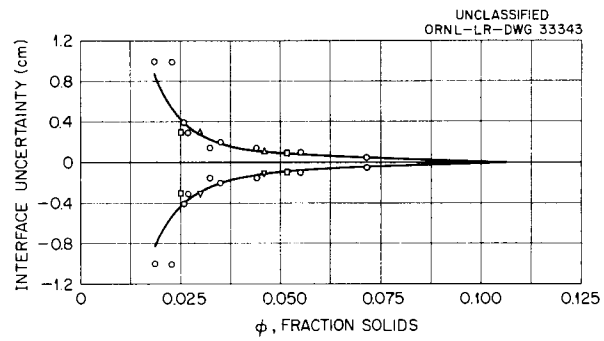

Fig. 8.26. Estimated Uncertainty in Position of Interface Between Fluid Bed and Supernatant Liquid, as a Function of Slurry Concentration.

fluidization velocity to settling rate is plotted vs volume fraction solids. This ratio remained close to unity over the range studied.

During rapid expansions of the fluidized bed, the interface between the fluidized bed and supernatant liquid became difficult to define. Eventually, however, a steady-state condition was reached, and the position of the interface could be estimated. The uncertainty in the position of the interface is shown in Fig. 8.26 as a function of slurry concentration. The uncertainty became significant at fraction solids less than 0.025 (256 g of Th per kg of H_2O).

The total thorium oxide concentration in the column, and thus the L/D ratio, was varied by a factor of 3, from 424 to 1246 g of thoria. In two runs with fluidized-bed concentrations of 413 and 329 g of Th per kg of H_2O, concentration samples were obtained as a function of bed height. In both runs the particle-size distribution was fairly constant throughout the bed; however, the thorium concentration decreased with increasing bed height. The decrease in concentration corresponded to about 1 g of Th per kg of H_2O per centimeter of bed height.

Part III

ENGINEERING DEVELOPMENT

R. N. Lyon

9. DEVELOPMENT OF FUEL AND SLURRY SYSTEM COMPONENTS

I. Spiewak

J. M. Baker
R. Blumberg
J. S. Culver
B. D. Draper
D. M. Eissenberg
C. H. Gabbard
B. A. Hannaford
J. K. Hayes
E. C. Hise
P. P. Holz
C. G. Lawson
J. E. Mott
J. C. Moyers
I. K. Namba
H. R. Payne
H. C. Roller
D. L. Snyder

9.1 RECOMBINER AND PRESSURIZER DEVELOPMENT

9.1.1 High-Pressure Recombiner Loop

The development of a reliable high-pressure recombiner could simplify the operation of homogeneous reactors in that gases evolved could be burned in place. The high-pressure recombiner loop has been operated to explore this problem.

A new horizontal Inconel boiler, replacing the stainless steel boiler which had failed as a result of caustic stress corrosion, was installed above the existing electrolytic cells. A natural-circulation attachment fabricated entirely from Inconel was installed over the new boiler. Both the boiler and the attachment were stress-relieved following welding. Operating conditions of the natural-circulation loop will be 1500 psi, 315 to 425°C, at stoichiometric H_2-O_2 concentrations of less than 5%. Exposure of titanium- and zirconium-alloy specimens will continue in the new loop.

9.1.2 Syracuse Contract

A knowledge of the reaction limits is required for conservative design of recombiners and pressurizers. Measurements of reaction limits of mixtures of stoichiometric H_2-O_2 and steam have been made in pipes 0.434, 0.957, and 2.9 in. in diameter. These data are summarized in Table 9.1. The indicated lower reaction limit is 6% $H_2 + \frac{1}{2} O_2$ in steam, in all three geometries. The method of ignition appears to exert a strong influence on the lower reaction limit.

The lower reaction limit, observed with $D_2 + \frac{1}{2} O_2$ in D_2O vapor in the 0.957-in. reactor at 100°C, was 16%, compared with 6% in the hydrogen system. The detonation limit was found to be 60% in the deuterium system, compared with 48% with

Table 9.1. Summary of Reaction Limits for $H_2 + \frac{1}{2}O_2$ in Steam*

Series	Reactor Diameter (in.)	Temperature (°C)	Ignition	Mole % $H_2 + \frac{1}{2}O_2$		
				No Reaction Range	Explosive Range	Detonation Range
1	0.957	100	Spark, 180 mj (millijoules)	Below 6	6–48	Above 48
2	0.957	100	Spark, 360 mj	Below 6	6–48	Above 48
3	0.957	100	Hot wire	Below 6	6–50	Above 50
4	0.434	100	Hot wire	Below 12	12–60	Above 60
5	0.434	100	Spark, 180 mj	Below 6	6–54	Above 54
6	0.434	200	Hot wire	Below 16	16–42	Above 42
7	0.434	300	Hot wire; rapid heating	Below 9	9–18	Not determined
8	0.434	300	Hot wire; slow heating	Below 16	16–18	Not determined
9	2.90	100	Spark, 360 mj	Below 6	6–48	Above 48

*J. A. Luker, Syracuse University, progress letters on UCNC Subcontract No. 548.

hydrogen. Similar results are being obtained in preliminary runs at 300°C.

9.1.3 Solubility of Oxygen and Hydrogen in Fuel Solution

Rocking-autoclave experiments were carried out to determine the solubility of oxygen and hydrogen in fuel solutions at 250°C. The solubility of oxygen in four different media was measured by sampling the liquid phase at equilibrium. These media were: D_2O; 0.04 *m* UO_2SO_4, 0.025 *m* H_2SO_4, 0.011 *m* $CuSO_4$ in H_2O; 0.04 *m* UO_2SO_4, 0.025 *m* H_2SO_4, 0.005 *m* $CuSO_4$ in D_2O; and 0.04 *m* UO_2SO_4, 0.025 *m* H_2SO_4, 0.03 *m* $CuSO_4$ in D_2O. The results, shown in Fig. 9.1, fall on a single line which may be expressed as a solubility of 0.00328 (std cc of O_2)/(psi of O_2)(g of soln). This line is within the experimental error of the solubility reported previously[1] for oxygen in H_2O.

Similar runs were made with stoichiometric $H_2 + \frac{1}{2} O_2$ in solvents of H_2O and a solution containing 0.04 *m* UO_2SO_4 and 0.025 *m* H_2SO_4. Solubilities were determined by two independent methods: sampling and material-pressure balance. The measurements indicated that the solubility of stoichiometric gas was about 50% greater than that of oxygen alone. Both gaseous components were equally soluble within the limits of experimental error.

[1] E. F. Stephan *et al.*, *The Solubility of Gases in Water and in Aqueous Uranyl Salt Solutions at Elevated Temperatures and Pressures*, BMI-1067 (Jan. 23, 1956).

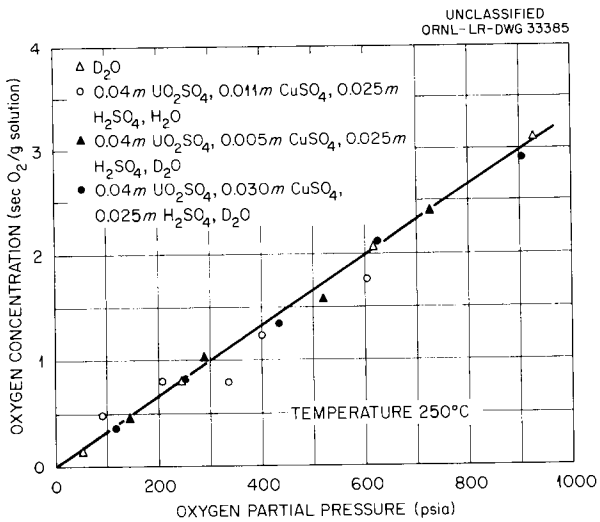

Fig. 9.1. Oxygen Solubility in D_2O and 0.04 *m* UO_2SO_4 at 250°C.

9.1.4 Titanium Equipment for Boiling UO_2SO_4 Solutions

In the pressurization of solution systems, severe corrosion of stainless steel has been observed when contacted by boiling uranyl sulfate. A small natural-circulation loop was constructed of titanium, and HRT fuel solution (0.04 *m* UO_2SO_4) was boiled for 1650 hr at 1500 psi; there were no deleterious effects on the solution or the container.

Following this run, the loop was refilled with 0.15 *m* UO_2SO_4 and the solution was boiled for 1000 hr at the same pressure. In this case heavy-phase uranyl sulfate solution was expected to appear, increasing the corrosiveness of the system. Inspection after the run showed that 97% of the uranium had precipitated, leaving a solution with a pH of 0.9. The loop piping showed loose films containing uranium and titanium oxides, but little corrosive attack. Pin specimens confirmed that the attack rate was below 1 mpy, except for one sample which experienced localized attack.

On the basis of these runs, boiling uranyl sulfate pressurization was deemed to be sufficiently attractive to warrant investigation in the HRT mockup.

9.1.5 Heating and Cooling of Steam-Oxygen Mixtures

A small system was constructed to investigate heat transfer operations such as would occur in a gas pressurizer. The over-all condensation rates from steam-oxygen mixtures were observed at 1500 psi total pressure, including oxygen partial pressures of 0 to 700 psi. The heat transfer rates appeared to be controlled by the coolant-air film coefficient on the secondary side of the double-pipe condenser. Heat fluxes up to 2600 Btu/hr·ft^2 were attained, and in the test system little effect of dilution of steam by oxygen was noted.

The system is being operated further to determine the resistance of stainless steel parts to corrosion by this environment.

9.2 CENTRIFUGAL PUMPS

9.2.1 20-cfm Allis-Chalmers Blower

The canned-motor blower operated on a steam-nitrogen mixture at 170°C and 1400 psi (4.8 lb/ft^3 density) for approximately 2700 hr with only minor difficulty, a leak in an instrument line fitting which was repaired. Additional heaters have been

procured to permit operation at higher temperatures.

9.2.2 4000-gpm Loop

It is planned to conduct tests of the Byron-Jackson pump in slurries to aid in developing erosion-resistant hydraulic parts for large slurry pumps. Three flowsheets for conversion of the 4000-gpm loop to slurry operation have been prepared. In two of these, the loop is pressurized by a pump relief-valve system; however, the methods of producing purge water for the pump motor are different. In the first flowsheet, slurry is let down continuously to low pressure, where it is evaporated, and both condensate and slurry are pumped to high pressure continuously. The second flowsheet utilizes a high-pressure water-slurry separator to manufacture purge water. The third flowsheet permits the loop contents to flash in a pressurizer, and purge water is obtained by condensation. Final selection of a flowsheet is being delayed pending further development of the various slurry components.

9.2.3 Reliance 6000-gpm Pump

The Reliance 6000-gpm pump is being purchased as a prototype for circulating UO_2SO_4 through intermediate-scale reactors. The over-all layout of the pump has been completed and detail design is continuing. The hydraulic design and the manufacture of the electrical test sample are in progress.

The flexible thermal-barrier seal, necessitated by the "top maintenance" feature, remains the major design problem. The usability of a Belleville spring gasket, with either stainless steel or gold insert contact surfaces, is being evaluated.

The insulation-test stator being irradiated in the HRT cell to provide information about its life expectancy suffered a partial short circuit to ground when water leaked in during a flooding operation of the cell. The stator has been partially dried by heating under a vacuum, and the winding resistance has improved to 12 megohms. Electrical testing will continue as soon as the resistance can be increased further to a satisfactory value. A test stator was installed in a Co^{60} source in the canal of the ORNL Graphite Reactor, and irradiation has begun.

9.2.4 300A Slurry Pump and Loop

Although the expected life of HRT solution circulating pumps is about two years, the life of similar slurry pumps is only about one-half year. Bearings and impellers wear out most frequently. The 300A loop was constructed (Fig. 9.2) in order to test improvements in the standard Westinghouse 300A pump. The loop contains an HRE-3 type of gas pressurizer in which a jet is used to contact pressurizer vapor with a sidestream from the loop. During water shakedown runs, gas was entrained from the pressurizer into the loop, and liquid was entrained from the loop into the condensate tank. This was corrected by reducing the flow of liquid through the jet eductor from 27 to 12 gpm and by reducing the gas flow from 10 to 1 cfm. The maximum condensation rate for purge water at operating conditions (280°C, 1500 psi) was greater than 10 gph.

The initial slurry run was terminated after 41 hr of operation at 280°C and 1500 psi owing to a large leak which developed around a tubing fitting. The failure was repaired, and the run will be resumed.

9.2.5 200Z Loop and Pump

The design of a second slurry-pump development loop, the 200Z loop, was completed, and fabrication is in progress. The 400A-2 solution loop is being modified so as to be similar to the 300A loop, except that a thermal-convection system will be used to condense purge water from the pressurizer rather than a jet pump.

The 200Z pump will be a modified 400A-2. It will contain a modified 200A impeller, with radial balancing vanes on both top and bottom shrouds to reduce wear-ring erosion. A vaned diffuser will reduce the radial thrust load. Cast Zircaloy hydraulic parts and aluminum oxide bearings have been purchased for the pump.

9.2.6 Byron-Jackson Slurry Pumps

Four 50-gpm slurry pumps and one 400-gpm slurry pump have been ordered from Byron Jackson Co. for general loop use. The over-all design and layout of the pumps has been approved, and delivery is expected early in 1959.

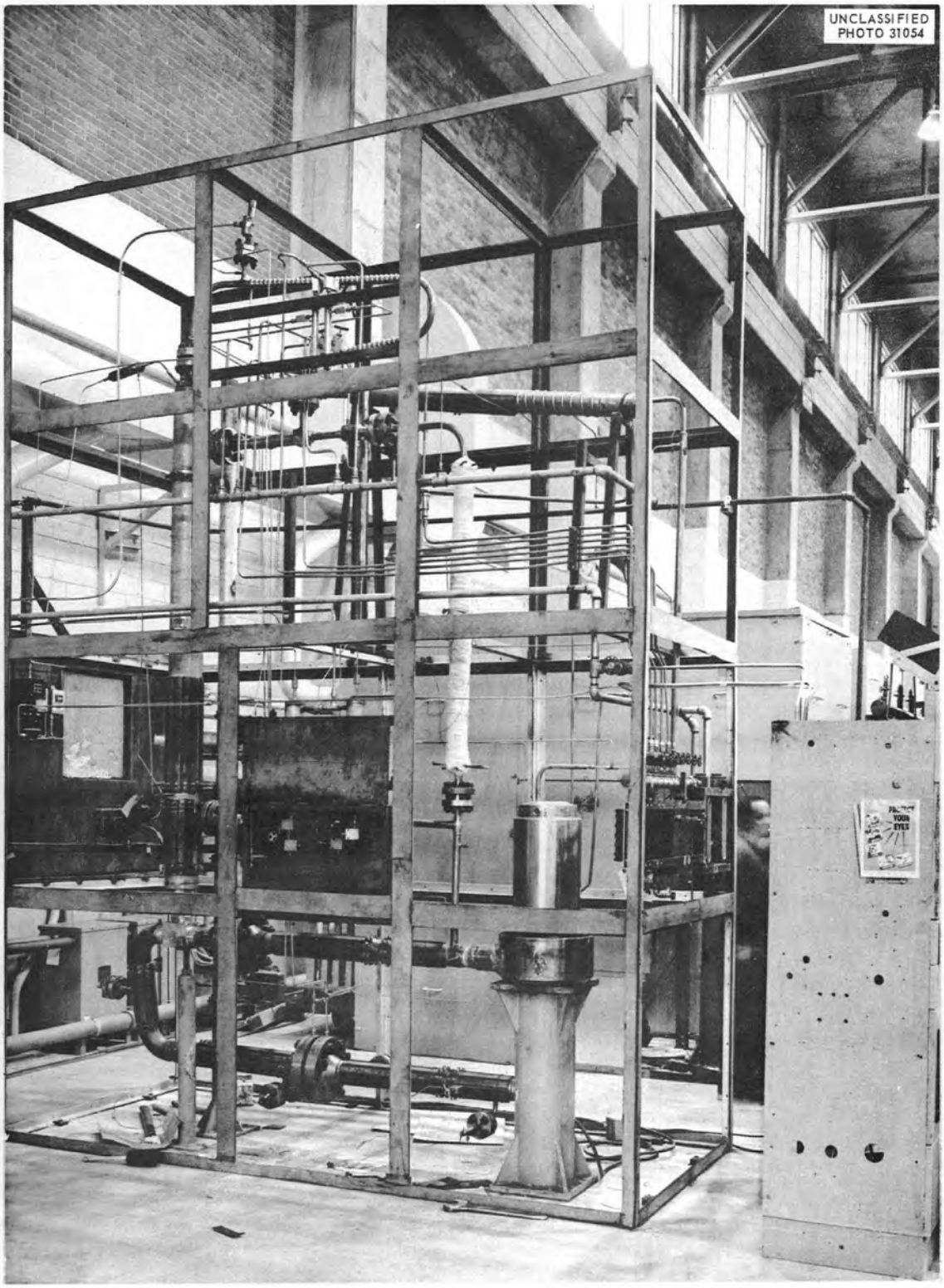

Fig. 9.2. 300A Slurry Loop.

9.2.7 Slurry Bearing-Test Program

A one-year contract was awarded to the Franklin Institute to determine the feasibility of operating hydrodynamic bearings in dilute slurries and to determine the proper design parameters for successful operation. Franklin will conduct tests on both radial and thrust bearings having Stellite-Graphitar and aluminum oxide bearing surfaces. The wear rate vs load will be determined for each type of bearing in water and in slurry.

An order has been placed for modified thrust bearings for a Westinghouse pump. These bearings will have line-contact leveling linkages rather than the point-contact type presently being used. This design should reduce the contact stresses on the linkage and therefore reduce the wear.

9.3 OXYGEN COMPRESSORS

The Pressure Products Industries diaphragm compressor has continued to deliver 2000-psi oxygen to the HRT mockup and has been satisfactory except for frequent plunger-packing failures. The water plunger drive has been replaced by a Scott & Williams purge-pump drive and intermediate system. This will permit remote operation of the compressor head comparable to the remote operation of the feed- and purge-pump heads.

Completely redesigned and rebuilt water-column cylinders have been received for the Harwood compressor. The Systems Development Section will place the Harwood unit in standby service for the HRT mockup.

Detail drawings for the Pressure Products Industries oxygen compressor (three-stage, 2-scfm, 2500-psi discharge, remote-drive) have been received and are acceptable. This unit will be a prototype of compressors used to recycle radioactive oxygen from a reactor low-pressure system back to high pressure.

9.4 FEED PUMPS

9.4.1 Solution Diaphragm-Pump Development

A diaphragm protected by 100-mesh screens, which are used in the HRT pumps and which will filter out particles larger than 0.006 in., was examined after 1000 hr of service. The diaphragm was nearly free of the small dents and scratches observed in diaphragms less well protected. Another diaphragm head has operated satisfactorily for 2200 hr in the valve test loop while protected by a 20-μ filter (0.0008-in. particle size). It is expected that filtration of such fine particles will eliminate mechanical damage as a factor in diaphragm failure.

The double-diaphragm feed pump has operated for 2000 hr under a variety of discharge conditions up to 2.7 gpm at 2000 psi. An endurance run has begun with a reciprocating drive with intermediate barrier; operation is at 2.2 gpm, 1500 psi, and 60 strokes/min. A single-diaphragm feed-pump head is being constructed with a 12-in.-dia contour, a 10.6-in.^{3} maximum displacement per stroke, 40-μ screening, and communicating holes to the diaphragm chamber over the entire contoured surface. The calculated diaphragm stress is 25,000 psi. A triplex arrangement of either of the above heads will supply the predicted 6-gpm fuel feed requirements of HRE-3.

A John Bean triplex power end, designed for 10-gpm service at 2000 psi, was installed with a variable-speed motor. It has been used to drive the double-diaphragm head with water cylinders, is now operating the double-diaphragm head with an oil cylinder and intermediate barrier, and will be used to drive the 12-in. contour head and other large developmental heads.

Several approaches are being tried to eliminate the phasing system presently necessary to obtain and maintain the correct amount of water in the intermediate drive line. Water-service hydraulic cylinders have been used as pulse generators to operate diaphragm heads directly without the use of intermediate barriers. Such a system needs no phasing, is self-regulating, and operates well, but the various cylinders used have been short-lived because the materials will not stand the high pressure drops with the low-viscosity liquid. However, with a conventional intermediate barrier and a reciprocating oil-pulse generator, it is possible to fill the intermediate system at any time so that the pump will operate properly at all pressures. This is accomplished by filling the intermediate system with water pressurized to 20 psig and then removing a predetermined amount. This simple method appears to eliminate phasing troubles.

9.4.2 Alternate Feed Pumps

The single-stage Roth turbine pump has been rebuilt with an impeller of Electrolyzed (trade name for hard-chrome surface of Electrolyzing Corporation) type 316 stainless steel and aluminum

oxide wear rings. It has since delivered 10 gpm of HRT fuel solution against a 300-psi head for 2000 hr with no change in characteristics. This type of pump can be staged to provide fuel feed to a reactor in the range of 5 to 30 gpm.

9.4.3 Slurry Feed Pumps

A remote-leg slurry pump, consisting of check valves mounted 3 ft below a standard diaphragm head and connected thereto by a glass vertical leg, was operated at atmospheric pressure for 1400 hr. A slurry-water interface was maintained in the vertical leg under a variety of conditions, thereby reducing slurry damage to the diaphragm. Tests were run with the following range of variables: slurry, 1600°C-fired ThO_2, as-fired and silicated; fluid density, 2.0 to 2.5 specific-gravity units; stroke volume, 3.5 to 7.0 in.^{3}; speed, 26 to 70 strokes/min; output, 0.3 to 1.5 gpm; vertical-leg diameter, 0.75 to 2 in.; average speed in vertical leg, 1 to 14 in./sec.

Within the range of variables tested, the elevation of the slurry interface above the check valves was a linear function of average speed in the vertical leg. This elevation varied from 6 in. at 1 in./sec to 32 in. at 14 in./sec.

With a 2-ft suction head, the Newtonian silicated slurry was pumped with nearly 100% volumetric efficiency at speeds up to 60 strokes/min. On the other hand, the untreated plastic slurries were pumped inefficiently at speeds above 25 strokes/min. This is illustrated in Fig. 9.3, which shows that at high speeds the denser the slurry (and the higher the yield stress), the less efficiently it is pumped. The magnitude of the net suction head as a function of the yield stress will be determined.

A second remote-leg pump (Fig. 9.4) has operated without difficulty for 1600 hr, pumping a slurry of density 1.4 to 1300 psi at 0.4 gpm. A continuous purge and vent system was developed for this pump to prevent gas collection in the head. This vent system is believed to be applicable to any remote-leg type of pump.

A high-pressure slurry feed-pump loop was constructed to evaluate the diaphragm remote-leg pump and the single-contour diaphragm pump.[2]

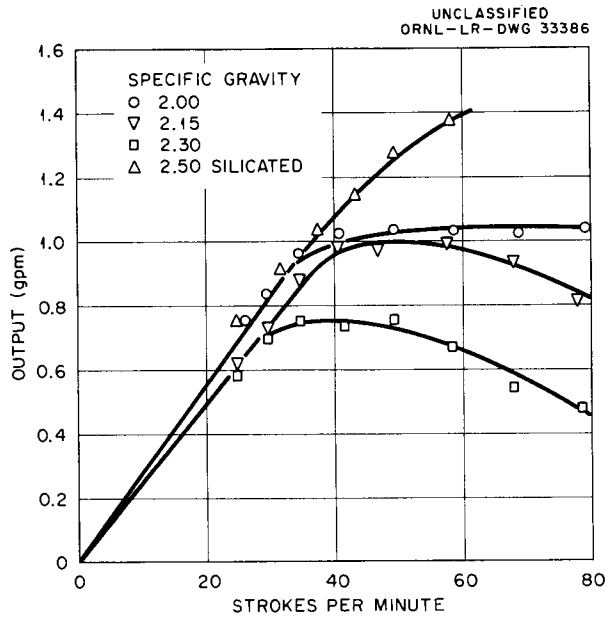

Fig. 9.3. Output of Remote-Leg Feed Pump with Various Slurries.

The pumps operated satisfactorily in a preliminary run circulating slurry with a specific gravity of 2 at 1.75 gpm to 1800 psi.

9.5 VALVE TRIM

9.5.1 Dump-Valve Trim for Solutions

The gold-ring-seal valve completed 4000 dumps. The valve, which had been leak free when checked after 2000 dumps, leaked 85 cc of water per minute at 2000 psi after completion of the test. Loop operation indicated that leakage started following a maintenance period and hydrostatic test. Damage to the seat, visible in Fig. 9.5, appears to be of mechanical origin rather than the result of corrosion.

A type 17-4 PH stainless steel plug and integral type 347 stainless steel seat have operated for more than 4000 dumps and still appear to be functioning properly.

A dump valve utilizing an aluminum oxide ball and seat has been designed and is being fabricated.

9.5.2 Slurry Hand Valves

A number of Pressure Products Industries ¼-in. high-pressure hand valves, equipped with replaceable trim, have been installed in various

[2] I. Spiewak *et al.*, *HRP Quar. Prog. Rep. Jan. 31, 1958*, ORNL-2493, p 59.

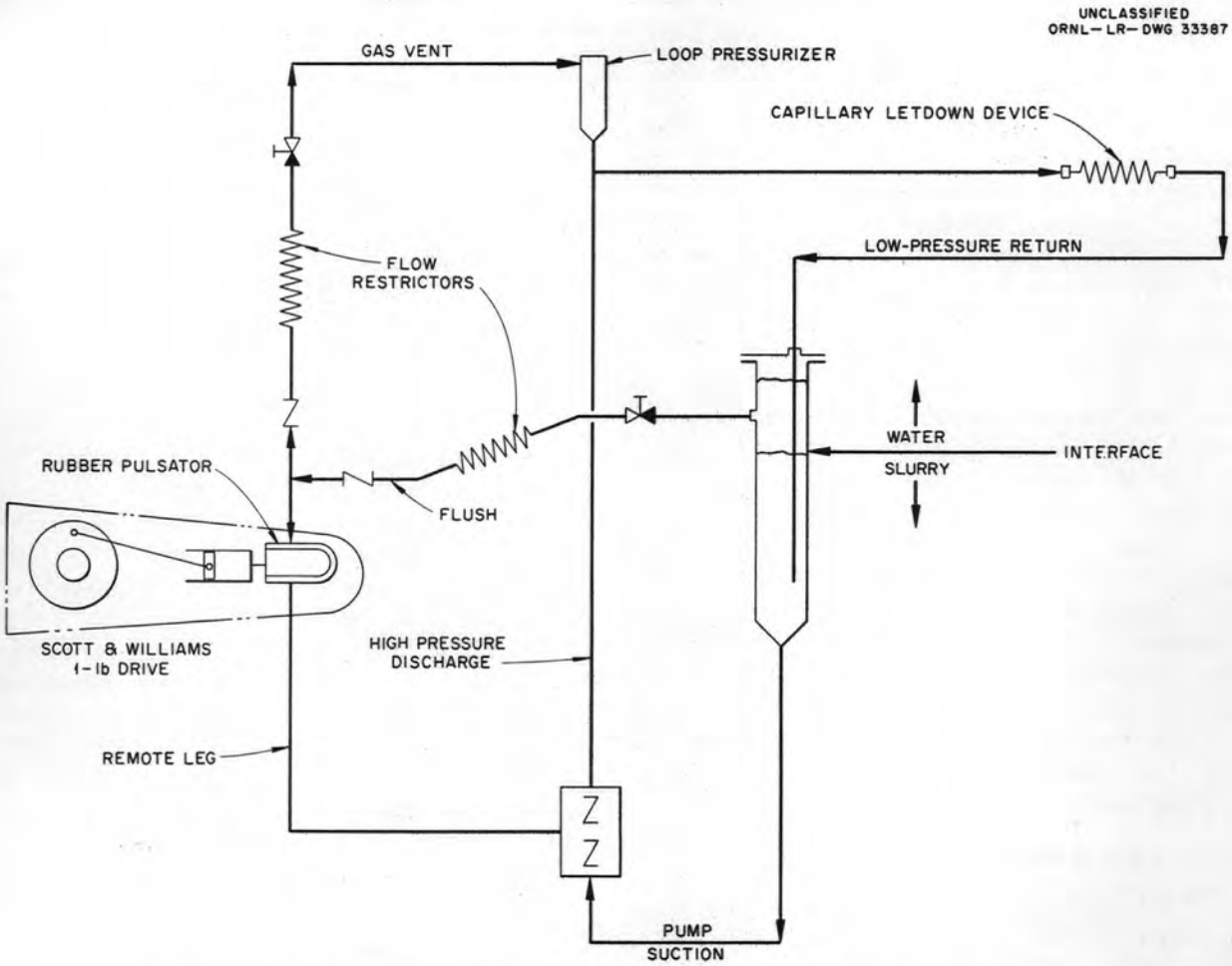

Fig. 9.4. High-Pressure Slurry Feed Pump Used in the Slurry Check-Valve Material Test.

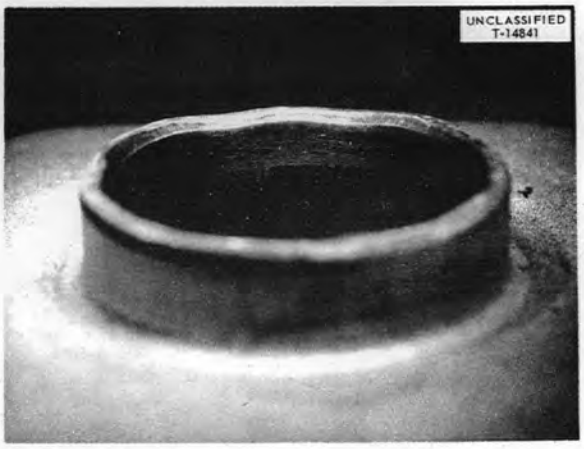

Fig. 9.5. Seat of Gold-Ring-Seal Dump Valve After 4000 Dumps.

loops to test trim materials under service conditions. Materials tested to date are types 18-8 and 17-4 PH stainless steels, Rexalloy, tungsten carbide, and gold. Other materials are on order. The experience with metals has been poor to fair, while that with tungsten carbide has been good. To illustrate, one application required a valve to throttle 2 cc of slurry per second with a pressure differential of 1300 psi at room temperature. While several metal-trimmed test valves failed to shut off after 10 min of throttling service, a valve with tungsten carbide trim was able to shut off after 3 hr of the same service.

Gold-trimmed hand valves, of the type selected for use on the PAR in-pile loop experiment, were tested on a slurry loop. They were cycled through 50 on-off operations with high and low pressure

drops and passed a 1600-psi hydrostatic test before removal from the loop.

9.5.3 Letdown Valves

A hole eroded through a 10-ft-long 0.063-in.-bore capillary tube about 1 in. downstream from the entrance after 1690 continuous hours of slurry letdown service. Average operating conditions were: slurry concentration, 660 g of ThO_2 per kg of water; pressure drop, 1250 psi; and velocity, 42 fps. Up to the time of the failure, no change in performance indicating wear or plugging was noted. About an inch of tubing above and below the hole was sectioned. The severe erosion was highly localized; the rest of the examined tubing showed some slight uniform wear. It is possible that the localized attack was initiated by damage to the wall from the drill used to clean out the weld at the end of the tube. However, the erosion had destroyed the evidence. The damaged section was replaced and the tubing has continued in service for another 1600 hr, making a total of 3300 hr for 9 of the 10 ft.

Fixed and variable capillary letdown systems in the 1-gpm range have been fabricated for use in the high-pressure slurry feed-pump test loop.

9.5.4 Slurry Check-Valve Material Test

Several slurry check-valve materials were evaluated while a 1600°C-fired thoria slurry was being pumped to 1300 psi at a flow of 0.4 gpm. Balls and seats made of stainless steels, titanium, and Stellites all failed in 100 hr or less. Kennametal K-501 (a platinum-bonded tungsten carbide) was in excellent condition after pumping 500-g/liter slurry for 164 hr. It failed in 16 hr, however, while circulating rinse water containing a few solids.

On the other hand, more promising results were obtained with ceramics. Boron carbide trim functioned for 1550 hr with negligible wear. Unfortunately, this material is very brittle and is a reactor poison. Aluminum oxide (85% purity) trim during operation up to 772 hr exhibited wear rates of from 45 to 76 mpy. The valve trim was tight after completion of tests. In comparison, aluminum oxide trim operating in distilled water showed wear rates averaging 30 mpy, while boron carbide showed no wear at all. Future testing will evaluate the commercially available ceramics, gold, Zircaloy, and zirconium alloys. Data thus far obtained indicates that check valves can be built now with slurry-service life expectancies of from six months to one year of continuous duty.

9.6 TITANIUM PROGRAM

Crane Company has decided that they are unable to fabricate titanium-lined $3\frac{1}{2}$-in. and 20-in. pipe in a manner which will withstand high pressures. Although they have spent much time and effort on this project, they have requested that they be released from the contract at no cost to ORNL. A fabrication history of the project, the $3\frac{1}{2}$-in. pipe as fabricated, and an account of findings on the 20-in. pipe when it is examined destructively are being purchased from the Crane Company for about 20% of the original contract price.

The small titanium-lined heat exchanger, constructed by The Pfaudler Company, has been received. It is being prepared for hydrostatic, thermal-cycle, and helium leak tests.

The $3\frac{1}{2}$-in. titanium A-110AT pipe extruded by Chase Brass & Copper Company was bored and honed by Watervliet Arsenal. Several small surface pits still remain, but no serious defects were found during x-ray and ultrasonic examination. Sound welds were produced in weld tests on the material. The pipe was fabricated into a boiling uranyl sulfate pressurizer for the HRT mockup.

9.7 BOLTING-MATERIAL PROGRAM

Several materials are being evaluated for high-strength bolting applications in contact with UO_2SO_4 fuel systems. Static corrosion tests of Allegheny Ludlum AM-355 and Universal-Cyclops 19-9 DL stainless steels in fuel solution at 300°C indicated an acceptable corrosion resistance. When stressed specimens were subjected to the same environment, AM-355 specimens failed in each of the heat treatments supplied, whereas 19-9 DL stood up unusually well. Both materials are to be heat treated again in an effort to arrive at an optimum treatment, and further corrosion tests will be made. Timken 16-25-6 and 16-15-6 stainless steels are now being heat treated for corrosion tests.

A $\frac{3}{8}$-in. titanium (A-110AT) screw and a $\frac{3}{8}$-in. screw of CD4MCU stainless steel have been stressed with nuts containing hardened stainless steel thread inserts. Both units were placed in fuel solution and have accumulated several

hundred hours of exposure. No galling has been observed during periodic disassembly.

9.8 HEAT EXCHANGERS

9.8.1 Tube-Joint Test

Thermal-cycle testing of the small tube bundles in an environment containing 50 ppm Cl and 10–25 ppm O_2 in 200°C boiling water was terminated. One of the units had operated 5000 hr when shut down. Metallographic examination is as yet incomplete. Some specimens have shown cracks which might be due to stress cracking or mechanical failure.

9.8.2 Heat Exchanger Test Facility

A contract for a heat input condenser and four test steam generators has been awarded to Griscom-Russell Company. The test bundles will contain tubes of type 347 stainless steel, type 304 stainless steel, type 347–carbon steel composite tubing, and type 347–Inconel composite tubing, respectively. Drawings of these units have been reviewed and returned to the vendor for fabrication. The vendor is investigating sources of composite tubing and initiating a tube-to-tubesheet welding program for the materials.

9.8.3 Slurry Heat Exchanger Flow Tests

A loop has been built to observe slurry behavior in plastic models of proposed heat exchanger designs. Equipped with a 100-gpm Moyno pump coupled to a variable-speed drive, the loop will have adequate head and a wide range of flow rates for room-temperature testing. To date, the loop has been flushed out and has received a shakedown run on water. Two plastic models are ready for testing.

9.9 HYDRODYNAMICS IN CORES AND BLANKETS

9.9.1 Heat Transfer from HRE-3 Core Wall to Core Solution

In order to prevent overheating of the HRE-3 core-tank wall, it is necessary to provide good thermal contact between the metal and adjacent fluids. Experimental measurements of the heat transfer coefficients between the core wall and circulating core fluid were completed in a full-scale 48-in. model of the HRE-3 core. Heat transfer rates were determined at four different latitudes, at flow rates of 1000 to 6000 gpm, and at two temperatures. The heat transfer coefficients at any one location were found to vary in a manner predicted by the standard Dittus-Boelter correlation, which was used to extrapolate to reactor temperature of 280°C. It can be seen in Fig. 9.6 that the minimum heat transfer coefficient predicted for HRE-3 is 2000 Btu/hr·ft^2·°F for the locations measured. This would permit only a very small increase in core wall temperature above fluid temperature during full-power reactor operation. The minimum heat transfer coefficient would be expected at the 180-deg angle, and measurements at this location are being made.

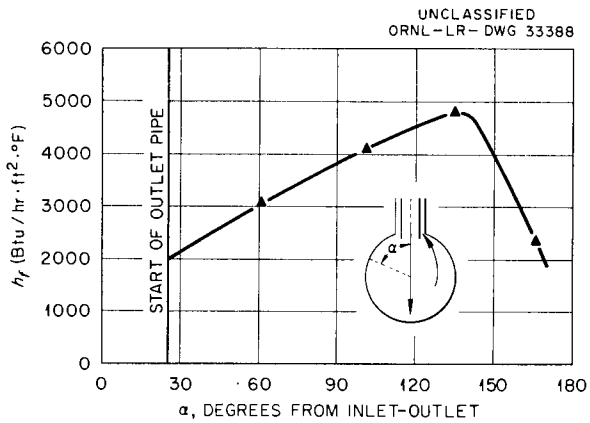

Fig. 9.6. Heat Transfer Rate Profile from HRE-3 Core Model (at 280°C). Flow rate, 6000 gpm.

9.9.2 Low-Pressure Model of HRE-3 Blanket[3]

A one-third-scale model of the proposed HRE-3 slurry blanket containing a jet pump, plastic core, and constant-flow-area shroud was operated with water to obtain measurements of flow behavior in the jet pump and shroud. The model was first operated with a single-nozzle, 1.625-in. dia, jet pump carrying a primary flow of up to 250 gpm. It was found necessary to replace the single nozzle in the jet pump with a multinozzle design to eliminate flow reversal and separation in the jet diffuser. With the multinozzle jet, shrouds of 24- and 34.4-in.^{2} flow areas were tested. The ratios of total shroud flow to primary jet flow for the two shrouds were 2.65 and 3.3, respectively. No areas of flow separation could be observed in either shroud.

[3] *Ibid.*, pp 60,61.

It was concluded from this work that a multi-nozzle jet pump coupled to a sizable slurry flow annulus surrounding the core would provide a very satisfactory method of removing heat from the high-power-density region adjacent to the core.

9.9.3 Single-Region Slurry Core

The 30-in. aluminum model of the HRE-3 blanket was converted to a one-half-scale model of a slurry core. This model will be used to develop the internals required to obtain a homogeneous slurry distribution within the core of HRE-4.

9.10 SEPARATION OF WATER FROM ThO_2 SLURRY

Tests on the separation of water from ThO_2 slurry were made with a small laboratory-model centrifuge on slurries of various concentrations. The results indicated that by varying the nozzle opening and bowl speed, separation could be controlled slightly, but, on the whole, the separation was not adequate. A characteristic of most runs was the plugging of one or more nozzles, causing buildup of slurry cake and severe rotational unbalance. It is possible that a more ruggedly constructed centrifuge would provide better results.

A small tubular filter containing 4-μ pore openings permitted separation of pure water from circulating slurries containing 100 to 1000 g of ThO_2 per liter. Water rates of 7 to 90 cc/min were obtained with a filter containing 6 in.^{2} of area; however, the capacity of the system was not reproducibile. The fragileness of the filter material tested limits its usefulness to laboratory applications. Tests of sturdier filters are planned.

Tests of both horizontal and vertical settling chambers indicated that sedimentation is a promising method of separation for slurries in the hindered-settling region, particularly at concentrations below 300 g of ThO_2 per liter. Further work is planned at higher concentrations.

9.11 SLURRY DUMP TANKS AND EVAPORATORS

The feasibility of using a steam-heated coil immersed in slurry to evaporate water for condensate production and for slurry resuspension depends on the absence of foam, the absence of slurry dehydration at the heated surface, and, in the case of slurry resuspension, reasonable energy requirements.

A 6-in.-dia glass model was tested with and without a draft tube and with both flat and conical bottom configurations.[4] A current production batch of 1600°C-fired thoria and 200A-14 pumped thoria slurry were used in the tests. In no case was foaming observed. The heating coils were operated at heat fluxes from 5000 to 50,000 Btu/ft^2·hr·°F, without caking on the submerged portions of the coil. During a rinsing operation, a portion of exposed coil was observed to have a thin hard film, which was easily removed when the coil was again submerged and heated. Heat transfer measurements from the coil to the slurry show the same results for pure water and for slurry containing 950 g of Th per kg of H_2O. The over-all boiling-heat-transfer coefficients increased from 350 Btu/ft^2·hr·°F at a heat flux of 5000 Btu/ft^2·hr·°F to 630 Btu/ft^2·hr·°F at a flux of 50,000 Btu/ft^2·hr·°F.

In all tests thoria was resuspended readily and maintained at uniform concentration, except for a small amount of sediment which was generally retained on the flat or conical bottom. Tests of steam-heated bottoms are planned in an attempt to eliminate this accumulation.

9.12 SETTLED-BED PROPERTIES OF THORIA SLURRIES

Settled beds of slurry can occur in reactor components as the result of processes such as sedimentation, centrifugal action, filtration of water from slurry deposited in semistagnant lines, and drying. An investigation was started to learn more about the properties of settled beds and their redispersion.

9.12.1 Low-Speed Centrifuge

A low-speed centrifuge, capable of subjecting any vessel less than 1 in. in diameter and 12 in. long to acceleration forces between 1 and 30 *g*, was constructed and operated. The centrifuge provided a convenient rapid method of producing compacted beds. The compaction settling rate of dense slurry was determined on the centrifuge as a function of acceleration for three thoria slurries. For two of these slurries [Figs. 9.7(*a*,*b*)] there was a fixed initial settling rate independent of acceleration. The greater the acceleration, however, the longer this settling rate was maintained.

---

[4] *Ibid.*, p 60.

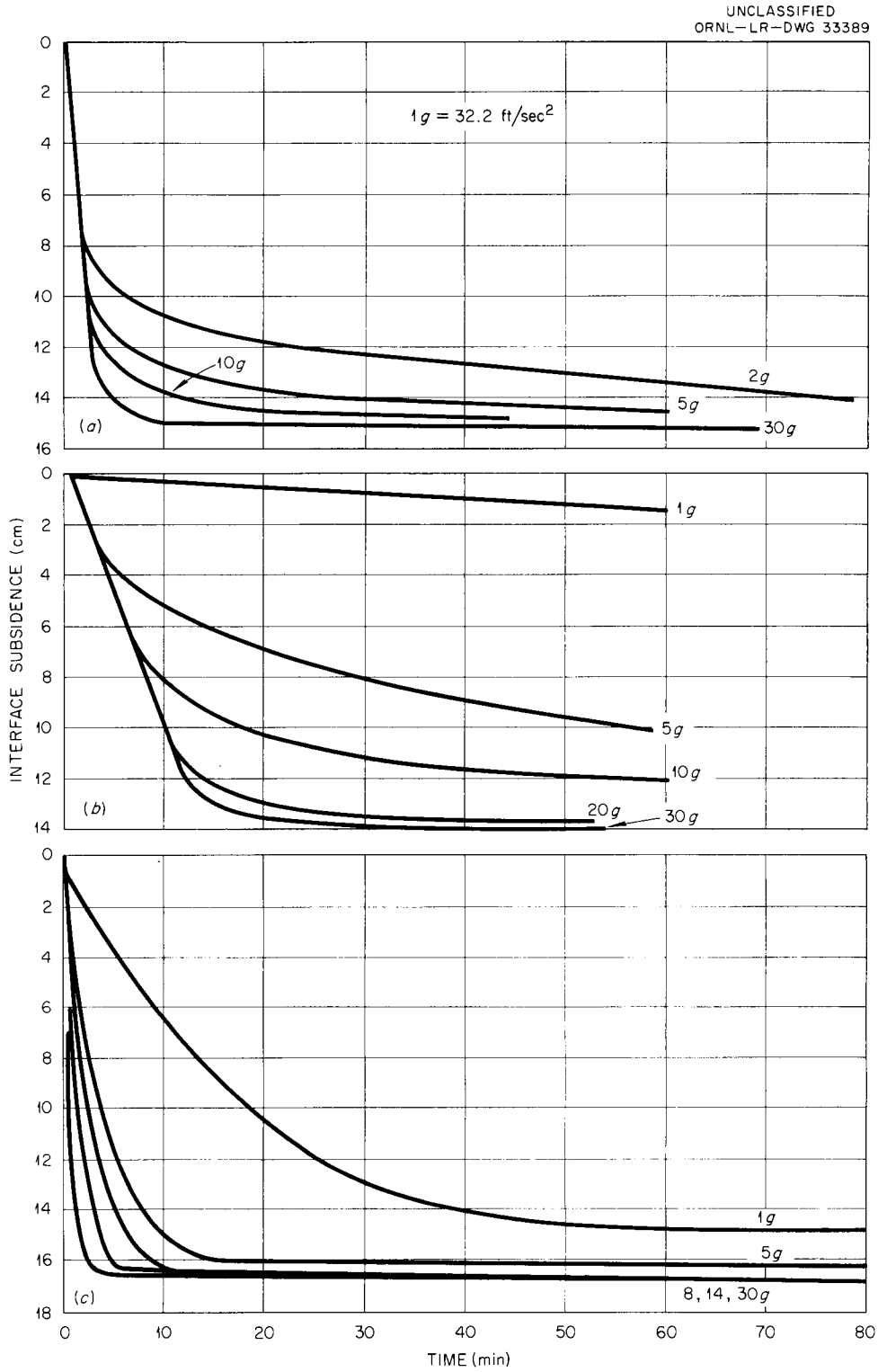

Fig. 9.7. Effect of Acceleration Forces on Initial Settling Rate of Three Thoria Slurries. (*a*) D-41 slurry; 800°C-fired; initial concentration, 790 g of ThO_2 per liter; particle size, 7 μ. (*b*) LO 35-37 slurry; 1600°C-fired; initial concentration, 790 g of ThO_2 per liter; particle size, 1.8 μ. (*c*) 3- to 5-μ cubical particles; initial concentration, 795 g of ThO_2 per liter.

These slurries consisted of random-shaped particles fired at 800 and 1600°C.

For the other slurry examined, there appeared to be no limiting settling rate in the range of acceleration forces examined [Fig. 9.7(*c*)]. This slurry consisted of closely sized cubical-shaped particles.

The centrifuge was used to examine the settled-bed density of many slurries at 30 *g* acceleration. Table 9.2 presents the settled-bed density at 1 *g* (gravity settling) and at 30 *g* for the slurries examined.

It is concluded from these data that particle size is an important variable in determining settled-bed density. Regular-shaped particles, such as cubes and spheres, appeared to settle more densely than irregular particles. Pumping changed the settled-bed characteristics, presumably because of corrosion-product additives and production of a larger proportion of fine particles.

9.12.2 Effect of Bed Depth

The effect of bed height on settled-bed density is being determined in a 1-in. vertical pipe. Results from a preliminary run with a slurry of 800°C-fired oxide show that the limiting density of the settled bed is reached at a distance of ~2 ft below the slurry level and that the density remains constant below that to at least the 6-ft level. This density is about twice the density of a 4-in.-high bed of the same slurry.

9.12.3 Slurry Plug Tester

A device was constructed to determine the force necessary to blow a compacted slurry plug up to 12 in. long from small-diameter pipe (¼ to 1 in. ID). Initial runs, with an 800°C-fired thoria slurry compacted initially under a 30 *g* acceleration force, demonstrated that the slurry will slip through a ¼-in.-ID pipe as a solid plug under less than 1 psig pressure, leaving a clean wall in the pipe. This slippage is probably due to a water film surrounding the plug. When the slurry is permitted initially to compact further by building up behind a cotton plug under pressure, a 1-in.-long plug did not flow in one case with 45 psig pressure applied. Further runs are scheduled to show the effect of corrosion products on plug behavior.

Table 9.2. Slurry Settled-Bed Concentration*

Slurry	Description	Final Concentration (g of ThO_2 per liter)	
		1 *g*	30 *g*
Houdry spheres	3–10 μ fraction	3900	5200
"Cubes"	4 μ	2700	3800
DT-2,3 irregular shape	3–7 μ, 1600° C fired	2200	2700
"Cubes"	1.8 μ	1800	2800
LO 35-37 irregular shape	1.8 μ, 1600° C fired	1400	2500
DT-1 irregular shape	1 μ, 1600° C fired	1300	2600
DT-1	After approximately 1500-hr loop operation (BS-22)	1800	3400
DT-1	Supernate washed out of BS-22 above	1800	2900

*Data taken in 1.6-cm-ID tube, 3-in.-high slurry level; initial concentration around 800 g of ThO_2 per liter of solution.

10. DEVELOPMENT OF REACTOR SLURRY SYSTEMS

R. B. Korsmeyer F. N. Peebles

D. G. Davis
R. B. Gallaher
C. H. Gibson
R. J. Kedl
V. L. Kenyon
L. F. Parsly
H. B. Piper
M. Richardson
A. N. Smith
R. W. Wansbrough
R. P. Wichner[1]

10.1 CIRCULATING-SLURRY BEHAVIOR

Slurry and water were circulated in S, T, and 200A loops for 8389 hr (65% of the time) during the last six months. A summary of these runs is given in Table 10.1.

10.1.1 200-gpm Loop Operation

Run 200A-15, to determine the circulation and degradation characteristics of 1600°C-fired oxide, was started on February 4 and was still continuing at the end of the report period. The initial loading was for a concentration of 1170 g of Th per kg of H_2O, and during the first 48 hr of circulation the concentration was increased to approximately 1500 g of Th per kg of H_2O. The loading was carried out in that manner so that the rise of the slurry-water interface in the pressurizer could be followed at the two concentrations. By means of gamma-ray attenuation across the pressurizer, the slurry-water interface was found to rise no higher than 10 in. above the inlet pipe into the pressurizer, even during the slurry additions. The difference between this behavior and that in run 200A-11[2] with 800°C-fired oxide, in which the slurry level rose to 44 in. above the inlet pipe, was attributed to differences in settling rates and rheologic properties of the two slurries.

The loop was operated with 1500 g of Th per kg of H_2O for 400 hr, after which the concentration was reduced to approximately 700 g of Th per kg of H_2O in order to lower the yield stress of the circulating slurry from 0.8 lbf/ft^2 to 0.1 lbf/ft^2. $UO_3 \cdot H_2O$ was added at 1544 hr to give a concentration of ½ wt % of uranium in order to determine the effect of this additive on the yield stress and the handling characteristics of the 1600°C-fired oxide.

MoO_3 was added at 2419 hr to give a concentration of 1.16 mole % of molybdenum to determine the effect of this addition on the yield stress and the handling characteristics of 1600°C-fired oxide.

The generalized attack rate indicated by iron accumulation in the slurry was 1.5 mpy with 1500 g of Th per kg of H_2O and 0.6 mpy with 700 g of Th per kg of H_2O. During 850 hr of circulation with uranium as the only additive, the generalized attack rate was 1 mpy and has remained at the same value during the 969 hr since the molybdenum addition.

The total iron accumulated during 3484 hr was 146 g, with the greater part coming from the type 347 stainless steel impeller. The attack on the titanium scroll liner was low; only 23 g of titanium, as determined by chemical analyses, accumulated in the slurry during the same period of operation.

The nitrogen absorption surface area of the slurry remained constant at 1.5 m^2/g for the first 2032 hr, with no later data available at this time. The average mean particle size for the first 100 hr was 1.78 ± 0.16 μ and decreased to 1.63 ± 0.09 μ for the period 100 to 1350 hr (intervals about the average values correspond to the 95% confidence level). There was no significant difference in the average mean particle sizes for the periods 100 to 500 hr and 500 to 1350 hr.

The only difficulties encountered during this run were mechanical. Two slurry sample valves failed, and then the sampling system was revised to permit back-flushing of the valves with water. A crack developed in the pump-flange seal weld, but it was successfully repaired. The only other difficulty occurred when a piece of tubing slipped out of a swaged fitting, momentarily releasing slurry to the atmosphere. Steps have been taken to eliminate this hazard.

10.1.2 100-gpm Loop Operation

Four runs were made in the 100A loops in continuation of the study of the effect of additives on the caking and sphere-forming tendencies of

[1]Attending Oak Ridge School of Reactor Technology.

[2]R. B. Korsmeyer *et al.*, *HRP Quar. Prog. Rep. April 30, 1957*, ORNL-2331, p 70.

Table 10.1. High-Temperature Slurry Circulation – Run Summaries

	Run No.								
	200A-15	S-111	S-112	S-113	S-114	S-115	S-116	S-117	S-118
Test dates	2/4 to 1*	1/6 to 1/20	1/27 to 2/10	2/20 to 3/5	3/15 to 3/21	3/31 to 4/1	4/7 to 4/10	4/28 to 4/30	5/8 to 5/25
Running time, hr	1	324	306	308	127	25	80	56.5	402.9
Objective	To determine circulation and degradation characteristics of 1600°C-fired ThO_2	To determine effect of uranium on coking and sphere-forming tendencies of 800°C-fired ThO_2 (rerun of T-95)	To determine circulation and degradation characteristics of 1600°C-fired ThO_2	To determine circulation and degradation characteristics of 1600°C-fired ThO_2 (rerun of S-112)	To determine effect of sulfate on the yield stress of 1600°C-fired ThO_2	To determine yield stress and pumping characteristics of 1600°C-fired ThO_2 containing 300 ppm sulfate	To determine yield stress and pumping characteristics of 1600°C-fired ThO_2 containing 300 ppm sulfate (rerun of S-115)	To determine yield stress and pumping characteristics of 1600°C-fired ThO_2 containing 300 ppm sulfate (rerun of S-116)	To determine yield stress and pumping characteristics of 1600°C-fired ThO_2 containing 300 ppm sulfate (rerun of S-116)
Charge									
ThO_2, kg	57.7 (LO-36-1600) 18.6 (LO-39-1600)	4.05 (LO-23)	4.6 (LO-36-1600)	4.7 (LO-39-1600)	8.0 (LO-40-1600)	11.2 (LO-40-1600)	15 (LO-40-1600)	15 (LO-40) from runs S-115 and -116	9.65 (LO-40) from runs S-116 and -117
Water, kg	60	12.1	12	12	12	12	12	12	11.5
Additives	75 liters O_2	29 g $UO_3 \cdot H_2O$	25 liters O_2	25 liters O_2	36.7 g conc H_2SO_4 25 liters O_2	3.7 g conc H_2SO_4 25 liters O_2	4.6 g conc H_2SO_4 25 liters O_2	25 liters O_2	25 liters O_2
Temperature, °C	300	290	290	290	290	290	290	290	290
Pressure, psig	2000	1600	1600	1700	1700	1700	1700	1700	1700
Average circulating concentration, g of Th per kg of H_2O	1	331	585	520	768	1225	1425	1600	1290
Reason for termination	1	Scheduled shutdown	Noisy pump; hydraulic unbalance due to wear in seal rings and orifice plate	Scheduled shutdown	Leak in pressurizer sample system	Noisy pump; oxide under rear weld pads	Leak in pressurizer sampling system	Noisy pump; front bearing failure	Leak in pressurizer sample valve
Equilibrium mean particle size, μ	1	1.0	2.2	1.5	1.6	1.3	Not available	1.2	1.2
Cake location	1	No cake	No cake	No cake	No cake	No cake	No cake	No cake	No cake
Fe buildup in slurry, g	1	23.2	80.7	16.1	84.6	2.53	5.33	8.3	32.5
Ni buildup in slurry, g	1	3.84	13.4	2.0	13.4	0.50	0.85	1.25	4.22
Cr buildup in slurry, g	1	3.98	15.3	2.0	9.9	0.52	0.82	1.36	0.69
Impeller weight loss, g	1	9.8	77.3	7.0	34	5.8	3.5	2.5	17.0
Orifice-plate weight loss, g	1	0.7575	Badly eroded; not removed from holder	0.475	1.6741	0.0080	0.1877	0.0975	0.7771

*Incomplete (still running).

Table 10.1 (continued)

	Run No.							
	S-119	S-120	T-97	T-98	T-99	T-100	T-101	T-102
Test dates	6/9 to 6/12	6/20 to 6/30	1/14 to 2/11	2/25 to 2/27	3/10 to 4/1	4/17 to 4/30	5/14 to 5/20	6/13 to 6/24
Running time, hr	56.5	237.4	678	48	531	353.5	142	269.1
Objective	To determine particle integrity and pumping characteristics of 1600°C-fired 3-μ-particle-size ThO_2	To determine effect of silica dry-film treatment of ThO_2 on yield stress and pumping characteristics	To determine effect of molybdenum and uranium on caking and sphere-forming tendencies of 800°C-fired ThO_2 at 1000 g of Th per kg of H_2O	To determine caking and sphere-forming tendencies of 800°C-fired ThO_2 with no additive (rerun of T-91)	To determine effect of molybdenum and uranium on caking and sphere-forming tendencies of 800°C-fired ThO_2 (rerun of T-96)	To determine caking and sphere-forming tendencies of 800°C-fired ThO_2 digested for 48 hr after oxalate precipitation	Same as T-100, at a higher concentration	Same as T-101, a continuation of the run
Charge								
ThO_2, kg	10 (DT-5)	8.8 (LO-40 dry-film)	12.4 (LO-23)	5.1 (LO-23)	4.9 (LO-23)	4.95 (LO-44-200)	8.62 (LO-44-200)	7.0 (from T-101 plus 1.3 kg fresh)
Water, kg	11.5	11.5	14.8	15.5	15.5	15.5	15	15
Additives	25 liters O_2	25 liters O_2	76 g $UO_3 \cdot H_2O$ 76 g MoO_3 25 liters O_2 50 g sodium aluminate after 300 hr of circulation	25 liters O_2	32 g $UO_3 \cdot H_2O$ 32 g MoO_3 25 liters O_2 12.3 g conc H_2SO_4 after 408 hr	25 liters O_2	25 liters O_2	25 liters O_2
Temperature, °C	290	290	290	290	290	290	290	290
Pressure, psig	1700	1700	1600	1600	1600	1700	1700	1700
Average circulating concentration, g of Th per kg of H_2O	1435	740	886	481	478	555	1024	990
Reason for termination	Excessive corrosion rate	Hydraulic unbalance in pump; weld pads came loose and scraped back of impeller severely	Scheduled shutdown	Noisy pump	Scheduled shutdown	Scheduled shutdown	Leak in $\frac{1}{4}$-in. pipe nipple	Pump noisy; front bearing failed
Equilibrium mean particle size, μ	2.3	1.2	0.5	15	0.34	1.5	1.7	1.6
Cake location	No cake	Some light film formed in loop piping and pump scroll	No cake	Eye and vanes of impeller	No cake	No cake	No cake	No cake
Fe buildup in slurry, g	51.1	159.5	61.1	8.77	21.9	31.6	40.7	26.7
Ni buildup in slurry, g	8.77	28.0	9.3	1.15	3.09	5.0	6.79	4.38
Cr buildup in slurry, g	9.0	25.6	10.1	1.66	2.22	6.1	8.72	3.04
Impeller weight loss, g	39.5	163.5	30	39.0	13.8	20.0	8.0	26
Orifice-plate weight loss, g	1.3316	1.5385	2.1906	0.0055	0.3445	0.2649	0.2692	0.8146

800°C-fired thorium oxide. Batch LO-23 oxide was used in the runs, three of which were check runs of prior tests.

In run T-98, slurry containing 481 g of Th per kg of H_2O with no additives was circulated for 48 hr, and the run was then terminated by cake formations in the impeller eye, balance holes, and vanes, which caused hydraulic unbalance in the pump. Spheres were formed within 3 hr after the start of the first slurry addition to the loop. No spheres or cakes were observed in run S-111 (containing 331 g of Th per kg of H_2O with ½ wt % of uranium), run T-97 (containing 886 g of Th per kg of H_2O with ½ wt % of uranium and 1.16 mole % of molybdenum), and run T-99, which was the same as T-97 except at a concentration of 478 g of Th per kg of H_2O. Apparently the presence of ½ wt % of uranium and/or 1.16 mole % of molybdenum was sufficient to prevent this slurry from forming spheres or cakes.

Nine tests were made in the 100A loop with 1600°C-fired thorium oxide. In run S-112 batch LO-36-1600 oxide was circulated for 306 hr at a concentration of 585 g of Th per kg of H_2O. The orifice plate showed severe wear after the run was terminated. The impeller, thermal barrier, and scroll were also heavily attacked. The attack rate had increased rapidly with time during the run, and the severe attack was probably due to a deficiency of oxygen in the slurry. The run was repeated as S-113 with batch LO-39-1600 oxide at a concentration of 520 g of Th per kg of H_2O and with the oxygen content of the slurry being maintained above 500 ppm. The generalized attack rate was approximately 4.5 mpy, which is similar to that of the better runs with 800°C-fired oxide containing additives.

As part of the program to find an acceptable slurry additive for lowering the yield stress of thoria slurries, the circulation characteristics of sulfated 1600°C-fired oxide were studied. Room-temperature tests indicated that a substantial reduction in the yield stress of 1600°C-fired oxide could be obtained with the addition of sulfate as sulfuric acid, and five loop tests were run to check the high-temperature behavior of the sulfated high-fired oxide. Run S-114 was loaded to 768 g of Th per kg of H_2O with batch LO-40-1600 oxide, and after 71 hr of circulatior 3000 ppm of sulfate was added as sulfuric acid. There was a marked reduction of the yield stress upon addition of the acid; however, the attack rate rose immediately by a factor of approximately 12. The run was terminated 56 hr later because of the excessive attack rate and a leak in the pressurizer sample system. The orifice plate and impeller were heavily attacked. The rapid attack rate after the acid addition also depleted the oxygen in the slurry. Runs S-115, -116, -117, and -118 were at concentrations of 1225 to 1600 g of Th per kg of H_2O with 300 ppm of sulfate. Of these, the first three runs were of short duration (<100 hr) and were terminated by difficulties with the loop not attributable to slurry behavior; run S-118 was completed without incident. The generalized attack rate for the sulfated slurry, as shown by data from all the runs, was approximately 9 mpy, which is not excessive for these slurry concentrations in the loop.

Run S-119 was made with batch DT-5 oxide which had been sized to give a mean particle size of 3 μ. However, there was a small amount (8%) of particles greater than 5 μ which caused excessive corrosion-erosion, and the run was terminated after 56 hr of operation. The average circulating concentration was 1435 g of Th per kg of H_2O.

The circulation characteristics of silica-coated 1600°C-fired thoria were examined in run S-120. The silica concentration in the slurry decreased rapidly so that only one-tenth of the initial concentration remained after 48 hr of circulation. Abrasion in the pump masked the general attack rate resulting from the slurry. No yield-stress data were obtained.

Three runs were made in T loop with 800°C-fired ThO_2, oxalate digestion time 48 hr (batch LO-44-200): runs T-100, -101, and -102, respectively, at 555, 1024, and 990 g of Th per kg of H_2O. No evidence of caking or sphere formation was observed in these runs. The average mean particle size decreased from 3.0 to 1.6 μ in approximately 36 hr. At the start of the runs the attack rate was high but decreased by a factor of 4 to a generalized attack rate of 10 mpy, which is not excessive in this loop at a concentration of 1000 g of Th per kg of H_2O. The change in the appearance of the particles can be seen by comparing the oxide before pumping (Fig. 10.1) with the oxide after pumping for ~300 hr at a concentration of 555 g of Th per kg of H_2O (Fig. 10.2). Figure 10.3 shows oxide which was prepared in a manner

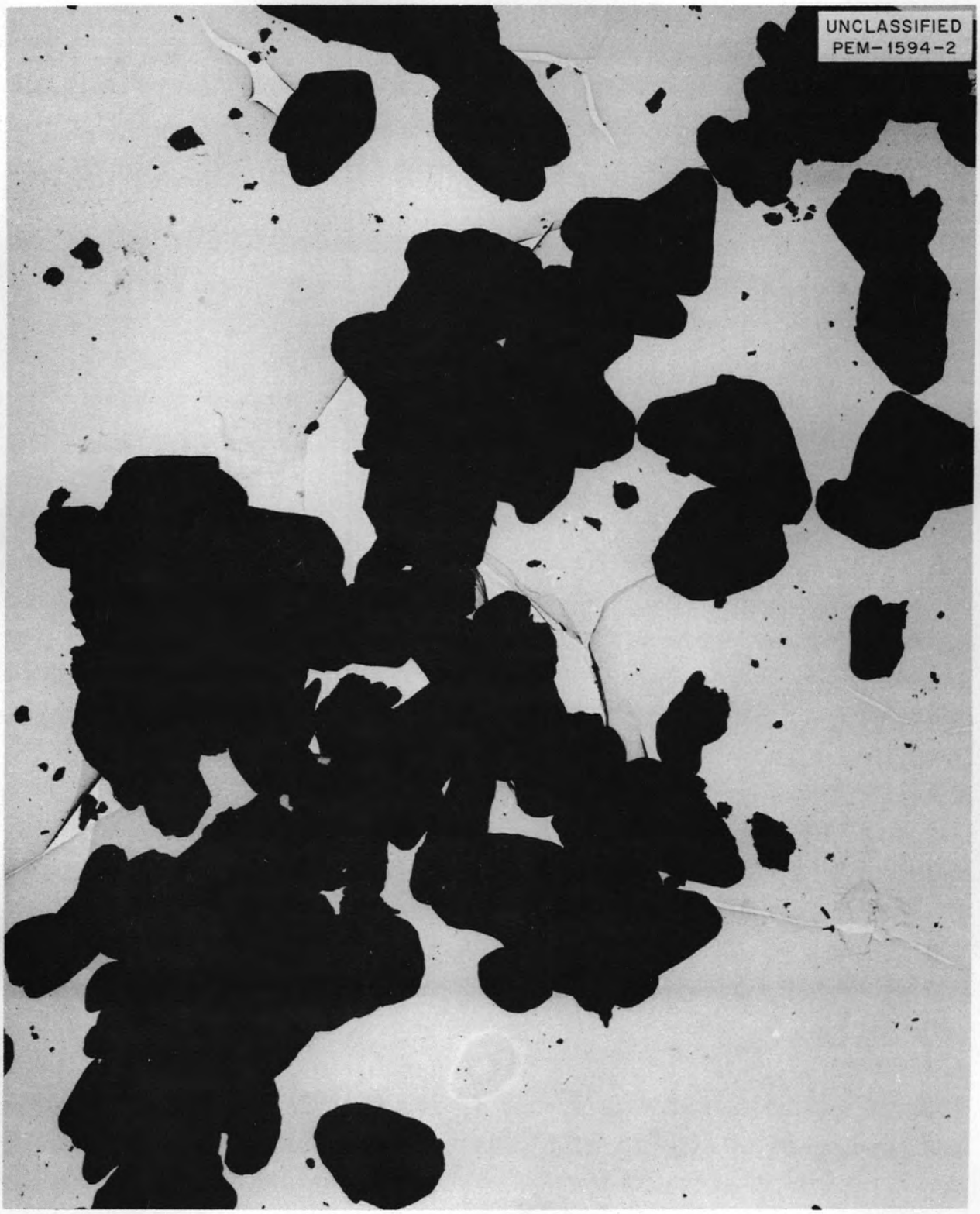

Fig. 10.1. Thorium Oxide, 800°C-Fired, Oxalate Digested 48 hr. 10,000X.

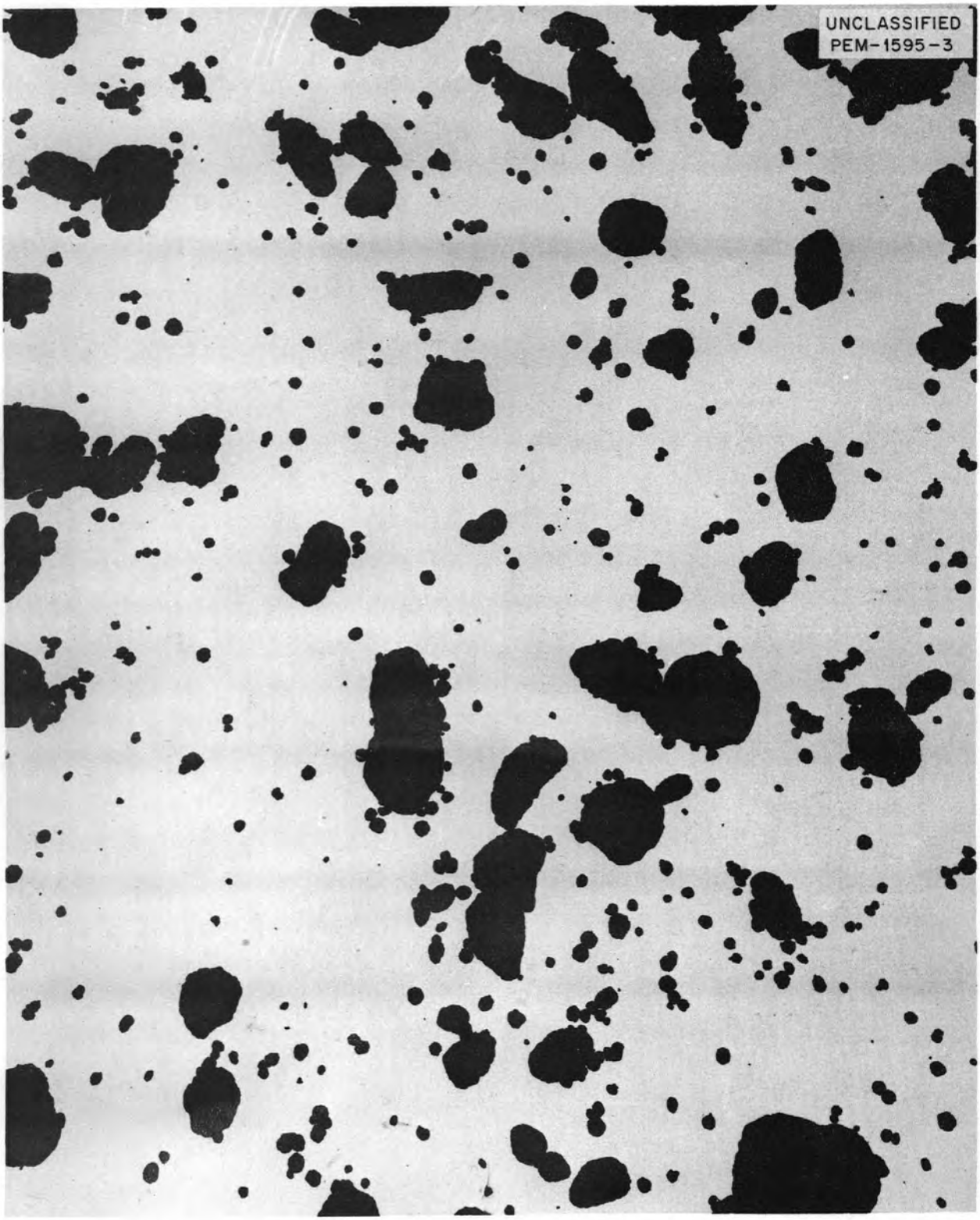

Fig. 10.2. Thorium Oxide, 800°C-Fired, Oxalate Digested 48 hr, Pumped 250–300 hr. 10,000X.

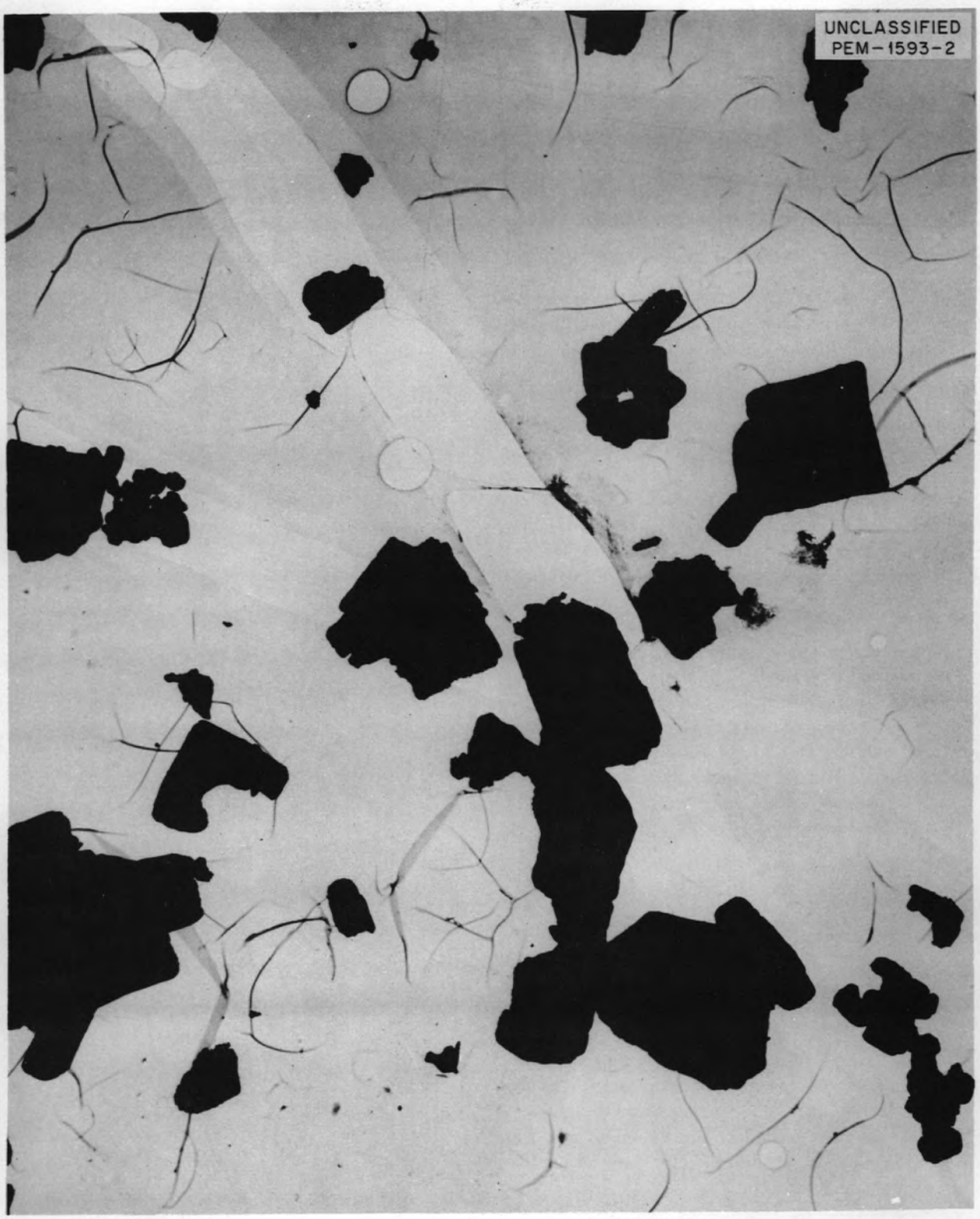

Fig. 10.3. Thorium Oxide, 800°C-Fired, Oxalate Not Digested. 10,000X.

similar to that for the above oxide, except without oxalate digestion, indicating that the digestion brings about a rounding of the sharp corners rather than a change in particle size.

10.1.3 High-Temperature Laminar Flow[3]

During the past six months the capillary-tube viscometer-sampler[4] was used to measure the rheological properties of thorium oxide slurries in 200A, T, and S loops at temperatures from 18 to 305°C and pressures from 1500 to 2000 psi. Figure 10.4 shows schematically the viscometer attached to the slurry loop. Data for the pseudo-shear diagram ($8V/g_cD$ vs $D\Delta P/4L$) were obtained by withdrawing slurry from the loop through the viscometer and measuring the slurry flow rate and pressure drop across the capillary tube of known dimensions. Data were taken after allowing a flush withdrawal equal to at least the volume of the viscometer at a flow rate in the turbulent range. The withdrawal flow rate was then gradually decreased to establish the laminar-flow portion of the pseudo-shear diagram. The apparent diameter of the capillary tube was found to be 0.080 ± 0.001 in. by distilled-water calibrations of the viscometer in laminar flow at room temperature and in turbulent flow at 282°C.

Figure 10.5 shows two pseudo-shear diagrams for the slurries of runs S-114 and T-99. The results of other capillary-tube viscometer-sampler tests are summarized in Table 10.2.

Included in the table is a factor K, defined by the following equation:

$$K = \frac{\tau_y}{(1-\epsilon)^3} ,$$

where τ_y is the yield stress of a slurry and $(1-\epsilon)^3$ is the volume fraction solids. K characterizes the deviation of a slurry from Newtonian behavior, and for many slurries at room temperature the K value is constant for a wide range of slurry concentrations. Preliminary data seem to indicate that K may also be constant for any slurry isotherm at high temperatures.

Also listed in Table 10.2 are values of modified Reynolds number calculated for the intersection

[3]See Secs 8.9 and 8.10 for supplementary discussion of viscometers and slurry flow properties.

[4]R. B. Korsmeyer *et al.*, *HRP Quar. Prog. Rep. Oct. 31, 1957*, ORNL-2432, p 57.

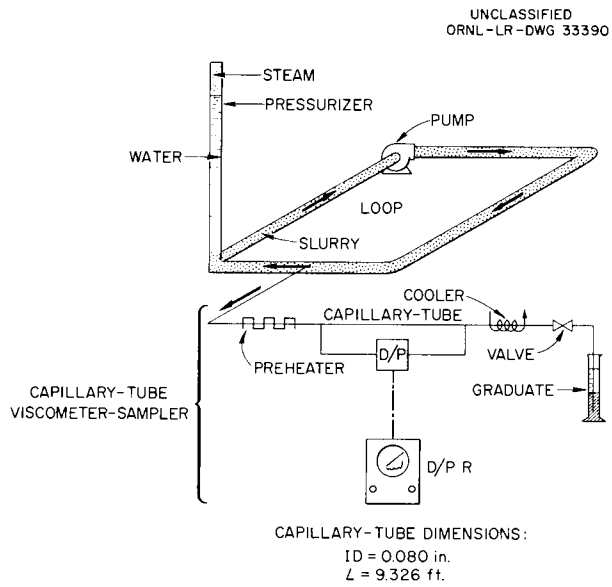

Fig. 10.4. Schematic Diagram of Capillary-Tube Viscometer-Sampler.

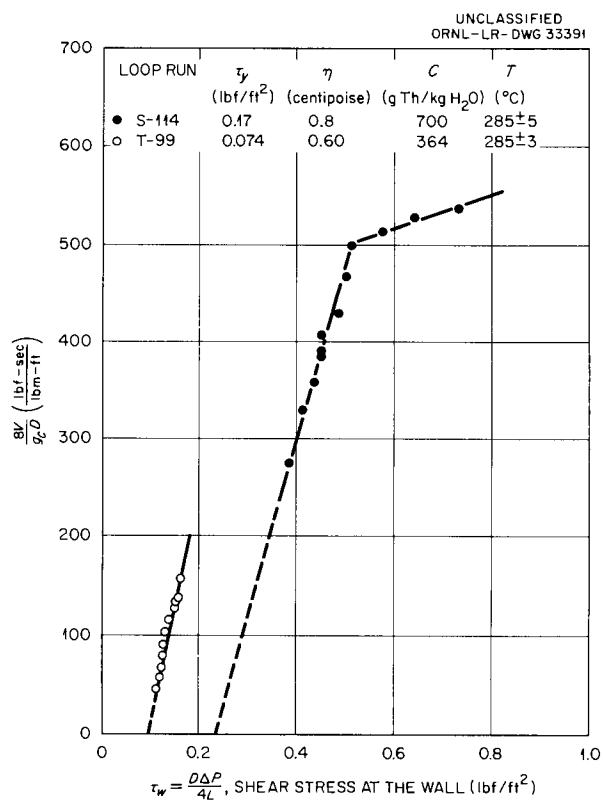

Fig. 10.5. Pseudo-Shear Diagrams, Runs S-114 and T-99.

Table 10.2. Summary of Viscometer Tests

Loop Run	Viscometer*	Temperature (°C)	Yield Stress, τ_y (lbf/ft^2)	Coefficient of Rigidity, η (centipoises)	$\frac{\tau_y}{(1-\epsilon)^3}$, K (lbf/ft^2)	Critical Modified Reynolds No., $DV\rho/\mu a_{crit}$	Thorium Concentration, C (g of Th per kg of H_2O)	Additives		Oxide
								mg per g of Th	mole %	
T-97	CTVS	240 ± 10	1.4–>3	1	2100–>6500		900–1030	U:5	Mo:1.16	800°C LO-23
	CTVS	275 ± 10	0.2–0.8	0.1–0.7	1500–2300	3200–3700	610–1030	U:5; $Na_2Al_2O_3$:5	Mo:1.16	800°C LO-23
	CTVS-LPV	18–25	0.006–0.09	1–3.6	6–180	2110	750–960	U:5; $Na_2Al_2O_3$:5	Mo:1.16	800°C LO-23
200A-15	CTVS	285 ± 10	0.18–0.65	1.2–1.3	400–540	3300–7700	720–1550			1600°C LO-36, 39
	LPV	23	0.06–0.38	2.2–4.3	120–175		650–1520			1600°C LO-36, 39
	LPV	23	0.56	5.0	195	2080	1470			1600°C LO-36, 39
	LPV	23	0.091	3.3	32	1970	1470	SO_4:5.8		1600°C LO-36, 39
	CTVS	275 ± 5	0.003–0.005	0.5–0.9	20–40	4900	640–670	U:5	Mo:1.16	1600°C LO-36, 39
S-114	CTVS	285 ± 5	0.17	0.8	980	6600	700			1600°C LO-40
	CTVS	285 ± 5	0–0.03	0.8	0–150		530	SO_4:1.6		1600°C LO-40
T-99	CTVS	285 ± 5	0.08	0.5	2700		400	U:5	Mo:1.16	800°C LO-23
	CTVS	285 ± 3	0.074	0.60	2700		360	U:5; SO_4:3.1	Mo:1.16	800°C LO-23
Unpumped	LPV	25	0.41	14	120		1550			800°C LO-44 digested
T-100	CTVS	275	0.01	0.55	110	4500	550			800°C LO-44 digested
	VTV-G	30	0.01–0.10	1.2–1.5	100–130	2200	440–1200			800°C LO-44 digested
T-101	CTVS	275	0.05	0.9	120	3400	900			800°C LO-44 digested
S-118	CTVS	282	0.18	2.2	370	>2700	1020			800°C LO-44 digested

*Viscometers identifiable as follows:
CTVS (capillary-tube viscometer-sampler); tube ID, 0.080 in.; L/D, 1400
LPV (low-pressure viscometer); tube ID, 0.1241 in.; L/D, 970
VTV-G (low-pressure vertical-tube viscometer); tube ID, 0.0390 in.; L/D, 1135.

of the laminar and turbulent flow lines of the pseudo-shear diagram:

$$[\text{Re mod}]_{\text{crit}} = \frac{DV\rho}{\mu a_{\text{crit}}} = \left(\frac{DV\rho/\tau_w}{8V/g_c D}\right)_{\text{crit}} .$$

Most of the low-temperature values were about 2100, but values at high temperature ranged from 3170 to 7700.

It is apparent that the rheological properties of the slurries tested varied widely with such factors as concentration, firing temperature, electrolyte additions, and slurry temperature.

The values of K for the 800°C-fired mixed-oxide slurry in run T-97 (LO-23 thorium oxide, ½ wt % U, 1.16 mole % Mo) were in the range 2100 to >6500 lbf/ft^2 at 240 ± 10°C. With the addition of ½ wt % sodium aluminate the range of K values was from 1500 to 2300 lbf/ft^2 at 275 ± 10°C, compared with 6 to 180 lbf/ft^2 at 18–25°C for the same slurry.

The high-temperature K values for the run 1600°C-fired-oxide slurry in run 200A-15 (batch LO-36, -39) were in the range of 400–540 lbf/ft^2 at 285 ± 10°C, compared with 120–195 lbf/ft^2 at 23°C. Sulfuric acid addition (5.8 mg of SO_4 per g of Th) to some 200A-15 slurry at a concentration of 1470 g of Th per kg of H_2O reduced the K value from 195 to 32 lbf/ft^2 at room temperature. The addition of ½ wt % U and 1.16 mole % Mo to the loop decreased the K value to 20–40 lbf/ft^2 at 275 ± 5°C, 640–670 g of Th per kg of H_2O.

The addition of 1.6 mg of SO_4 per g of Th as sulfuric acid to the slurry of run S-114 (LO-40, 1600°C-fired oxide) decreased K from 980 to less than 150 lbf/ft^2 at 285 ± 5°C. The addition of 3.1 mg of SO_4 per g of Th as sulfuric acid to the slurry of T-99 (LO-23, 800°C-fired oxide, ½ wt % U, 1.16 mole % Mo) had no appreciable effect on the K value of 2700 lbf/ft^2 at 285 ± 5°C.

Slurries of an oxide which was digested as the oxalate before being fired to 800°C (LO-44, 200–800°C-digested) were found to have K values of 115 ± 15 lbf/ft^2 at 25–275°C, 440–1550 g of Th per kg of H_2O, before and after pumping for more than 500 hr in two loop runs (T-100, -101).

Coefficients of rigidity for the slurries tested ranged from 1 to 14 centipoises at 18 to 25°C and from 0.1 to 2.2 at 230 to 295°C.

10.1.4 Low-Temperature Laminar Flow

A vertical-capillary-tube viscometer (Fig. 10.6) was designed and built and was used to determine the rheological properties of small samples (50

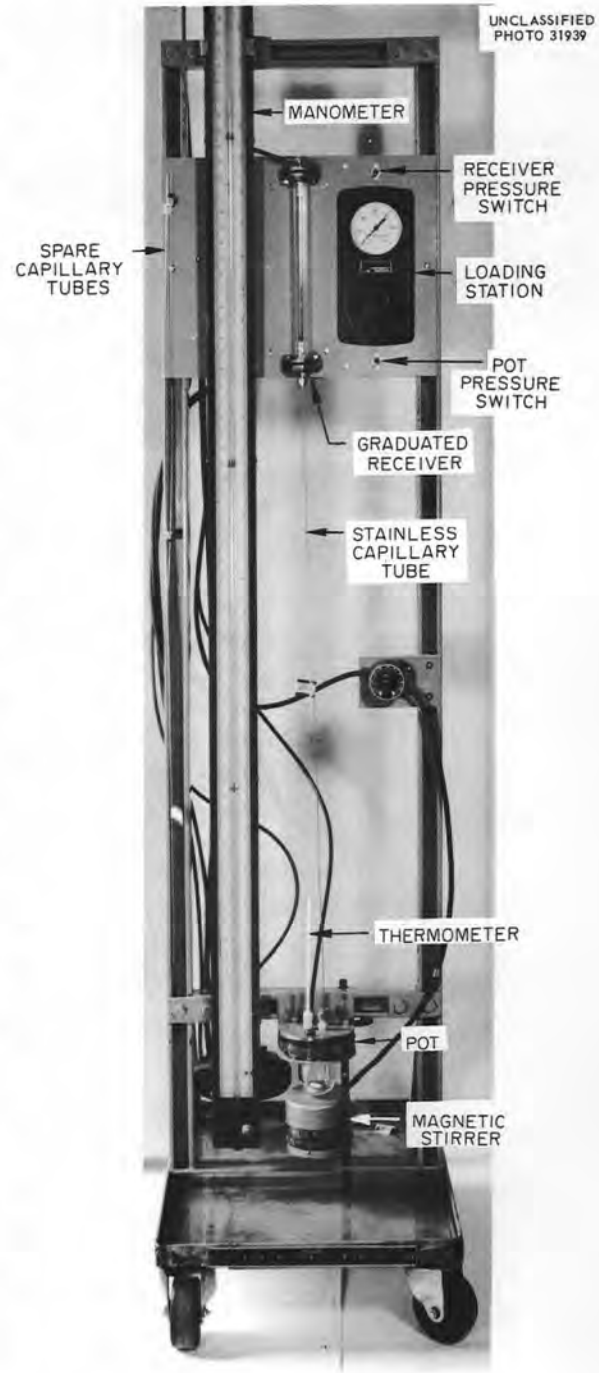

Fig. 10.6. Low-Pressure Vertical-Tube Viscometer.

to 100 cc) of thorium oxide slurries at room temperature. A schematic diagram of the viscometer is shown in Fig. 10.7. Slurry is blown through the capillary tube between the magnetically stirred glass pot and the graduated receiver by pressurizing one or the other with air. Rheological data are taken by measuring the time required for the graduated receiver to be filled or emptied at a given pressure setting measured by the 100-in. mercury manometer. The first pseudo-shear diagrams for the instrument are shown in Fig. 10.8.

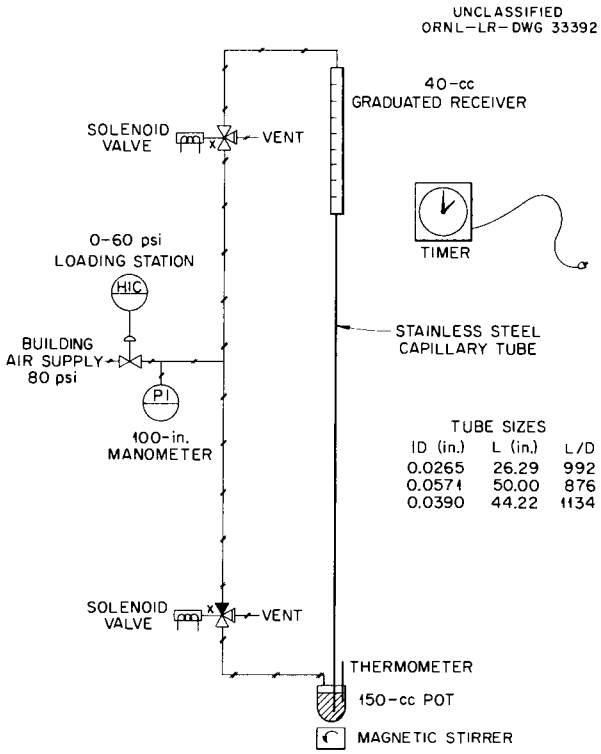

Fig. 10.7. Schematic Diagram of Low-Pressure Vertical-Tube Viscometer.

By proper selection of the capillary tube from the three different sizes which have been calibrated, a wide range of rheological properties may be measured.

10.2 BLANKET SYSTEM DEVELOPMENT

10.2.1 Alterations to the 300-SM System

The following alterations were made to the 300-SM slurry blanket test facility during the report period. The $1\frac{1}{2}$-in. inlet nozzles used during

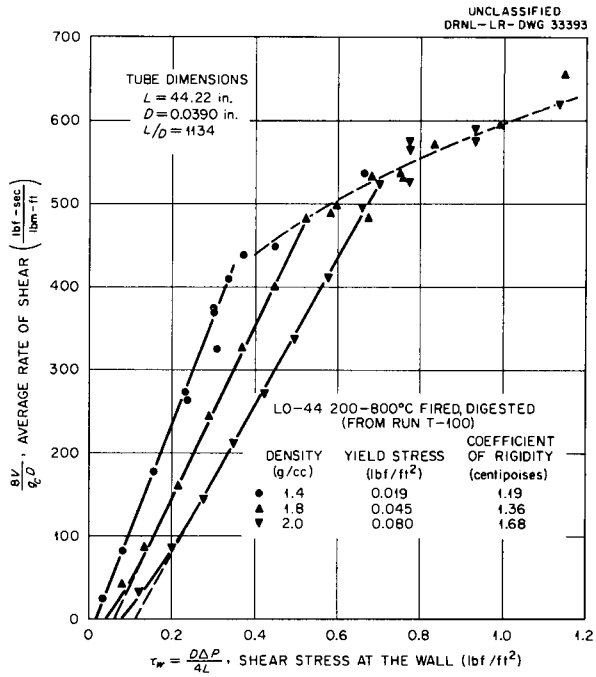

Fig. 10.8. Pseudo-Shear Diagrams from Low-Pressure Vertical-Tube Viscometer (Slurry Temperature, 30°C).

runs SM-3 and -4 were replaced with the 2-in. nozzles used during run SM-2; the blanket exit assembly was modified; a continuously metering density bridge was installed in the circulating loop; the pressurizer was modified for gas pressurization; gamma-transmission survey facilities for the pressurizer were added; and a Zircaloy impeller was installed in the circulating pump.

The inlet nozzles were changed to provide a basis for comparing the relative importance of blanket flow and inlet velocity in determining the degree of suspension in the blanket. Runs SM-3 and -4 gave data on the effectiveness of suspension with the $1\frac{1}{2}$-in. nozzles over the range 200–350 gpm, and run SM-2 gave data on the effectiveness of suspension with 2-in. nozzles at 230 gpm only.

The blanket exit assembly was modified by closing the annulus at the top of the pressure vessel, thus forcing all the flow to leave the blanket at the top of the core. Data from run SM-4 indicated that the annulus at the top of the core was obstructed by settled slurry during most of the run.

A bridge[5] for continuous measurement of densities was installed in the main circulating loop near the exit from the pressure vessel to monitor the circulating concentration. Figure 10.9 is a schematic diagram of the installation.

The pressurizer was altered, as shown in Fig. 10.10, to permit operation with either steam or gas pressurization. The original ½-in. overhead vapor line from the pressurizer was replaced with a 2½-in. line to provide adequate flow area for an overhead thermal-convection loop. Four parallel condensing coils were wrapped on the downflow leg of the 2½-in. line, and the condensate tank was attached just below the return line to the pressurizer. A flow restrictor was installed in the main circulating loop downstream of the pump, and a ¾-in. bypass was provided from the pump discharge to the top of the pressurizer. On the present assembly of the system, the bypass has been extended inside the pressurizer so that it will discharge into the center of the pressurizer about 6 in. below the condensate overflow. The pressurizer baffles were omitted. Additional heaters were installed as shown in the figure. The 4- and 10-kw heaters on the pressurizer wall are controlled either from the core-to-blanket differential pressure for steam-pressurized operation or from the wall temperature for gas-pressurized operation. The 3-kw flange heater and the 1-kw vapor-line heater are connected for manual control to assist in establishing convection through the vapor line when pressurizing with gas. All heaters are provided with high-temperature cutouts.

Because of the slurry buildup in the heated section of the pressurizer, experienced in run SM-4, a gamma-ray transmission facility was installed so that this section of the pressurizer can be scanned.

[5] R. P. Wichner and C. F. VandenBulck, *The Pressure Bridge Density Meter for Continuously Metering Densities of Flowing Streams*, ORNL CF-57-1-49 (Jan. 10, 1957).

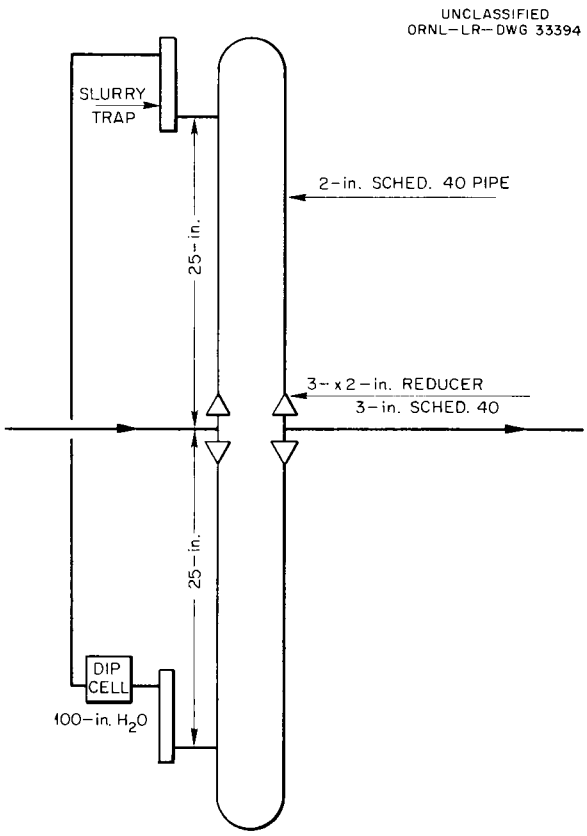

Fig. 10.9. Bridge for Continuous Density Measurement.

10.2.2 Run SM-5

(*a*) **Operating Summary.** – From May 2 through June 24 the 300A circulating pump ran for 452 hr with water in the loop and for 645 hr with slurry. For the last 500 hr the charged inventory was maintained at 522 ± 9 kg of thorium, and a series of 25 samples at each of nine operating conditions was obtained. Gamma surveys were also made of the blanket at the time the samples were withdrawn. These samples were used to study the slurry concentration gradient and distribution within the system and to determine both the sampling error and the accuracy of analytical procedures.

The slurry was dumped from the loop because the iron accumulation in the slurry exceeded 1000 g. In previous runs, severe local attack had been found for this level of iron accumulation.

In the first slurry dump, completed in approximately 15 min, 85% of the charged inventory was recovered. Of the 75 kg remaining in the loop, 33% was found in the bottom of the blanket below the inlet nozzles, as shown in Fig. 10.11. An additional 48 kg was recovered from the loop in three rinse runs. About 1 kg was back of the thermal barrier in the pump, and some fines were lost in decanting. Twenty-five kilograms, or 6% of the charged inventory, was not recovered.

The expected localized corrosion at the bond between the type 309 stainless steel and the carbon-steel pressure vessel was not found when

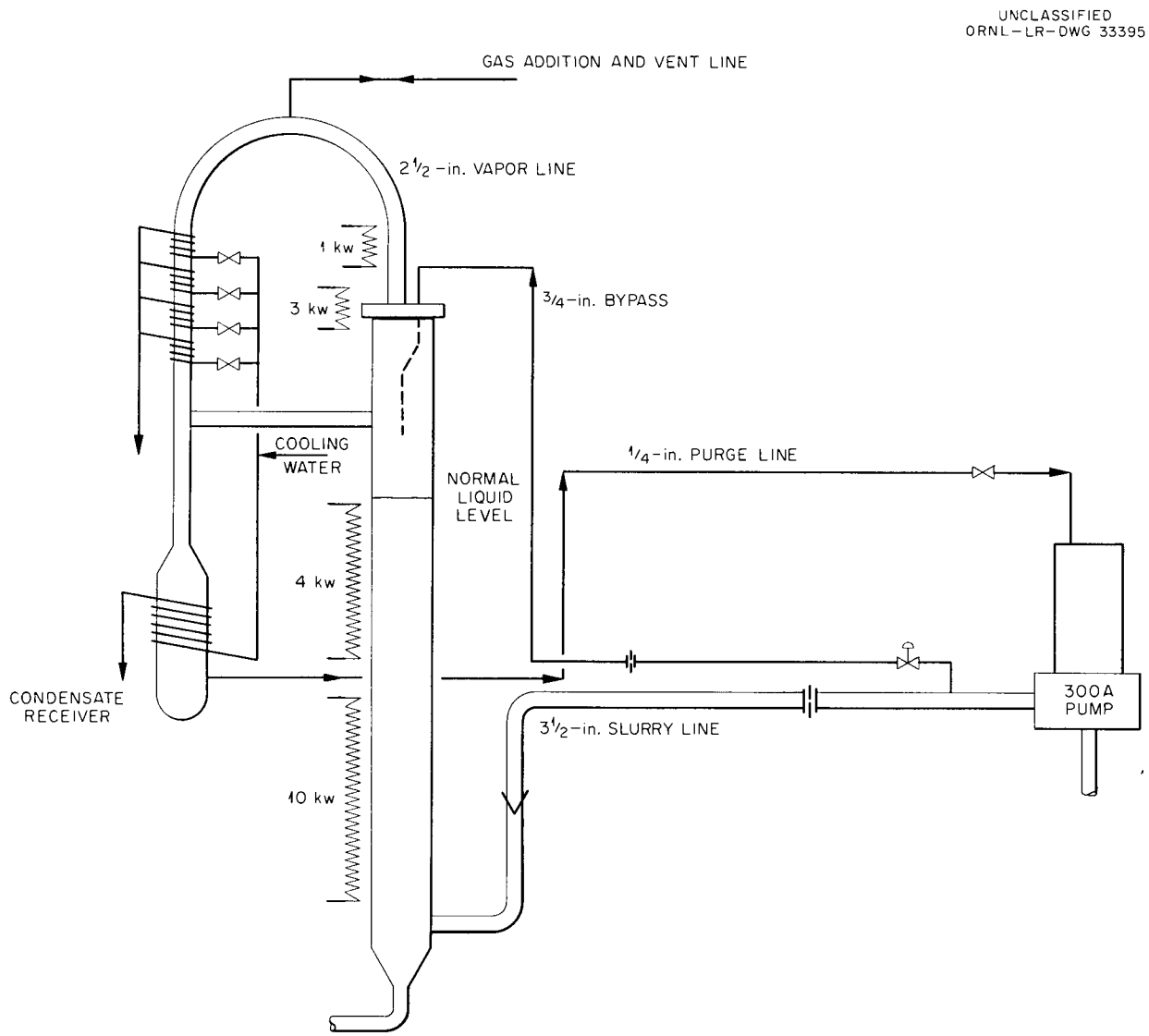

Fig. 10.10. Slurry Blanket Test Pressurizer for Gas Pressurization.

the pressure vessel was opened. There was some localized pitting, but no deep pits were observed.

After the pump was disassembled, examination showed that no repairs would be required. The Zircaloy impeller had lost 6 g, or 0.42% of its weight. The lower radial bearing was scored slightly, and as can be seen in Fig. 10.12, the lower hub of the impeller was worn.

(*b*) Pressurization Tests. – On May 2, after gamma scans of the blanket and pressurizer had been obtained at 25°C, the pump was started and an attempt was made to pressurize the system with nitrogen. Large quantities of gas were drawn from the pressurizer and accumulated in the back of the pump and in the top of the pressure vessel. The gas was vented and the loop was brought up to pressure with steam. About 60 hr were required to remove enough gas for the system to operate smoothly.

Operation with steam was continued until May 9, when gas pressurization was again attempted by slowly opening the bypass to the pressurizer and adding nitrogen to the vapor space at the top of the pressurizer. In about 6 hr, after the nitrogen had diffused throughout the system, operational difficulties began. The liquid level in the

Fig. 10.11. Bottom View of Blanket After First Dump.

Fig. 10.12. Zircaloy Impeller After Run SM-5.

pressurizer rose uncontrollably, and the pump secondary flow became low and erratic. After the excess gas was vented from the loop, operation became stable.

A third gas-pressurization test was made on May 19 with the loop at 150°C. Gas accumulated in the back of the pump in less time than in the previous test, which was made at a loop temperature of 200°C. It is concluded, therefore, that the present system of gas pressurization is not feasible.

(c) Slurry Operation. – Slurry additions began on May 21, and 525 kg of thorium had been charged by May 27. Systematic sampling of the facility was started on May 28, and the first series of samples, with the loop at 150°C and the circulating pump running on 60-cycle current, was completed the next day. The loop was then heated to 170°C, and another set of samples was withdrawn.

On June 5, as the loop was being heated to 200°C, a leak was found at the flange between the sphere and the top spool piece. The loop was then cooled to about room temperature, and the flange was tightened. Because of mixing between the pressurizer and the loop, the pump had to be stopped before the loop could be cooled to below 140°C.

During the shutdown the blanket pressure recorder was recalibrated, and a different type of pressure transmitter was installed on the density bridge in an effort to obtain a signal free of excessive noise. The pressure recorder for the density bridge was recalibrated with the new d/p cell.

These operations required a full week, by far the longest shutdown to date with slurry in the circulating system. A very smooth startup was achieved. The circulating concentration increased gradually after the startup and leveled off after approximately 16 hr of circulation. Figure 10.13 shows the variation of circulating concentration with time during the startup. The circulating density estimated from the pump power was used as the basis for computing the circulating concentration (the power-density relationship was established by observations taken during the period of operation on water). Similar data could be obtained from the loop flowmeter and pump-head meter readings.

The loop was brought up to 200°C and the third set of samples was taken, with the pump still at 60 cycles, on June 16. The pump was then operated on 50-cycle current, and the fourth series of samples was withdrawn. A fifth set of samples, at 200°C and 50 cycles, was obtained on June 18. Samples were then withdrawn at 43 and 50 cycles

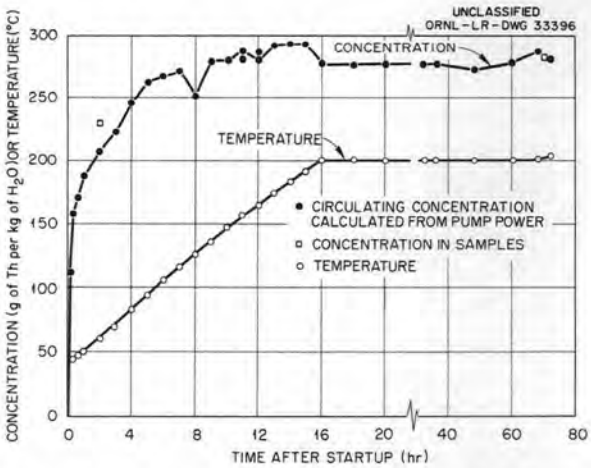

Fig. 10.13. Circulating Concentration of ThO_2 vs Time During Startup.

with the loop at 170°C and at 50 and 43 cycles with the loop at 150°C. The series of samples at three pump speeds for each of three loop temperatures was completed on June 24.

Chemical analysis of the samples from the circulating loop indicated that the total iron buildup in the slurry was in excess of a kilogram; so the slurry was dumped from the loop upon completion of sampling on June 24.

Table 10.3 presents the results of sampling during run SM-5. The circulating-loop sample values are means of sets of 10 to 12 samples taken at intervals over a period of several hours. The blanket sample values are means of sets of two taken successively. It is evident that the 150°C, 60-cycle operation gave the most uniform slurry distribution. The 200°C, 43-cycle operation gave decidedly the worst distribution, with extremely dilute slurry at the outer wall at the top (gamma surveys indicated water at the top of the scan, which goes about 15 deg higher than the sample point), a high concentration near the core wall indicating deposits in that region, and a high concentration on the outer wall at the lowest level.

Figure 10.14 presents a correlation of the relative circulating concentration (ratio of observed concentration to loop charge) vs flow rate times the 1.2 power of the ratio of viscosity at the observed temperature to viscosity at 170°C. It is felt that the relative circulating concentration may be indicative of the degree of suspension achieved in the blanket. The curve shows that the relative concentration varied as $[Q(\mu/\mu_{170})^{1.2}]^{0.5}$.

(d) Density-Bridge Performance. – The density bridge performed unsatisfactorily. Table 10.4 shows typical observations. With the original installation, in which a Swartwout diaphragm cell was used to measure the bridge differential, excessive line noise was experienced, the recorder trace covering 9 to 14% of the range. Observed densities were low with the pump running, which suggested some hydraulic unbalance in the metering system.

During the extended shutdown in the middle of the run, the Swartwout cell was replaced with a Barton bellows-type cell. This cell contains an internal damping mechanism, and after the damping was adjusted on June 17, the trace became much

Table 10.3. Slurry Distribution During Run SM-5; Concentrations in Grams of Thorium per Kilogram of H_2O

	150°C			170°C			200°C		
	Frequency (cycles)			Frequency (cycles)			Frequency (cycles)		
	60 (317 gpm)	50 (223 gpm)	43 (170.5 gpm)	60 (318 gpm)	50 (223 gpm)	43 (166 gpm)	60 (314 gpm)	50 (222 gpm)	43 (159 gpm)
Calculated charge	349	356	350	359	358	363	366	366	374
Loop piping	321	293	256	304	263	246	281	246	176
Blanket, 55 deg above center line									
Outer wall	331	219	216	291	222	173	219	179	55
6 in. into blanket	306	265	234	302	232	216	245	268	144
12 in. into blanket	294	266	265	302	312	362	277	256	502
Blanket, 30 deg above center line									
Outer wall	277	253	245	307	283	274	281	272	235
6 in. into blanket	333	261	242	302	305	273	263	289	294
12 in. into blanket	318	249	288	322	282	334	274	292	332
Blanket, 30 deg below center line									
Outer wall	320	257	306	331	298	302	324	339	381
6 in. into blanket	306	274	367	260	285	260	239	289	291
12 in. into blanket	331	261	241	294	263	287	262	326	313
Blanket, 55 deg below center line									
Outer wall	307	274	317	305	339	289	274	305	420
6 in. into blanket	279	271	269	313	290	303	274	265	322
12 in. into blanket	325	275	259	316	266	294	338	293	333

more stable. Deviations from the calculated density based on loop sampling became much smaller after this equipment charge, although deviations in excess of 5% were observed on June 18 and on June 23. The behavior on June 18 could be accounted for by development of a concentration gradient in the piping, but no explanation is available for the behavior on June 23.

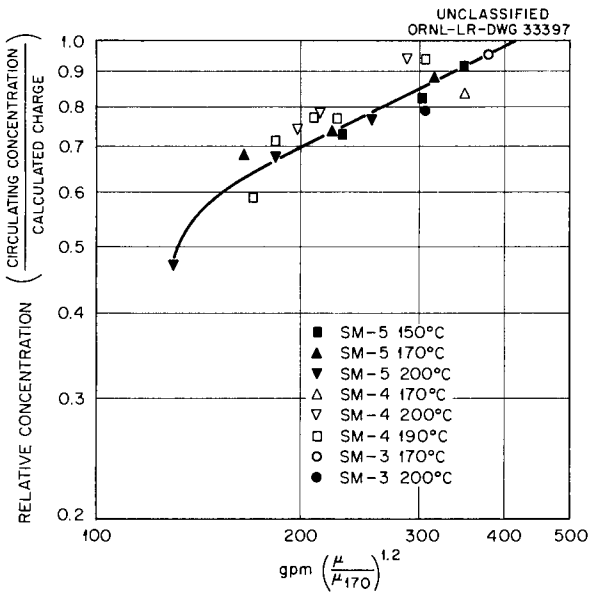

Fig. 10.14. Effect of Flow Rate and Temperature on Circulating ThO_2 Concentration, Runs SM-3, -4, and -5.

During the first rinse run on June 27, the bridge gave an indicated density of 0.92 before the pump was started, and showed a noise-band width of approximately 6% during the run. This suggested that the freedom from noise during the latter part of the run may have been due to slurry plugging the instrument connections.

(e) Gamma-Survey Results. – Gamma scans of the pressure vessel and pressurizer were made at the same time that samples were taken throughout the run. No slurry was carried up into the pressurizer during the run. Table 10.5 presents a comparison of the data obtained by sampling and by gamma surveys of the pressure vessel. Considerable deviations are found between the two sets of data, particularly for the position 55 deg above the equator. Figure 10.15 presents the concentration distribution found by the gamma survey for 150°C, 60-cycle operation. Dilute regions are indicated at the top and bottom, with more concentrated material in between. The four sampler positions are at 15, 32, 71, and 88 in. along the gamma track. The most puzzling feature of the gamma surveys is the dilute region indicated

Table 10.4. Density-Bridge Performance

Date	Time	Thorium Concentration (g of Th per kg of H_2O)	Cell in Use	Pump Frequency (cycles)	System Temperature (°C)	Calculated Specific Gravity	Upper Limit of Noise Band (%)	Lower Limit of Noise Band (%)	Mean Reading (%)	Specific Gravity from Bridge	Bridge Specific Gravity Minus Calculated Specific Gravity
5/4	1700	0	Swartwout	60	200	0.815	43.0	34.0	38.5	0.770	–0.045
5/14	0900	0	Swartwout	60	150	0.916	47.5	39.0	43.3	0.866	–0.050
5/19	1430	0	Swartwout	0	156	0.910	47.8	47.8	47.8	0.956	+0.046
5/19	1500	0	Swartwout	60	156	0.910	46.5	37.8	41.8	0.836	–0.074
5/28	0900	321	Swartwout	60	156	1.200	64.0	50.0	57.0	1.14	–0.06
6/4	0900	316	Swartwout	60	171	1.178	62.0	51.0	56.5	1.13	–0.048
6/4	1415	316	Swartwout	0*	171	1.178	56.0	56.0	56.0	1.12	–0.058
6/16	0900	281	Barton	60	200	1.046	55.0	50.5	52.8	1.056	+0.010
6/17	1300	246	Barton	50	200	1.039			53.0	1.06	+0.021
6/18	0900	176	Barton	43	200	0.962			51.0	1.02	+0.058
6/19	0900	246	Barton	43	173	1.115			55.0	1.10	–0.015
6/20	0900	263	Barton	50	170	1.134			55.5	1.11	–0.024
6/23	0900	293	Barton	50	150	1.185			56.5	1.13	–0.055
6/24	0900	256	Barton	43	150	1.151			57.0	1.14	–0.011

*Instantaneous reading when pump stopped.

Table 10.5. Comparison of Gamma Surveys and Sampling Results; Concentrations in Grams of Thorium per Kilogram of H_2O

Position	Method	150°C Frequency (cycles)			170°C Frequency (cycles)			200°C Frequency (cycles)		
		60	50	43	60	50	43	60	50	43
55 deg above equator	Sample	310	250	238	298	250	250	247	232	234
	Gamma	305	375	405	280	450	413	322	392	377
30 deg above equator	Sample	309	254	258	310	284	297	273	281	287
	Gamma	320	335	365	293	390	305	305	350	325
30 deg below equator	Sample	319	264	271	295	279	283	275	318	362
	Gamma	355	325	340	327	326	283	307	320	300
55 deg below equator	Sample	304	273	282	311	291	281	295	288	358
	Gamma	335	280	327	315	285	275	300	276	255
Average through blanket	Sample	311	260	262	304	285	281	273	279	299
	Gamma	308	302	321	287	313	279	304	331	273

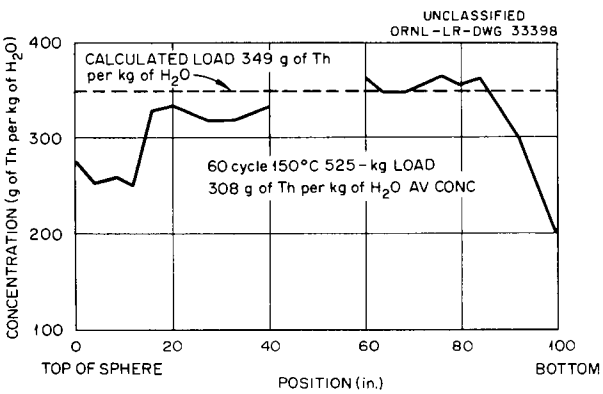

Fig. 10.15. ThO_2 Concentration Distribution vs Position in Blanket, Run SM-5.

below 80 in. The concentration in this region calculated from the gamma surveys is substantially lower than that of the slurry circulating through the piping.

This was the final run of the series made with the simulated HRT blanket system. In these runs it was shown that slurry at concentrations up to 500 g of Th per kg of H_2O cannot be circulated with a uniform blanket concentration in the presently designed HRT system at the design flow rate of 230 gpm. Experiments were run at higher flow rates (run SM-5) and with smaller inlet nozzles over a range of flow rates (runs SM-3 and -4). These runs demonstrated that a substantial improvement in slurry suspension can be made by either of these procedures. Sampling and gamma survey systems were designed, installed, and improved so that more useful data could be obtained on the slurry distribution in the blanket. Examination of the information obtained to date suggested two useful criteria for blanket performance: (1) the ratio of the concentration circulating through the external loop to the charge concentration and (2) the variance between samples taken at various locations in the blanket. Performance, in terms of uniformity of distribution and freedom from dense accumulations, was not satisfactory under any conditions tested, but the data indicated that the desired uniformity could be achieved at higher flow rates.

A satisfactory procedure for obtaining good slurry removal during a moderately slow (15–20 min) dump was developed. Steam was used to agitate the slurry and maintain suspension during the dump operation. Prior to use of this procedure, most of the solids tended to remain in the pressure vessel when the loop was dumped.

10.2.3 Conversion of 300-SM Loop to High-Pressure Operation

The present HRT slurry mockup is limited to a maximum operating pressure of 325 psi by the design of the pressure vessel; it is limited therefore at 100 psi overpressure to a maximum temperature of 200°C. Experience during run SM-2

(confirmed by later runs) indicated[6] temperature-dependent effects on slurry suspension. Thus it seemed advisable to carry out tests in a system capable of operating up to reactor design conditions of 300°C and 2000 psi. A new pressure vessel conforming to the proposed HRE-3 design, but of smaller size to permit utilization of the present 300-gpm pump, was designed. Dimensional-similitude studies led to the selection of a 30-in.-dia pressure vessel with a 12-in.-dia core. The vessel (Fig. 10.16) is designed with suitable nozzles to permit investigation of three different blanket flow patterns:

1. entering at the bottom, flowing up between the core and a surrounding flow guide, and flowing down outside the flow guide;
2. straight-through flow, up or down, with the flow guide removed;
3. swirling flow, with the slurry entering two tangential nozzles on the equator and leaving at the top and bottom.

By replacing the closure flange carrying the core with a similar flange without a core, similar flow tests can be carried out for a 30-in. single-region reactor system. Initial use of the new equipment will be for tests of single-region systems.

A contract for the mechanical design and fabrication of the new pressure vessel was awarded to Combustion Engineering Corp.; the vessel is scheduled for delivery in November 1958.

Because of the heavier walls of the new pressure vessel, it is estimated that a gamma source of approximately 3 curies will be required to permit attenuation measurements equivalent to those currently being made. A source-handling facility capable of safe storage and handling of a 10-curie gamma source and a new survey track and drive were designed by Vitro Engineering Corp.

It is planned to retain the existing pump, pressurizer, and approximately 50% of the piping. These components are adequate for the new operating conditions. A test heat exchanger will be incorporated in the new section of the loop, as a means of cooling the system and to provide experience with a slurry system containing at least one heat exchanger design.

The existing low-pressure system for the HRT slurry mockup is inadequate for the new design because (1) it is unable to cool and contain a dump from 300°C, (2) the tanks are incorrectly sized for the new high-pressure system, and (3) slurry cannot be completely suspended in the large tanks. A new low-pressure system was designed around a dump tank based on an experimental prototype tested previously.[7] During a dump the pressure will be allowed to rise to a maximum of 135 psig; the condenser was designed with sufficient capacity to limit the pressure to this value. Dump cooling will be accomplished by condensing the steam flashing from the dump stream. All components were designed for 150 psig internal pressure and full vacuum.

10.2.4 Gamma-Survey Development

An experimental program of gamma-absorption measurements was undertaken to increase confidence in the quantitative interpretation of the gamma-survey results obtained on the HRT blanket mockup vessel and in an attempt to explain the anomalous shape of the transmission pattern at the top and bottom.[8] In the mockup pressure vessel, an uncollimated Co^{60} gamma source is placed at the geometric center of the vessel, and a counting device is moved around the periphery of the vessel along a great circle inclined 18 deg off the vertical to avoid various fittings on the vessel, such as sample ports.[9] The anomaly lies in the marked decrease in transmission near the top of the track and in the slight decrease in transmission (as contrasted to an expected slight increase due to the effect of the conical part of the core tank in reducing the blanket thickness) at the bottom.

The experimental tank shown in Fig. 10.17 was built in order to obtain transmission measurements under controlled conditions through a system resembling the HRT blanket mockup. This is a full-scale model of a sector of the blanket pressure vessel. Measurements were made with the vessel empty, with the vessel full of water, and with thorium nitrate solution of various concentrations. High-density local thorium concentrations were

[6] R. B. Korsmeyer *et al.*, *HRP Quar. Prog. Rep. Jan. 31, 1957*, ORNL-2272, p 68–71.

[7] C. S. King *et al.*, *Thoria Dump Tank Test*, EPS-X-326 (Nov. 13, 1957).

[8] R. B. Korsmeyer *et al.*, *HRP Quar. Prog. Rep. Oct. 31, 1957*, ORNL-2432, p 68.

[9] L. F. Parsly, Jr., *Report of Slurry Blanket Test Run SM-3*, ORNL CF-57-10-2 (Oct. 15, 1957).

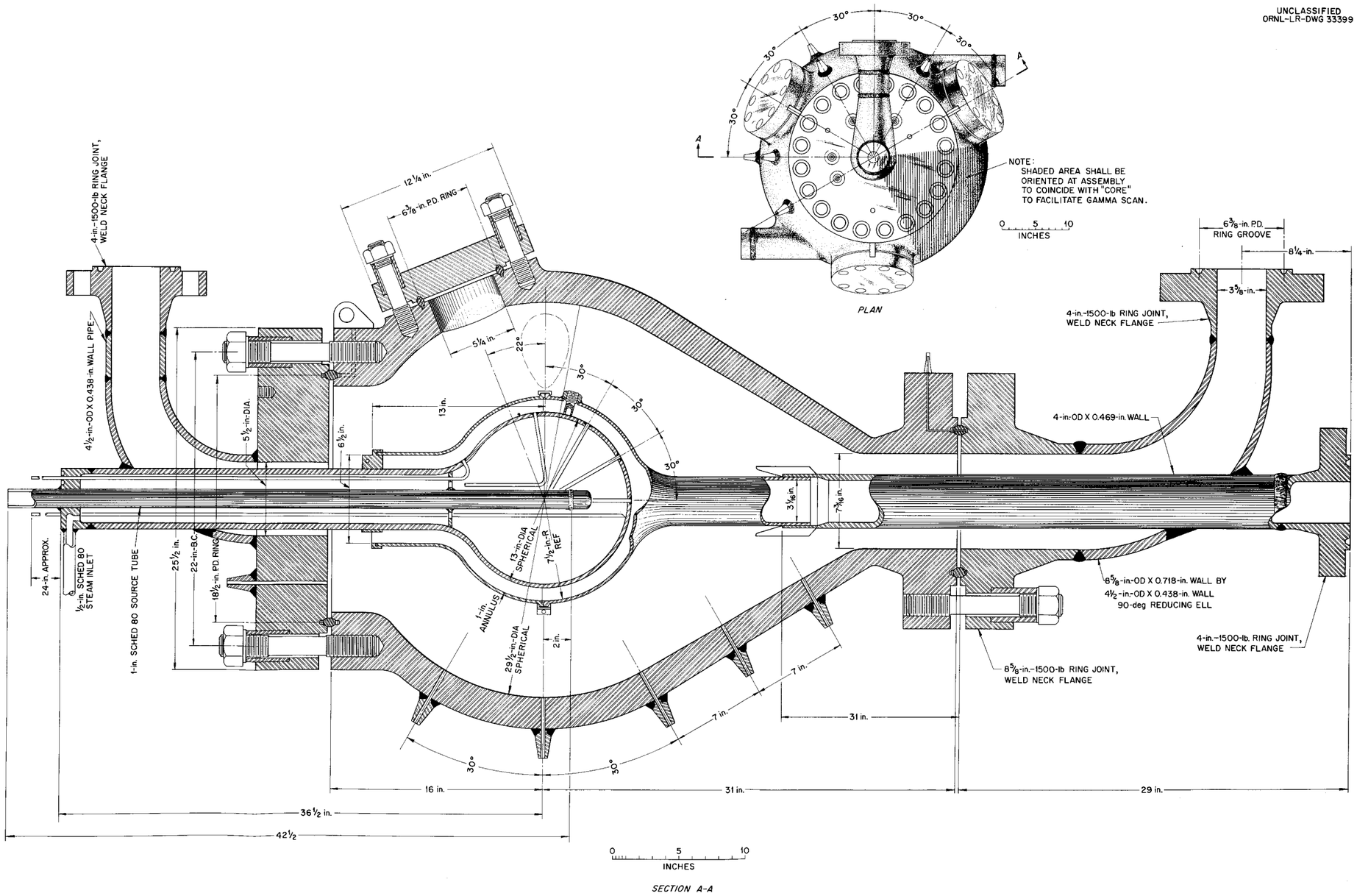

Fig. 10.16. High-Pressure Experimental Blanket Vessel.

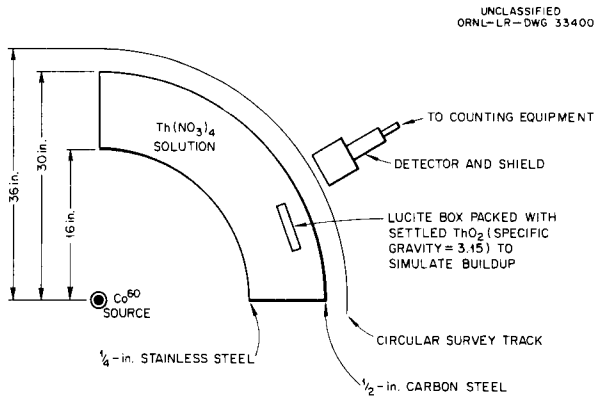

Fig. 10.17. Gamma-Absorption Calibration Tank.

simulated by inserting Lucite containers of various thicknesses filled with settled thorium oxide of specific gravity 3.15.

The results indicated that, for any pulse-height setting, the expected relationship of count rate to mean thorium density is valid. Figure 10.18 presents typical results. For the 1.2-Mev pulse height used to date in the slurry-blanket test measurements, the experimental absorption coefficient was found to be 0.055 cm^2/g, in excellent agreement with the 0.054 cm^2/g suggested by J. A. Lane and used for the calculation of thorium density in the blanket mockup.

It was also found, as would be expected, that it is impossible to differentiate between cake and uniformly distributed thorium. The gamma absorption measurement can give only the average density along the line of sight from source to detector.

A possible explanation for the peculiar shape of the pressure-vessel scans was found from the experiments with the quadrant tank, which was made from rolled steel plate. The pressure vessel in the 300-SM loop is a spun tank, and audigage

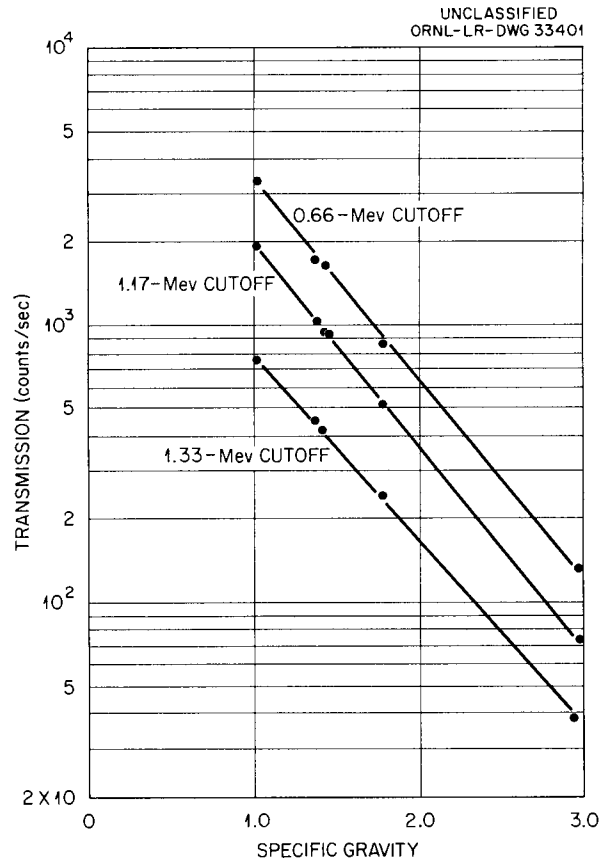

Fig. 10.18. Gamma-Ray Transmission Through Thorium Nitrate Solutions and Through Thorium Oxide Beds (750-mc Co^{60} Source).

measurements of the vessel taken on the top hemisphere showed a change in thickness from the top of the sphere to the center line of as much as $\frac{3}{8}$ in., the thicker area being at the top. Audigage measurements of the lower hemisphere were not taken because of the interference of various vessel fittings, but the gamma scans indicated that the variation in wall thickness is approximately the same as that of the top hemisphere.

11. INSTRUMENT AND VALVE DEVELOPMENT

D. S. Toomb

S. J. Ball
A. M. Billings
E. H. Bell
R. L. Moore
J. L. Redford
H. D. Wills

11.1 INSTRUMENT DEVELOPMENT

11.1.1 High-Temperature Radiation-Resistant Differential Transformers

The development of differential transformers for sensing instrument primary-element motions and capable of operating for long periods at high temperatures and in radiation fields was continued. Further tests at 300°C of the ORNL-designed transformer wound with 30-gage anodized aluminum wire[1] indicate that impregnation of the winding is necessary to avoid zero and null shifts with temperature. As silicone-varnish impregnation is not satisfactory for long-time operation at 300°C, it is planned to impregnate the coils with Sauereisen No. 1 cement.[2] An experimental coil was vacuum-impregnated with this cement, with excellent penetration of the winding being achieved.

Extended tests of the anodized aluminum coils have resulted in failure of the terminal connections due to oxidation of the solder at the terminal. To avoid this problem, a new transformer was designed and is being constructed. This unit will use anodized aluminum wire on an aluminum bobbin with Sauereisen impregnation. Aluminum leads will be brought out through an aluminum-clad mineral-insulated cable. The connection of the coil wires to the lead wires will probably be effected by a pressure-crimped joint which was shown to be promising in preliminary experiments. The new coil will also be hermetically sealed to allow operation under water or in environments where the humidity is high.

11.1.2 Heated-Thermocouple-Probe Liquid-Level Sensor

A heated-thermocouple probe of the type illustrated in Fig. 11.1 is being used as a static low-liquid-level sensor in a high-pressure boiler. When the liquid level drops below the thermocouple junction, the reduced heat transfer from the probe to the surrounding vapor causes the temperature of the probe to rise owing to the constant heating produced by the electrically excited Nichrome-V heating element surrounding the junction. The increased signal from the thermocouple is made to close a contact-making millivoltmeter circuit which pilots an alarm or safety relay. In preliminary tests the probes were operated for six weeks at 300°C in air; no change in insulation resistance was noted.

[1] D. S. Toomb *et al.*, *HRP Quar. Prog. Rep. Jan. 31, 1958*, ORNL-2493, p 78.

[2] A slurry of feldspar in sodium silicate manufactured by Sauereisen Cements Co., Pittsburgh, Pa.

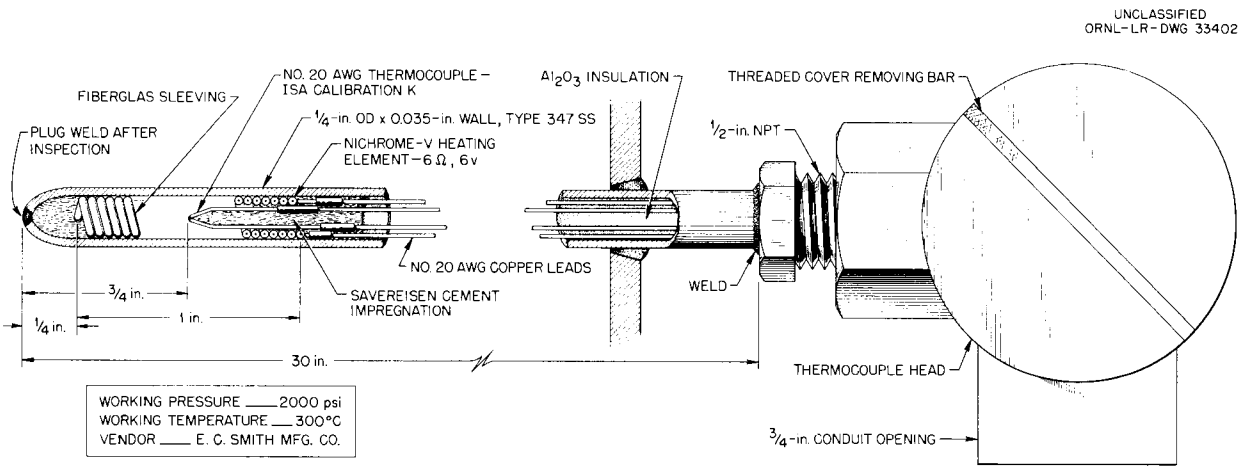

Fig. 11.1. Heated-Thermocouple-Probe Liquid-Level Sensor.

The probes are an improvement over a previously described type[3] in that the heating is localized at the thermocouple junction, which provides increased liquid-level sensitivity and response rate. The electrical insulation is completely inorganic; so the units are amenable to reactor applications where radiation damage to insulations is a consideration.

11.1.3 Variable-Area-Type Transmitting Flowmeters

A transmitting flowmeter of the variable-area type was specified and was purchased for evaluation as to suitability of primary elements of this type for measurement of the very low purge-water flows to the pressurizers and circulating pumps in HRP systems. The prototype design illustrated in Fig. 11.2 is superior to that incorporated in a higher flow-range transmitter tested earlier[4] because the in-line flow connection avoids stagnant areas which might fill with sediment and plug the meter. Other features of this meter include the linear output signal necessary to produce a true average of the pulsing flow when damped by a suitable filter and a low head loss which allows the transmitter to be installed in the low-pressure suction line of the pumps.

A similar, but higher range, transmitter purchased for feed-pump output flow measurement and of a design that eliminates the midsection flange is shown in Fig. 11.3.

11.1.4 Transistorized Electropneumatic Converter

A transistorized electropneumatic converter has been developed by the University of Virginia Engineering Experiment Station on a subcontract from ORNL to provide a more reliable instrument for critical control loops by the elimination of vacuum tubes.

The transducer is shown in block diagram form in Fig. 11.4. Operation is as follows:

1. A 3-v, 1000-cps signal is supplied to the primary of a linear variable differential transformer from an oscillator.

2. The output of the linear variable differential transformer is a 1000-cps signal varying in amplitude proportionally to the linear displacement of the ferrite core slug which is positioned by the instrument sensing element.

3. This signal is amplified and converted to a d-c voltage by a phase-sensitive demodulator.

4. The d-c output of the first stage is passed through a low-pass filter to remove frequencies above 1 cps. This eliminates signals caused by vibration or turbulence in primary elements, which might saturate the amplifier.

5. After filtering, the d-c signal is amplified by a d-c amplifier consisting of a 1000-cps transistor chopper, an a-c amplifier, and a phase-sensitive demodulator.

6. The amplified d-c voltage is used to control a power amplifier stage which supplies a d-c current of 0–5 ma to a commercial electromechanical electric-to-pneumatic transducer giving a 3- to 15-psi proportional output signal.

7. The output also supplies a pneumatic-to-electric converter, the output of which is a 1000-cps signal which is proportional to the pneumatic signal and which is in phase opposition to the input signal. This signal is fed back to the input amplifier to provide over-all feedback around the instrument. This feedback stabilizes the instrument and increases linearity.

8. An adjustable d-c feedback loop is also provided around the d-c amplifier to provide damping and prevent oscillation of the instrument.

9. The reference voltages for the phase-sensitive demodulator, transistor chopper, and the primary voltage for the feedback transducer are supplied via phase-shift and buffer amplifiers from one secondary of the transmitting differential transformer. This method of phasing eliminates the attendant reduction in signal amplitude experienced when phasing is accomplished by phase-shifting the signal voltage and provides automatic compensation for variations in phase shift of the transmitting differential transformer such as occur when the resistance of the transformer primary winding changes with temperature.

The supply power requirements of the instrument are 250 ma at 48 v dc. Twenty-six transistors are utilized to replace ten vacuum-tube functions (six tubes, some twin types) in the presently used vacuum-tube equipment.

---

[3] D. S. Toomb *et al.* *HRP Quar. Prog. Rep. July 31, 1956*, ORNL-2148, p 67.

[4] D. S. Toomb *et al.*, *HRP Quar. Prog. Rep. April 30, 1956*, ORNL-2096, p 75.

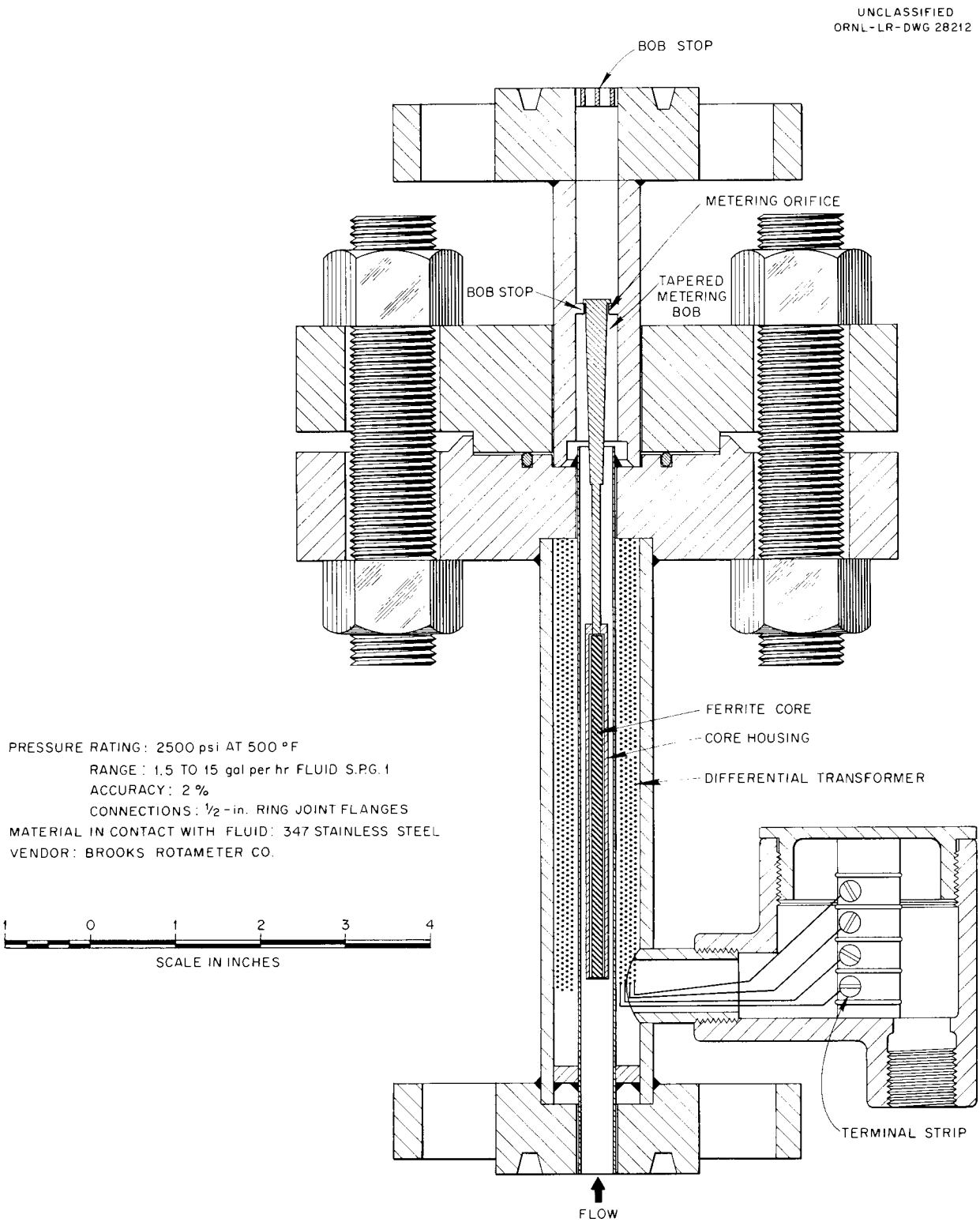

Fig. 11.2. Low-Range Variable-Area-Type Transmitting Flowmeter.

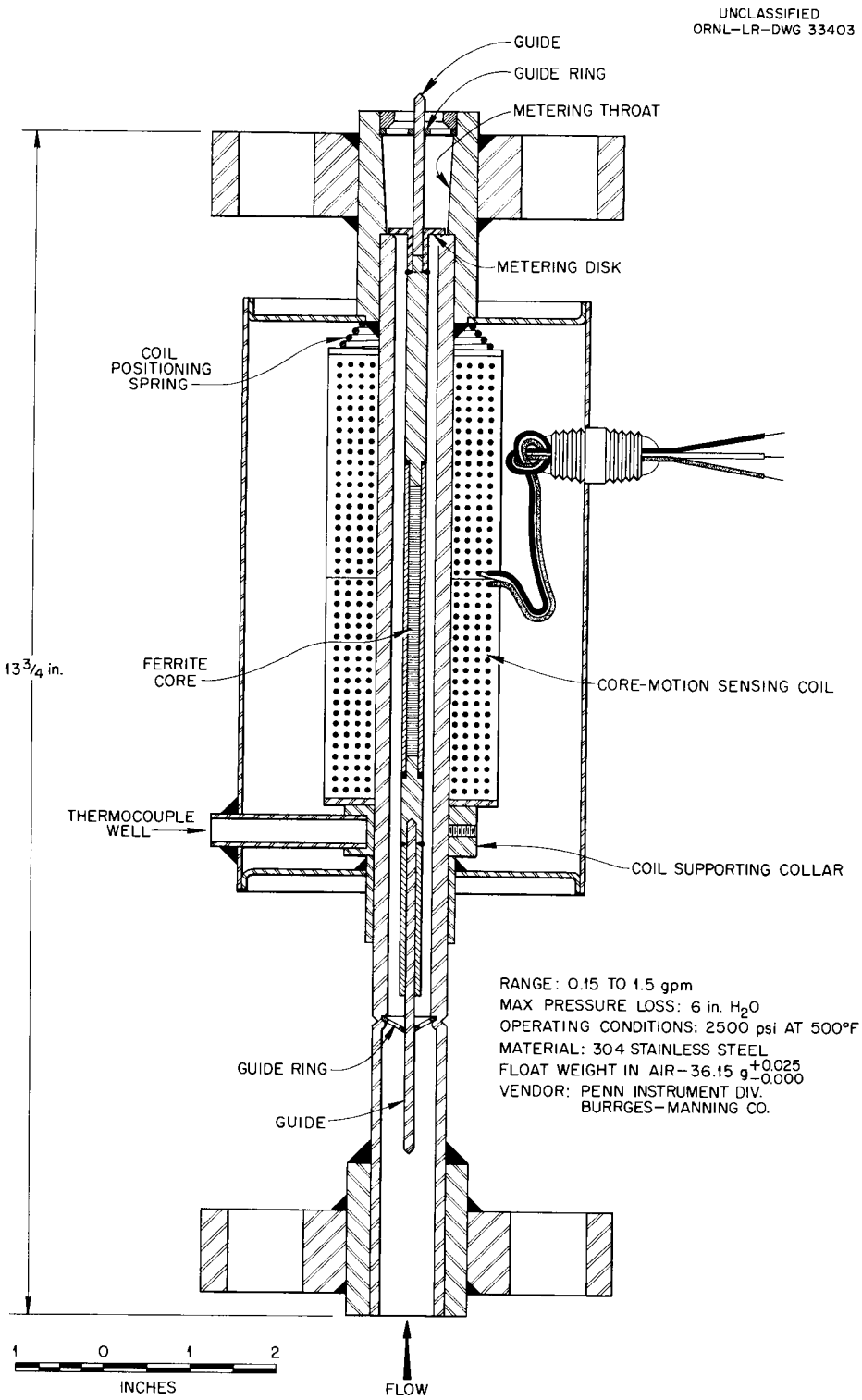

Fig. 11.3. High-Range Variable-Area-Type Transmitting Flowmeter.

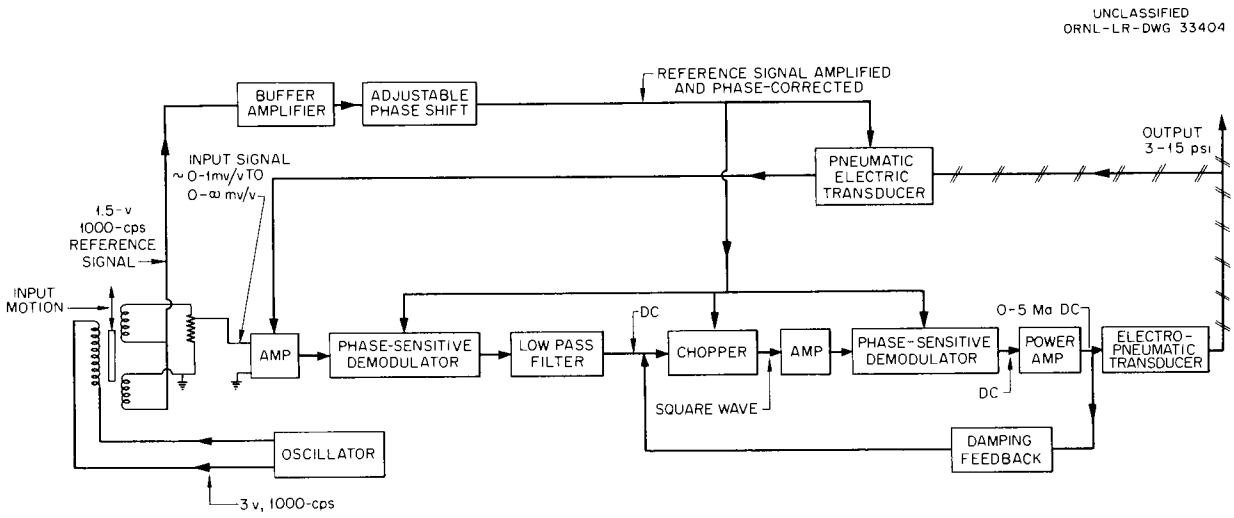

Fig. 11.4. Block Diagram of Transistorized Electropneumatic Converter.

During test operation to date, trouble has been experienced with intermittent open circuits caused by the mounting of condensers on the flexible printed-circuit boards with the leads under too much tension. All these condensers are now being replaced. Figure 11.5 illustrates the construction of the modular printed-circuit board of the amplifier-oscillator chassis. The four circuit boards slide into side-mounted connectors on the left. The entire chassis slides into a housing with an integral connector to permit fast interchange of units. The electric-to-pneumatic output stage and the pneumatic-to-electric feedback unit are mounted on a separate chassis illustrated in Fig. 11.6.

11.1.5 Control Analysis of HRT Heat Exchanger Feedwater System

A systems-analysis review of the existing HRT heat exchanger feedwater control system was made[5–7] which indicated that with proper operation the present system is capable of smooth performance in the power range of 1 to 5 Mw. This conclusion has been verified in subsequent operation of the reactor.

The analysis indicated that a larger feedwater control valve for the blanket heat exchanger will be necessary for 10-Mw operation.

The frequency-response technique of analysis was utilized in which the system response to sinusoidal perturbations is considered and theorems permit conclusions regarding stability and transient response. Preliminary controller adjustments were calculated and a method of optimizing the control system during operation was suggested.[5]

11.2 VALVE DEVELOPMENT

11.2.1 Valve Actuators

A new all-metal reversible valve actuator supplied to ORNL specifications is shown in Fig. 11.7. The 40-in.^{2}-effective-area actuator is considerably shorter than earlier used models, which reduces side-stem loading when the valve and associated actuator are mounted horizontally. Horizontal valve mounting has been used to facilitate remote maintenance. The more compact assembly is also important from space-layout considerations. Other interesting features include the internal stem-sealing bellows to eliminate actuating-air leakage and provision for fail-action spring loads from 50 to 3600 lb by the use of different springs and spring tension adjustments in six springs equally spaced radially. The new unit will be life-tested with a valve load simulated by an opposing spring.

---

[5] R. L. Moore, *Review of HRT Feedwater System*, ORNL CF-58-4-63 (April 9, 1958).

[6] H. D. Wills, *HRT Steam System Feedwater Pressure Control*, ORNL CF-58-4-8 (April 15, 1958).

[7] S. J. Ball, *Frequency Response Analysis of the HRT Feedwater Control System*, ORNL CF-58-4-10 (April 4, 1958).

UNCLASSIFIED
PHOTO 31566

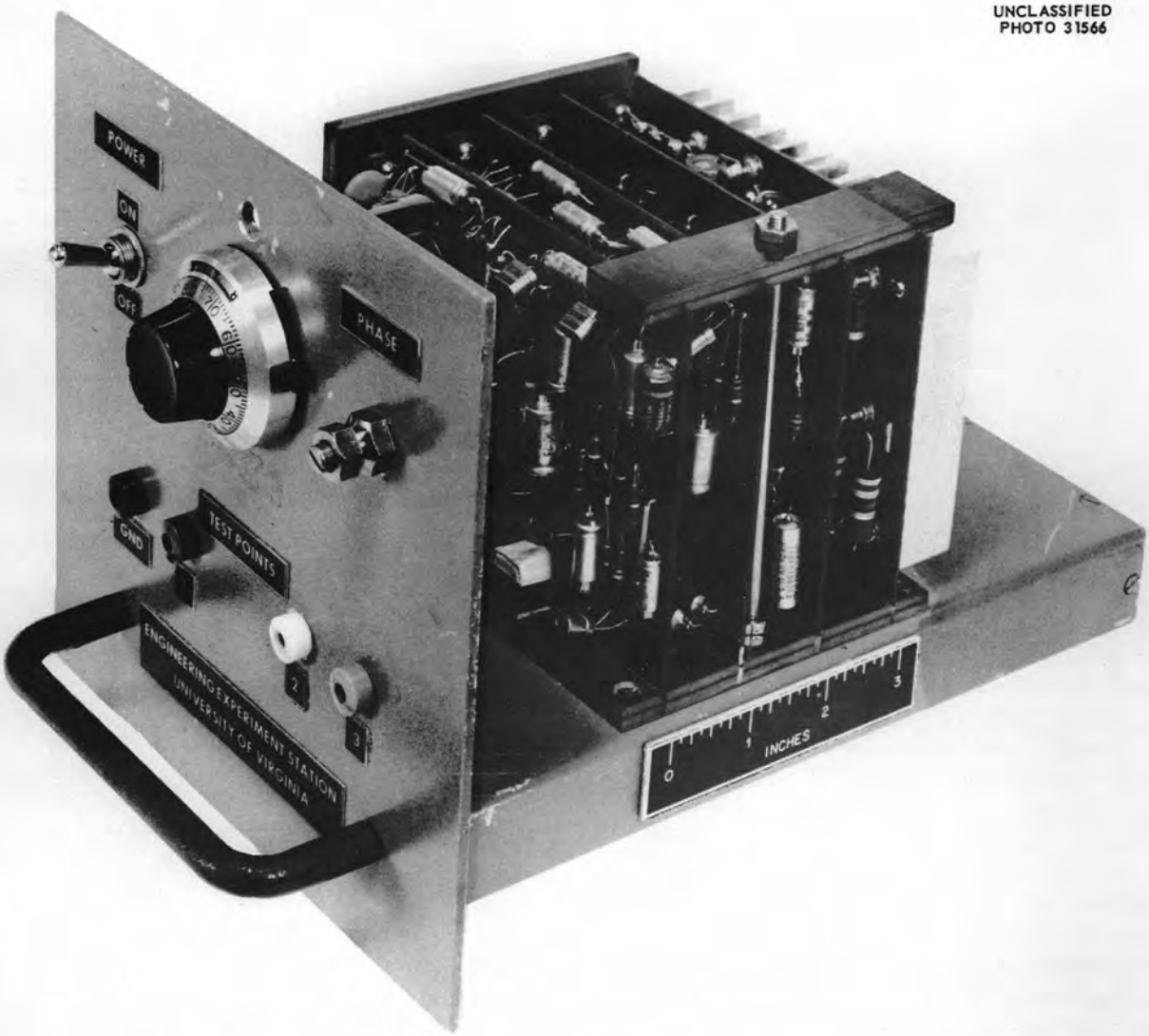

Fig. 11.5. Oscillator-Amplifier Chassis of Transistorized Electropneumatic Converter.

A control-valve actuating system (shown schematically in Fig. 11.8) using 500-psi water as the working fluid is now being tested. Possible advantages of this system for a large valve actuating system are the reduced size of the cylinders necessary, compared with sizes possible with compressed air as the working fluid, and the relative immunity of water to radiation damage as compared with the conventionally used oils. Some difficulty was experienced with pump packing during the first 15,000 cycles, but cylinder operation remained satisfactory to approximately 35,000 cycles. At this point, an appreciable leak developed, apparently by the piston rings and out the shaft packing. However, the system is still operable, and after a 30-min warmup period, the leak disappears. Operation has proceeded to a total of 55,000 cycles with no further increase in leakage. When leakage becomes so great as to preclude operation, the Moyno pump and Askania cylinder will be dismantled and examined.

The previously described[8] stacked-bellows actuator for large valves was cycled 18,083 times

[8]D. S. Toomb *et al.*, *HRP Quar. Prog. Rep. Jan. 31, 1958*, ORNL-2493, p 83.

UNCLASSIFIED
PHOTO 31567

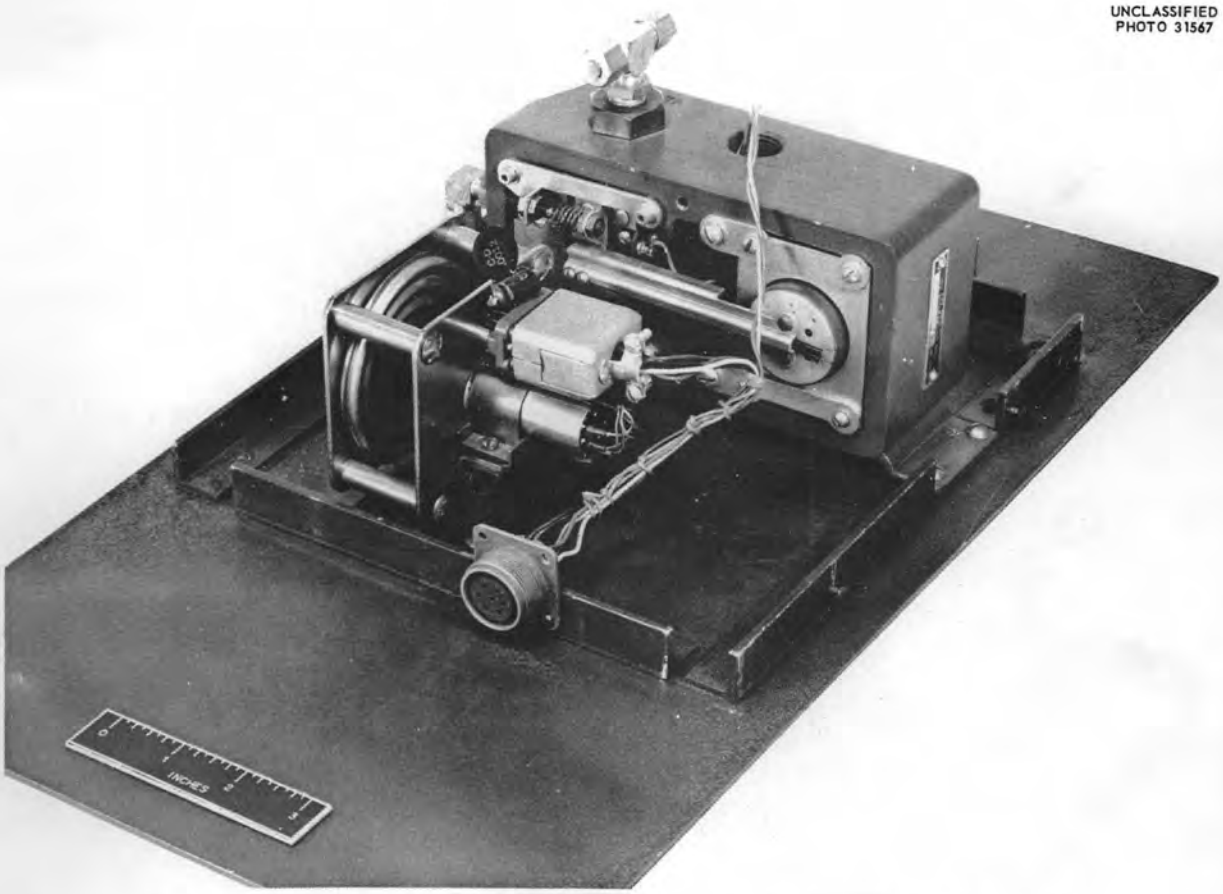

Fig. 11.6. Electropneumatic Output Stage of Transistorized Electropneumatic Converter.

with 80-psig air pressure against a maximum spring load of 5000 lb (see Fig. 11.9) before a leak developed in one of the prime-mover bellows. At 9000 cycles the lower Oilite bronze quide bushing slipped from the housing into which it was press-fitted and had to be reinserted. A more positive method of attaching this guide will be utilized in future models.

11.2.2 Stem-Sealing Bellows

Single- and three-ply titanium bellows were successfully formed by the Fulton Sylphon Division, Robertshaw-Fulton Controls Corp., on an ORNL order. The three-ply bellows formed of grade 55 titanium was specified for 2500-psi 300°C service. Dimensions of the three-ply prototypes were:

Thickness per ply	0.007 in.
Outside diameter	$1\frac{1}{4}$ in.
Inside diameter	$1\frac{3}{16}$ in.
Length	$2\frac{1}{8}$ in.

While being tested in uranyl sulfate at 2300 psi and 300°C with a stroke of $\frac{1}{8}$ in., the first bellows failed at 78 cycles. A second unit was cycled at 1000 psi and 250°C with a stroke of 0.090 in. and failed at 5390 cycles.

On the basis of these tests and their own experimental findings, Fulton Sylphon has increased the ply thickness of this bellows to 0.010 in. and has doubled its length. Prototypes of the modified design are now being fabricated and will be available for testing in the near future.

A three-ply, seamless, type 347 stainless steel bellows was selected as the stem seal for all HRT valve applications where packing-gland leakage might jeopardize reactor operation. The choice of this particular bellows (Fulton Sylphon Division drawing number 10716-R3) was based on the HRE experience of no failures with similar units and has now been substantiated by the

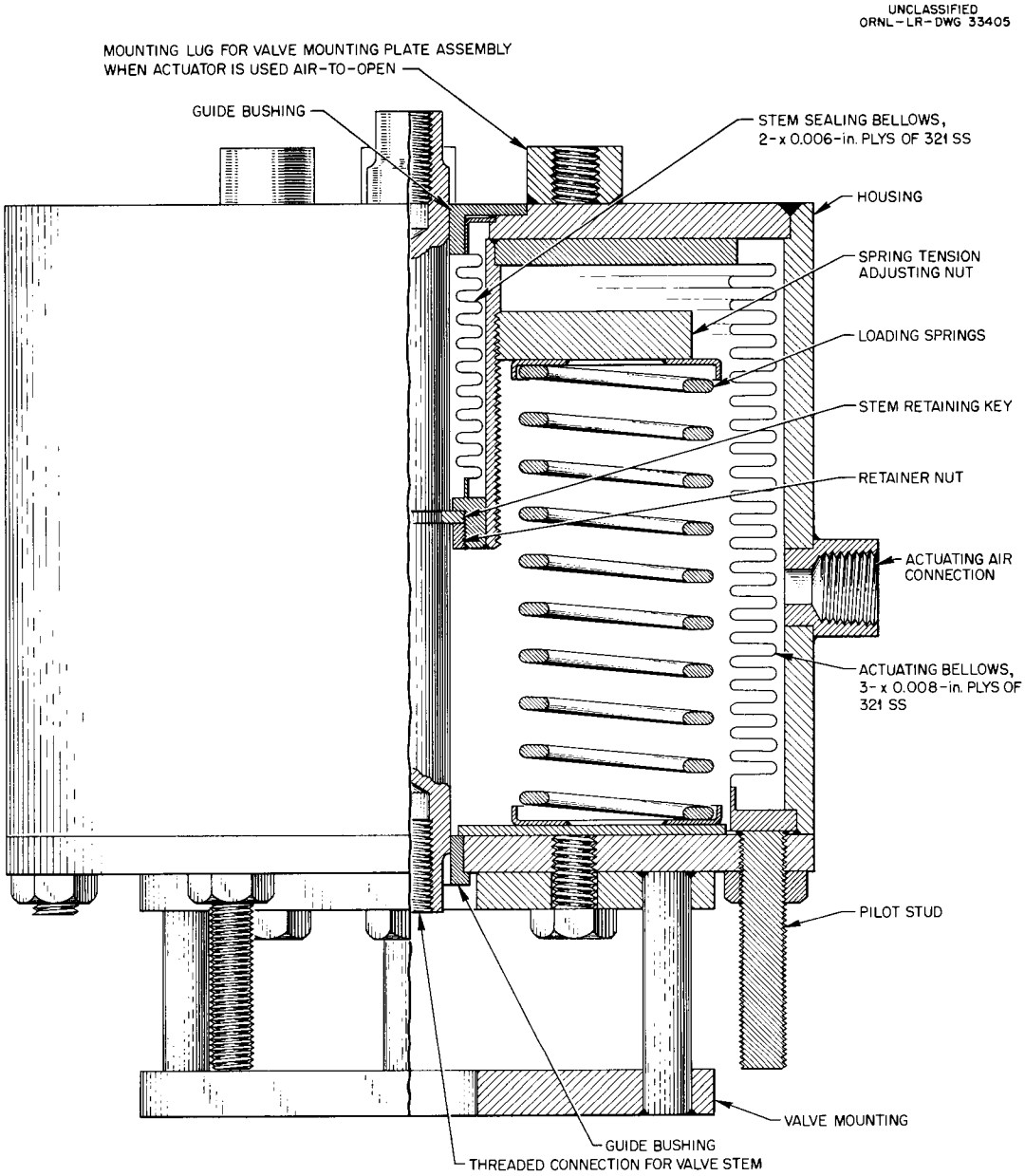

ACTION — REVERSIBLE, SHOWN AIR-TO-CLOSE
EFFECTIVE AREA — 40 in.^{2}
MAXIMUM STROKE — $^1/_2$ in.
MAXIMUM ACTUATING AIR PRESSURE — 75 psi
MAXIMUM TEST PRESSURE — 100 psi
SPRING LOADING — 50 lb MIN, 3600 lb MAX
MAXIMUM SPRING RATE — 1500 lb/in.
INSIDE SURFACE — ZINC PLATED
VENDOR — FULTON-SYLPHON DIV.

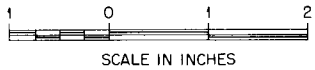

Fig. 11.7. Metal-Bellows Type of Control-Valve Actuator.

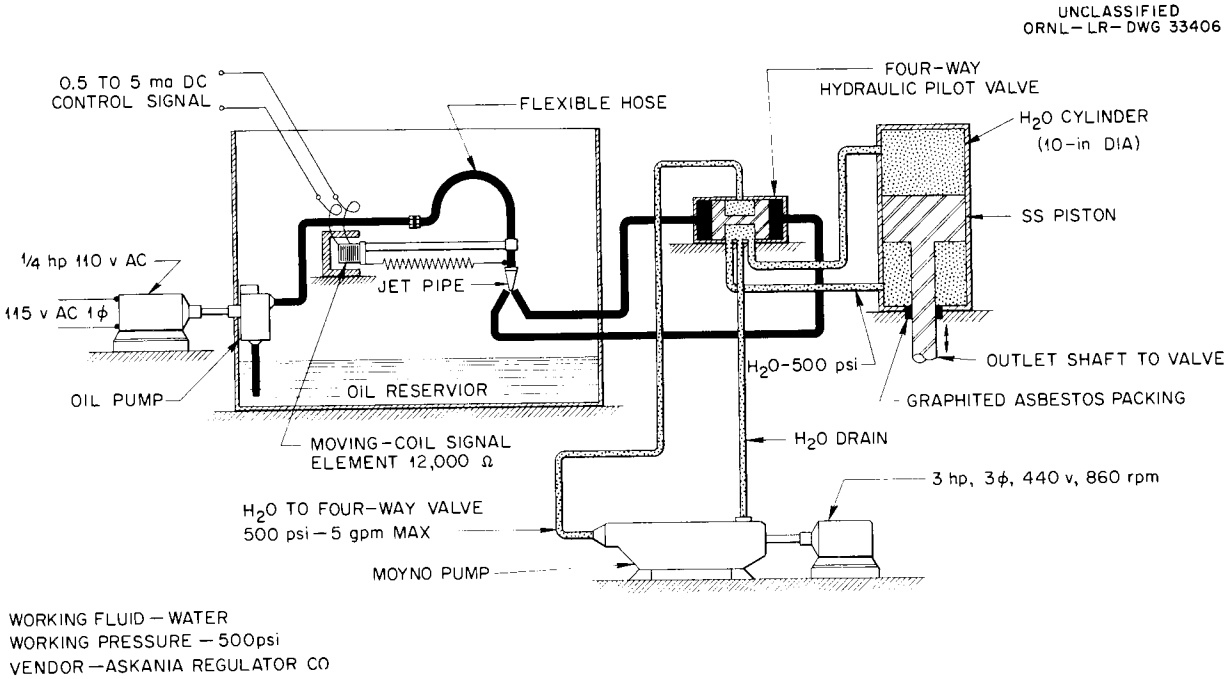

Fig. 11.8. Hydraulic Type of Control-Valve Actuating System.

results of a recently completed life-testing program.[9]

Of four Fulton Sylphon 28-convolution light seal-welded bellows cycled at 2300 psi and 285°C in uranyl sulfate, the average number of $^9/_{32}$-in.-stroke cycles before failure was 135,000. The minimum number was 59,000 and the maximum was 185,000.

A 26-convolution version of the bellows described above is shown at the bottom of Fig. 11.10. The bellows shown at the top of the figure is a three-ply type 316 stainless steel bellows with backup rings rated at 10,000 psi by the manufacturer, The Foxboro Company. The construction of the backup rings is illustrated in Fig. 11.11. Two units were tested at 2000 psi and 250°C in water with a stroke of 0.076 in.; cycles failure were 26,450 and 30,783. The backup rings probably do not lend much support to the bellows at the 2000-psi test pressure.

[9]A. M. Billings, *Life Test of Stem-Sealing Bellows for HRT Valves*, ORNL CF-58-3-39 (March 17, 1958).

11.2.3 Slurry-Service Valve

A prototype pneumatically actuated sampling valve has been constructed for slurry test-loop service. The valve, shown in Fig. 11.12, has a bellows stem seal and a replaceable plug and seat. A type 17-4 PH stainless steel plug and seat will be tested initially; however, as replacement of the plug and seat is relatively simple, various materials will be tried.

A bellows-sealed pneumatically actuated control valve installed as a flow control element in the 30-gpm slurry loop was removed after 907 hr of service in an 800°C-fired slurry which was expected to, and did, form cakes in other parts of the loop. The valve design, illustrated in Fig. 11.13, incorporates a bellows-compartment flushing connection and an angle body design; tungsten carbide was used as the material for the plug, seat, and plug guide.

Upon disassembly, the tungsten carbide plug and plug guide were found to be bound so tightly that movement of the plug was impossible. The

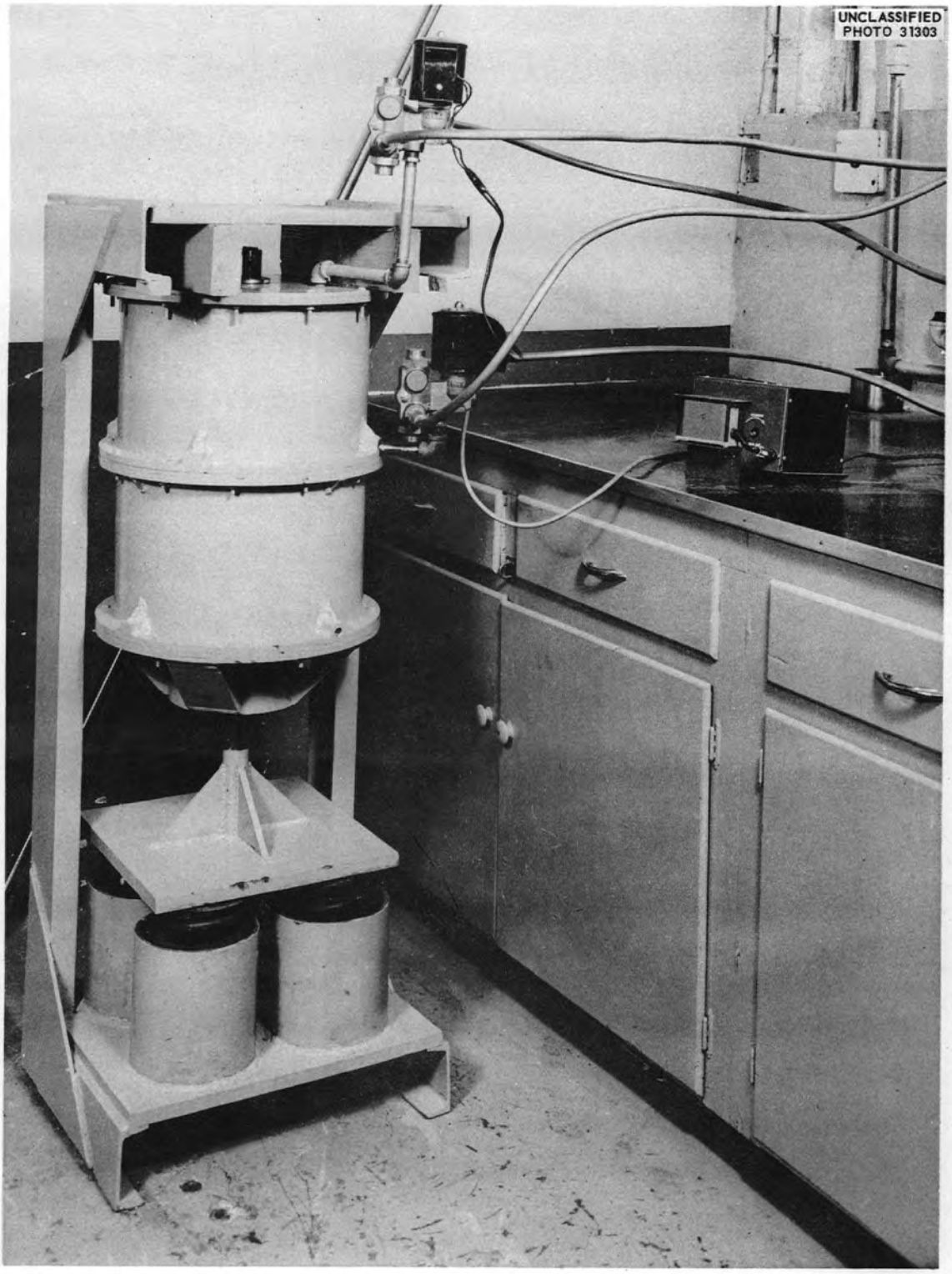

Fig. 11.9. Test Stand for Stacked-Bellows Control-Valve Actuator.

UNCLASSIFIED
PHOTO 25835

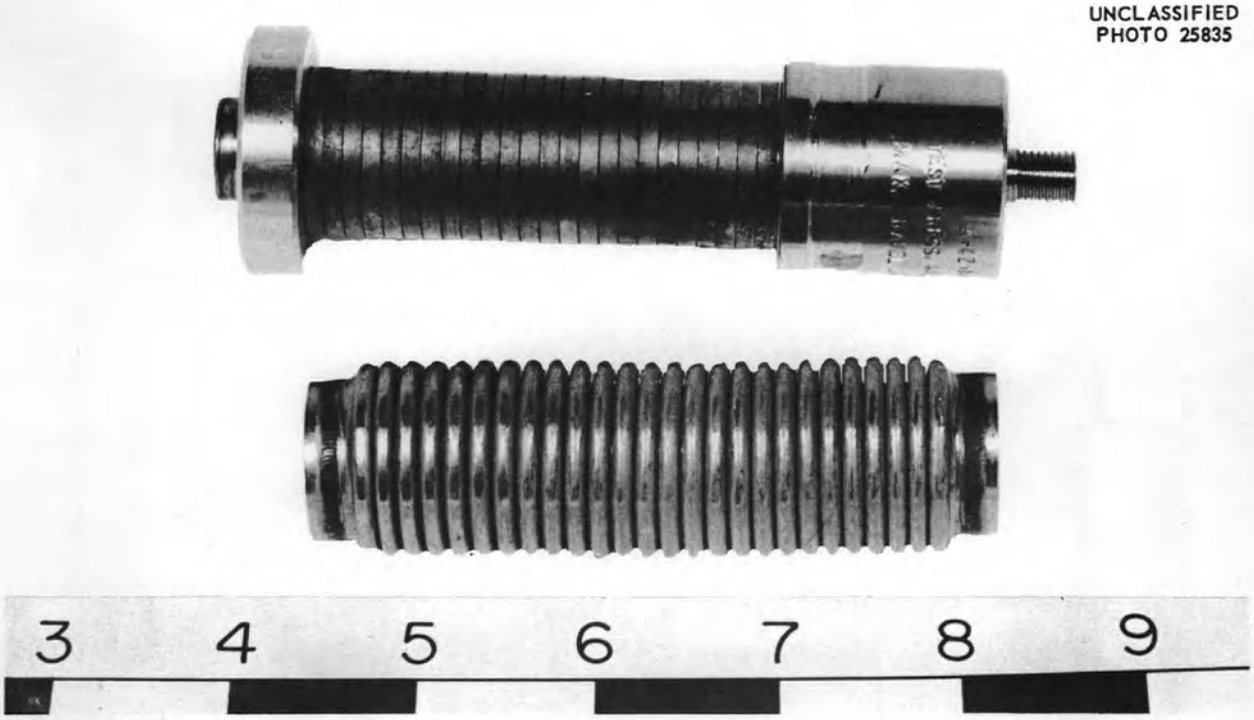

Fig. 11.10. Foxboro and Fulton Sylphon Stainless Steel Bellows Before Testing.

plug guide was cracked and was displaced $\frac{1}{4}$ in. from its press-fit with the stainless steel holder. A thin layer of slurry was visible in the annulus between the plug and plug guide. After removal of the plug from the plug guide, a thick greenish and bluish scale was found on the portion of the plug frozen in its guide. The plug and guide assembly, after removal, is shown in Fig. 11.14.

Service to which this valve was subjected follows:

Valve wide open	825 hr
Valve 40% open (50% flow)	75 hr
Flow, wide open	40 gpm
ΔP across valve	5 to 10 psi
Loop pressure	1650 psig
Loop temperature	280°C
Direction of flow in valve	From top of seat
Slurry concentration	450 g of Th per kg of H_2O

The replacement valve for this application utilizes a chrome carbide plug and seat with a tungsten carbide guide. For subsequent loop operation, the condensate purge of the bellows compartment will also be increased as a precaution against plugging of the guide-to-plug passage with slurry.

UNCLASSIFIED
ORNL-LR-DWG 28847

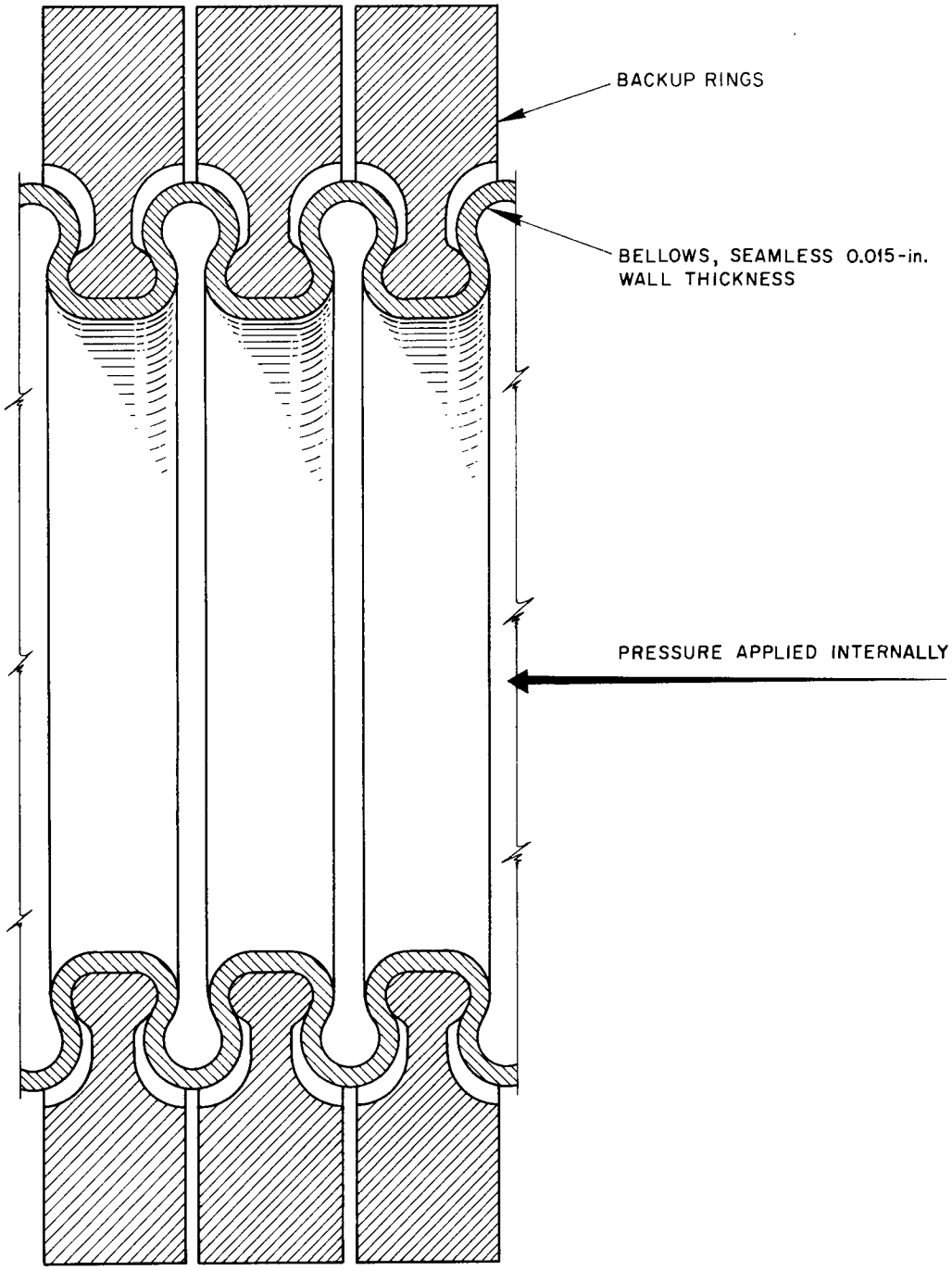

Fig. 11.11. Section Through Foxboro Super-Pressure Bellows.

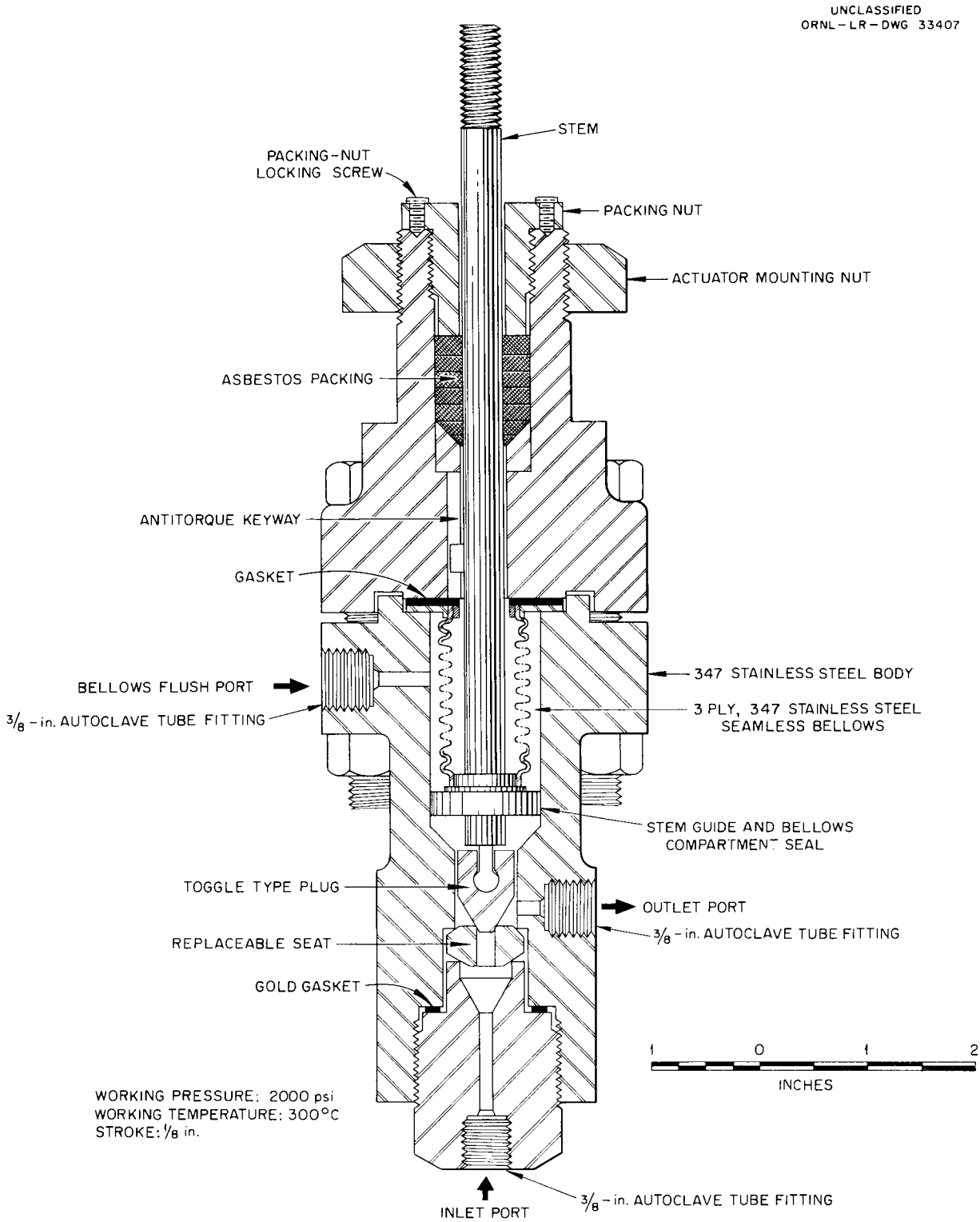

Fig. 11.12. Slurry Sampling Valve.

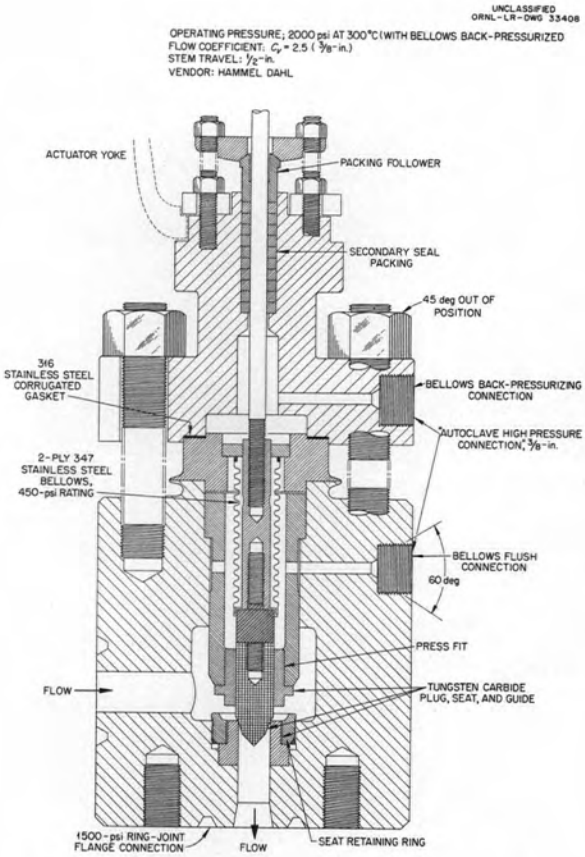

Fig. 11.13. High-Pressure Slurry Control Valve.

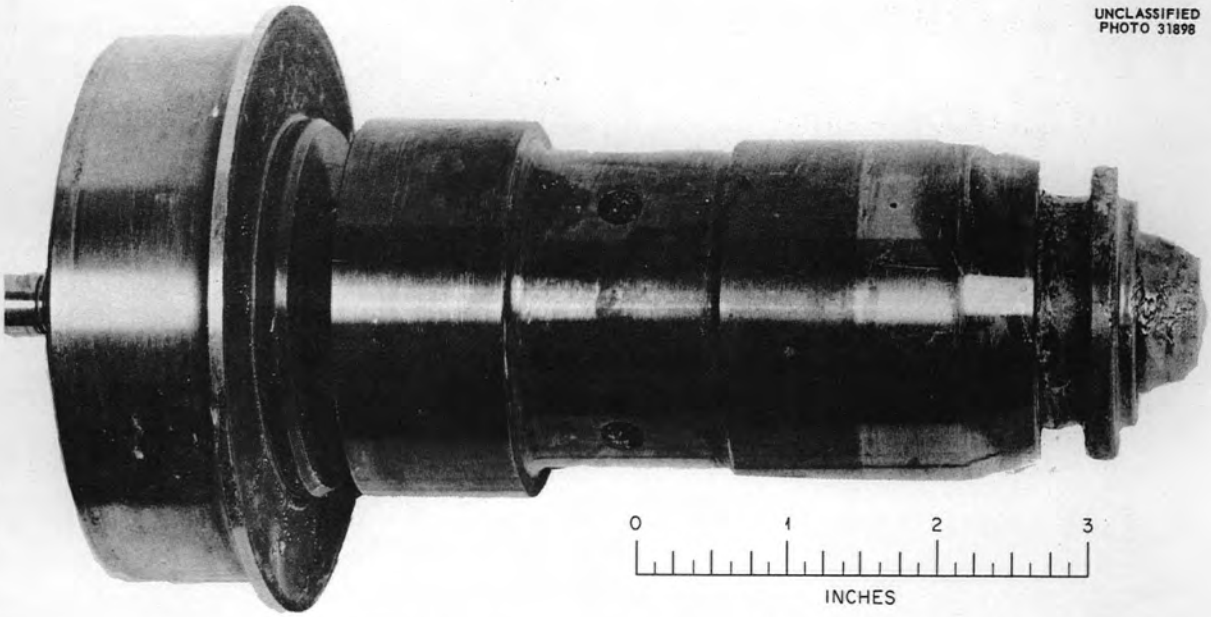

Fig. 11.14. Plug-and-Guide Assembly from High-Pressure Slurry Control Valve.

Part IV

REACTOR MATERIALS RESEARCH

E. G. Bohlmann

12. SOLUTION CORROSION[1]

J. C. Griess H. C. Savage
S. E. Bolt D. N. Hess
S. R. Buxton P. D. Neumann
J. L. English E. S. Snavely
R. S. Greeley W. C. Ulrich
N. E. Wisdom[2]

12.1 DYNAMIC SOLUTION CORROSION

12.1.1 Solution Stability Studies

The rapid buildup of nickel concentration due to stainless steel corrosion during run 13 of the HRT has simulated interest in the effect of nickel ions on the chemical stability of dilute uranyl sulfate solutions. Since most out-of-pile tests had been run in normal water with relatively low nickel concentrations, the effect of changing the solvent from normal to heavy water and the effect of nickel(II) concentration on solution stability needed investigation. For these reasons a run was made at 300°C in a stainless steel loop with 0.04 *m* UO_2SO_4 containing initially 0.025 *m* D_2SO_4 and 0.03 *m* $CuSO_4$ in heavy water. Additions of nickel sulfate dissolved in deuterium oxide were later made to bring the nickel(II) concentration successively to about 400, 750, and 1700 ppm.

It appeared that the solution was stable with up to 750 ppm nickel(II). When the nickel concentration was increased to 1700 ppm, about 35% of the nickel and 7% of the copper were lost from solution. The temperature of the system was lowered to 150°C; and the precipitated nickel dissolved, but the precipitated copper did not. At both temperatures and all nickel concentrations the uranium concentration of the solution remained constant.

The run was restarted with fresh solution containing 1800 ppm nickel(II) as $NiSO_4$, the loop was brought to 175°C, and the temperature was raised in 25°C increments to a final temperature of 300°C with several days of circulation at each temperature. Table 12.1 lists the compositions of the solutions which were stable for the short periods of circulation at each temperature. As can be seen, some of the copper and nickel precipitated on startup and more nickel precipitated at 200°C. Above 200°C the nickel showed an increasing solubility up to 275°C, and then some reprecipitated at 300°C. The copper concentration fluctuated around 1800 ppm up to 275°C, and then more precipitated at 300°C. No uranium was lost from solution at any temperature during the run.

Table 12.1. Steady-State Concentrations of Copper* and Nickel* in Heavy-Water Solution Containing 0.04 *m* UO_2SO_4 + 0.025 *m* D_2SO_4 at Various Temperatures

Temperature (°C)	Time (hr)	Concentrations	
		Copper (ppm)	Nickel (ppm)
		1900**	1800**
175	260	1750	1600
200	140	1800	1050
225	120	1800	1100
250	120	1750	1350
275	170	1750	1600
300	240	1600	1200

*Added as the sulfate salt.
**Initial concentration.

Two other runs were made to investigate the interrelationship between the solubility of copper and nickel. For the first run the solution was made up to simulate the solution circulating in the HRT at the end of run 13 [viz., 0.036 *m* UO_2SO_4, 0.022 *m* D_2SO_4, 0.009 *m* $CuSO_4$, 0.013 *m* $NiSO_4$ (760 ppm Ni), and 0.0016 *m* $MnSO_4$ in heavy water]. The run was started at 250°C, increased to 280°C after 72 hr, increased to 300°C after 300 hr, and held at 300°C for 165 hr. The solution was stable throughout the test. For the second run the solution

[1]Reported in greater detail by J. C. Griess *et al.*, *Quarterly Report of the Solution Corrosion Group for the Period Ending April 30, 1958*, ORNL CF-58-4-131, and *July 31, 1958*, ORNL CF-58-7-132.

[2]Summer employee.

contained a uranium concentration similar to that in the blanket of the HRT during run 16 [viz., 0.01 *m* UO_2SO_4, 0.02 *m* D_2SO_4, and 0.01 *m* $CuSO_4$ in heavy water]. The solution was stable at 300°C. Additions of nickel sulfate were made batchwise to the circulating solution, and the solution remained stable with up to 800 ppm nickel. Further additions of nickel sulfate caused precipitation of both nickel and copper.

In addition to the above solution stability tests, four runs were made in a titanium loop to study the stability of solutions containing added alkali or alkaline-earth metal sulfates. The results are shown in Table 12.2. The solutions containing lithium and rubidium sulfate lost, respectively, 30 and 15% of their copper. The solution containing beryllium sulfate gave a high corrosion rate at high velocity (770 mpy at 70 fps). All solutions produced small amounts of solids containing up to 15% uranium; the solids were collected in a hydroclone underflow pot attached to the loop. The total amount of solids collected was not enough to affect significantly the concentration of uranium in solution. The solution containing magnesium sulfate produced the least amount of solids; these contained only 3% uranium by spectrographic analysis.

Since the solution containing magnesium sulfate appeared more stable and less corrosive than the others, further runs were made with it. In one, J-95, shown in Table 12.2, nickel sulfate was added twice. Nickel, copper, and magnesium precipitated; but no uranium was lost from solution, and the resulting solutions were stable at the concentrations shown in Table 12.2.

In two other runs with the solution containing magnesium sulfate, the corrosion of type 347 stainless steel was investigated at 250°C. In the presence of magnesium sulfate, corrosion of stainless steel was two to five times less at all velocities than in a similar run containing no magnesium sulfate. Also, the critical velocity was increased from 10 to 20 fps to 30 to 40 fps.

Therefore, of the solutions discussed above, the solution containing magnesium sulfate is the least corrosive and most stable (except perhaps for the 0.01 *m* UO_2SO_4 solution which has not been tested at 250°C). Its instability with regard to nickel but not uranium could be an advantage from the standpoint of removing a significant neutron poison from solution. Further tests with magnesium sulfate at higher temperatures are in progress.

12.1.2 Oxygen Exhaustion Studies

The probability that oxygen exhaustion occurred during the first few hours of power operation in HRT run No. 13 (ref 3) prompted a further investigation of the behavior of uranyl sulfate solutions in stainless steel systems in the absence of

[3] R. Van Winkle, oral report, HRP Monthly Information Meeting (March 13, 1958).

Table 12.2. Final Concentrations of Solutions Initially Containing 0.04 *m* UO_2SO_4, 0.025 *m* D_2SO_4, 0.04 *m* Added Sulfate, and 0.03 *m* $CuSO_4$ (1900 ppm Cu) in Heavy Water Circulated for 200 hr at 300°C

Run No.	UO_2SO_4 (*m*)	D_2SO_4 (*m*)	Added Sulfate (*m*)	Copper (ppm)	Nickel (ppm)
G-108	0.04	0.036	Li_2SO_4, 0.04	1300	<20
G-109	0.04	0.029	Rb_2SO_4, 0.025*	1600	<30
G-107	0.04	0.025	$BeSO_4$, 0.04	1900	<30
G-105	0.04	0.025	$MgSO_4$, 0.04	1900	<20
J-95 after first nickel sulfate addition	0.04	0.029	$MgSO_4$, 0.028	1650	250**
J-95 after second nickel sulfate addition	0.04	0.026	$MgSO_4$, 0.020	1400	500**

*No Rb_2SO_4 was lost from solution; the initial concentration was 0.025 *m*.
**Nickel added batchwise as nickel sulfate.

oxygen. It has been general knowledge that in the absence of oxygen, uranyl ions are reduced and precipitated as U_3O_8 or UO_2, but no loop runs had been made in which the reduction of uranium was allowed to go to completion and during which the composition changes in solution were followed closely. Therefore two runs were made in a stainless steel loop, one at 250 and one at 280°C with 0.04 *m* UO_2SO_4 containing 0.025 *m* H_2SO_4 with oxygen excluded from the system. During these runs the solutions were sampled frequently to determine the rate of uranium precipitation, the generalized corrosion rate of the system (from nickel analyses), and the behavior of the constituents of the solution.

Figure 12.1 shows the concentration of several constituents as a function of time during the run at 250°C. The data for the run at 280°C were similar. The uranium concentration in solution dropped to less than 0.5 g/liter within 3 hr, and simultaneously the free-acid concentration increased from 0.025 *m* to 0.041 *m*. The liberation of hydrogen ions intensified the attack on the steel, and in this sense the corrosion was autocatalytic.

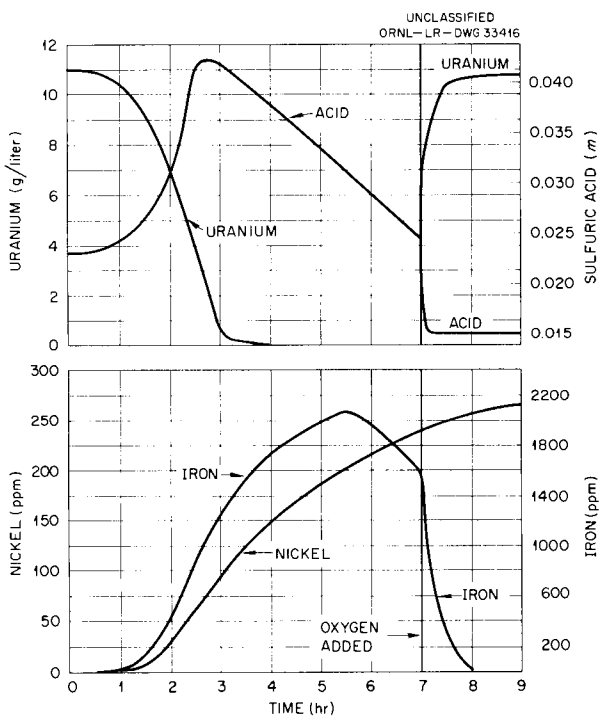

Fig. 12.1. Changes in Composition of a Uranyl Solution Circulated at 250°C in a Stainless Steel Loop in the Absence of Oxygen.

When all the uranium had precipitated, the free acid was steadily used up in the corrosion process and the pH increased. If the amount of free acid is calculated on the basis that the uranium precipitated as U_3O_8, good agreement is obtained with the observed amounts of free acid, iron, and nickel found in solution.

Also, in the absence of oxygen, iron from the corrosion of steel remained soluble as ferrous ions. As can be seen in Fig. 12.1, the iron and nickel concentrations reached high values in the ratio Fe(II):Ni(II) = 10:1. The corrosion rate of the stainless steel loop calculated from the steepest portion of the nickel curve was about 150 mpy. As the acid was used up in corrosion, the ferrous iron began to precipitate, presumably as ferrous sulfate (or perhaps basic sulfate) since the sulfate concentration decreased simultaneously.

After 8 hr of running without oxygen, 350-psi oxygen was added to the loop. Within ½ hr about 95% of the uranium had redissolved, and within 1 hr essentially all the uranium was in solution. Within 2 hr the nickel concentration leveled off, and the pH steadied at 1.65 to 1.70. The addition of oxygen oxidized the ferrous ions to ferric ions, which hydrolyzed and precipitated from solution.

A third run was made in which oxygen was removed from a stainless steel–uranyl sulfate system. In this run the solution contained 0.04 *m* UO_2SO_4, 0.01 *m* $CuSO_4$, 0.025 *m* H_2SO_4, and 0.04 *m* $MgSO_4$ and was circulated at 250°C. The magnesium sulfate was added to determine whether it would suppress the corrosiveness of the sulfuric acid solution resulting from the reduction and precipitation of uranium. As in the first two cases, the data were similar to those shown in Fig. 12.1. The conclusion was drawn that the magnesium sulfate did not inhibit corrosion. In addition to precipitation of uranium, copper was lost from solution.

Thus it may be concluded that if oxygen exhaustion occurred with 0.04 *m* UO_2SO_4 in a stainless steel system at elevated temperatures, precipitation of uranium would occur within a few hours, the actual length of time depending on the temperature and the previous history of the system. As the uranium precipitated, acid would be produced, the attack on the steel would be intensified, and ferrous and nickelous ion concentrations in solution would increase sharply. If oxygen exhaustion continued, the acid would be consumed

in the corrosion process, and the ferrous iron would precipitate. If oxygen were added, the uranium would quickly reappear in solution, the ferrous iron would precipitate as ferric oxide, and the corrosion rate of the steel would decrease to a low value.

The analysis of solution samples taken from the fuel system during HRT run 13 showed no significant concentrations of iron and no evidence of solid oxide particles in the circulating stream as was observed in the tests described above. Based on data obtained out-of-pile, it appears that oxygen depletion was not the cause of the observed high corrosion rate during HRT run 13. However, the effect of radiation on the chemistry of the solution exposed to stainless steel in the absence of oxygen has not been investigated, and this fact precludes a definitive statement as to whether or not oxygen exhaustion was the reason for the high corrosion rate in run 13.

12.1.3 Corrosion of York Mesh in an Iodine-Containing Uranyl Sulfate Solution at 100°C

The possibility existed that the high nickel concentration experienced in HRT run 13 was due to corrosion of the type 304 stainless steel York mesh in the entrainment separator. Therefore tests were run in which samples of the same mesh used in the HRT were exposed in the gas phase (loop pressurizer) and in the liquid phase to a solution containing 0.04 *m* UO_2SO_4 and 0.025 *m* H_2SO_4 circulated at 100°C. The system was pressurized with 40-psi hydrogen and 20-psi oxygen. No significant corrosion occurred during a 60-hr exposure of either as-received mesh or mesh which had been sensitized at 1200°F for 30 min.

The specimens were replaced in the loop without defilming for a second test in which two additions of potassium iodide were made to simulate the appearance of fission-product iodine in the HRT. The amount of iodine added each time, 300 mg as potassium iodide, was equivalent to the total amount of iodine generated during HRT run 13. No iodine appeared in solution after the first addition, but 20 to 30 ppm iodine was detected in solution throughout the run after the second addition. No deleterious effect of the iodine in solution or in the vapor phase was detected on the mesh after a 240-hr exposure at 100°C. It appears unlikely, therefore, that the corrosion experienced in HRT run 13 occurred in the entrainment separator, although it is possible that the radiation associated with the HRT exposure could have influenced the corrosion.

12.1.4 Sixth Test of the HRT Core–Pressure-Vessel Flange and Transition-Joint Mockup

A sixth test of the mockup of the Zircaloy-2–stainless steel transition and expansion joint used in the HRT reactor vessel has been made in 100A dynamic loop F. The first five tests were described previously.[4] The sixth test lasted 4084 hr, 29 hr on water and 4055 hr on fuel solution (0.04 *m* UO_2SO_4, 0.02 *m* H_2SO_4, 0.005 *m* $CuSO_4$). The system was thermally cycled 144 times, each cycle consisting of 4 hr cooling to 100°C, 4 hr heating to 300°C, and 16 hr isothermal operation at 300°C. The thermal cycles were made once each day except during two periods (approximately 10 days each) of continuous isothermal operation at 300°C. During each thermal cycle the expansion joint was mechanically deflected $\frac{5}{8}$ in.

At the conclusion of the run and prior to disassembly, no leakage was detected through the 10-in.-IPS 1500-lb test-vessel oval-ring joint when tested with 200 psig of helium. Neither leakage of fuel solution into the gasket grooves of the oval-ring joint nor leakage of fuel solution through the bellows or across the transition joint occurred during the run. After disassembly the bellows and transition joint were leak-tight to 50 psi of helium.

The pitting attack on the bellows at the edge of the reinforcing rings[5] did not occur perceptibly during the sixth test. This fact was surprising since the previous test had indicated that the mechanical deflections of the bellows were causing the pitting.[6] Why the pitting did not continue is unknown.

The solution remained stable throughout the test. The increase in nickel ion concentration corresponded to a generalized corrosion rate of about 0.1 mpy, the same rate as observed in the previous two tests.[6]

The shiny black oxide film, which had protected the type 347 stainless steel coupons at flow rates

---

[4] H. C. Savage *et al.*, *HRP Quar. Prog. Rep. Oct. 31, 1956*, ORNL-2222, p 77–79; *April 30, 1957*, ORNL-2331, p 83; *July 31, 1957*, ORNL-2379, p 69; *Oct. 31, 1957*, ORNL-2432, p 79.

[5] J. C. Griess *et al.*, *HRP Quar. Prog. Rep. Jan. 31, 1957*, ORNL-2272, p 77–78.

[6] J. C. Griess *et al.*, *HRP Quar. Prog. Rep. Oct. 31, 1957*, ORNL-2432, p 79.

up to 50 fps in the previous tests, broke down at bulk flow rates of 30 fps and above at the edges of the coupons where slight turbulence took place. Localized attack occurred at a rate estimated to be approximately 15 mpy. Since the critical velocity is greater than 50 fps at 300°C, the breakdown of the film must have occurred at the intermediate temperatures during thermal cycling of the loop. The breakdown of the film, which had remained intact during the previous 4500 hr of operation under the same conditions, illustrates the fact that well-established films are not completely reliable at flow rates greater than the critical velocity in the given system.

The total exposure of the mockup has been 9153 hr, including 8600 hr on fuel solution, 312 thermal cycles, and 518 mechanical deflections. It is believed that the design has been proved insofar as an out-of-pile mockup can test it; disassembly and complete examination of the components are planned.

12.1.5 Corrosion of Stainless Steel, Titanium, and Zircaloy-2 in the Heavy Second Liquid Phase of Uranyl Sulfate Solution

Controlled studies of the attack by the heavy phase of two-liquid-phase uranyl sulfate solution at elevated temperatures have not been made previously, although instances of drastic attack on stainless steel by the heavy phase have occurred.[7] Since hot spots which could cause two-phase separation could conceivably occur in a reactor, further investigation was desirable. An all-titanium loop was modified to include a ¼-in. titanium bypass line into which could be inserted with Swagelok fittings a ¼-in.-OD, 6-in.-long, weighed tubing specimen. The tubing specimen was encased with a close-fitting aluminum jacket around which was wound a 300-w heater. A 1500-w preheater was installed on the ¼-in. titanium line preceding the specimen. During operation, the main circulating stream was controlled at 295 to 300°C, while the bypass line was heated to 310 to 312°C. The latter temperature was above the second-liquid-phase temperature of the 0.17 *m* UO_2SO_4 solution used in these runs. Boiling was prevented by gas pressurizing the system to 1700 psig. The bypass line was tilted slightly in relation to the horizontal in order that any heavy liquid phase which formed in the preheater would run down into the tubing specimen and cause local corrosion there. The solution flow rate through the specimen was about 3 fps.

Three 200-hr runs were made, one each with a type 347 stainless steel, a type A-55 titanium, and a Zircaloy-2 tubing specimen. No evidence of localized attack was found on any of the specimens on visual examination after the runs. The corrosion rate from the loss in weight was 76 mpy for the stainless steel, 1.6 mpy for the titanium, and 0.7 mpy for the Zircaloy-2. The high corrosion rate of the stainless steel suggests that heavy phase was present on the tubing walls during the run. However, the absence of localized attack indicates that the heavy phase, if present, was swept past the tubing by the flowing solution, even though it has been observed in quartz tubes that heavy phase strongly wets the three metals tested.[8] It was concluded that heavy-phase attack was severe only on the stainless steel and was not so catastrophic as has been observed in static systems[6] so long as the solution flow rate was 3 fps.

12.1.6 Corrosion of Stainless and Carbon Steels at 300°C in Chloride-Containing Boiler Water

In a continuation of the study of corrosion of materials by boiler water,[9] the effect of chloride contamination was investigated. Three runs were made, one each with <0.1, ~4, and ~9 ppm oxygen in solution. The solution was maintained at pH 10 to 10.5, with 60 ppm phosphate as trisodium phosphate by continuous addition and letdown. The chloride concentration was 50 to 60 ppm as potassium chloride, and all other ions were less than 1 ppm.

The variation in corrosion rate with oxygen concentration for the austenitic stainless steels and the carbon steels was similar to that reported previously for the same system without chloride.[9] This fact is brought out in Table 12.3, which shows

[7] J. C. Griess *et al.*, *HRP Quar. Prog. Rep. July 31, 1957*, ORNL-2379, p 76.

[8] I. Spiewak, *Monthly Program Report of the Component Development Section for July 1958*, Central Files memorandum (to be published).

[9] J. C. Griess *et al.*, *HRP Quar. Prog. Rep. Jan. 31, 1958*, ORNL-2493, p 89.

Table 12.3. Comparison of Corrosion Rates of Steels in Boiler Water at 300°C With and Without Chloride

	Corrosion Rate (mpy)		
	O_2 Concentration <1 ppm	O_2 Concentration ~4 ppm	O_2 Concentration ~9 ppm
<1 ppm chloride			
Average austenitic stainless steels	0.4	1.6	1.8
Average carbon steels	12	18	24
50 ppm chloride			
Average austenitic stainless steels	0.4	1.9	1.8
Average carbon steels	12	21	24

the corrosion rates for the steels at several oxygen concentrations in the presence and in the absence of chloride. From Table 12.3 it can be seen that the corrosion rate of both stainless and carbon steel increased as the oxygen concentration increased and was independent of the 50 ppm chloride.

Stress specimens were included in each run and were totally immersed at a solution flow rate of about 3 fps. Stress-corrosion cracks were found on only two specimens, and both of these were type 347 stainless steel specimens exposed in the run with 9 ppm oxygen. One of the cracked specimens was stressed on top of a similar carbon steel specimen; that is, the stainless steel was galvanically coupled to carbon steel over its entire length. The other cracked specimen was stressed over another stainless steel specimen. The cracks in both cases started from the side which was in tension. It appeared that the crevice formed between the specimens mounted on top of one another did not influence the cracking behavior; and it is also obvious that, at least in the one case, the carbon steel coupled to the stainless steel did not cathodically protect it.

12.1.7 Effect of Ruthenium Nitroso Sulfate on the Behavior of Dilute Uranyl Sulfate and Sulfuric Acid Solutions

The relatively stable ruthenium nitroso complex was previously tested[10] for its corrosion-inhibition properties in 0.17 *m* UO_2SO_4. It was found that the complex salt was not stable at 250°C, that at least 90% of the ruthenium precipitated from solution as a mixture of the metal and ruthenium dioxide, and that a large increase in the hexavalent chromium concentration occurred. Corrosion of the stainless steel was markedly inhibited at low velocities, and the critical velocity was substantially increased by the chromium(VI) (ref 11).

More recently, the effect of ruthenium nitroso sulfate in other solutions has been studied. In 0.04 *m* UO_2SO_4 containing 0.025 *m* H_2SO_4, 0.01 *m* $CuSO_4$, and about 1000 ppm O_2, the presence of 100 ppm ruthenium as the nitroso sulfate caused the appearance of 600 ppm chromium(VI) within 50 hr at 250°C. Normally, in the absence of ruthenium, the chromium(VI) concentration in this solution reaches only about 5 ppm in 50 hr. In the presence of ruthenium, corrosion was markedly inhibited, presumably as a result of the chromium(VI), and as in the previous run, at least 90% of the ruthenium was lost from solution very early in the run.

Normally when sulfuric acid solutions are circulated in a stainless steel loop, no chromium(VI) is formed, regardless of oxygen concentration or temperature, and corrosion damage is severe. It was of interest, therefore, to determine whether the addition of ruthenium to such solutions would result in the formation of chromium(VI), which

[10] J. C. Griess *et al.*, *HRP Quar. Prog. Rep. Oct. 31, 1957*, ORNL-2432, p 81.

[11] J. C. Griess *et al.*, *HRP Quar. Prog. Rep. July 31, 1954*, ORNL-1772, p 79.

would minimize corrosion.[12] Solutions of 0.025 and 0.05 *m* H_2SO_4 containing 100 ppm of ruthenium and about 1000 ppm of oxygen were circulated in stainless steel loops at 250°C. In each case most of the ruthenium was lost from solution, and substantial concentrations of chromium(VI) formed; as expected, little corrosion occurred.

In all cases the amount of chromium present in solution exceeded that which resulted from corrosion in that run. Apparently the ruthenium was effective in oxidizing the chromic oxide in the scale (from previous runs) to the soluble hexavalent state. Furthermore, at the end of the run the ruthenium lost from solution could not be rinsed from the system, and even though no ruthenium was added in subsequent runs, the system retained its ability to form substantial quantities of chromium(VI).

In view of the ability of ruthenium to cause the rapid oxidation of chromium to the hexavalent state, it is possible that the addition of ruthenium to in-pile solutions could result in a residual concentration of chromium(VI), which presumably would be an effective corrosion inhibitor. Further tests are necessary to investigate this possibility.

12.2 LABORATORY CORROSION STUDIES

12.2.1 Stress-Corrosion Cracking

(a) Stress-Corrosion Cracking by Chloride-Containing Cooling Water. – The stress-corrosion cracking behavior of type 347 stainless steel and other alloys has been examined under conditions in which pipe U-bends of the test materials were heated internally with 60-psig steam at approximately 150°C while undergoing spray-cooling of external surfaces by chloride-containing potable water. The construction and operational characteristics of the bent-pipe spray test have been reported previously along with results of the initial tests.[13–16] Testing has been continued to determine the effects of annealing after bending, surface condition of the pipe, and cathodic protection on cracking susceptibility of type 347 stainless steel and also to examine the cracking behavior of other alloys.

Generally, the pipe bends were cold formed from ½-in. sched-40 pipe; in some cases, ½-in.-dia tubing was used. The chloride content of the cooling water ranged between 3 and 7 ppm. At the end of 1000-hr runs the chloride content of the scales deposited on the external surfaces of the pipes was 150 ppm or greater. Under the test conditions, cold-formed pipe bends of type 347 stainless steel developed many cracks during 1000-hr runs.

Efforts to minimize or eliminate cracking in type 347 stainless steel consisted in (1) annealing cold-formed pipe bends for ½ hr at 1066°C (1950°F) followed by water quenching, (2) shot-blasting the external surface of a cold-formed pipe bend to place the surface under compressive stress, and (3) cathodically protecting the cold-formed pipe. In the latter case one half of the surface of the cold-formed pipe was wrapped with 1/16-in.-dia aluminum wire on ½-in. centers. The other half of the pipe was left unwrapped. Results of the tests with type 347 stainless steel and other alloys of interest are summarized in Table 12.4.

Annealing at 1950°F was not completely effective in eliminating cracking in type 347 stainless steel, but beneficial effects were evident. In two cases, annealed pipes were exposed for periods of 2000 and 4990 hr without cracking. In a third case cracking occurred, but the number of cracks was appreciably smaller than was observed on cold-formed pipes that had not been annealed.

Placing the surfaces of a cold-formed pipe bend under compressive stress by shot-blasting has prevented cracking during 4990 hr of exposure. During the last 1000 hr, a small group of cracks developed on a non-shot-blasted surface where the pipe bend was connected to the steam manifold. From this group of cracks a major crack extended for approximately ¼ in. into the shot-blasted surface. Although it was not possible to determine with certainty the starting point of the crack, the geometry suggested that it originated in the cluster of small cracks. No cracks were found elsewhere on the shot-blasted surface.

---

[12] J. C. Griess *et al.*, *HRP Quar. Prog. Rep. April 30, 1955*, ORNL-1895 p 90–91.

[13] E. L. Compere and J. L. English, *HRP Quar. Prog. Rep. July 31, 1954*, ORNL-1772, p 94.

[14] J. L. English *et al.*, *HRP Quar. Prog. Rep. April 30, 1956*, ORNL-2096, p 85.

[15] J. C. Griess *et al.*, *Quarterly Report of the Solution Corrosion Group for the Period Ending April 30, 1956*, ORNL CF-56-4-138, p 31–32.

[16] J. C. Griess *et al.*, *Quarterly Report of the Solution Corrosion Group for the Period Ending Jan. 31, 1957*, ORNL CF-57-1-144, p 35–37.

Table 12.4. Stress-Corrosion Cracking of Steam-Heated* Pipe Bends of Several Alloys Cooled with Chloride-Containing Potable Water**

Material	Initial Treatment	Total Time (hr)	Observations
347 SS	Cold formed	1000	Many cracks
	Cold formed; annealed ½ hr at 1950°F	1000	Several cracks
	Cold formed; annealed ½ hr at 1950°F	2000	No cracks
	Cold formed; annealed ½ hr at 1950°F	4990	No cracks
	Cold formed; shot blasted	4990	Cracks in unblasted area extending into blasted area
	Cold formed; one half of stressed area wrapped with aluminum wire; other half unwrapped	2000	Several cracks on unwrapped area; no cracks on wrapped area
MST grade 3 titanium	Cold formed	4990	No cracks
Croloy 16-1	Cold formed	4990	No cracks
Incoloy T	Cold formed	1990	Few cracks
Ni-o-nel	Cold formed	1990	No cracks
Inconel	Cold formed	990	No cracks

*60-psig steam (~150°C).

**Chloride content in water, 3 to 7 ppm.

The use of cathodic protection, achieved by wrapping aluminum wire around one half of the stressed surface of a cold-formed type 347 stainless steel pipe bend, prevented cracking during a 2000-hr test. The unprotected half of the pipe developed cracks during the interval between 1000 and 2000 hr.

Materials which have been completely resistant to stress-corrosion cracking in the cold-formed condition to date include MST grade 3 titanium, Croloy 16-1 stainless steel, Ni-o-nel, and Inconel. An Incoloy T pipe bend developed several cracks during a 1990-hr test.

Although only one test has been completed to date, cathodic protection appears to be a possible and practical means of eliminating cracking, even in the case where the stainless steel and the anodic member are not totally submerged. For example, in underwater maintenance where chloride-containing water is used, it may be possible to prevent cracking of austenitic stainless steels by attaching an active metal to the surface of the steel. Presumably the active metal not only would protect the austenitic stainless steel while it was submerged but also would protect it after the water had been drained and during the time the pipe dried. Once dry, stress-corrosion cracking would be of no concern. Tests are currently being conducted to determine the effective range of aluminum, magnesium, and carbon steel in preventing stress-corrosion cracking of type 347 stainless steel in the spray-bend test.

(*b*) Stress-Corrosion Cracking by High-Temperature Chloride-Containing Water. – Corrosion tests have been continued to determine the stress-corrosion cracking behavior of a number of alloys immersed at 300°C in oxygenated distilled water to which has been added 100 ppm of chloride. The initial pH is adjusted to values of 2.8, 6.5, or 10.5 by use of sodium hydroxide or hydrochloric acid. Standard U-bend specimens are used. Among the alloys undergoing test are a group of the austenitic

stainless steels, a ferritic stainless steel, and two high-nickel-content alloys. The results of the tests appear in Table 12.5. Initial results have been reported previously.[17]

The present and the previously reported results[17] have confirmed the susceptibility of the 300-series austenitic stainless steels to cracking in all the chloride-containing environments that were examined at 300°C. Carpenter 7-Mo stainless steel, a precipitation-hardenable alloy, developed cracks in the hardened condition (50 Rockwell C) in pH 2.8 water but was otherwise crack-resistant in pH 2.8 and 10.5 chloride-containing water in the annealed and hardened conditions.

Croloy 16-1 stainless steel cracked during 200 hr in pH 6.5 water but did not crack during 2000 hr of exposure at a pH of 10.5. Incoloy cracked during a 500-hr exposure in pH 2.8 water but resisted cracking during periods of 500 and 1500 hr, respectively, in pH 6.5 and pH 10.5 water. Exposure periods of 300 and 400 hr in pH 2.8 and 6.5 water

[17] J. C. Griess *et al.*, *HRP Quar. Prog. Rep. Jan. 31, 1958*, ORNL-2493, p 94–95.

Table 12.5. Stress-Corrosion Cracking Behavior of Various Alloys at 300°C in Air-Saturated* Distilled Water Containing 100 ppm of Chloride

Alloy Type	Condition Prior to Stressing	Initial Water pH	Total Time (hr)	Observations
304 SS	Annealed	2.8	100	Cracks
	Annealed	10.5	100	Cracks
	Sensitized	2.8	200	Cracks
	Sensitized	10.5	400	Cracks
304L SS	Annealed	2.8	1000	Many cracks
309SCb SS	Annealed	2.8	500	Many cracks
316 SS	Annealed	2.8	500	Cracks
321 SS	Annealed	2.8	200	Cracks
	Annealed	10.5	500	Suspected cracks
Carpenter 7-Mo SS	Annealed	2.8	2000	No cracks
	Annealed	10.5	1000	No cracks
	Full hard	2.8	100	Cracks
	Full hard	10.5	500	No cracks
Croloy 16-1 SS	Annealed	6.5	200	Cracks
	Annealed	10.5	2000	No cracks
Incoloy	Annealed	2.8	500	Cracks
	Annealed	6.5	500	No cracks
	Annealed	10.5	1500	No cracks
Ni-o-nel	Annealed	2.8	300	Cracks
	Annealed	6.5	400	Cracks
	Annealed	10.5	1500	No cracks

*Saturated with air at room temperature.

produced cracking in Ni-o-nel, but the alloy did not crack during 1500 hr in pH 10.5 water.

Thus far, the data indicate that under conditions where both oxygen and chloride are present the high-nickel alloys, such as Ni-o-nel and Incoloy, are more resistant to stress-corrosion cracking in a chloride-containing alkaline environment than the austenitic stainless steels. However, the high-nickel alloys do not appear more resistant to cracking than the austenitic stainless steels in pH 2.8 and 6.5 chloride-containing water. The tests are being continued in those cases where cracking has not been observed.

Tests have been continued also to determine the effect of the complete removal of oxygen from chloride-containing water on the stress-corrosion cracking behavior of type 347 stainless steel at 300°C. With sodium sulfite being used as an oxygen scavenger, no cracks have been found in eight specimens exposed for 2000 hr. Under similar test conditions with oxygen present, all the type 347 stainless steel stress specimens developed cracks during exposure periods of 500 hr or less.

(c) Stress-Corrosion Cracking by Chloride-Containing Uranyl Sulfate Solution. – An evaluation of the effectiveness of a preformed film for preventing stress-corrosion cracking of type 347 stainless steel in chloride-containing uranyl sulfate solution at its atmospheric boiling temperature has been continued. Preliminary results of the evaluation have been reported.[18] Prefilming of elastically stressed U-bend specimens was accomplished by immersion in chloride-free 0.04 *m* UO_2SO_4 solution containing 0.02 *m* H_2SO_4 and 0.005 *m* $CuSO_4$ at temperatures of 100, 125, 150, 175, and 200°C. At temperatures of 125°C and above, the prefilming solution was pressurized with oxygen. After prefilming, the stressed specimens were tested in boiling and aerated 0.04 *m* UO_2SO_4–0.02 *m* H_2SO_4–0.005 *m* $CuSO_4$ solution containing 50 ppm of chloride as potassium chloride.

Initial studies concerned with pretreatment in boiling chloride-free uranyl sulfate showed that pre-exposure times of 50, 100, or 500 hr were completely effective in preventing cracking when the specimens were subsequently exposed to the chloride-containing environment. In the case of the 500-hr pretreatment, specimens were stressed both before and after the prefilming, and in neither case was cracking observed for exposures up to 3000 hr. In the absence of any pretreatment more than half of the specimens would have cracked in 500 hr or less in the chloride-containing environment.

Other studies were concerned with the effectiveness of films formed at temperatures above the atmospheric boiling point of the solution. Stressed U-bends were exposed for 100-hr periods in chloride-free 0.04 *m* UO_2SO_4–0.02 *m* H_2SO_4–0.005 *m* $CuSO_4$ solution at temperatures of 125, 150, 175, and 200°C. The prefilmed specimens were then placed in the boiling uranyl sulfate solution containing 50 ppm of chloride.

Accumulated exposure times in the chloride-containing solution thus far are 1500 hr for 125°C specimens, 1000 hr for 150°C specimens, 500 hr for 175°C specimens, and 200 hr for 200°C specimens. Although the exposure times are relatively short, particularly for the specimens pretreated at 175 and 200°C, none of the specimens have exhibited cracking. The tests are being continued.

Thus the experimental evidence to date clearly indicates the beneficial effect of preformed films in preventing stress-corrosion cracking of type 347 stainless steel in boiling chloride-containing uranyl sulfate solution. The effectiveness of such preformed films for preventing cracking in chloride-containing uranyl sulfate solutions at elevated temperatures remains to be investigated.

12.2.2 Miscellaneous Corrosion Tests

A number of corrosion tests have been made on materials of possible interest to the Homogeneous Reactor Project. The materials included niobium, types 17-4 PH and Croloy 16-1 stainless steel, Ni-o-nel, Flame-Plated stainless steel, and type 202 stainless steel.

(a) Niobium. – Niobium was tested in boiling 5% HNO_3 and in 0.04 *m* UO_2SO_4 containing 0.02 *m* H_2SO_4 and 0.005 *m* $CuSO_4$. Tests in the latter solution were run at its atmospheric boiling temperature and at 200 and 300°C. In all cases except at 300°C, the 1000-hr corrosion rates were 0.1 mpy or less. Some shallow pitting attack (<0.5 mil) was noted on all specimens. At 300°C in the uranyl sulfate solution the specimens underwent severe exfoliation during a 500-hr test. Although not expected to crack, the material was stressed

[18] J. C. Griess *et al.*, *Quarterly Report of the Solution Corrosion Group for the Period Ending January 31, 1958*, ORNL CF-58-1-72, p 46–48.

and exposed in the boiling uranyl sulfate solution to which 50 ppm of chloride had been added; no cracking was experienced during a 1000-hr test.

The catastrophic corrosion attack encountered at 300°C precludes the use of niobium in uranyl sulfate solution at that temperature and probably at somewhat lower temperatures.

(b) Type 17-4 PH Stainless Steel. – Type 17-4 PH stainless steel is a precipitation-hardenable alloy which could find use as a bolting or valve-trim material. Corrosion tests have been completed in which the alloy in various degrees of hardness was exposed to a number of reactor-related environments. The conditions of the tests and the results appear in Table 12.6.

The corrosion resistance of the alloy was excellent under all conditions of the test. Corrosion rates were 1 mpy or less, and the attack was uniform. No cracking around the stencil marks on fully hardened specimens (44 Rockwell C) was noted, although such cracking had been found previously in similar environments.[19] However, partially hardened (37 Rockwell C) bolt-type specimens, of a different heat of steel and stressed at a room-temperature value of 40,000 psi, cracked in the solution and vapor phases of oxygenated chloride-free 0.04 *m* UO_2SO_4–0.02 *m* H_2SO_4–0.005 *m* $CuSO_4$ solution at 280°C. The time required for cracking in either phase was less than 1000 hr.

The inconsistency of the above results on the cracking susceptibility of 17-4 PH stainless steel shows why the use of the alloy under tensile conditions in uranyl sulfate environments should be avoided if possible. In cases where no substitute exists, thorough testing of the heat of steel to be used should be performed to demonstrate the dependability of the particular lot of material for the application.

(c) Croloy 16-1 Stainless Steel. – Croloy 16-1 stainless steel, containing 16% Cr, 1% Ni, 0.03% C (maximum), and balance iron, was one of several alloys considered for fabrication of heat-exchanger tubes. In addition to a study of its stress-corrosion cracking behavior in chloride-containing high-temperature water, reported in Sec 12.2.1, static autoclave tests were run to determine the corrosion resistance of the alloy in a solution containing 0.04 *m* UO_2SO_4, 0.02 *m* H_2SO_4, and 0.005 *m* $CuSO_4$ at atmospheric boiling temperature and at 200 and

[19] E. L. Compere, J. L. English, and G. E. Moore, *HRP Quar. Prog. Rep. April 30, 1955*, ORNL-1895, p 124–25.

Table 12.6. Corrosion of 17-4 PH Stainless Steel by Several Reactor-Related Environments

Environment	Temperature (°C)	Total Time (hr)	Atmosphere	Metal Hardness (Rockwell C)	Corrosion Rate (mpy)
Distilled water	80	1000	Oxygen	44	<0.1
	Boiling	1000	Air	32	0.1
UO_2SO_4 solution[a]	80	1000	Oxygen	44	0.2
	Boiling	1000	Air	32	0.3
	Boiling	1000	Air	44	0.2
	300	1000	Oxygen	32	0.3
UO_2SO_4 solution[b]	90	672	Oxygen	28.5	0.8
	90	672	Oxygen	28.5	0.6[c]
5% HNO_3	Boiling	1000	Air	32	1.0

[a] 0.04 *m* UO_2SO_4–0.02 *m* H_2SO_4–0.005 *m* $CuSO_4$.
[b] 0.04 *m* UO_2SO_4–0.4 *m* H_2SO_4–0.03 *m* $CuSO_4$.
[c] Specimens pretreated for 24 hr in test solution at room temperature before start of test.

300°C. Under all conditions, the corrosion resistance was poor; corrosion rates ranged between 9 and 265 mpy. Poor agreement between results was obtained in duplicate tests. Severe end-grain corrosion attack was noted on a number of the specimens. In view of the results, Croloy 16-1 stainless steel is not considered an acceptable material for use with uranyl sulfate solutions at boiling temperature and above.

(d) Ni-o-nel. – Another material of general interest for homogeneous reactor applications is Ni-o-nel, which contains approximately 40% Ni, 20% Cr, 30% Fe, 3% Mo, 1.75% Cu, and 0.05% C. Specimens prepared from cold-rolled and annealed $\frac{1}{8}$-in.-thick sheet were subjected to a number of conventional screening tests. The results of the tests appear in Table 12.7.

With the exception of the 200 and 300°C tests in uranyl sulfate solution, the corrosion resistance of Ni-o-nel was excellent, with observed rates less than 0.1 mpy. In the uranyl sulfate solution at 200 and 300°C, the rates were 2 mpy or slightly less. One significant feature of the corrosion behavior of Ni-o-nel was its resistance to stress-corrosion cracking in boiling uranyl sulfate solution containing 50 ppm of chloride and in boiling 42% $MgCl_2$ solution. In comparison, $\frac{1}{16}$-in.-thick type 347 stainless steel stress specimens are cracked consistently in periods of 100 hr or less in the former solution and in a few hours in the latter environment. Further critical examination and consideration of the alloy for possible reactor use are merited.

(e) Flame-Plated Stainless Steel. – Recently tests were completed with a hard-facing material, Flame-Plate, a product of Linde Company. The plate composition is reported to be 64% W, 23% Ni, 6% Cr, and 7% C. The deposited plate has an average hardness of 930 DPH (~68 Rockwell C). Test specimens of type 347 stainless steel were Flame-Plated on one flat surface and subjected to exposure in deionized water, nitric acid, and oxygenated uranyl sulfate solutions. The deposited Flame-Plate was reported to be 0.003 in. thick after polishing. Results of the tests are included in Table 12.8. Corrosion rates were based on the Flame-Plated surface area only; attack on type 347 stainless steel is not more than several tenths of a mil per year in all environments tested.

The corrosion resistance of the Flame-Plate was generally poor in all environments tested. The attack on the deposit was characterized by heavy granulation. Therefore, Flame-Plate is not recommended for homogeneous reactor application.

(f) Type 202 Stainless Steel. – Test results obtained with annealed type 202 stainless steel

Table 12.7. Corrosion of Ni-o-nel by Several Reactor-Related Environments

Environment	Temperature (°C)	Total Time (hr)	Corrosion Rate (mpy)	Observations
5% HNO_3	Boiling	1000	<0.1	Negligible attack
42% $MgCl_2$[a]	154	100		No cracks
UO_2SO_4 solution[b]	Boiling	1000	<0.1	Negligible attack
	Boiling	1000	<0.1[c]	Very shallow pitting, <0.5 mil
	200	1000	1.7	Numerous shallow pits, <0.5 mil
	300	1000	2.0	Mild attack along polish lines
	300	1000	2.0[a]	No cracking
UO_2SO_4 solution plus chloride[d]	Boiling	1000	<0.1	Negligible attack
	Boiling	2500	<0.1[a]	No cracking

[a]Stress-corrosion cracking test with U-bend specimen.
[b]0.04 *m* UO_2SO_4–0.02 *m* H_2SO_4–0.005 *m* $CuSO_4$.
[c]Specimens heated for 1 hr in air at 677°C (1250°F).
[d]0.04 *m* UO_2SO_4–0.02 *m* H_2SO_4–0.005 *m* $CuSO_4$ with 50 ppm chloride as HCl.

have been reported previously.[20] Recent tests have been concerned with the behavior of the alloy in the sensitized condition, such as could result from welding operations. The sensitizing treatment consisted in heating specimens for 1 hr in air at 677°C (1250°F) followed by air cooling. The corrosion behavior of the sensitized material and that of the annealed material are compared in Table 12.9.

[20] J. C. Griess *et al.*, *Quarterly Report of the Solution Corrosion Group for the Period Ending July 31, 1957*, ORNL CF-57-7-121.

Table 12.8. Corrosion of Flame-Plate on Type 347 Stainless Steel by Several Reactor-Related Environments

(Test time, 1000 hr)

Environment	Temperature (°C)	Corrosion Rate* (mpy)
Deionized H_2O	300	19
5% HNO_3	Boiling	2
UO_2SO_4 solution**	Boiling	4
	200	3
	300	20

*Based upon Flame-Plated surface only.
**0.04 *m* UO_2SO_4–0.025 *m* H_2SO_4–0.01 *m* $CuSO_4$.

In the annealed condition, the corrosion resistance of type 202 stainless steel compared favorably with that of type 347 stainless steel exposed in similar environments. The corrosion resistance of the former, however, was lowered by the sensitizing treatment. This was particularly true in the boiling 5% HNO_3 and the boiling uranyl sulfate solutions. The behavior of sensitized specimens in the latter solution was very erratic. In one case, severe blistering of the metal and reduction of copper from solution were observed, while specimens corroded at a rate of 22 mpy. A repeat test with specimens from the same source resulted in a corrosion rate of 2 mpy; neither metal blistering nor copper reduction occurred. For comparative purposes, sensitized type 302 stainless steel specimens were exposed for 1000 hr in the boiling uranyl sulfate solution. The specimens underwent negligible attack and showed no blistering.

Weld specimens of the type 202 alloy were exposed in the as-welded and in the welded-and-annealed condition in oxygenated 0.04 *m* UO_2SO_4–0.02 *m* H_2SO_4–0.005 *m* $CuSO_4$ solution at its atmospheric boiling temperature and at 200 and 300°C and in boiling 5% HNO_3 solution. Type 308 stainless steel rod was used for the welding. The results of 1000-hr tests for as-welded and welded-and-annealed specimens were in excellent agreement. Corrosion rates, with one exception, were 0.6 mpy or less in the environments tested. The exception was the uranyl sulfate solution at

Table 12.9. Corrosion of Type 202 Stainless Steel in Annealed and Sensitized[a] Conditions by Several Reactor-Related Environments

(Test time, 1000 hr)

Environment	Temperature (°C)	Corrosion Rate (mpy)	
		Annealed	Sensitized
5% HNO_3	Boiling	0.1	18
UO_2SO_4 solution[b]	Boiling	<0.1	2, 22
	200	0.9	2
	300	0.4	0.4
UO_2SO_4 solution[c]	Boiling	<0.1	

[a]Heated 1 hr in air at 1250°F; air cooled.
[b]0.04 *m* UO_2SO_4–0.02 *m* H_2SO_4–0.005 *m* $CuSO_4$.
[c]1.33 *m* UO_2SO_4.

200°C; observed corrosion rates were 1.5 and 2.0 mpy. No evidence of localized corrosion attack resulting from sensitization during welding was observed on the as-welded specimens or on the specimens that were annealed after welding.

The stress-corrosion cracking behavior of annealed type 202 stainless steel was examined in boiling 0.04 *m* UO_2SO_4–0.02 *m* H_2SO_4–0.005 *m* $CuSO_4$ solution containing 50 ppm of chloride as potassium chloride. Cracking of both unstressed control specimens and stressed specimens occurred around the edges of drilled holes during 1000 hr. The control specimens were also subject to blistering.

In view of the irregular behavior of the type 202 stainless steel, it appears unlikely that the alloy would be suited to homogeneous reactor applications.

13. SLURRY CORROSION

E. L. Compere H. C. Savage

S. E. Bolt
J. W. Brown
V. A. DeCarlo
D. W. Hubbard
D. T. Jones
R. A. Lorenz
A. R. Olsen
S. A. Reed
L. Rice
W. C. Ulrich
R. M. Warner
L. F. Woo

13.1 100A PUMP LOOPS

13.1.1 Loop Engineering: Corrosion Test Loop ES

The construction and testing of a third slurry corrosion test loop, designated ES (Figs. 13.1 and 13.2), were completed. The loop is fabricated entirely of type 347 stainless steel. However, the pump scroll, where excessive corrosion-erosion damage is sometimes observed, is lined with titanium, which can be removed and replaced with other materials for evaluation if desired. Pump impellers of type 347 stainless steel, titanium, and Zircaloy-2 are available.

Six standard 30-in.-long horizontal sample barrels identical to those used in the solution corrosion loops[1] are incorporated in the loop as shown in Fig. 13.2 to provide a wide range of flow conditions for corrosion testing. Capillary-tube letdown sample units,[2] a slurry addition device,[3] a condensate system[4] to supply pump-bearings purge, and venturi flowmeters are incorporated in the loop. These devices have all been used satisfactorily on slurry loops BS and CS, previously described.[5,6] The pump bearings and journal bushings are of pure sintered alumina;[7] these have been more satisfactory in the slurry loops than the Graphitar 14–Stellite 98M2 combination usually employed. Loop ES was designed for operation at pressures to 2000 psia and at temperatures from 130 to 325°C with steam pressurization or for isothermal operation with gas overpressure. Results of operating tests with water were satisfactory. One test run (Sec 13.1.5) with thorium oxide slurry at an average concentration of 1154 g of Th per kg of H_2O and at 280°C was completed satisfactorily.

13.1.2 Loop Engineering: Venturi Performance

As reported previously,[8] calibrated venturis were installed in the pump suction lines and pressurizer bypass lines of slurry loops BS and CS as an aid in monitoring changes in density and/or flow rates of the thorium oxide slurry. These are important variables in evaluating corrosion-erosion by thorium oxide slurries.

A correlation was made of the pressure-drop readings of these venturis with changes in the slurry flow rate (calculated from changes in the pump speed) and the density (concentration) of the slurry, as obtained from analyses of slurry samples removed from the loops. Figures 13.3 and 13.4, respectively, are plots of the data obtained during runs BS-22 and CS-46D.

For run BS-22 (Sec 13.1.8), operation was at a temperature of 280°C in both loop and pressurizer with oxygen overpressure. The average concentration of the circulating slurry was 1010 g of Th per kg of H_2O. There were no operational difficulties with either one of the two venturi flowmeters: one in the 1½-in. sched-80 pump suction line, which indicated total loop flow, and one in the ½-in. sched-80 pressurizer mixing line to meter the flow bypassed through the top of the pressurizer (~15% of the total flow).

The circulating slurry density based on the sampled concentration at loop operating temperature, along with the actual pressure-drop measurements of the two venturis in run BS-22, is shown in Fig. 13.3. The calculated pressure drops, based on the slurry density and flow rates, are also

[1] H. C. Savage *et al.*, *HRP Quar. Prog. Rep. March 15, 1952*, ORNL-1280, p 46, Fig. 16.

[2] E. L. Compere *et al.*, *HRP Quar. Prog. Rep. April 30, 1957*, ORNL-2331, p 96.

[3] E. L. Compere *et al.*, *HRP Quar. Prog. Rep. April 30, 1956*, ORNL-2096, p 87.

[4] *Ibid.*

[5] E. L. Compere *et al.*, *HRP Quar. Prog. Rep. April 30, 1957*, ORNL-2331, p 96 and Fig. 12.1 and 12.2.

[6] E. L. Compere *et al.*, *HRP Dynamic Slurry Corrosion Studies: Quarter Ending April 30, 1956*, ORNL CF-56-4-139.

[7] J. C. Griess *et al.*, *HRP Quar. Prog. Rep. July 31, 1956*, ORNL-2148, p 73, Fig. 11.3

[8] E. L. Compere *et al.*, *HRP Quar. Prog. Rep. July 31, 1957*, ORNL-2379, p 84.

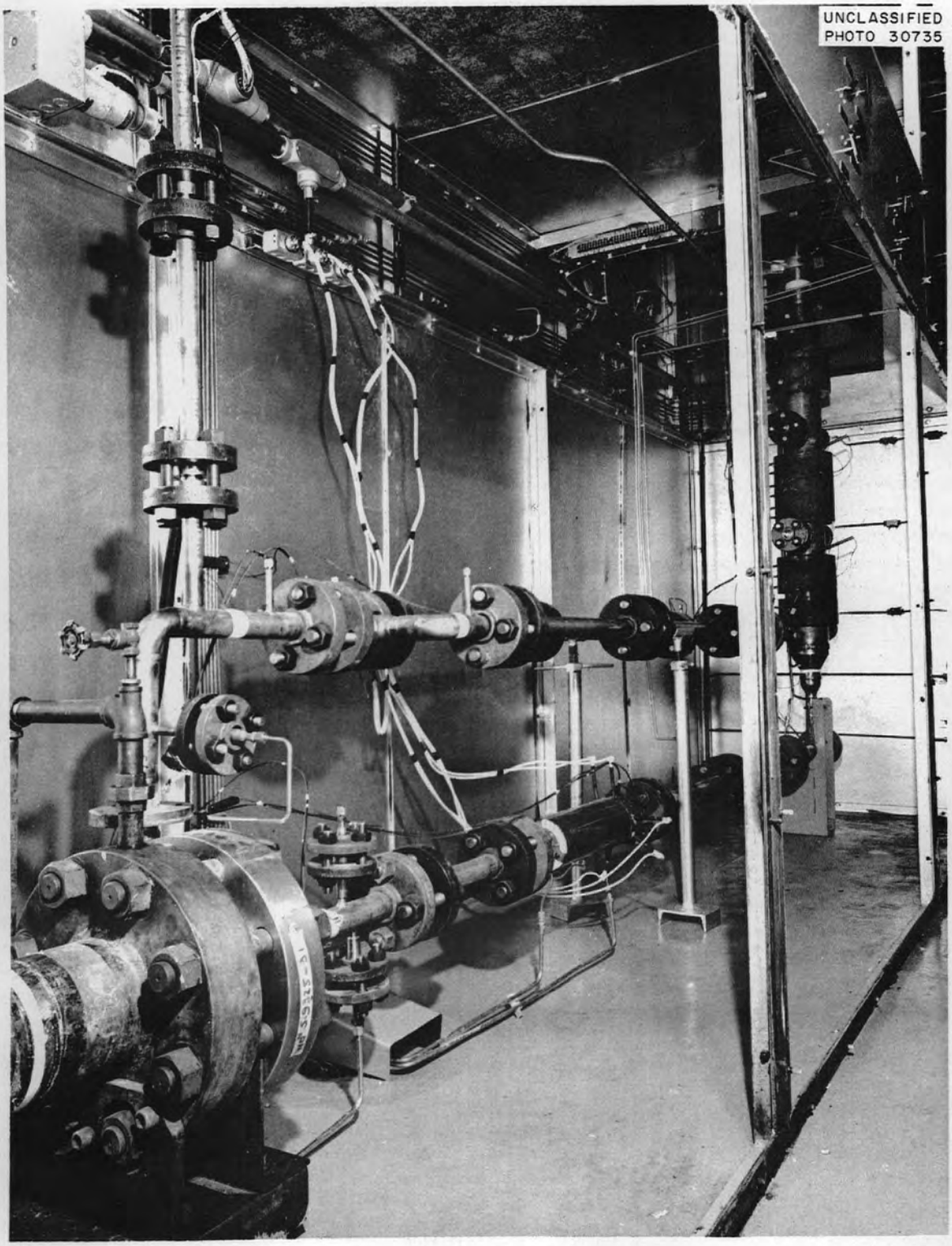

Fig. 13.1. Photograph of Slurry Loop ES.

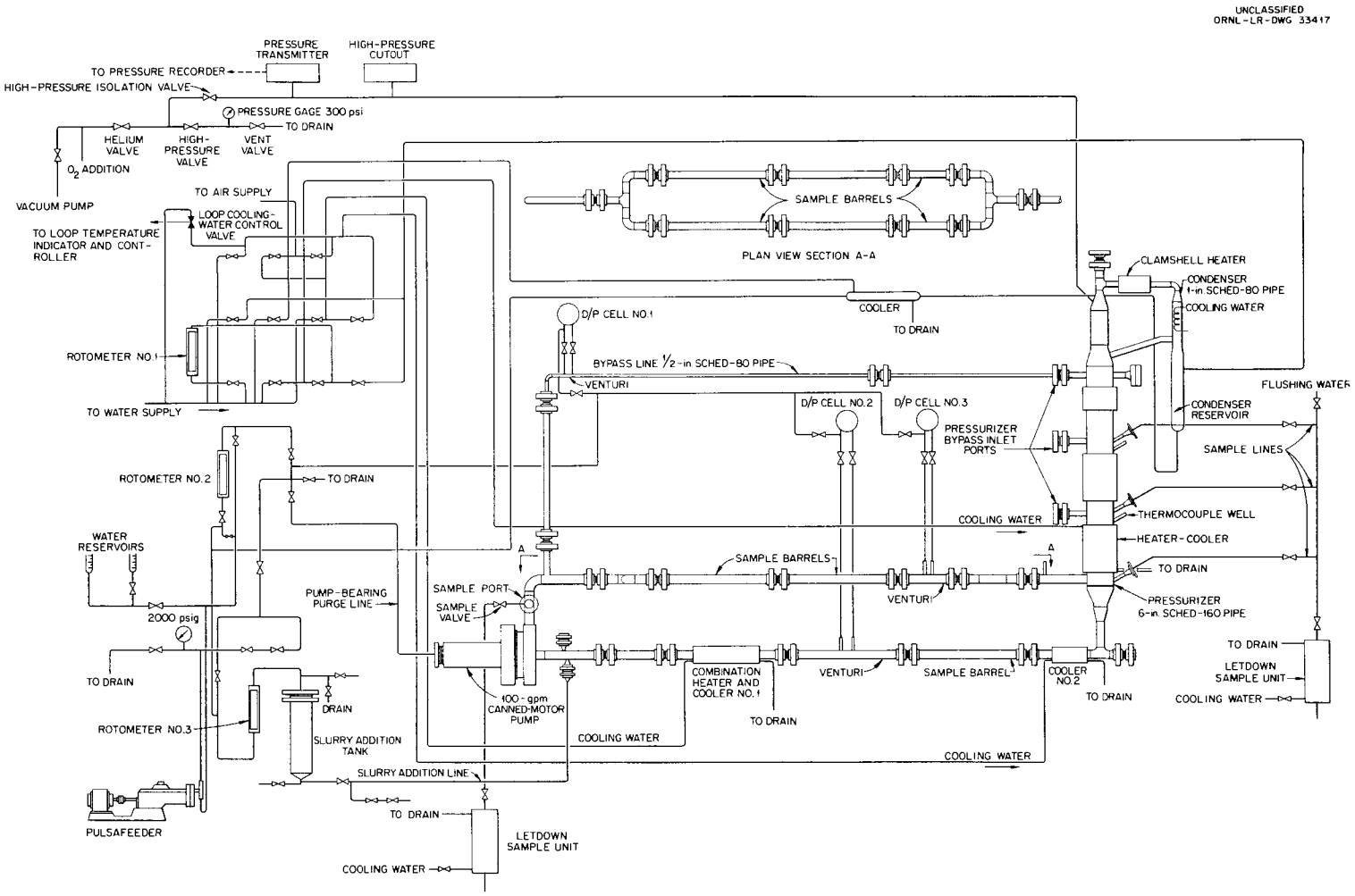

Fig. 13.2. Schematic Diagram of Loop ES.

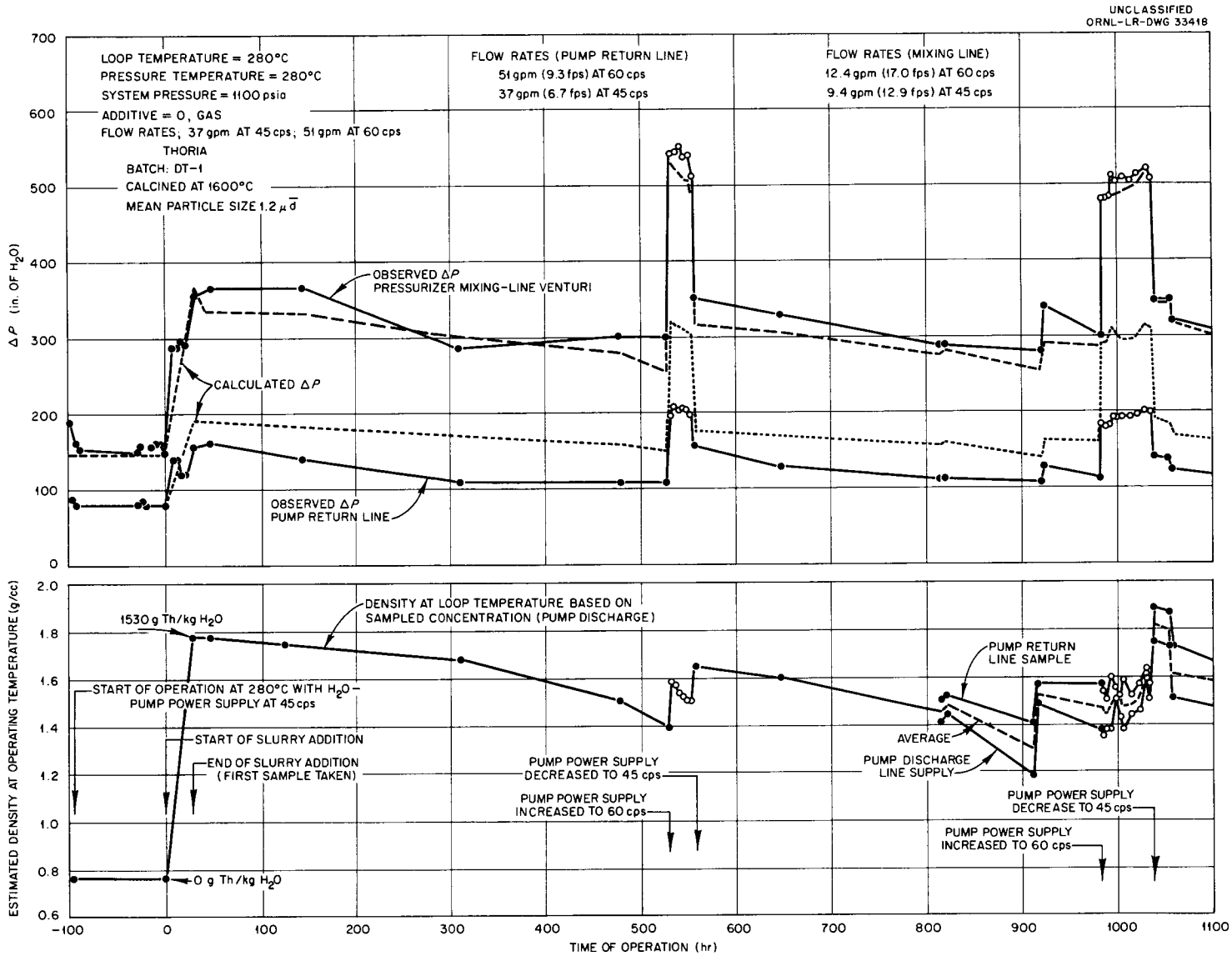

Fig. 13.3. Comparison of Observed Venturi ΔP Readings with Values Calculated from Slurry Sample Densities and Estimated Flow Rates, Run BS-22.

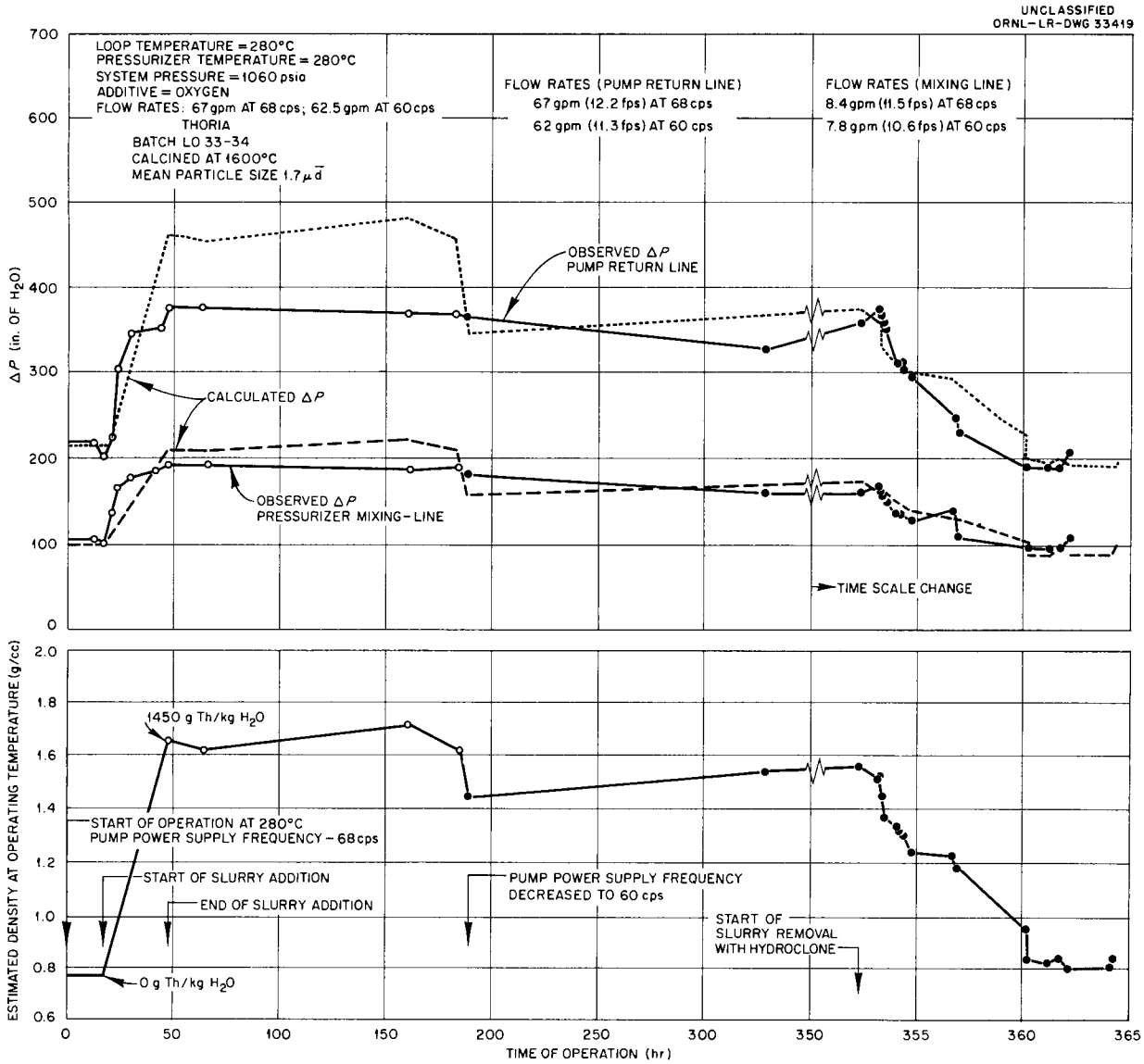

Fig. 13.4. Comparison of Observed Venturi ΔP Readings with Values Calculated from Slurry Sample Densities and Estimated Flow Rates, Run CS-46D.

shown. Since water was circulated in the loop at temperature and pressure for 100 hr prior to the addition of thorium oxide slurry, the venturi flow measurements during this period are also shown. There is good agreement between the actual and calculated values during the operating period with water.

In general, the pressurizer-mixing-line venturi measurements are in good agreement with the theoretical values after the addition of thorium oxide, including the brief periods when flow rates were increased by increasing the pump speed. However, the pressure-drop measurements obtained from the venturi in the pump return line were consistently below the calculated values. This can be seen particularly well during the periods when the pump speed was increased. The low pressure-drop readings observed on the venturi in the pump suction line may have resulted from a slurry concentration in the bottom of the line. The existence of a concentration gradient is supported by the fact that ~60% of the slurry

charged to the loop was left in this line after the slurry circulating in the loop was removed by means of a hydroclone prior to shutdown.

Figure 13.4 is a plot of the venturi pressure-drop readings taken from loop CS during run CS-46D (Sec 13.1.6). As in loop BS, there were no operating difficulties with either one of the two venturi flowmeters.

There is again good agreement between the measured and calculated values during the initial operating period with water at 280°C. The major discrepancy is in the pump-return-line pressure-drop measurements (monitoring total loop flow) as compared with the calculated values immediately after thoria was added to the loop. The slurry concentration based on samples removed during this period was ~1350 g of Th per kg of H_2O.

When the loop flow rate was decreased, by decreasing the pump speed from 68-cps operation to 60-cps operation, some loss in thorium oxide concentration was noted (down to ~1150 g of Th per kg of H_2O). The calculated and actual venturi pressure drops are in good agreement from this point to the end of the run. It can be seen that the venturi pressure drops in both the pump suction line and the pressurizer mixing line decreased, as expected, when the slurry was removed from the loop by means of a hydroclone at the end of the run.

From Figs. 13.3 and 13.4 it is concluded that the venturi pressure-drop measurements reflect the changes in the concentration of slurry in the 100A slurry test loops and can be a valuable aid in this respect. In some cases the venturi readings did not respond as expected to the changes in slurry flow rate as calculated from changes in the pump speed. Whether this means that the actual slurry flow rate did not change as expected when the pump speed was changed is not known. Since all slurry flow rates in the loops are based on measurements made with water at room temperature, a change in the pump efficiency when circulating thorium oxide slurries at 250–280°C may result in a lower-than-predicted flow rate under these conditions.

13.1.3 Loop Engineering: Hydroclone for Slurry Removal

At the completion of slurry runs BS-22 (Sec 13.1.8), CS-46C, and CS-46D (Sec 13.1.6), a hydroclone[9] was connected to each of the loops by means of a bypass line so that a portion of the slurry flow could be continuously circulated through the hydroclone in an attempt to remove the slurry from the loop and to concentrate it in the hydroclone underflow pot. If successful, this procedure would eliminate the difficult and time-consuming operation of discharging the slurry by means of draining, followed by repeated washings. In addition, the hydroclone and underflow pot could be used to vary the slurry concentration in the loop as desired. The results of the hydroclone performance in removing the slurry from the loops after runs BS-22, CS-46C, and CS-46D are discussed below.

Run BS-22 had been in progress for 1500 hr at the time slurry flow was started through the hydroclone. Although run BS-22 was made at a temperature of 280°C, the loop temperature was reduced to 225°C to observe the effect on slurry flow behavior just prior to use of the hydroclone. The operating conditions are shown in Table 13.1.

A 0.4-in. titanium hydroclone (ORNL drawing D-26410) with a 6.5-liter underflow pot fabricated from 4-in. sched-80 pipe was used. The underflow

[9] P. A. Haas, *Hydraulic Cyclones for Application to Homogeneous Reactor Chemical Processing*, ORNL-2301 (Nov. 18, 1957).

Table 13.1. Operating Conditions During Slurry Removal with a Hydroclone, Run BS-22

Pressurizer temperature	225°C
Loop temperature	225°C
Loop pressure	550 psia
Additives	Oxygen
ThO_2 in loop	11.75 kg
Slurry volume in loop	17.5 liters (at 25°C)
Hydroclone feed rate	~0.5 gpm
Flow time through hydroclone	50 min
Slurry concentration	700 g of ThO_2 per kg of H_2O
Slurry concentration, sampled (initial)	365 g of ThO_2 per kg of H_2O (average)*
Slurry concentration, sampled (final)	11 g of ThO_2 per kg of H_2O*

*Sampled from pump discharge line at hydroclone feed line take-off point.

pot was the same tank used for slurry additions to the loop as previously described.[10]

When slurry flow was started through the hydroclone, the pump power demand started decreasing, indicating a reduction of thorium oxide concentration. After approximately 15 min of hydroclone operation, no further reduction in pump power was noted. Since it was not known whether the underflow pot would contain the entire loop inventory of thorium oxide (11.75 kg), the hydroclone feed was stopped after 98 min and the slurry was removed from the underflow pot. A total of 4.55 kg ThO_2 was removed from the 6.5-liter underflow pot. After refilling the underflow pot with water, feed to the hydroclone was restarted. Although only 4.55 kg of ThO_2 out of the total inventory of 11.75 kg of ThO_2 had been removed at this point, samples removed from the pump discharge and suction lines showed a very low thorium oxide concentration. A plot of the thorium oxide concentration based on samples removed from the pump discharge line (at the point of the hydroclone bypass take-off) against flow time through the hydroclone is shown in Fig. 13.5. Even though the slurry flow rate in the loop was increased by increasing the pump speed with a motor generator from 45-cps operation to 60-cps operation (9.3 fps in the 1½-in. sched-80 loop piping), no additional slurry was picked up by the circulating fluid.

When the loop was drained and opened, the remaining 7.2 kg of ThO_2 was found in the bottom, horizontal 1½-in. sched-80 pipe between the pressurizer and pump suction. It is concluded that the hydroclone had removed essentially all the slurry circulating in the loop and that the 7.2 kg was stagnant in the pump return line. The sampled concentration of the circulating slurry was reduced from 365 to <1 g of ThO_2 per kg of H_2O in ~50 min, as shown in Fig. 13.5.

For the removal of slurry from the loop at the termination of run CS-46C, the same hydroclone as in run BS-22, described above, was used. Table 13.2 lists the loop operating conditions during removal of the slurry.

As in run BS-22, the pump power demand started decreasing when feed was started through the hydroclone. After 35 min of operation the pump power demand leveled off, which was taken as an indication that the hydroclone underflow pot was full of slurry. The hydroclone feed was stopped and 11.05 kg of thorium oxide was removed from the 6.5-liter underflow pot. The underflow pot was then refilled with water and the feed restarted. After an additional 39 min the pump power demand again leveled off, and 12.05 kg of thorium oxide was removed from the underflow pot. The procedure was repeated for a third removal, and an additional 1.48 kg of ThO_2 was removed.

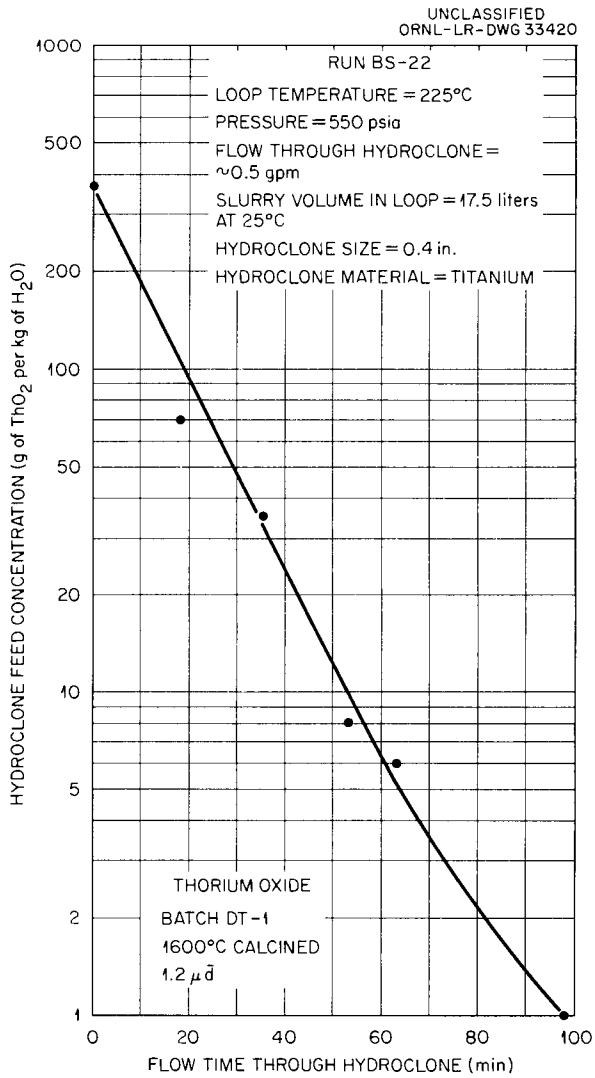

Fig. 13.5. Removal of ThO_2 with a Hydroclone, Run BS-22.

[10] E. L. Compere *et al.*, *HRP Dynamic Slurry Corrosion Studies: Quarter Ending April 30, 1956*, ORNL CF-56-4-139.

Table 13.2. Operating Conditions During Slurry Removal with a Hydroclone, Run CS-46C

Pressurizer temperature	280°C
Loop temperature	280°C
Loop pressure	1000 psia
Additives	Oxygen
ThO_2 in loop	25.1 kg
Slurry volume in loop	18.0 liters (at 25°C)
Hydroclone feed rate	~0.7 gpm
Flow time through hydroclone	151 min
Slurry concentration, load	1580 g of ThO_2 per kg of H_2O
Slurry concentration, sampled (initial)	1680 g of ThO_2 per kg of H_2O*
Slurry concentration, sampled (final)	7 g of ThO_2 per kg of H_2O*

*Sampled from pump discharge line at hydroclone feed line take-off point.

The total time of flow through the hydroclone was 125 min at a feed rate of ~0.7 gpm; 24.6 kg of ThO_2 was removed from the loop at the end of run CS-46C by means of the hydroclone. This represented 99% removal of the ThO_2 (24.8 kg) in the loop. The concentration of ThO_2 circulating in the loop was reduced from 1680 to 10 g per kg of H_2O, as shown in Fig. 13.6.

A third test of the removal of the ThO_2 from a dynamic test loop was made at the end of run CS-46D. Again the same hydroclone as in the two previous tests was used. Table 13.3 shows the loop conditions at the time feed to the hydroclone was begun and the initial and final concentration of ThO_2 in the loop.

After 25 min of operation, feed to the hydroclone was stopped and the slurry was removed from the underflow pot. When feed to the hydroclone was restarted, the pump power demand did not decrease as expected. From this and visual observation of samples removed from the loop during the next hour, it appeared that the hydroclone was not removing slurry from the loop, although all indications were that slurry was flowing through the bypass line to the hydroclone. The underflow pot was drained, and it contained a small amount of slurry.

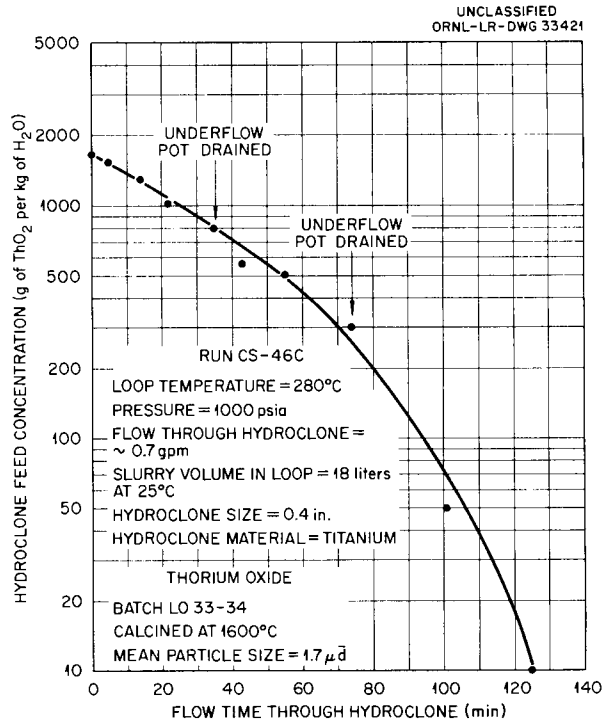

Fig. 13.6. Removal of ThO_2 with a Hydroclone, Run CS-46C.

Table 13.3. Operating Conditions During Slurry Removal with a Hydroclone, Run CS-46D

Pressurizer temperature	280°C
Loop temperature	280°C
Pressure	1050 psia
Additives	Oxygen
ThO_2 in loop	22.1 kg
Slurry volume in loop	17.5 liters (at 25°C)
Hydroclone feed rate	~0.7 gpm
Flow time through hydroclone	4 hr*
Slurry concentration, load	1400 g of ThO_2 per kg of H_2O
Slurry concentration, sampled (initial)	1330 g of ThO_2 per kg of H_2O**
Slurry concentration, sampled (final)	5 g of ThO_2 per kg of H_2O**

*For 1 hr of this time the hydroclone did not appear to function properly and was replaced with a new unit.

**Sampled from pump discharge line at hydroclone feed line take-off point.

The hydroclone was removed and replaced with a new hydroclone of identical design. The rapid removal of slurry from the loop with the new hydroclone is illustrated in Fig. 13.7. Approximately 4 hr were required to reduce the loop concentration from 1250 to 5 g of ThO_2 per kg of H_2O. Approximately 21.5 kg of thorium oxide of the original inventory of 22.1 kg was removed in this test.

The original hydroclone removed after 92 min of operation in run CS-46D did not appear to be excessively corroded and/or eroded. The inside diameter of the vortex finder was increased by 0.010 in. (0.100 in. to 0.110 in.), and the inside diameter of the underflow port was increased by 0.004 in. (0.100 in. to 0.104 in.). The hydroclone had accumulated 5.3 hr of operation with thorium oxide slurry during runs BS-22, CS-46C, and CS-46D with thorium oxide concentrations varying from 1600 to <5 g per kg of H_2O. Feed rates were from 0.5 to 0.7 gpm, with temperatures ranging between 220 and 280°C. The unit was returned to the Chemical Technology Division for a performance check, and tests indicated no loss of efficiency. Thus it would appear that the hydroclone became partially plugged during operation.

From the above tests the hydroclone appears to be effective in removing slurry from loops operating at temperatures to 280°C with slurry concentrations to 1600 g of ThO_2 per kg of H_2O. Based on the observed attack during the relatively short operating period of 5.3 hr, the life of titanium hydroclones may be short under these conditions and must be investigated further.

13.1.4 Pump Loop Tests: Introduction

Tests in the 100A loops continued to be concerned with the evaluation of new preparations of high-temperature-calcined thoria. An improvement in the erosion characteristics of thoria as a result of the removal of large particles by sedimentation classification, which was demonstrated during the previous quarter,[11] prompted additional tests with slurries of classified and sized thoria.

Runs were made with five new experimental lots or batches of thoria produced in the Chemical Technology Division. One of these lots was a composite of four batches. Seven of eight batches, each prepared from 10°C-precipitated thorium oxalate, had been calcined for 4 hr at 1600°C. An eighth preparation was calcined at 1400°C for 4 hr. The oxide had been subsequently classified by sedimentation to provide mean particle sizes of 1.7 to 0.9 μ. Conditions and results of the various runs are given in Table 13.4.

13.1.5 Circulation of Slurries of 0.9-μ, 1400–1600°C-Calcined Thoria

As part of the program to study the effect of particle size on the attack by thoria slurries and on their circulation properties, three loop tests were made with preparations of thoria which had mean particle sizes of 0.9 μ. One preparation, batch LO-37, which was used in run CS-45, was calcined at 1400°C. The other two preparations, batches LO-38 and LO-39, each calcined at 1600°C, were circulated in runs BS-21 and ES-4, respectively. All runs were to be made at 280°C at a circulating concentration of ~1500 g of thorium per kilogram of water and with oxygen gas pressurization.

(a) 1600°C-Calcined Thoria, Runs BS-21 and ES-4. – For run BS-21 the loop was charged to a slurry concentration of 1475 g of thorium per kilogram of water. The performance of the system was satisfactory during the first 75 hr of slurry circulation. Thorium concentrations of samples withdrawn from the loop during that period were in excellent agreement with the calculated charge concentration. However, at slurry circulation hour 82, the operation of the system became generally unstable after a sharp decrease in system temperature. At that time G-M survey-meter scans of the vertical pressurizer indicated that a moderate deposit of thoria had accumulated on the pressurizer pipe walls. Over the following 12-hr period, the deposit became so heavy that it was impossible to keep the system temperature in control. Consequently, the test was terminated after 94 hr of operation at an average circulating concentration of 964 g of thoria per kilogram of water. Based on the thorium concentration of a sample taken just before shutdown and the charge inventory, 69% of the thoria in the loop had deposited in the pressurizer.

After the system had cooled to room temperature, 30% of the thoria charge was recovered by draining. The system was then rinsed by use of the circulating pump with the loop filled with water to the

[11] E. L. Compere *et al.*, *HRP Quar. Prog. Rep. Jan. 31, 1958*, ORNL-2493, p 99.

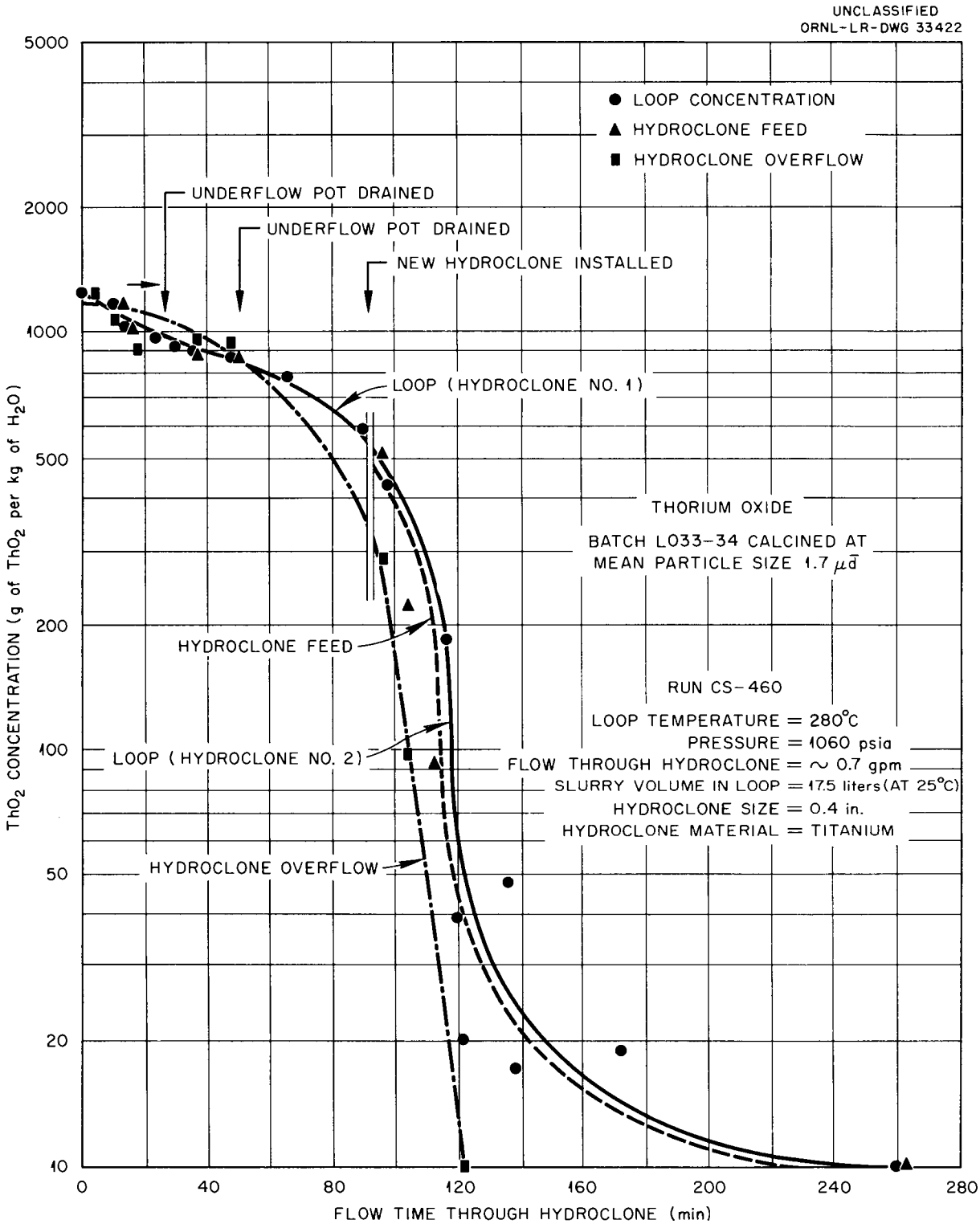

Fig. 13.7. Removal of ThO_2 with a Hydroclone, Run CS-46D.

Table 13.4. Corrosion by Circulating Thorium Oxide Slurries in Loop Tests

	Run Number						
	CS-45	BS-21	ES-4	BS-22	CS-46	BS-20	CS-44
Hours	78	94	719	1559	579	1003	421
Temperature, °C	280	280	280	280	280	280	200
Concentration, g Th/kg H_2O							
Load	1526	1475	1836	1393	1228	1514	1278
Average	848	964	1154	1010	1213	1454	1151
Calcination temperature, °C	1400	1600	1600	1600	1600	1600	1600
Thoria batch No.	LO-37	LO-38	LO-39	DT-1	LO-33-36[a]	LO-33-36	LO-33-36
pH of slurry	7.1	7.4	5.0	4.9	4.5	5.9	6.0
Oxygen, ppm	~600	200	1400	260	1200	850	1400
Average particle size, μ							
Prerun	0.9	0.9	0.9	1.2	1.4	1.7	1.7
Postrun	0.9	0.9	0.9	1.2	1.4	1.4	1.7
Impeller weight loss, g	4.5 (347 SS)	1 (347 SS)	5 (Zr-2)	18.5 (347 SS)	2.5 (Zr-2)	27 (347 SS)	1 (347 SS)
Loop corrosion rate (except impeller), mpy	3.2	2.7	1.0	1.1	3.3	0.9	0.7
Range of pin attack rates, mpy, at given flow velocity							
Velocity, fps							
Austenitic Stainless Steels							
9–10	1, 1[b]		0.6–1				<0.2[b]
19–21	0.3–1[b]	3–6	0.5–1, 0.1[b]	1–2	<0.2–0.3	1–2	0–0.7
25–29	1, 3–5[b]		1–5		0–0.5[b]		
38–45	3–6, 21–30[b]	13–22	3–7	16–27	1–5	19–28	0–0.2
63–73	49–55[b]				18–65		
Martensitic Stainless Steels							
9–10	1		<0.2				
19–21		4	1	1		2	0
25–29	1		4				
38–45	4	10	5	14		16	0
Titanium Alloys							
9–10	0.8		0				0–<0.2
19–21		4.2–6.5	0.8	0.4–0.9	0.3–0.6	1.5–2.1	0–2.6
25–29	3.2		0.6				
38–45	1.8	8.1–9.4	0.5	3–5	0.8, 0.2–0.5[b]	5.3–7.0	
63					5–6		
Zirconium Alloys							
9–10	<0.2		0				0
19–21	<0.2	0.5–1.1	0	<0.2	WG[c]	0.1–1.4	0–<0.2
25–29	<0.2		0				
38–45	0.2	0–3.7	0.5	0.4–1	0	0.8–1.4	0.7
63–73			3		2		0.9[b]
Noble Metals							
9–10	Nb, WG[c]		Pt-Ir,[d] <0.2; Au, WG				
19–21		Au, 0.5; Pt, 2.7	Pt-Ir,[d] 1.0; Au, 0.8	Au, WG; Pt, 0	Au, 0; Pt, <0.2	Au, 0.3; Pt, 1.3	Au, 0.7; Pt, 0.7
25–29	Nb, 4.6		Pt-Ir,[d] 1.6; Au, 1.6				
38–45	Nb, 16.3	Au, 7; Pt, 10	Pt-Ir,[d] 2.1; Au, 4.3	Au, 3; Pt, 15	Au, 0.4; Pt, 1.5	Au, 4.0; Pt, 12	Au, 9.4; Pt, 5.0
63					Au, 10; Pt, 25		

[a]Thoria was pumped in a previous loop run.
[b]Coupon specimens.
[c]WG = weight gain shown by defilmed specimens.
[d]Pt–5% Ir alloy.

normal operating level. After ten consecutive rinses using a total of 60 gal of water, an additional 52% of the thoria was recovered. Two additional rinses were required to recover the residual thoria. When the system was disassembled, no deposits were found in the loop piping, pressurizer, or pump.

The second loop test, run ES-4, which employed 0.9-μ thoria, batch LO-39 (1600°C-calcined), was the first slurry run made in the new 100A pump loop ES. The system was initially charged to a concentration of 1333 g of thorium per kilogram of water by making five injections of thoria slurry to the loop over a period of 48 hr. A sample withdrawn from the loop immediately after the fifth slurry addition contained 1192 g of thorium per kilogram of water, which indicated that about 10% of the thoria charged to the system was not circulating. At that time loop instruments, including a G-M meter survey, showed no evidence of localized deposits in the system. Consequently a sixth addition of slurry was made, which increased the charge concentration to 1488 g of thorium per kilogram of water. The average concentration of three samples taken during the following 94-hr period was 1091 g of thorium per kilogram of water.

In an attempt to reach a circulating concentration of ~1500 g of thoria per kilogram of water, another charge of slurry was made to the system, which raised the inventory concentration of the loop to 1836 g of thorium per kilogram of water. The average concentration of samples taken during the following 475-hr period of circulation was 1197 g of thoria per kilogram of water.

The test was terminated after a total of 719 hr of operation at an average concentration of 1154 g of thorium per kilogram of water.

Because of pump trouble (a cracked Al_2O_3 journal, causing a change in balance), the normal draining and rinsing sequence could not be followed, and an accurate material balance for the loop was not obtained. However, when the system was disassembled after flushing with water, no deposits of thoria were found.

(*b*) 1400°C-Calcined Thoria, Run CS-45. – The 1400°C-calcined thoria, batch LO-37, was to be circulated in run CS-45 at conditions comparable to run BS-21; that is, the test loop was to be operated with gas pressurization and was to be loaded by five incremental charges of thoria. During the injection of the third increment of thoria to the loop, the bypass mixing line became plugged with slurry, which necessitated stopping the test. The bypass line was blocked off and the run was continued by operating the system steam-pressurized. Loading to the target concentration, 1526 g of thorium per kilogram of water, was then accomplished without incident.

However, immediately after the injection of the final charge of slurry to the loop, operation became very erratic, as was experienced in run BS-21, owing to deposition of thoria in the pressurizer. Consequently it was necessary to terminate the run after 78 hr of operation at an average circulating concentration of 848 g of thorium per kilogram of water.

The loop was drained and rinsed in the same manner as described for run BS-21. Fifty-one per cent of the thoria in the system was removed by draining. The loop was then rinsed 21 times by use of the pump and a total of 65 gal of water. After the last rinse 98% of the thoria had been recovered. That remaining in the system was found as a thin, pasty deposit in the header to the low-flow (~6-fps) sample barrel and as a loosely adherent sludge in the lower section of the pressurizer.

Sedimentation-particle-size data and chemical analyses of slurry samples withdrawn from the test loops during runs BS-21, CS-45, and ES-4 and of the slurries drained and rinsed from the systems afforded no explanation for the cause of the thoria deposits in runs BS-21 and CS-45 or for the apparent dropout of slurry during run ES-4. At room temperature all postrun slurries of the three 0.9-μ thoria batches were highly flocculated and free flowing. No degradation was noted in any of the runs.

The poor circulation properties of batches LO-37, -38, and -39 appeared to be a general characteristic of the small particle size or of the particle-size distributions of these preparations rather than of the presence of impurities or changes in slurry properties as a result of circulation.

(c) Corrosion-Erosion Results. – Attack rates of corrosion specimens and of loop piping and impeller weight-loss data for the runs are presented in Table 13.4. In all the tests some abrasive attack was noted on the upstream sides of pin specimens exposed at velocities of 20 fps and above.

It should be noted that the higher attack rates computed for runs CS-45 and BS-21 reflect the shorter circulation periods. However, the weight loss of the type 347 stainless steel impeller used in run CS-45 was significantly higher than the weight loss of the one used in run BS-21. Attack on both impellers was uniform.

In run ES-4 the circulating pump was fitted with a cast Zircaloy-2 impeller and a titanium 75A scroll liner. Thus, by analyzing for zirconium and titanium ions in slurry samples withdrawn from the loop, it was possible to estimate attack rates for these components and to separate them from the generalized attack rate of the type 347 stainless steel loop piping. Attack on the Zircaloy-2 impeller was uniform and the computed attack rate, using the 5-g weight loss, was 4.0 mpy. No titanium was found in the slurry. The rate for the loop piping, calculated from total iron, chromium, and nickel ions in the slurry samples, was 1 mpy.

No unusual attack was noted on any of the steel and titanium specimens exposed in the three runs. Pins of platinum and gold exposed at 40 fps in run BS-21 displayed higher-than-normal weight losses as a result of localized upstream abrasion. Zircaloy-2 specimens displayed normal low rates at all velocities, with a maximum of 3 mpy at 73 fps in run ES-4.

Attack rates of a number of miscellaneous materials tested in connection with the component development program are reported in Table 13.5 and are discussed in Sec 13.1.7.

13.1.6 Circulation of 1.7-μ High-Calcined Thoria at 200 and 280°C

Three loop runs employed slurries prepared from a composite of four 1600°C-calcined thoria preparations, batches LO-33 to -36, whose mean particle size was 1.7 μ. These preparations were circulated as oxygenated aqueous slurries in run CS-44 at 200°C and in runs CS-46 and BS-20 at 280°C.

For run CS-44 the loop was operated at 200°C with steam pressurization and with the addition of gaseous oxygen which provided an average concentration of 1000 ppm of oxygen. The 421-hr test was made at an average circulating concentration of 1151 g of thorium per kilogram of water.

Run BS-20, a 1003-hr test, was made at 280°C at an average circulating concentration of 1454 g of thorium per kilogram of water. The test loop was operated isothermally with the addition of oxygen gas which provided a concentration of 650 ppm of oxygen.

Run CS-46 was charged with slurry which had been circulated in run BS-20. The 579-hr test was made at an average circulating concentration of 1213 g of thorium per kilogram of water. The loop was operated isothermally with oxygen addition. Average oxygen concentration during the run was 1200 ppm. Because of mechanical difficulties, adequate pump balance was not achieved for some time, and it was necessary to unload and reload the loop several times, the same slurry being used. This is not believed to have affected corrosion results or slurry properties.

The corrosion-erosion attack data for the three runs are presented in Table 13.4.

The effect of operating temperature on attack by slurry is exemplified by comparing the data shown in Table 13.4 for runs BS-20 and CS-44. Both tests utilized the same thoria preparation at comparable conditions of pH and of slurry and oxygen concentrations. At similar flow velocities, attack rates of specimens of the austenitic stainless steels and zirconium alloys were significantly lower in run CS-44 at 200°C than in run BS-20 at 280°C. A direct comparison of titanium alloys is not possible because duplicate specimens of the same alloys were not exposed in both tests.

The similar attack of platinum and gold specimens, which essentially measure the erosiveness of the thoria, was to be expected since the attack is not chemical in nature. It should be noted that in the higher velocity range relative attack levels of the noble metals were reversed in the two runs.

In run CS-44 a lower attack on the type 347 stainless steel piping was also seen. The generalized system attack rate, calculated from corrosion ions detected in slurry samples withdrawn from the loops, for run BS-20 was 0.9 mpy, while for run CS-44 it was 0.7 mpy even though the run was shorter. Over half the total corrosion products (Fe, Cr, Ni) detected in the slurry in run BS-20 were contributed by the impeller.

Attack on the type 347 stainless steel impellers used in the circulating pumps was markedly different. The impeller used in run CS-44 lost only 1 g; the one used in run BS-20 lost 27 g and was heavily abraded. Pits resulting from apparent eddy attack on the shroud edge of the latter impeller

Table 13.5. Attack of Miscellaneous Materials by Aqueous Oxygenated Thoria Slurries at 280°C in Pump Loop Tests

	Specimen Attack Rates (mpy) at Given Flow Velocity				
	9–10 fps	19–21 fps	25–30 fps	38–41 fps	63–73 fps
Austenitic stainless steels	1,[a] 0.6–1[b]	0.5–1,[b] 0–0.7	1,[c] 1–5[d]	3–6,[c] 3–7,[d] 1–5,[a] 0–0.2[b]	18–65[a]
Zircaloy-2	0	0	0,[d] 0,[a] 0–0.3[b]	0.5–0.8,[d] 0,[a] 0.7[b]	2–3,[d] 2[a]
Sintered Al_2O_3	340,[c] 31[d]	35,[d] 93[a]	700,[c] 57[d]	1100,[c] 56,[d] 120[a]	
CD4MCu cast stainless steel	1[c]		2[c]	6[c]	
Elgiloy		5[a]		6–8[a]	170–180[a]
Hastelloys (B, C, L)		10–23[b]	13–45[b]		
Incoloy	0.7[c]		1[c]	6[c]	
Kennametal K-501 (WC in Pt matrix)	>1200[c]		>1200[c]		
Norbide (boron carbide)		>1500[a]		>1500[a]	>1500[a]
Rexalloy A-33	140,[c] 5[d]	180,[d] 125[a]	190,[c] 200[d]	270,[c] 190,[d] 180[a]	250[a]
Stellite (1, 3, 12, Star J)	9–90,[c] 1–6[d]	10–170[d]	12–140,[c] 55–210[d]	24–260,[c] 72–210[d]	
Flame-sprayed tungsten carbide on 347 SS	33[d]	39[d]	40[d]	43[d]	

[a]Run CS-46.
[b]Run CS-44.
[c]Run CS-45.
[d]Run ES-4.

were more than 100 mils deep. The eddy attack, characterized by deep gouged pits undercut in the direction of the flow, was localized along about a ¼-in. area of the peripheral edge of the shroud. (The velocity in that region was approximately 70 fps.) A photograph of the impeller used in run BS-20 is shown in Fig. 13.8. An enlarged photograph of the eroded area is presented in Fig. 13.9. The greater attack during run BS-20 may be associated both with increased temperature-velocity effects, as noted on pin specimens, and also with the operational history of the runs.

It is possible that the aggravated localized attack on the impeller used in run BS-20 was caused in part by cavitation during the test. In common, both tests were interrupted twice by power outages, which were of sufficient duration to reduce the system temperature and pressure to borderline operational limits. Venturi flowmeters in the systems and samples taken from the loops after restarting the circulating pumps indicated that complete resuspension of the solids occurred within 5 min after circulation was resumed. For each run the pump became gas bound during the startup operations. However, additional periods of unstable operation occurred during run BS-20 owing to leakage of water from the loop, and it is possible that gas became entrained because of

UNCLASSIFIED
PHOTO 30889

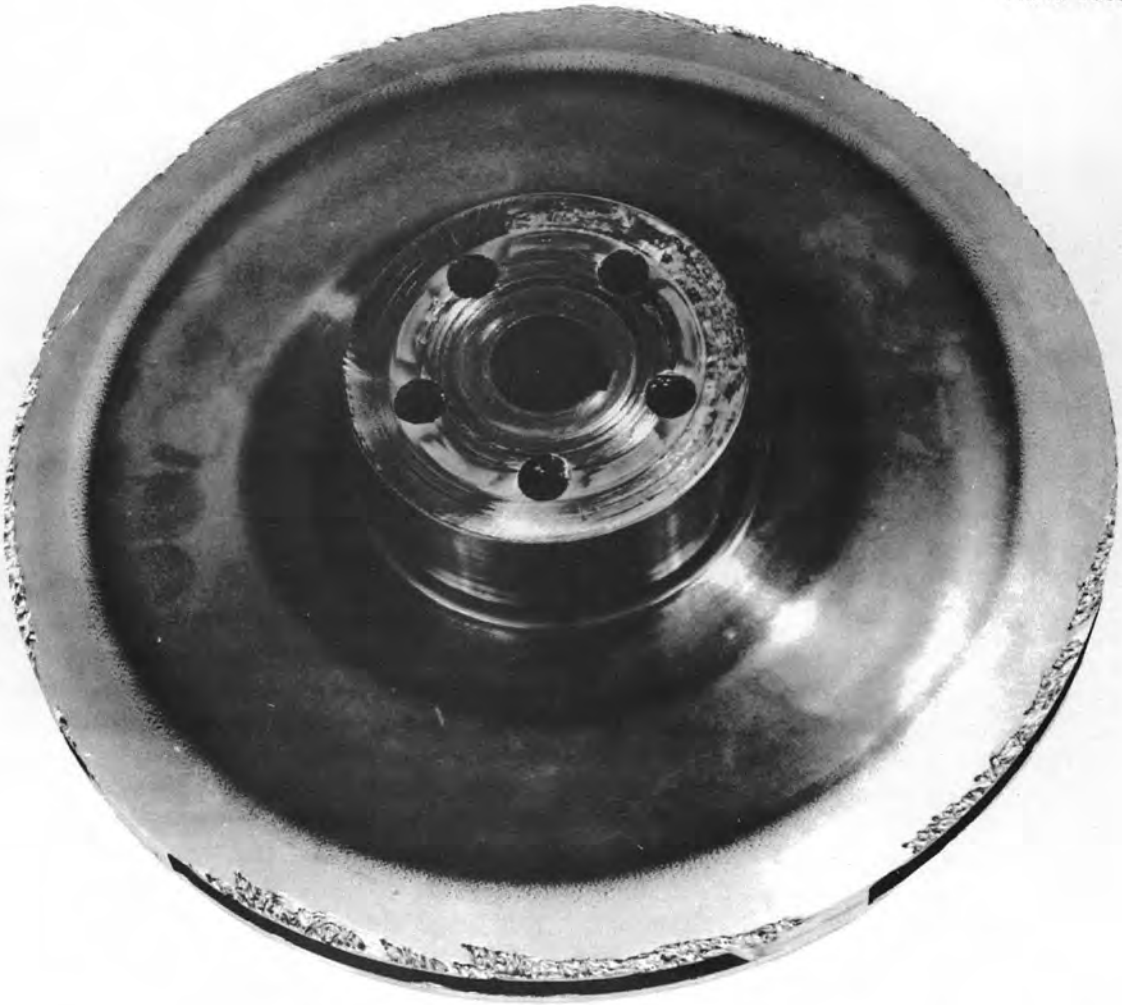

Fig. 13.8. Erosion of Type 347 Stainless Steel Pump Impeller Used in Slurry Run BS-20.

Fig. 13.9. Detail of Eroded Surface (9.5X) of Type 347 Stainless Steel Pump Impeller; Slurry Run BS-20.

lowered pressurizer levels, leading to cavitation and possible increased attack on the pump impeller and on pin specimens at the higher velocities.

In general, the handling properties of the slurries in both tests were satisfactory. No deposits or films of thoria were found after the loops were drained and rinsed in the usual manner.

It was indicated by sedimentation particle-size distribution analyses that the extended circulation of the slurry in run BS-20 effectively degraded the 3 wt % of thoria particles >3 μ to particles 1 μ or less in size. Major degradation took place during the first 100 hr of circulation. When the slurry was recirculated in run CS-46, no additional degradation was detected.

A comparison of the attack data shown in Table 13.4 for runs BS-20 and CS-46 is of particular interest. When the slurry which was moderately degraded in run BS-20 was subsequently recirculated in run CS-46 at essentially the same conditions of temperature and slurry concentration, markedly lower attack rates were observed on all specimens.

Similar reductions in attack rates have been observed previously when degradation has occurred as a result of circulation. It is indicated that the relatively low weight fraction of particles >3 μ increased the attack rates about tenfold.

The cast Zircaloy-2 impeller used in run CS-46 was attacked uniformly and lost 2.5 g during the 279-hr circulation period. Based on that weight loss, the attack rate was 4.3 mpy.

13.1.7 Corrosion-Erosion Resistance of Miscellaneous Materials

A number of miscellaneous materials, of interest for possible use in slurry feed pumps and valves and other special components, were exposed in runs CS-45 and ES-4 and in runs CS-44 and CS-46, which utilized slurries of other thoria preparations of larger mean particle size. Data for these materials are presented in Table 13.5. For comparison, data for austenitic stainless steels and Zircaloy-2 are also included.

Sintered Al_2O_3, the Hastelloys, and Elgiloy showed a normal dependence on flow velocity.

Kennametal K-501, Norbide, Rexalloys, and tungsten carbide were mainly chemically attacked and showed little or no velocity dependence. Attack of Stellites varied with composition and velocity. Also, it is known that attack of these alloys is dependent upon temperature and atmosphere. At the test conditions, Stellite Nos. 1 and 12 showed greatest resistance to attack; Stellite Nos. 3 and Star J were an order of magnitude poorer. A limited number of CD4MCu experimental alloy pins used in the tests displayed rates comparable to those of the austenitic stainless steels. Rates of pin specimens of Incoloy exposed in one test compared favorably with those of the austenitic stainless steels.

It may be noted in Table 13.5 that the corrosion of Zircaloy-2 was substantially less than that of any of the other materials cited; Zircaloy-2 frequently showed no attack, the maximum being 2–3 mpy at 63–73 fps.

13.1.8 Circulation of 1.2-μ Thoria Slurry; Observation of Sludge Dropout

(a) Run BS-22. – One other thoria preparation, batch DT-1, a 1600°C-calcined oxide classified to a mean particle size of 1.2 μ, was circulated in run BS-22 for a period of 1559 hr at an average circulating concentration of 1010 g of thorium per kilogram of water. The system was operated isothermally at 280°C with oxygen gas injection which provided an average concentration of 260 ppm dissolved oxygen.

The purpose of the test was twofold. Principally it was of interest to observe the attack rates of various materials during an extended period of exposure to such a circulating slurry. Second, the test was designed to observe the variations in slurry concentration at different locations in the loop to provide a better understanding of the circulation characteristics of high-concentration slurries of 1600°C-calcined thoria. For this purpose the system included two venturi flowmeters, one placed in the bypass mixing line which was connected between the pump-discharge line and the system pressurizer, and a second placed in the return line of the loop which was connected to the suction of the pump.

The circulating pump was operated from a motor-generator set so that bulk flow velocities could be changed during the test. A hydroclone was affixed to the slurry addition system in such a manner that the hydroclone underflow could be accumulated in the slurry addition tank. By this means the thoria inventory in the system could be adjusted while the loop was at operating temperature and pressure.

During operation, samples were withdrawn from the pump discharge line through a valve affixed to the side of the loop piping and from the pump suction line through a valve connected to the bottom of the pipe.

The target concentration for the test was 1500 g of thorium per kilogram of water. Slurry was charged in the usual manner by making incremental injections of thoria by means of the addition system while the loop was operated at 280°C and 1400 psi pressure. A normal charging schedule was followed to attain the desired circulating concentration. Five injections of slurry, made over a period of 26 hr, brought the system to an inventory concentration of 1486 g of thorium per kilogram of water.

The response of the venturi meters with varying flow conditions and slurry concentrations and the operations involving the use of the hydroclone are discussed in more detail in Secs 13.1.2 and 13.1.3.

The circulating concentration, indicated by samples withdrawn from the loop and by venturi flowmeter readings, varied less than 0.2% for the initial 238 hr of circulation. Over the following 64-hr period a sharp decrease in concentration to 1135 g of thorium per kilogram occurred, after which time the concentration, indicated by samples from the pump-discharge sample port, became constant.

During the remainder of the test, bulk flow rates in the loop were varied from 25 to 60 gpm, with corresponding pipeline velocities of 6 to 13 fps, by using the motor-generator set. No significant variations in circulating concentration were effected by these changes. As the flow rates were varied, samples withdrawn from the valve on the bottom of the pump suction line were consistently higher by 30 to 35% in thorium concentration than samples removed from the pump discharge line. It was concluded that during this period the noncirculating thoria remained as a sludge in the lower section of the loop.

Charging additional thoria to the system did not significantly change the circulating concentration or the proportionate difference in concentrations of samples removed from the two sampling positions.

Withdrawal of slurry from the loop lowered the concentrations of samples removed from both valves, but the proportionate difference between the two positions was little changed.

Late in the run, after the circulating concentration had been lowered to ~500 g of thorium per kilogram of water, the temperature of the loop was lowered to 225°C to observe the effect on flow behavior. Concentrations were unchanged.

The test was concluded by removing the circulating thoria with the hydroclone (see Sec 13.1.3). Forty per cent of the charge inventory in the system was removed in this manner. After shutdown, an additional 20% of the charge was drained from the lower sample valve. When the loop was disassembled, the remainder of the thoria was found as a free-flowing sludge in the pump suction line.

Because chemical and physical property measurements of the various slurry samples from the test are not complete, the cause of the dropout of thoria has not yet been ascertained.

Particle-size distribution data for most of the samples taken during the test indicate that no particle degradation took place as a result of circulation. High-temperature sedimentation data for several of the slurry samples taken during the tests are presented in Sec 19.7.

(*b*) **Corrosion-Erosion.** – Attack data for run BS-22 are shown in Table 13.4. Pin attack rates are in excellent agreement with those rates observed in run BS-20, which was made at similar conditions. Except for Zircaloy-2, localized upstream erosion was pronounced on pin specimens exposed at 40 fps.

The generalized attack rate for the type 347 stainless steel loop piping was 1.1 mpy.

Attack on the type 347 stainless steel impeller used in the pump was less severe than that which occurred on the impeller used in run BS-20. In general, attack was uniform except for minor localized areas around the welds which joined the shrouds to the vanes. A generalized attack rate for the impeller, computed from the 18.5-g weight loss, was 5.4 mpy.

13.1.9 Field Corrosion Tests

In cooperation with the Systems Development Section, two sets of corrosion specimens were exposed in run SM-4[12] of the slurry blanket mockup. One set of 16 in-line coupon-type corrosion specimens and a set of 8 stress specimens were exposed in the 2396-hr test.

The in-line specimens, which were exposed at a relative velocity estimated as approximately 20 fps, consisted of four coupons each of type 347 stainless steel, SA-212-B carbon steel, titanium RC-55, and Zircaloy-2. Each coupon was machined to the dimensions 2.35 × 1.00 × 0.20 in. from special ¼-in. plate from controlled-materials stock.[13] The coupons, contained in a type 347 stainless steel holder, were not insulated.

The stress specimens consisted of two samples each of type 347 stainless steel, type AM-350 stainless steel, Ti-6Al-4V alloy, and Zircaloy-2. One specimen of each of the materials was suspended in the vapor space of the vertical pressurizer, while the comparison specimen was placed on the lower section of the specimen holder, which was normally below the level of liquid in the pressurizer. Flow over these specimens was negligible. The stress specimens were mounted, uninsulated, on a type 347 stainless steel holder with type 347 stainless steel bolts.

The in-line assembly was inserted in a flanged section of 3-in. sched-40 pipe in the main loop of the mockup. The flow rate past the specimens was 360 gpm except for intermittent periods of operation when the circulating pump was operated at increased or reduced speeds by use of a motor-generator set.

The specimens were exposed for a period of 160 hr in water before slurry charging was begun. The total exposure in slurry was 2236 hr.

During slurry loading and circulation, loop temperatures varied from 150 to 200°C. The system was initially charged, at 170°C over a period of 240 hr, to 350 g of thoria per kilogram of water. After 600 hr of circulation at 200°C at that concentration, an additional loading, which took place over the next 220 hr, was made to increase the concentration to 595 g of thoria per kilogram of water. The mockup operated at the higher concentration for an additional 1176 hr in the temperature range 150 to 190°C.

The slurry charges to run SM-4 consisted of a composite of batches of LO-series 800°C-calcined thoria to which was added approximately 3500 ppm SO_4^{--}, based on thoria, as sulfuric acid. The

[12] R. B. Korsmeyer *et al.*, *HRP Quar. Prog. Rep. Jan. 31, 1958*, ORNL-2493, p 67.

[13] E. L. Compere *et al.*, *HRP Quar. Prog. Rep. Oct. 31, 1957*, ORNL-2432, p 95.

pH of the slurry ranged from 4.8 to 6.8 during the test. No oxygen was added to the mockup.

Corrosion rates, except for SA-212-B carbon steel, were low. Attack of type 347 stainless steel ranged from 0.5 to 0.9 mpy on three specimens; the fourth, the coupon at the entrance in the specimen array, showed 4.2 mpy. The higher attack on that coupon was attributed to entrance effects and increased impingement attack by the slurry particles. The pattern of attack may be seen in Fig. 13.10. Three of the four specimens of titanium RC-55 were not detectably attacked; the fourth showed a corrosion rate of <0.1 mpy. Attack of Zircaloy-2 ranged from 0.1 to 0.3 mpy.

All four of the coupons of SA-212-B carbon steel dissolved during the run, indicating a corrosion rate in excess of 350 mpy. It is probable that the addition of sulfuric acid to the slurry and the lack of oxygen in the system greatly enhanced the attack of these specimens.

No evidence of stress-corrosion cracking was observed with any of the stressed specimens, exposed in the pressurizer.

The attack rates of coupon specimens exposed in the main line of the loop appear to be in good agreement with the general attack observed in the blanket mockup system. Based on corrosion products present in the slurry from the blanket mockup, a generalized stainless steel attack rate of 0.6 mpy was estimated. However, much of the attack was localized in high-velocity regions of the system. Eroded areas up to $^{3}/_{16}$ in. deep were

UNCLASSIFIED
PHOTO 30562

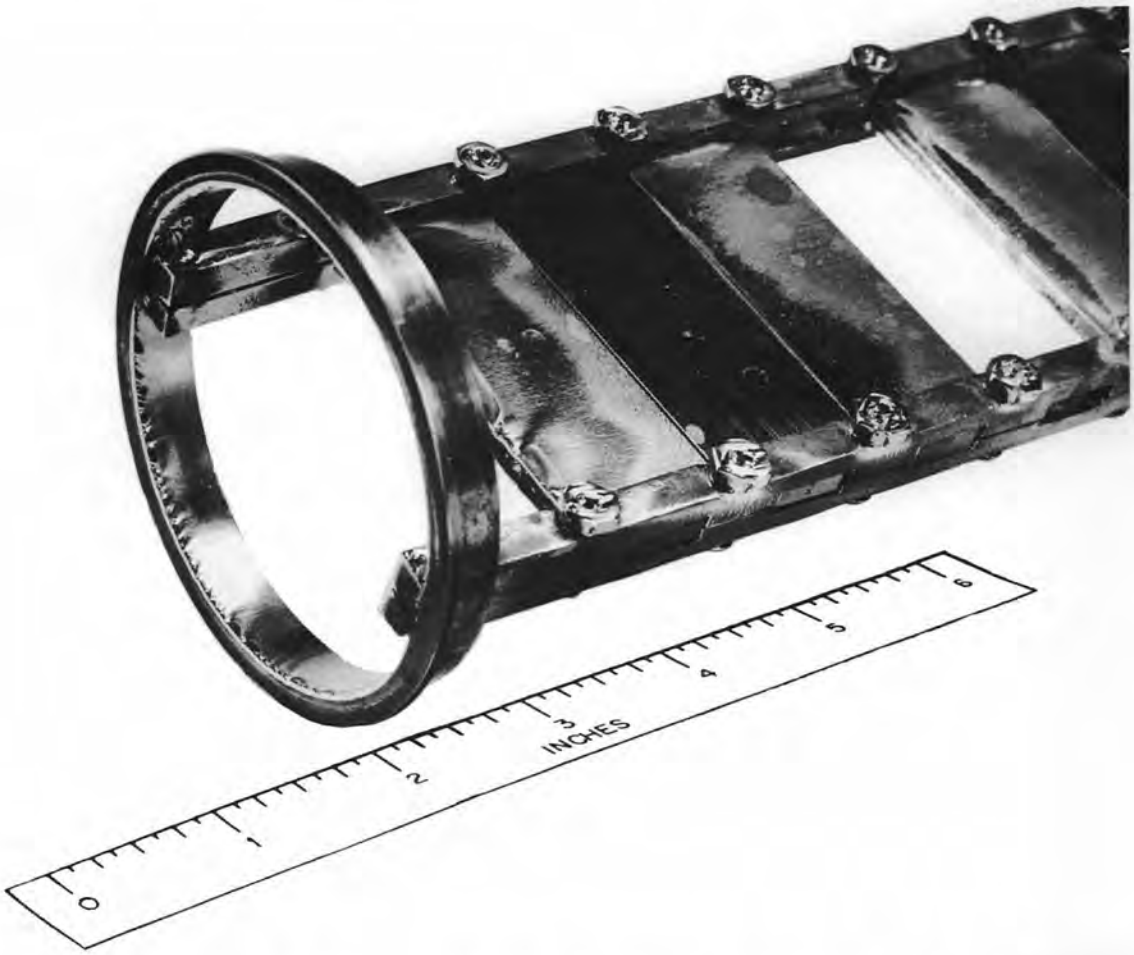

Fig. 13.10. In-Line Corrosion Specimens After Exposure in Slurry Blanket Mockup Run SM-4. Flow left to right.

observed in the carbon-steel sphere in localized areas opposite the slurry inlet jets where the metallized stainless steel coat was penetrated.

13.2 TOROIDS

13.2.1 Introduction

During this report period, a series of toroid tests was completed in which basic slurry corrosion variables were studied. Other tests were concerned with the degradation of 1600°C-calcined thoria, with the effect of additions of sodium aluminate to slurries, with the effect of additions of molybdenum trioxide to slurries, with the corrosion-erosion characteristics of thoria spheres, and with a large number of special and unusual thoria preparations.

13.2.2 Effect of Atmosphere, Circulation Temperature, and ThO_2 Properties on Attack by Aqueous Slurries

A series of tests was initiated during the previous quarter[14] to study the effect of operating temperature, ThO_2 properties, and gaseous atmosphere on the corrosion-erosion attack of selected alloys by circulating aqueous slurries in toroids. Slurries at concentrations of 1000 g of thorium per kilogram of water of 550, 650, 800, and 1600°C-calcined thoria were circulated for 300 hr at 26 fps with hydrogen and oxygen atmospheres at circulation temperatures of 100, 150, 200, 250, and 280°C. Pin specimens of type 347 stainless steel, titanium-75A, Zircaloy-3A, and SA-212-B mild steel were exposed in each test. Oxygen overpressure was obtained from the thermal decomposition of an appropriate amount of hydrogen peroxide. In the hydrogen series, the toroids were purged with hydrogen for 15 min and then sealed. Tests made at 100, 150, and 200°C were reported last quarter.

Additional tests were made during this report period at 250 and 280°C. Attack data for all tests are shown in Table 13.6. The attack rates are corrected for slug flow based on 45% liquid volume fill at temperature.

[14] E. L. Compere *et al.*, *HRP Quar. Prog. Rep. Jan. 31, 1958*, ORNL-2493, p 103.

The corrosion data of Table 13.6 were examined by use of a factor analysis method, which permitted the separation of the effect of different variables as multiplicative factors. This treatment is regarded as a suitable pattern for the interpretation of many kinds of corrosion data. Because of the balanced experimental pattern, over-all effects of variables were obtained by comparing suitable averages. More detailed comparisons taking into account interdependence of effects between particular conditions or materials are not shown. Results of this examination are shown in Table 13.7.

Substantial generalized effects of the various variables may be noted. A great difference in response of the different metals was exhibited. Atmosphere exerted a significant effect: hydrogen rather than oxygen atmosphere generally increased corrosion by a factor of 4 in these neutral slurries, the effect ranging from a factor of 2 for Ti-75A to a factor of 9 for carbon steel. Corrosion rate generally increased with circulation temperature, an over-all doubling being noted for each 35°C increase in temperature. An apparent reversal of 150 and 200°C factors was observed and is to be investigated further.

A difference between batches of thoria may be noted, with batch LO-2A showing the most aggressive behavior. This may be due to halide (5 ppm) and phosphate (15 ppm) contamination present in this preparation. The 10°C-precipitated 1600°C-calcined thoria, which was a bench-scale preparation with low original particle size, gave the lowest attack rates.

If it is assumed that the aggressive behavior of batch LO-2A was due to the impurities noted above, then for the remaining batches aggressiveness may be correlated with original particle size for the 300-hr runs. However, because the particles degrade at different rates and degraded particles in many cases are less aggressive, these results should not be generalized.

The apparent growth of particles in the hydrogenated tests which circulated slurries of 800 and 1600°C thoria was believed to be caused by the interference of corrosion products, especially iron, in the sedimentation-particle-size analyses.

Table 13.6. Toroid Experiments Studying the Effect of Hydrogen and Oxygen Atmospheres in Relation to Calcination Temperature and Operating Temperature

Time: 300 hr
Velocity: 26 fps
Concentration: 1000 g of Th per kg of H_2O

Thoria	Temperature (°C)	Attack Rate (mpy)*								pH Postrun		Average Particle Size (μ)			
		347 SS		Ti-75A		SA-212-B		Zircaloy-3A				Prerun		Postrun	
		O_2	H_2	O_2	H_2	O_2	H_2	O_2	H_2	O_2	H_2	O_2	H_2	O_2	H_2
LO-17R	100	1.3	2.0	WG**	0.2	15.8	103.0	1.8	1.0	7.7	9.0	2.3	2.3	0.7	0.6
550°C-	150	1.8	10.7	1.8	2.9	13.3	244.2	1.8	4.0	8.2	8.3	2.3	2.3	0.7	
calcined	200	WG	2.2	WG	0.7	WG	267.0	WG	1.6	7.4	8.9	2.3	2.3	0.8	0.6
	250	2.4	21.7	2.0	3.3	7.1	233.0	0.7	4.2	6.0	6.8	2.3	2.3	0.6	0.6
	280	3.4	31.1	11.1	4.2	17.3	91.1	4.2	2.0	5.4	6.0	2.3	2.3	0.7	0.7
LO-18	100	0.7	1.8	0.4	1.1	24.4	180.0	0.9	1.3	7.6	8.6	3.3	3.3	0.7	0.5
650°C-	150	3.8	9.8	<0.1	1.3	20.7	378.0	1.3	6.9	7.4	7.9	3.3	3.3	0.6	
calcined	200	1.3	12.9	1.3	5.6	2.7	289.0	0.2	3.3	7.1	7.9	3.3	3.3	0.4	0.9
	250	3.3	44.4	4.2	10.4	10.9	133.2	2.2	3.1	5.6	6.4	3.3	3.3	0.6	0.5
	280	4.0	14.5	14.2	7.8	27.5	53.3	5.3	1.3	5.2	6.3	3.3	3.3	0.6	0.8
LO-2A	100	0.2	WG	0.2	WG	24.4	357.0	0.2	0.9	7.7	7.6	1.4	1.4	0.7	0.8
800°C-	150	1.6	3.8	5.1	9.8	8.5	266.5	0.4	7.3	7.3	7.3	1.4	1.4	0.8	0.8
calcined	200	7.6	12.7	10.7	2.9	13.1	155.5	4.2	2.2	6.1	7.3	1.4	1.4	0.8	0.9
	250	8.4	53.3	5.3	11.8	13.8	37.8	1.6	1.8	6.3	7.5	1.4	1.4	0.7	2.2
	280	5.1	71.2	13.5	19.3	14.8	46.7	3.8	4.2	5.7	6.5	1.4	1.4	0.8	3.3
TO-10-1000	100	WG	1.1	WG	WG	4.0	8.5	0.2	1.3	7.4	8.4	1.2	1.2	1.2	1.8
1600°C-	150	0.4	1.8	0.7	18.7	6.0	8.7	0.9	3.8	7.0	8.1	1.2	1.2	2.0	1.6
calcined	200	0.9	4.7	0.9	1.1	1.1	6.0	4.2	1.3	6.2	8.8	1.2	1.2	0.8	3.2
	250	1.8	21.1	0.7	3.6	17.1	8.4	WG	3.1	5.6	9.7	1.2	1.2	1.2	2.6
	280	7.1	33.3	3.6	4.0	17.1	26.7	WG	9.3	4.6	9.9	1.2	1.2	1.2	5.3

*Corrected for slug flow.
**WG = weight gain.

Table 13.7. General Effects of Atmosphere, Circulation Temperature, and Thoria Properties on Attack of Various Metals

Data from Table 13.6; results expressed as multiplicative factors relative to normalized attack rate of type 347 stainless steel at 280°C with O_2 atmosphere = 4 mpy (26 fps)

Variable	Relative Factor	Variable	Relative Factor
Metal		Atmosphere	
Zircaloy-3A	0.43	O_2	1.0
Ti-75A	0.52	H_2	4.0
347 SS	1.00		
SA-212-B	7.7		
Thoria batch		Circulation temperature, °C	
LO-17R (550°C)	0.88	100	0.14
LO-18 (650°C)	1.4	150	0.51
LO-2A (800°C)	1.5	200	0.30
TO-10-1000 (1600°C)	0.56	250	0.67
		280	1.00

13.2.3 Degradation of 1600°C-Calcined ThO_2 Prepared by Jet Precipitation

It has been generally observed in previous toroid and pump loop circulation tests that thoria calcined at 1600°C does not degrade.[15,16] Moderate particle degradation was noted, however, in several toroid runs made during the previous quarter with slurries of 1600°C-calcined ThO_2 prepared from jet-precipitated thorium oxalate.

An inspection of the particle-size-distribution curves of the slurries used in those tests indicated that only a small weight fraction of particles >3 μ had degraded and that the particles resulting from the degradation were generally less than ~0.5 μ.

A series of tests was completed during the present report period to investigate this phenomenon further. The fraction of large-particle ThO_2 contained in batch JP-1 was used in the tests. A sized fraction of particles was separated from the batch by sedimentation classification.[17] The material obtained by the classification ranged in size from 40 to 120 μ. Its apparent mean Stokes diameter was 60 μ. A photograph of the thoria is shown in Fig. 13.11.

By microscopic examination the particles appeared to be composed primarily of coarse sintered aggregates. The crystallite size of the material, measured by x-ray line broadening, was >2500 Å.

Aqueous oxygenated slurries of the sized oxide were circulated at concentrations of 50 to 1000 g of thorium per kilogram of water at 250°C. Tests at each slurry concentration were made at circulation velocities of 10 and 26 fps. The results of the runs are shown in Table 13.8.

Without exception, the large particles were degraded during circulation to a mean size of 0.5 to 0.7 μ. Also there was a pronounced decrease in crystallite size.

Attack rates of all corrosion specimens exposed in the tests were high. A pronounced dependence of attack rate on concentration was manifested.

These tests demonstrated the unique degradation properties of 1600°C-calcined ThO_2 prepared from thorium oxalate produced by the jet-precipitation technique. It appears that the large particles present in this batch were essentially aggregates which resulted from sintering during the calcination of $Th(C_2O_4)_2$. Although the aggregates were broken down rather readily during circulation,

[15] E. L. Compere *et al.*, *HRP Quar. Prog. Rep. July 31, 1957*, ORNL-2379, p 92.

[16] E. L. Compere *et al.*, *HRP Quar. Prog. Rep. Oct. 31, 1957*, ORNL-2432, p 87.

[17] E. L. Compere *et al.*, *HRP Quar. Prog. Rep. Jan. 31, 1958*, ORNL-2493, p 99.

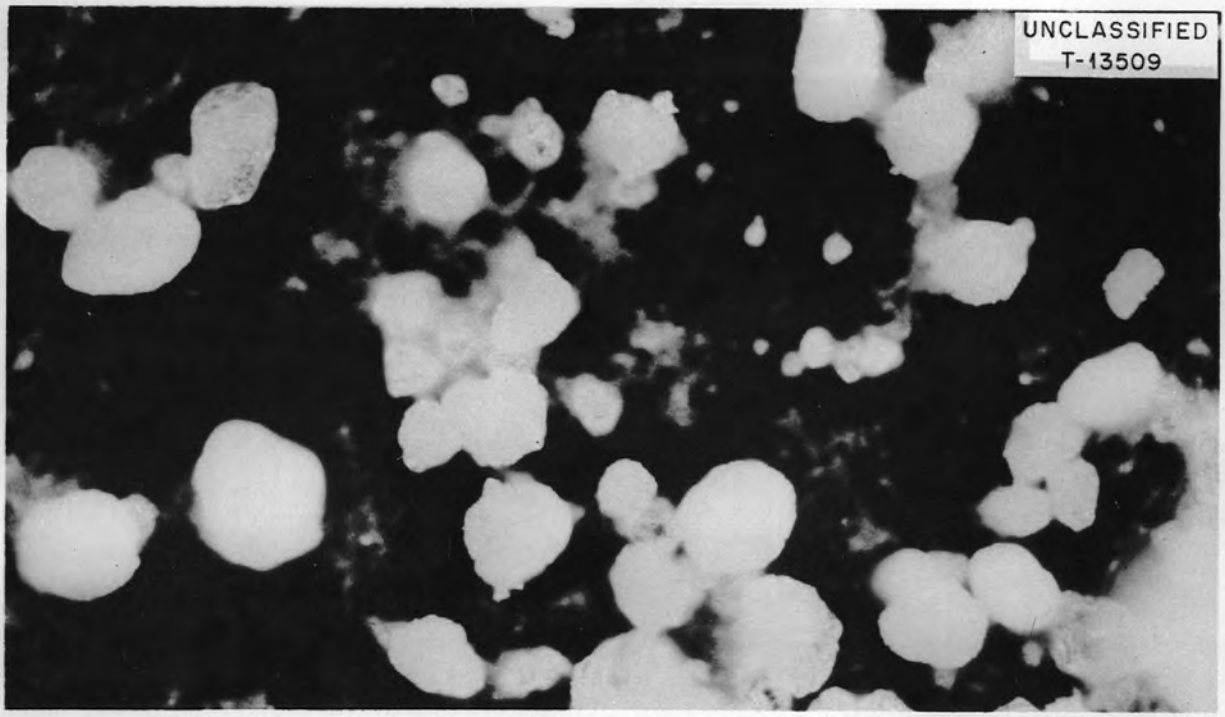

Fig. 13.11. Large-Particle Fraction of Batch JP-1 ThO_2 Used in Toroid Degradation Tests. 400X.

Table 13.8. Results of Toroid Tests with Slurries of Thoria Prepared from 1600°C-Calcined Jet-Precipitated Thorium Oxalate

Time: 300 hr
Thoria: Batch JP-1, 1600°C-calcined
Mean particle size: 60 μ
Crystallite size: >2500 Å
Atmosphere: Oxygen
Temperature: 250°C

Concentration (g of Th per kg of H_2O)	Postrun Crystallite Size[a] (Å)	Postrun Particle Size[b] (μ)	Pin Attack Rates[c] (mpy)				
			347 SS	Ti-75A	Zircaloy-3A	SA-212-B	Armco Iron
10-fps Circulation Velocity							
50	195	0.5	1	1	1	5	
250	140	0.5	6	2	4	8	
500	590	0.6	3	2	6	23	
1000	140	0.5	9	9	10	8	
26-fps Circulation Velocity							
50	150	0.7	5	5	4		15
250	180	0.5	3	0.5	9		11
500	105	0.5	11	9	15		14
1000	120	0.5	9	16	24		13

[a]Measured by x-ray line broadening.
[b]Measured by gravitational sedimentation.
[c]Corrected for slug flow.

they produced undesirably high abrasive attack during degradation.

13.2.4 Circulation of Slurries Containing Sodium Aluminate

In conjunction with laboratory studies being performed in the Research and Analysis Section, eight toroid tests were completed during the quarter to determine the circulation behavior and corrosion-erosion attack of thoria slurries containing additions of $NaAlO_2$. Two thoria preparations were submitted for toroid circulation tests. Both batches, LO-7 and LO-12, were 800°C-calcined oxides prepared from 70°C-precipitated thorium oxalate in the Chemical Technology Division pilot plant.

In previous loop tests conducted by the Systems Development Section, batch LO-12 formed spheroids and deposits in the test loop; batch LO-7 circulated satisfactorily. Addition of approximately 0.5 wt % $NaAlO_2$ to the LO-12 thoria slurry had significantly lowered its yield stress and had minimized the tendency toward deposition and spheroid formation. Further, it was reported that additions of $NaAlO_2$ dispersed flocculated thoria slurries and that the dispersing effect was retained after autoclaving at 250°C for several days.[18]

Each batch was circulated in toroid tests at a concentration of 500 g of thorium per kilogram of water with and without the addition of $NaAlO_2$. Similar tests at a concentration of 1000 g of thorium per kilogram of water were made with batch LO-12. One test circulated a slurry from which the sodium ion had been essentially removed by dialysis. Test variables and the results of the runs are shown in Table 13.9. The attack data were examined by use of the factor analysis method which permitted the separation of the effect of variables as multiplicative factors. Results of this examination are also presented in Table 13.9.

The corrosion rates of type 347 stainless steel and titanium-75A were markedly increased in all tests employing slurries containing $NaAlO_2$. Severe attack of titanium-75A at the highest concentration of sodium aluminate was noted and was presumably associated with the alkalinity of the slurry. Steel, SA-212-B, specimens displayed slightly higher rates when aluminate was present. The attack of Zircaloy-3A was little affected by the addition of sodium aluminate to slurries at a concentration of 500 g of thoria per kilogram of water. However, a proportionally higher attack occurred with Zircaloy-3A pins exposed in slurries containing 1000 g of thoria per kilogram of water with $NaAlO_2$ added.

In a single test which circulated the dialyzed slurry, type 347 stainless steel, Zircaloy-3A, and titanium-75A displayed low rates; the attack of carbon steel increased slightly.

Thoria was deposited on stainless steel and titanium pins in tests with LO-12 ThO_2, regardless of the presence or absence of $NaAlO_2$ or the slurry concentration. Film formation was not noted with batch LO-7 slurries, but they were somewhat more abrasive.

All postrun slurries containing aluminate additions were agglomerated, and, as noted in Table 13.9, spheroids were present in slurries from several of the tests. No correlation of spheroid formation with any test variable was evident.

13.2.5 Circulation of Slurries Containing Molybdenum Trioxide

One of the proposed recombination catalysts, molybdenum trioxide, was added to circulating aqueous slurries to determine its relative effect on corrosion-erosion in both hydrogen and oxygen atmospheres. The operating conditions and results of the tests are shown in Table 13.10.

The general effect of molybdenum trioxide addition was to increase the attack rate, and in general rates were also higher under hydrogen atmosphere.

The corrosion data presented in Table 13.10 were examined by use of the factor analysis procedure, and results of this examination also appear in the table. Based on this analysis it appears that the addition of molybdenum trioxide substantially increased the attack of SA-212-B mild steel and Zircaloy-3A. Hydrogen atmosphere, compared with oxygen atmosphere, caused substantial increases in the attack of type 347 stainless steel and titanium-75A and reduced the attack of SA-212-B mild steel.

13.2.6 Circulation of Thoria Spheres

In cooperation with the Chemical Technology Division, a series of toroid tests was undertaken

[18] P. R. Kasten *et al.*, *HRP Quar. Prog. Rep. Jan. 31, 1958*, ORNL-2493, p 43.

Table 13.9. Toroid Tests with ThO_2 Slurries Containing Sodium Aluminate

Time: 300 hr — Temperature: 280°C
Velocity: 26 fps — Atmosphere: Oxygen

ThO_2 Preparation	Concentration of $NaAlO_2$ (m)	Slurry Concentration (g of Th per kg of H_2O)	pH of Slurry Postrun	Spheroid Formation	Metal Attack Rates[a] (mpy)			
					347 SS	Ti-75A	SA-212-B	Zircaloy-3A
LO-7	None	500	5.2	Yes	6	5	14	2
LO-7	0.033	500	6.4	No	13	8	17	0.4
LO-12	None	500	6.7	No	1	3	8	0.9
LO-12	0.033	500	7.3	No	17	2	12	0.6
LO-12	0.033[b]	500	5.9	Yes	1	WG	18	0.2
LO-12	None	1000	6.0	Yes	6	2	14	1
LO-12	0.064	1000	10.1	Yes	19	14	14	1
LO-12	0.135	1000	9.5	No	33	140	38	3

Statistical Analysis into Multiplicative Factors [Relative to Normalized Rate of Type 347 Stainless Steel at 1000 g of Th per kg of H_2O (Batch LO-12) $\cong$ 8 mpy]

Average Effect of Major Variables

Metal	Relative Factor	Concentration and Batch	Relative Factor
347 SS	1.0	1000 g of Th per kg of H_2O	1.0
Ti-75A	0.6	500 g of Th per kg of H_2O	0.6
SA-212-B	1.6	Batch LO-7	1.7
Zr-3A	0.1	Batch LO-12	1.0
Additive		Further Effect of Special Combinations	
No Additive	1.0	$NaAlO_2$ (dialyzed), SA-212-B	5
$NaAlO_2$ Addition[c]	2	$NaAlO_2$ (dialyzed), Ti-75A	0.1
$(NaAlO_2/Th) \times 2$	2	$(NaAlO_2/Th) \times 2$, Ti-75A	5
$NaAlO_2$ (dialyzed)	0.2		

[a] Corrected for slug flow.
[b] Sodium ion removed by dialysis.
[c] At lower $NaAlO_2/Th$ ratio.

Table 13.10. Toroid Tests with ThO_2 Slurries Containing Molybdenum Trioxide

Thoria preparation: LO-33 to 36 (1600°C-calcined, classified, 1.7 μ)
Concentration: 1500 g of Th per kg of H_2O
Temperature: 280°C
Time: 300 hr
Velocity: 26 fps

Concentration of MoO_3 (m)	Metal Attack Rates (mpy), Corrected for Slug Flow					pH of Slurry, Postrun	Average Particle Size (μ), Postrun
	Toroid	347 SS	Ti-75A	SA-212-B	Zircaloy-3A		
Oxygen							
None	1.3	10.0	5.3	12.6	0.7	4.7	1.4
0.03	2.0	6.5	1.1	125.0	2.0	7.8	1.2
Hydrogen							
None	2.0	78.0	8.2	7.8	1.6	7.7	2.1
0.03	3.6	40.0	15.5	14.5	4.9	8.4	1.7

Statistical Analysis into Multiplicative Factors
(Relative to Normalized Rate of Type 347 Stainless Steel in Oxygen Without Additive = 12 mpy)

Average Effect of Major Variables

I. Metal	Relative Factor
Toroid (347 SS)	0.1
347 SS	1.0
Ti-75A	0.3
SA-212-B	1.0
Zircaloy-3A	0.09
II. Atmosphere	
Oxygen	1.0
Hydrogen	2.0

III. Additive	Relative Factor
None	1.0
0.03 m MoO_3	1.5

IV. Alternate Statement of Factors (Instead of II, III)

Metal	Results in Hydrogen Relative to Oxygen: Factor	Results in 0.03 m MoO_3 Relative to Additive: Factor
Toroid	1.6*	1.6*
347 SS	7**	0.6*
Ti-75A	5**	0.6*
SA-212-B	0.3**	4**
Zircaloy-3A	2	3

*Trivial factors >0.7, <1.4 (50% CI).
**Definitely significant factors <0.3, >4 (95% CI).

to study the corrosion-erosion attack and behavior on circulation of aqueous slurries of thoria spheres. The 1000°C-calcined spheres, prepared by the Houdry Process Corporation, were of random shape and size, ranging from 3 to 150 μ (mean diameter 55 μ). Portions of the preparations were recalcined for 4 hr in the Chemical Technology Division laboratory at 1200, 1600, and 1700°C. Those calcined at 1700°C were too badly sintered to be included in the toroid tests. Tests were also made with the same preparation after it had been sized[19] by sedimentation into fractions <3, 3–10, 10–25, and >25 μ. Portions of each fraction were recalcined at 1200, 1400, and 1600°C. No effort was made to classify any of the preparations as to shape (see Fig. 13.12). A small quantity of <3-μ spheres available from another preparation was also tested.

Oxygenated aqueous slurries of the original and recalcined unsized spheres and of each size

[19] J. P. McBride *et al.*, *HRP Quar. Prog. Rep. Jan. 31, 1958*, ORNL-2493, p 167.

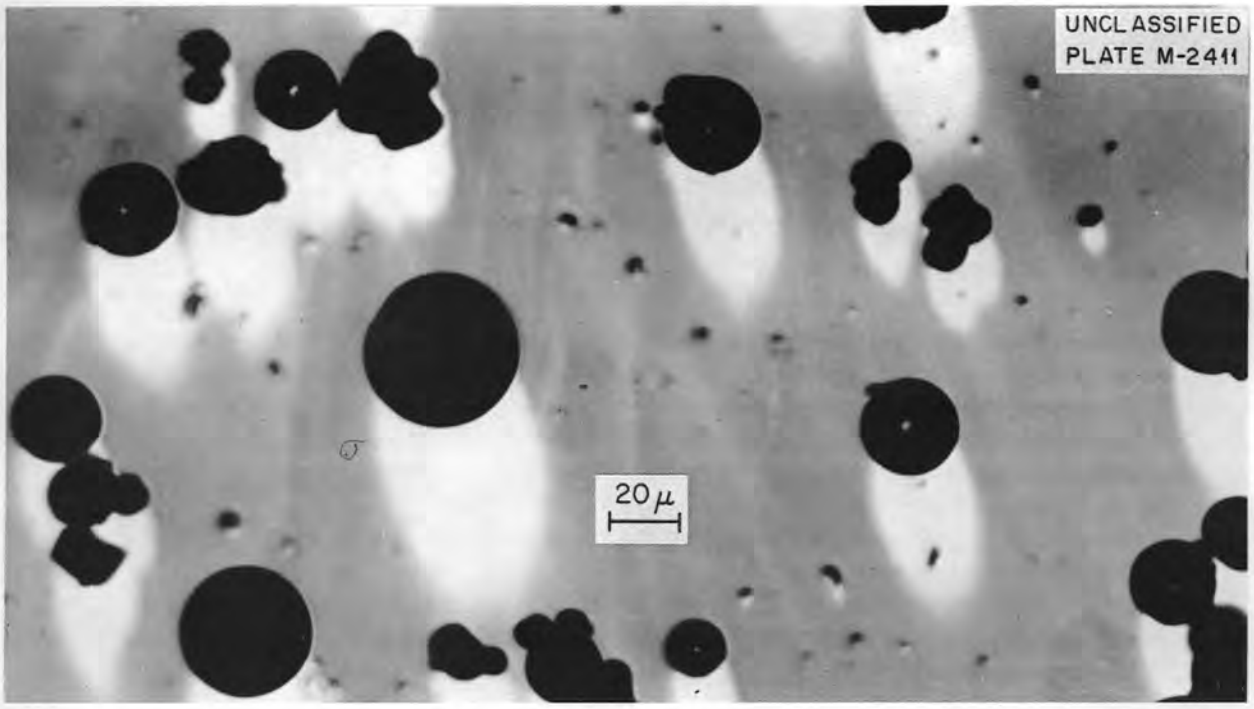

Fig. 13.12. Thoria Spheres Calcined at 1000°C and Sized by Sedimentation To Be > 25 μ in Diameter. 500X.

fraction of the original and recalcined sized spheres were circulated at 280°C at a concentration of 1500 g of Th per kg of H_2O at velocities of 10 and 26 fps. The duration of each run was approximately 300 hr. The results of the tests are presented in Table 13.11.

In those cases where excessive attack rates were observed, both a high pressure and a strong odor of ammonia were observed when the toroids were opened at the termination of the run. Chemical analyses revealed nitrogen-containing impurities present in the spheres. Organic amines and nitrates were used in the manufacture of the thoria spheres and were most probably the source of the impurities.

Slurries that had been circulated at 26 fps poured readily from the toroids after the tests. Those that had been circulated at 10 fps were recovered with difficulty. Thin, tightly adherent thoria films formed on most of the pin specimens during circulation of the unsized spheres.

Examination of the data indicated that those experiments showing the highest pH's (above 10) generally exhibited severe corrosion, and those showing postrun pH values below 9.5 had much less corrosion. For purposes of discussion the data are separated in this way.

In the lower pH group, the following conclusions were drawn: the general level of corrosion appeared to be comparatively low – possibly lower than for nonspherical material. There appeared to be general effects of velocity and calcination temperature, with corrosion becoming more severe as these increased in value. These factors exerted relatively less effect as the particle size became larger. There was no other strong effect observed for particle size. In general, the levels of attack were about the same for all size ranges. Under all conditions the carbon steel exhibited the same range of corrosion susceptibility, and this could well have been largely a water-corrosion phenomenon. The more spherical <3-μ fraction, also tested, showed results slightly higher than other comparable material. The unsized 3–150-μ original thoria gave results comparable with the >25-μ sized fraction.

In the higher pH group, the evidence indicated that the systems became oxygen deficient and that there was production of ammonia which in some manner had been retained by or generated

Table 13.11. Effect of Size Range, Velocity, and Calcination Temperature on Corrosion-Erosion by Thoria Spheres

Time: 300 hr
Concentration: 1500 g of Th per kg of H_2O
Atmosphere: oxygen
Temperature: 280°C

Size Range (μ)	Velocity (fps)	Calcination Temperature (°C)	pH After Run	Attack Rate[a] (mpy)					Average Particle Size (μ)	
				Toroid	347 SS	Ti-75A	SA-212-B	Zircaloy-3A	Prerun	Postrun
				Postrun pH <9.5						
<3	10	1000	6.0	0.4	2	0.7	7	WG[b]	2.1	2.2
	10	1200 (4 hr)	6.1	0.2	1.5	0.2	11	0.2	c	1.6
	10	1400 (2 hr)	5.8	1.1	2.2	2	10	4	c	1.0
	10	1600 (2 hr)	5.5	3	13	13	13	19	c	0.7
	26	1200 (4 hr)	6.2	4.0	10	8	7	8	c	2.1
<3-SPH[d]	26	1000	6.9	5	24	10	34	4	2.2	2.5
3–10	10	1000	5.6	1.1	3	2	10	WG	7	7
	10	1200 (4 hr)	5.3	0	1.1	1.1	10	0	10	7
	10	1400 (2 hr)	5.9	0.2	1.3	2	8	0.2	11	8
	10	1600 (2 hr)	5.5	0.7	5	3	6	0.7	12	8
	26	1000	6.8	2	15	5	9	20	7	6
10–25	10	1000	5.9	0.2	1	WG	11	WG	14	>10
	10	1200 (4 hr)	6.8	0.2	13	WG	17	1.3	15	15
	10	1400 (2 hr)	5.5	3	2	3	7	2	18	28
	10	1600 (2 hr)	5.4	2	2	2.4	5	0.1	16	15
	26	1000	6.9	0.4	0.7	WG	3	WG	14	14
	26	1200 (4 hr)	7.9	0.6	3	WG	10	WG	15	13
	26	1400 (2 hr)	9.4	3	4	2	11	21	18	8
>25	10	1000	5.8	0	0.7	WG	5	WG	26	>25
	10	1200 (4 hr)	6.8	0	0.7	WG	10	WG	24	24
	10	1400 (2 hr)	5.9	0.2	0.7	0.2	6	0.9	36	e
	10	1600 (2 hr)	6.1	0.2	0.6	WG	5	0	>50	28
Unsized[f]	10	1000	6.5	0.2	WG	WG	13	WG	55	>50
	10	1200 (4 hr)	6.5	0	3	WG	10	WG	e	>50
	10	1600 (4 hr)	8.0	0.2	0	WG	6	WG	50	>50
>25	26	1000	7.1	0.4	0.4	WG	4	WG	26	24
	26	1200 (4 hr)	7.8	1	0.4	WG	5	0.1	24	30
	26	1400 (2 hr)	9.0	0.6	1.1	WG	16	WG	36	19
	26	1600 (2 hr)	7.5	1.8	1.2	0.8	6	3	>50	20
Unsized[f]	26	1000	7.5	0.2	WG	WG	11	0.5	55	>50
	26	1200 (4 hr)	8.1	2	0	WG	7	WG	e	>50
	26	1600 (4 hr)	8.8	0.9	8	2	10	3	50	13

Table 13.11 (continued)

Size Range (μ)	Velocity (fps)	Calcination Temperature (°C)	pH After Run	Attack Rate[a] (mpy)					Average Particle Size (μ)	
				Toroid	347 SS	Ti-75A	SA-212-B	Zircaloy-3A	Prerun	Postrun
				Postrun pH > 10						
<3	26	1000	10.2	53	290	13	4	13	2.1	6
	26	1600 (2 hr)	10.9	6	22	18	23	27	c	0.7
3–10	26	1200 (4 hr)	10.5	160	730	73	890	47	10	7
	26	1400 (2 hr)	10.4	120	1600[g]	140	680	62	11	17
	26	1600 (2 hr)	10.6	100	1900[g]	83	1800[g]	67	13	14
10–25	26	1600 (2 hr)	10.5	100	390	90	290	26	16	9

[a]Corrected for slug flow.
[b]WG = weight gain shown by defilmed specimens.
[c]Aggregates easily broken up; reportea >50 μ.
[d]Spherical material from different batch; s. d <3-μ material was not spherical.
[e]Insufficient sample to make determination.
[f]Unsized spheres of 55 μ mean diameter (particle sizes range from 3 to 150 μ).
[g]Pin consumed; value computed from dimensions of pin and represents a minimum rate.

from the recalcined material. Oxygen deficiency or alkalinity has been observed to be associated with higher corrosion rates in other tests. The combination of these effects with high circulation velocity resulted in generally very severe attack of all materials. There was somewhat higher attack by the 3–10-μ size range, but in general the effect did not appear to be closely associated with size. Examination of the attack pattern of such specimens as survived left little doubt that the thoria had indeed circulated.

13.2.7 Tests with Micropulverized Thoria

As part of the cooperative test program with the Chemical Technology Division, a series of toroid tests was made to ascertain the corrosion-erosion characteristics of slurries of micropulverized thoria. Batch LO-25-1 was recalcined at 1600°C and then attrited in a Mikropulverizer to a mean particle size of 1.7 μ. A portion of the ground material was also classified by sedimentation to a mean particle size of 1.6 μ.

To compare the erosiveness of the two products, toroid tests of 100-hr duration were made at 280°C and 26 fps at a concentration of 1500 g of Th per kg of H_2O. A summary of the tests and the results of an examination by the factor analysis method are presented in Table 13.12.

Both preparations produced high attack rates on type 347 stainless steel, titanium-75A, and Armco iron. Attack of Zircaloy-3A was more moderate. Except for stainless steel, attack of the alloys was less severe with the slurry of the classified thoria. The lower attack produced by the classified material appeared to be associated with the extent of particle degradation which occurred in the two tests.

13.2.8 Toroid Tests with Thoria Sols

Although the major effort at ORNL in the development of a thorium blanket for a breeder reactor has been directed toward the perfection of aqueous thoria slurries, attention has also been given to possible application of thoria sols.[19] Toroid tests were completed recently to ascertain the stability and corrosion attack of three experimental sol preparations furnished by the Davison Chemical Company. The sols, as furnished, contained ~300 g of thorium and 200 g of SiO_2 per liter. Conditions and corrosion results for the tests are shown in Table 13.13.

Initially, two of the preparations were circulated at 280°C. During the 300-hr circulation period

Table 13.12. Toroid Tests with Classified and Unclassified Micropulverized Thoria

Time: 100 hr
Velocity: 26 fps
Temperature: 280°C
Concentration: 1500 g of Th per kg of H_2O
Atmosphere: Oxygen

Batch	Corrosion Rate* (mpy)				pH, Postrun	Average Particle Size (μ)	
	347 SS	Ti-75A	Armco Iron	Zircaloy-3A		Prerun	Postrun
LO-25-1 (unclassified)	11.3	10.5	31.0	2.7	5.9	1.7	0.9
LO-25-1 (classified)	19.5	6.7	18.2	WG	5.7	1.6	1.5

Statistical Analysis into Multiplicative Factors
(Relative to Normalized Rate of Type 347 Stainless Steel in Unclassified Micropulverized Thoria = 11 mpy)

Average Effect of Major Variables

Metal	Relative Factor	Micropulverized thoria	Relative Factor
Toroid	0.4	Unclassified	1.0
347 SS	1.0	Classified	0.5
Ti-75A	0.5		
Armco iron	1.6		
Zircaloy-3A	0.03		

*Corrected for slug flow.

Table 13.13. Attack Data from Toroid Tests with Thoria Sols

Time: 300 hr
Relative velocity: 26 fps
Atmosphere: Oxygen

Test No.	Sol Concentration (g of Th per kg of H_2O)	Operating Temperature (°C)	pH, Postrun	Corrosion Rates* (mpy)			
				347 SS	Ti-75A	SA-212-B	Zircaloy-3A
1	281	280	7.8	2	4	21	0.4
1	278	280	7.2	WG**	WG	2	WG
2	350	280	6.7	6	3	27	1
3	308	250	8.6	1	1	11	WG
3	198	280	7.4	3	2	23	2
3	350	280	6.7	6	3	27	1

*Corrected for slug flow.
**WG = weight gain.

both sols broke; that is, they were flocculated after circulation. The third preparation was then circulated at 250°C. It also was flocculated after circulation.

Because the stability of sols is often affected by changes in concentration, it appeared possible that the water lost to vapor at 280°C was sufficient to cause supersaturation of the sols and thereby promote flocculation. Therefore an additional run was made at 280°C. In one toroid sufficient water was added to compensate for liquid lost to vapor at 280°C. In the second, the sol was diluted with an equivalent volume of water. In both tests the preparations were flocculated after 300 hr of circulation.

Corrosion rates in one test were low. In the other four tests the rates were moderate but significantly higher. By chemical analysis, the sols were found to contain appreciable chloride contamination (up to 800 ppm) and 8000 to 9000 ppm of sodium ion. Undoubtedly, these contaminants contributed to the corrosiveness of the sols. In general, attack rates were lower in the purer preparations.

13.3 IN-PILE AUTOCLAVE SLURRY CORROSION TESTS

13.3.1 Introduction to Autoclave Experiments

A series of in-pile autoclave slurry corrosion experiments discussed here includes a six-week run containing an initial overpressure of oxygen and a seven-week run containing an initial overpressure of deuterium. The experiments were performed in the HB-6 facility of the LITR at a maximum fission power density of 0.6 w/ml. These runs utilized newly modified equipment and a special thoria-urania preparation which contained 0.5 wt % enriched uranium, based on thorium. Studies of the catalytic recombination of radiolytic gases by added MoO_3 were made during in-pile operation and in a separate experiment by the Chemical Technology Division before loading. Observations of the pressure in the bomb from time to time, including periods of different relative pile operation time, permitted a consideration of the effect of time and radiation as separate factors in the generalized corrosion. The examination of the autoclaves and contents after irradiation has not yet been completed.

Contents of the autoclaves from the previous in-pile and control experiments have been examined, and results are presented below. A summary of operating conditions of various in-pile autoclave experiments is given in Table 13.14.

13.3.2 Development, Construction, and Operation

Three HB-6 type rocking-autoclave experiments, L6Z-122S, -125S, and -126S2, containing thorium-uranium oxide slurries were assembled and operated in beam hole HB-6 of the LITR to obtain radiation-corrosion data with slurries. These were the first in-pile HB-6 experiments to use the new MTR type of plug and rocking mechanism. Figure 13.13 is a photograph of the autoclave assembly as installed in the LITR. Because of the solid stainless steel plug and gear rocking mechanism, operation was much smoother, and it was possible to rock the experiment in a retracted position at a reduced flux level. There was also less flexing of the service lines, thus increasing their life.

Experiment L6Z-122S was removed from the reactor after operating satisfactorily for 1070 hr at 280°C (680 hr with the reactor at 3 Mw). The autoclave was fabricated from Zircaloy-2 and contained six pin-type corrosion specimens: two of Zircaloy-2, one of Zr–15% Nb–2% Pd, one of Zr–15% Nb (as quenched), one of Zr–15% Nb–5% Mo, and one of Zr–15% Nb (beta quenched, heat treated at 550°C for two weeks, and air cooled).

The autoclave was loaded with dry thorium oxide coprecipitated with 0.5 wt % enriched uranium, based on thorium, and D_2O was added to obtain a thorium oxide slurry with a nominal concentration of 1000 g of Th per kg of D_2O. Properties of the slurry are given in Table 13.15. Molybdenum trioxide was also added to catalyze the recombination of radiolytic gas. An initial oxygen overpressure of approximately 460 psi at 25°C was obtained by the addition of gaseous oxygen to the vapor space of the autoclave by use of a technique reported previously.[20] The autoclave was operated in the out-of-pile mockup for approximately 21 hr at 250°C and 1250 psia as a final test before insertion in the LITR.

Autoclave L6Z-125S, which operated satisfactorily in beam hole HB-6 of the LITR for 1100 hr at 280°C (774 hr with the reactor at 3 Mw), was also fabricated from Zircaloy-2 and contained six pin-type corrosion specimens of the following compositions: two of Zircaloy-2, one of Zr–15% Nb–2%

[20] E. L. Compere *et al.*, *HRP Quar. Prog. Rep. Jan. 31, 1958*, ORNL-2493, p 112.

Table 13.14. In-Pile Autoclave Slurry Experiments

	Experiment No.				
	117[a]	120S[b]	121S	122S	125S
Temperature, °C	280	280	280	280	280
g of Th per kg of D_2O		1000	1000	990	950
U in Th, %				0.5	0.5
MoO_3, *m*				0.02	0.02
Atmosphere	O_2	O_2	O_2	O_2	D_2
Flux ($\times 10^{13}$)	0.7	None	0.5	0.5	0.5
Power density (w/ml)				0.6	0.6
Hours at temperature	993	480	319	1069	1232
Hours irradiated[c]	670		261	690	774
Radiolytic gas, psi	Not obs		Not obs	21-60	Not obs[d]
Over-all rate, mpy	0.3	0.4	0.9	0.8	0.4

[a]Experiment by G. H. Jenks and R. J. Davis.
[b]Unirradiated control for comparison with test 121S.
[c]LITR at 3 Mw.
[d]6–21 psi at 175°C.

Pd (heat treated at 900°C for 1 hr, water quenched), one of Zr–15% Nb–5% Mo (heat treated at 900°C for 1 hr, water quenched), one of Zr–15% Nb–5% Mo (heat treated at 900°C for 1 hr, capsuled and water quenched), and one of Zr–15% Nb (beta quenched, heat treated at 550°C for two weeks, air cooled). The autoclave was loaded with the same thorium oxide material containing 0.5 wt % enriched uranium, based on thorium, and MoO_3 catalyst as was L6Z-122S, and D_2O was used as the dispersant to give a nominal concentration of 1000 g of Th per kg of D_2O. However, a deuterium gas atmosphere at a pressure of approximately 80 psi at 25°C was used instead of the oxygen atmosphere used in previous in-pile slurry autoclaves. The capillary line through which the deuterium gas addition was made was then filled with D_2O using a micropulsafeeder as in L6Z-122S. The autoclave was operated in the out-of-pile mockup facility for about 90 hr at 280°C and 1100 psia as a final test before insertion in the LITR.

Table 13.15. Examination of Thoria Charged to In-Pile Autoclave Test L6Z-122S and -125S

Preparation method*	Coprecipitation of Th and U(IV) oxalates
Maximum calcination temperature	1300°C
Analysis	
Th	87.47%
U (93% enriched)	0.44%
Surface area	2.0 m^2/g
Particle size	
Average diameter	0.8 μ
Over 20 μ	19 wt % (corrected average)
5–20 μ	4 wt %
1–5 μ	13 wt %
0.5–1 μ	44 wt %
Below 0.5 μ	20 wt %

*Prepared by Chemical Technology Division.

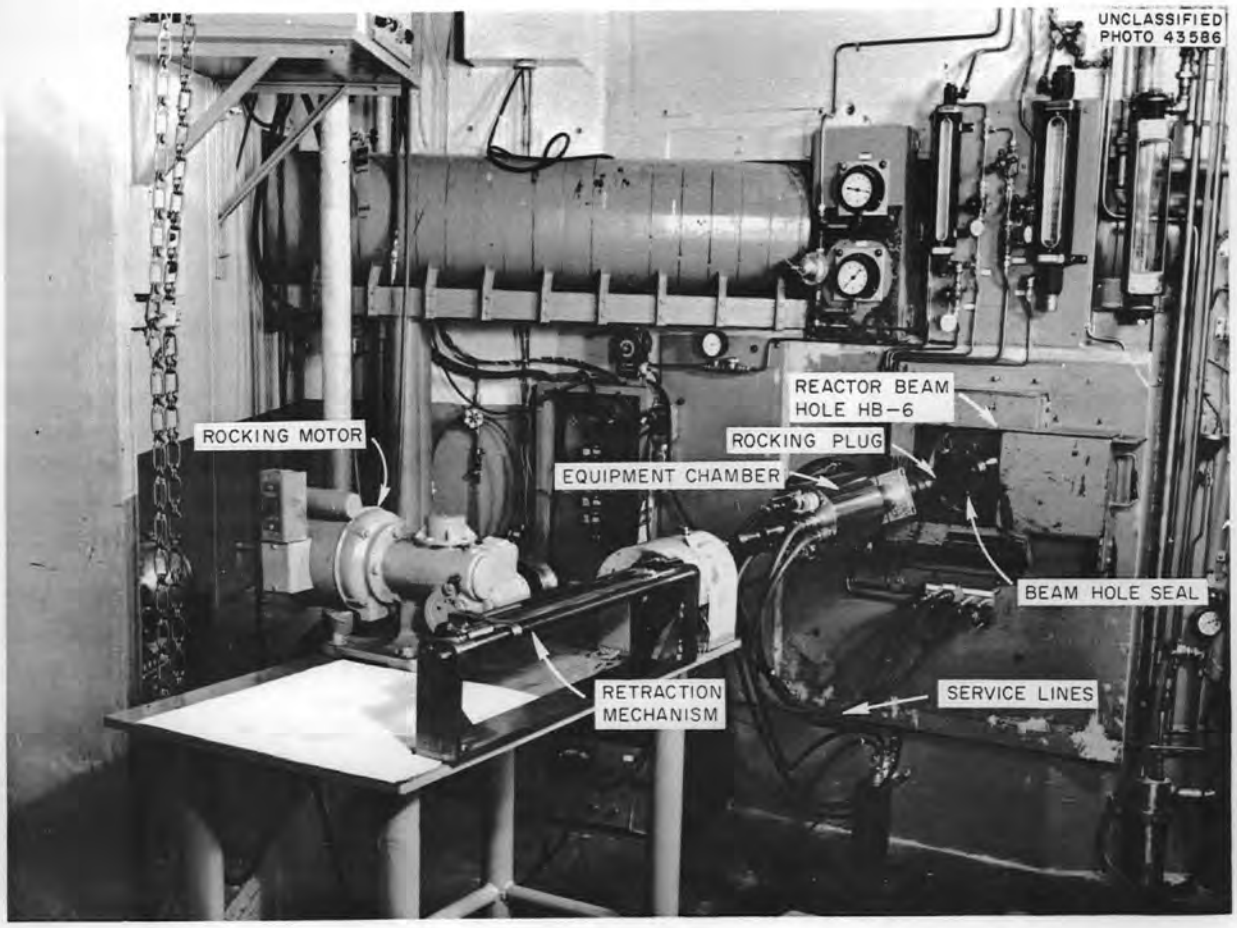

Fig. 13.13. LITR HB-6 Rocking-Autoclave Experimental Assembly.

Autoclave L6Z-126S2, which was inserted in the LITR on July 15, 1958, and is now in operation in beam hole HB-6, was also fabricated from Zircaloy-2 and contained six pin-type corrosion specimens of the following composition: two of Zircaloy-2, one of Zr–15% Nb–2% Pd (heat treated at 900°C for 1 hr, water quenched), one of Zr–15% Nb (heat treated at 900°C for 1 hr, water quenched), one of Zr–15% Nb–5% Mo (heat treated at 900°C for 1 hr, capsuled, water quenched), and one of Zr–15% Nb (beta quenched, heat treated at 550°C for two weeks, air cooled). The autoclave was loaded with thorium oxide material containing 5 wt % enriched uranium, based on thorium, molybdenum trioxide catalyst, and slurried in D_2O to give a nominal composition of 1000 g of Th per kg of D_2O. A deuterium gas atmosphere of about 100 psi at 25°C was obtained after the capillary gas-addition line was filled with D_2O from a micro-pulsafeeder. The autoclave was operated in the out-of-pile mockup facility for about 144 hr at 280°C and 1100 psia as a final test before insertion in the LITR.

13.3.3 Recombination of Radiolytic Gases

The new retraction mechanism permits a rapid movement of the autoclave into or from the region of high neutron flux; with the LITR at full power the experiment can be either retracted or inserted, and from following the change in total pressure the ingrowth or recombination of radiolytic gas may be deduced. From this the catalytic activity of the MoO_3 may be estimated.

The kinetics generally could be treated as first order with respect to stoichiometric radiolytic gas (presumably first order with respect to D_2). Catalyst activities were computed from observed rates and equilibrium D_2 pressures on this assumption. An insertion experiment with autoclave L6Z-122S at a 1500-kw LITR power at

280°C gave results consistent with those obtained at 3000 kw, providing additional evidence of first-order kinetics with respect to radiolytic gas.

(*a*) **Oxygen Atmosphere.** – Table 13.16 presents the results of recombination studies in experiment L6Z-122S, which utilized oxygenated slurry. These values should be compared with catalyst activities of 0.57 and 0.32 moles D_2/liter-hr at 100 psi D_2 which were determined in repeated out-of-pile experiments on the same materials by the Chemical Technology Division. Good agreement with the out-of-pile activity is noted.

A moderate downward trend in catalyst activity is indicated, with the activity approximately halved in about 1000 hr. Results of tests at 250 and 220°C are also shown.

It is possible to compute from the observed rate, equilibrium pressure, and LITR power a value of

Table 13.16. In-Pile Recombination of Radiolytic Gas Under Oxygen Atmosphere; Experiment L6Z-122S

990 g of Th per kg of D_2O; 0.5% enriched U/Th
1000 psi O_2
3000 kw LITR power = 0.5×10^{13} neutrons·cm^{-2}·sec^{-1} (HB-6)
Catalyst, 0.02 *m* MoO_3

Hours Heated	Hours Radiotion	Type of Experiment[a]	Observed Rate[b] (moles D_2/liter-hr)	D_2 Equilibrium (psi)	Calculated Catalyst Activity at 100 psi D_2 (moles D_2/liter-hr)	Calculated G_{D_2}
			280°C, 3000 kw			
72	0	I	0.15	26	0.58	0.66
73	1	R	0.12	26	0.46	0.53
93	16	R	0.20	43	0.48	0.88
96	16	I	0.14	30	0.45	0.62
165	76	R	0.14	23	0.59	0.62
168	76	I	0.17	24	0.70	0.74
328	220	R	0.10	25	0.40	0.44
652	495	I	0.14	46	0.30	0.62
978	604	R	0.14	66	0.22	0.62
1056	673	R	0.13	64	0.21	0.57
1057	674	I	0.20	58	0.34	0.88
			280°C, 1500 kw			
330	220	I	0.07	14	0.50	0.62
				Confidence interval (95%) of mean		0.57–0.71
			250°C, 3000 kw			
485	359	R	0.17	123	0.14	0.80
487	359	I	0.19	46	0.40	0.85
				Estimated confidence interval (95%)		0.6–1.1
			220°C, 3000 kw			
979	604	I	0.39	233	0.17	1.6
				Estimated confidence interval (95%)		1.0–2.4

[a] I = insertion experiment; R = retraction experiment.
[b] Recombination rate at the equilibrium pressure equals the production rate.

G_{D_2} (molecules of D_2 produced per 100 ev absorbed) for the radiolytic production of D_2 (more properly, a value of G for radiolytic gas, $\frac{3}{2}$ G_{D_2}, may be deduced; the identification with D_2 is conjecture). It was assumed that the flux was 0.5×10^{13} neutrons/cm^2, as is reported further below for the similar experiment L6Z-121S, based on determination of the activation of Zircaloy-2 specimens in the autoclave. A cross-section of 478 barns was used for U^{235} at 50°C LITR temperature, and an effective fission energy of 170 Mev was assumed.

Values for G_{D_2} are shown in Table 13.16. No trend was noted. The value at 280°C may be estimated from the data to lie between 0.57 and 0.71. A similar percentage uncertainty of individual values was assumed in estimating the confidence interval for observation at 250 and 220°C. A somewhat higher value of G was calculated for these temperatures, but in view of the high uncertainty associated with so few observations no significance is yet attributed to this possible temperature effect.

(*b*) Deuterium Atmosphere. – Table 13.17 presents the results of recombination studies in the deuterium-atmosphere slurry experiment, L6Z-125S. No detectable quantity of radiolytic gas was observed in four retraction experiments and one insertion experiment at 280°C and 3000 kw. An insertion experiment was performed at 220°C with similar results. Small but measurable quantities of radiolytic gas were generated with insertions at 175 and 150°C. The kinetics appeared to be first order with respect to stoichiometric radiolytic gas. Since the maximum radiolytic deuterium pressure produced was only 14 psi, not very precise values of the G_{D_2} and of the activity of the MoO_3 catalyst were obtained. However, a significant difference in the G_{D_2} in this experiment, which was initially charged with 80 psi D_2 at room temperature, was observed as compared with experiment L6Z-122S, which was initially charged with 470 psi O_2. At 95% confidence interval of the mean, the 280°C experiment L6Z-122S gave a G_{D_2} value of 0.57 to 0.71 while at 175°C experiment L6Z-125S gave a G_{D_2} value of 0.01 to 0.03.

13.3.4 Effects of Time and Radiation on Generalized Corrosion

In experiment L6Z-122S generalized corrosion of the autoclave and contents was followed in the usual way[21,22] by observing the temperature and pressure of the autoclave at suitable times, especially at room temperature during reactor shutdown periods. Loss in pressure (after suitable correction for steam, etc.) was attributed to consumption of oxygen by general corrosion, and the uniform thickness of metal thus required was computed.

The results of pertinent experiments, given in Table 13.14, are shown in Fig. 13.14. Results from experiment L52Z-117, performed by the In-Pile Bomb Group of the Radiation Corrosion Section, are included. This experiment, with D_2O and oxygen in a Zircaloy-2 autoclave at 280°C in the HB-5 facility, provides a valuable in-pile comparison experiment. The lines shown on the graph pertain to run L6Z-122S and are results of an attempt to separate time and radiation effects in this experiment as described below.

During its fifth week, experiment L6Z-122S received a much smaller irradiation than normal because of special operation of the LITR in connection with another experiment. This, together with usual fluctuations in radiation time for other weeks, caused the experiment to encounter periods of considerably varied integrated power.

Corrosion rates for each week were calculated from the data shown on Fig. 13.14 and are shown in Fig. 13.15. Actual values are shown on horizontal dotted lines where they differ from the averages used in correlations. A graphical multiple correlation analysis by the method of Ezekiel[23] permitted the corrosion rate to be estimated as: mpy = 75/hr + 1.2 (w/ml), where time is in hours at temperature beginning with loading and where radiation is expressed as the time-averaged fission power density, w/ml.

---

[21] E. L. Compere *et al.*, *HRP Quar. Prog. Rep. Jan. 31, 1958*, ORNL-2493, p 113.

[22] K. S. Warren and R. J. Davis, *In-Reactor Autoclave Corrosion Studies – LITR I Outline of Methods and Procedures*, ORNL CF-57-5-110 (May 22, 1957).

[23] M. Ezekiel, *Methods of Correlation Analyses*, 2d ed., chaps. 14, 16, Wiley, New York, 1941; also, O. B. Ellis, *Corrosion* 9, 203–8 (1953).

Table 13.17. In-Pile Recombination of Radiolytic Gas Under Deuterium Atmosphere; Experiment L6Z-125S

950 g Th/kg D_2O, 0.5% enriched U/Th
0.017 *m* MoO_3
0.5×10^{13} neutrons·cm^{-2}·sec^{-1} at 3000-kw reactor power*

Temperature (°C)	Power Level (kw)	Hours Above 100°C	Radiation Hours	Type of Experiment	Observed Rate** (moles D_2/liter-hr)	Equilibrium D_2 Pressure (psi)	Calculated Catalyst Activity at 100 psi D_2 (moles D_2/liter-hr)	Calculated G_{D_2}
175	3000	395.6	265.2	Insertion	0.0055	13.6	0.040	0.022
		629.1	307.1	Insertion	0.0037	6.3	0.059	0.015
		1141.2	686.9	Insertion	0.0046	4.2	0.109	0.019
						Confidence interval of mean (95%)		0.010–0.027
150	3000	655.3	329.4	Insertion	0.0045	12.8	0.035	0.018
		1096.5	647.1	Insertion	0.0066	4.8	0.137	0.026
						Confidence interval of mean (95%)		0.012–0.032

*Based on neutron activation analysis of Zircaloy-2 pins in L6Z-121S.
**Observed rate or production rate equals recombination rate at equilibrium.

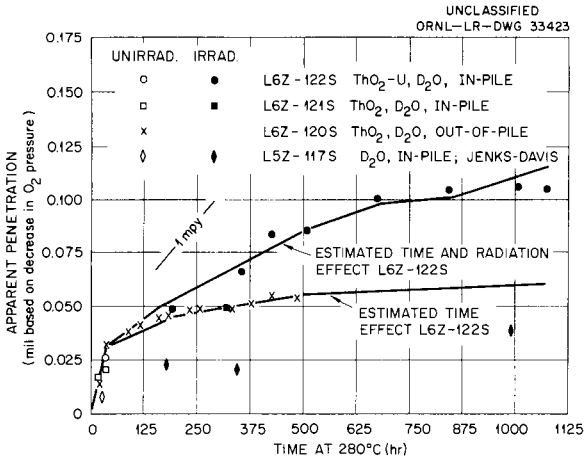

Fig. 13.14. Generalized Corrosion Attack of Zircaloy-2 Autoclaves Associated with In-Pile Slurry Studies (280°C, O_2).

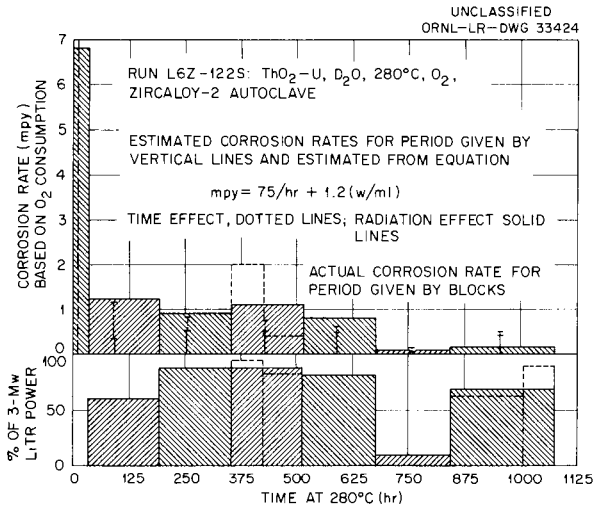

Fig. 13.15. Effects of Time and Radiation on In-Pile Slurry Corrosion.

The results of this procedure are shown as estimated rates in Fig. 13.15. These estimated rates for the respective periods were used in constructing the integrated curves of Fig. 13.14.

The over-all agreement is reasonably satisfactory. The time component of run L6Z-122S agrees very well with the data of runs L6Z-120S and -121S. Agreement with run L52Z-117 in which only D_2O was present is less good in level, but primarily appears to be due to a difference in oxygen consumption during the pretreatment period of the first 10–30 hr. It is not certain whether this lower pretreatment requirement is due to the absence of thoria.

The presence of a radiation effect in experiment L6Z-122S and its apparent absence in run L6Z-121S imply that the radiation effect could be attributed to the fissioning which was the cause of the higher power density in experiment L6Z-122S.

It should be noted that the effects considered above are quite small and that adequate evaluation of radiation effects must await subsequent experiments at higher power densities.

Following experiment L6Z-122S, experiment L6Z-125S was performed to compare the effect of an atmosphere of deuterium gas on the corrosion of Zircaloy-2 by the thoria–urania 0.5 wt % slurry with that observed under an oxygen atmosphere. Since the corrosion of the Zircaloy-2 in a deuterium atmosphere can be assumed to follow the reaction metal + D_2O → metal oxide + D_2, the corrosion may be followed by observing the increase in pressure. After 400 hr at temperature the autoclave was retracted for ~200 hr to compare the effect of changes in power level on the corrosion; it was subsequently reinserted. During a later one-week period, it was retracted on alternate days to diminish the radiation during the period.

Figure 13.16 presents the corrosion results of experiment L6Z-125S, as estimated from the values of D_2 pressure at room temperature during

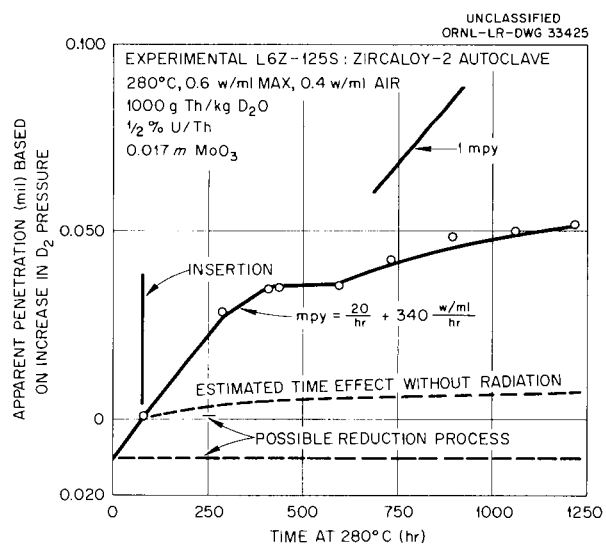

Fig. 13.16. Radiation Corrosion Under Deuterium Atmosphere.

reactor shutdown periods. An attempt was made to fit an equation of the same form as was used in the oxygen-atmosphere experiment L6Z-122S described above; that is, mpy = A/hr + B × (w/ml). Coefficients which permitted the best fit here were not physically possible, as a constant term had to be included, which implied negative corrosion in the latter parts of the run in the absence of radiation. It was found possible to fit the data using the equation: mpy = 20/hr + (340/hr) × (w/ml). The results of this equation under the time and radiation conditions of experiment L6Z-125S are shown in Fig. 13.16 along with the actual results of the experiment. The over-all corrosion rate for the experiment was 0.4 mpy. It is possible that some deuterium may have been consumed during the pretreatment period, to reduce molybdenum trioxide and uranium oxide, and that this may have been compensated for by corrosion deuterium indicated by the equation (see Fig. 13.16) to have been produced during this period. It will be of interest to see in later experiments under D_2 atmosphere whether the radiation effect is diminished as the experiment is continued, as implied by the equation given above.

13.3.5 Examination of Irradiated Thoria and Autoclave Corrosion Specimens

The operating results of the first in-pile slurry autoclave corrosion test, L6Z-121S, and the unirradiated control, L6Z-120S, were reported previously.[21] During the present quarter, the autoclaves have been opened and the contents examined and analyzed.

Analysis of slurry from the experiments is given in Table 13.18. Recovery was satisfactory, with no deposits of thoria noted after sufficient rinsing. The analysis for corrosion products did not provide useful information: there was less Fe, Cr, and Ni than there was in the original material, a 10°C oxalate precipitated thoria calcined at 1600°C, which had been previously circulated in a 100A

Table 13.18. Analysis of Irradiated Thoria from Autoclave Experiments

	Original Material*	L6Z-120S, Unirradiated Test	L6Z-121S, Irradiated Test
Settled volume, %		67	37
Volume recovered, ml		2.4	3.0
Th recovered, g		2.52	1.48
Fe, μg per g of Th	380	500	170
Cr, μg per g of Th	90	800	0
Ni, μg per g of Th	60	0	0
Zr, μg per g of Th		240	110
U^{233}, counts/min per g of Th			4.4×10^5
Particle size by sedimentation**			
Average diameter, μ	1.7	1.3	0.8
Weight per cent over 3 μ	6	3–4	7
1.5–3 μ	55	30	19
1–1.5 μ	12	32	19
Below 1 μ	28	34	55

*Original material was pumped thoria from 100A loop run BS-16. It had been prepared by 10°C precipitation with oxalic acid, with 1600°C calcination.

**The determination on original material was performed in 0.001 m $Na_4P_2O_7$; determinations for L6Z-120S and -121S performed in 0.005 m $Na_4P_2O_7$

pump loop. The zirconium result was higher than anticipated, corresponding to generalized attack rates of 13 and 5 mpy, respectively. The analytical method could have permitted thorium carry-over, which would be reported as zirconium. In view of this, the determinations were performed several times but with similar results.

Particle size analysis indicated that a decrease in particle size was encountered on the irradiated material, which increased the fraction below 1 μ from about 30% to about 55% and reduced the average particle size from 1.3 to 0.8 μ.

The generation of U^{233} was observed in agreement with theory; assuming a thorium cross section of 7.0 barns and a flux of 0.50×10^{13} neutrons/cm^2 for 261 hr, followed by decay of protactinium for approximately 42 days, it may be estimated from ORNL-1818[24] that a quantity of 0.022 mg of U^{233} per g of Th should have been found (with 31% of the Pa^{233} yet to decay). The observed yield corresponds to 0.021 mg of U^{233} per g of Th.

All pin corrosion specimens showed slight increases in defilmed weight, amounting to a few tenths of 1 mg/cm^2. The Zircaloy-2 specimens had clean, shiny films; the niobium-containing zirconium alloys had darker gray, glossy films. In all cases no localized attack was evident, although grain patterns and very slight etching were noted on the niobium-containing alloys. No irradiation effects were observable.

Pin specimen corrosion rates were calculated from the observed weight gains. Values are shown in Table 13.19. Results for all specimens fell within a reasonable experimental error range, and no distinctive corrosion behavior was identified. Comparison of the activation of a Zircaloy-2 specimen from experiment L6Z-121S with similar material having received a known amount of irradiation indicated that the specimen had been exposed to a neutron flux of 5.0×10^{12} neutrons/cm^2. This value has therefore been used as the flux applied in this experiment.

13.4 IN-PILE SLURRY TOROID

13.4.1 Engineering Development

Development work on an in-pile slurry toroid has been interrupted during this period because of the work on the HRT core and blanket specimen assemblies (see Sec 14.3.2), as well as a decision, based on certain encouraging tests, to assemble a test model of an in-pile slurry loop (see Sec 13.5). However, the method of temperature control which encloses the toroid bundle within an ambient whose temperature is controlled by air-water

[24] A. T. Gresky and E. D. Arnold, *Products Produced in Batch Neutron Irradiation of Thorium*, ORNL-1818 (Dec. 5, 1955).

Table 13.19. Comparison of Corrosion Data for Pin Specimens from Irradiated Autoclave Slurry Experiment and Control

280°C, 1000 g of Th per kg of D_2O, O_2 Atmosphere, Zircaloy-2 Autoclave

	Experiment L6Z-120S	Experiment L6Z-121S
Hours at temperature	480	319
Hours radiation (LITR at 3000 kw)	0	261
Autoclave generalized corrosion rate,* mpy	0.4	0.9
Pin Material	Pin Corrosion Rate (mpy), Based on Weight Gain	
Zircaloy-2	0.6, 0.6, 0.9	0.0, 0.9, 1.7
Zr–15% Nb, quenched	0.9	1.4
Zr–15% Nb–2% Pd, quenched	0.9	0.3
Zr–15% Nb–5% Mo, quenched	0.9	0.5

*Based on changes in oxygen pressure after pretreatment period.

and/or steam mixtures[25] was tested during the past period. These tests indicated the necessity of changes in the system to obtain a faster response to changes in the toroid temperature. The system would maintain a constant toroid temperature under steady-state or slowly changing toroid heat loads but was relatively insensitive to fast changes in heat loads, and thus temperature, as would be encountered during a reactor scram.

A new temperature control system has been installed which uses two continuously flowing, constant-temperature supply streams which are mixtures of air and water – one high temperature and one low temperature – for heating and cooling. Both these streams are controlled and mixed as required to control the ambient temperature surrounding the toroids by proportional control-throttling valves. Since only a portion of each coolant and/or heating stream may be required at any given heat load for control of the toroid temperature, the excess is discharged to the drain.

13.5 IN-PILE SLURRY LOOP

13.5.1 Loop Development

The experimental in-pile slurry loop run, previously described,[26] was terminated because of a bearing failure in the circulating pump after 790 hr of operation at room temperature with a slurry containing approximately 550 g of Th per kg of H_2O.

The failure is not attributed directly to the slurry but is believed to have been a mechanical failure. The particular pump being used was an early model of the present in-pile type 5-gpm pump with aluminum oxide bearings and journal bushings. The pump components were not fabricated to the more rigid dimensional tolerances now employed, and the bearings and bearing housings were not pinned in place to prevent slippage as is the current practice. Excessive pump temperatures were frequently observed during the run and are attributed to leakage of high-temperature slurry past the thermal spacer into the rotor cavity.

The circulation of a thorium oxide slurry of approximately 550 g of thorium per kilogram of water for 790 hr in the experimental loop was encouraging. Therefore slurry tests were carried out with models of components for an in-pile loop designed to operate in beam hole HB-2 or HB-4 of the LITR. Slurry was circulated through a transparent plastic model of the loop core[27] as designed for the ORR in-pile loop. Visual observation of the slurry flow indicated that this core would be suitable for a slurry loop. In addition, a transparent plastic model of the horizontal pressurizer as used in the present in-pile loops was fabricated and tested with slurry. Visual observations of the slurry flow in this pressurizer indicated that the slurry could be prevented from settling by introducing the slurry into the pressurizer through several jets spaced along the bottom of the pressurizer.

Since the pump test with thorium oxide slurry, reported previously,[26] indicated that the pump bearing purge, and thus a condensate system, could be eliminated from the loop design, a test model of an in-pile loop, designated L-4-24S, designed to fit into the existing HB-4 facility of the LITR was assembled. The core section of the loop was identical to that designed for the ORR in-pile loop, and the horizontal pressurizer, fabricated from $1\frac{1}{2}$-in. sched-80 pipe, contained three jets spaced at intervals along the bottom. The total flow through the pressurizer was equally divided between the three jets. There were no provisions for purging the pump bearings. Total loop volume is 1750 cc, of which 750 cc is the pressurizer volume.

Loop operation with water at 285°C and 1100 psi (60 psi of oxygen gas added at room temperature) was satisfactory. Following the water run, the loop was charged with thorium oxide slurry to a load concentration of 500 g of Th per kg of H_2O. Immediately after charging, the loop concentration was approximately 180 g of Th per kg of H_2O and gradually decreased to less than 10 g of Th per kg of H_2O during the 30-hr operating period of this run. Operating conditions were 75°C and 100 psi pressure. The slurry lost from the circulating stream was found in the loop pressurizer. The flow rate through the pressurizer did not appear to decrease, and no adverse effect on loop operation was noted.

[25] E. L. Compere *et al.*, *HRP Quar. Prog. Rep. Jan. 31, 1958*, ORNL-2493, p 114.

[26] *Ibid.*, p 115.

[27] J. H. Jenks *et al.*, *HRP Quar. Prog. Rep. July 31, 1957*, ORNL-2379, p 100, Fig. 14.3.

A second run, at a temperature of 140°C and 200 psi, was made, 60 psi of oxygen gas being added to the loop before starting the run. The loop was charged, by means of an addition tank, to a concentration of 340 g of Th per kg of H_2O. Immediately after charging, the sampled concentration was 120 g of Th per kg of H_2O. After 3 hr of operation at 140°C and 200 psi, the loop concentration had decreased to 73 g of Th per kg of H_2O. The loop was shut down, and the thoria lost from the circulating stream was again found in the pressurizer. Again over-all loop operation was satisfactory, with no evidence of plugging or pump malfunction.

From the above test runs the loop appears to operate satisfactorily. The major problem is the accumulation of slurry in the horizontal pressurizer section. Additional runs are being made in an attempt to solve this problem.

The reason for slurry accumulation in the loop pressurizer, which did not occur in the plastic test model, could be accounted for by the increase in settling rate and proportional increase in dropout velocity at the 70 to 140°C loop temperature; the plastic-model tests were at room temperature. All tests have been made with a thorium oxide slurry from mixed batch LO-17 and TO-10-1000, calcined at 1600°C and with a mean particle size of 0.7 μ. The material had been previously pumped in 100A test loop BS for ~1000 hr.

14. RADIATION CORROSION

G. H. Jenks H. C. Savage

A. L. Bacarella
J. E. Baker
S. J. Ball
J. C. Banter
S. E. Bolt
J. W. Brown
R. J. Davis
V. A. DeCarlo
D. T. Jones
F. A. Knox
R. A. Lorenz
J. R. McWherter
A. R. Olsen
A. J. Shor
M. D. Silverman
W. C. Ulrich
R. M. Warner
K. S. Warren
S. H. Wheeler
W. C. Yee

14.1 IN-PILE LOOPS

14.1.1 Development and Construction

(a) HB-2 Loop Package. – Assembly of loop L-2-22 was completed. This is a type 347 stainless steel loop containing tapered-channel coupon corrosion specimens, low-velocity coupon corrosion specimens, and multiple-break tensile specimens. Zircaloy-2 tapered-channel coupon holders in the core and line positions contain Zircaloy-2, type 347 stainless steel, niobium, crystal-bar zirconium, Zr–5% Sn, and Zr–15% Nb corrosion specimens. Four Zircaloy-2 tensile specimens are in the core and two in the line. Four low-velocity coupon holders in the core, two in the line sample holder, and two in the pressurizer contain a variety of zirconium alloys of various heat treatments. Two cobalt-aluminum flux monitors encased in type 347 stainless steel are located in the core.

The loop was operated out-of-pile for a cumulative time of 686 hr at 280°C with D_2O and a D_2O solution containing 0.04 *m* UO_2SO_4, 0.10 *m* D_2SO_4, 0.003 *m* $CuSO_4$, and 0.20 *m* Li_2SO_4. At that time a leak developed in the pump rotor housing[1] (0.130 in. thick). The leak was a result of severe localized corrosion attack in the pump rotor housing adjacent to the thermal shield, as shown in Fig. 14.1. Figures 14.2 and 14.3 show the attack on the thermal shield in the same location. This is a crevice region, with a temperature gradient from 280 to about 100°C through the thermal shield. The heavy, loosely adhering film shown in Fig. 14.2 was localized on the thermal shield.

The remaining interior areas of the loop which could be observed had the usual clean, hard film, as illustrated by the photograph of the 280°C side of the thermal shield (Fig. 14.3). Metallographic examination of the capillary drain line and radiographic examinations of all crevice areas of the loop were made. There was no excessive attack in these areas or in the rest of the system external to the pump thermal shield. The pump was replaced with another ORNL 5-gpm pump, and out-of-pile pretreatment and operational tests were completed.

(b) ORR Loop Package. – Construction of the ORR loop mockup facility, including instrumentation and auxiliary equipment, was completed. Figure 14.4 is a photograph of the first test loop, designated O-1-20. The loop includes additional heaters for the simulation of reactor heat generation during operation in the mockup facility.

Except for minor modifications, the core section of the loop is as described in a previous report.[2] The loop layout, with the exception of a rearrangement of the pressurizer and the addition of a purge line from the pressurizer discharge to the rear of the pump, is substantially the same as formerly shown.[3] The purpose of the pump purge line is to maintain a low, controlled concentration of radiolytic gas in the pump-rotor-cavity region during in-pile operation and, also, through control of temperature in this region, to minimize the possibility of uranyl peroxide precipitation.

Preliminary operation of the test loop, including cleaning, leak testing, and instrument calibration, was initiated. The reactor beam-hole liners, shield plugs, and parts of the loop retraction gear were received, inspected, and tested, with satisfactory results.

---

[1] G. H. Jenks *et al.*, *HRP Quar. Prog. Rep. Oct. 31, 1955*, ORNL-2004, p 124, Fig. 12.4.

[2] G. H. Jenks *et al.*, *HRP Quar. Prog. Rep. July 31, 1957*, ORNL-2379, p 100.

[3] G. H. Jenks *et al.*, *HRP Quar. Prog. Rep. April 30, 1957*, ORNL-2331, p 113.

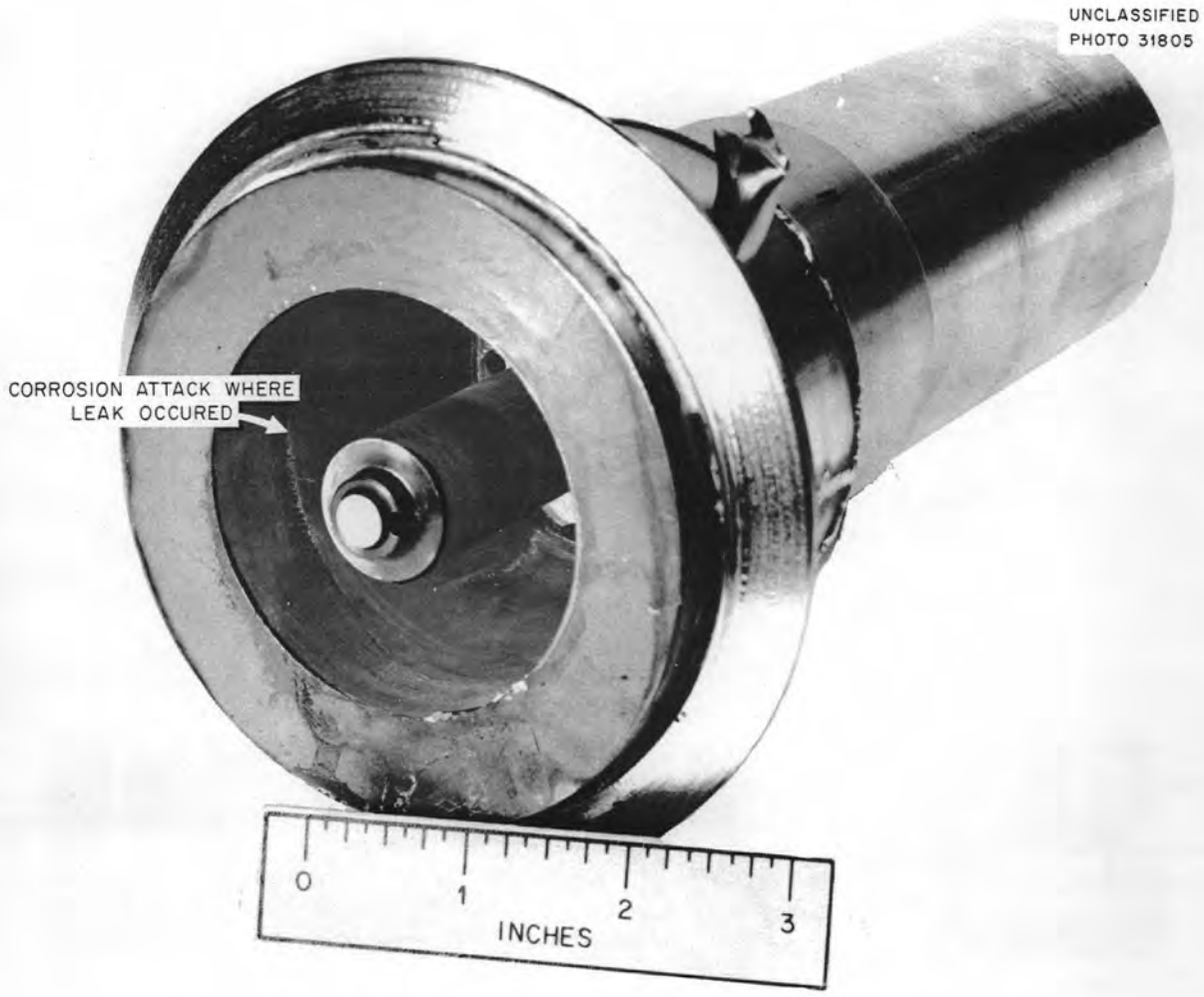

Fig. 14.1. Pump Rotor Housing as Removed from Loop L-2-22.

14.1.2 General Description of In-Pile Loop Experiment L-4-18

With the exception of metallographic examination, stainless steel loop experiment L-4-18 has been completed. This was the fourteenth in-pile loop experiment and the tenth to be irradiated in the HB-4 beam hole at the LITR. This experiment was with a solution of 0.17 *M* UO_2SO_4 in D_2O operating at 235°C in the main stream and 265°C in the pressurizer. Concentrations will be given in terms of molarity at room temperature throughout this report of the L-4-18 experiment.

A set of 24 corrosion coupons, eight each of types 347 and 430L stainless steel and of Zircaloy-2, was installed in the core in a type 347 stainless steel tapered-channel coupon holder. Contained in the core annulus were two assemblies with 15 coupons each, an all-Zircaloy-2 stress-specimen assembly, and a 4-in.-long cobalt-wire flux monitor canned in stainless steel. One annulus coupon holder, fabricated of type 347 stainless steel, contained eight coupons of type 430L stainless steel and seven coupons of type 347 stainless steel. The other holder, fabricated of titanium 75A, contained four coupons each of Zircaloy-2, Zr–15% Nb, and Ti–3% Al, and three coupons of Ti-55A. The Zr–15% Nb alloy was fabricated in the following manner: annealed for 2 hr at 1000°C, water quenched, rolled to 0.090-in. thickness, annealed 2 hr at 900°C, water quenched; sandblasted to remove oxide, pickled to mirror finish, sawed to size, surface-ground to 0.065-in.

UNCLASSIFIED
PHOTO 31752

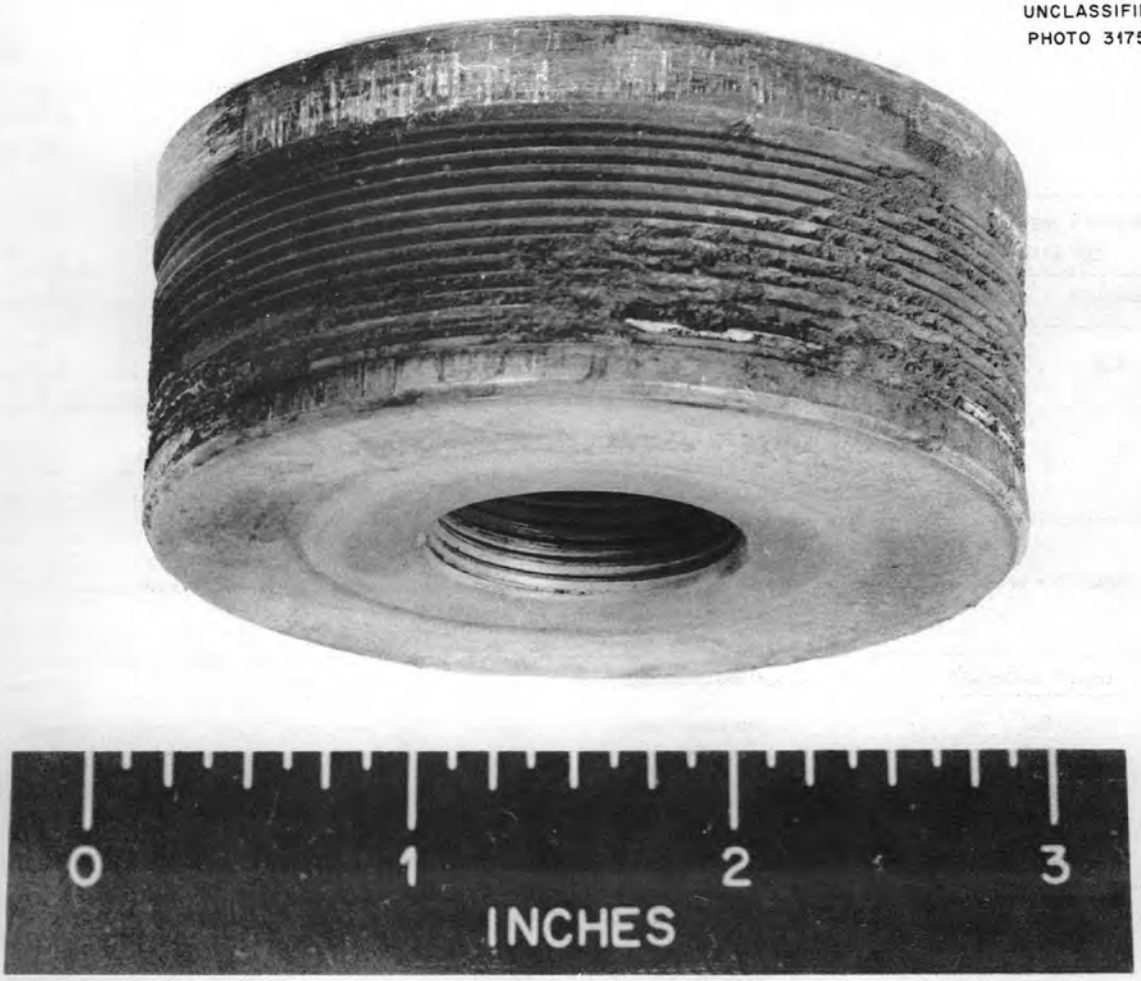

Fig. 14.2. Pump Thermal Shield as Removed from Loop L-2-22.

thickness, and chemically polished to 0.060-in. thickness.

All the above-described specimen arrays, excluding the cobalt monitor, were duplicated in the in-line position.

The structure of the loop was essentially the same as in previous HB-4 experiments. The 5-gpm ORNL pump was of the outboard-bearing design and contained aluminum oxide bearings and journal bushings. The technique of pinning the rear-bearing housing to the rear of the pump housing, and both front and rear bearings to the bearing housings, initiated with L-2-17,[4] was again employed to prevent movement of the aluminum oxide bearings. Setscrews were used as pins.

The loop was operated for short periods with seven different solutions during the out-of-pile tests and pretreatment. A 4.5-hr run with 3% trisodium phosphate solution was made at 95°C, followed by a 24-hr run with a 5% HNO_3 solution at the same temperature. After removal of the acid solution from the loop, three charges of water were circulated at 235°C in the main stream and at 275°C in the pressurizer, for periods of 12, 25, and 5 hr, respectively. Two runs of 107 and 54 hr were made at the test temperatures with identical natural-uranium solutions: 0.17 *M* UO_2SO_4, 0.025 *M* H_2SO_4, and 0.10 *M* $CuSO_4$. The over-all loop corrosion rates during the natural-uranium runs were 3.6 and 0.2 mpy, respectively,

[4]G. H. Jenks *et al.*, *HRP Quar. Prog. Rep. Jan. 31, 1958*, ORNL-2493, p 119.

based on oxygen consumption, and 2.0 and 0.4 mpy, respectively, based on the amount of nickel found in the solutions.

The enriched solution initially charged to the loop for in-pile operation was 0.17 *M* UO_2SO_4, 0.02 *M* H_2SO_4, and 0.07 *M* $CuSO_4$. The makeup solution was essentially the same, with the exception that it was 0.05 *M* in excess H_2SO_4 and contained 100 ppm Cr. The additional acid was included to replace that consumed in corrosion, and the chromium was included to inhibit corrosion of the stainless steel valve stems during solution additions. The enriched-uranium solution was circulated for about 59 hr in the loop before the reactor went to power. The experiment was terminated when the loop pump failed after 860 hr of circulation. The energy output of the LITR during the inserted time was 1926 Mwhr, essentially all of which was at 3-Mw operation.

The failure of the circulating pump appeared similar in nature to the pump failure in L-2-17.[5,6] Resistance measurements of the start and run windings, taken before and after the pump failure, indicated turn-to-turn or winding-to-winding shorts in the run windings. Some circulation was obtained during attempts to rinse the loop with water after the fuel solution had been drained.

The average fission power during operation of the loop at 3 Mw, determined from Cs^{137} analyses, was 694 w. The over-all average total fission and gamma heat, as determined[7] by electric-heater power requirements, was 849 w. The thermal-neutron fluxes to which core specimens were exposed were determined from induced-activity measurements on representative Zircaloy-2 coupons from the core channel and core annulus arrays, and from the cobalt flux monitor. The latter was cut into 12 pieces, each of which was measured. Flux values obtained from the coupons and the monitor were in agreement and indicated the usual axial flux gradient and the absence of a radial gradient in the core. This agreement is in contrast with the results of similar measurements in L-2-17,[8] the only previous experiment to contain a cobalt flux monitor. In L-2-17 the flux

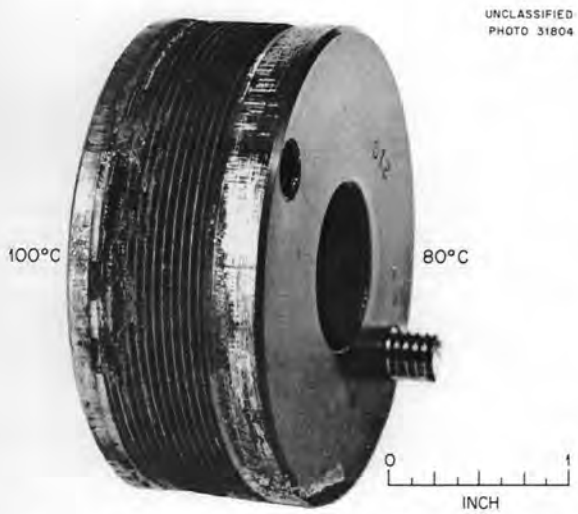

Fig. 14.3. Pump Thermal Shield from Loop L-2-22 (After Scale Removal).

[5]G. H. Jenks *et al.*, *HRP Quar. Prog. Rep. Jan. 31, 1958*, ORNL-2493, p 119.

[6]F. J. Walter, *HRP In-Pile Corrosion Test Loops, Operation of In-Pile Loop L-4-18*, ORNL CF-57-8-113 (Aug. 30, 1957).

[7]F. J. Walter, *HRP In-Pile Corrosion Test Loops, Operation of In-Pile Loop L-4-18*, ORNL CF-57-8-113 (Aug. 30, 1957).

[8]G. H. Jenks *et al.*, *HRP Quar. Prog. Rep. Jan. 31, 1958*, ORNL-2493, p 120.

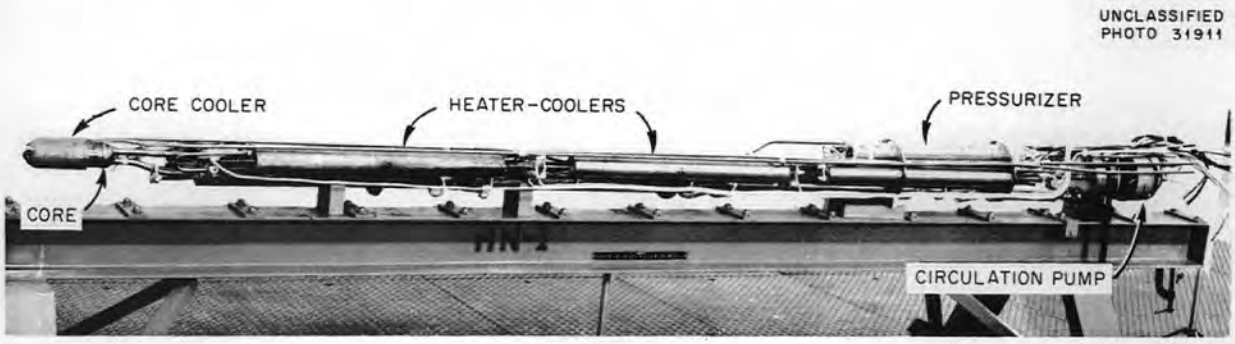

Fig. 14.4. ORR HN-1 Test Loop.

values indicated by the cobalt were about 75% of those obtained from core coupon measurements. The thermal-neutron flux in the core of L-4-18 ranged from 3.7×10^{12} neutrons·cm^{-2}·sec^{-1} at the location of the leading core channel coupon to 7.7×10^{11} neutrons·cm^{-2}·sec^{-1} at the rear coupon. The flux at the core nose, obtained by extrapolation of the data, was 4.8×10^{12} neutrons·cm^{-2}·sec^{-1}. Solution fission power densities at the specimen locations as calculated from the thermal-flux values varied from 5.2 w/ml for the leading core channel coupon to 1.1 w/ml for the rear coupon; the estimated value at the nose of the core was 7.0 w/ml.

The calculated free-acid concentration was maintained reasonably constant throughout the experiment, and there was no evidence of solution instability.

The over-all stainless steel corrosion rate based on oxygen was 0.6 mpy uncorrected for oxygen loss in zirconium and titanium corrosion and 0.5 mpy corrected. The over-all rate based on the nickel in solution was 0.3 mpy.

14.1.3 Qualitative Results of Inspection and Evaluation of Loop L-4-18

The dismantling operations on loop L-4-18 were completed without difficulty. Components removed from the loop included the core, the two in-line sample holders, the pressurizer, two sections of the pressurizer heater, a section of the main loop piping adjacent to the pump outlet, a section of the sampler-line capillary tubing, and the pump.

Before the pump was dismantled, it was noted that the impeller rotated freely and that there was adequate end-play. After the pump was dismantled, examination of the rotor can and of the aluminum oxide bearings and journals showed no evidence of wear. The shaft in the region of the thermal barrier and the thermal barrier itself were also examined. Although no evidence of localized attack was apparent, the appearance of the surface scale in different positions in this region varied markedly. The first three rings of the barrier at the high-temperature end were free from any scale accumulations, while the remainder of the barrier was covered with a dark brown-black scale. The shaft in the same area was covered at the forward end by a thin dark-brown scale. The appearance of the scale changed along the shaft, and in the low-temperature region of the pump the shaft exhibited a light-gray, essentially film-free, surface. The portion of the shaft in the scale-covered barrier region was also covered by a similar band of scale.

The components outside the core region were generally covered with a relatively thin dark-gray to dark brown-black, rustlike scale. The vapor region of the pressurizer was almost free of this scale, particularly at the outlet end. The liquid region of the pressurizer was uniformly covered with a heavy, black, velvetlike scale. The interior surface of the pressurizer is shown in Fig. 14.5. There was no evidence of localized attack on any of the components examined.

All the stainless steel and Zircaloy-2 coupons in the line channel array were covered with the rustlike scale, but the in-line annulus coupons were not. This is the first time that all the components of a stainless steel loop located outside the core area were not uniformly covered by a scale of this type. The type 430L stainless steel in-line annulus coupons were covered with a light-gray scale with an overlay of dark-brown to black scale, while the type 347 stainless steel coupons contained in the same array were covered with a darker gray scale and a similar overlay. The Zircaloy-2 and Zr–15% Nb coupons contained in the second in-line annulus array were covered with dark shiny scales and some dark-brown scale, with the 15% Nb alloy scale being darker and showing some grain patterns. The Ti-55A and Ti–3% Al coupons from the same array were covered with heavy bronze-colored scale and spots of the dark-brown transported scale.

The interior surface of the type 347 stainless steel core body and the type 347 stainless steel coupon holders, spiders, and coupons were covered with a glossy rust-colored scale at the high-flux end of the core. This scale tapered gradually into a thick dull-black scale at the low-flux end. The type 430L stainless steel coupons were similar in appearance to those in the in-line annulus coupon array. The Zircaloy-2 coupons and stress specimens were generally covered with a thin irridescent film which was predominantly gray but with varying amounts of brown flakes of scale retained on the surfaces. The apparent film thickness and amounts of retained scale increased with decreasing flux. The Zr-Nb alloys were covered with a dark scale in a definite grain pattern with some retained flakes of dark-brown

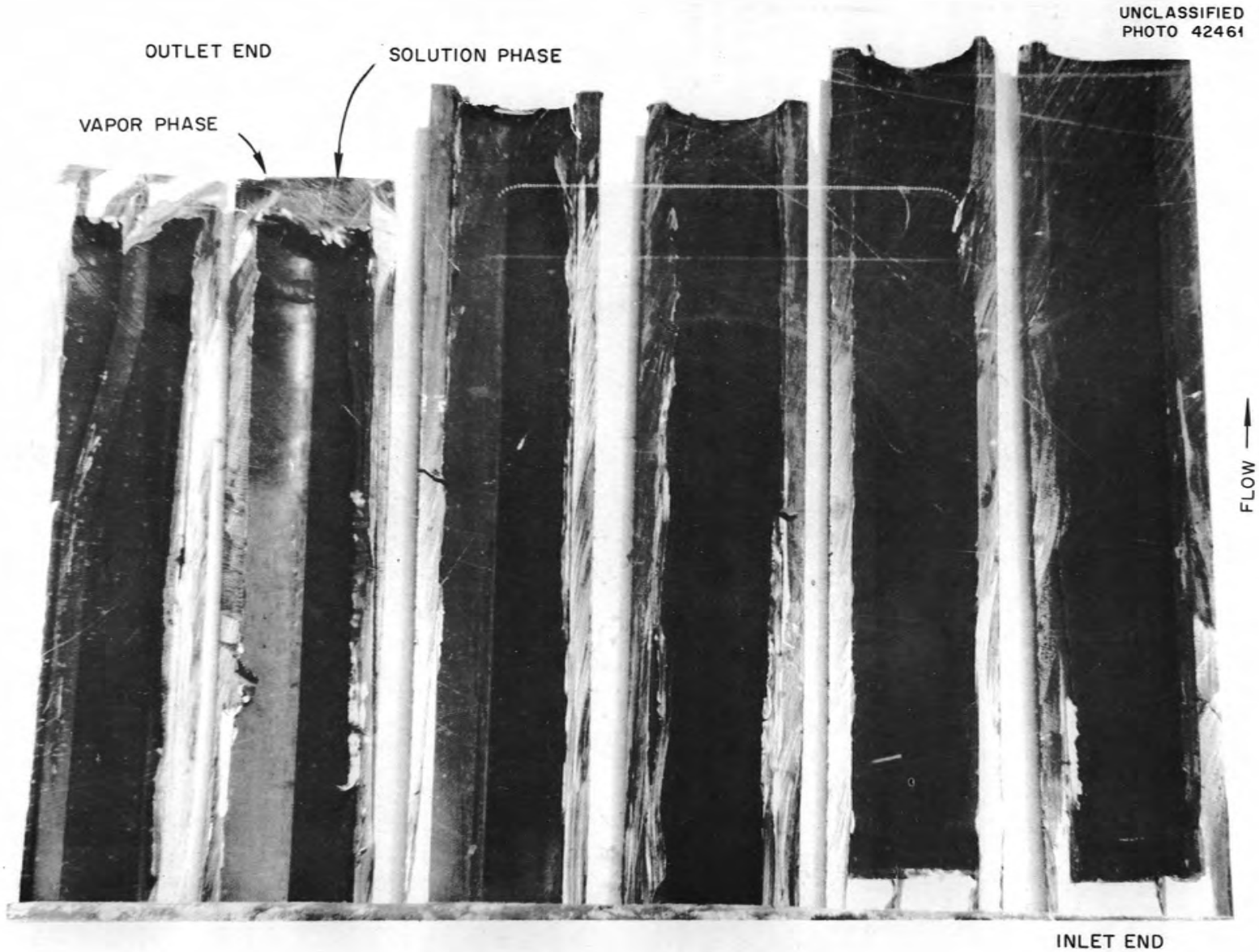

Fig. 14.5. In-Pile Loop L-4-18 Pressurizer.

scale. The Ti-55A coupons were covered with the typical thin bronze-colored film. The Ti-Al alloy coupons also were covered with a shiny bronze film, but all the surfaces had a rough etched appearance.

As with previous loops, repeated attempts to defilm the zirconium and titanium alloys by the standard cathodic defilming technique were only partially effective, and some scale was retained.

Several specimens of each material from the core and in-line coupon arrays, together with the stress specimens and sections cut from the core cap, pressurizer, pressurizer heater, main loop piping, and sampler-line capillary tubing, were sent to the Solid State Division for metallographic examination. A $\frac{3}{8}$-in.-long piece of the sampler-line capillary tubing has been examined at this time. In longitudinal section, the piece exhibited a wide variance in corrosive attack. The area near the loop piping junction showed severe intergranular attack to a depth of about 5 mils. Other areas showed intergranular penetrations of about 1 mil. All surfaces were covered with an oxide scale approximately 2 mils thick.

Samples of the bulk scale scraped from the rear of the core, the in-line annulus holders, the pressurizer, and the pump volute were submitted for chemical analyses. In addition, analyses were performed on solutions resulting from dissolution of the scale from one half of the type 347 stainless steel core coupon holder.

14.1.4 Quantitative Results of Inspection and Evaluation of Loop L-4-18

(a) Analyses of Scale from Low-Power-Density Regions. – (1) *Procedure and Results.* – An attempt was made to determine the distribution of corrosion products and uranium throughout the loop system by chemical analyses of samples of bulk scale removed from surfaces in various portions of the loop. The analytical results are listed in Table 14.1.

A material balance of Fe, Ni, and Zr was attempted by employing these results together with the results of oxygen, nickel, and weight measurements. The average of the samples was assumed to be representative of the average scale in portions of the loop outside the core. The amount of scale in the core was considered negligible. The method of testing the balance in Table 14.2 and the assumptions involved are the same as those previously used for experiments L-4-16[9] and L-2-17,[10] with the exception that a different value was used for the ratio of nickel to iron in the stainless steel. An examination of the certified analyses sheets for the steels used in the various loop components showed that the probable average value of the ratio is 0.19 rather than the previously employed value of 0.15. The steel averages about 12.5% nickel instead of the 10% previously assumed. The specimen material, however, contained about 10% nickel.

(2) *Discussion of Results.* – The analytical results show wide variation in the composition of the scales taken from different loop locations, and the material balance is not considered to be of quantitative significance. Qualitatively, the results indicate a transport of zirconium from the core to the out-of-core locations, and a good balance for the nickel, with more than half of the nickel in the scale.

[9] G. H. Jenks *et al.*, *HRP Quar. Prog. Rep. July 31, 1957*, ORNL-2379, p 110.

[10] G. H. Jenks *et al.*, *HRP Quar. Prog. Rep. Jan. 31, 1958*, ORNL-2493, p 123.

Table 14.1. Analyses of Scale from L-4-18

Source of Scale	Scale Weight (mg)	Scale Composition (wt %)						
		U	Zr	Fe	Ni	Cu	Cs^{137}	*
Rear of core	19.9	0.05	4.5	48.0	7.0	0.78	0	40
In-line annulus holders	17.0	0.06	6.5	20.6	2.1	0.18	0	71
Pump volute	6.5	0.21	13.3	42.7	3.5	9.0	0	31

*Weight per cent of scale not represented by listed constituents.

Table 14.2. L-4-18 Material Balance of Scale Constituents

Element	Mass Ratio of Element to Iron in Scale	Mass Ratio of Element to Iron in Stainless Steel	Element Oxidized During In-Pile Exposure (g)	Element in Scale Based on Iron (g)	Excess of Element in Scale over Amount Calculated from Corrosion Data (g)
Zr	0.22		0.11[a]	0.77	0.66
Ni	0.11	0.19	0.61[b]	0.39	0.01[c]
Fe	(1)	(1)	3.5[b]	(3.5)	(0)

Type 347 Stainless Steel Oxidized During In-Pile Exposure

Basis of Calculation	Amount Oxidized (g)
Oxygen consumption	4.85
Dissolved nickel	1.84[d]

[a]Based on weight-loss data.
[b]Based on oxygen-consumption data.
[c]Nickel in scale plus nickel in solution less nickel oxidized based on oxygen data.
[d]Extrapolated to end of run.

Chromium was also sought in the scale solutions. None was found, but the scale dissolution procedure may have led to the loss by volatilization of chromium as CrO_2Cl_2. It should be noted that the previously reported analyses which show a negligible amount of chromium in scales taken from the L-2-17 loop[11] are subject to a similar qualification. The values for copper in the scales from both the L-4-18 and L-2-17 experiments appear to be higher than is reasonable if the average value for the given loop is assumed to be representative of all the scale in that loop. No evidence for a significant loss of copper from the loop solution was indicated during either experiment.

(*b*) Analyses for Uranium on Steel Surfaces from High-Power-Density Regions. – (1) *Procedure and Results.* – As mentioned above, analyses were performed on solutions containing the scale dissolved from one half of the type 347 core coupon holder. The analyses were carried out primarily to determine the amount of uranium on the steel surfaces. The as-removed holder-half was sectioned into four approximately equal lengths; after being measured and weighed, three were treated separately with a 10% HCl solution and one piece was treated with an HCl plus HNO_3 solution. Visually, the samples appeared clean after this treatment. The solution samples were analyzed for U, Cr, Cu, Ni, Fe, and Zr. The amount of each constituent is listed in Table 14.3 as the percentage by weight of the entire sample. Also shown, in the next-to-last column of the table, is the weight per cent of each scale sample not represented by the reported analyses.

Five to eight micrograms of uranium per square centimeter were found on the steel surfaces, and there was little difference between amounts found at the front and at the rear of the core.

(2) *Discussion of Results.* – As discussed in a previous report,[12] fission fragments originating in sorbed uranium can contribute an appreciable fraction of the total intensity of the fission-fragment irradiation of the wall during exposure. In the case of an annulus specimen from L-2-17, 21 μg of uranium per square centimeter was found on the specimen surface, and it was estimated that the contribution of this uranium to the total of

[11]G. H. Jenks *et al.*, *HRP Quar. Prog. Rep. Jan. 31, 1958*, ORNL-2493, p 124.

[12]G. H. Jenks *et al.*, *HRP Quar. Prog. Rep. Jan. 31, 1958*, ORNL-2493, p 126.

Table 14.3. Analyses for Uranium in Scale from Loop L-4-18 Type 347 Stainless Steel Core Coupon Holder

Location	Total Area* (cm^2)	Sample Weight (mg)	Sample Weight per Unit Area (mg/cm^2)	Amount in Scale (wt %)							Weight of Uranium per Unit Area ($\mu g/cm^2$)
				U	Cr	Cu	Ni	Fe	Zr	Other	
Front	25	31.2	1.2	0.53	0.45	1.34	4.55	55.2	0	37.9	6
Center front	23			125**	106**	0	1017**	9375**	0		5
Center rear	25	360.1	14.4	0.05	0.09	2.72	11.86	55.5	0	29.8	7
Rear	23	27.0	1.2	0.64	0.42	0	4.53	55.5	0	38.9	8

*Total area of half-holder approximately 95 cm^2.

**Sample weight unreliable; results reported as total weight in micrograms.

fission-fragment energy deposited in the wall might have been five times as great as that from the uranium in the 0.04 *m* UO_2SO_4 solution circulated in the loop. In the same manner and with the same assumptions, it can be estimated that the 5–8 μg of uranium per square centimeter of steel surface in the L-4-18 experiment contributed only 0.35 times as much energy to the steel wall as did the uranium in the 0.17 *m* UO_2SO_4 solution. The corrosion data for steel core specimens in this experiment (see Fig. 14.7, Sec *c*-4 below) show that at the highest power densities the rate changes rapidly with changing power density, and a change of a factor of 1.35 in effective power density has an appreciable effect. Below a solution power density of about 3 w/ml, the effect of this increase in power density on the steel corrosion rate would be small.

The significance of the analytical results for constituents other than uranium in these samples is uncertain because unknown amounts of metal may have been dissolved along with the oxides. It is of interest, however, that the ratio of nickel to iron is about the same as the average found in scales taken from out-of-core positions (Table 14.1) and that little chromium was found in the samples. The analytical procedure for chromium in this case probably did not lead to a loss of chromium. It is also of interest that the steel surfaces apparently held no zirconium.

(c) Results of Specimen Weight Measurements and Discussion. – (1) *General.* – Unless otherwise stated, all corrosion-rate values reported below were calculated from weight-loss data, with the exposed specimen area and total radiation time (equivalent to 642 hr of LITR operation at 3 Mw) used as the bases for the calculations. Average solution velocities across the coupons contained in the tapered-channel holders were 9.6 to 42.8 fps. Power-density values were calculated on the bases of the thermal-neutron flux at the coupon location and an energy per fission of 200 Mev. The core channel and core annulus specimens are designated as CC and CA specimens, respectively, and the corresponding in-line specimens as LC and LA, respectively.

(2) *Zircaloy-2.* – The results of weight measurements (presented as corrosion rates) for the Zircaloy-2 core coupons are listed in Table 14.4 and plotted, along with curves representing Zircaloy-2 data obtained in previous loop experiments, in Fig. 14.6. Weight data for the two CA stress specimens are also represented. Each stress specimen was exposed to an average power density of 2.6 w/ml and exhibited an average corrosion rate of 1.3 mpy. The specimens were stressed at room temperature to 17,500 and 20,400 psi, respectively. The rates for the CC coupons and CA coupons and stress specimens are in near agreement.

All specimens from the LC and LA coupon arrays as well as the LC stress specimens exhibited weight gains following the usual defilming

Table 14.4. L-4-18 Core Coupon Corrosion Rates

Core Channel Coupons			Core Annulus Coupons			
Power Density (w/ml)	Average Velocity (fps)	Corrosion Rate (mpy)	Array	Power Density (w/ml)	Approximate Velocity (fps)	Corrosion Rate (mpy)
			Zircaloy-2			
4.86	9.8	1.94	TB-4	4.50	1.0	1.94
4.56	10.6	1.83	TB-4	3.93	1.0	1.59
3.29	19.0	1.59	TB-4	3.44	1.0	1.09
2.69	33.2	1.47	TB-4	3.01	1.0	0.84
2.20	42.8	1.41				
2.06	38.8	0.88				
1.49	14.3	0.52				
1.21	10.4	0.71				
			Type 347 Stainless Steel			
4.26	11.7	0.53	SA-12	4.34	1.0	1.96
4.00	12.9	0.05	SA-12	4.07	1.0	0.14
3.47	16.4	0.43	SA-12	3.93	1.0	0.33
2.86	28.1	0.14	SA-12	3.57	1.0	0
2.34	38.7	0.66	SA-12	3.33	1.0	0
1.70	19.4	0.05	SA-12	3.01	1.0	0.19
1.39	12.8	0.14	SA-12	2.93	1.0	0
1.14	9.6	0.98				
			Type 430L Stainless Steel			
5.16	9.6	5.27	SA-12	4.50	1.0	2.88
3.71	14.3	1.04	SA-12	4.21	1.0	1.36
3.06	22.4	0.65	SA-12	3.83	1.0	0.60
2.50	35.7	0.79	SA-12	3.70	1.0	0.78
1.93	28.9	0.89	SA-12	3.44	1.0	0.90
1.81	23.3	0.75	SA-12	3.26	1.0	0.84
1.59	16.5	0.75	SA-12	3.14	1.0	0.79
1.30	11.5	0.94	SA-12	2.84	1.0	0.75
			Titanium–3% Aluminum			
			TB-4	4.07	1.0	0.51
			TB-4	3.57	1.0	0.51
			TB-4	3.14	1.0	0.60
			TB-4	2.84	1.0	+0.2 mg
			Titanium-55A			
			TB-4	4.21	1.0	0.25
			TB-4	3.70	1.0	0.17
			TB-4	3.26	1.0	0.25

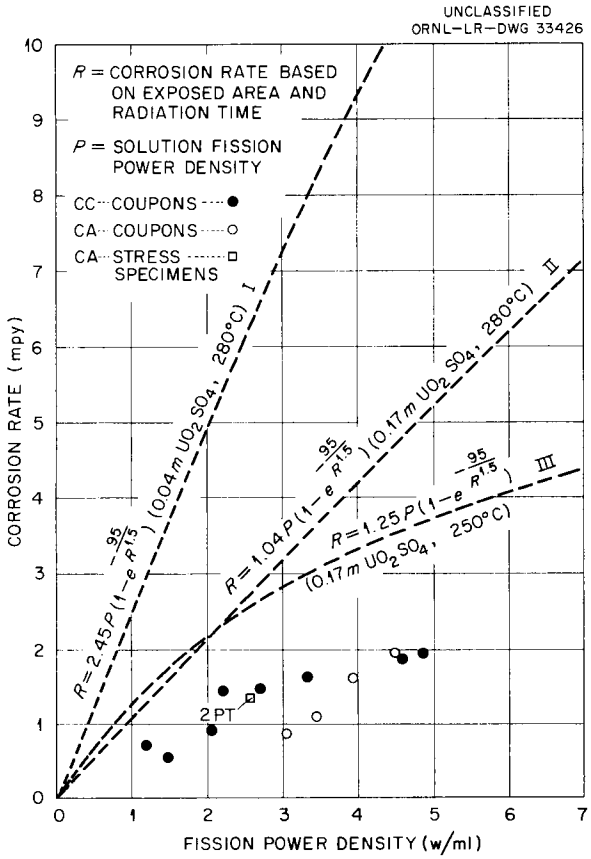

Fig. 14.6. Loop L-4-18 Zircaloy-2 Corrosion Data.

operation. The weight increases averaged 0.9, 0.8, and 0.3 mg/cm^2, respectively.

As illustrated in Fig. 14.6, the corrosion rates observed in this 235°C loop experiment were lower than those observed at 250°C in previous experiments. This decrease in rate with decreasing temperature is in qualitative agreement with the temperature effect noted in autoclave experiments at 250°C and below. However, the autoclave experiments below 250°C have not been operated at conditions which permit a quantitative comparison between loop and autoclave results at this time.

(3) *Zirconium-Niobium Alloy.* – All the Zircaloy-2 and Zr–15% Nb CA coupons were contained in one ladder-type array. As reported above (Sec 14.1.2), the Zr–15% Nb coupons were pickled before installation in the loop. Corrosion rates observed for the Zr–15% Nb and Zircaloy-2 CA coupons are presented in Table 14.5 as the ratios of the observed Zr–15% Nb coupon corrosion

Table 14.5. Ratio of Zr–15% Nb CA Coupon Corrosion Rates to Zircaloy-2 CA Coupon Corrosion Rates at Similar Power Densities

Power Density (w/ml)	Ratio
4.34	0.57
3.83	0.22
3.33	0.56
2.93	0.28

rates to those for Zircaloy-2 at similar power densities. The niobium-alloy specimens exhibited corrosion rates 22 to 57% of those shown by the Zircaloy-2 coupons.

Four coupons each of pickled Zr–15% Nb and Zircaloy-2 contained in one LA coupon array exhibited weight increases, following defilming, of from 0.3 to 0.5 mg/cm^2 and from 0.7 to 0.8 mg/cm^2, respectively.

(4) *Type 347 and 430L Stainless Steels.* – CC and CA specimen results for types 347 and 430L stainless steel are listed in Table 14.4 and are plotted in Fig. 14.7 as the logarithm of the corrosion rate versus the reciprocal of the fission power density in solution. The average corrosion rate for the one half of the type 347 stainless steel channel holder which was defilmed was 1.1 mpy at an average power density of 2.7 w/ml.

In-line specimens of type 347 stainless steel showed either weight gains after defilming or weight losses which correspond to low corrosion rates. All specimens of 430L stainless steel from the LC and LA arrays lost weight as measured after defilming. The average corrosion rates for these specimens were 1 mpy or less, with the exception of one annulus specimen which exhibited a rate of 2.3 mpy. These in-line results are summarized in Table 14.6.

The manner in which the results are plotted in Fig. 14.7 implies that the relationship between corrosion rate and fission power density can be described by an equation of the form

$$R = Ae^{-B/P} ,$$

where R = average corrosion rate, P = fission power density, and A and B are constants. This equation has been employed previously for presenting the steel results from 280 and 300°C loop

experiments[13] and is also used in discussing the L-2-19 results in Sec 14.1.7(*c*). The L-4-18 results plotted in this form are of the same general nature as those obtained at the higher temperatures. Above a rate of about 1 mpy, the points fall on a straight line, and below 1 mpy the rates decrease only slightly with decreasing power density.

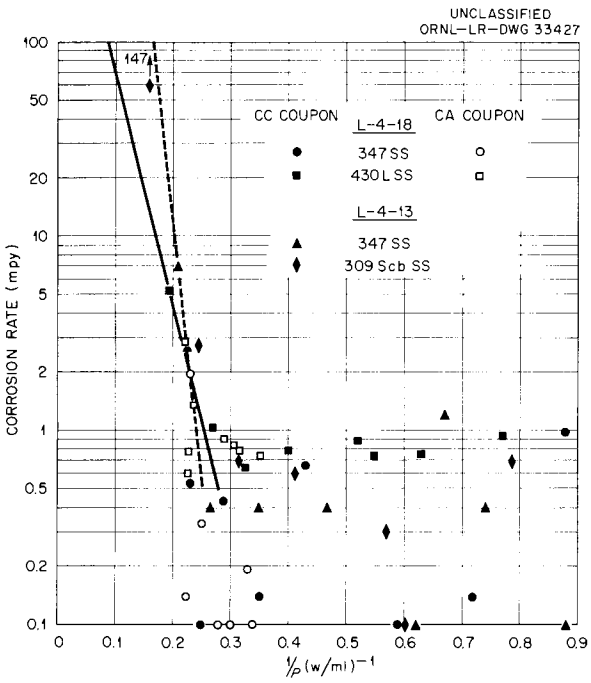

Fig. 14.7. Stainless Steel Corrosion Data for 235 and 250°C Experiments with 0.17 *m* UO_2SO_4 Solutions in D_2O.

For fission power densities above about 4 w/ml, there is no significant difference between the corrosion rates observed for type 347 and 430L specimens, nor between the core and annulus specimens. At power densities below 4 w/ml, the 430L specimens, in general, exhibited rates higher than those for type 347, but below about 1 mpy. It should be noted that this attack of 430L at low power densities in the core did not exceed that of the in-line specimens, which also corroded at average rates of about 1 mpy.

The data obtained on type 347 and 309 SCb stainless steel CC specimens in loop L-4-13,[14] a similar D_2O experiment run at 250°C, are compared with these results in Fig. 14.7. The behavior of type 347 stainless steel at 235°C does not appear to differ appreciably from that demonstrated in the 250°C experiment. However, a type 309 SCb CC specimen in L-4-13, exposed to a power density of 6.3 w/ml, corroded at 147 mpy.

CA specimens of type 347 stainless steel were not employed in experiment L-4-13, but the average rate for half of the steel core channel holder was observed to be in near agreement with that determined for the holder in L-4-18 (0.94 mpy at an average power density of 3.0 w/ml in L-4-13, compared with 1.1 mpy at 2.7 w/ml in L-4-18).

(5) *Titanium-55A.* – The Ti-55A CA coupon corrosion results are listed in Table 14.4. The

[13] G. H. Jenks *et al.*, *HRP Quar. Prog. Rep. Jan. 31, 1958*, ORNL-2493, p 131.

[14] G. H. Jenks *et al.*, *HRP Quar. Prog. Rep. April 30, 1957*, ORNL-2331, p 116.

Table 14.6. Summary of Data for Steel Specimens from In-Line Positions in Loop L-4-18

Stainless Steel Type	Position	Number of Specimens	Velocity (fps)	Corrosion Rate (mpy)
347	LC	3	12.9–28.1	(0.1–0.6 mg)*
		1	9.6	1.2
		4	11.7–38.7	0.05–0.3
	LA	4	~1.0	(0.3–0.5 mg)*
		3	~1.0	0.05–0.1
430L	LC	8	9.6–35.7	0.7–1.1
	LA	8	~1.0	0.8–2.3

*Weight gains.

three LA coupons exhibited weight gains of 0.05 to 0.9 mg/cm^2, as measured after the defilming operation.

(6) *Titanium–3% Al.* – Corrosion rates observed on the Ti–3% Al CA coupons are listed in Table 14.4. Ratios of these rates to those for Ti-55A at similar power densities show that the aluminum alloy corrodes twice as fast as Ti-55A. Both groups of specimens were contained in one ladder coupon array. Two of the four Ti–3% Al LA coupons exhibited weight gains of 0.05 and 0.14 mg/cm^2, as measured after the defilming operation. A third coupon showed no weight change, and the fourth exhibited a weight loss corresponding to a corrosion rate of 0.1 mpy.

14.1.5 General Description of In-Pile Loop Experiment L-2-19

A previous loop experiment, L-2-14,[15] with high concentrations of excess H_2SO_4 and $CuSO_4$ in a 0.17 *m* UO_2SO_4 solution demonstrated a beneficial effect of this combination of additives on the in-pile corrosion of Zircaloy-2. Autoclave experiments with a high concentration of excess H_2SO_4 in a UO_2SO_4 solution in one case[16] and with Li_2SO_4 in a UO_2SO_4 solution in other cases[17] have indicated a beneficial effect on Zircaloy-2 in-pile corrosion for additions of either chemical. The loop experiment to be described here, L-2-19, was designed primarily as a continuation of the studies of the effect of Li_2SO_4 additions.

With the exception of metallographic examination, experiment L-2-19 has been completed. This was the fifteenth in-pile loop experiment and the fifth to be irradiated in the HB-2 beam hole at the LITR.

One set of 24 corrosion coupons in Zircaloy-2 tapered-channel coupon holders was installed in the core, and one set in the in-line position. Each contained an equal number of titanium 110AT, Zircaloy-2, and type 347 stainless steel coupons arranged identically. Holders fabricated of titanium 75A contained five annulus ladder-type coupon arrays. Each array contained eight $\frac{1}{2} \times \frac{1}{2}$ in. scalloped coupons. Three arrays were mounted in the core annulus and two in the in-line position. Of the 40 coupons in the ladder arrays, 14 were stainless steel, 19 were zirconium, 6 were Incoloy, and 1 was TiO_2.

Five stress-specimen assemblies were contained in the loop: two in the core annulus, one in the in-line position, and two in the liquid-phase region of the pressurizer. The specimens were fabricated from titanium 110AT or type 430L stainless steel. The holders, screws, and fulcrums in the stress assemblies that contained steel specimens were fabricated from type 347 stainless steel, and in the assemblies that contained titanium specimens, from MST grade III titanium. The locations of the ladder coupon arrays and stress-specimen assemblies and the types of materials contained in each are given in Table 14.7.

In addition, single $\frac{3}{8} \times \frac{1}{2}$ in. coupons of type 347 stainless steel and Zircaloy-2 and a piece of ZrO_2 rod were mounted in the high-flux end of the core. They were contained in brackets fabricated from 0.010-in.-thick type 347 stainless steel and attached to the forward face of the core spider.

The structure of the stainless steel loop was essentially the same as in previous HB-2 experiments. However, the pressurizer was fabricated from 1.5-in. instead of 1.25-in. sched-80 pipe, resulting in an increase in pressurizer volume from about 550 to 700 ml.

The ORNL 5-gpm pump was of the outboard-bearing design and contained aluminum oxide bearings and journal bushings. The rear bearing housing was pinned to the rear of the pump housing, and both front and rear bearings were pinned to their housings by means of setscrews.

The loop was operated for short periods with seven different solutions during the out-of-pile tests and pretreatment. A 5-hr run with 3% trisodium phosphate solution was made at 95°C, followed by a 19-hr run with a 5% HNO_3 solution at the same temperature. After the acid solution was drained from the loop, water was circulated for 5 hr at temperatures of 280°C in the main stream and 295°C in the pressurizer. Following the H_2O run, a 90-hr run at the same temperatures was made with a natural-uranium solution: 0.04 *m* UO_2SO_4, 0.0075 *m* $CuSO_4$, 0.025 *m* H_2SO_4, and 0.20 *m* Li_2SO_4 (natural). A slight decrease in the concentration of uranium, lithium, copper, and sulfate was noted during the first portion of the

[15] G. H. Jenks *et al.*, *HRP Quar. Prog. Rep. Oct. 31, 1957*, ORNL-2432, p 117.

[16] G. H. Jenks *et al.*, *HRP Quar. Prog. Rep. April 30, 1956*, ORNL-2096, p 92–94.

[17] G. H. Jenks *et al.*, *HRP Quar. Prog. Rep. Oct. 31, 1956*, ORNL-2222, p 100 esp 107–8.

Table 14.7. Alloy Specimens Contained in Experiment L-2-19

I. Alloys Contained in Tapered-Channel Holders

Core

8 – Type 347 stainless steel
8 – Zircaloy-2
8 – Titanium 110AT

In-Line

8 – Type 347 stainless steel
8 – Zircaloy-2
8 – Titanium 110AT

II. Alloys Contained in Ladder Coupon Arrays

Core

Array TB-1

3 – Zircaloy-2
5 – Zircaloy-2 weld[a]

Array TB-2

3 – Type 304L stainless steel (annealed)[b]
2 – Type 304L stainless steel (sensitized)[c]
3 – Type 430L stainless steel

Array TB-3

4 – Incoloy
3 – Crystal-bar zirconium[d]
1 – TiO_2

In-Line

Array TB-4

3 – Crystal-bar zirconium[d]
5 – Zircaloy-2 weld[a]

Array TB-5

2 – Incoloy
2 – Type 304 L stainless steel (annealed)[b]
2 – Type 304L stainless steel (sensitized)[c]
2 – Type 430L stainless steel

III. Alloys Contained in Stress-Specimen Assemblies

Core

2 – Type 430L stainless steel
2 – Type 110AT titanium

In-Line

2 – Type 110AT titanium

Pressurizer

2 – Type 430L stainless steel
2 – Type 110AT titanium

IV. Alloys Located in High-Flux End of Core

1 – Type 347 stainless steel
1 – Zircaloy-2
1 – ZrO_2

[a]Newport News Shipbuilding & Dry Dock Co. scrap weldment.

[b]Annealed 30 min at 1950°F, water quenched.

[c]Sensitized 60 min at 1250°F, air-cooled.

[d]Reactor-grade, arc-melted crystal-bar zirconium. Cold-rolled from 0.130 to 0.075 in.; annealed at 600°C for 15 min, air-cooled; machined and ground to 0.065 in.; samples chemically polished to thickness of 0.060 in.

run. The over-all corrosion rate for the loop, based on oxygen consumption, was 1.7 mpy.

The solution was drained, a 5% HNO_3 solution was charged to the loop, and operation was resumed for an additional 4 hr at 95°C. After removing the acid solution, circulation was resumed with a second natural-uranium solution of the same composition as the original except for an increase in H_2SO_4 to 0.03 *m*. The main-stream and pressurizer temperatures were maintained at 270 and 280°C, respectively, for the first 48 hr of this run, during which time the over-all corrosion rate based on oxygen consumption was 1.8 mpy. The main-stream and pressurizer temperatures were then raised to 280 and 295°C, respectively, and maintained there for the rest of the run. During the next 53 hr of circulation the over-all corrosion rate based on oxygen was computed to be 1.6 mpy. The concentrations of uranium, copper, lithium, and sulfate decreased during both periods of operation with the second uranium solution. Before continuing, the H_2SO_4 was adjusted to 0.06 *m*. An immediate increase in copper, uranium, lithium, and sulfate in solution was noticed. Circulation was then continued for an additional 45 hr, during which time the over-all corrosion rate based on oxygen was 0.6 mpy. Corrosion rates based on nickel in solution were

all less than 0.1 mpy. After the uranium solution was drained from the loop, a 5% HNO_3 solution was circulated for 4 hr at 95°C.

The enriched-uranium solution initially charged to the loop for in-pile operation was 0.17 *m* UO_2SO_4, 0.02 *m* $CuSO_4$, 0.10 *m* H_2SO_4, and 0.20 *m* Li_2SO_4 (99.9% Li^7). Two makeup solutions, similar to the original but containing 0.12 and 0.195 *m* excess H_2SO_4, respectively, and 100 ppm Cr, were used to replace solution withdrawn as samples. The main-stream and pressurizer temperatures during the in-pile run were 280 and 295°C, respectively. Enriched solution was circulated for approximately 93 hr in the loop before radiation was initiated, and samples of solution during this operation indicated that the solution was stable. The in-pile experiment was terminated when the loop pump failed after 1149 hr of circulation. The energy output of the LITR during the inserted time was 2705 Mwhr, essentially all at the 3-Mw level.

Electrical measurements made on the pump windings and power supply indicated turn-to-turn or winding-to-winding shorts in the run windings.[18]

The average fission power density during operation of the loop at 3 Mw, determined from Cs^{137} analyses, was 1959 w. The over-all average total fission and gamma heat at 3 Mw, determined by electric-heater power requirements, was 2558 w.[18]

The thermal-neutron fluxes to which core specimens were exposed were determined from induced-activity measurements on representative Zircaloy-2 coupons from the core channel and from one core annulus coupon array. The determinations indicated the usual axial but no radial flux gradient in the experiment. The flux values determined ranged from 1.5×10^{13} neutrons·cm^{-2}·sec^{-1} at the location of the leading core channel coupon to 3.2×10^{12} neutrons·cm^{-2}·sec^{-1} at the rear coupon. The flux at the core nose, obtained by extrapolation of the coupon data, was 2.0×10^{13} neutrons·cm^{-2}·sec^{-1}. The flux at the stainless steel and Zircaloy-2 coupons and at the ZrO_2 specimen located in a bracket at the high-flux end of the core was similarly estimated to be 1.7×10^{13}, 1.7×10^{13}, and 1.6×10^{13} neutrons·cm^{-2}·sec^{-1}, respectively.

Thermal-neutron flux levels in the core were measured also by means of a cobalt-aluminum flux monitor which was encased in type 347 stainless steel. The values determined in this manner, 1.7×10^{13} neutrons·cm^{-2}·sec^{-1} at the core nose and 2.8×10^{12} neutrons·cm^{-2}·sec^{-1} at the location of the rear channel coupon, were only about 87% of those obtained by analyses of the zirconium specimens. It is interesting to note that in L-2-17, the one previous HB-2 loop experiment to contain a cobalt flux monitor, flux values determined from cobalt were only 75% of those obtained by analyses of Zircaloy-2 core coupons. In the case of L-4-18, an HB-4 experiment, and the only other experiment to contain a cobalt monitor, flux levels were in agreement with values obtained from the Zircaloy-2 core specimens. Agreement in flux values obtained from analyses of Zircaloy-2 core channel and core annulus coupons indicated no radial flux gradient for any of the three loops.

The flux values determined from Zr^{95}-Nb^{95} measurements were employed in solution fission-power-density calculations for experiment L-2-19. The power density at a given position was corrected to include the estimated power density associated with fast-neutron moderation. The corrected power densities ranged from 20.6 w/ml for the leading core channel coupon to 4.4 w/ml for the rear coupon. These included estimated contributions from fast-neutron moderation of 0.5 and 0.1 w/ml, respectively. Estimated solution power densities were 27.4 w/ml at the nose of the core, 22.7 w/ml at the stainless steel and Zircaloy-2 core nose coupons, and 21.9 w/ml at the ZrO_2 core nose specimen.

The calculated free-acid concentration was maintained reasonably constant throughout the run at about 0.1 *m*. The corrected over-all stainless steel corrosion rate was 1.3 mpy based on oxygen consumption and 0.7 mpy based on the nickel in solution.

14.1.6 Qualitative Results of Inspection and Evaluation of Loop L-2-19

The dismantling operations on loop L-2-19 were completed without difficulty. Components removed from the loop included the core, the two in-line sample holders, the pressurizer, two sections of the pressurizer heater, a section of the main loop piping adjacent to the pump, the pump,

[18] R. A. Lorenz, *HRP In-Pile Corrosion Test Loops, Operation of In-Pile Loop L-2-19*, ORNL CF-58-6-74 (June 19, 1958).

and a section of the capillary line leading from the loop to the sampling system.

The pump from this loop was completely dismantled and examined. Before dismantling there was evidence of adequate end-play, and the impeller rotated freely. After disassembly the thrust face of the rear aluminum oxide journal was found to be broken into several large and many small pieces. Examination of the stainless steel rear-bearing housing showed a few scratches, but there was no evidence of rubbing on the rear of the impeller, the pump volute, or the front of the thermal spacer. Although inconclusive, the evidence indicates that the journal was probably broken sometime during the disassembly operation. There was no evidence of damage to the other bearing surfaces or the rotor can.

As shown in Fig. 14.8, considerable corrosive attack had occurred on the thermal barrier and on the pump shaft in the region of the barrier. On the basis of an estimate of the temperature distribution across the thermal barrier as shown in Fig. 14.9, the most severely attacked area on the thermal barrier was in the temperature region 190 to 210°C. The shaft in this region also showed evidence of attack. In a narrow region corresponding to the 200°C location (Fig. 14.8), the shaft diameter was reduced from an original 0.867 in. to at least the minimum measured diameter of 0.828 in. The actual deepest penetration was probably greater than the indicated 0.02 in. Sections of the thermal spacer and the shaft have been submitted for metallographic examination.

All components and specimens outside the core region were generally covered with a relatively thin reddish-brown rustlike scale except for the vapor region of the pressurizer wall, which was covered with a very thin film ranging in color from a metallic blue-gray at the inlet to a dark gray-black at the outlet. There was no appreciable scale accumulation at the pressurizer interface region.

The interior surface of the type 347 stainless steel core body was covered with a glossy reddish-brown film, which retained a dark rustlike scale deposit increasing in abundance from the high- to the low-flux end of the core. The appearance

UNCLASSIFIED
PHOTO 43006

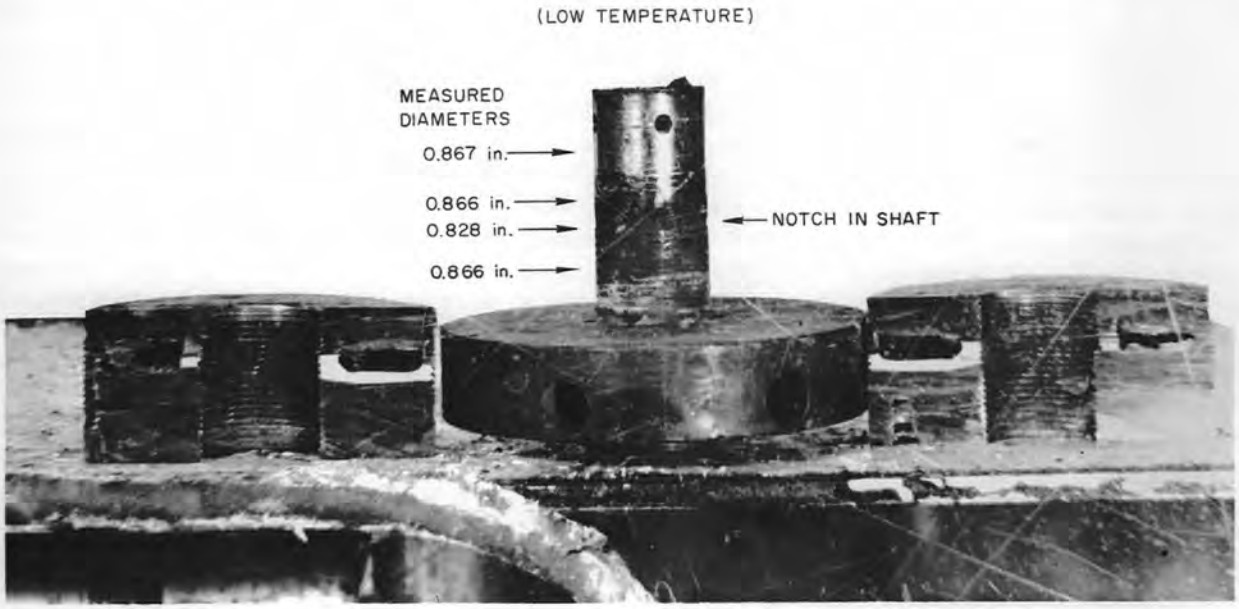

Fig. 14.8. In-Pile Loop L-2-19 Pump Sections.

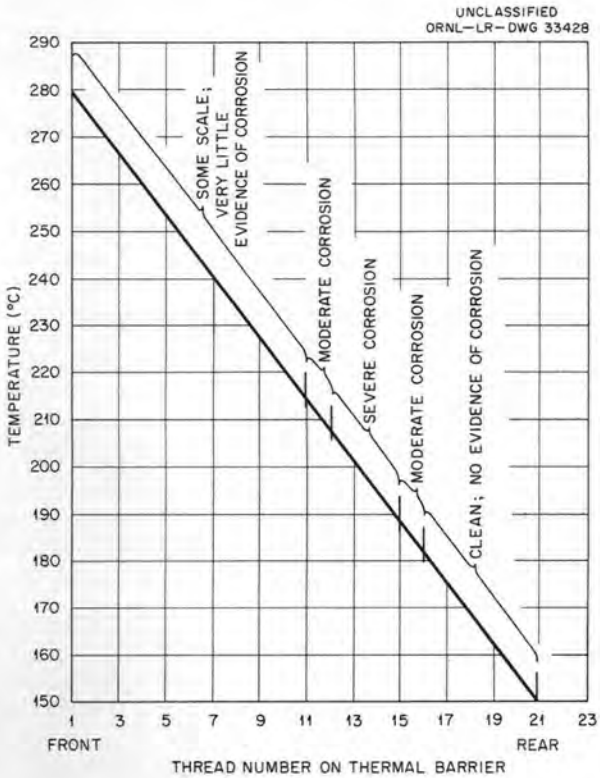

Fig. 14.9. Estimated Temperature Plot Across the Pump Thermal Barrier, Loop L-2-19, and Descriptions of Corrosive Attack at Several Positions.

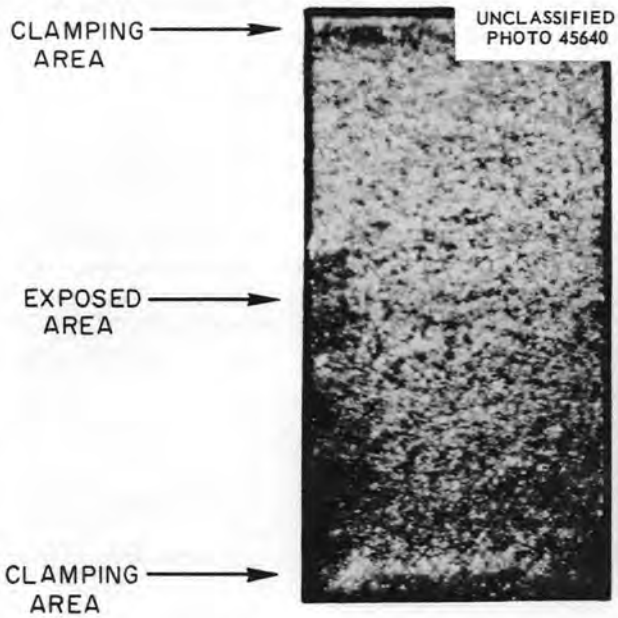

Fig. 14.10. Type 347 Stainless Steel Coupon from Position 4 of the Core Channel Array from Loop L-2-19.

of the type 347 stainless steel coupons, bands, and spiders was similar to that of the core walls.

There was no evidence of attack on the interior core-body wall; however, the type 347 stainless steel coupon located in the core nose, as well as the steel coupons from the higher flux region of the core channel array, was severely pitted. The attack was concentrated in, but not limited to, the exposed surfaces. Figure 14.10 is a photograph of the type 347 stainless steel coupon from position 4 of the core channel array. One peculiarity of the pits on these specimens was the smooth craterlike conformation of the individual pits.

The type 430L and 304L stainless steel coupons and type 430L stress specimens in the core annulus array were covered with a dull reddish-brown film which increased in thickness with decreasing flux. The coupon surfaces were roughened, but there was no distinct pitting attack. The type 430L stress specimens located in the core annulus and in the pressurizer liquid region showed distinct localized attack on the crevice regions. Similar specimens from the line annulus positions were free of this kind of attack. Incoloy coupons from the core annulus array also were covered with the reddish-brown deposit. The surfaces of these coupons were etched and pitted in the manner usually observed on type 347 stainless steel coupons exposed to irradiation in previous experiments; shallow pits had spread laterally to give a fairly uniform attack.[19]

Surfaces of the Zircaloy-2 core channel and annulus coupons and of the channel holders were roughened and covered with the typical shiny gray film. The degree of roughness decreased and the film thickness appeared to increase with decreasing flux. The core holder also retained some transported iron oxide scale at the low-flux end and in areas under the stainless steel clamping bands. The welded Zircaloy-2 and the crystal-bar zirconium coupons from the core annulus arrays were covered with gray films and exhibited grain patterns with interference colors. The zirconium oxide core nose specimen was completely gone at the time of disassembly.

[19] G. H. Jenks *et al.*, *HRP Quar. Prog. Rep. July 31, 1957*, ORNL-2379, p 110.

All the titanium core specimens, including the core annulus stress specimens and the annulus coupon holders of this material, were covered with the typical bronze-colored film. Some accumulation of iron oxide was observed in the lower flux regions. The stress specimens showed some evidence of very small pits and possibly cracks. The one TiO_2 coupon was covered with a whitish-bronze scale. After defilming, the specimen exhibited a light-tan color and small surface pits.

As with previous loops, repeated attempts to defilm the zirconium and titanium in-line specimens by the standard cathodic defilming technique were only partially effective, and some scale was retained. The stainless steel coupons from these locations could not be completely defilmed either, some spots of scale being retained.

14.1.7 Quantitative Results of Inspection and Evaluation of Loop L-2-19

(a) Analyses of Scale from Low-Power-Density Regions. – (1) *Procedure and Results.* – Chemical analyses were made of samples of bulk scale removed from the rear core wall, the in-line channel and annulus coupon holders, the liquid- and vapor-phase areas of the pressurizer, and the pump volute. The samples were analyzed for U, Cu, Ni, Fe, and Zr. Amounts of each constituent are listed in Table 14.8 as percentages by weight of the entire sample. The weight per cent of each scale sample not represented by the reported analyses is shown in the final column. An analysis for chromium was attempted, but the results are considered unreliable.

A material balance of Fe, Ni, and Zr was attempted for this experiment by combining these analyses with those of oxygen, nickel, and specimen-weight measurements and by employing assumptions previously described.[20] The results are presented in Table 14.9.

(2) *Discussion of Results.* – Bulk-scale analyses from the present loop, in line with previous results,[20–22] show wide variations in scale composition from different parts of the loop, and the results of the material balance are not considered to be of quantitative significance. Qualitatively, the results indicate that only a small part of the zirconium which was oxidized in the core (and the ZrO_2 from the ZrO_2 specimen) is accounted for in the scale contained in regions outside the core. This is in contrast to the results of previously attempted material balances, which have indicated complete transfer of ZrO_2. Little nickel was found in the scales, again in contrast with the results obtained in previous loops. Compared in Table 14.10 are the average analytical values for the constituents found in bulk-scale samples from the various loops for which analyses are available. Values for the mass ratio of a given element to iron are also listed. The amount of nickel found in solution in L-2-19 is in near agreement with the amount predicted on the assumption that (1) the value obtained from oxygen data for the amount of steel oxidized is valid, (2) no selective oxidation of the stainless steel

[20] G. H. Jenks *et al.*, *HRP Quar. Prog. Rep. July 31, 1957*, ORNL-2379, p 105.

[21] G. H. Jenks *et al.*, *HRP Quar. Prog. Rep. Jan. 31, 1958*, ORNL-2493, p 123.

[22] G. H. Jenks *et al.*, sec 14.1.4.1 (this report).

Table 14.8. Chemical Analysis of Bulk Scale from In-Pile Loop L-2-19

Sample No.	Location	Scale Weight (mg)	Scale Composition (wt %)					
			U	Cu	Ni	Fe	Zr	*
S-1	Rear of core	18.1	0.07	0	0	18.0	2.2	80
S-2	In-line channel holder	13.0	0.02	0	1.6	14.8	5.0	79
S-3	Pressurizer liquid	57.5	0.03	0.2	0	23.9	2.3	74
S-4	Pressurizer vapor	57.3	0.01	0	0.8	11.1	1.4	87
S-5	Pump volute	15.8	0.05	0.8	0	38.0	0.8	60
S-6	In-line annulus holder	63.3	0.02	0	0	25.7	1.3	73

*Weight per cent of scale not represented by listed constituents.

Table 14.9. L-2-19 Material Balance of Scale Constituents

Element	Mass Ratio of Element to Iron in Scale	Mass Ratio of Element to Iron in Type 347 SS	Element Oxidized During In-Pile Exposure (g)	Element in Scale Based on Iron (g)	Excess of Element in Scale over Amount Calculated from Corrosion Data (g)
Zr	0.10		2.23[a]	0.44	−1.79
Ni	0.02	0.19	0.78[b]	0.09	0.14[c]
Fe	(1)	(1)	4.1[b]	(4.1)	(0)

Type 347 Stainless Steel Oxidized During In-Pile Exposure

Basis of Calculation	Amount Oxidized (g)
Oxygen consumption	6.21[d]
Dissolved nickel	6.65[e]

[a]Based on weight-loss data of all zirconium in core plus ZrO_2 specimen (0.53 g).
[b]Based on oxygen-consumption data.
[c]Nickel in solution plus nickel in scale less nickel oxidized based on oxygen data.
[d]Corrected for O_2 consumed by Zr, Ti, Incoloy, and 430L SS.
[e]Extrapolated to end of run and corrected for 0.07 g of nickel from Incoloy.

Table 14.10. Comparison of Bulk-Scale Analyses from Several Loop Experiments

Experiment No.	Per Cent Scale Represented by Constituents	Amount of Constituent in Scale (wt %) and Mass Ratio of Element to Iron in Scale										
		Fe	U	U/Fe	Zr	Zr/Fe	Ni	Ni/Fe	Cr	Cr/Fe	Cu	Cu/Fe
L-4-16	63.9	42.8	0.07	0.002	8.5	0.20	6.7	0.16	5.8	0.14	0.06	0.001
L-2-17	53.8	25.3	0.20	0.04	8.3	0.37	8.4	0.33			4.4	0.17
L-4-18	52.7	37.1	0.11	0.03	8.1	0.22	3.2	0.09			3.3	0.09
L-2-19	25.0	21.9	0.03	0.001	2.2	0.10	0.40	0.02			0.17	0.01

constituents occurred, and (3) all the nickel which was oxidized entered solution.

(*b*) Analyses for Uranium in Scale from Surfaces of Zirconium Alloys Exposed in Loop L-2-19 Core. – (1) *Procedure and Results.* – The surfaces of four core zirconium corrosion specimens in experiment L-2-19 were analyzed for uranium by using the procedure followed with loop L-2-17.[23] Two of the specimens were Zircaloy-2 channel coupons, ZB-48 and ZB-71, exposed at solution power densities of 10.6 and 5.8 w/ml and solution velocities of 32.6 and 14.1 fps, respectively. The other two were annulus coupons – one a zirconium weld, ZNN-4, and the other of crystal-bar zirconium, ZZ-3. They were exposed at solution power densities of 8.8 and 10.0 w/ml, respectively, and at a solution velocity of about 1 fps. The results of the analyses, given in Table 14.11, are expressed in a form used previously for loop L-2-17.

(2) *Discussion of Results.* – The analytical results indicate that very little uranium was

[23]G. H. Jenks *et al.*, *HRP Quar. Prog. Rep. Jan. 31, 1958*, ORNL-2493, p 124.

Table 14.11. Scale Analyses for L-2-19 Core Specimens

Specimen			Weight Dissolved (mg)	Analyses			
Material	Number	Type*		Element	Element in Sample (%)	Total Element in Scale (μg)	Element in Scale (μg/cm^2)
Zircaloy-2	ZB-48	CC	25.8	U	0.0	0	0.0
				Ni	0.11	12**	5.5**
				Cu	0.08	21	9.5
				Cr	0.54	121**	55.0**
				Fe	0.21	32**	14.5**
				Zr	71.20		
	ZB-71	CC	16.5	U	0.006	1	0.5
				Ni	0.43	70**	31.8**
				Cu	0.18	30	13.6
				Cr	0.0	0	0.0
				Fe	0.42	68**	30.9**
				Zr	1.91		
Zircaloy-2 weld	ZNN-4	CA	60.8	U	0.0	0	0.0
				Ni	0.05	8**	3.6**
				Cu	0.04	23	10.5
				Cr	0.0	0	0.0
				Fe	0.16	44**	20.0**
				Zr	73.13		
Crystal-bar zirconium	ZZ-3	CA	32.1	U	0.002	0.6	0.3
				Ni	0.0	0	0.0
				Cu	0.37	119	54.0
				Cr	0.0	0	0.0
				Fe	0.17	55	25
				Zr	68.64		

*CC, core channel coupon; CA, core annulus coupon.

**Corrected for amount of element in Zircaloy-2.

sorbed on Zircaloy-2 surfaces in the core in this experiment. The largest amount, 0.5 μg/cm^2, is a factor of 10 less than the amount found on the channel specimen and a factor of 40 less than that found on the annulus specimen in the 0.04 *m* UO_2SO_4 experiment, L-2-17.[24]

(c) Results of Specimen Weight Measurements and Discussion. – (1) *General.* – Unless otherwise stated, all corrosion-rate values reported below were calculated from weight-loss data, with the exposed specimen area and total radiation time (equivalent to 902 hr of LITR operation at 3 Mw) used as the bases for the calculations. Average solution velocities across the coupons contained in the tapered-channel holders were from 8.8 to 42.0 fps. Solution velocity across the ladder coupon arrays was estimated at 1 fps. Power-density values for the core specimens are based on flux values determined from the induced activity in zirconium and include the estimated fast-neutron contribution at the specimen positions. The core channel and core annulus specimens are designated as CC and CA, respectively, and the corresponding in-line specimens as LC and LA. The pressurizer specimens are designated as P.

(2) *Zircaloy-2, Zircaloy-2 Weld, and Crystal-Bar Zirconium.* – Weight data for the core specimens,

[24] G. H. Jenks *et al.*, *HRP Quar. Prog. Rep. Jan. 31, 1958*, ORNL-2493, p 125.

expressed as corrosion rates, are listed in Table 14.12 and plotted in Fig. 14.11. For comparison, the L-2-14[25] results are also shown in Fig. 14.11. The L-2-14 experiment and the present loop were both operated at 280°C with 0.17 *m* UO_2SO_4 in light-water solutions. The solution in L-2-14 was 0.4 *m* H_2SO_4 and 0.15 *m* in $CuSO_4$; that in the present loop was 0.1 *m* in H_2SO_4 and 0.2 *m* in Li_2SO_4.

[25]G. H. Jenks *et al.*, *HRP Quar. Prog. Rep. Oct. 31, 1957*, ORNL-2432, p 115.

Table 14.12. L-2-19 Core Coupon Corrosion Rates

Core Channel Coupons			Core Annulus Coupons			
Power Density (w/ml)	Velocity (fps)	Corrosion Rate (mpy)	Array	Power Density (w/ml)	Velocity (fps)	Corrosion Rate (mpy)
			Zircaloy-2			
19.4	9.5	10.8	TB-1	15.1	1.0	5.8
17.9	10.4	10.2	TB-1	10.0	1.0	4.4
16.6	18.6	7.8	TB-1	6.7	1.0	2.8
10.6	32.6	Film analysis	TB-1	17.3	1.0	6.3*
8.7	42.0	5.4	TB-1	13.2	1.0	5.3*
8.1	38.0	5.0	TB-1	11.5	1.0	4.8*
5.8	14.1	Film analysis	TB-1	8.8	1.0	Film analysis*
4.8	10.1	2.9	TB-1	7.7	1.0	3.3*
			**	22.7		14.1
			Crystal-Bar Zirconium			
			TB-3	17.3	1.0	5.8
			TB-3	13.2	1.0	4.8
			TB-3	10.0	1.0	Film analysis
			Type 347 Stainless Steel			
16.7	11.4	35.0	**	22.7	1.0	30.5
15.9	12.6	31.9				
13.8	16.0	29.2				
11.3	27.5	24.1				
9.4	38.0	14.3				
6.6	19.0	3.4				
5.4	12.5	1.4				
4.4	9.4	0.58				
			Titanium 110AT			
20.6	8.8	1.8	***	11.0	1.0	1.2
14.9	13.5	1.9	***	11.0	1.0	1.2
12.1	21.8	1.8				
9.9	35.0	1.5				
7.6	28.4	1.1				
7.1	45.7	1.2				
6.2	16.2	1.1				
5.1	11.2	0.87				

*Zircaloy-2 weld specimens.

**Core nose coupon.

***Stress specimen (stressed by hand beyond yield point).

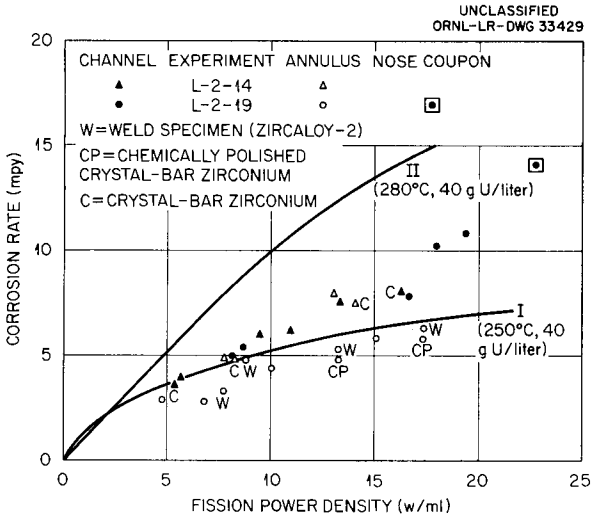

Fig. 14.11. Corrosion of Zirconium and Zircaloy-2 in Loops L-2-19 and L-2-14 Based upon Exposed Specimen Area.

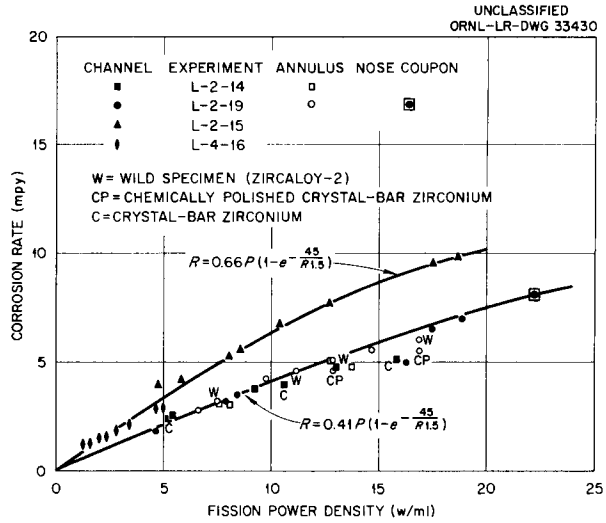

Fig. 14.12. Corrosion of Zirconium and Zircaloy-2 in L-2-19 and Other Experiments Based upon Total Specimen Area and Radiation Time.

With the exception of one crystal-bar zirconium coupon, all specimens from the in-line positions, after defilming by the usual technique, exhibited weight gains. The eight LC Zircaloy-2 coupons showed weight increases which varied from 1.5 to 3.0 mg/cm^2 and averaged 2.0 mg/cm^2. The five Zircaloy-2 weld-specimen LA coupons showed weight increases which ranged from 1.9 to 3.8 mg/cm^2 and averaged 2.9 mg/cm^2. Two of the three crystal-bar zirconium LA specimens showed weight increases of 2.4 and 2.8 mg/cm^2; the third specimen exhibited a weight loss corresponding to a corrosion rate of 1.0 mpy.

The CA specimens employed in experiment L-2-19 were of a new scalloped design[26] for which the total-to-exposed-area ratio is 1.07; the CC coupons were of the usual type, with a ratio of 1.57. As shown in Fig. 14.11, the rates based on exposed specimen area are greater for the CC than for the CA coupons. However, when total specimen area is employed in the rate calculation, the values for the differently located specimens are in near agreement, as shown in Fig. 14.12. There is no reason, from the results to date, to expect an adverse effect of velocity on the corrosion of Zircaloy-2. A beneficial effect has been noted in all previous 280 and 300°C experiments with the exception of L-2-14, but as previously discussed, this beneficial effect appears to be correlated with the surface sorption of less uranium at high velocities.[27] The analytical results for L-2-19 indicate an insignificant sorption of uranium on Zircaloy-2 exposed in either the CA or CC positions. From these considerations and from the observation of close agreement of the rates based on total area, it appears likely that all portions of a given Zircaloy-2 and zirconium specimen in this experiment were attacked at about the same rate.

As computed on the basis of total area, the rates for core specimens in L-2-19 are in near agreement with those in L-2-14, and are significantly less than the rates for CC specimens in the other 280°C experiments with 0.17 *m* UO_2SO_4 solutions but with low concentrations of other solute additives (L-4-16 and L-2-15). Various experiments have indicated that uranium is sorbed on Zircaloy-2 surfaces exposed in UO_2SO_4 solutions with low concentrations of solute additives, and as discussed previously, this sorbed uranium may be responsible for a large fraction of the total intensity of radiation at a surface. The indicated absence of surface uranium from the L-2-19

[26] G. H. Jenks *et al.*, *HRP Quar. Prog. Rep. July 31, 1957*, ORNL-2379, p 115.

[27] G. H. Jenks *et al.*, *HRP Quar. Prog. Rep. Oct. 31, 1957*, ORNL-2432, p 118.

specimens leads to the conclusion that the beneficial effect of the combination of Li_2SO_4 and H_2SO_4 additives is, in part at least, due to inhibition of uranium sorption by the additives. It also appears likely that the combination of H_2SO_4 and $CuSO_4$ additives in experiment L-2-14 acted to benefit the corrosion behavior in the same manner.

Average corrosion rates for the Zircaloy-2 weld specimens are in near agreement with those for the as-machined Zircaloy-2. The chemically polished crystal-bar zirconium specimens exhibited somewhat lower rates than those for as-machined Zircaloy-2. A similar difference between as-machined and pickled Zircaloy-2 specimens has been noted in autoclave experiments.[28]

(3) *Stainless Steel.* – Results for core channel and core nose specimens of type 347 stainless steel are listed in Table 14.12 and plotted in Fig. 14.13, where core channel data from all previous 280 and 300°C loop experiments are included for comparison. Core annulus data for the stainless steel (304L, 430L, and 347) and for the Incoloy specimens are plotted in Fig. 14.14. For comparison, data are also plotted for CA steel specimens in the other experiment, L-2-17,[29] which contained several different steel

[28] G. H. Jenks *et al.*, *HRP Quar. Prog. Rep. Oct. 31, 1956*, ORNL-2222, p 107–11.

[29] G. H. Jenks *et al.*, *HRP Quar. Prog. Rep. Jan. 31, 1958*, ORNL-2493, p 128–32.

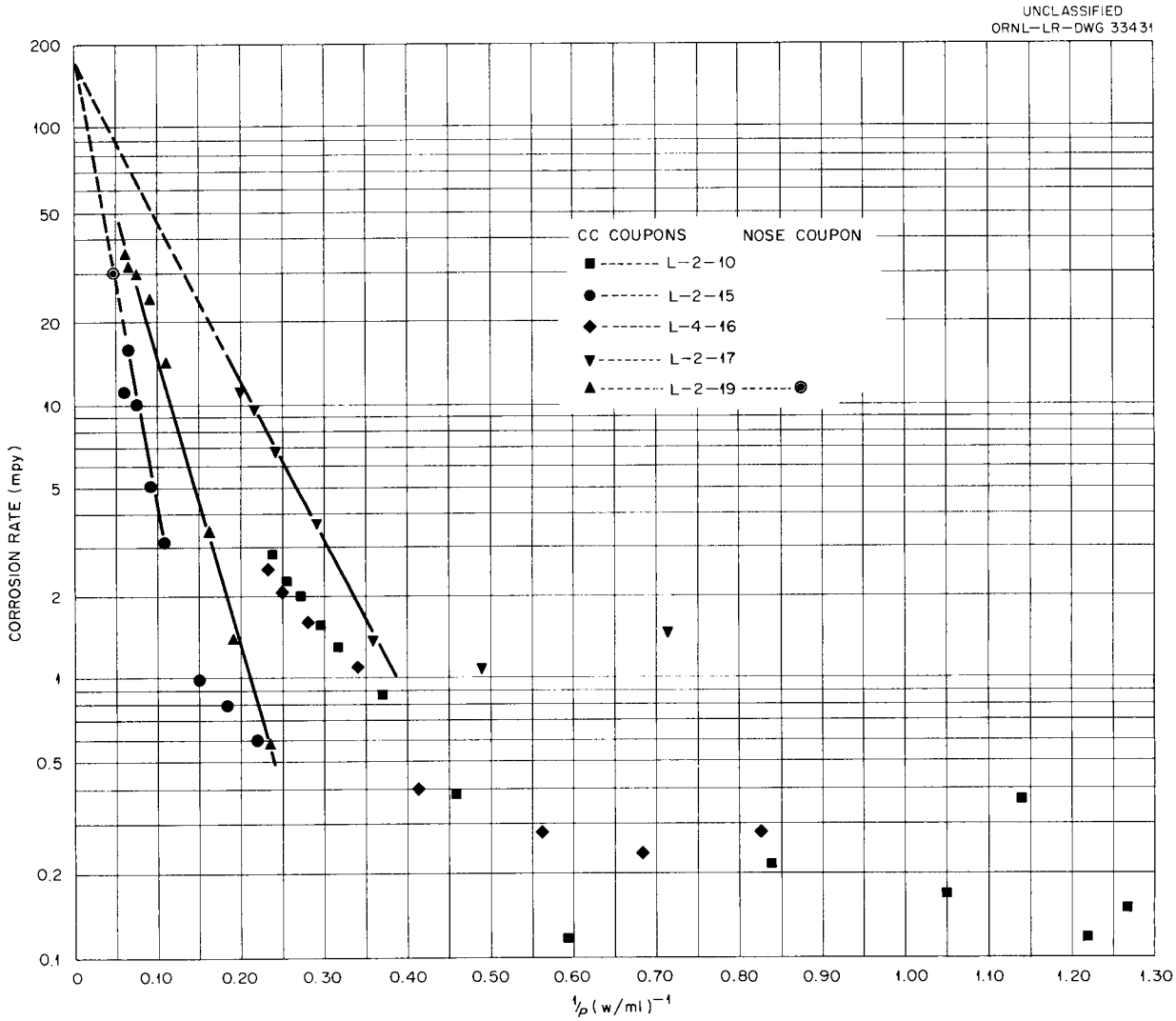

Fig. 14.13. Type 347 Stainless Steel Corrosion Data for 280 and 300°C In-Pile Loop Experiments, Core Channel Specimens.

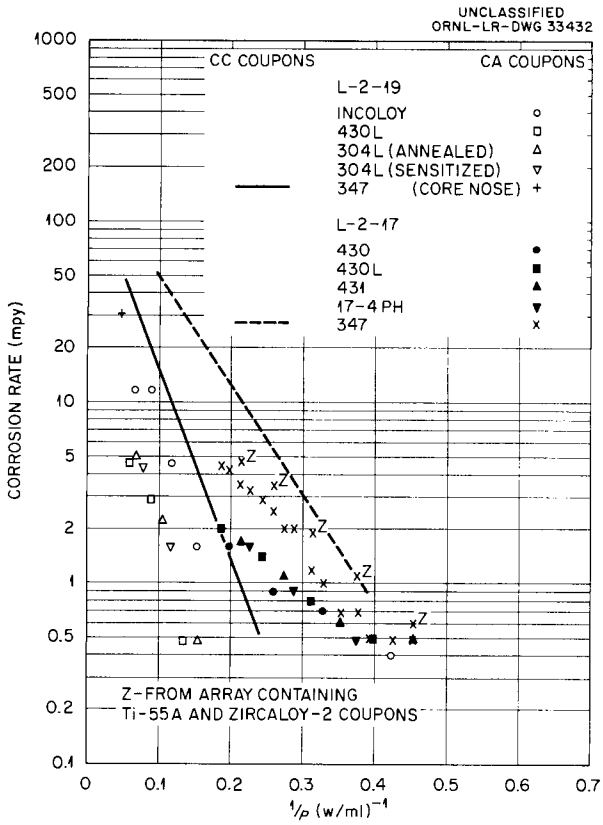

Fig. 14.14. Corrosion of Various Stainless Steels in In-Pile Loop Experiments L-2-19 and L-2-17.

alloys. Lines which represent the type 347 steel CC data for each experiment are also shown. The power-density values employed do not include any fast-neutron contribution.

In-line samples of all types of stainless steel showed either weight gains or no change in weight after defilming. One Incoloy specimen exhibited a rate of 0.01 mpy, and the other a weight gain. Two specimens of 430L exposed in the liquid region of the pressurizer corroded at rates of 6.1 and 2.0 mpy, respectively. These results are summarized in Table 14.13.

As shown in Fig. 14.13, the average corrosion rates for type 347 stainless steel CC specimens in this experiment appear to fall between those observed for the other 280°C experiments. The explanation for the indicated difference in steel behavior in different experiments is not known, but a correlation has been noted between the slope of the line through the data at high corrosion rates and the steady-state pressure of radiolytic gas in the main stream during exposure. The estimated pressures of radiolytic gas in the 280°C experiments are: L-2-15, 100 psi; L-2-19, 55 psi; L-4-16 and L-2-10, 30 psi. The absolute value of the slope increases roughly as the square root of the estimated gas pressure. If the radiolytic gas has, in fact, a beneficial effect on the steel corrosion it is probably associated with the hydrogen

Table 14.13. Summary of Data for Steel and Incoloy Specimens from In-Line and Pressurizer, In-Pile L-2-19

Material	Position	Number of Specimens	Velocity (fps)	Corrosion Rate (mpy)	Stress (psi)	Strain (μin./in.)
347 SS	LC	6	11.4–38.0	(0.8–2.1 mg)*		
		2	9.4 and 12.5	0.0		
430L SS	LA	2	1.0	(0.6 and 1.0 mg)*		
	P	2	1.0	6.1	58,000	2000
				2.9	70,000	2415
304L SS (annealed)	LA	2	1.0	(0.6 and 1.0 mg)*		
304L SS (sensitized)	LA	2	1.0	(0.6 and 1.0 mg)*		
Incoloy	LA	1	1.0	(1.1 mg)*		
		1	1.0	0.01		

*Weight gains.

component of the gas. The pressure of excess oxygen normally exceeds that of the oxygen component of the radiolytic gas and varies between about 140 and 40 psi during an experiment. No consistent effect has been noted of this variation of oxygen pressure on over-all rates for steel in a given loop or autoclave experiment.

The annulus results shown in Fig. 14.14 indicate considerably better performance for the 430L, 304L, and Incoloy in the CA positions than for 347 steel in the CC positions of L-2-19. The L-2-17 results given in Fig. 14.14 exhibit a similar difference between the stainless steel alloys other than type 347 in the CA positions and the type 347 in the CC. A large number of type 347 specimens were also mounted in the CA of L-2-17, and the rates for these were less than those for the CC specimens but greater than those for the other steel alloys. These results in L-2-17 suggest that the noted difference in performance between type 347 in the CC positions and other stainless steels in the CA is not due entirely to differences in solution velocities at the different exposure positions. The difference cannot be ascribed entirely to galvanic effects either. With the exception of a few of the type 347 stainless steel specimens in L-2-17 (marked with a Z), all the CA steel specimens in that experiment were mounted in steel holders which contained only steel specimens. However, some deleterious effect on steel corrosion of contact with dissimilar metals is indicated by the observation that the rates for the "Z" marked specimens were consistently greater than those for the other type 347 stainless steel specimens in the CA. The "Z" specimens were also mounted in stainless steel holders but were in contact with titanium and/or Zircaloy-2 specimens within the array. The type 347 CC specimens were in Zircaloy-2 holders. In L-2-19, CA steel specimens were in titanium holders, with the exception of the type 347 nose coupon, which was held in a bracket of type 347 stainless steel. The CC holder in L-2-19 was of Zircaloy-2.

(4) *Titanium.* – The results for CC coupons and CA stress specimens of titanium 110AT are listed in Table 14.12. Over-all rates of about 1 to 2 mpy were observed.

The single TiO_2 CA coupon was exposed at a power density of 6.7 w/ml and exhibited an over-all rate from weight loss of 5.5 mpy. It is interesting to note that if a protective TiO_2 film on titanium were being removed at this constant rate, the titanium metal would corrode at about 3.6 mpy; that is, within about a factor of two of the rate exhibited by titanium in the majority of loop experiments.

All LC coupons except two exhibited weight gains as measured after the defilming operation. The weight gains ranged from 0.3 to 1.8 mg/cm^2 and averaged 0.9 mg/cm^2. Corrosion rates observed for the exceptions were 0.06 and 0.18 mpy. Following defilming, one of the LA stress specimens exhibited a weight gain of 0.005 mg/cm^2; the other showed no weight change.

14.1.8 General Description of In-Pile Loop L-2-21

Stainless steel loop L-2-21, irradiated in hole HB-2 at the LITR, was removed after 889 hr of circulation time in-pile when unusually high corrosion rates and possible solution instability were encountered. This time was accumulated during three separate periods of operation with three different enriched-uranium solutions. The reactor was at zero-power for approximately 25% of the time, and the energy output of the LITR was 1709 Mwhr. Although the loop temperatures and reactor energy level were varied during the run, the main-stream and pressurizer temperatures were maintained at 280 and 296°C, respectively, and the reactor energy level at 3 Mw, for most of the experiment. The solutions employed were all 0.17 *M* UO_2SO_4 in heavy water but varied slightly in copper and sulfuric acid concentrations. This was the first loop to employ heavy-water solutions at these elevated temperatures and was also the first loop to utilize a pump with the newly developed three-phase 220-v stator.[30] The loop contents have been reported previously.[31,32] No difficulty was encountered with the pump; however, the short duration of the experiment did not permit a satisfactory evaluation of the pump performance.

Although examination of the loop has not been completed, the available data indicate that very heavy corrosion occurred on the type 347 stainless

[30] A. Weitzberg and H. C. Savage, *Performance Test of 220-v Three-Phase Stator for Use with 5-gpm In-Pile Loop Pump*, ORNL CF-57-10-24 (Oct. 4, 1957).

[31] G. H. Jenks *et al.*, *HRP Quar. Prog. Rep. Oct. 31, 1957*, ORNL-2432, p 106.

[32] G. H. Jenks *et al.*, *HRP Quar. Prog. Rep. Jan. 31, 1958*, ORNL-2493, p 117.

steel in the forward half of the core (which constitutes about 5% of the total stainless steel area in the loop), while very slight corrosion occurred on the steel surfaces in the rear of the core and in the in-line positions. During the second and third periods of operation, the over-all corrosion rates for the entire loop, based on oxygen consumption, were observed to rise to about 25–30 mpy during the periods when the reactor power level was raised to 3 Mw. It can be estimated that during these periods the stainless steel in the forward part of the core must have been corroding at about 600 mpy.

Preliminary examination of the circulation pump also showed some pitting near the outlet of the stainless steel volute and on the steel impeller shaft in the region of the thermal barrier.

14.2 IN-PILE AUTOCLAVE TESTS – LITR

14.2.1 Development, Construction, and Operation

(a) HB-5. – The assembly and operation of rocking autoclaves for solution radiation-corrosion studies in beam hole HB-5 of the LITR continued. Five experiments, L52Z-117, L53Z-118, L51Z-119, L52S-130, and L51Z-131, were assembled, were operated in the LITR, and were removed from the facility after operating times of 1040, 1495, 140, 1337, and 882 hr, respectively. The early termination of experiment L51Z-119 was caused by a leak in the closure fitting. Autoclave L53T-132 was inserted in the reactor on June 4 and is still in operation.

The experiment L53T-132 assembly contains a nose bearing[33] with a thin aluminum cover-plate attached to protect the bearing during operation. In some previous experiments the nose bearing (without cover-plate) was found to be frozen when removed from the reactor. The bearing failures were attributed to dirt particles entering the bearing. Other bearings with built-in shields have also been obtained for this application, but have not been utilized as yet.

The design of the corrosion test coupons has been changed from a rectangular shape[34] to that shown in Fig. 14.15. The first experiment to utilize the new type of specimens was L51Z-131.

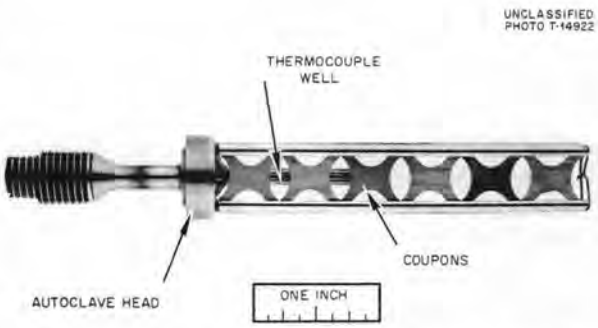

Fig. 14.15. HB-5 Rocking-Autoclave Coupon Rack Assembly.

The new specimen shape is designed to obtain better mixing of solution during operation and to increase the fraction of coupon area exposed to solution during in-pile exposure to simplify the calculation of corrosion rates.

(b) HB-6. – One solution autoclave, L6Z-133, for beam hole HB-6 of the LITR was assembled and was operated for 300 hr at 280°C. This experiment was designed to test the effect of hydrogen, by means of high radiolytic-gas pressure (~500 psi), on the corrosion of stainless steel by uranyl sulfate solution. The autoclave was operated in beam hole HB-6, rather than HB-5, since other experiments with which L6Z-133 is to be compared were also operated in HB-6. Experiments in beam hole HB-6 are operated in a position such that the long axis of the autoclave is approximately parallel to the reactor lattice rather than perpendicular to the reactor lattice as in HB-5. This results in a more uniform neutron flux distribution in the HB-6 experiments.[35]

14.2.2 Results and Discussion

(a) Introduction. – Examinations are complete or nearly complete for nine autoclave experiments which were exposed in the new HB-5 facility of the LITR. Five of these experiments were designed primarily to test the effect of the addition of various solutes to 0.17 *m* UO_2SO_4 solution on the in-pile corrosion of Zircaloy-2. Other experiments were concerned with studies of the anomalous buildup of pressure which has been observed in Zircaloy-2 autoclaves in previous experiments[36]

[33] G. H. Jenks *et al.*, *HRP Quar. Prog. Rep. Oct. 31, 1957*, ORNL-2432, p 121, Fig. 14.8.

[34] G. H. Jenks *et al.*, *HRP Quar. Prog. Rep. July 31, 1957*, ORNL-2379, p 116, Fig. 14.9.

[35] K. S. Warren and R. J. Davis, *In-Reactor Autoclave Corrosion Studies – LITR I Outline of Methods and Procedures*, ORNL CF-57-5-110 (May 22, 1957).

[36] G. H. Jenks *et al.*, *HRP Quar. Prog. Rep. April 30, 1957*, ORNL-2331, p 120–22.

and with studies of corrosion of Zircaloy-2 in solutions of depleted UO_2SO_4. One experiment was primarily concerned with steel corrosion. No previous reports have been given of experiments in the new facility.

(b) General Characteristics of Experiments in the HB-5 Multiple-Hole Facility. – The experimental conditions which prevail in the HB-5 autoclaves and the type of data which are obtained differ from those for previously reported LITR autoclave experiments. All previous data were obtained from autoclaves of the type I or II design,[35] in which the autoclaves are oriented so that the cylindrical axis of the autoclave is perpendicular to the cylindrical axis of the beam hole. This arrangement provides a nearly uniform thermal-neutron flux throughout the autoclave.[37] In the type III autoclave system[35] now employed in HB-5, the cylindrical axis of the autoclave is parallel to the cylindrical axis of the beam hole, and a thermal-flux gradient along the length of the autoclave is observed. The flux at the forward end is two to three times that at the rear (Fig. 14.16). Specimens within the autoclave are thus exposed to a range of solution power densities.

The mixing of solution by the back-and-forth rolling action of the type III bomb is less vigorous than that prevailing in autoclaves of the previous designs. Visual observations in a plastic mockup of the autoclave have demonstrated the poorer mixing. The poor mixing probably allows larger gradients of temperature and radiolytic-gas concentration in the HB-5 autoclave than in those for the previous systems.

Coupon specimens[34] with a total-to-exposed-area ratio of 1.62 were used in most of the HB-5 autoclaves reported. Experiment L51Z-131 contained scalloped coupons (Fig. 14.15) with a total-to-exposed-area ratio of 1.16. The pin type specimens previously employed[35] have a ratio of about 1.

Temperatures in the HB-5 autoclave are measured by a thermocouple located in a well and by thermocouples attached to the outer autoclave surface.

(c) Experimental Consitions and Results. – The conditions and some of the results for the experiments under discussion are listed in Table 14.14.

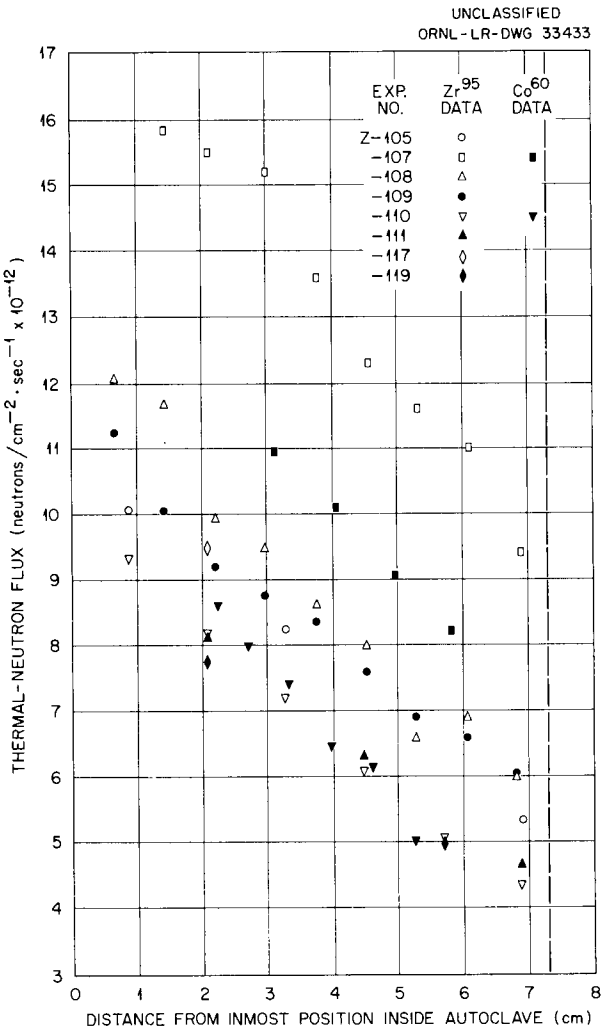

Fig. 14.16. Data from Flux Measurements in Several HB-5 Autoclave Experiments.

Both the initial solution composition and the analyses of the solution recovered after exposure are given where available. The results of quartz-tube tests of the solutions prior to exposure indicated that all were stable at the exposure temperature.

The temperature for in-pile operation is that indicated by the well thermocouples except for Z-107 for which the solution temperature was estimated from the temperatures of the thermocouples located on the autoclave walls.

The power densities (or thermal-neutron fluxes) in these autoclaves varied in a nearly linear manner with position in the autoclave as can be seen in Fig. 14.16. The average power densities

[37] G. H. Jenks *et al.*, *HRP Quar. Prog. Rep. Oct. 31, 1957*, ORNL-2432, p 128.

Table 14.14. In-Pile Autoclave Corrosion Data; LITR Beam Hole HB-5; Type III Autoclaves

Autoclave Designation	Dates In and Out	Solution Concentration (Before and After Exposure)						Pretreatment		Exposure Conditions and Average Corrosion Rates											Remarks
		UO_2SO_4 (m)	Enrichment (% U^{235})	$CuSO_4$ (m)	H_2SO_4 (m)	Other (m)	pH	Time Exposed to Water – to Solution (hr)	Temp. (°C)	Temp. (°C)	Radiation Time (hr)	Total Time at Elevoted Temp. After Pretreatment (hr)	Average Power Density (w/ml)	Average Power Density Corrected for Scale Uronium (w/ml)	Average Radiolytic-Gas Pressure (psi)	Oxygen Pressure, Initial and Final (psi)	Average Corrosion Rate (mpy)		Average Penetration (mils)		
																	O_2 Consumption	Specimen Wt	O_2 Consumption	Specimen Wt	
L51Z-105	12-26-57	0.160	93.2	0.018	0.038		1.80	8	310	280	168.2	208	10.5	16.2	190	1465	16.9	15.8	0.333	0.303	1.89% U in Zircaloy-2 scale from coupons;
	1-3-58	0.18		0.006			1.75	21	280							295					0.42% U in Zr–5% Sn scale from coupons
L52Z-107	6-25-57	0.169	93.2	0.040	0.040	0.179	1.80	7	310	295	15.2	15				1330	11.7	13.8	0.053	0.053	No thermocouple well; Co-Al flux monitor; 0.2% U,
	6-28-57	0.17		0.030		0.18 Li_2SO_4 (natural)	1.5	18	280	280	18.6	46	14.2	15.0		1170					0% Li in Zircaloy-2 scale from coupons
L53Z-108	10-22-57	0.167	93.2	0.039	0.059	0.010 W as	1.10	8	310	280	80.2	162	12.0	21.0	20	1570	17.5	15.5	0.168	0.142	Co-Al flux monitor failed; 2.7% U in Zircaloy-2
	10-29-57	0.08		0.015		$H_8SiW_{12}O_{42}$	2.20	28.5	280							930					scale from coupons
L51Z-109	9-24-57	0.166	93.2	0.039	0.039	0.006 $KReO_4$	1.15	6	310	280	139.2	151	11.4	23.3	134	1460	15.4	15.0	0.253	0.238	Co-Al flux monitor foiled; 3.8% U in Zircaloy-2
	10-1-57	0.18		0.025			1.35	16.3	280							480					scale from coupons
L52Z-110	11-19-57	0.171	93.2	0.040	0.040	0.171 $BeSO_4$	1.45	8	310	280	189.7	231	9.6	12.8	255	1215	12.5	11.9	0.278	0.258	Co-Al flux monitor; snorkel; 1.3% U in Zircaloy-2
	11-29-57	0.19		0.029			1.60	16	280							365					scale from coupons
L52Z-117	1-28-58					D_2O solvent		7	310	280	669.5	1040			0	1285	0.4	0.2	0.040	0.03	Specimen data from as-removed weights; one
	3-11-58							24.0	280							1155					specimen gained weight; five lost weight
L53Z-118	2-11-58	0.167	0.02				2.45	7.5	310	280	1093.2	1495			0	1306	0.4	0.9	0.064	0.12	Specimen data from weight gains in the as-
	4-15-58	0.143		0.0005				16.9	280							999					removed condition
L52S-130	3-11-58	0.039	0.02	0.00014	0.018		1.7	8	310	280	369.7	503			0	226–125	0.4		0.04	0.06	Specimen data from weight gains in the as-
	5-6-58	0.046		0.00011		0.015 $NiSO_4$ D_2O solvent	2.2	19.8	280	250	726.0	834				130–119	<0.1				removed condition; pD reported equals glass-electrode value plus 0.25
L51Z-131	4-15-58	0.180	0.02				2.45	6.5	310	250	719.0	822			0	762	0.7		0.062		Specimen weight data and analyses of irradiated
	5-20-58							23.5	280							596					solution not yet available

listed in Table 14.14 are simply the power densities at the midpoint of the autoclave. In two instances, Z-107 and Z-110, flux values and hence power densities are available from the cobalt flux monitors as well as from the Zr^{95} activities in the specimens. The Co^{60} values are believed to be more reliable and are employed in the Z-107 case, where the Co^{60} and Zr^{95} results are in disagreement. For the Z-110 data, the Co^{60} and Zr^{95} values are in agreement, and in this case, as well as in the others where only Zr^{95} results are available, the power-density values are calculated from thermal-neutron flux values determined from Zr^{95} activity in specimens.

The average radiolytic-gas pressures, as shown by pressure increases on reactor startup and pressure decreases on reactor shutdown, and the approximate partial pressures of oxygen (excluding radiolytic oxygen) at the beginning and end of the exposure period are listed. In experiments Z-117, Z-118, Z-119, S-130, and Z-131, which contained little or no U^{235}, no radiolytic-gas pressure was detected.

During each exposure a series of pressure observations was made at the operating temperature. Initial and final pressures were also observed at about 25°C. The results of the 25°C measurements were in disagreement with the high-temperature results in several of the experiments. This difference was marked for experiments Z-107, Z-108, and Z-109, in which the 25°C data indicated a larger amount of oxygen initially in the autoclaves and a larger consumption of oxygen during exposure. The present interpretation is that the room-temperature measurements of oxygen consumption are more reliable, and that the high-temperature data may be in error as a result of a thermal gradient and stratification of oxygen and water vapor along the length of the autoclave. The corrosion rates based on oxygen-consumption data were calculated from the room-temperature measurements. The oxygen consumed by specimens of material different from that of the bomb was calculated from the weight measurements on those specimens. The values for average penetration determined from oxygen consumption represent, in each case, the average of the corrosion penetration indicated by the pressure measurements made before and after the exposure plus the estimated penetration during pretreatment.

Average corrosion rates of the autoclave material from specimen weight-loss data were obtained as follows: Values for corrosion penetration of each specimen during the experiment were estimated from the weight-loss data together with the values for total specimen area. The average corrosion rate during the exposure period on each specimen was calculated from the penetration values and the radiation times. These rates were plotted as a function of position in the autoclave, and the average rate over all the surfaces in the autoclave was obtained by a graphical integration of a smooth curve drawn through the data. In this connection it may be noted that the distribution of interior area along the length of the autoclave is very nearly linear. Values of average penetration for all autoclave surfaces determined from these average rate values and exposure time are listed.

Experiments Z-107, Z-108, Z-109, and Z-110 each contained as flux monitors a cobalt aluminum wire encased in Zircaloy-2.[38] In the Z-108 and Z-109 experiments, the Zircaloy-2 cases failed during exposure, and the wire showed definite evidence of corrosive attack by the solution. The particular batch of Zircaloy-2 used as case material showed evidence of white oxide after pretreatment and probably had poor corrosion resistance. Subsequent tests did not include a flux monitor. The "snorkel" included in Z-110 was a tube which extended the pressure-tap on the autoclave to a position at the top part of the middle portion of the bomb. The snorkel was constructed of the same, apparently inferior, Zircaloy-2 batch.

Specimen data from each of the experiments are listed in Table 14.15 together with calculated values of corrosion rates and, for high-power-density experiments, values for corrected power densities. Total specimen areas were employed in the rate calculations. The significance of the corrected power density has been discussed previously[39] and defined as follows:

$$P_c = P_s(1 + 8.3\, U_f/U_s)$$

[38] G. H. Jenks *et al.*, *HRP Quar. Prog. Rep. Oct. 31, 1957*, ORNL-2432, p 126–27.

[39] G. H. Jenks *et al.*, *HRP Quar. Prog. Rep. Oct. 31, 1957*, ORNL-2432, p 120–24.

Table 14.15. In-Pile Autoclave Corrosion Data from Specimens

Experiment Designation	Specimen No.	1	2	3	4	5	6	7	8	9
L51Z-105	Material	Zr-2	Zr–5% Sn	Zr-2	Zr-2	Zr–5% Sn	Zr-2			
	Corrosion rate, weight loss (mpy)	19.2	15.2	16.8	14.3	10.9	11.0			
	Power density (w/ml)	12.8	11.6	10.5	9.2	8.0	6.8			
	Corrected power density (w/ml)	19.8		16.2	14.2		10.5			
	Corrosion rate of alloy/corrosion rate of Zircaloy-2		0.84			0.85				
L52Z-107	Material	Zr-2	Zr-2	Zr-2	Zr-2	Zr-2	Zr-2	Zr-2	Zr-2	Zr-2
	Corrosion rate, weight loss (mpy)	18.2	18.2	18.4	13.0	11.4	14.0	7.8	8.6	11.1
	Power density (w/ml)	18.3	17.2	16.3	15.1	14.0	12.9	11.8	10.8	9.7
	Corrected power density (w/ml)	19.3	18.1	17.2	15.9	14.8	13.6	12.4	11.4	10.2
L53Z-108	Material	Zr-2	Zr-2	Zr-2	Zr-2	Zr-2	Zr-2	Zr-2	Zr-2	Zr-2
	Corrosion rate, weight loss (mpy)	18.3	19.3	18.6	17.9	16.5	14.5	12.8	12.4	9.8
	Power density (w/ml)	15.6	14.7	13.9	12.8	11.9	10.9	10.0	9.1	8.1
	Corrected power density (w/ml)	27.2	25.7	24.3	22.3	20.8	19.0	17.5	15.9	14.1
L51Z-109	Material	Zr-2	Zr-2	Zr-2	Zr-2	Zr-2	Zr-2	Zr-2	Zr-2	Zr-2
	Corrosion rate, weight loss (mpy)	17.9	17.8	17.3	16.4	15.3	14.4	12.8	12.3	10.9
	Power density (w/ml)	14.7	13.9	13.1	12.2	11.3	10.4	9.6	8.8	7.9
	Corrected power density (w/ml)	30.0	28.4	26.8	24.9	23.1	21.3	19.6	18.0	16.2
L52Z-110	Material	Zr-2	Zr-2	Zr-2	Zr-2	Zr-2	Zr-2			
	Corrosion rate, weight loss (mpy)	15.2	14.0	12.6	11.0	9.4	7.9			
	Power density (w/ml)	12.8	11.4	10.0	8.7	7.3	5.9			
	Corrected power density (w/ml)	17.1	15.2	13.3	11.6	9.7	7.9			
L52Z-117	Material	Zr-2	Zr-2	Zr-2	Zr-2	Zr-2	Zr-2			
	Corrosion rate, as-removed weight losses (mpy)		0.4	0.4	0.1	0.1	0.1			
	Corrosion rate, defilmed weight losses (mpy)		0.5							
	Corrosion rate, as-removed weight gain (mpy)	0.8								
L53Z-118	Material	Zr-2	Zr-2	Zr-2	Zr-2	Zr-2	Zr-2			
	Corrosion rate, as-removed weight gain (mpy)	1.2	0.9	1.0	0.9	0.9	0.7			
L52S-130	Material	347 SS	347 SS	347 SS	347 SS	347 SS	347 SS			
	Corrosion penetration, as-removed weight gain (mils)	0.020	0.072	0.072	0.066	0.086	0.066			

where P_c is the corrected power density, w/ml; P_s is the power density in solution as listed in Tables 14.14 and 14.15; U_f is the weight per cent of uranium in the scale; and U_s is the concentration (g/liter) of uranium in solution at the test temperature.

(*d*) Results of Tests of the Effect of Several Different Solute Additives on the Corrosion of Zircaloy-2 by 0.17 *m* UO_2SO_4. – Five experiments were designed primarily to test the effect of several different solute additives on the corrosion of Zircaloy-2 by 0.17 *m* UO_2SO_4 solutions. The additives tested were lithium sulfate, Z-107; silicotungstic acid, Z-108; potassium perrhenate, Z-109; and beryllium sulfate, Z-110. The fifth experiment, Z-105, was a control in which the solution composition duplicated that of several previous autoclave experiments. Specimen corrosion-rate data for these experiments are plotted against uncorrected power densities in Fig. 14.17. Average rate values from oxygen and

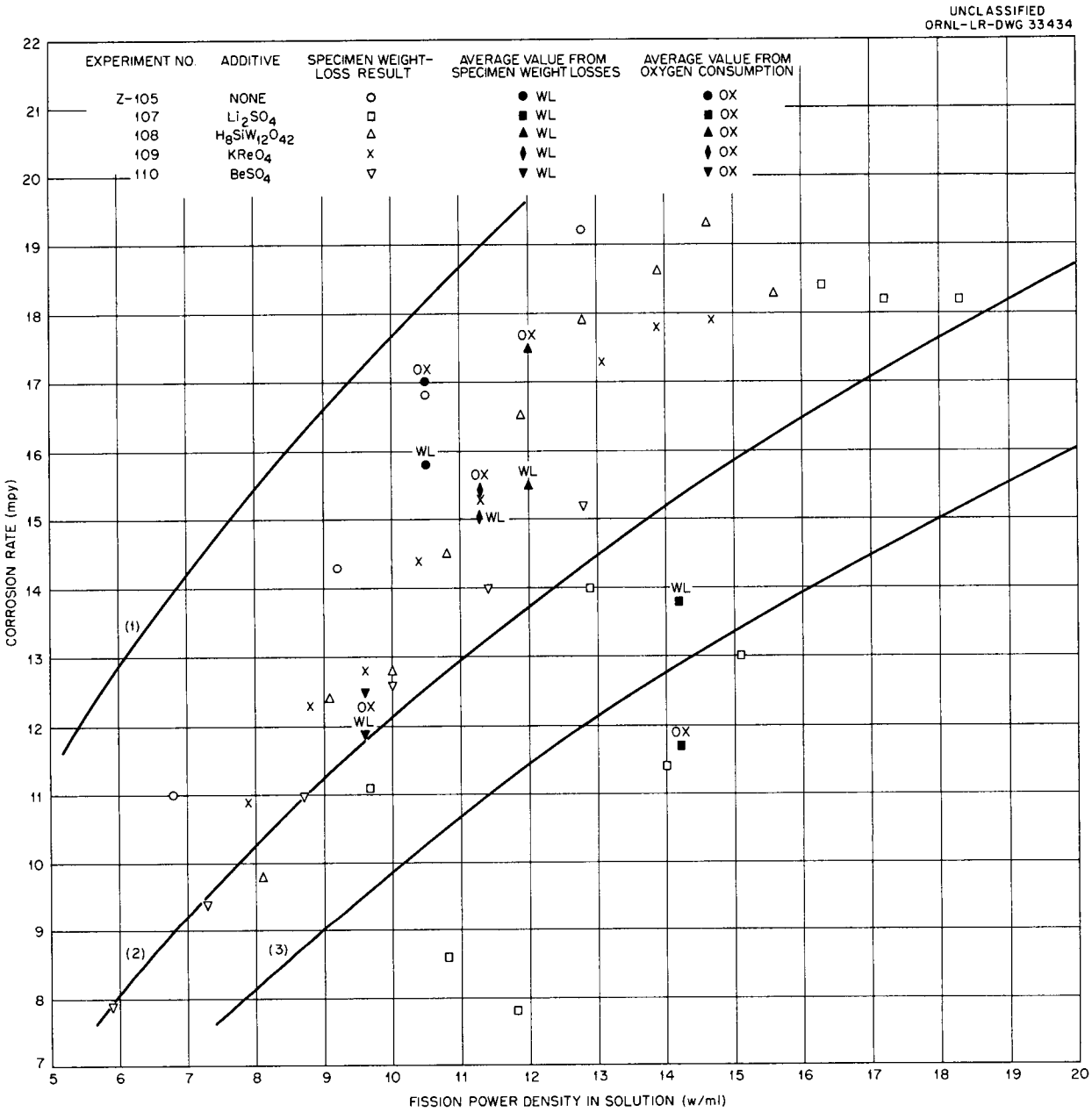

Fig. 14.17. Zircaloy-2 Corrosion Rates vs Solution Power Density from Autoclave Experiments of the Effect of Solute Additives in UO_2SO_4 Solution.

specimen data are also shown. The curves in Fig. 14.17 have the following significance:

Curve 1 obeys the equation:

$$(1) \qquad R = 2.45P\left(1 - e^{-95/R^{1.5}}\right) ,$$

which was found to apply to previous data obtained with 0.17 *m* UO_2SO_4 reference solutions[40] with no excess H_2SO_4.

Curve 2 obeys the equation:

$$(2) \qquad R = 1.36P\left(1 - e^{-95/R^{1.5}}\right) ,$$

which was found to apply to previous data[40] obtained with 0.17 *m* UO_2SO_4 reference solutions with 0.04 *m* excess H_2SO_4.

[40] G. H. Jenks, *Effect of Radiation on the Corrosion of Zircaloy-2*, ORNL CF-57-9-11, p 22–23 (Sept. 30, 1957).

Curve 3 obeys the equation:

$$R = 1.04P\left(1 - e^{-95/R^{1.5}}\right) , \quad (3)$$

which the previous autoclave data obtained in reference solutions were assumed to obey when corrected for scale uranium.[39] Corrosion-rate values plotted against corrected power densities are shown in Fig. 14.18. (Analytical data for uranium in scale are given under Remarks in Table 14.14.) The curves are the same as those in Fig. 14.17.

In addition to the above-mentioned measurements, the surfaces of two specimens, one of Zircaloy-2 and one of Zr–5% Sn, from experiment Z-105 were analyzed for the amount of uranium retained after descaling. The specimens were treated with acetone and dried to remove heavy scale and were cathodically treated in 5% H_2SO_4 at 85°C prior to the surface analyses. The analyses were carried out as previously described for specimens from loop experiment L-2-17.[41] The results listed in Table 14.16 indicate uranium in the adherent scale in amounts comparable to those found on specimens in the as-removed condition in the 0.04 *m* UO_2SO_4, 300°C loop experiment, L-2-17.

(e) Discussion of Results of Tests of Additives on the Corrosion of Zircaloy-2. – The control experiment, Z-105, employed a solution composition similar to that in several previous autoclave tests[40] for which the observed rates fell

[41] G. H. Jenks *et al.*, *HRP Quar. Prog. Rep. Jan. 31, 1958*, ORNL-2493, p 124–26.

Table 14.16. Chemical Analyses of Film Retained on L51Z-105 Coupons After Defilming

	Film Composition ($\mu g/cm^2$)	
	Sample No. 4, Zircaloy-2	Sample No. 5, Zr–5% Sn
Uranium	9.4	10.4
Chromium	2.5	4.9
Nickel	25.8	12.5
Iron	20.6	24.4
Copper	0	0

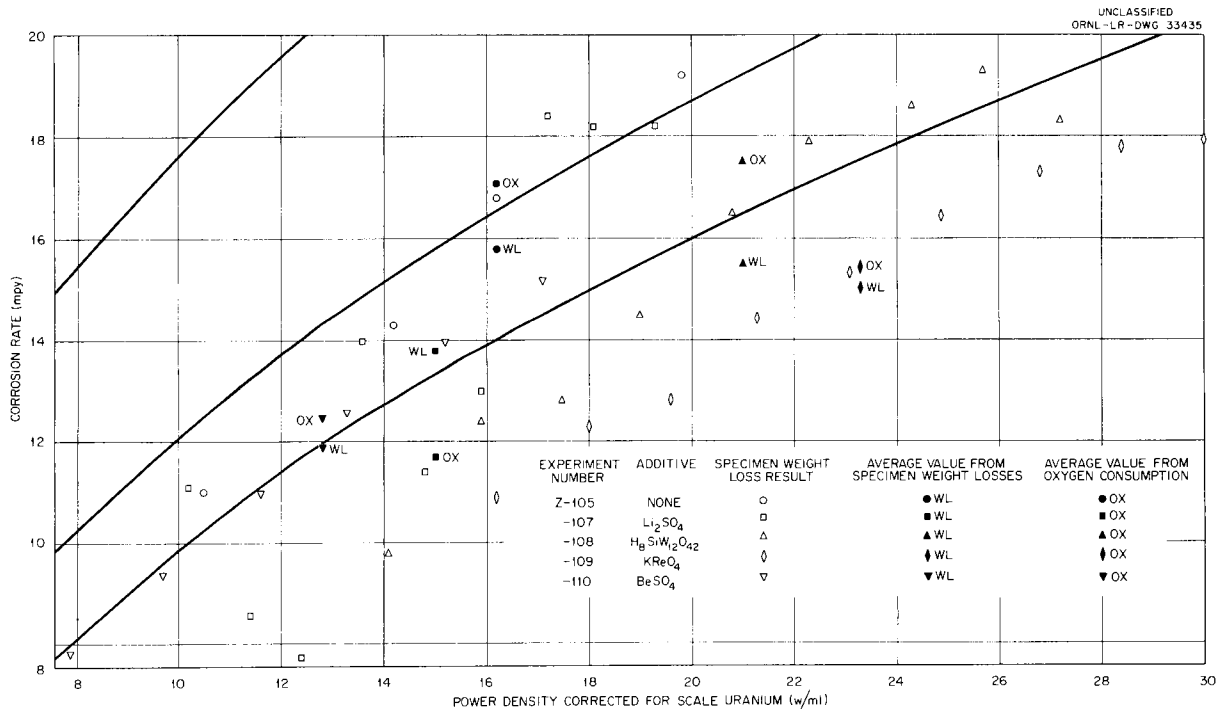

Fig. 14.18. Corrosion Rate vs Power Density Corrected for Scale Uranium from Autoclave Experiments of the Effect of Solute Additives in UO_2SO_4 Solution.

along curve 2. The rate points from Z-105 fell well above line 2, with the greatest divergence at the highest power densities. The average value from oxygen data for Z-105 is in near agreement with the specimen data. The rates indicated by specimen data from the experiments with silicotungstic acid, $KReO_4$, and $BeSO_4$ (Z-108, Z-109, and Z-110) diverge from line 2 in a similar manner but to a lesser extent than those for Z-105. The average rate values from oxygen data from experiments Z-108, Z-109, and Z-110 each agree well with those indicated by specimen data.

The explanation for the indicated difference between specimens in HB-5 and previous types of autoclaves is unknown. However, it may be due to gradients of temperature between specimens, thermocouple well, and walls in the HB-5 autoclave, which increase with increasing power density. The data correlated in terms of corrected power densities in Fig. 14.18 indicate that the additives $KReO_4$ and silicotungstic acid were probably effective in reducing the in-pile corrosion of Zircaloy-2. Little beneficial effect for the $BeSO_4$ or Li_2SO_4 additions in these experiments is indicated. Previous tests with Li_2SO_4 additives have indicated considerable reduction in Zircaloy-2 corrosion so that these results should not be considered as proof that Li_2SO_4 or indeed $BeSO_4$ would not inhibit Zircaloy-2 corrosion in some other system.

The two Zr–5% Sn specimens in Z-105 corroded less rapidly than the Zircaloy-2. A comparison of the alloy corrosion rates with a smooth curve through the Zircaloy-2 data indicates that the 5% tin alloy corroded about 85% as fast as Zircaloy-2 at similar solution power densities. It should be noted (Table 14.16) that the amount of uranium found on the defilmed surface of the alloy coupon was comparable to that on the Zircaloy-2 coupon. However, analyses of the heavy scales (Table 14.14) showed considerably less uranium in the alloy scale than in the Zircaloy-2 scale. The difference in the power-density contribution from the heavy scales may be sufficient to account for the difference in corrosion behavior.

(f) Investigation of Pressure-Peaking Phenomenon in Depleted UO_2SO_4 Solution and Corrosion in Depleted 0.17 *m* UO_2SO_4 Solution at 280°C. – In two previous experiments, Z-13 and Z-22,[36] operated as perpendicularly rocked autoclaves in facility HB-5 with depleted uranyl sulfate solution (0.17 *m* UO_2SO_4 and 0.02 *m* $CuSO_4$ at 250°C), an anomalous pressure behavior was observed. No radiolytic-gas pressure was anticipated, but, in each case, the pressure within the autoclave started to increase following the initial exposure to radiation. The pressure reached a peak after about 60 hr of radiation and then decreased to essentially zero excess pressure. It has been postulated that this increase was due to a loss of copper catalysis by a loss of a large fraction of the copper ion from solution, possibly by plating out as metallic copper on the corroding metal, and to an inhibition of gamma-ray catalyzed recombination of H_2 and O_2 by a small amount of copper remaining in solution.[42] The copper, in this postulated picture, must re-enter the solution after being lost, in order to account for the return of the radiolytic-gas pressure to the normal negligible value.

To test this general postulate, experiments Z-131 and Z-118 were carried out with depleted uranyl sulfate solutions, 0.17 *m* UO_2SO_4, containing no copper, in the multiple facility in HB-5 (autoclaves axially rotated). The exposure temperature for Z-131 was 250°C; that for Z-118 was 280°C.

The results of pressure measurements in these experiments together with those of the previous experiments, Z-13 and Z-22, are illustrated in Fig. 14.19 with the total pressure of gas, including excess oxygen, within an autoclave plotted against the radiation time. The pressure at zero time is the pressure of excess oxygen in each case. No increase in pressure or other unusual effects were noted for either experiment Z-131 or Z-118.

Specimen weight data from the 280°C experiment, Z-118, are included in Tables 14.14 and 14.15. The Z-131 specimen results are not yet available. All the specimens from Z-118 exhibited weight gains as-removed, and there was no definite evidence of larger weight gains for those specimens exposed at the forward, high-flux end of the autoclave. The average gain in weight of the specimens is nearly twice as great as that expected if all Zircaloy-2 surfaces within the autoclave corroded at the average rate of 0.4 mpy indicated by the oxygen data and if no transfer of

[42] G. H. Jenks *et al.*, *HRP Quar. Prog. Rep. July 31, 1957*, ORNL-2379, p 118–19.

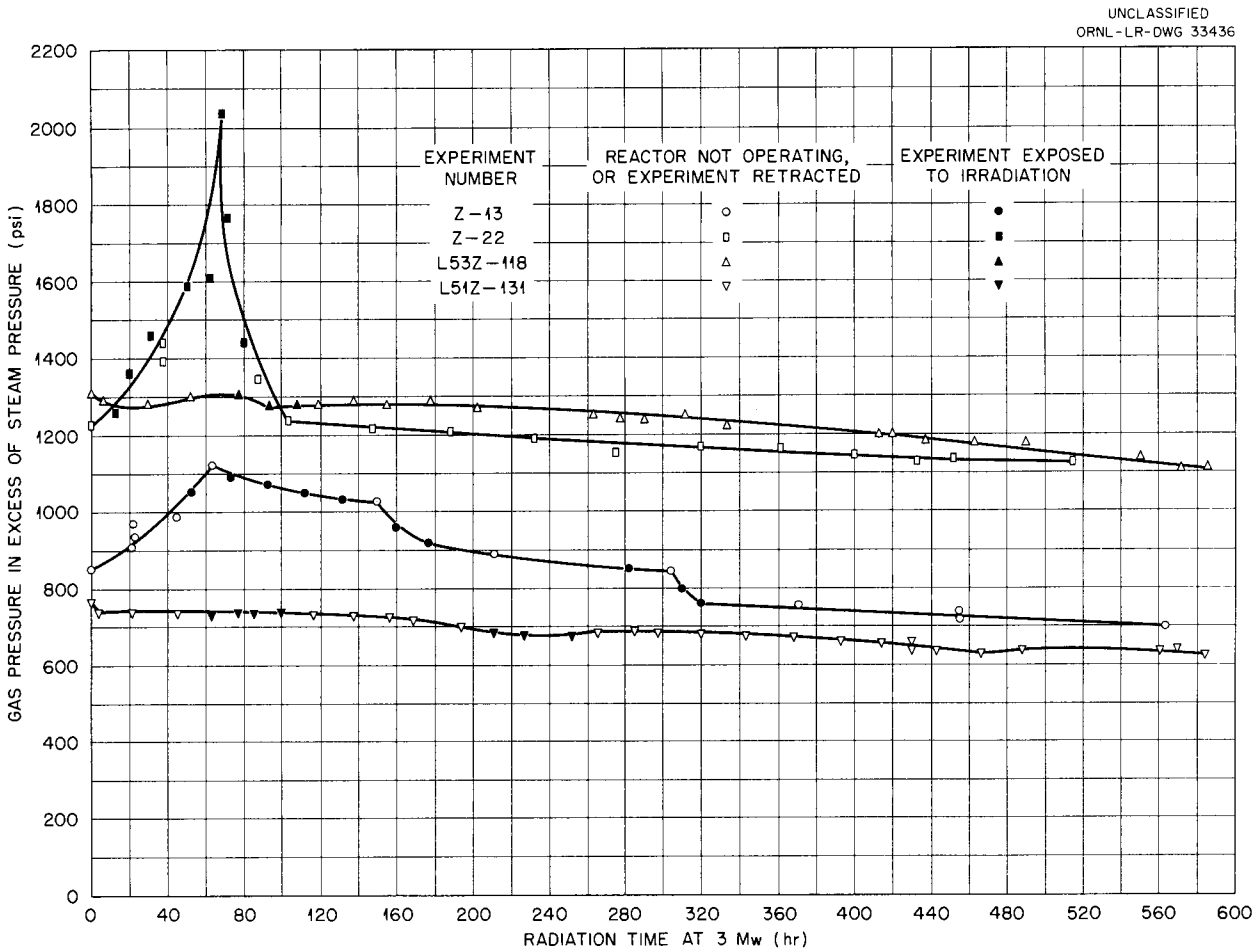

Fig. 14.19. Anomalous Pressure Peaking Observed in Some Depleted UO_2SO_4 Experiments.

oxide took place within the autoclave. The specimens were not defilmed but were retained for future studies.

The average corrosion rate of 0.4 mpy for Zircaloy-2 as indicated by oxygen data in Z-118 is less than that observed in the two previous autoclave experiments at 280°C with solution of the same composition. The observed rate in Z-13 was 1.2 mpy; that in Z-22 was 0.8 mpy. However, all the Zircaloy-2 surfaces in these previous autoclave experiments were exposed to a fairly uniform radiation intensity which was probably about the same as or a little greater than that at the forward portion of the autoclave in Z-118. Hence, the average rate of 0.4 mpy in Z-118 is reasonable in comparison with those in Z-13 and Z-22. It may be noted, however, that the average rate observed in Z-118 is only about a factor of two greater than that expected for Zircaloy-2 out-of-radiation as indicated by the results of a long-term autoclave test with a solution 0.17 *m* UO_2SO_4 and 0.02 *m* $CuSO_4$ at 290°C.[43] The specimen weight results (high weight gains, as removed, and lack of change in weight gain as a function of position in the autoclave) indicate that a transfer of scale took place from the autoclave walls to the specimen.

Direct comparison between the results of pressure measurements in the present experiment and in the previous ones which exhibited pressure peaking is precluded because radiation facilities of different types were employed with the two different sets of experiments. Perpendicularly oriented autoclaves were employed with the former experiments, while

[43] G. H. Jenks, *Effect of Radiation on the Corrosion of Zircaloy-2*, ORNL CF-57-9-11, p 13–14 (Sept. 30, 1957).

the axially oriented autoclaves were employed with the present experiments. As described in Sec 14.2.2(*b*), the axially oriented autoclaves in HB-5 are subjected to a gradient of intensity of radiation from the reactor, and the average intensity of radiation is less than in the perpendicularly oriented autoclaves in HB-5. The effect of these differences in radiation intensity and distribution is unknown. Tentatively, the results of pressure measurements in these several different experiments are considered to support the postulate that the pressure-peaking phenomenon is associated with the copper initially present in the depleted uranyl sulfate solutions.[42]

(*g*) Corrosion of Zircaloy-2 in Oxygenated D_2O at 280°C, Z-117. – Experiment Z-117 contained oxygenated D_2O in a Zircaloy-2 autoclave with six Zircaloy-2 specimens. It was exposed to radiation in the multiple HB-5 facility at 280°C for 670 hr (1040 hr total time). Although there was some scatter of the data, the rate of oxygen consumption appeared to be linear with radiation time and at a rate corresponding to an average corrosion rate of 0.4 mpy. The specimen at the forward, high-flux position showed a weight gain in an amount which corresponds to an average corrosion rate of 0.8 mpy, assuming that the weight increase was due to oxidation and retention of the oxide on the specimen. The other five specimens showed weight losses, as-removed, with values which decreased with decreasing flux. Rate values computed from weight losses ranged from 0.4 to 0.1 mpy. One specimen showing a weight loss as-removed was cathodically defilmed. An additional loss of weight occurred which was sufficient to raise the calculated apparent corrosion rate from the 0.4 mpy initially measured to 0.5 mpy. The remaining five specimens were not cathodically defilmed but were reserved for further studies. The average corrosion rate of 0.3 mpy from specimen weight data listed in Table 14.14 is a linear average of the values computed from as-removed weight changes. The additional loss in weight which was observed upon cathodically defilming the one specimen is evidence that appreciable amounts of scale remained on the specimens which exhibited weight losses as-removed.

The loss in weight observed with specimens in this experiment is an exception to the behavior normally observed in nonfissioning solutions. Out-of-pile exposures of Zircaloy-2 in autoclave experiments carried out at this laboratory and in-pile autoclave tests with depleted uranyl sulfate solutions have invariably led to observations of weight gains on specimens.

The average corrosion rate of 0.4 mpy determined from oxygen pressure measurements is the same as that observed for Zircaloy-2 in contact with 0.17 *m* UO_2SO_4 depleted of U^{235} at 280°C in experiment Z-118. In view of this apparent agreement, it is interesting to note that, in autoclave tests at the MTR, Zircaloy-2 in contact with oxygenated water in the temperature range 280–300°C corroded at about the same rate as that in contact with oxygenated 0.017 *m* H_2SO_4 solution at the same temperatures.[44]

The rates observed in the MTR were about a factor of 10 greater than those in the LITR. However, the estimated radiation intensity at the MTR was also about a factor of 10 greater than that employed in the LITR experiments. The orientation of the MTR autoclaves within the beam hole was similar to that for the LITR experiments Z-117 and Z-118. Though by no means conclusive, these various results indicate that the corrosion of Zircaloy-2 in either H_2O, D_2O, 0.17 *m* UO_2SO_4, depleted, or 0.02 *m* H_2SO_4, all oxygenated, is accelerated to about the same extent by reactor radiations and that the degree of acceleration is roughly proportional to the intensity of radiation within the range of intensities investigated.

(*h*) Radiation Corrosion of Stainless Steel by 0.04 *m* UO_2SO_4 Solution Depleted of U^{235}. – Experiment S-130 employed a type 347 stainless steel autoclave and specimens of the same material. The solution composition was about the same as that employed in HRT run 13. The autoclave was exposed in the multiple-hole HB-5 facility at 280°C for 370 hr of radiation and then at 250°C for 726 hr of additional radiation.

The results of oxygen pressure measurements during exposure are shown graphically in Fig. 14.20, where the average corrosion penetration calculated from the oxygen data is plotted against the radiation time. Pressure data obtained with a previous experiment, H-95[45] (0.04 *m* enriched UO_2SO_4, 0.05 *m* $CuSO_4$, and 0.04 *m* H_2SO_4 in light water), exposed at temperatures of

[44] G. H. Jenks *et al.*, *HRP Quar. Prog. Rep. July 31, 1957*, ORNL-2379, p 119–21.

[45] G. H. Jenks *et al.*, *HRP Quar. Prog. Rep. April 30, 1956*, ORNL-2096, p 93–94.

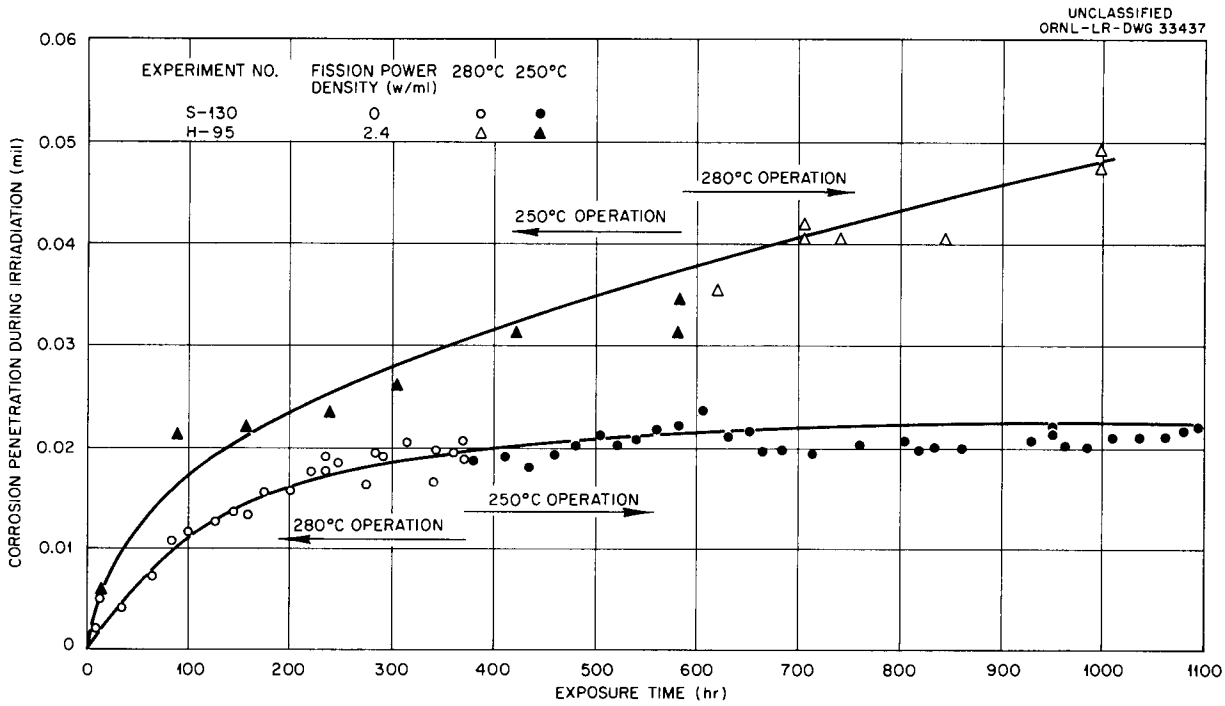

Fig. 14.20. Corrosion of 347 Stainless Steel in In-Pile Autoclave.

250 and 280°C and at a fission power density of 2.4 w/ml are included in Fig. 14.20 for comparison with the S-130 data.

The specimens in S-130 exhibited weight gains as-removed, with little difference in the amount of weight gained with the exception of the forward, highest flux specimen. This specimen gained about one-third as much weight as the average of the weight gained by the others. The weight-gain data are reported in Table 14.15 as calculated average values of penetration rather than as corrosion rate because the experiment was exposed at two different temperatures and because the corrosion rate was not constant during exposure. No pressure of radiolytic gas was detected during exposure at either temperature.

The results show that the corrosion of steel in the depleted UO_2SO_4 solution employed in S-130 is accelerated during the initial exposure to reactor radiations. The rate decreased with radiation and became very small after a penetration of about 0.02 mil had taken place. In general, the corrosion-time behavior in this depleted experiment did not appear to differ appreciably from that in the former experiment H-95, which employed an appreciable fission power density in solution. Autoclave data obtained in other previous in-pile experiments of steel corrosion in UO_2SO_4 solutions containing excess H_2SO_4 have exhibited a similar behavior pattern. Most of the earlier tests were exposed at 250°C and to a range of solution power densities of about 2–10 w/ml. Moderate attack rates (1–5 mpy) occurred for an initial period of 100–300 hr of exposure, and the later continuing rates were quite low (0.2–0.5 mpy).

14.3 HRT SERVICE CORROSION

14.3.1 HRT Specimen and Scale Examinations

(a) Introduction. – Following HRT runs 13 and 14, several metallic specimens were removed from the reactor high-pressure system and transferred to the Materials Research Section for examination. Samples of scale accumulations in the high-pressure system were also taken after these runs and transferred to the Materials Section. A list of components, specimens, and samples which have been received in connection with runs 13 and 14 is given in Table 14.17. The operations which have been performed or which are in progress with each of these samples are also shown in the table.

Table 14.17. List of Components, Specimens, and Samples Removed from HRT After Runs 13 and 14, with Examinations and Operations Performed

Run No.	Sample Identification	Examinations and Operations*												Scale Analysis*			
		As Removed							Descaled								
		Visual	Photo-graphy	X-Ray	Spectrometer Scan	Weight	Scale Removal: Mechanical	Scale Removal: Defilming	Weight	Visual	Photo-graphy	Metallographic or Microscopic	Induced Activity Analysis	Chemical	Radio-chemical	Specific Fe^{59} Activity	Others
13	Core access flange																
	Solution side	C	C	C**	C**		C			C	C			C	C	C	
	Exterior side	C					C							C			
13	Line 103 coupon array	I	I	C	C	C		C***	C	C	I	P	P	I	I	I	
13	Line 100 scale accumulation	C	C	C	C							P		C	C	C	Particle property determinations proposed
13	Core scale	C	C	C	C							P		C	C	C	Particle property determinations proposed
14	Core access flange	C	C				C							C	C	C	
	347 SS specimen	C	C			C	C	C	C	C	I	P	P	C	C	C	
	Titanium spacers	C	C			C	C	C	C	C	I			C	C	C	
14	Core scale	I	I	P	P									P			
14	Blanket corrosion specimen array	I	I			C		P	P			P	P	P	P		Tensile and impact testing proposed

*Legend: C – completed; I – incomplete; P – proposed.
**Analysis of scale removed from component.
***Only one coupon of each material (347 SS, 309 SCb SS, titanium, and Zircaloy-2) has been defilmed to date (7-21-58).

A sketch of the reactor which shows the general location of specimens during exposure is given in Fig. 14.21. A brief discussion and description of some of the samples and of the sampling techniques are given below.

The results of these examinations are being reported as they become available. Some of the data which are available have not been correlated as yet. Discussion in this report is limited to the results of specimen weight measurements and chemical analyses of scale.

(*b*) Specimen Description and Results of Examination. – (1) *Line 103 Samples, Run 13.* – The line 103 coupon assembly which was received after run 13 contained eight coupons, two each of type 347 stainless steel, 309 SCb stainless steel, Ti-75A, and Zircaloy-2. A description of the assembly and information regarding exposures prior to run 13 have been reported.[46] To date, one coupon of each material has been defilmed. The remaining four coupons and holder have been retained for future evaluation. A separate defilming bath was employed for each specimen, and the separate defilming solutions were transferred to the Analytical Chemistry Division for chemical and radiochemical analyses.

The results of microscopic examination of the specimens indicated that all components of the assembly retained some transported iron oxide film. There was clear evidence of solution penetration into the crevice areas between the coupons and the titanium holder. Each of the stainless steel coupons exhibited evidence of accelerated attack in some portions of the crevice region.

The results of weight measurements on these specimens are listed in Table 14.18. The order of listing is the same as the order of arrangement of coupons in the holder, with the solution flowing from H-87 to H-78. The average depths of corrosion penetration calculated from the weight losses are shown in the next to last column. The value for the 347 stainless steel coupon is about 0.06 mil and that for the 309 SCb coupon is 0.23 mil. For comparison, if corrosion of steel in

[46] R. M. Warner, *HRT Corrosion Sample Data and Fabrication – Circulating Lines* – Addendum No. 1, ORNL CF-56-6-62 (Aug. 1, 1957).

UNCLASSIFIED
ORNL–LR–DWG 32901

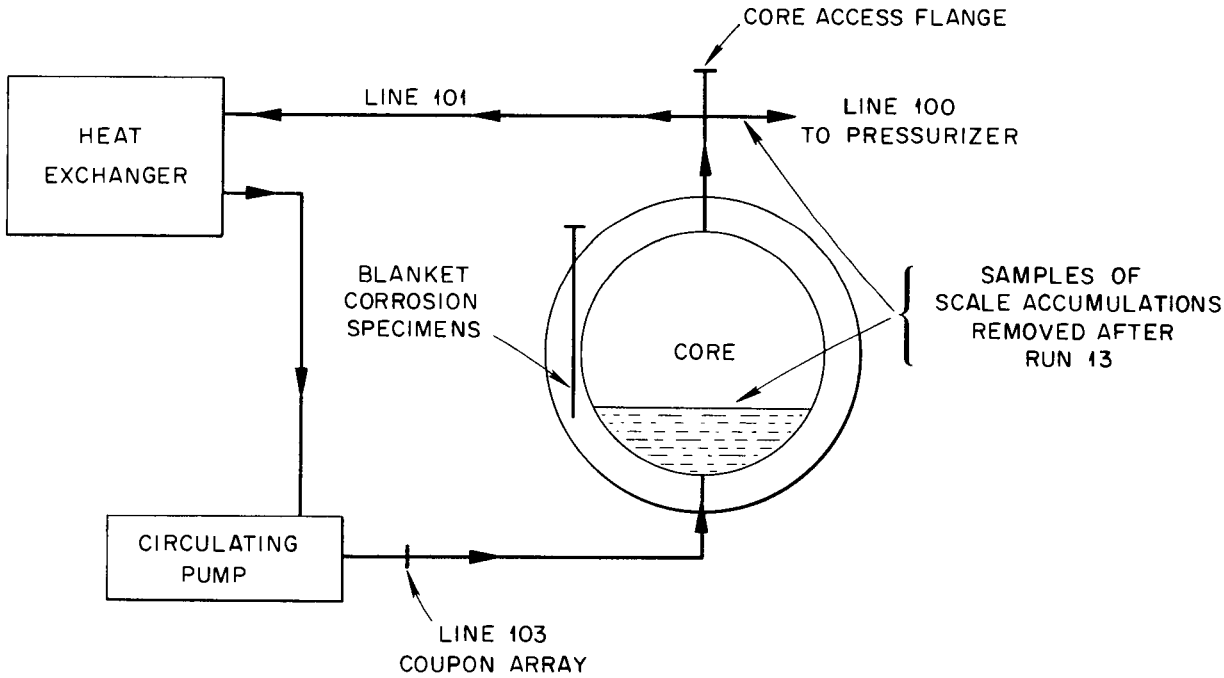

Fig. 14.21. In-Reactor Location of Metal and Scale Specimens Examined After HRE-2 Runs 13 and 14.

Table 14.18. Weight Data for Corrosion Coupons From HRT Holder 103 After Run 13 and for Core Access Corrosion Coupon Exposed During Run 14

Run Number	Sample Number	Material	Area (cm^2)	Initial Weight (g)	First As-Removed Weight* (g)	Second As-Removed Weight** (g)	Defilmed Weight (g)	Weight Change Between Final and Initial (mg)	Corrosion Penetration (mils)	Removed Scale Weights (mg/cm^2)
13	H-87	Ti-75A	20.7	16.6105	16.6115	16.6492				
13	H-88	Ti-75A	20.7	16.5430	16.5438	16.5860	16.5411	−1.9	0.008	2.17
13	H-95	Zircaloy-2	20.7	24.0233	24.0287	24.0406	24.0290	+5.7		0.56
13	H-96	Zircaloy-2	20.7	24.1542	24.1604	24.1693				
13	H-70	347 SS	20.7	29.0756	29.0805	29.1144	29.0523	−23.3	0.055	3.00
13	H-71	347 SS	20.7	29.0955	29.1013	29.1332				
13	H-77	309 SCb SS	20.7	28.8648	28.8703	28.8587				
13	H-78	309 SCb SS	20.7	28.9662	28.9714	28.9100	28.8679	−98.3	0.23	2.04
14	Specimen A	347 SS	61.7	82.5274		83.2610	82.5166	−10.8	0.009	12.1

*Weight after HRT run 7 reported in ORNL CF-56-6-62 Addendum No. 1.
**Weight after HRT power run.

only the high-pressure system accounted for the 500 g of nickel entering solution during run 13, and if this corrosion were uniform over the various steel surfaces, the average corrosion penetration would be about 0.5 mil. The amount of oxide removed in defilming a given specimen is shown in the final column.

The results of chemical analyses for various constituents in the different defilming solutions are given in Table 14.19. No reliable control analysis of the defilming solution is available, but the solution, as prepared, is known to contain nickel and copper in amounts sufficient to influence the results. It is also known that iron is present in the defilming solution, but the concentration of this element is probably small compared with the amounts in the scale sample. No correction has been applied for the presence of any of these materials in the as-prepared solution. Chromium was sought in the scale solution but was not detected. No explanation other than experimental uncertainty is offered for the anomalously high values for iron in the H-95 sample.

(2) *Core Access Flange for Run 13.* – During run 13, the core access was closed with a blind flange (six threaded mounting holes were in the flange). The flange was removed after run 13 and transferred to the Materials Section. Examination showed that the interior recessed portion of the flange was covered with a reddish-brown, rustlike scale. There was some evidence of an effect of solution flow on the scale in that the rust accumulation was heavier in the center and along the outer edges of the recess than in a circular ring between these areas. There was some evidence of surface roughening in areas where the scale had flaked off. From the visual and microscopic examination, it was judged that scale thickness on the flange was about the same as that on the 347 stainless steel specimen H-70, Table 14.18.

A sample of scale scraped from the flange surface was analyzed chemically and spectrographically for several elements by members of the Analytical Division; the results are included in Table 14.20. The scale was dissolved by the Analytical group, and both chemical and spectrographic analyses were made with the one solution. As may be seen in the table, the two methods gave different results for the concentration of a given element in the scale. The scale was identified by x-ray diffraction to be predominantly Fe_2O_3.

(3) *Core Access Flange and Sample for Run 14.* – Following the run 13 flange examination, a triangular-shaped type 347 stainless steel specimen was attached to the flange with titanium

Table 14.19. Chemical Analyses of Scale Removed by Defilming Coupons from HRT Holder 103 After Run 13

Sample No.	Material	Weight* (mg)	Per Cent of Scale Represented by Constituents	Amount of Constituent in Scale (wt %) and Mass Ratio of Element to Iron in Scale									
				Fe	U	U/Fe	Zr	Zr/Fe	Ni	Ni/Fe	Cu	Cu/Fe	Ti
H-70	347 SS	62.1	35	30	1.5	0.05	2.0	0.07	<1	<0.03	<1	<0.03	
H-78	309 SCb SS	42.1	80	75	0.5	0.007	1.0	0.01	<2	<0.03	<4	<0.05	
H-88	Ti-75A	44.9		80	1.0	0.01	2.0	0.03	<3	<0.04	<5	<0.06	34
H-95	Zircaloy-2	11.6		120	0.5	0.004	7.0	0.06	<6	<0.05	<5	<0.04	

*The weight of the material analyzed was determined by the difference between the as-removed and defilmed coupon weights.

Table 14.20. Analyses of Scale Removed from HRT After Runs 13 and 14

Run No.	Source of Scale	Sample Weight (g)	Analytical Technique	Per Cent of Scale Represented by Constituents	Amount of Constituent in Scale (wt %) and Mass Ratio of Element to Iron in Scale										
					Fe	U	U/Fe	Ni	Ni/Fe	Cu	Cu/Fe	Cr	Cr/Fe	Zr	Zr/Fe
13	Core I*	1.7329	Chemical		18.2	0.32		0.18	0.010	0.09		0		0.01	
			Spectrographic		18.5			0.35	0.019	0.15		2.3		0.17	
13	Core II	1.2033	Chemical	13.5	10.4	2.0	0.2	0.6	0.06	0.4	0.04	0.1	0.01	0	0
13	Line 100	0.4437	Chemical	12.0	7.7	2.5	0.3	0.8	0.10	0.2	0.03	0.8	0.10	0	0
13	Core access flange, fuel side	0.0655	Chemical	36.0	34.6	0.4	0.01	0.5	0.015	0	0	0	0	0.2	0
			Spectrographic	75.0	65.0			1.3	0.020	0.2	0.003	7.1	0.11	1.5	0.023
14	Access flange	0.0292	Chemical	43.9	36	0.14	0.004	0.6	0.016	0.7	0.019	6.5	0.18	Nil	
14	Core access, type 347 SS sample A	0.0658	Chemical	41.6	39.5	0.11	0.003	0.4	0.010	0.6	0.015	1.0	0.025	Nil	
14	Titanium spacer employed with type 347 SS sample A	0.0489	Chemical	42.7	40.2	0.23	0.006	0.6	0.015	0.6	0.015	1.1	0.027	Nil	

*This sample splattered during the dissolving process after a dilute HNO_3 leach. The contents of the leach solution were not included in this sample.

bolts and spacers. The spacers were used to offset the specimen and permit free access of solution to all surfaces. The steel specimen was pretreated in 280°C water. The titanium spacers were identified, degreased, dried, weighed, and installed without further pretreatment. The flange was installed for HRT run 14 and, at the conclusion of the run, was returned to the Materials Section for examination.

Examination of the flange and specimen assembly revealed that all surfaces exposed to the solution were heavily coated with a loosely adherent, granular, reddish-brown scale. The thickness of scale on the specimen was estimated from visual shadow-comparison to be between 5 and 10 mils.

Separate samples of scale scraped from the specimen, spacers, and a portion of the flange which had not been scraped following run 13 were analyzed chemically by the Analytical group. The results are included in Table 14.20.

The results of weight measurements on the installed, as-removed, and defilmed flange specimen are shown in Table 14.18. The average corrosion penetration indicated by the loss in weight of the specimen during exposure is 0.009 mil. A penetration of this depth certainly occurred during the pretreatment of the specimen, and, hence, the indicated corrosion during run 14 is extremely small. The weight lost by the specimen during defilming shows that the average weight of the scale was 12 mg/cm^2. As mentioned above, the scale was 5 to 10 mils in thickness; hence the indicated bulk density of the scale is 0.5 to 1.

(4) *Core and Line 100 Scales Following Run 13.* – A sample of scale from the core, mostly

from the top diffuser plate, was obtained by the Reactor Operations Section following run 13. An aspirator with a shielded Filtron filter unit as a collection chamber was employed in the recovery. A sample of scale from line 100 (the connecting line between the core and the pressurizer) was also recovered, with a mechanically driven auger and a catch bucket. No material was found in the catch bucket, but the flutes of the auger were coated, and a sample was thus obtained.

Visually, the scales appeared to be highly porous accumulations of rust-colored material, similar to hematite or limonite ore concentrates. The core scale was largely made up of chunks or flakes. Some large ripples were noted on this material, but none of the irregularities simulated machine marks. These materials were analyzed chemically and spectrographically by the Analytical group. The results are given in Table 14.20. The results for core sample 1 are not considered representative of the original sample, since the original material was leached in dilute HNO_3 before dissolving, and, in addition, considerable splattering occurred during the dissolution step. The results are included in Table 14.20 for comparison between the chemical and spectrographic analyses.

(c) **Discussion of Results of Specimen Weight Measurements.** – The type 347 stainless steel coupon from line 103 which was examined after run 13 exhibited a weight loss which corresponds to an average corrosion penetration of 0.06 mil. The results for the similarly located 309 SCb stainless steel coupon correspond to an average penetration of 0.23 mil. In comparison, an average penetration of about 0.5 mil would be expected if all of the probable steel corrosion in this run was in the high-pressure system with uniform attack of the different steel surfaces in this system. The only other high-pressure steel surface which was examined closely after this run, that of the core access flange, showed evidence of surface roughening. Such roughening is indicative of some corrosion attack. In general, it is believed that the specimen data are not inconsistent with the postulate that the majority of the steel corrosion in run 13 was in the high-pressure system, with fairly general attack of the different surfaces. The sample data, however, show that the attack was not entirely uniform.

The only type 347 stainless steel specimen examined after run 14 was the core access specimen. Weight results of the examination showed that the corrosion attack of the specimen during the run was negligibly small.

(*d*) **Discussion of Results of Scale Analyses.** – Visual examination of the core and of line 100 by the Reactor Operations Group and by others after run 13 indicated that a large amount of scale had accumulated in these regions. The results of scale weight measurement on line 103 coupons and of visual examination after run 13 are consistent with the postulate that most of the scale estimated to have been formed during the run was not on the stainless steel surfaces in the high-pressure system. Only 20% or less of the amount expected could be accounted for in uniform distribution of oxide over the different high-pressure steel surfaces.

The large amount of scale deposited on the core access flange and specimen array after run 14 and the negligible change in weight of the metal specimen during the run indicate that appreciable quantities of oxide were transported through the solution during the run. This scale may have come from the accumulation observed in the core after run 13. Such a transfer from the regions of high fission power density in the core to the surfaces at low power density outside the core is in accord with the results of in-pile loop experiments. In these experiments, there is evidence that bulk scale is transferred from the core to surfaces in regions external to the core.[47] Visual examination of the reactor core by the Reactor Operations Section and by others after run 14 indicated[48] that the quantity of scale in that region was less than after run 13.

14.3.2 HRT Corrosion Specimens

The assembly of a corrosion specimen holder[49–51] for installation in the core tank of

[47] G. H. Jenks *et al.*, *HRP Quar. Prog. Rep. Jan. 31, 1958*, ORNL-2493, p 120–22.

[48] R. B. Briggs, oral communication.

[49] W. R. Gall *et al.*, *HRP Quar. Prog. Rep. Oct. 31, 1956*, ORNL-2222, p 7–10, Figs. 2.1 and 2.2.

[50] G. H. Jenks *et al.*, *HRP Quar. Prog. Rep. Jan. 31, 1958*, ORNL-2493, p 139–40.

[51] R. M. Warner, D. T. Jones, and B. W. Scott, *HRT Corrosion Specimens and Holder: Core Region of Pressure Vessel (Loading No. 1)*, ORNL CF-58-7-68 (July 11, 1958).

the HRT was completed during the past period. Three thermocouples sheathed with stainless steel–titanium were installed in the assembly so as to extend to three different locations in the core. These thermocouples, which are for use in estimating the temperature of the corrosion test specimens, penetrate the top flange closure of the assembly and are made leak-tight by means of gold gasket seals as shown in Fig. 14.22. A backup seal weld is also used in the event of leakage past the gasket seal.

A temperature calibration and response-time measurements were obtained on these thermocouples prior to installation. The response-time

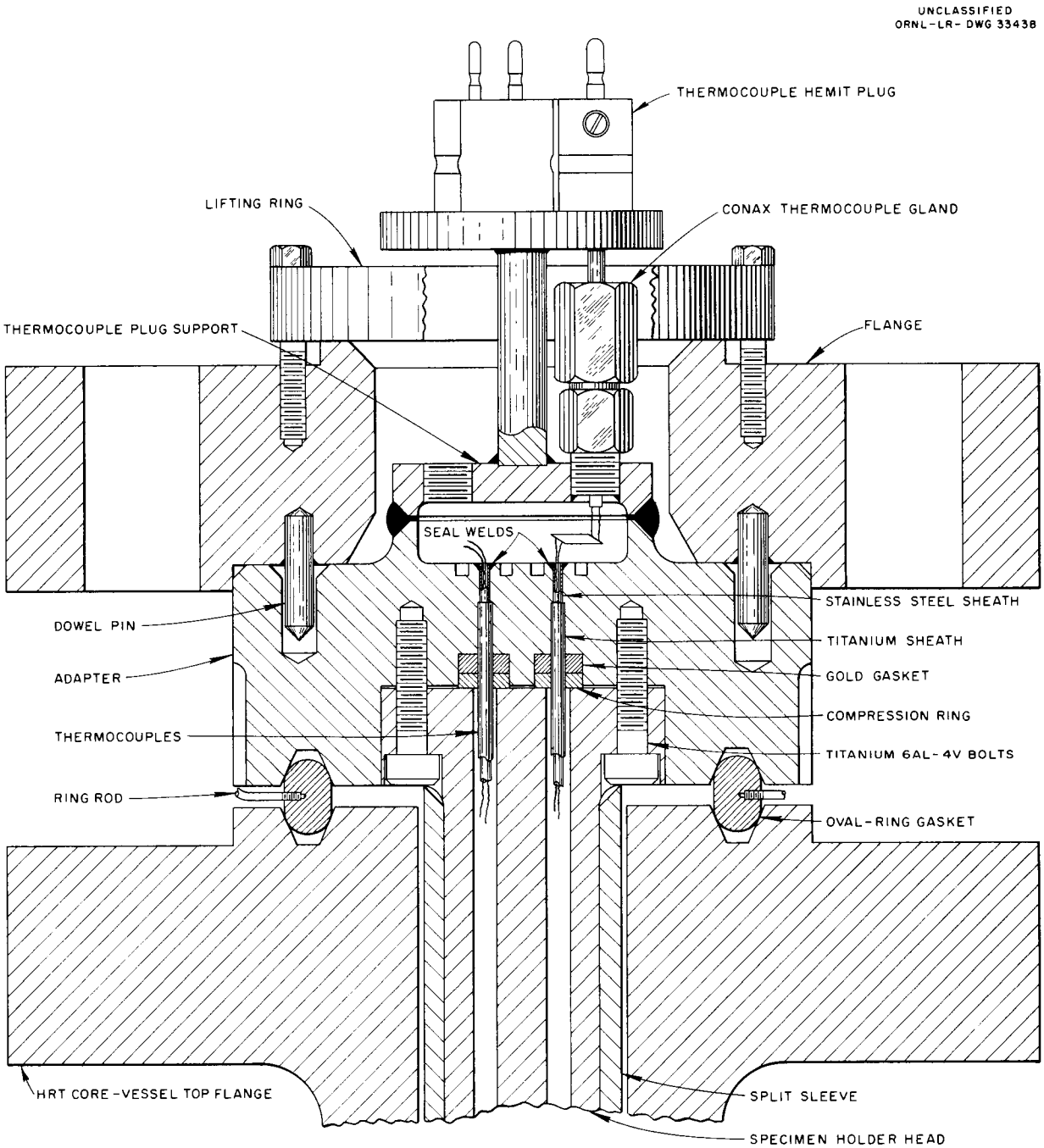

Fig. 14.22. Thermocouple Assembly for HRT Core-Vessel Specimen Holder.

checks were made in both heated water and oil baths under varying degrees of agitation to permit an evaluation of the effect of the film heat transfer coefficient on the over-all temperature response time.

The sample holder adapter was bored, and a set of gold gaskets and a compression ring were selectively fabricated for each individual thermocouple sheath. A torque of approximately 40 ft-lb was used in tightening the bolts to create the seal between the thermocouple sheaths, the gaskets, and the adapter. The joint assembly was then temperature-cycled from room temperature to 300°C three times with retorquing of the bolts. A helium leak test followed each thermal cycle. No leakage was detected after the initial tightening of the bolts or after each of the three temperature cycles. The backup seal welds between the stainless portions of the sheath and the adapter have been made satisfactorily.

The first core specimen holder assembly was installed in the HRT during the week of July 21, 1958.

Two blanket sample holders with samples installed[52] were delivered to the HRT during the report period. The first holder[53] was installed in the HRT at the beginning of run 12 and was removed after run 14 for sample examination. The second holder[54] was installed during the week of July 21, 1958.

---

[52]ORNL DWG D-25626, "Corrosion Specimen Blanket Assembly."

[53]R. M. Warner, D. T. Jones, and W. J. Leonard, *HRT Corrosion Specimens and Holder-Blanket Region of Pressure Vessel (Loading No. 1)*, ORNL CF-58-4-38 (April 18, 1958).

[54]D. T. Jones and B. W. Scott, *HRT Corrosion Specimens and Holder-Blanket Region of Pressure Vessel (Loading No. 2)*, ORNL CF-58-7-69 (July 18, 1958).

15. METALLURGY

G. M. Adamson

R. G. Berggren
E. S. Bomar
F. W. Cooke
C. E. Curtis
T. M. Kegley
W. J. Leonard
M. L. Picklesimer
J. J. Prislinger
P. L. Rittenhouse
R. L. Stephenson
J. K. White
J. C. Wilson
C. H. Wodtke

15.1 PHYSICAL METALLURGY

15.1.1 Zirconium-Alloy Development

Zirconium-base alloys containing niobium have shown the greatest promise in the development of a corrosion-resistant alloy to replace Zircaloy-2 as the core-tank material for aqueous homogeneous reactors. The information necessary for the development of these alloys is being procured in basic physical metallurgical studies and in in-pile corrosion tests.

Data on the transformation occurring in the Zr-Nb-*X* alloy systems have been reported.[1–6] Quench-and-reheat transformation data were obtained during the present report period for the Zr-15Nb-*X* alloys, with *X* as 2 and 5 wt % Mo, 5 wt % Pd, and 3 wt % V, over the temperature range of 300 to 600°C for times up to three weeks, and for Zr-20Nb and Zr-20Nb-*X*, with *X* as 2Mo and 2Pd, from 350 to 600°C for times up to 2 hr. No hardness increases were found in the Zr-20Nb or the Zr-20Nb-*X* alloys after they were held for 2 hr at any of the temperatures studied. The hardness data obtained for the Zr-15Nb-*X* alloys indicate that for the alloy containing 5Pd the minimum incubation time for the beginning of the hardening reaction was approximately 2 hr and occurred at a temperature between 400 and 450°C; for the 3V alloy, approximately 1.3 hr at about 525°C; for the 2Mo alloy, approximately 4 hr at about 400°C; and for the 5Mo alloy, more than two weeks at any temperature. These times are all sufficient to permit multipass welding without hardening in the heat-affected zone.

The Zr-Pd and Zr-Pt alloy systems have shown some promise as heat-treatable, corrosion-resistant alloys in in-pile tests. Since nothing is known of these alloy systems, with the exception of the phase diagram for the Zr-Pt system, physical-metallurgical studies are now being made. Specimens of Zr-Pd and Zr-Pt alloys containing 5 and 10 wt % of the alloying element have been quenched and aged for the early determinations of structure and transformations. Isothermal transformation studies have been started on the Zr-5Pd alloy at temperatures from 350 to 600°C for times up to 2 hr. Metallographic preparation of these alloys is very difficult, and etching and polishing procedures must be developed further before the specimens already prepared can be evaluated.

The Zr-Nb-*X* alloy specimens exposed in in-pile loop L-2-17 (0.04 *m* UO_2SO_4, 300°C, 2625 Mwhr, 1300 hr at temperature) are being examined microscopically. From the work that has already been accomplished, it may be concluded that the radiation exposure caused no major differences in microstructures in comparison with the in-line specimens and with out-of-pile control specimens aged for similar times.

15.1.2 Zircaloy-2 Fabrication Study

The Zircaloy-2 produced by the normal commercial practice of rolling from 840°C (1550°F) contains intermetallic and gas stringers and an undesirable amount of preferred orientation with its accompanying anistropy of mechanical properties.[6] A new fabrication schedule has been

[1] G. M. Adamson *et al.*, *HRP Quar. Prog. Rep. Oct. 31, 1956*, ORNL-2222, p 114–16.

[2] G. M. Adamson *et al.*, *HRP Quar. Prog. Rep. Jan. 31, 1957*, ORNL-2272, p 119–23.

[3] G. M. Adamson *et al.*, *HRP Quar. Prog. Rep. April 30, 1957*, ORNL-2331, p 124.

[4] G. M. Adamson *et al.*, *HRP Quar. Prog. Rep. July 31, 1957*, ORNL-2379, p 122–26.

[5] G. M. Adamson *et al.*, *HRP Quar. Prog. Rep. Oct. 31, 1957*, ORNL-2432, p 131–33.

[6] G. M. Adamson *et al.*, *HRP Quar. Prog. Rep. Jan. 31, 1958*, ORNL-2493, p 141–48.

developed and reported.[7] While the material produced by the new schedule is free of intermetallic stringers and, as described in Sec 15.2.1, possesses much more isotropic mechanical properties, it has not been shown to produce material of optimum properties for use in general construction. The isotropy of mechanical properties and the degree of preferred orientation will be determined as functions of the variables of fabrication. The completed study should permit fabrication schedules to be specified so that material can be produced with almost any degree of preferred orientation and anistropy of mechanical properties.

A study of fabrication schedules is being conducted that involves, as variables, the number of beta quenches, cold and hot reductions, cross-rolling, annealing temperatures, and total reductions between anneals. An annealing study has been completed on material fabricated to nine schedules, and it has been shown by metallography that the optimum annealing time and temperature were 30 min and 775°C. Impact and tensile blanks from the materials have been annealed and air cooled. The tensile specimens for all nine schedules have been machined and broken. The tensile data are being analyzed, as are the specimens themselves.

All the tensile specimens have shown elliptical cross sections after fracture, the eccentricity varying with the fabrication schedule and the orientation of the specimen within the rolled plate. Considerable variations in yield and tensile strengths and elongations have been observed, but no obvious correlation to fabrication variables or eccentricity has been found. An optical comparator is being used to obtain the measurements of the cross sections of the broken specimens from the fracture to the shoulder. These measurements provide information on the reduction of area, eccentricity, and flow pattern along the length of the specimen.

15.1.3 Zirconium Hydride Layer Study

It has been claimed, from evidence obtained by x-ray diffraction techniques, that a hydride layer exists between the metal and the oxide layer formed in aqueous corrosion of zirconium-base alloys. The existence of such a layer might explain some of the corrosion data obtained on zirconium and Zircaloy-2, and some of the lack of reproducibility in testing.

A study has been initiated to develop a method for identifying and examining a very thin hydride layer on the surface of a zirconium-base alloy. Zircaloy-2 specimens have been hydrided to total contents of 100 and 250 ppm H_2 at 300°C in the Sievert's apparatus to produce a layer of hydride on the surface of the specimens. The hydride was found to exist as discrete patches, or spots, scattered over the surface of the specimens without any apparent relationship to the underlying metal structure. If any hydride layer existed between the patches, it could not be detected. Specimens hydrided at 400°C to 100 ppm H_2 have been slant-polished, electro-polished, chemically polished, and replicated with Faxfilm in the as-polished condition in an attempt to detect and examine the surface layer. In all cases, the edge-rounding of the specimen was sufficient to obscure the hydride layer if it does exist.

Specimens were hydrided at 600°C just long enough for a decrease in pressure to occur and were immediately cooled to 300°C in an attempt to activate the entire surface at high temperature but to form a layer characteristic of 300°C and 500 ppm H_2. The specimen showed a hydride layer that could be examined, but, unfortunately, it had apparently reached an equilibrium condition with the hydrogen atmosphere at a temperature near 500°C. The center of the specimen showed hydride particles of a density and size equivalent to those of a specimen equilibrated at 500°C to a total content of about 200 ppm H_2.

The examination of a slant-polished specimen hydrided to 500 ppm H_2 at 400°C has shown that the fine "needles" of hydride reported by several observers to exist in the grains of Zircaloy-2 just under the hydride layer, rather than as the expected films in the grain boundaries, are actually small deformation twins. The twins result from the deformation of the surface layer of the specimen during the formation of the layer of hydride and are caused by the rather large volume increase occurring in the conversion of zirconium to hydride. The microstructures observed are shown in Fig. 15.1 in bright-field illumination and in polarized light and are of the same area. These structures show how the deformation twins can be easily mistaken for hydride needles if the examination is made only in bright field. A normal

[7] M. L. Picklesimer and G. M. Adamson, *Development of a Fabrication Procedure for Zircaloy-2*, ORNL CF-56-11-115 (Nov. 21, 1956).

cross-section examination of the interface between the specimen and the surface hydride showed that the twins were observed only as very thin lines which could be easily mistaken for the so-called hydride "etch-pitlines" found in some high-purity zirconium specimens water-quenched from temperatures above about 500°C.

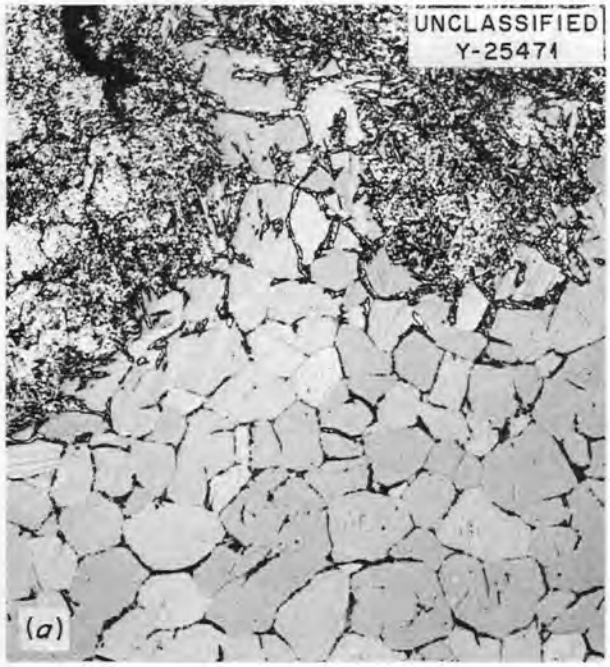

Fig. 15.1. Deformation Twins Under Surface of Hydrided Zircaloy-2. (*a*) Bright field; (*b*) polarized light.

15.1.4 Recombiner-Loop Specimens

Specimens of iodide zirconium, iodide titanium, titanium A-55, titanium A-110AT, Zircaloy-2, Zr-15Nb, and type 430 stainless steel were held in the cell liquid, cell vapor, and recombiner sections of a recombiner loop.[8] The loop was operated by the Component Development Section of REED to study the effects of several variables and catalysts on the high-temperature recombination of electrolytically generated H_2 and O_2. The cell liquid was operated at a temperature of 230°C; the specimen location in the cell vapor was at a temperature of 235 to 280°C; and the recombiner section was operated at 430 to 500°C. Hydrogen analyses of the specimens have been obtained and are reported in Table 15.1.

Comparison of the data with data obtained in prior loops[9] (listed as footnotes in the table) shows several discrepancies in the hydrogen contents for a given material in a particular position. Metallographic examination of the specimens confirmed generally the hydrogen contents determined by equilibrium pressure analysis. Appreciable corrosion was shown by all the titanium alloys and by the type 430 stainless steel in both the liquid and the vapor section of the boiler, but the hydrogen contents could not be correlated with the amount of corrosion which occurred on the specimens.

The data presented in Table 15.1, plus data obtained in prior tests, show that the titanium alloys pick up large amounts of hydrogen in the cell-liquid and -vapor positions but not in the recombiner section, while the zirconium alloys pick up major amounts of hydrogen in the recombiner section but not in the cell-liquid or -vapor positions. The type 430 stainless steel specimens picked up some hydrogen in all positions, but the effects of hydrogen on this steel are not known.

---

[8] I. Spiewak, *HRP Quar. Prog. Rep. Jan. 31, 1958*, ORNL-2493, p 53.

[9] M. L. Picklesimer, *Examination of Recombiner Loop Specimens of Zr and Ti Alloys*, ORNL CF-56-10-37 (Oct. 2, 1956).

Table 15.1. Hydrogen Contents of Recombiner-Loop Specimens

Specimen Position	Hydrogen (ppm)						
	Zr	Zircaloy-2	Zr–15Nb	Ti	A-45 Ti	Ti A-110AT	430 SS
Control	80	60	44	92	27	73	4
Cell liquid (230°C)	28	63	46	1800	1100	4500[a]	47
Cell vapor (235–280°C)	30	78[b]	62	120[c]	51[d]	1400	14
Recombiner (430–500°C)	8000[e]	140	90	140	70	190	9

[a]Estimated pressure too high for accurate reading in analysis.
[b]71, 480, 350 on prior runs.
[c]1200, 1000, 1500 on prior runs.
[d]290, 470, 540 on prior runs.
[e]1600, 40, 32 on prior runs.

15.2 MECHANICAL METALLURGY

15.2.1 Zirconium Alloys

A study is being made of the mechanical properties of zirconium alloys. This study includes the application and interpretation of the various mechanical-property testing methods when applied to, or used with, the hexagonal metals. To determine the effect of fabrication practice on isotropy, various tests have been made with plates from the fabrication study (see Sec 15.1.2).

Full-size Charpy V-notch impact energy curves from samples cut from a commercial Zircaloy-2 plate were presented previously.[6] These curves showed that both transition temperature and fracture energy varied considerably with notch and specimen orientation. The former was the more critical variable of the two. Shear lips were found on samples fractured with low energies but not on those requiring high energies.

In Fig. 15.2 are presented impact curves from a plate of Zircaloy-2 fabricated by the developed schedule. The ingot for this plate was not vacuum melted and therefore contained a higher hydrogen content than was desired. Since hydrogen is known to embrittle zirconium, the two lower sets of curves separate this variable. Even in the "as-received" condition, the four curves show much less spread than curves for the commercial plate. With the material produced by the developed schedule, shear lips were found on all samples broken above 100°C. Flat brittle breaks appeared below this temperature. Notch orientation no longer appears to be the primary variable.

In the tests reported in the two lower sets of curves, the effect of the hydrides was minimized – in one, by quenching and holding them in solution, and in the other, by removing the hydrogen by vacuum annealing. These two sets of curves are similar, and show, by the lower transition temperature and the higher fracture energies below the transition temperature, that a further improvement in impact properties may be obtained by controlling the hydrides. No brittle-appearing fractures were found on any of these samples even at the lowest temperatures.

The anisotropy of these materials was not revealed by conventional tensile tests, as shown by the data in Table 15.2. Listed in the table are tensile data from both longitudinal and transverse subsize specimens cut from the plates previously discussed, as well as scrap from the HRE-2 core tank. The differences in tensile values both at room temperature and 300°C are within the experimental limits. Even with the commercial plate, these differences are not large. Anisotropy of these materials is, however, shown by the three columns on the right side of the table. With

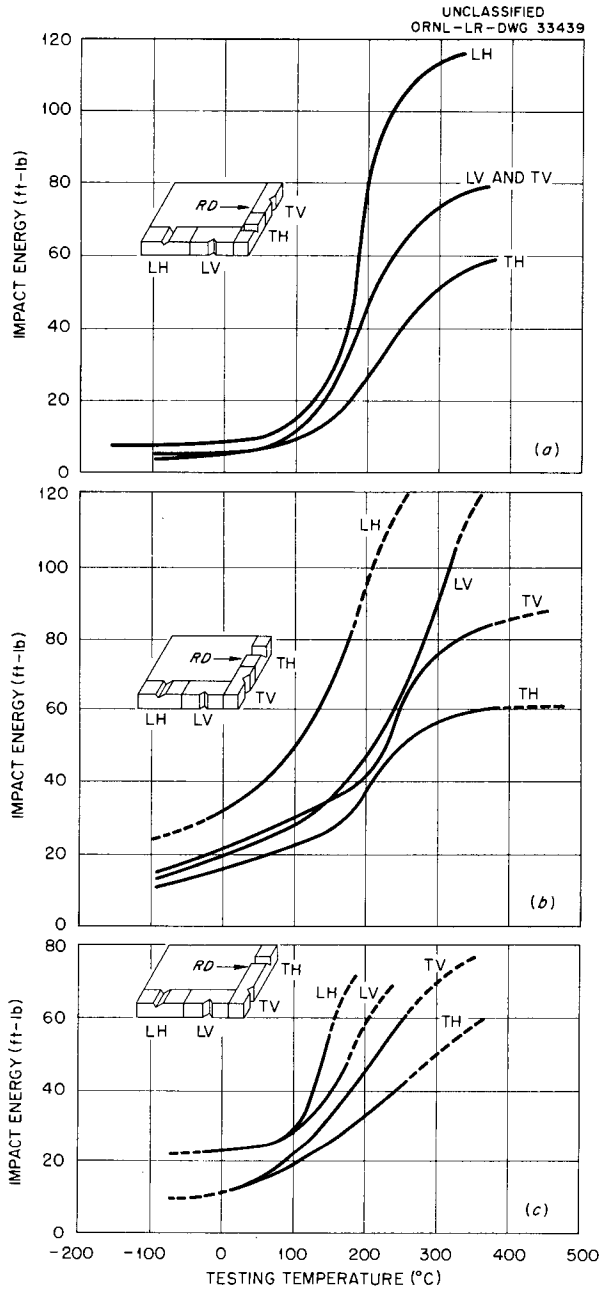

Fig. 15.2. Impact-Energy Curves of Experimentally Fabricated Zircaloy-2. (*a*) As-received; (*b*) water-quenched from 400°C; (*c*) vacuum-annealed at 800°C.

Zircaloy-2, the necked sections of fractured tensile specimens have elliptical, rather than round, cross sections. In these columns are tabulated the percentage reductions in length of both the major and minor axes of the ellipse and the ratio between them. In isotropic material the percentage reduction would be the same in both directions, and the ratio would therefore be one. The variations in these ratios appear to be a sensitive index of anisotropy. They confirm the improved mechanical properties of plate fabricated by the developed procedure.

Subsize Izod impact specimens of Zr-15Nb and Zr-20Nb alloys were heat-treated and broken to determine the effects of alloy content and some heat treatments on the impact energy curves. From the data obtained in the physical metallurgical studies of these alloys,[1,2] it is known that the beta-quenched Zr-20Nb alloy is essentially free of an embrittling omega phase. Beta-quenched Zr-15Nb alloy contains omega phase, but it too should be low in omega phase if cooled rapidly after an additional aging of 48 hr at 600°C. The impact energy curves presented in Fig. 15.3 all show apparent transition regions, which for both of the 15% Nb alloys occurred at temperatures above room temperature, and very low energy values at low temperatures. While the presence of omega phase may be a contributor to the embrittlement, omega is not a complete explanation since the embrittlement was found in all three alloys. Metallographic and x-ray diffraction studies of specimens of a 20% Nb alloy quenched in liquid nitrogen and examined at room temperature do not show any changes which could explain the low impact values obtained below room temperature. The decrease in impact energies with increasing

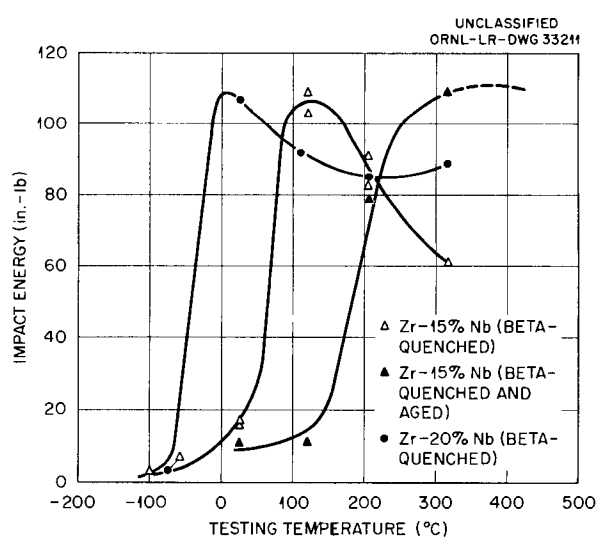

Fig. 15.3. Impact Strength of Various Zirconium-Niobium Alloys.

Table 15.2. Tensile Properties of Zircaloy-2

Plate Source*	Specimen Direction	Ultimate Strength (psi)	Yield Strength (psi)	Elongation (%)	Percentage Reduction			Isotropic Ratio, Long./Normal
					Area	Long. or Trans. Direction	Normal Direction	
				Room Temperature				
Core tank	Long.	61,400	52,300	30.7	60.6	56.6	10.0	5.7
	Trans.	63,300	59,000	24.5	62.1	57.8	10.0	5.8
Commercial	Long.	64,900	54,800	31.1	47.7	45.5	4.4	10.4
	Trans.	69,000	58,300	25.8	43.3	40.6	3.3	13.7
Experimental No. 1	Long.	73,200	63,300	31.0	46.4	35.5	16.7	2.1
	Trans.	75,200	59,400	29.1	44.0	28.4	21.6	1.3
Experimental No. 2	Long.	73,800	66,400	32.2	46.0	37.2	14.4	2.6
	Trans.	74,200	58,400	32.7	44.3	25.5	25.5	1.0
				300°C				
Core tank	Long.	28,400	22,200	38.8	77.6	68.9	27.2	2.5
	Trans.	32,200	29,600	27.9	76.2	71.1	17.8	4.0
Commercial	Long.	32,600	25,500	35.5	43.5	38.4	7.8	4.9
	Trans.	29,300	21,200	29.3	68.4	65.5	13.3	4.9
Experimental No. 1	Long.	38,600	31,400	30.4	64.5	52.2	24.4	2.1
	Trans.	37,600	29,000	31.5	61.5	43.8	31.6	1.4
Experimental No. 2	Long.	32,800	27,800	32.9	76.5	63.3	35.5	1.8
	Trans.	35,000	25,100	32.1	68.7	48.3	39.4	1.2

*Core tank – scrap material from HRT core-tank fabrication.
Commercial plate – commercial plate similar to above but straight rolled.
Experimental plate 1 – fabricated commercially by developed procedure in Sec 15.1.2 except inert-gas melted.
Experimental plate 2 – same plate as item 3 but refabricated in laboratory using same procedure.

break temperature above the transition was probably caused by aging during heating to fracture temperature.

15.2.2 Mechanical Properties of Irradiated Titanium and Zirconium Alloys

Subsize mechanical-property specimens have been exposed in in-pile loops to determine whether any adverse mechanical-property changes should be expected under homogeneous reactor conditions. Such samples are exposed directly to the fissioning uranyl sulfate solution and will therefore show effects from both the loop environment and the neutron irradiation.

Data from subsize Izod-type impact specimens from two titanium alloys exposed in loop L-4-16[10] (0.17 *m* UO_2SO_4, 280°C, estimated fast-neutron dose 4.9 to 9.5×10^{18} *nvt*) are plotted in Fig. 15.4. The control samples were as-machined and had

[10]G. H. Jenks *et al.*, *HRP Quar. Prog. Rep. July 31, 1957*, ORNL-2379, p 101–14.

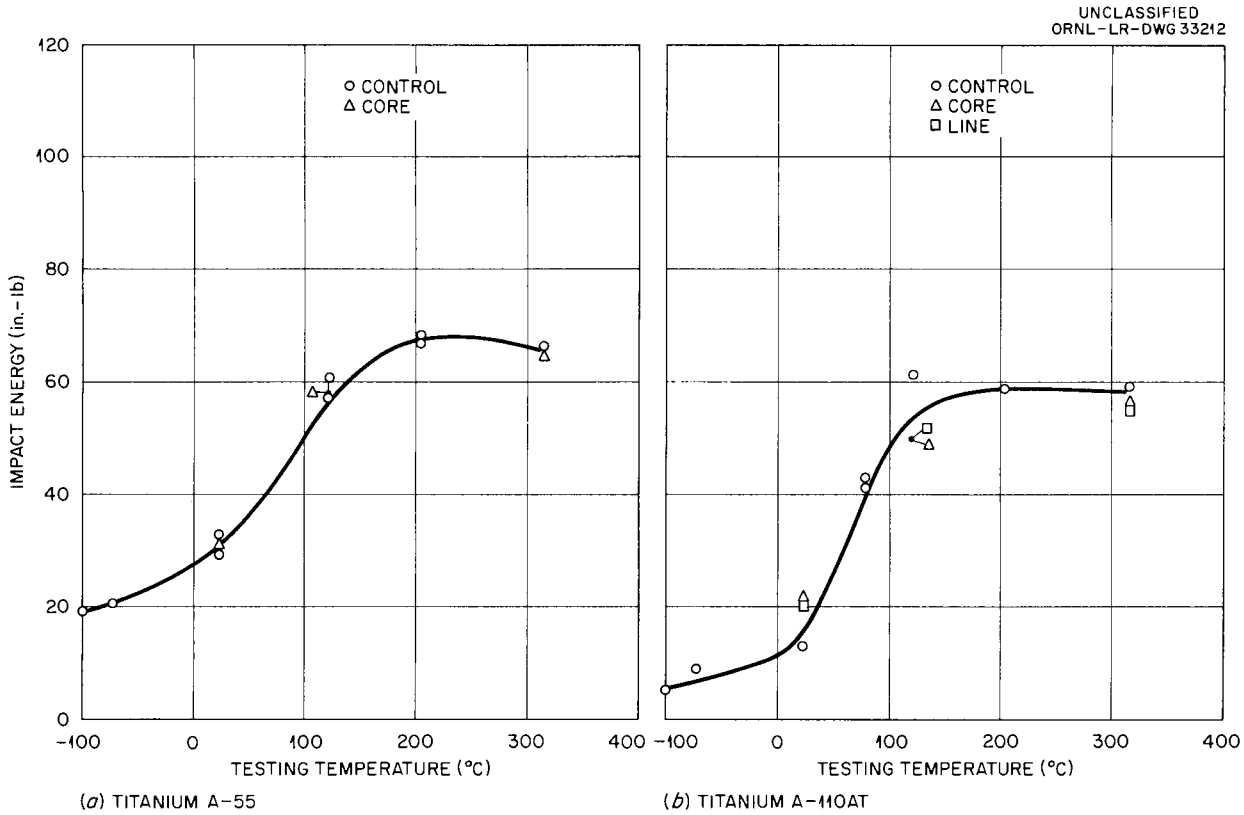

Fig. 15.4. Impact Strength of Titanium Alloys After Exposure in In-Pile Loops. (*a*) Titanium A-55; (*b*) Titanium A-110AT.

not received a thermal treatment similar to that to which the loop samples had been subjected. The line and core specimens were exposed to the same circulating solution and were maintained at the same temperature. The samples in the core were subjected to neutron irradiation, while those in the line were exposed to negligible fluxes. With both A-55 and A-110AT titanium the impact energy values for the three types of samples fall within a normal spread; therefore it may be assumed that no change of properties occurred under the environmental conditions encountered in this loop.

Similar impact data for several zirconium alloys are shown in Fig. 15.5. Samples of Zircaloy-3a (0.25% Fe, 0.25% Sn, Zr) were irradiated in loop L-4-13[11] (0.17 *m* UO_2SO_4, 250°C, estimated fast dose 2.5 to 5.1 × 10^{18} *nvt*), and specimens of crystal-bar zirconium were exposed in loop L-2-15[12] (0.17 *m* UO_2SO_4, 280°C, estimated fast dose 0.7 to 1.4 × 10^{19} *nvt*). Again, since no consistent differences were found between the control, line, and core samples, it appears that no change in mechanical properties occurred with either of these materials. This conclusion confirms the lack of change previously reported[5] and based on tests with tensile specimens of these alloys.

The impact curves in Fig. 15.5*c* are for a group of Zr-20Nb alloys that had been irradiated in loop L-4-13.[11] Comparison of these curves with the curve in Fig. 15.3 shows that a large change in impact properties occurred during loop exposure. The transition region shifted to a temperature several hundred degrees higher than in the original samples. However, since the values are the same for the line and core samples, the change is not a

[11] G. H. Jenks *et al.*, *HRP Quar. Prog. Rep. April 30, 1957*, ORNL-2331, p 113–16.

[12] G. H. Jenks *et al.*, *HRP Quar. Prog. Rep. July 31, 1957*, ORNL-2379, p 101–14.

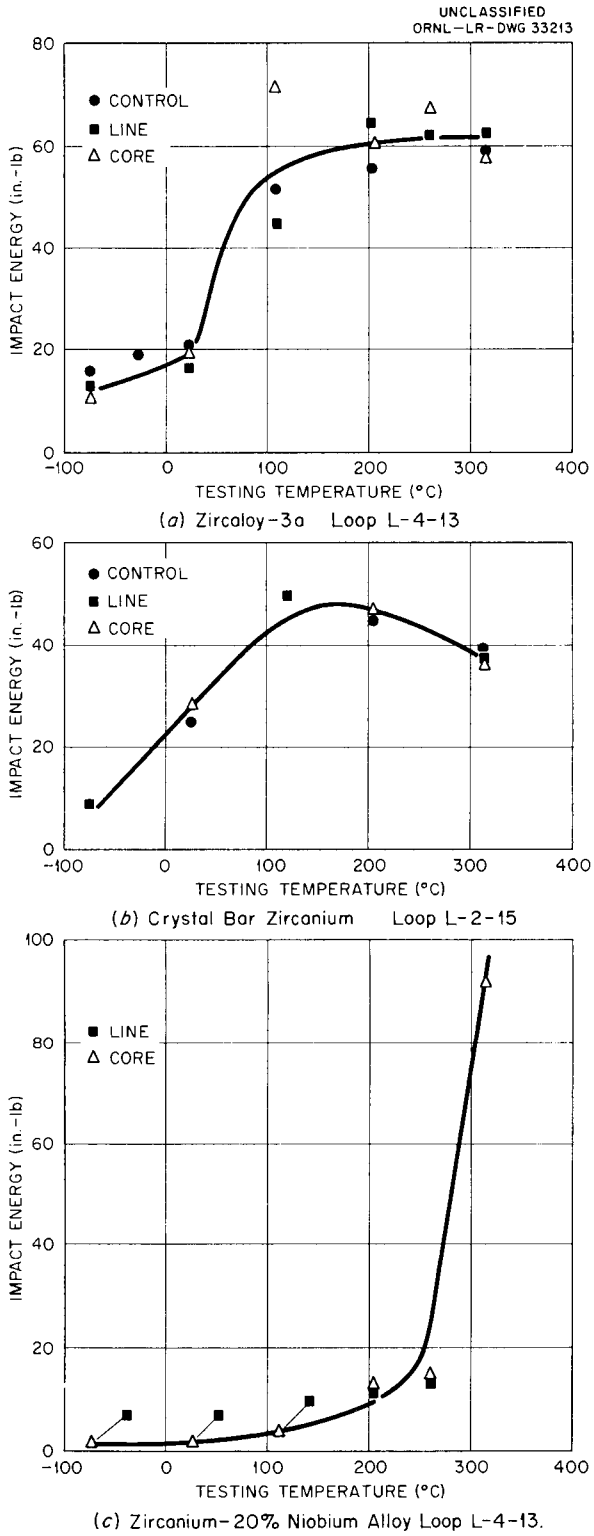

Fig. 15.5. Impact Strength of Zirconium Alloys After Exposure in In-Pile Loops. (*a*) Zircaloy-3a, Loop L-4-13; (*b*) crystal-bar zirconium, Loop L-2-15; (*c*) zirconium–20% Nb, Loop L-4-13.

radiation-induced change. The major portion of the increase was caused by an embrittling transformation occurring in the alloy at loop-operating temperature or in cooling from it.

Alloys of Zr-15Nb both beta-quenched and aged at 600°C for 48 hr were exposed in loop L-4-16.[10] All these samples fractured with very low energies, and no differences were found for core and line specimens. No definite transition temperature was noted up to the maximum break temperature at 315°C; however, with the aged sample there was some indication of it just appearing at this temperature. A higher transition temperature for these alloys over the 20% alloy might be expected since this was also a characteristic of the unexposed samples.

15.2.3 Creep Testing of Zirconium- and Titanium-Base Alloys

Long-time creep tests are being conducted on Zircaloy-2, A-45 titanium, and A-110AT titanium at stresses just below the 0.2% yield strength between room temperature and 315°C. There are very few data in the literature on the creep properties of these materials in excess of 1000 hr. Design considerations make it desirable to know the creep characteristics of these materials and also the shape of the time-deformation curves, especially whether the transition from second- to third-stage creep is abrupt. At present, creep tests up to 4500 hr indicate a constant rate of second-stage creep with no indication of the start of third-stage creep.

15.3 WELDING DEVELOPMENT

15.3.1 Titanium Alloys

Welding techniques have been developed which are suitable for making field welds in titanium A-110AT (2.5% Sn, 5% Al), a high-strength alpha-titanium alloy which shows promise as a material for process piping. A section of extruded 4-in.-dia pipe with a $^3/_8$-in. wall was welded by using A-110AT filler wire and applying procedures developed for welding commercial titanium. The welds were satisfactory as shown by visual, radiographic, and penetrant inspections. After encountering variable results in bend test specimens in the early phases of the investigation, consistent bend results were obtained by more closely controlling the grinding during sample preparation. Welds were produced from which specimens could

be satisfactorily bent 105 deg over a mandrel having a radius four times the plate thickness. Commercial producers of this alloy require only a bend radius of 8T for wrought plate. Mechanical-property test coupons from the welded pipe gave results within the limits of the commercial base-metal specifications. The procedure was successfully applied in the construction of an A-110AT pressurizer in which uranyl sulfate will be boiled.

A paper on air welding of unalloyed titanium was presented at the annual meeting of the American Welding Society and has been published.[13]

15.3.2 Zircaloy-2

Previous developments in the welding of Zircaloy-2 resulted in air welds, trailer welds, and dry-box welds all having essentially the same properties as determined by mechanical-property tests. However, some evidence of minor contamination in the air welds was shown by their average microhardnesses of 220–230 DPH (3-kg load), as compared with 180–185 DPH for dry-box and trailer welds.[6]

Subsequent welding development now permits air welds to be made with microhardnesses comparable with those of welds made by the other two methods. The reduction in contamination was obtained by improved gas coverage and by more careful cleaning. Gas coverage was improved by the use of larger size gas cups on the torch and by more careful control of flow rates. Greater cleanliness was achieved by removing all surface discoloration from each weld pass before the following one was made; grinding with tungsten carbide wheels is recommended. With the modified procedure, three test air welds were made with resultant average microhardnesses between 180 and 185 DPH.

15.3.3 Composite Welds

To minimize corrosion failures, it may be necessary to construct heat exchangers and other special components from duplex material, the most likely combination being type 347 stainless steel clad with either Inconel or a low-alloy steel. Consequently, a welding program on duplex materials has been instigated.

To evaluate the welding problems, $\frac{1}{2}$-in.-dia, $\frac{1}{16}$-in.-wall type 316 stainless steel externally clad with Inconel was welded into a $\frac{1}{2}$-in. Inconel tube sheet. The root pass was successfully made by using an Inconel filler wire. This practice is desirable since process water may contact this surface by seepage through the crevice between the tube and tube sheet. Type 347 stainless steel filler metal was then used to complete the weld. Extensive cracking occurred in all passes of stainless steel weld metal, owing to conversion of all the ferrite by the dilution from the high-nickel alloy. The cracks were visible on the surface. A second series of welds was made with an Inconel root pass, followed by a pass with an alloy (Hastelloy W) intermediate in nickel content between stainless steel and Inconel. This material did not crack when deposited on Inconel. The rest of the weld was made with type 347 stainless steel filler metal with no cracking. These results indicate that it may be possible to control weld cracking by use of a barrier filler metal between Inconel weld metal and type 347 stainless steel weld metal. The particular rod used is not considered to be the best as it contains appreciable amounts of elements, such as molybdenum, which are foreign to both type 347 stainless steel and Inconel.

15.4 NONDESTRUCTIVE-TESTING DEVELOPMENT

15.4.1 Ultrasonic Attenuation in Metals

Earlier work[6] established the fact that ultrasonic attenuation and other losses were so great and so variable in type 347 stainless steel weld metal, as well as in welds in many other materials, that straightforward inspection was not possible. Efforts to solve the problem have taken two primary directions: (1) improvement of the ultrasonic transmission characteristics of the weld, either by heat treatment or changing the welding technique or chemistry, and (2) increasing the sound input so that a satisfactory inspection might be made despite high attenuation.

A series of heat treatments, over a range up to 2300°F and up to 1 hr at temperature, was undertaken in an attempt to dissolve interstitials and make a more uniform microstructure. No improvement in the ultrasonic attenuation was obtained with the solution of the interstitials, so this approach has been abandoned until such time as investigations into the mechanism of attenuation indicate that heat treatments would be of value.

[13] G. M. Adamson and W. J. Leonard, *Welding J. (N.Y.)* 37, 673 (1958).

It is known that a number of factors affect ultrasonic attenuation in metals. Metals whose grain size is large usually show higher ultrasonic attenuation than fine-grained metals.[14] Cast metals and anisotropic structures usually show poorer transmission of ultrasound than wrought metals and isotropic crystalline structures. Precipitated carbides have been linked to high ultrasonic attenuation, and the presence, even in low percentages, of ferrite in austenitic stainless steel is suspected as a factor. In order to make quantitative determinations of these factors, some accurate means of measuring attenuation is required. To meet this need, an attenuation comparator has been purchased and techniques have been developed for its use.

The following is a brief résumé of the method. A disk of x-cut quartz crystal is cemented to the sample with a couplant having a low melting point. The quartz is then excited with pulsed high-frequency energy so that it vibrates at its fundamental resonant frequency or at an odd harmonic thereof. Pulses of ultrasound are thus set into reverberation between the walls of the specimen. The rate of decay of the reverberations is indicative of the attenuation of ultrasound at that particular frequency. This rate is compared with an electrically generated, calibrated, exponential curve in order to describe the attenuation quantitatively. Experimentation has shown that phenyl salicylate forms a more stable bond than several other couplants that have been used and is more suited to high-frequency measurements. A series of experiments was performed to determine the best shape and the smallest sample size which will allow attenuation measurements free of interference from "side effects." In the range investigated, side effects appeared to cause negligible interference, but resolution requirements caused adoption of a $\frac{3}{4} \times \frac{3}{4}$ in. square rod sample.

Comparative measurements of the attenuation losses found in a variety of materials are listed in Table 15.3. With present equipment the maximum measurable loss is 3.5 db, and a value below 1 db would probably be necessary for routine inspection.

In type 347 stainless steel plate, measurable differences were noted in ultrasonic attenuation depending on whether propagation was in the direction of rolling or perpendicular to it. In the specimens of plate used for this study, attenuation values measured in the rolling direction averaged about 10% lower than the values measured perpendicular to the rolling direction. This is not always a clear-cut difference because the variations from point to point along a sample of commercial plate are of the same order of magnitude as the directional variation. Thus a large number of measurements must be made before this differential becomes apparent.

Since with the $\frac{1}{2}$-in. Zircaloy-2 plate the attenuation varied with the fourth power of the frequency, as shown in Fig. 15.6, the major loss was Rayleigh scattering.[15] This plot shows why low frequencies

[14] D. L. Worlton, *J. Soc. Non-Destructive Testing* 13(6), 24 (1955).

[15] J. W. Strutt, baron Rayleigh, *The Theory of Sound*, Dover Publications, New York, 1945.

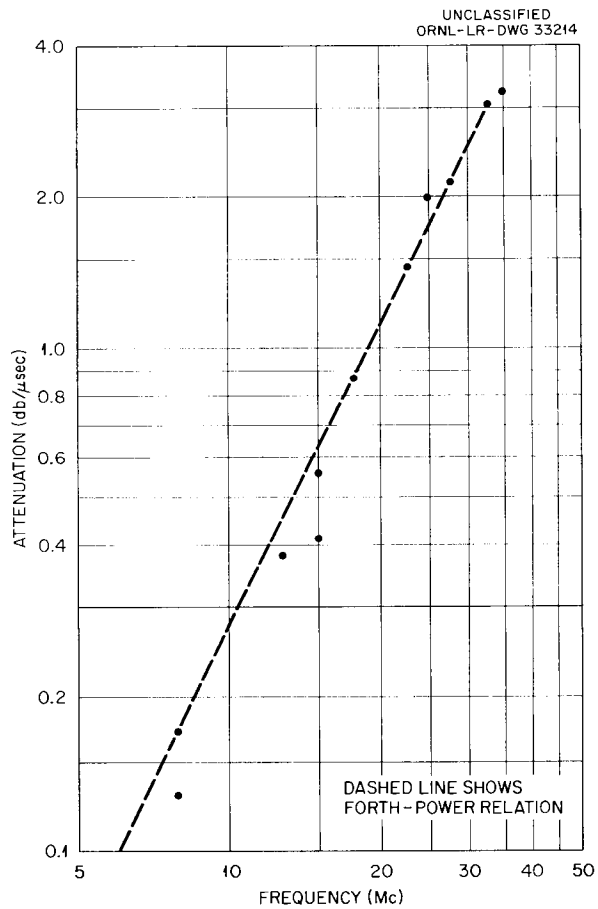

Fig. 15.6. Variation in Attenuation with Frequency for Zircaloy-2.

Table 15.3. Five-Megacycle Attenuation Measurements of Various Alloys

Metal	Original Form	Grain Count per Inch	Attenuation at 5 Mc (db/μsec)	Inspection Grouping
Type 420 stainless steel	1½-in. rod	1500	0.02	Very large sections (~2 ft) inspectable at 5 Mc
Zircaloy-2	½-in. plate	1600	0.06	Medium-to-small sections (<2½ in.) inspectable at 25 Mc
Type 347 stainless steel	1-in. plate	800	In rolling direction, 0.10; across rolling direction, 0.15	Medium sections (1–5 in.) inspectable at 5 Mc
Type 316 stainless steel	1-in. plate	550	0.2	Same as above
Inconel	Annealed 1-in. plate		0.3	Small sections (<¾ in.) inspectable at 10 Mc
INOR-8	1-in. plate		0.4	Same as above
Type 430 stainless steel	1½-in. rod		0.5	Same as above
Type 420 stainless steel	1½-in.-diameter casting	80 × 200	1	Small sections (~½ in.) inspectable at 5 Mc
Type 316 stainless steel	1½-in.-diameter casting	40 × 100	Not measurable at 5 Mc*	Frequencies lower than 5 Mc required
Type 347 stainless steel	1½ × 2 × 6 in. casting	30 × 120	Not measurable at 5 Mc	Same as above
Type 347 stainless steel weldments	Type H (high manganese)	100 × 200	Not measurable at 5 Mc	Same as above
	High ferrite	60 × 180	Not measurable at 5 Mc	Same as above
	Low ferrite	70 × 115	Not measurable at 5 Mc	Same as above

*Low-frequency measurements in process.

may be required for the inspection. Since the ratio of wavelength to grain size was appropriate in many of the other samples, Rayleigh scattering was expected, but has not been demonstrated.

In an attempt to concentrate higher ultrasonic energies into a small region, two magnesium ultrasonic lenses were designed and machined. One of the lenses proved to have excessive internal reflections and was discarded. The other improved the concentration of ultrasound by almost 100%. A further increase is necessary to obtain a satisfactory inspection, and to achieve this an ultrasound focusing transducer was made to order from a high-gain Z-type ceramic. This transducer to date has failed to provide the necessary improvement. A variable-focal-length liquid lens has been purchased for the same purpose but has not yet been evaluated.

15.5 ACTIVE-METAL REACTIONS

15.5.1 Titanium

Under an ORNL subcontract, Stanford Research Institute is studying combustion reactions of titanium and zirconium in aqueous solutions and vapors. The purpose of the study is to establish the limiting conditions for such reactions. The work discussed below is summarized from Stanford's quarterly report.[16] A topical report on the year's work has been issued.[17]

In tests similar to those described previously,[18] it was found that the conditions for autoignition of titanium at 300°C were not appreciably different from those at room temperature. No difference in conditions was found in comparing combustion in oxygen-helium mixtures with that in oxygen-steam systems.

A series of tests was made in which the energy for ignition was supplied by external means and the conditions for propagation of the combustion reaction were studied. The oxygen pressure required to sustain combustion was much lower than that required for ignition, as shown in Fig. 15.7. It might also be noted that for propagation steam-oxygen mixtures are more active than are helium-oxygen mixtures. While pure steam would not support the reaction, even at 1900 psi, the addition of less than 5% oxygen was all that was required even at moderate pressures (300 psi or more). It was also determined that air at atmospheric pressure would not support the reaction.

15.5.2 Zirconium

When Stanford tested Zircaloy-2 under conditions similar to those used for titanium, it was found to ignite less readily. Under dynamic conditions where the titanium disks ignited with only 50 psi oxygen pressure, the Zircaloy disks required between 500 and 1000 psi. In the static tests 0.012-in. Zircaloy-2 strips required 750 psi pure oxygen,

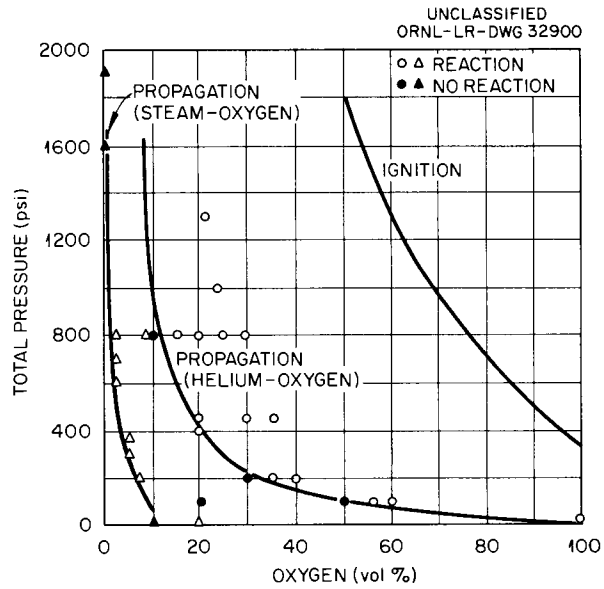

Fig. 15.7. Limits of Ignition and Propagation of Combustion for Titanium in Oxygen Diluted with Helium or Steam.

while ¼-in. rods did not ignite with 1500 psi pure oxygen. With titanium, ignition was obtained in both cases with 350 psi oxygen.

After zirconium has been ignited, however, it is more difficult to quench. Identical strips of Zircaloy-2 and titanium were held partly in water and partly in a vapor region containing 750 psi oxygen at room temperature. When the strips were ignited in the vapor region and allowed to burn, the titanium reaction was quenched at the water line, but the Zircaloy-2 sample burned for several inches below the water line before it was quenched. When Zircaloy-2 strips were heated to the melting point by external means, it was found that the combustion reaction would propagate itself in mixtures containing in excess of 3% oxygen at total pressures ranging from atmospheric to 800 psi.

Work was completed and a report issued[19] on the reactive-metal contract with Aerojet General Corporation. No differences were found between the reactions of Zircaloy-2 with water and with oxygenated uranyl sulfate solutions. In no case was any self-sustaining reaction found that started in the solutions. With both zirconium and Zircaloy-2 wires in the vapor space, propagation did not

[16] F. E. Littman and F. M. Church, *Reactions of Titanium with Water and Aqueous Solutions*, Stanford Research Institute Quar. Rep. No. 4, Dec. 16, 1957–March 15, 1958.

[17] F. E. Littman and F. M. Church, *Reactions of Titanium with Water and Aqueous Solutions*, Stanford Research Institute final report, March 15, 1957, to June 15, 1958, SRI Project No. SD-2116.

[18] F. E. Littman and F. M. Church, *Reactions of Titanium with Water and Aqueous Solutions*, Stanford Research Institute Quar. Rep. Nos. 1, 2, 3, March 15, 1957–Dec. 15, 1957.

[19] H. M. Higgins, *Reaction of Zircaloy-2 with Water and with Uranyl Sulfate Fuel Solution*, AGC-AE-40.

occur in pure steam, but did with as little as 0.5 vol % oxygen. After the reaction was started in the vapor space, whether it continued into the water or not varied with test conditions and requires additional study for complete understanding.

15.6 METALLURGICAL SERVICES

An investigation[20] of trim from the HRP dump-valve test loop revealed that performance improved with increasing poppet hardness. From this it was hypothesized that deformation of softer poppets increased the poppet-seat contact area and thus reduced the closing pressure. The deformation areas of a number of poppets were measured and the closing pressures calculated. A plot of closing pressure vs leak rate (Fig. 15.8) shows a fair correlation and tends to support the hypothesis.

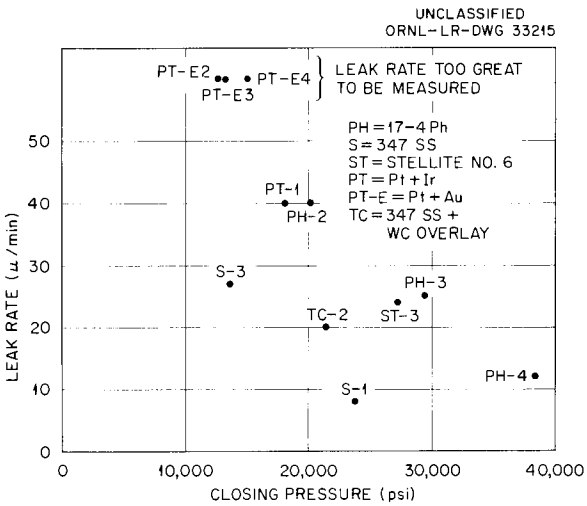

Fig. 15.8. Dump-Valve Leak Rate vs Closing Pressure.

A number of commercially pure titanium and Zircaloy-2 corrosion-test specimens were surface hardened, in an attempt to increase the abrasion resistance, by treatments in an oxygen-nitrogen atmosphere. The process, developed by Armour Research Foundation,[21] produced in both titanium and Zircaloy-2 a surface hardness of 550 DPH units which extended to a depth of several mils. These samples are now being tested.

15.7 CERAMIC DEVELOPMENTS[22]

The Ceramic Laboratory has cooperated with the HRP in investigating various methods of pelletizing thorium oxide powder. The product desired was spherical pellets of $\sim 1\mu$ diameter and with sufficient strength to resist breakdown in pumping.

The following possible methods have been tried since January:

1. subjection of previously calcined ThO_2 to mechanical pressure in a steel mold to break down the particles;
2. calcination of the powdered ThO_2 in an oxy-acetylene flame by means of a flame-spray gun;
3. electric-arc treatment; in one case the ThO_2 powder was merely dropped through the arc flame; in another approach the powder was passed through one of the arc electrodes which had been drilled previously.

The products are now being tested by the Project. Cursory examination indicated that the flame-spray did not heat the ThO_2 (mp $\sim 3000°C$) sufficiently to cause much sintering. In the arc calcination the powder tends to form hollow bubbles which are fragile, and the ThO_2 tends to be converted to the carbide or even reduced to the metal.

15.8 EFFECTS OF RADIATION ON STRUCTURAL METALS AND ALLOYS[23]

15.8.1 Equipment and Facilities

Irradiations of MTR 10-6 and MTR 10-9 were completed in the MTR; the experiments were disassembled and were received at ORNL. An earlier experiment, ORNL 10-8, was also received at ORNL. No further MTR irradiations are anticipated, because the ORR is now available.

A new subsize impact machine was modified for remote operation and has been used satisfactorily for several months. The results obtained have been checked against the old machine (now retired), and the energy values check closely. A second new machine is nearing completion as an operating spare.

[20] F. W. Cooke, *Metallurgical Examination of Valve Trim from HRP Dump Valve Test Loop*, ORNL CF-58-5-110 (May 28, 1958).

[21] Armour Research Foundation Project B-056-0 for Watertown Arsenal, *Surface Hardening of Titanium with Metaloid Elements*, progress reports 28 to 51, July 28, 1953, to June 21, 1955.

[22] Reported by C. E. Curtis of the Ceramic Section of the Metallurgy Division.

[23] Work conducted in the Solid State Division.

Progress is being made in irradiation techniques, engineering design, and instrumentation planning for the ORR experiments. A successful "canning" method for irradiating specimens in the lattice is being tested. Hydrostatic pressure is utilized to hydroform a 0.002- to 0.005-in. stainless steel sheet in contact with large numbers of jigged specimens. Good heat transfer to cooling water, protection from corrosion, relatively simple construction, and efficient use of reactor space appear achievable.

The fast-neutron flux above 0.7, 1.5, and 3 Mev has been measured (by D. Binder, Solid State Division) in the HB-3 facility of the LITR at the position at which Charpy specimens are irradiated. Similar measurements will be made in the HRT in order to establish the relative fast-neutron dose in these two facilities.

An LITR irradiation of Charpy V-notch specimens of pressure-vessel steels at 575°F has started. A dose of 1×10^{19} fast neutrons/cm^2 (>1 Mev) will be reached. Sufficient specimens for some postirradiation annealing have been included.

15.8.2 Impact Tests

Groups of V-notch Charpy specimens, representing three ASTM specification steels in several heat-treated conditions, were irradiated simultaneously at two neutron-flux levels and at two temperatures in the LITR. The test results for these specimens, Figs. 15.9 through 15.11, show

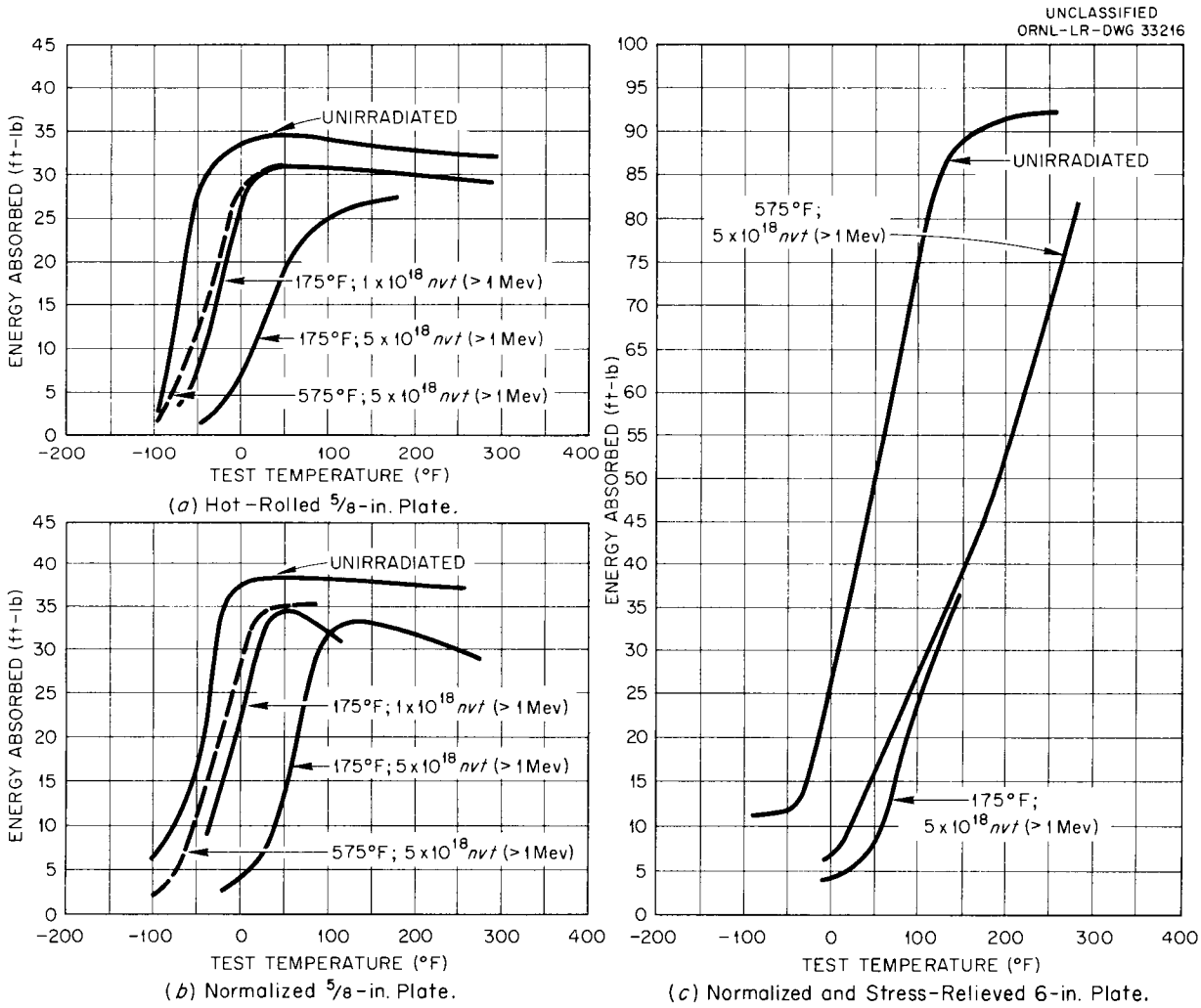

Fig. 15.9. Charpy V-Notch Impact Strength of Various Irradiated A-212B Steel. (*a*) Hot-rolled $\frac{5}{8}$-in. plate; (*b*) normalized $\frac{5}{8}$-in. plate; (*c*) normalized and stress-relieved 6-in. plate.

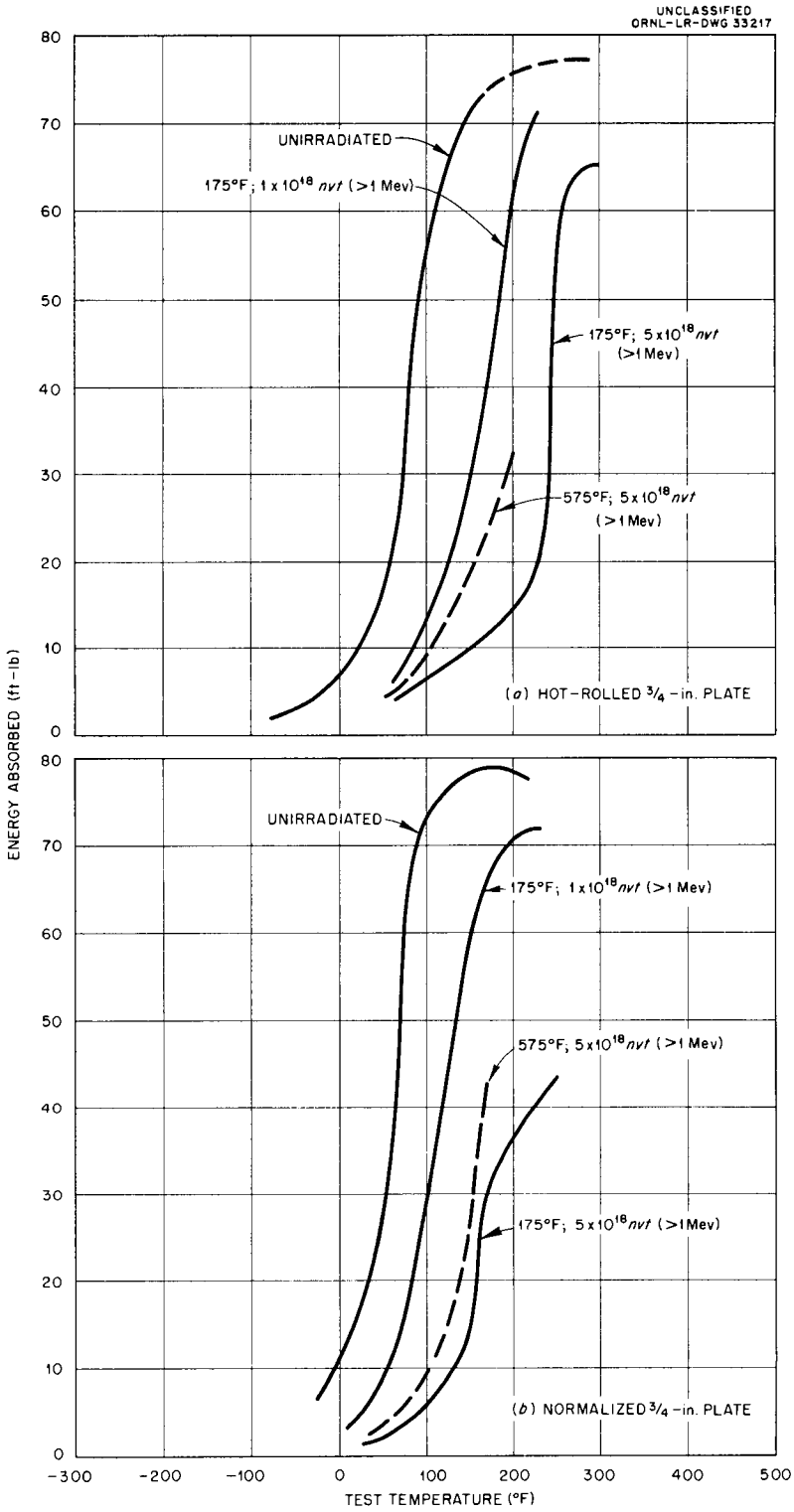

Fig. 15.10. Charpy V-Notch Impact Strength of Irradiated A-285 Steel. (*a*) Hot-rolled $\frac{3}{4}$-in. plate; (*b*) normalized $\frac{3}{4}$-in. plate.

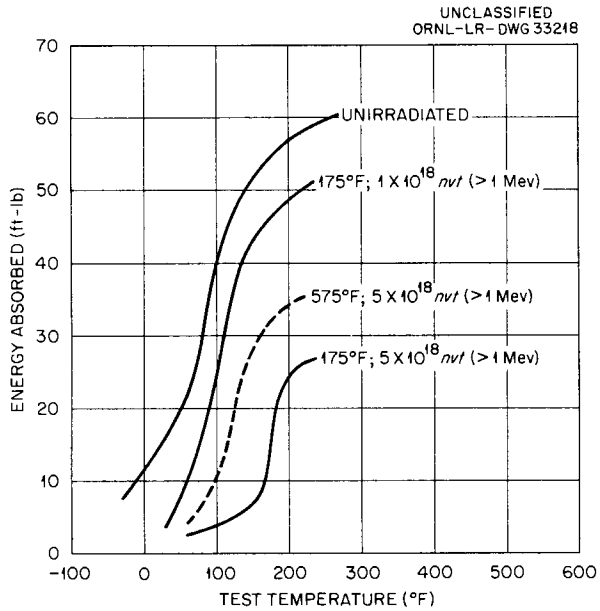

Fig. 15.11. Charpy V-Notch Impact Strength of Irradiated A-301B Steel.

the variable effects of irradiation temperature. It will be noted that the shift in transition temperature caused by a dose of 5×10^{18} fast neutrons/cm^2 (>1 Mev) at 175°F may, or may not, be reduced appreciably if the irradiation is carried out at a higher temperature (575°F). The reason for this difference is not known at the present. The Charpy V-notch data indicate larger transition-temperature shifts than had been observed on subsize Izod specimens. Thus there may be a specimen-size effect in irradiated steels.

Subsize Izod impact tests were conducted with specimens cut from a 4-in.-thick plate of ASTM A-212B carbon steel and irradiated in the MTR at various temperatures and neutron fluxes. The data in Fig. 15.12 show that irradiation at temperatures below 500°F results in little, if any, improvement over irradiation at 175°F. The effects of irradiation temperatures between 440 and 540°F are indicated by the three samples broken at 200°F. The specimen irradiated at 440°F was brittle at the 200°F test temperature, while the specimen

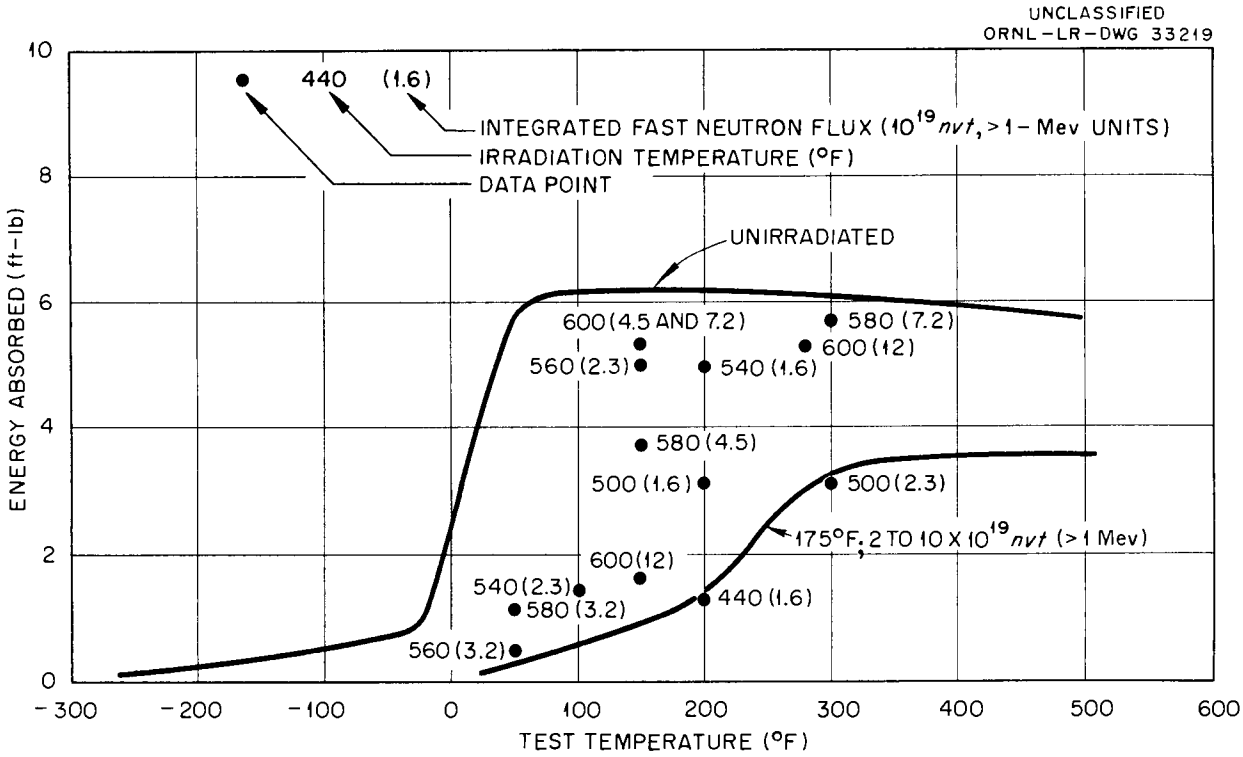

Fig. 15.12. Subsize Izod Impact Strength of A-212B Steel Irradiated for Varying Times and Temperatures.

irradiated at 540°F was ductile. The specimen irradiated at 500°F was of intermediate ductility. Other comparisons in this figure show the effect of integrated fast-neutron flux at a given irradiation temperature. Three specimens were irradiated simultaneously at 600°F and tested at 150°F but were exposed to three different fast-neutron fluxes and thus different integrated fast-neutron fluxes. The two specimens exposed to 4.5 and 7.2 × 10^{19} *nvt* were ductile, but the specimen exposed to 12 × 10^{19} fast neutrons/cm^2 was brittle at these test conditions.

Subsize Izod impact specimens cut from a 4-in.-thick multipass butt weld of E-7016 carbon-steel electrode (HRT weld-qualification plate) were irradiated in the experiment discussed in the previous paragraph. The effects of irradiation temperature and integrated fast-neutron flux, Fig. 15.13, are similar to those shown in Fig. 15.12 but differ in magnitude. With the weld metal, irradiation temperatures of 560°F and above were much more effective in reducing the transition temperature.

The data in Figs. 15.12 and 15.13 have been replotted in Figs. 15.14 and 15.15, respectively,

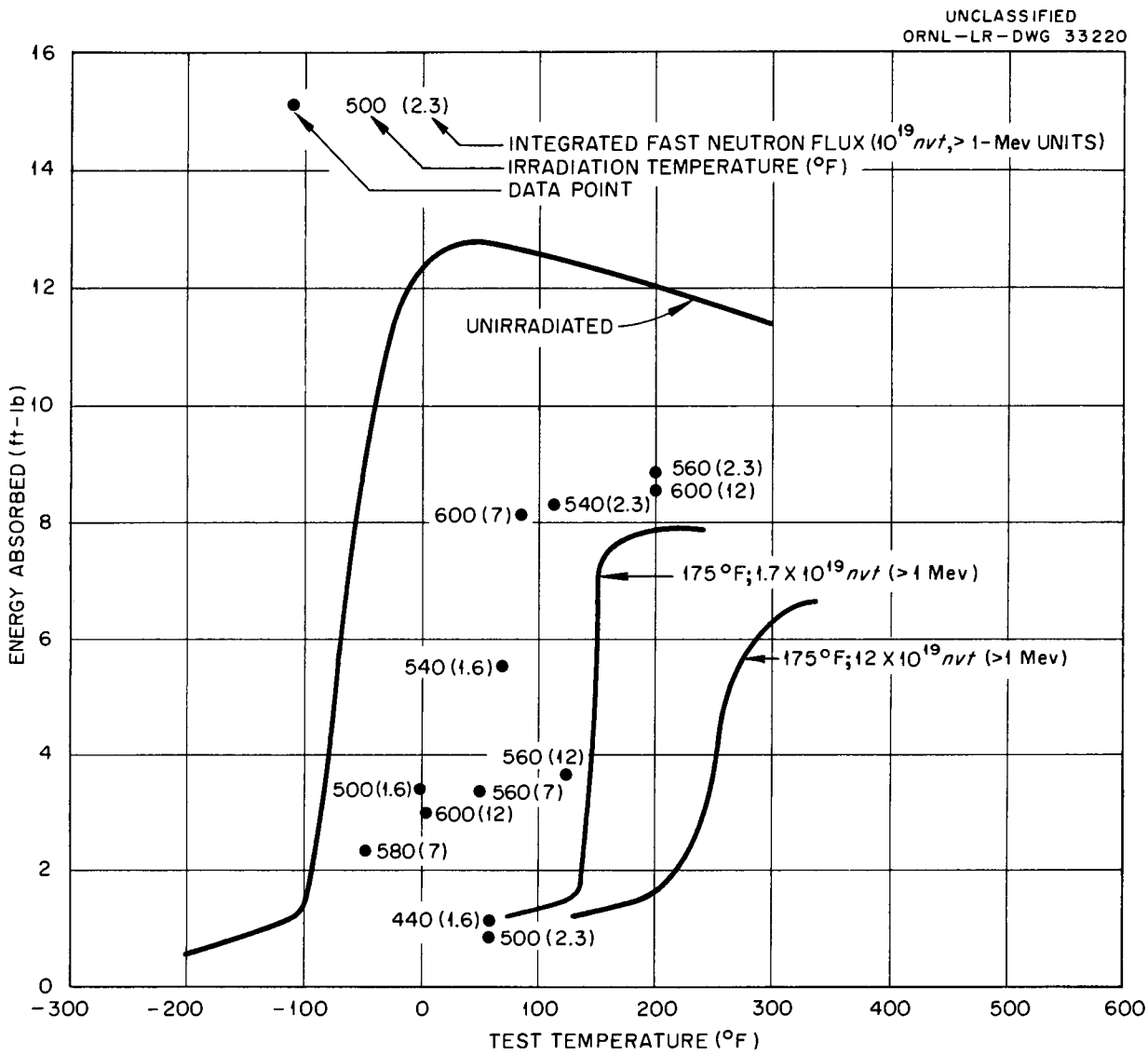

Fig. 15.13. Subsize Izod Impact Strength of E-7016 Weld Metal After Irradiation for Varying Times and Temperatures.

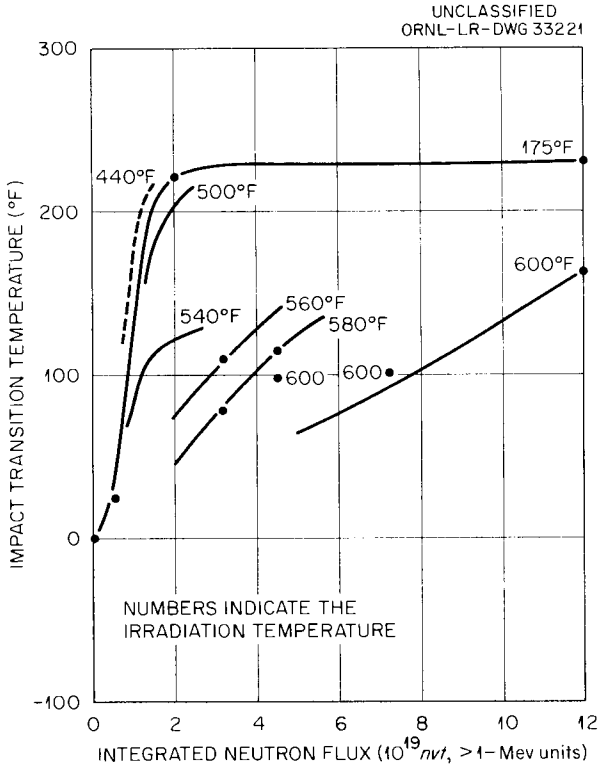

Fig. 15.14. Estimated Impact Transition Temperatures of Irradiated A-212B High-Tensile-Strength Carbon-Silicon Steel; Subsize Izod Test, 4-in. Plate, Hot-Rolled (Item 65).

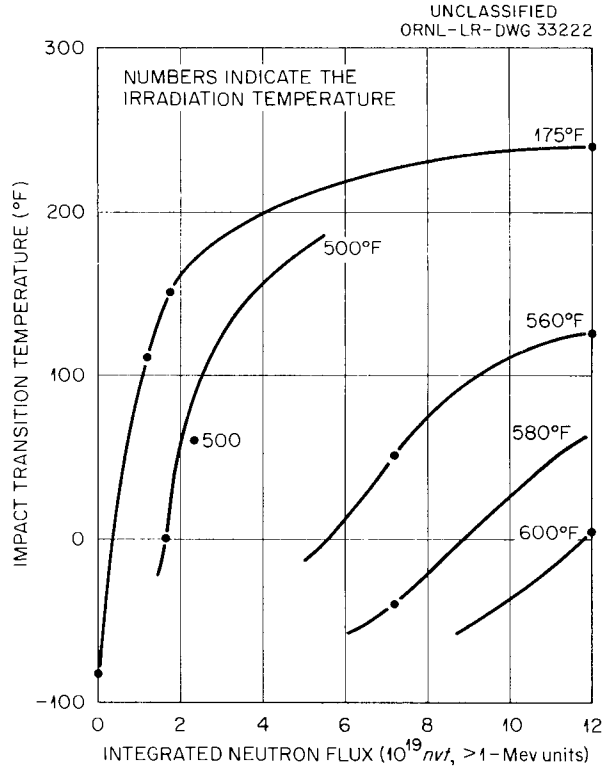

Fig. 15.15. Estimated Impact Transition Temperatures of Irradiated Carbon-Steel Weld Metal; Subsize Izod Test, 4-in.-Thick Multipass Butt Weld, E-7016 Electrode, Stress-Relieved (Item 65W).

to indicate the general dependence of transition-temperature shift on fast-neutron dose and irradiation temperature based on the present interpretation of the data. Similar information on three other steels is consistent with this picture. It is apparent that in the flux and temperature ranges of interest to the HRP, the magnitude of irradiation effects is extremely sensitive to dose and temperature of irradiation. The strong temperature dependence also explains the marked difference in radiation effects in the Charpy V-notch specimens (Figs. 15.9, 15.10, and 15.11) at the same irradiation temperature; apparently the temperature of annealing of radiation effects is slightly different in different steels (as in Figs. 15.14 and 15.15).

15.8.3 Tensile Tests

The results of tensile tests of several irradiated steels, presented in Table 15.4, indicate that (1) at fast-neutron doses of 5×10^{18} fast neutrons/cm^2 and irradiation temperatures from 150 to 600°F the increase of strength and loss of ductility do not appear large; (2) at fast-neutron doses of 2×10^{19} fast neutrons/cm^2 and greater and irradiation temperatures of about 575°F the yield strength is more than doubled, the uniform elongation is seriously reduced, and in some cases failure occurred without localized deformation (necking); and (3) at the higher fast-neutron doses, irradiation temperatures in excess of 700°F are required to keep the irradiation-induced changes within reasonable values.

In several instances (lines 5, 12, and 20 in Table 15.4) fracture took place without necking after a few per cent plastic deformation. Failure without necking has never occurred in specimens irradiated at lower temperature, even after higher neutron exposures. The fracture stresses were also considerably reduced by irradiation. It must be concluded that elevated irradiation temperatures do not unequivocally reduce the extent of ductility loss. The ductility loss at low (<200°F) irradiation temperatures is seen as reduced uniform

elongation, and high doses are necessary to affect the reduction of area. At higher irradiation temperatures (500–700°F) ductility loss, as evidenced by uniform elongation, is not so great, but loss of reduction of area becomes more prominent.

In comparing notch-impact and tensile results, it is difficult to decide whether the tensile or notch-impact data give the more pessimistic results. The effects of specimen size (notch-impact tests) and testing temperature (tensile tests) must be studied to resolve this question.

An earlier indication that the tensile properties might prove more limiting than the impact properties was found in comparing the results of a steel and a weld metal. The uniform elongation was found to be reduced to much lower values in an E-7016 weld metal than in the corresponding wrought metal (type A-212 grade B), although the notch impact results were similar.

Table 15.4. Tensile Properties of Irradiated Steels

Line	Alloy	Dose (fast neutrons/cm^2)	Temperature of Irradiation (°F)	Yield Strength (psi)	Tensile Strength (psi)	Uniform Elongation (%)
				$\times 10^3$	$\times 10^3$	
1	A-106:	0		40	76	18
2	fine grain,	2×10^{19}	580	81	102	8
3	0.24% C	2×10^{19}	680	55	87	11
4		2×10^{19}	760	48	82	12
5		8×10^{19}	580	79	106*	6
6		8×10^{19}	780	47	79	11
7		1×10^{20}	175	97	102	4
8	A-106:	0		46	80	14
9	coarse grain,	2×10^{19}	580	93	115	8
10	0.24% C	2×10^{19}	680	67	98	9
11		2×10^{19}	760	43	84	14
12		7×10^{19}	580	87	103*	3
13		7×10^{19}	780	64	94	11
14		1×10^{20}	175	116	121	2
15	A-212:	0		40	75	25
16	0.2% C	2×10^{19}	175	92	98	6
17		2×10^{19}	560	76	102	9
18		2×10^{19}	680	61	90	12
19		2×10^{19}	760	56	84	14
20		6×10^{19}	700	82	105*	6
21		6×10^{19}	780	59	81	13
22		1×10^{20}	175	109	116	4

Table 15.4 (continued)

Line	Alloy	Dose (fast neutrons/cm^2)	Temperature of Irradiation (°F)	Yield Strength (psi)	Tensile Strength (psi)	Uniform Elongation (%)
23	A-301:	0		41	66	23
24	0.1% C,	5×10^{18}	150	55	69	23
25	1% Cr, ½% Mo	5×10^{18}	575	47	71	26
26		0		44**	68	21
27		5×10^{18}	150	57**	71	23
28		5×10^{18}	575	52**	73	23
29		1.5×10^{19}	740	53	78	18
30		4.5×10^{19}	740	63	86	12
31		4.5×10^{19}	700	91	103	
32	E-7016:	0		59	73	16
33	weld metal	5×10^{18}	175	69	78	11
34		5×10^{18}	600	61	77	17
35		2×10^{19}	175	108	108	0
36		6×10^{19}	700	83	94	12
37		6×10^{19}	740	77**	85	12
38		6×10^{19}	780	69	77	15
39		1×10^{20}	175	115	115	0

*Broke without necking; work-hardening rate greater than for unirradiated specimen.

**2.0/min testing rate; all others 0.05/min.

Part V

CHEMICAL ENGINEERING DEVELOPMENT

D. E. Ferguson

16. URANYL SULFATE FUEL PROCESSING

R. A. McNees P. A. Haas
S. Peterson J. W. Snider

16.1 IODINE CHEMISTRY

16.1.1 Laboratory Experiments

The effect of Co^{60} gamma irradiation at an intensity of 1.7 w per kg of H_2O on the valence of iodine in simulated fuel solution under oxygen overpressure was studied at 257 and 300°C. The solution was contained in a titanium bomb, and samples were withdrawn through a titanium capillary line and were cooled in ice after only a few inches travel from the bomb. The results (Table 16.1) indicate that the iodate content of the solution was affected only slightly, if at all, by the irradiation, although it is not certain whether these results measure actual iodate in the bomb or iodate formed during sample cooling. The latter possibility is supported by repeated observations that the iodate content is greater in samples taken at the higher temperature where, thermodynamically, iodate is less stable. However, oxygen solubility is increased at the higher temperature, and therefore, during cooling, the greater O_2 concentration would favor oxidation of elemental iodine.

When the silvered Yorkmesh used as an iodine absorber in the low-pressure system of the HRT was immersed in simulated HRT fuel solution at 110°C, the silver was rapidly loosened from the supporting metal and dissolved, but at 98°C the rate of attack was much lower. Specimens of the silvered Yorkmesh exposed to boiling uranyl sulfate solutions containing either 10 or 40 g of uranium per kilogram of H_2O and 25 mole % excess sulfuric acid lost only traces of silver after seven days at 98°C. However, identical specimens were stripped of silver after 24 hr at 110°C, to give solutions containing as much as 3 g of Ag per kg of H_2O. Gamma radiation appeared to accelerate the rate of attack. Silvered Yorkmesh was not attacked when heated with only water at 98 or 110°C. These data indicate the need for preventing fuel solution from coming into contact with the iodine absorption unit in the HRT system.

At 150°C iodine absorption by silvered Yorkmesh was eight times faster than at 120°C when specimens were exposed to an atmosphere of oxygen, steam, and iodine of fixed composition and flow rate. At 150°C silvered Yorkmesh which had absorbed 60% of the stoichiometric amount of iodine continued to function efficiently in a steam-oxygen-iodine mixture containing traces of iodine and 1% oxygen. When the O_2 content was increased to 10%, rapid oxidation of the stainless steel supporting wire occurred, with consequent destruction of the absorption bed. Silvered Yorkmesh containing no iodine was not affected by the oxygen-rich atmosphere. This indicates that dilution of oxygen by steam in the low-pressure system at the iodine absorption unit must be maintained whenever there is a possibility that the absorption-bed temperature will exceed 120–130°C.

Table 16.1. Effect of Co^{60} Irradiation on Valence of Iodine in Simulated Fuel Solution at 257 and 300°C

Fuel: 0.04 *m* UO_2SO_4, 0.005 *m* $CuSO_4$, 10^{-5} *m* HIO_3, sulfuric acid; oxygen overpressure

H_2SO_4 in Fuel (*m*)	Temperature (°C)	Iodate Content (% of total iodine)	
		No Irradiation	Irradiated 24–96 min at 1.7 w/kg
0.03	257	5.4	7.1
	300	10.3	9.3
0.02	257	6.9	9.8
	300	12.1	11.9

16.1.2 HRT Operating Experience

The behavior of iodine in the HRT was followed during the three completed power runs by analyzing samples taken from the high-pressure system for both I^{133} and I^{131}. These analyses indicated that iodine did not accumulate in the reactor fuel solution during operation but was removed to such an extent that only 2 to 3% of the iodine calculated to have been produced was found in the samples (Table 16.2). In many cases the iodine found in the samples was less than would be expected if iodine was being removed from the

Table 16.2. Behavior of Fission-Product Iodine in the HRT

Sample No. (from Fuel High-Pressure System)[a]	Reactor Operation (Mwhr)	Total I^{131} Activity (d/sec)		Found by Analysis	Iodine (%) Remaining in Fuel[b]
		Calculated as Produced and Not Decayed by Sampling Time	Calculated as Present If Removed at Letdown Rate		
		First Power Run			
13-22	2.5	9×10^{12}	2.4×10^{12}	5×10^{11}	0.5
13-59	20	6×10^{13}	3.2×10^{11}	1.6×10^{12}	2.7
13-71	36	1.1×10^{14}	5.1×10^{12}	2.3×10^{12}	2.0
		Second Power Run			
14-88	5.4	1.8×10^{13}	7×10^{12}	5×10^{11}	2.8
14-103	21	7×10^{13}	8×10^{12}	1.6×10^{12}	2.3
14-134	72	2.1×10^{14}	1.2×10^{13}	5×10^{12}	2.4
14-190	223	6×10^{14}	1.9×10^{13}	2.5×10^{13}	4.2
		Third Power Run			
16-171	74	1.8×10^{14}	5.5×10^{12}	2.2×10^{11}	0.1
16-224	136.5	3.2×10^{14}	8×10^{12}	2.0×10^{12}	0.6
16-313	399	9×10^{14}	2.1×10^{13}	1.2×10^{12}	0.1
16-388	765	1.5×10^{15}	2.7×10^{13}	1.1×10^{12}	0.07
16-422[c]	923	1.7×10^{15}	2.2×10^{13}	1.4×10^{13}	0.8
16-425	926.5	1.7×10^{15}	2.3×10^{13}	3.3×10^{12}	0.2
16-437	1027	1.9×10^{15}	2.9×10^{13}	5.4×10^{12}	0.3
16-452[c]	1171	2.1×10^{15}	3.5×10^{13}	1.3×10^{13}	0.6

[a]Data from other samples available but not reported here.

[b](Calculated iodine produced and not decayed × 100)/(iodine found by analysis).

[c]Sample from blanket high-pressure system.

fuel solution at a rate equal to the rate at which fuel was let down from the high-pressure system to the low-pressure system, in which the iodine absorption unit is located. These low iodine concentrations, coupled with the somewhat erratic results observed with some samples and previous laboratory experience in handling samples containing very low (10^{-5} *m*) concentrations of iodine, indicate that some iodine may have been lost from the samples prior to analysis. Therefore the concentration of iodine in the fuel during operation may have been somewhat higher than is indicated by the data.

16.2 SOLIDS BEHAVIOR

The thermal-cycling corrosion loop at Y-12 from which corrosion-product solids were being isolated by a hydroclone was shut down and was examined for solids accumulation in various parts of the system. The accumulation of nickel in the loop solution indicated the formation of 80 to 85 g of mixed Fe_2O_3-Cr_2O_3. Of this amount, 10 g was collected by the hydroclone, and 7 g was removed from the bellows housing and pressurizer, 90% of this being from the bellows housing. The Fe_2O_3-Cr_2O_3 remaining in the loop would account

for a film thickness of 0.2 mil, or 1.8 mg/cm^2, if uniformly distributed over the loop surface. Experience with corrosion test pins indicates that the oxide film will accumulate to about 2.1 mg/cm^2 at 250 to 300°C at low velocities. Since this level was not reached during operation of the loop, the recovery of 12% of the solids produced, or 60% of the solids known to be loose in the system, is most encouraging.

In fundamental studies of solids deposition by Stanford Research Institute,[1] mixed Fe_2O_3-Cr_2O_3 solids were deposited on stainless steel surfaces by collection of particulate matter and not by precipitation from solution. In these tests two to four times as much solids accumulated on the upper portions of test coupons as on the bottom, apparently as a result of gravity settling of solids on the coupons. X-ray examination of the corrosion-product surface so formed indicated that preferred orientation of the depositing solids may have occurred.

16.3 ALTERNATE CORE PROCESSING DEVELOPMENT

Studies of methods to improve the performance of hydroclones for separating solids from liquids at reactor temperature and pressure indicated that an over-all gain in solids removal could result from an increased flow through the clone. With the increased capacity and concurrent decrease in pressure drop through the system, some ability to remove 1-μ-dia particles would be lost, but this loss would be offset by decreased settling in other portions of the reactor system.

To obtain this performance, a hydraulic centrifugal separator of the fixed-impeller or axial-flow hydroclone type was fabricated, and flow-rate–pressure-drop tests were made at room temperature. The entering liquid is accelerated by a finned core to give a high velocity at almost 90 deg to the inlet axis. This whirl velocity results in a centrifugal field that can be used for phase separation or for particle-size classification. The exit streams leave through concentric axially centered ports, which may use recovery fins to minimize head losses. Depending on the exit-stream split and exit-port areas, the axial-flow hydroclone can eliminate the forced vortex and high shear rates inherent in the conventional conical hydroclone. Much higher capacities, lower centrifugal fields, and somewhat more difficult fabrication techniques are inherent in the axial-flow type of design.

The 1-in.-dia axial-flow hydroclone at 15 gpm requires a pressure drop equivalent to 27 ft of water and (based on several assumptions) gives about 1250 G at the wall and 650 G at the core surface. The average holdup time is about 0.03 sec, and a theoretically calculated d_{50} particle would be about 5.0 μ for ThO_2 at room temperature or corrosion-product oxides at 300°C.

[1] H. Eding, *Mechanisms of Surface Adsorption in Homogeneous Reactor Loops*, Stanford Research Institute Prog. Rep. Nos. 10, 11, and 12, Jan.–March 1958, SRI Project No. SD-2080-2.

17. GASEOUS-FISSION-PRODUCT DISPOSAL

R. A. McNees
R. D. Ackley
R. E. Adams
W. E. Browning
J. M. Funderburg[1]
M. H. Lloyd
L. I. Moss[1]

17.1 DYNAMIC STUDIES

Evaluation of various adsorber materials at temperatures from 25 to 300°C was completed. The materials were compared on the basis of adsorption of a pulse of Kr^{85} from an oxygen stream flowing through a 1-in.-dia adsorber column. All materials had been previously dried at elevated temperatures. The charcoal and carbon wool were dried at 150°C, the Linde sieve material at 300°C, the silica gel at 230°C, the alumina at 200°C, and the Driocel at 230–260°C. By injecting a brief pulse of Kr^{85} into the krypton-carrier gas sweep stream and measuring its residence time in the adsorber column, the dynamic adsorption coefficient (k) of the adsorbent was determined from the relation[2]

$$k = \frac{F \cdot t_{max}}{m} ,$$

where F = gas flow (cc/min), t_{max} = residence time for krypton (min), and m = mass of charcoal (g). Graphs of k (dynamic adsorption coefficient, cc/g) as a function of temperature for the several groups of materials are presented in Figs. 17.1 through 17.3. Of the groups studied, activated charcoals were the most efficient for adsorption of krypton. Of the charcoals, Columbia G was the most efficient under the conditions used. The dynamic data reported here on Linde molecular sieves supersede similar data previously reported[3] and are in agreement with static equilibrium data.

In studies on the effect of drying on the adsorptive capacity of Columbia G charcoal for krypton, the adsorption efficiency of the charcoal was increased 33 to 44% by decreasing the moisture content of the adsorbent from 3.4 to 0.1–0.2 wt %.[4] These results agree with preliminary results.[5] Several methods of drying the charcoal were studied: purging the adsorption trap with dry oxygen at room temperature or at 100 to 150°C and drying under vacuum with occasional purge with dry oxygen. Purging with dry oxygen at 100 to 150°C was the fastest and most efficient method.

The identity of the diluent or sweep gas plays an important role in determining the dynamic

[1] MIT Practice School.

[2] W. E. Browning and C. C. Bolta, *Measurement and Analysis of Holdup of Gas Mixtures by Charcoal Adsorption Traps*, ORNL-2116 (July 27, 1956).

[3] W. E. Browning *et al.*, *HRP Quar. Prog. Rep. Jan. 31, 1958*, ORNL-2493, p 157–61.

[4] J. M. Funderburg and L. I. Moss, *Drying of Charcoal Used for Adsorption of Gaseous Fission Products from Homogeneous Reactors*, KT-307 (Dec. 20, 1957).

[5] R. A. McNees *et al.*, *HRP Quar. Prog. Rep. July 31, 1957*, ORNL-2379, p 138.

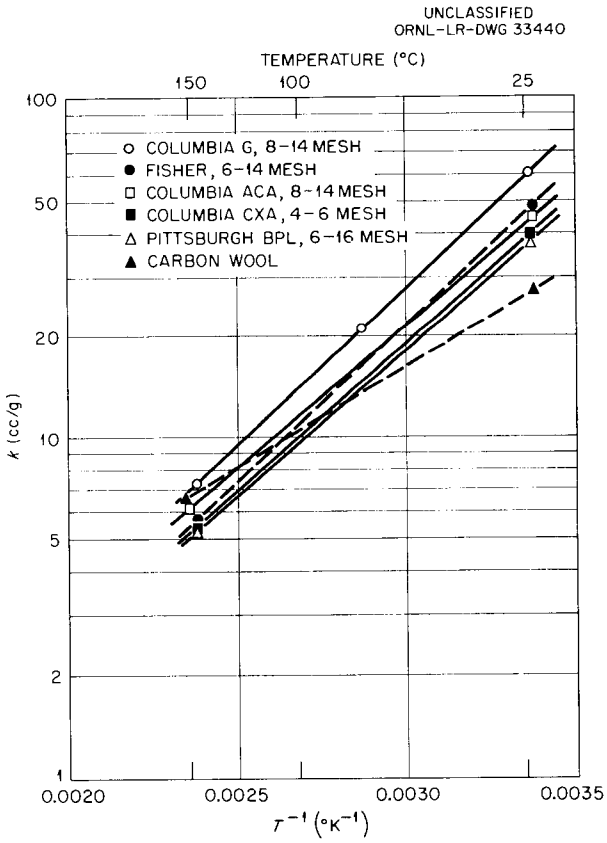

Fig. 17.1. k Values for Krypton on Various Types of Activated Carbon.

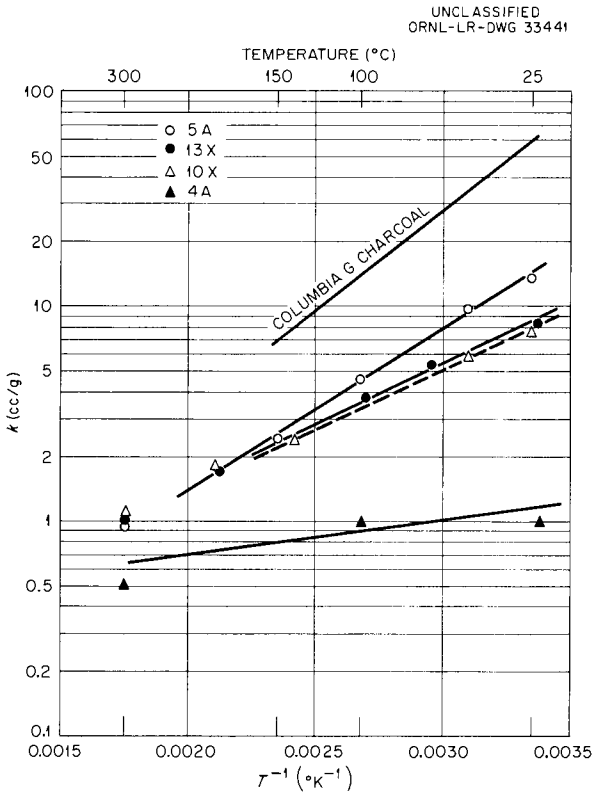

Fig. 17.2. *k* **Values for Krypton on Linde Molecular Sieves.**

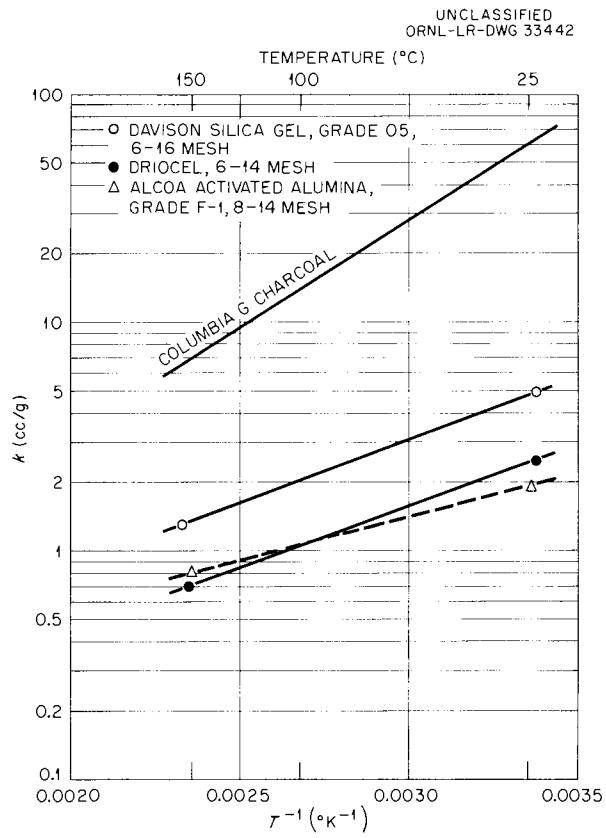

Fig. 17.3. *k* **Values for Krypton on Miscellaneous Adsorbents.**

adsorption coefficient (k) of an adsorber material for krypton. Of the sweep gases studied (helium, hydrogen, argon, nitrogen, oxygen, air, and Freon-12), helium and hydrogen gave the least interference and Freon-12 gave the most. While it is not anticipated that Freon-12 will have reactor applications, it was selected for study to demonstrate the consequences of a significantly large interference with krypton adsorption. A graph of k as a function of temperature for Columbia G charcoal with the various sweep gases is given in Fig. 17.4.

The partial pressure of krypton in the sweep gas is also of importance in determining the efficiency of charcoal for krypton adsorption. In the tracer experiments reported previously, the krypton partial pressure was only a very small fraction of a millimeter, although in some reactor applications higher partial pressures of the fission gases in the sweep gas may be expected. Therefore the effect of krypton partial pressure was studied. As the krypton partial pressure in an oxygen stream was increased from less than 0.1 to 760 mm, the dynamic adsorption coefficient decreased 51% (Fig. 17.5). The krypton partial pressure was varied by adding stable krypton to the oxygen sweep gas.

An investigation of the probability and consequences of ignition of the charcoal contained in the HRT charcoal beds was completed. Based on experiments and on calculations of heat generation and heat transfer in the HRT beds, it appears that the probability of ignition of the charcoal in the HRT beds is very slight. An ignition temperature of 290°C was determined for Columbia G charcoal in a system similar to the inlet section of the HRT beds, without external water cooling but with oxygen flow rates of 250 and 500 cc/min. This compares with an ignition temperature of 362°C reported for charcoal in oxygen at a very low flow rate.[6] The higher

[6] J. E. Bigelow *et al.*, *The Action of Oxygen on Activated Charcoal*, KT-107 (June 29, 1951).

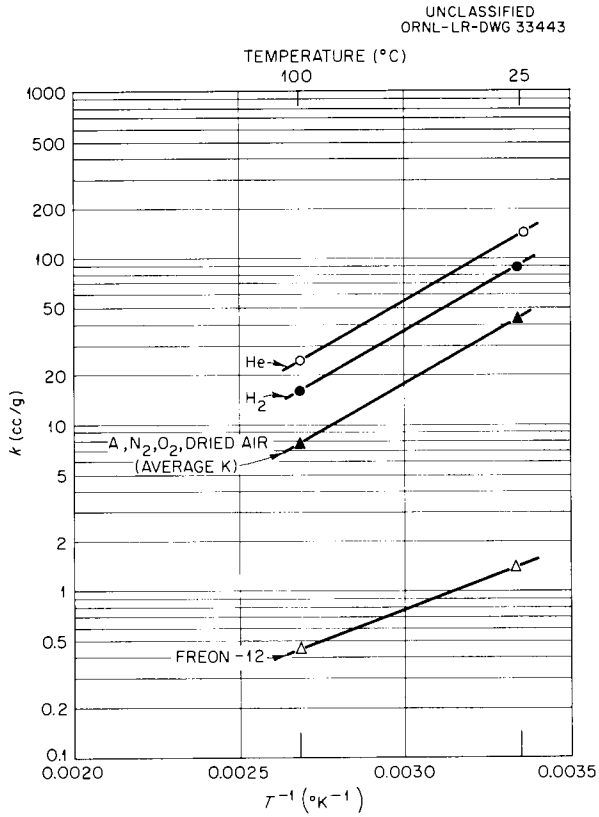

Fig. 17.4. *k* Values for Krypton on Columbia G Charcoal with Various Sweep Gases.

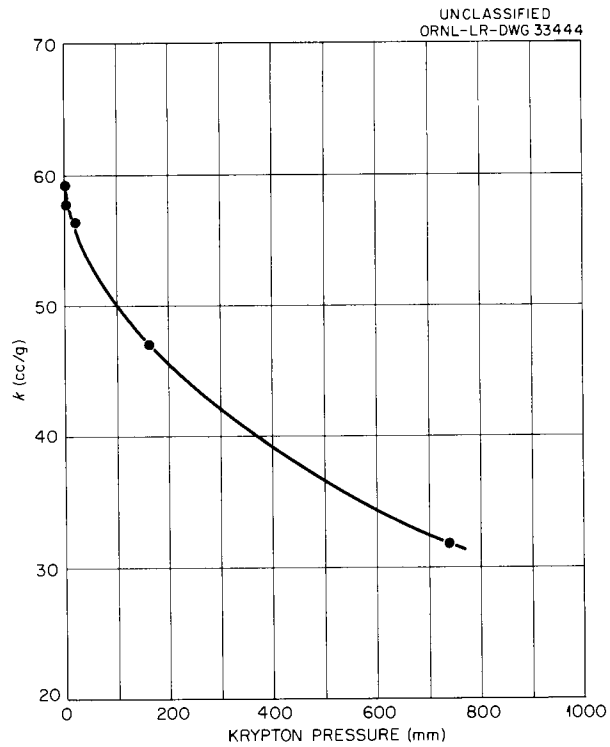

Fig. 17.5. Variation of Dynamic Adsorption Coefficient, *k*, with Krypton Pressure on Charcoal at 23°C.

ignition temperature for low flow conditions no doubt results from the accumulation of carbon oxides which dilute the oxygen and raise the ignition point. Neither of these experimentally measured ignition temperatures involved radiation conditions or ozone production by the irradiation of oxygen, and it is possible that the ignition temperature may be somewhat different in the actual HRT beds.

After ignition occurred, oxygen flow was continued and temperatures in the vicinity of 1000°C were measured at the combustion front. Since the combustion rate of charcoal is dependent on the supply of oxygen, stopping the oxygen flow to the charcoal decreased the combustion rate sharply. Charcoal temperatures dropped very rapidly in the experiment when the oxygen flow was stopped; however, the resumption of oxygen flow caused the charcoal to burn again unless the charcoal had cooled to below 200°C.

A second series of experiments was run to determine the outside pipe-wall temperature while charcoal was burning inside a 0.5-in.-ID water-cooled pipe (0.625-in. OD), and the propagation rate of the combustion front was determined at oxygen flow rates of 250, 500, and 1000 cc/min (Table 17.1).

If, by a combination of circumstances, one of the HRT charcoal beds should ignite, it will be possible to extinguish the fire by stopping the oxygen flow in that particular bed and allowing a cooling period. Operation of the reactor could be continued by diversion of the stream of oxygen and fission-product gas to an alternative charcoal bed. A more detailed report on these charcoal-ignition experiments has been issued.[7]

[7] R. E. Adams and W. E. Browning, *Estimate of the Probability and Consequences of Ignition of the HRT Charcoal Beds*, ORNL CF-58-6-6 (June 3, 1958).

Table 17.1. Combustion of Columbia G Charcoal in a Water-Cooled Pipe

Oxygen Flow Rate (cc/min)	Maximum Temperature (°C)		Downstream Propagation Rate of Combustion Front (cm/min)
	Charcoal	Outside Wall	
250	800	58	0.145
500	900	75	0.391
1000	1060	80	1.11

17.2 EQUILIBRIUM STUDIES

Static adsorption isotherms were determined for xenon on Columbia charcoal grade G at temperatures of 2, 28, and 85°C (Fig. 17.6) and for Linde molecular sieves 5A, 10X, and 13X and Davison silica gels grades 35 and 70 at temperatures of 2 and 28°C (Figs. 17.7 and 17.8). At all temperatures and pressures studied, these materials adsorbed more xenon than krypton. At pressures of 25 to 30 mm, silica gel grades 70 and 35, respectively, adsorbed about 4.5 and 7 times more xenon than krypton. Molecular sieves 10X and 13X adsorbed about 10 times more, and molecular sieve 5A and Columbia charcoal about 11.5 times more.

The ratio of static adsorptive capacities of the various adsorbents was about the same for xenon as was found for krypton and reported in previous quarterly reports. Charcoal was again the best adsorbent, and molecular sieve 5A was the best noncarbon adsorbent. As with krypton, xenon adsorption decreased with increasing adsorbent pore size of the molecular sieves; the 4A material was not examined.

Xenon adsorption isotherms were measured for Columbia charcoal grade G and for molecular

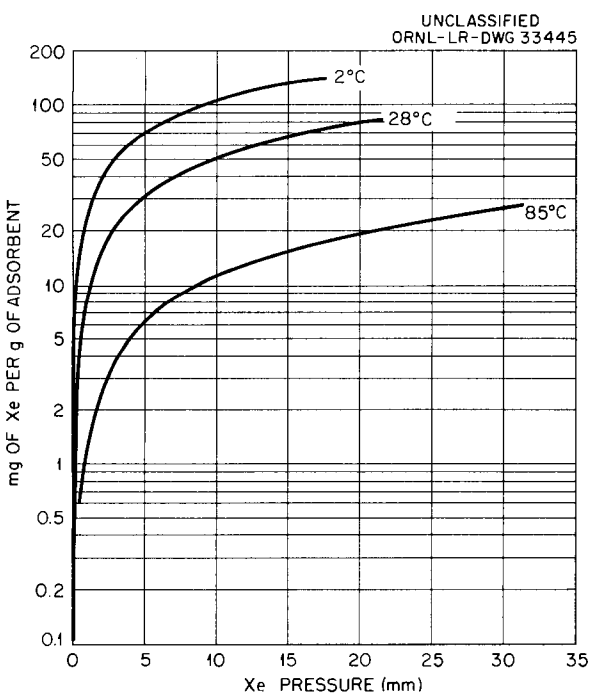

Fig. 17.6. Effect of Temperature on Xenon Adsorption on Columbia Charcoal at 2, 28, and 85°C.

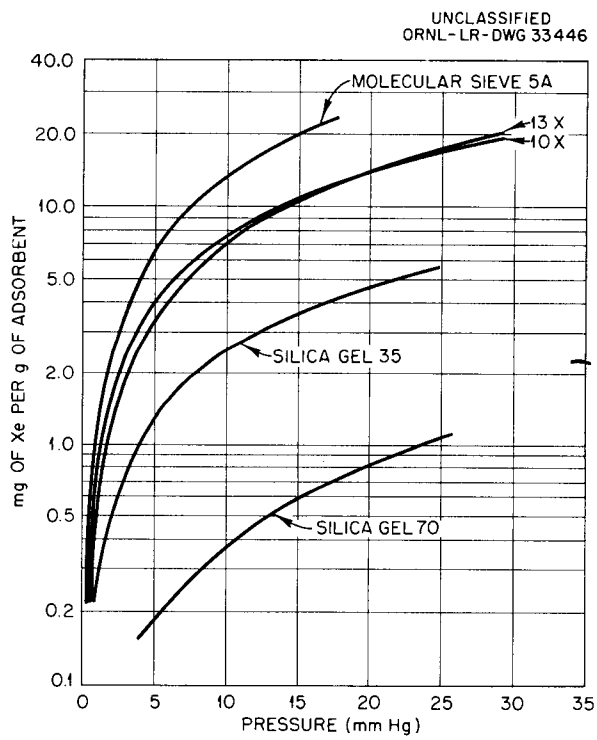

Fig. 17.7. Adsorption Isotherms for Xenon on Various Materials at 2°C.

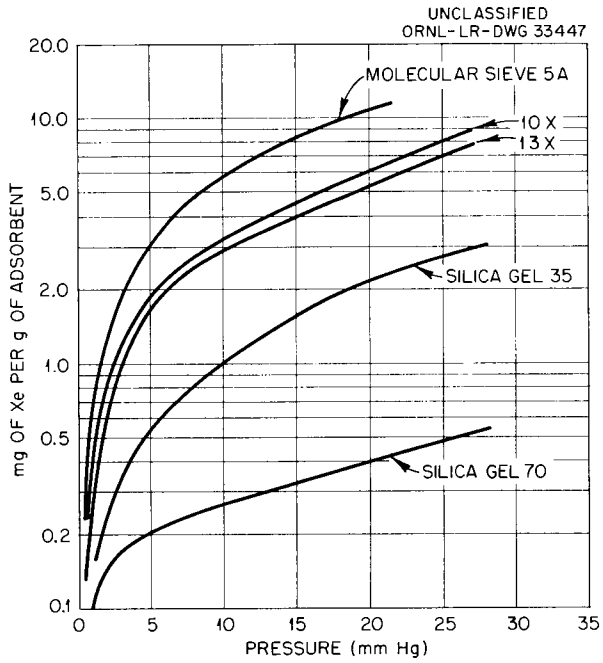

Fig. 17.8. Adsorption Isotherms for Xenon on Various Materials at 28°C.

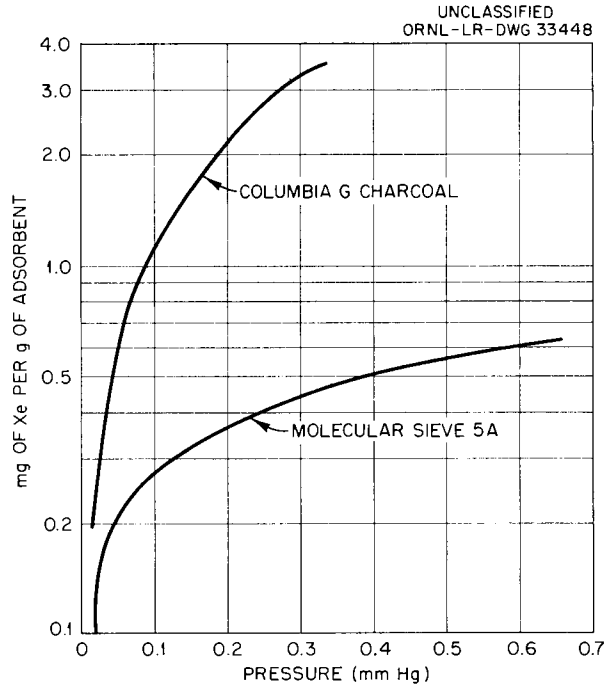

Fig. 17.9. Adsorption of Xenon on Charcoal and Molecular Sieve 5A at 24°C and Xenon Pressures Less Than 0.8 mm.

sieve 5A at pressures ranging from 0.014 to 1.0 mm at 24°C (Fig. 17.9), and the same relation in adsorptive capacity was noted at these pressures as at higher pressures. In these studies the amount of xenon adsorbed on a known mass of adsorbent at a known pressure was determined by observing with a precision cathetometer the displacement of a calibrated McBain balance.

When attempts to use the same technique for krypton studies at low pressure produced erratic results, the system was modified to allow the use of radioactive-tracer techniques. Stable krypton was spiked with Kr^{85} tracer, and the specific activity of the mixture was determined. The amount of traced krypton adsorbed at known pressure by a known mass of adsorbent was determined by removing the adsorbed gas from the adsorbent into a suitable counting tube in which Kr^{85} activity was measured. The data obtained at krypton pressures ranging from 0.01 to 0.60 mm at 28°C are shown in Figs. 17.10

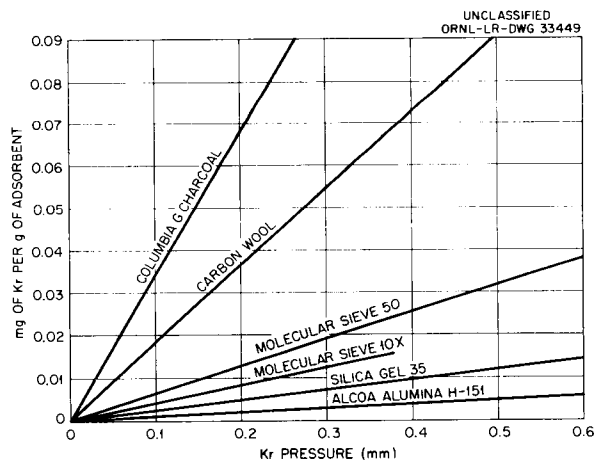

Fig. 17.10. Adsorption of Krypton at Low Pressures on Various Materials at 28°C.

and 17.11. Although the adsorptive-capacity values obtained by the McBain sorption-balance technique at low pressures are larger than those obtained by the tracer technique, the capacity ratio of various materials was the same by the two methods.

Studies on the effect of water on the adsorptive capacities of Columbia charcoal and Linde molecular sieve 5A for krypton at 28°C showed the capacity of either of the materials to be 35 to 45% greater when dry than when they contained 7% water. This is in agreement with the results of dynamic experiments reported in the preceding section for charcoal. The capacity of dry 5A sieve was 410% greater than when it contained 15% water (Fig. 17.12). An important difference between these materials is that 28 mm water vapor pressure (vapor pressure at 28°C) is necessary to maintain 7% water in charcoal, while the molecular sieves will adsorb 15% water in an essentially universal fashion. This indicates that once the sieve material becomes wet it cannot be dried, as can charcoal, by simply passing dry oxygen through the material for several hours.

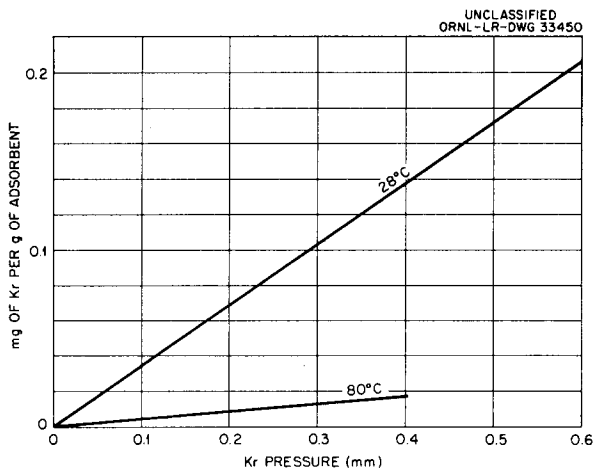

Fig. 17.11. Adsorption of Krypton at Low Pressures on Columbia G Charcoal at 28 and 80°C.

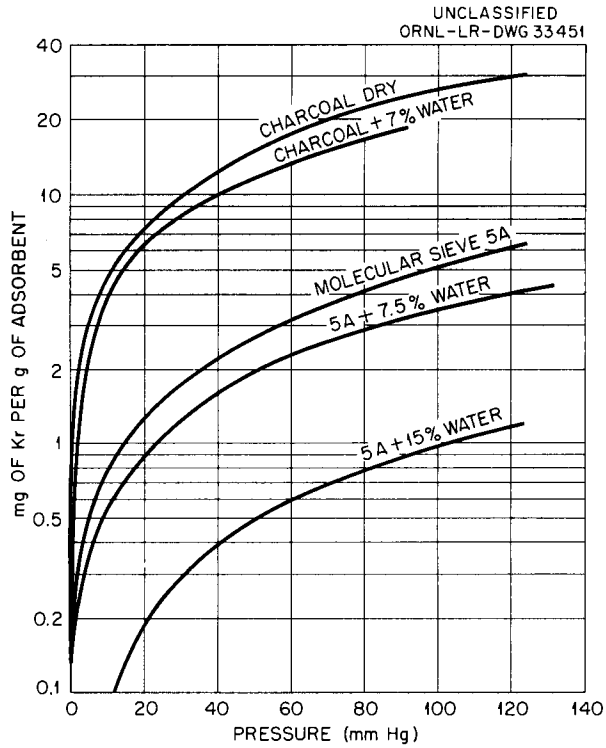

Fig. 17.12. Adsorption Isotherms for Krypton on Charcoal and Molecular Sieve 5A Containing Various Amounts of Water.

18. URANYL SULFATE BLANKET PROCESSING

R. E. Leuze P. A. Haas
J. M. Chilton J. W. Snider

The final P-1 loop experiments, to study plutonium behavior in 1.4 *m* UO_2SO_4 circulating at 250°C, were completed. The loop was then treated with chromous sulfate in dilute sulfuric acid to remove the corrosion film and adsorbed plutonium and was transferred to the burial grounds, where it will be disassembled and inspected. Laboratory tests in static bombs were made to study plutonium adsorption in an all-titanium system, and sorption of plutonium from 1.4 *m* UO_2SO_4 onto cation exchange resin was investigated as a possible processing method.

18.1 PLUTONIUM BEHAVIOR IN THE P-1 LOOP

After the four plutonium runs previously reported,[1] an attempt was made to remove or redissolve the plutonium adsorbed on the loop walls by circulating plutonium-free 1.4 *m* UO_2SO_4 at 250°C (run P-32). Essentially none of the plutonium was dissolved or removed as PuO_2 by the hydroclone during the 10 hr. The final plutonium run (P-33) was made to determine the behavior of plutonium at concentrations of several hundred milligrams per liter. Unfortunately, the hydroclone line became plugged shortly after the run started, and thus no information on solids removal was obtained. However, the results were similar to those obtained previously when dissolved plutonium sulfate was added to circulating 1.4 *m* UO_2SO_4 at 250°C. Of the 7.5 g of plutonium added, only about 4% (26 mg per kg of H_2O) remained in solution as Pu(VI). The remainder was apparently adsorbed on the loop walls. The loop was rinsed several times with water to remove the uranium left in the heel; however, this procedure removed essentially none of the plutonium.

18.1.1 Solids Removed

In the run with uranyl sulfate solution (run P-32) the hydroclone removed a total of 2.8 g of solids during 10 hr of operation. This material was quite similar to that found in previous runs – presumably an oxide containing 93% uranium, 5% iron, 1% chromium, and 0.2% plutonium. A small amount of solids found in the flowing-stream samples was also composed chiefly of uranium. Since the hydroclone line was plugged early in run P-33, no solids were removed in the final experiment.

18.1.2 Plutonium Solubility

During the final experiment (run P-33) about 1 g of plutonium as the dissolved sulfate was injected every 8 hr into a circulating stream of 1.4 *m* UO_2SO_4 at 250°C under 350 to 400 psi O_2. The graph in Fig. 18.1 compares the analytical values for the plutonium solution with the theoretical amount that would have been in solution with no adsorption or precipitation. The amount actually in solution, all Pu(VI), decreased from a little more than 200 mg per kg of H_2O early in the run to 26 mg per kg of H_2O at the end of the run. Although the solubility of plutonium in a reactor cannot be predicted from these experiments, all indications are that it will be low even under

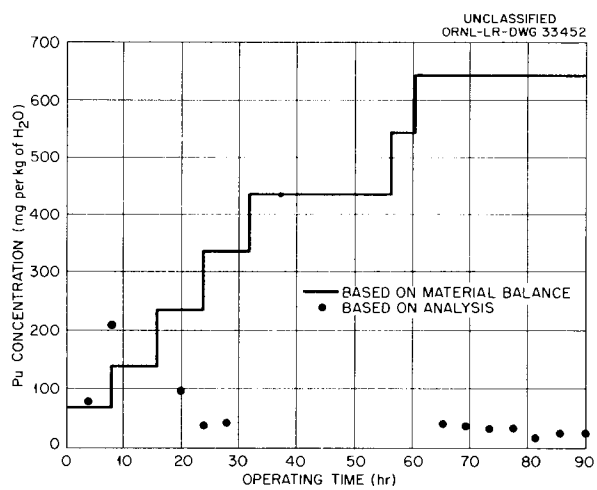

Fig. 18.1. Plutonium Concentration in Circulating Uranyl Sulfate of Run P-33. About 13 liters of 1.4 *m* UO_2SO_4 circulated at 250°C under O_2; dissolved plutonium sulfate injected at intervals.

[1] R. E. Leuze *et al.*, *HRP Quar. Prog. Rep. Jan. 31, 1958*, ORNL-2493, p 163–66.

conditions that oxidize plutonium to the hexavalent state.

18.1.3 Plutonium Adsorption on Metal

The sample coupons were removed at the end of run P-33, and the adsorbed plutonium was determined by direct alpha counting. Results agreed very well with results obtained by dissolution of the metal surface and determination of plutonium in solution. The individual sample coupons showed a wide variation in the amount of plutonium adsorbed, from 0.25 to 2.19 mg/cm^2. Assuming uniform distribution throughout the loop, the lowest figure would correspond to a total adsorption of 2.43 g of plutonium and the highest to 21 g. Since only 7.5 g was injected and practically none remained in solution or was removed by the hydroclone, it can be assumed that the 7.5 g was practically all adsorbed. Combined with adsorption from previous runs, this corresponds to an average plutonium adsorption of 1.1 mg/cm^2.

18.1.4 Corrosion

The corrosion rate for the loop, as determined by analysis of flowing-stream samples for dissolved nickel, was 15 mpy in run P-32 and 13 mpy in run P-33.

18.2 CHROMOUS SULFATE DESCALING OF P-1 LOOP

A chromous sulfate descaling procedure was used after run P-33 in an attempt to remove all plutonium remaining in the loop. The loop was evacuated, filled with nitrogen, and evacuated a second time. Chromous sulfate solution containing 0.36 *N* chromous ion and 0.77 *N* acid as sulfuric acid was drown into the loop. The plutonium on the walls, calculated from material balances for the six plutonium runs, was approximately 8 g. The first chromous sulfate solution was held in the loop for 76 hr, during which time it was cycled between room temperature and 90°C three times. When drained from the loop, the solution analysis was: chromous ion, 0.13 *N*; H^+, 0.39 *N*; plutonium, 312 mg/liter; nickel, 306 mg/liter; iron, 3.53 g/liter. The loop was rinsed with water and the same procedure was followed a second time. The drain from this run contained a total of 283 mg/liter of plutonium. After a water rinse, the loop was treated with chromous sulfate a third time. The drain from this run contained a total of 68 mg/liter of plutonium, 193 mg/liter of nickel, and 321 mg/liter of iron.

The plutonium removed in the first, second, and third runs, respectively, was 4.06, 3.68, and 0.88 g, for a total of 8.62 g, somewhat more than was calculated to be present on the walls of the system. The corrosion rate, based on the nickel content of the drained solutions, was about 25 mpy for these descaling operations.

18.3 PLUTONIUM BEHAVIOR IN A TITANIUM SYSTEM

Static bomb tests were made in which soluble plutonium was added in daily increments to a 1.4 *m* UO_2SO_4 solution which was held at 250°C overnight. The solution was contained in an all-titanium vessel, and titanium sample disks were suspended in the solution. Adsorption of plutonium on the walls was determined both by material balance and by counting the sample disks in an alpha counter. Runs were made under both oxygen overpressure and stoichiometric hydrogen-oxygen overpressure.

Under an oxygen overpressure of 190 psi (at 250°C) essentially no plutonium was lost from the solutions until the concentration exceeded approximately 40 mg per kg of H_2O. Essentially all the plutonium added in excess of 40 mg per kg of H_2O hydrolyzed and either precipitated as PuO_2 or adsorbed on the titanium. From 12 to 20% of the hydrolyzed plutonium adsorbed on the titanium, and at the end of this experiment the total plutonium adsorption was 2–5 μg/cm^2.

When a stoichiometric overpressure of hydrogen and oxygen was used, plutonium behavior was similar to behavior in a type 347 stainless steel system. Plutonium in excess of 5 mg per kg of H_2O hydrolyzed and adsorbed on the equipment walls. No loose PuO_2 precipitate was formed. At the end of this experiment, plutonium adsorption was 51 μg/cm^2. Material balances were excellent in all runs; the material adsorbed on the walls was easily removed by 6 *N* HNO_3 containing a trace of HF.

18.4 PLUTONIUM SORPTION ON CATION EXCHANGE RESIN

Scouting studies showed that tetravalent plutonium can be sorbed from 1.4 *m* UO_2SO_4 onto Dowex-50 cation exchange resin in the uranyl form. Higher cross-linked resin was superior in all respects to lower cross-linked resin. A total of 1.56 mg of plutonium per gram of dry 16% cross-linked resin was loaded, with no indication of saturation. From a feed containing 20 mg of Pu per kg of H_2O, the effluent contained less than 2 mg of Pu per kg of H_2O. The plutonium was completely eluted with 6 *M* H_2SO_4.

19. THORIUM OXIDE SLURRY DEVELOPMENT

J. P. McBride P. A. Haas E. M. Shank
C. V. Ellison N. A. Krohn C. E. Schilling
C. C. Haws K. H. McCorkle W. J. Watt
K. O. Johnsson L. E. Morse W. M. Woods
E. V. Jones R. L. Pearson E. L. Youngblood

19.1 SLURRY IRRADIATION STUDIES

19.1.1 Slurry Irradiations in the LITR

Seven short-term slurry irradiations were carried out in the C-44 vertical-tube facility of the LITR. The first (LITR-40) was on a slurry of 1300°C-fired thorium–enriched-uranium oxide (0.5% U^{235}) containing 750 g of Th per kg of D_2O. The concentration of MoO_3 used as a gas recombination catalyst was 0.05 *m*; 0.05 *m* MoO_3 was used in previous tests with enriched uranium. The dash-pot-stirred irradiation bomb, which contained the slurry, operated successfully at 300°C in pile for the entire test period of 355 hr. The reactor was at full power for 322 hr. No gas pressure in excess of steam was observed.

Two irradiations (LITR-41 and -42) were with slurries (750 g of Th per kg of D_2O) of 800°C-fired ThO_2 which had been coated with Dri-film (see Sec 19.4), washed, and refired at 1000°C to give a silicated surface. The stirrer failed in the first test, and the slurry was irradiated for 305 hr at 300°C in the settled condition. In the second test the stirrer failed after 24 hr, and the irradiation continued for 329 hr at 300°C. When the autoclaves were opened, both slurries were thick and required dilution with distilled water before they could be poured from the autoclave.

The fourth test (LITR-43) was made on a thoria-urania sol submitted for evaluation by the Davison Chemical Company. The sol was irradiated for 145 hr at 286°C without agitation. When the autoclave was opened after three weeks' decay, the sol had separated into a dilute slurry of gray material and a hard cake of yellowish material. A control out-of-pile test heated for 352 hr at 290°C showed a lesser degree of separation and essentially no color change.

The other three short-term irradiations (LITR-44, -46, and -47) were made with D_2O slurries of the same material – a thorium–natural-uranium oxide (5% U^{238}) prepared by firing the coprecipitated oxalates at 1000°C and grinding the product for 1 hr in a mullite mortar. The tests were made primarily to observe radiolytic-gas production and recombination phenomena; so no catalyst was added. The first test (750 g of Th per kg of H_2O) was irradiated for 49 hr, when a leak forced its removal. No pressure in excess of steam was noted at temperatures from 280 to 290°C. The second test (500 g of Th per kg of D_2O) was irradiated for 361 hr at temperatures from 260 to 300°C. Pressure readings in excess of steam were observed during the run, but upon termination it was discovered that the zero set on the pressure recorder had changed during the run by an amount larger than the observed pressure increases. The third test, containing 250 g of Th per kg of D_2O, was irradiated for 354 hr. No pressures in excess of steam were observed at temperatures from 270 to 280°C for the first seven days of operation. The pressure readings for the remainder of the test were inconsistent because of plugging of the capillary tube.

A long-term irradiation of a settled slurry of 1600°C-fired pilot-plant ThO_2 was terminated after 3235 hr of irradiation ($\sim 3 \times 10^{20}$ *nvt*). No gas pressures in excess of steam were observed. Approximately 0.2 wt % of mass-233 isotopes should be present. The material has not yet been recovered.

19.1.2 Postirradiation Examination

Analyses of several of the recovered slurries, including that from the Davison thoria-urania sol irradiation, showed essentially all the fission products associated with the solid phase (Table 19.1), in agreement with previous results. Particle size measurements of the slurries from LITR-38, -40, and -41 showed no significant differences between the irradiated and control samples.

19.1.3 ORNL Graphite Reactor Irradiations

Radiolytic-gas production and recombination studies in the ORNL Graphite Reactor were continued. The test with a slurry (500 g of Th per kg

Table 19.1. Distribution of Fission Products in Irradiated Slurries

Component	Amount in Supernatant (% of total)				
	LITR-38[a]	LITR-40[b]	LITR-41[c]	LITR-42[c]	LITR-43[d]
Gross β	0.02	0.04	0.17	1.8	0.06
Gross γ	0.02	0.11	0.28	2.3	0.05
TRE	0.45	0.02	5.2	1.7	0.08
Sr	3.6	0.04	9.9	4.4	0.05
Ru	0.54	0.9	27.9	9.8	0.12
Cs	9.8	86.3	3.3	12.5	100.0
Nb	0.27	0.02	0.11	2.2	0.10
Zr	0.03	0.01	0.06		
Zr-Nb				11.8	0.05
Pa	0.01	0.02	0.05	1.4	0.05
I	0.43				

[a] 1000°C-calcined ThO_2–0.5% U in D_2O.
[b] 1300°C-calcined ThO_2–0.5% U in D_2O.
[c] 1000°C-calcined Dri-filmed ThO_2.
[d] Davison sol NB53273.

of H_2O) of thorium–enriched-uranium oxide (2.8% U^{235}) calcined to 900°C was terminated after operating for 3018 hr in pile, with the reactor at full power of 3500 Mw for 2624 hr. Equilibrium pressures were measured from 200 to 280°C. From 200 to 240°C, radiolytic-gas pressures were in reasonable agreement with those observed in a previous test[1] with a similar slurry of 650°C-fired oxide. Above 240°C, however, the observed radiolytic-gas pressures remained nearly constant instead of decreasing as expected. The phenomenon occurred several times. It could be caused by an accumulation of radiolytic hydrogen as a result of oxygen consumption by corrosion, or it could indicate a change in the rate-controlling step of the recombination reaction. There is some experimental evidence for both these possibilities, but the data are insufficient to indicate whether these conditions existed.

19.1.4 Equipment Development

Two mockups of a proposed ORR slurry bomb (0.98 in. dia × 10 in. long) were assembled and were tested for temperature control at simulated gamma heat loads up to 5 kw and a bomb wall temperature of 300°C. Control by spraying the bomb wall with an air-water mixture was attempted on the first mockup. Required heat removal rates were attained, but temperature control was poor and problems of uncontrollable vapor binding were encountered. A method termed "conductance control" was tested on the second mockup. It gave excellent temperature uniformity and control over a wide range of cooling loads up to the maximum of 5 kw.

"Conductance control" utilized the conductance of a gas stream flowing through a narrow annulus (0.007 to 0.008 in. wide) surrounding the bomb as a variable thermal resistance between the bomb wall and its jacket. Water, boiling outside the jacket wall at 100°C, removed the heat from the system. Helium, air, and air-helium mixtures were used as the conducting gas for heat loads ranging between 1.1 and 4.9 kw at a constant wall temperature of 300°C. Pure argon and Freon-12 permitted lower heat loads of 0.6 and 0.4 kw, respectively. The maximum deviation from the mean temperature along the bomb wall at the 5 kw load was 14°C.

[1] J. P. McBride *et al.*, *HRP Quar. Prog. Rep. Oct. 31, 1957*, ORNL-2432, p 156.

A dash-pot bomb similar in geometry to those used for slurry irradiation[2] was blanketed with a 40-mil-thick gas layer in a cylindrical water-cooled aluminum jacket to test the feasibility of adapting the conductance-control method to control bomb temperature. Heat transfer coefficients, based on the area at the mean radius of the gas layer, were 6 Btu/hr·ft^2·°F for air and 15 for helium. Dependence of heat transfer rate on gas flow rate was slight in the range of flow rates of 2–28 scfh. The rate of heat dissipation at bomb operating temperature, 300°C, was approximately 110 w with air and 275 w with helium.

By assuming that the coils do not touch the aluminum jacket, a nominal thermal conductivity of the coils was calculated to be 0.66 Btu/hr·ft^2·°F per foot, which is in the range of thermal conductivity of glass. The fraction of the total resistance to heat transfer that is presented by the coils varies from slightly over half with helium to slightly less than one-quarter with air. The rate of heat transfer and range of control are not great enough to be of significant advantage compared to the present method of cooling the slurry-irradiation bombs in the LITR.

19.2 GAS RECOMBINATION STUDIES

Out-of-pile tests were carried out in support of in-pile corrosion studies to determine the MoO_3 catalyst concentration required in heavy-water slurries of thorium-uranium oxide to maintain a steady-state radiolytic-gas pressure in pile at $\leq$100 psi D_2 partial pressure at 280°C. The slurries used contained 1000 g of Th per kg of H_2O, and the thorium-uranium oxides had U^{235}/Th ratios of 0.005 and 0.05. Studies with the slurry containing the U/Th ratio of 0.005 indicated that a catalyst concentration of 0.02 *m* MoO_3 would be required. In-pile results confirmed this (see Sec 13.3.3). Initial experiments with slurries of the higher percentage uranium oxide with MoO_3 concentrations from 0.013 to 0.3 *m* MoO_3 showed little catalytic activity as prepared. After activation by treating with D_2 overpressure, slurries with MoO_3 concentrations from 0.001 to 0.038 *m* MoO_3 showed activities of 2–4 moles D_2/hr·liter, sufficient to be considered for use in the in-pile experiment. Experiments on the addition of silver to slurries of this oxide and on seeding in catalytically active solids were also investigated.

19.2.1 Studies with Thorium-Uranium Oxide Containing U^{235}/Th = 0.005

The thorium-uranium oxide containing U^{235}/Th = 0.005 was prepared by coprecipitating the thorium-uranium oxalates at 10°C (ref 3) and decomposing the material by a multistage calcination ending with a 24-hr firing at 1300°C. The final firing temperature was selected in order to produce a mixed oxide with a surface area approximating that of a 1600°C-fired pure oxide. The surface area obtained was 2 m^2/g.

The gas recombination experiments were carried out with slurries (1000 g of Th per kg of D_2O) to which MoO_3 was added. The anticipated deuterium production rate, and hence the required combination rate at 100 psi D_2, with this slurry in the LITR was 0.3 mole D_2/hr·liter. With 0.025 and 0.05 *m* MoO_3, recombination rates were too high (Table 19.2). The rate was too low with 0.015 *m* MoO_3, but adding more MoO_3 to a final concentration of 0.02 *m* MoO_3 resulted in the desired recombination activity at 275°C and 100 psi deuterium partial pressure of 0.32 mole D_2/hr·liter. On further heating of this slurry at 280–285°C

Table 19.2. Reaction Rates of Stoichiometric D_2-O_2 Mixtures at Several MoO_3 Concentrations in Heavy-Water Slurries of Thorium-Uranium Oxide (U^{235}/Th = 0.005)

Thorium-uranium oxide prepared by 24-hr calcination at 1300°C of coprecipitated oxalates

MoO_3 Concentration (*m*)	Reaction Temperature (°C)	Reaction Rate, P_{D_2} = 100 psi (moles D_2/hr·liter)
0.015	284	0.05
0.02*	278	0.32
0.02	280	0.57**
0.0228	280	0.84
0.025	277	2.7
0.05	258	5.4

*Catalyst concentration increased by adding 0.005 *m* MoO_3 to slurry containing 0.015 *m* MoO_3.

**Rate after slurry was heated at 280–285°C for 64 hr under O_2 overpressure.

[2] D. E. Ferguson *et al.*, *HRP Quar. Prog. Rep. Jan. 31, 1956*, ORNL-2057, p 111.

[3] *Ibid.*, p 112.

for 64 hr in the presence of oxygen, the rate increased to 0.57 mole D_2/hr·liter at 200°C and P_{D_2} = 100 psi. Prior to use in recombination experiments, all the slurries were heated a short time at 280°C with an oxygen overpressure.

The effect of prolonged heating of the thorium-uranium oxide slurry (U^{235}/Th = 0.005) containing 0.023 *m* MoO_3 at 280–285°C on the catalytic activity of the slurry for the stoichiometric D_2-O_2 mixture was determined for heating periods up to 543 hr. The reaction rate was relatively unaffected by heating for 100 and 213 hr, but at the end of the 543 hr the rate decreased about 20% (Table 19.3). This experiment was carried out in a stationary bomb with a small oxygen overpressure. The bomb was cooled to add the hydrogen and oxygen and shaken during the ½ hr required to raise the temperature to 280°C.

Table 19.3. Effect of Hydrothermal Treatment on Catalytic Activity

Conditions: Thorium-uranium oxide (U^{235}/Th = 0.005) prepared by 24-hr firing at 1300°C of coprecipitated oxalates, 1000 g of Th per kg of D_2O, 0.023 *m* MoO_3, 280°C

Heating Time (hr)	Reaction Rate, P_{D_2} = 100 psi (moles D_2/hr·liter)
0	0.84
100	0.87
213	0.84
543	0.68

19.2.2 Studies with Thorium-Uranium Oxide Containing U^{235}/Th = 0.05

The slurry containing 1000 g of Th per kg of D_2O and prepared from the thorium-uranium oxide with a U^{235}/Th ratio of 0.05 will require, in the LITR, a catalyst that will recombine the radiolytic gases at a rate of 3 moles D_2/hr·liter to maintain 100 psi D_2 partial pressure when there is a slight excess O_2 overpressure. In the presence of excess D_2 there is an indication that a recombination rate as low as 0.2 mole D_2/hr·liter may be sufficient (Sec 13.3.3). Experiments to determine the conditions required to yield the desired reaction rate are still in progress.

Reaction rates in the slurries as prepared and containing 0.012 to 0.3 *m* MoO_3 have been less than 0.1 mole of D_2 reacted per hour per liter of slurry at 280°C and 100 psi D_2 partial pressure (Table 19.4). It also appeared from these results that further increase in the MoO_3 concentration would not increase the reaction rate appreciably. For MoO_3 concentrations of 0.038 to 0.09 *m*, activation by heating with a deuterium overpressure at 270°C increased the reaction rate tenfold, but the rates were still far short of the 3 moles D_2/hr·liter required. The maximum rate was 0.9 mole D_2/hr·liter at 280°C and a partial pressure of 100 psi D_2 at 0.046 *m* MoO_3. The minimum value was 0.2 mole D_2/hr·liter for the same conditions of temperature and pressure at 0.09 *m* MoO_3.

Activated slurries containing MoO_3 concentrations of 0.001 to 0.032 *m* showed rates approximating the desired rate of 3 moles D_2/hr·liter. Some anomalies appeared, however, in that the apparent order of the reaction with respect to

Table 19.4. Reaction Rates of Stoichiometric D_2-O_2 Mixtures at Various MoO_3 Concentrations in Heavy Water Slurries of Thorium-Uranium Oxide (U^{235}/Th = 0.05)

Thorium-uranium oxide prepared from coprecipitated oxalates fired 24 hr at 1000°C; all slurries heated 3 hr at 280–285°C under O_2 overpressure

MoO_3 Concentration (*m*)	Reaction Rate, P_{D_2} = 100 psi (moles D_2/hr·liter)
0.013	0.006
0.016	0.007
0.026	0.004
0.032	0.003
0.038	0.005
0.048	0.007
0.064	0.007
0.080	0.005
0.096	0.007
0.15	0.06
0.20	0.06
0.30	0.07

pressure varied with the conditions, being apparently zero order at high gas pressures and changing to first order or less as the pressure decreased. The pressure dependence for gas recombination in the slurries in the absence of catalyst appeared to be less than first order at the higher temperatures.

The catalytic properties of thorium-uranium oxide (U/Th = 0.05) slurries containing silver were studied. The reaction rate was about 1.0 mole D_2/hr·liter at 280°C and 100 psi D_2 over the silver concentration range 0.0125 to 0.05 *m*. The results were the same whether the silver was added as the metal powder or as silver carbonate. The low surface area of the oxide (2 m^2/g) may explain the lack of change of reactivity with increasing silver concentration.

The possibility of obtaining the desired reaction rate by the addition of an acceptable amount of MoO_3-bearing ThO_2 was also studied. The material added to the thorium-uranium slurry was the dried solid phase of a slurry prepared from 900°C 24-hr calcined D-16 ThO_2 containing about 0.6% MoO_3, which showed very high activity for the H_2-O_2 reaction after being activated with H_2. After a slurry containing 10 wt % of the catalyst "seed" was heated with D_2 for 2 hr at 270°C, the reaction rate for the stoichiometric gas mixture was 14.1 moles D_2/hr·liter at 280°C and a partial pressure of 100 psi D_2. Slurries containing 5 and 7.5 wt % of "seeded" catalyst had reaction rates of 0.3 mole D_2/hr·liter of slurry under the same conditions of temperature and pressure.

As with the slurries containing lower percentages of uranium, the mixed oxide used in the above studies was prepared from the 10°C-coprecipitated oxalates, which were converted to the oxides by calcining at 1000°C for 24 hr. The oxide was milled for 1 hr in a mullite mortar previous to use. The slurry was prepared by heating the dry tumbled oxide and catalyst in D_2O for 3 hr at 280°C under a low O_2 overpressure. The slurries were activated by heating with D_2 (500 psi at 25°C) for 2 hr at 270°C.

19.3 MOLYBDENUM OXIDE CHEMISTRY IN THORIUM AND THORIUM-URANIUM OXIDE SLURRIES

The inactivity (i.e., for catalytic H_2-O_2 reaction) shown by molybdenum oxide in slurries of low-fired thorium oxide or those containing uranium oxide may result from the reaction of the molybdenum oxide with the thorium and/or uranium oxide to form catalytically inactive species.[4] Studies to delineate the chemistry of molybdenum oxide in slurries of thorium oxide and thorium-uranium oxide were carried out. Possible variables were the firing time and temperature of the oxide, the amount of uranium, the method of incorporating the uranium, the concentration of molybdenum, and equilibration time. The objective was to determine, if possible, the nature of the catalytic species and the rate and extent of reaction of the molybdenum oxide with the other oxides.

The program was mainly one of searching for analytical techniques to determine molybdenum-containing species. The following analytical procedures were adopted: (1) a total molybdenum determination involving complete dissolution of the slurry solids and a colorimetric estimation of molybdenum;[5] (2) a leaching of the solids with cold concentrated ammonia, which apparently removes all molybdenum oxide species except those tightly bound to the surface; and (3) a subsequent leaching of the solids with hot concentrated HCl to dissolve molybdenum which has reacted to form molybdate salts.

The data indicate that, when molybdenum oxide is autoclaved at 280°C in thorium oxide or thorium-uranium oxide slurry, a part of the molybdenum oxide is connected to acid-soluble species and another part is either strongly adsorbed on the thoria or converted to a form insoluble in both the base and the acid (Table 19.5). For the pure oxides the nonleachable molybdenum oxide increases with increasing oxide firing temperature if the data are considered in terms of micrograms of MoO_3 per square meter of surface area (see Fig. 19.1). For the higher fired oxides, 900 and 1600°C, the quantity of nonleachable MoO_3 approximates a monolayer, leading one to believe that this species may be associated with recombination activity in these systems (i.e., MoO_3 forms active systems only with the high-fired oxides).

Thermogravimetric Studies. – Preliminary to the above-described development work, a thermogravimetric analysis was made of a simple mixture of

[4] W. D. Fletcher, C. C. Thomas, Jr., and D. E. Byrnes, *PAR Quar. Prog. Rep. Aug. 31, 1957*, WACP-668, p 104.

[5] O. Menis, personal communication.

Table 19.5. Reaction of Molybdenum Oxide with Thorium and Thorium-Uranium Oxide Slurries

5.7 g of $ThO_2 \cdot MoO_3$ per 10 ml of H_2O, autoclaved at 280°C

Experiment No.	Slurry Oxide	Time Autoclaved (hr)	Total Molybdenum Oxide (mg)	Molybdenum Leached (%)		Residual Molybdenum	
				Cold NH_4OH	Hot HCl	%	$\mu g/m^2$
38	650°C ThO_2	44	70.8	25.9	30.5	43.6	180
28	900°C ThO_2	44	61.0	21.8	25.5	52.7	805
17	1600°C ThO_2	44	66.0	36.4	54.1	9.5	1100
42	1000°C ThO_2–0.5% U	44	74.2	43.0	59.8		
11	1600°C ThO_2–0.5% U	22	73.2	39.4	63.4		
410	1000°C ThO_2–5% U	22	149.6	11.53	81.9	6.53	

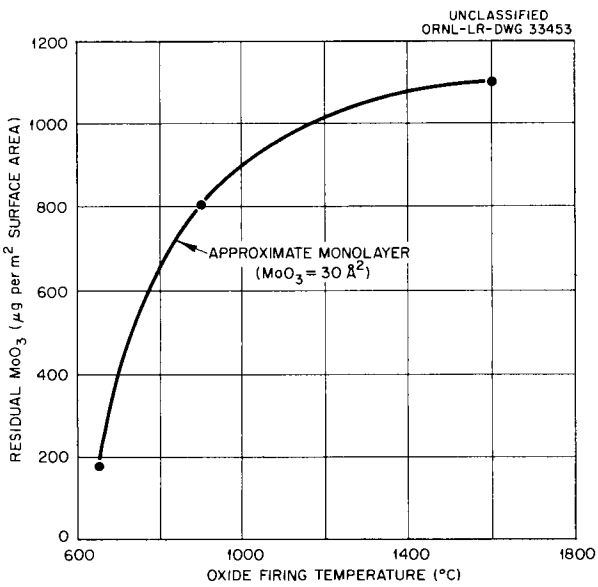

Fig. 19.1. Effect of Oxide Firing Temperature on Surface Reaction of Thorium Oxide with Molybdenum Oxide. Slurry: 500 g of Th per kg of H_2O, 0.05 *m* MoO_3, autoclaved 44 hr at 280°C; solids leached with cold concentrated NH_4OH and hot concentrated HCl.

650°C ThO_2 and MoO_3. The sample lost weight steadily up to 750°C and even to 800°C, but then there was no appreciable loss between 800 and 1000°C. The loss at 1000°C was very slow, but was rather rapid from 1000 to 1100°C. From 1150 to 1200°C, and for 36 min at 1200°C, there was no further loss. Pure MoO_3 is completely volatile at 800°C.

These data indicated that a thermogravimetric method for total molybdenum weight might be developed. Experiments did not confirm this but did suggest that simple heating of the MoO_3 with ThO_2 at 800 to 1000°C might be a convenient method for incorporating the molybdenum oxide in a thorium oxide slurry. Solids were prepared by autoclaving at 280°C slurries of 650, 900, and 1600°C fired ThO_2 and MoO_3. The samples were dried at 150°C and then heated from 750 to 800°C and left overnight at this temperature. They were then cooled and weighed and were calcined at about 1125°C for 4 hr; the loss in weight was considered as MoO_3. The results were:

Initial ThO_2 Calcination Temperature (°C)	MoO_3 Recovery (%)				
	Exp. 1	Exp. 2	Exp. 3	Exp. 4	Exp. 5
650	109.9	106.0	129.4	130.2	
900	112.8	108.8	134.4	142.0	105.9
1600	77.1	105.0	71.0	98.1	

19.4 PROPERTIES OF SILICA-COATED THORIUM OXIDE

High-temperature slurry settling studies have shown that the effect of an additive on the settling rate becomes relatively less with increasing temperature and is sometimes negligible at 300°C. Altering the surface characteristics of the thoria

could give a slurry showing better dispersion at high temperatures. Thorium oxides with chemically bonded silicated surfaces were prepared by treatment with chlorosilane vapors (G-E Dri-film SC-77), washing to remove chloride ion, and refiring to remove organic groups and leave a silicate surface. Thoria (650°C, D-16) so treated showed no crystallite growth on being refired to as high as 1000°C and, as an aqueous slurry, showed complete dispersion in high-temperature settling studies up to 280°C.

19.4.1 Dri-film Chemistry

General Electric Dri-film SC-77 is a 50-50 mixture of dimethyldichlorosilane and methyltrichlorosilane, a clear liquid with a boiling point of 66–70°C. It is applied by simply equilibrating the oxide with the vapors at room temperature. The Dri-film reacts chemically with the adsorbed water as hydroxyl groups on the thoria surface, releasing HCl. Subsequent heating of the oxide (110°C) drives off most of the HCl and forms a polymer, bound by silicon-oxygen linkages to the thoria surface by the splitting-out of water between hydroxyl groups:

$$CH_3SiCl_3 + 3H_2O \longrightarrow CH_3Si(OH)_3 + 3HCl$$
$$\xrightarrow{\Delta} CH_3SiO{\cdot}OH \text{ (polymer)} + H_2O$$
$$\xrightarrow{\Delta} CH_3SiO_{1.5} \text{ (polymer)} + H_2O$$

Thorium oxide treated with the Dri-film vapors is not wet by water. Subsequent burning of the Dri-film-treated oxide removes all the methyl groups, leaving a silica film bonded chemically to the thoria surface.

19.4.2 Preparation and Washing

The oxides were exposed to the Dri-film vapors overnight in an evacuated desiccator and then heated at 150°C for 5 hr or more. The resulting materials were washed six or more times with 6 *N* NH_4OH to which some alcohol had been added to improve the wetting. This was followed by several washes with 3 *N* NH_4OH and finally with water. The washed products were dried overnight at 150°C and analyzed for chloride. At this point the chloride content is usually less than 50 ppm. Firing the oxides at 650°C for 24 hr yielded free-flowing white powders containing less than 10 ppm of chloride.

19.4.3 Characteristic Properties

The effect of firing temperature on the characteristic properties of the silica-coated oxides is shown in Table 19.6. Data obtained previously on the D-16 oxide are included for comparison. No change in particle size resulted from the Dri-film treatment, but at firing temperatures up to 1000°C crystallite growth was prevented and the decrease in specific surface area was inhibited. At 1200°C pronounced sintering of the oxide occurred, with consequent increase in crystallite size and decrease in specific surface area. The products from the 1600°C firing were completely sintered, dense cakes.

19.4.4 Slurry Properties

Slurries of the silica-coated oxides were prepared at a concentration of 250 g of Th per kg of H_2O, and the pH, settling rate, and settled densities were determined after the slurries had been autoclaved for 22 hr at 300°C. The pH's of the slurries were only slightly lower than those of the untreated oxide, but the slurries settled very slowly (too slowly to be read conveniently), and the settled beds were more dense, indicating a higher dispersion characteristic than the untreated oxide (Table 19.7).

19.4.5 High-Temperature Settling Behavior

The settling behavior of a slurry (250 g of Th per kg of H_2O) of D-16 thorium oxide that had been silica-coated was observed between room temperature and 320°C with x-ray equipment. No settling was observed in 7 min at temperatures below 200°C. At 280°C there was a slight indication that settling had begun, although a small accumulation, with time, of solid on the bottom of the bomb indicated that dispersion was essentially complete. At 320°C the system flocculated and settled rapidly. Lowering the temperature to 240°C restored the complete dispersion.

19.5 RELATION OF OXIDE PARTICULATE PROPERTIES TO YIELD STRESS

One of the specifications set for the slurry to be used in HRE-3 requires a yield stress equal to or less than 0.1 lb/ft^2 at a concentration of 1500 g of Th per kg of H_2O. Measurements on the first batches of 1600°C oxide produced at the pilot plant (LO-33, -34, -35, -36) showed yield-stress

Table 19.6. Characteristic Properties of Silica-Coated Thorium Oxide

Oxide	Treatment	Firing Temperature (°C)	Particle Size (μ)	Surface Area (m^2/g)	X-Ray Crystallite Size (Å)	Relative Surface for N_2 Adsorption* (S/θ)
D-16-650°C	None	650	2.1	33.5	115	0.64
		800		13.1	263	0.58
		1000	3.1	6.5	745	0.81
D-16-650°C	Silica-coated	650	3.0	32.7	111	0.61
		800	2.5	27.6	118	0.54
		1000	3.3	13.4	104	0.23
		1200	10	1.3	404	0.09
		1600		0.24		
SO-B-10-650	Silica-coated	650	0.9	28.8	100	0.48
		800	0.9	24.9	105	0.44
		1000	1.0	17.4	111	0.32
		1200	1.0	1.6	530	0.14

*Relative area of the crystallite available for N_2 adsorption: $S/\theta = (1.67 \times 10^{-4})$ (x-ray crystallite size)(surface area).

Table 19.7. Slurry Properties of Silica-Coated Thorium Oxide

Conditions: 250 g of Th per kg of H_2O; autoclaved 22 hr, 300°C

Oxide	Treatment	Firing Temperature (°C)	pH	Settling Rate (cm/sec)	Settled Concentration (g of Th per kg of H_2O)
D-16-650°C	None	650	8.3*	0.03*	1300
		800	6.6	0.06	1350
		1000	7.1	0.08	1750
D-16-650°C	Silica-coated	650	5.9	**	1900
		800	4.6	**	2050
		1000	6.3	**	1850
		1200	6.1	0.0002	2000
SO-B-10-650	Silica-coated	650	3.9	**	1700
		800	4.3	**	1950
		1000	4.2	**	2150
		1200	5.1	**	3050

*500 g of Th per kg of H_2O.

**Settling rate too slow to be read conveniently.

values close to 0.8 lb/ft^2. Hence a study was made on the influence of thorium oxide average particle size, uniformity, shape, and firing temperature on the yield stress of thorium oxide slurries.

The particle-size data agreed with those of D. G. Thomas (Sec 8.9), who found that τ_y was proportional to $1/d_g^2$ where d_g is the geometric mean particle size (see Fig. 19.2). The uniformity of the oxide had little or no influence on the yield

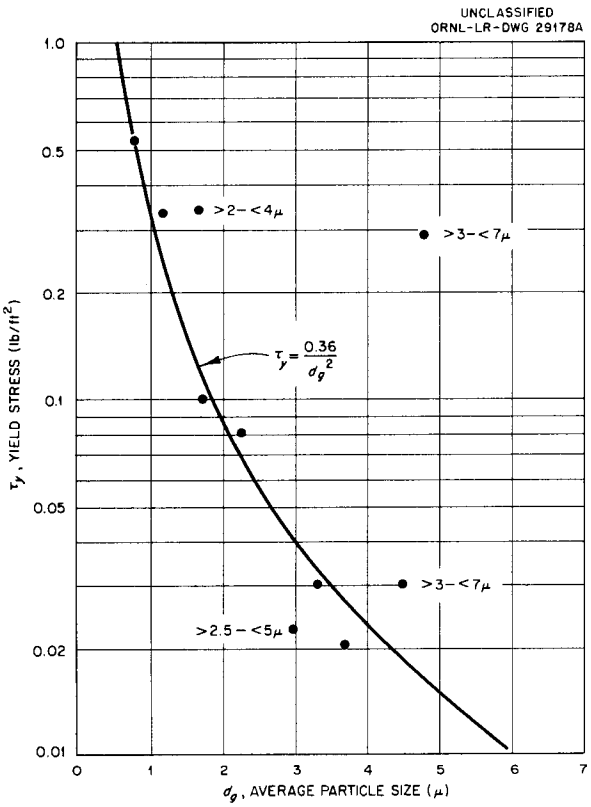

Fig. 19.2. Effect of Particle Size on Yield Stress.

stress (Table 19.8), but the presence of a fine fraction lowered the yield stress somewhat. For example, a slurry of DT-1 (density = 2 g/cc) classified to contain particles between 2 and 4 μ had a yield stress of 0.34 lb/ft^2, which was lowered to 0.26 lb/ft^2 by the addition of 3.34 wt % LO-38 (d_g = 0.82 μ).

Slurries (density = 2 g/ml) of Houdry spheres classified to contain particles between 3 and 10 μ and less than 3 μ had essentially zero yield stress (Table 19.8). Both the yield stress and coefficient of rigidity decreased with increasing firing temperature from 650 to 1600°C (Fig. 19.3). The yield stress gradually decreased with increasing firing temperatures from 0.8 to 0.2 lb/ft^2 for slurries of density 2 g/ml and average particle size 1 μ, but the coefficient of rigidity decreased to 5 centipoises for the same slurries at 800°C oxide firing temperature and to only 3 centipoises for the 1600°C firing.

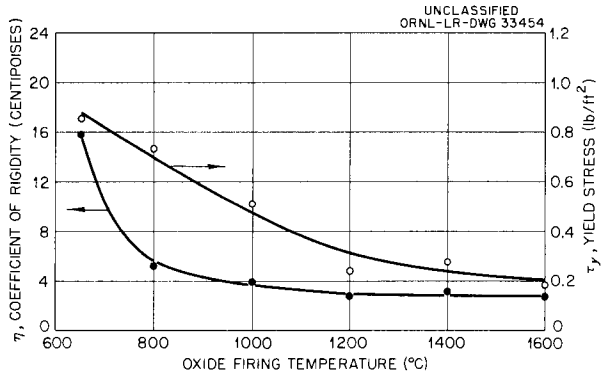

Fig. 19.3. Yield Stress and Coefficient of Rigidity as a Function of Oxide Firing Temperature. Average particle size, 1 μ; slurry density, 2 g/cc.

19.6 PARTICULATE PROPERTIES OF COMPRESSED, HIGH-FIRED THORIUM OXIDE

The effect of pressing at pressures up to 72,500 psi on the particulate properties of 1600°C-fired thorium oxide (LO-36) was determined in a series of experiments in a cylindrical 1-in.-ID steel punch-and-die set. The thorium oxide used (LO-36) had been packed in trays prior to its final calcination to roughly double its ordinary bulk density (as 800°C-fired oxide). The purpose of the tests was to find an alternative to the laborious dispersion operation now used to break up the hard lumps of oxide to a material suitable for use in the classification step for production oxide. Also, it was possible that a simple dry pressing operation to break up oversize agglomerates might be developed, which could be substituted for the classification step entirely and thus eliminate the additional firing step required to decompose the oxalic acid dispersing agent. The data indicated that pressure of 20,000 psi was sufficient to break up the hard lumps of oxide to produce a material suitable for classification in the usual manner. A pressure of 50,000 psi was sufficient to break up the microscopic agglomerates and to

Table 19.8. Yield-Stress Values for Slurries of Production Oxides

Oxide	Slurry Preparation	Slurry Density (g/ml)	Geometric Mean Particle Size, d_g (μ)	Geometric Mean Standard Deviation, σ_g	Yield Stress (lb/ft^2)
LO-31-1600-4	As prepared	1.95	3.6	2.6	0.02
LO-36-1600-4	Classified, <5 μ	1.90	1.0	1.5	0.14
LO-38-1600-4	Classified, <3 μ	2.00	0.8	1.4	0.53
LO-41-1600-4	As prepared	2.00	1.7	1.7	0.10
DT-1-1600-4	As prepared	1.95	1.5	1.5	0.29
	Classified, <5 μ	2.00	1.2	1.4	0.33
	Classified, >2 to <4 μ	2.00	1.7	1.3	0.34
	Classified, >2 to <4 μ plus 3.4% LO-38	2.00			0.26
DT-2 and -3	Classified, >3 to <7 μ (No. 1)	2.00	4.8	1.5	0.28
	Classified, >3 to <7 μ (No. 2)	2.00	4.5	1.5	0.03
	Classified, <3 μ	2.00	2.3	1.7	0.08
DT-5-1600-4	As prepared	2.00	3.7	1.3	0.02
	Classified, <5 μ	2.00	3.0	1.3	0.02
	Classified, <5 μ	2.32	3.0	1.3	0.07
	Classified, >2.5 to <5 μ	2.00	3.3	1.3	0.03
Houdry spheres	Classified, >3 to <10 μ	2.00	7.6	1.4	0.00
	Classified, <3 μ	2.00	2.3	1.4	0.00

disperse the oxide into the individual particles of the oxalate relic structure. If scale-up of this procedure is possible, it might be used either as a preliminary to the present classification step or as a substitute.

The effect of pressure on percentage yield of classified product from a single decantation at the 5-μ settling rate is shown in Fig. 19.4. Pressures less than 1000 psi had little effect. The yield increased markedly with pressure up to 20,000 psi, beyond which the increase in yield was relatively slight. While a series of decantations was not run to determine ultimate yield, it appears from these and subsequent data that a second decantation could have been carried out immediately, eliminating the prolonged steeping in oxalic acid now used, with prospective yields as good as or better than those now obtained in the pilot plant.

The effect of pressure on the weight fraction of particles greater than 20 μ in diameter and on the weight fraction greater than 1.05 μ in diameter is shown in Fig. 19.5. The "oversize" fractions were affected only slightly by pressures less than 20,000 psi. A maximum in the >20-μ fraction appeared to occur at about 2500 psi, but its extent does not greatly exceed the scatter of the data from the average in that pressure range. When the pressure exceeded 50,000 psi, the fraction of oversize material was essentially the same as that in a typical classified product from the pilot plant.

Production oxides ordinarily show a break in the plot of log of particle size vs weight fraction on

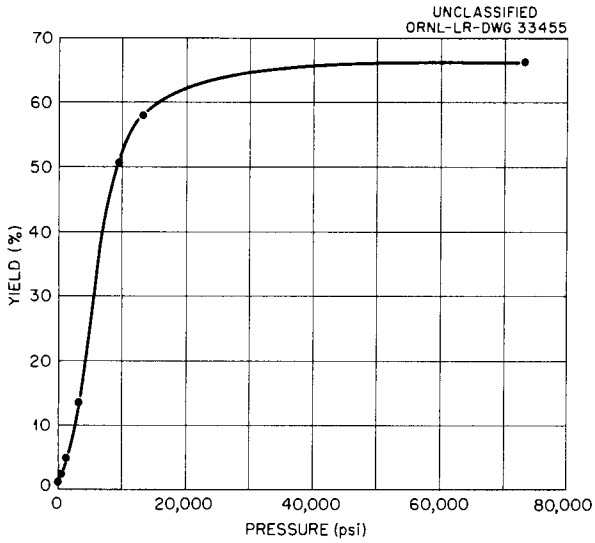

Fig. 19.4. First-Decantation Yield as a Function of Pressure. Oxide: 1600°C-fired (LO-36), compacted; oxalic acid dispersion decanted at a rate to yield particles of $< 5\ \mu$.

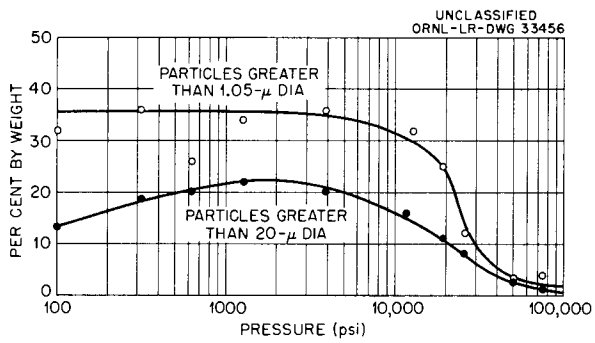

Fig. 19.5. Weight Per Cent of Particles Greater Than 1.05 and 20 μ in Diameter as a Function of Pressure. Oxide: 1600°C-calcined (LO-36), compacted.

the probability scale at about 1 μ, the material below this particle size being quite uniform (shallow slope) and that above having a rather wide dispersion (steep slope). Pressures up to 72,500 psi, while decreasing the oversize fraction in LO-36 oxide (Fig. 19.5), did not change the point at which the break in the particle-size curve occurred (1 μ) nor the uniformity of the material below 1 μ. Electron micrographs of LO-36 prior to and after pressing, Figs. 19.6(*a*) and (*b*), confirmed the impression that the effect of pressure was to break up lumps and agglomerates, leaving the original particles intact.

The nitrogen adsorption surface area appeared to be relatively unaffected by the pressing (Table 19.9), again indicating that pressing was not breaking up the individual particles. Iron contamination also remained within acceptable limits (Table 19.10).

Thorium oxides with preparation histories and structures different from those of LO-36 responded to compressing in markedly different ways. The nitrogen adsorption area of LO-30 1600°C-calcined oxide, a comparatively coarse, nonuniform oxide from 70°C-precipitated oxalate increased from

Table 19.9. Nitrogen-Adsorption Surface Area of Compressed 1600°C-Calcined Thorium Oxide (LO-36) Samples

Pressure (psi)	Area (m^2/g)
318	1.3
636	1.3
1,270	1.3
3,175	1.3
6,360	1.4
12,700	1.5
25,400	1.7
50,800	1.8
72,500	1.8

Table 19.10. Iron Analysis of Compressed 1600°C-Calcined Thorium Oxide (LO-36) Sample

Pressure (psi)	Iron (ppm)
318	26
636	24
1,270	25
3,175	21
6,360	26
12,700	25
25,400	48
50,800	25
72,500	24

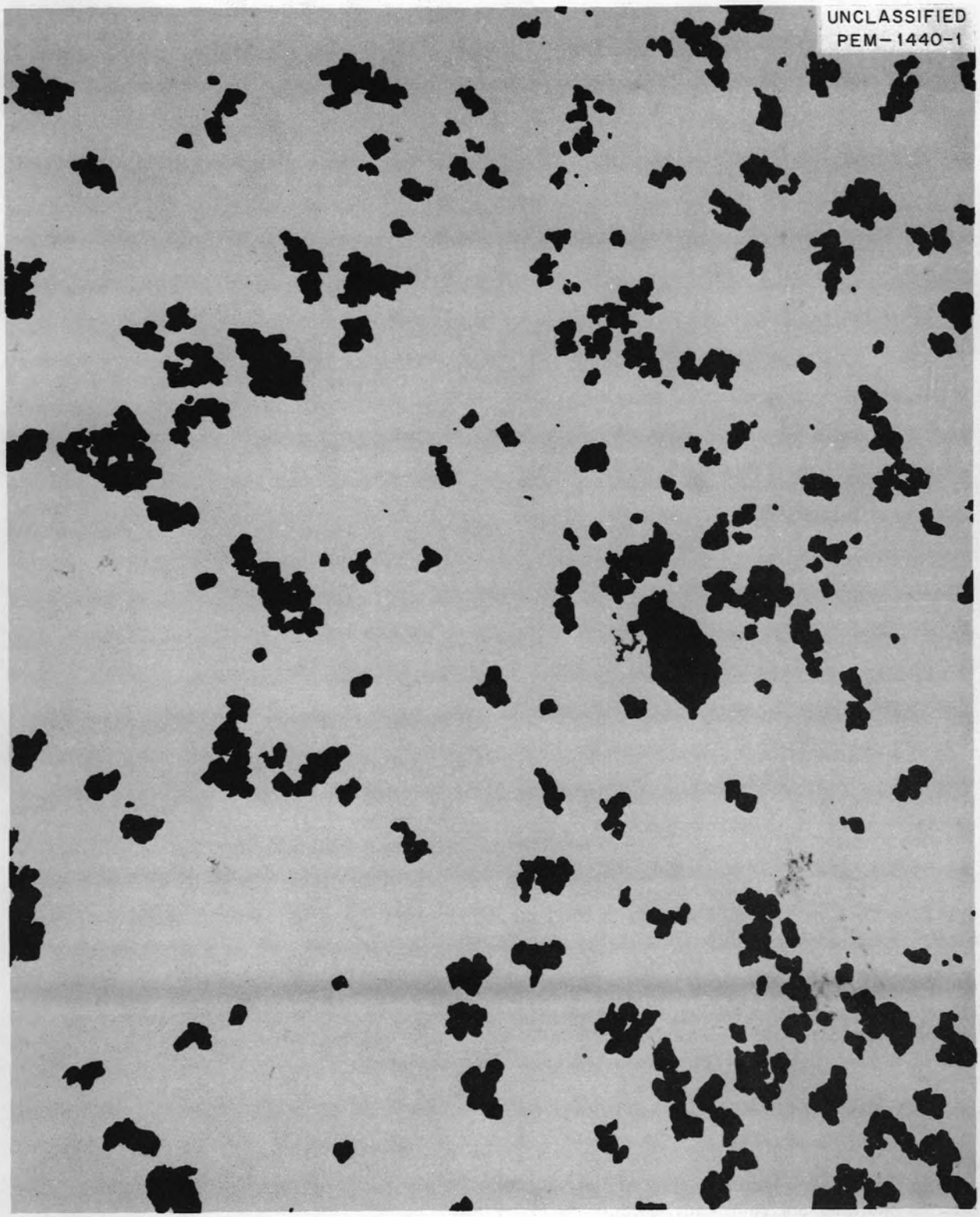

Fig. 19.6a. LO-36 Thorium Oxide Before Pressing. 8000X.

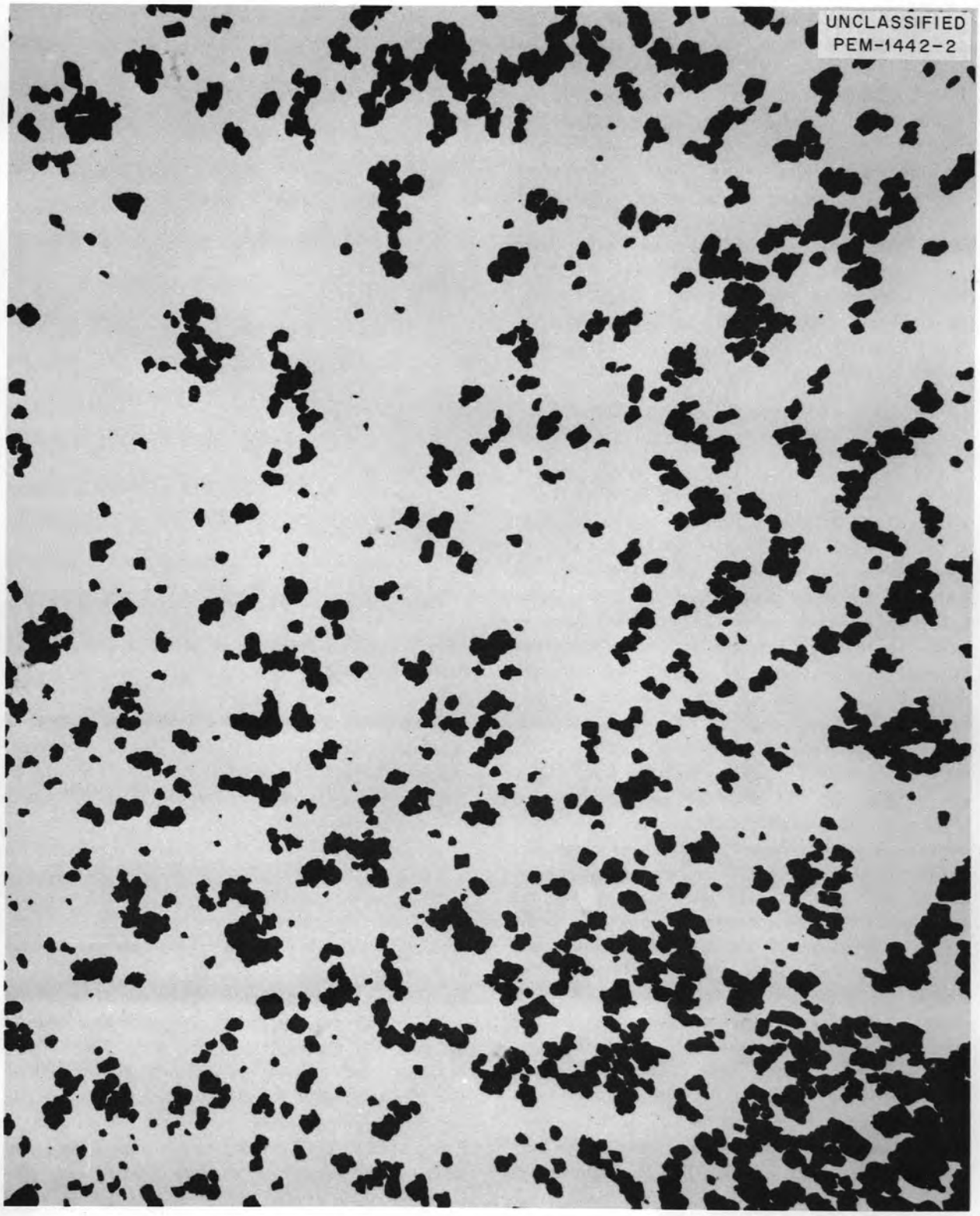

Fig. 19.6b. LO-36 Thorium Oxide After Pressing at 72,500 psi. 8000X.

0.6 to 2.4 m^2/g at a pressure of 72,500 psi. The average particle size, 3 μ, was not greatly affected, however. A comparatively coarse, 1600°C-fired, uniform oxide, composed of agglomerated crystal clusters formed in the oxalate precipitation step, shattered into a less uniform material of smaller average particle size when compressed at 12,700 psi. Before compression the average particle size was 7 μ, and the geometric mean standard deviation was 1.5. After compressing, the average particle size was 1.3 μ and the deviation 2.0. This suggests that a dry-pressing test might be used to predict the likelihood of particle degradation in an oxide when pumped as a slurry.

19.7 EVALUATION OF PUMPED HIGH-FIRED OXIDE

In a high-temperature loop run, BS-22, carried out by the Materials Research Section of REED with a slurry of 1600°C-fired pilot plant oxide at a concentration of 1500 g of Th per kg of H_2O, about 40% of the slurry charged settled along the bottom of the loop system and could not be resuspended. The suspended material was removed from the loop by hydroclones, and the settled material was removed by cooling the loop and draining it. Samples of each were characterized by chemical analysis, particle-size analysis, settling rates from room temperature to 300°C (at a concentration of 250 g of Th per kg of H_2O), and yield-stress and coefficient-of-rigidity measurements. No significant differences were found between the hydrocloned and drained materials.

The results of chemical analyses of the hydrocloned and drained materials, both solids and supernatants, were nearly the same except in the loss on ignition and the titanium, sodium, and potassium contents of the solids. Loss on ignition was 0.15% in the drained solids and 0.06% in the hydroclone solids. The titanium, sodium, and potassium contents of the drained and hydrocloned materials, respectively, were 0.35%, 33 ppm, and 27 ppm, and 0.63%, 92 ppm, and 142 ppm.

The original oxide for run BS-22 was DT-1, 1600°C-fired pilot-plant oxide. Its average particle size, d_g, was 1.2 μ, with a geometric mean standard deviation (σ) of 1.36. The drained solids had a d_g of 0.96 μ and a σ of 1.3; the hydroclone solids, 1.1 μ and 1.4.

Essentially no differences were found in the settling rates of the two materials (Fig. 19.7).

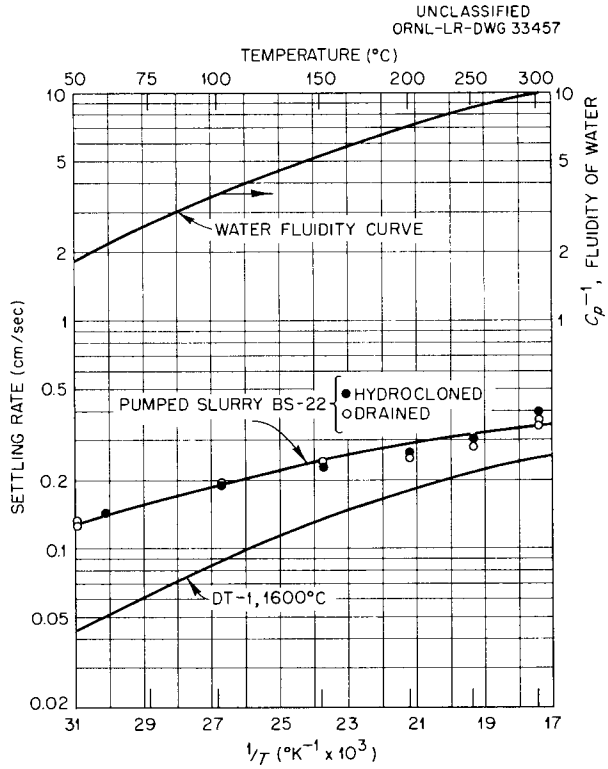

Fig. 19.7. Settling Rates of Pumped High-Fired Oxide: Run BS-22.

The temperature-dependence curves were typical of pumped 1600°C-fired material. The yield stress and coefficient of rigidity of 2-g/ml slurries of the two materials were the same: 0.27 lb/ft^2 and 3.8–4.0 centipoises.

19.8 THORIUM-URANIUM OXIDE

The present concept of the HRE-4 one-region slurry reactor calls for slurry fuel of thorium-uranium with a U/Th mole ratio of about 0.08 and a slurry concentration of 200 to 400 g of Th per kg of H_2O. Two methods of preparing the mixed oxide on an engineering scale are under investigation: (1) coprecipitation of the thorium-uranous oxalates and subsequent thermal decomposition and (2) adsorption or precipitation of a uranium compound on the thoria surface followed by a firing step to bind the uranium to the surface and cause it to diffuse into the thoria particles. The first method, which has been described previously,[3] has the possible advantage of distributing the uranium homogeneously in the solid, but will require laboratory development of the precipitation step to permit particle-size control; the second

takes advantage of the methods of particle-size control already developed in the thorium oxide preparation studies and shares with the other preparation method the necessity of investigating the effects of temperature-time phenomena in the firing step and hydrothermal treatment on the oxide particle size and the approach to an equilibrium condition.

19.8.1 Coprecipitation

In the coprecipitation step the mixed oxalate is precipitated by adding to a thorium nitrate solution an oxalic acid–ammonium oxalate solution of uranous oxalate. Previous studies have indicated that thorium-uranium oxides with U/Th mole ratios of 0.005 and 0.05 could be readily prepared by this technique, the limitation on uranium content being the solubility of the uranous oxalate in the oxalic acid–ammonium oxalate reagent.

Only one attempt has been made to coprecipitate thorium-uranous oxalate at U/Th mole ratios greater than 0.05. The ammonium oxalate–oxalic acid–uranous oxalate reagent used had an NH_4^+/H^+ ratio of 9.4, as opposed to the ratio of 0.02 or less used in the other preparations, and was 2.2 *M* in $H_2C_2O_4$. The mixed oxalate was precipitated from 0.1 *M* $Th(NO_3)_4$ solution. The uranous oxalate was precipitated quantitatively. The solid formed by firing the mixed oxalate at 650°C had a U/Th ratio of 0.4. The estimated uranium valence from the weight, assuming a U/Th ratio of 2, was 5.4. This may be compared with the value obtained by Anderson[6] of 5.3 for a thorium-uranium oxide with the same U/Th ratio and fired at 500°C.

19.8.2 Adsorption

Adsorption studies were carried out with suspensions of 650°C-fired thoria, surface area 20 to 30 m^2/g, using solutions of uranyl nitrate, formate, and acetate, ammonium-uranyl carbonate and an alkaline-peroxide complexed uranium. Simple agitation of the suspension and recovery of the solid resulted in only partial adsorption of uranium. Boiling or steam distillation was more effective, but only in the case of the ammonium-uranyl carbonate was there a complete decomposition of the solution and deposition of the uranium on the thoria surface. The dried solids from all suspensions except those in uranyl nitrate were peach colored. Those from the nitrate solution were dark red and had hardened into irregularly shaped agglomerates.

19.9 THORIUM OXIDE PREPARATION DEVELOPMENT

19.9.1 Laboratory Studies

Investigation of the effect of the oxalate precipitation variables on the properties of oxide produced by the thermal decomposition of thorium oxalate is complete, and a report[7] has been issued. With a 10°C precipitation temperature, vigorous agitation, a high oxalic acid addition rate (to the thorium nitrate; each reagent 1 *M*), and long digestion time, it was possible to produce engineering-scale quantities of very uniform oxide products, 1 μ in average size and with a small fraction >5 μ after firing at 1600°C. Additional laboratory studies indicated that the particle size could be further controlled by installing a draft tube with a variable opening (Fig. 19.8) around the agitator and varying the rate of recirculation of the precipitating medium through the draft tube (Table 19.11). Oxide produced with the draft tube was as uniform as oxide produced without its use and had as low an oversize fraction after 1600°C firing. More than 1100 lb of oxide was produced in the pilot plant with the draft tube, with average particle sizes varying from 1 to 4.8 μ.

19.9.2 Continuous Thorium Oxalate Precipitation

Results of experiments on the continuous precipitation of thorium oxalate showed that major changes occur during the oxalate digestion period even though mixing and initial precipitation are completed within seconds. The oxalate slurry initially produced underwent a change upon standing from a stiff whipped-cream appearance to a quite fluid, settleable slurry. The time required for this change was between 1 and 5 min.

In an attempt to prevent digestion effects, the product was discharged into methyl alcohol at dry-ice temperature. The resulting mixture was filtered and washed as quickly as practical. The

[6] J. S. Anderson *et al.*, *J. Chem. Soc. (London)* **1954**, 3324.

[7] R. L. Pearson *et al.*, *Preparation of ThO_2 for Homogeneous Reactor Blanket Use*, ORNL-2509 (May 26,

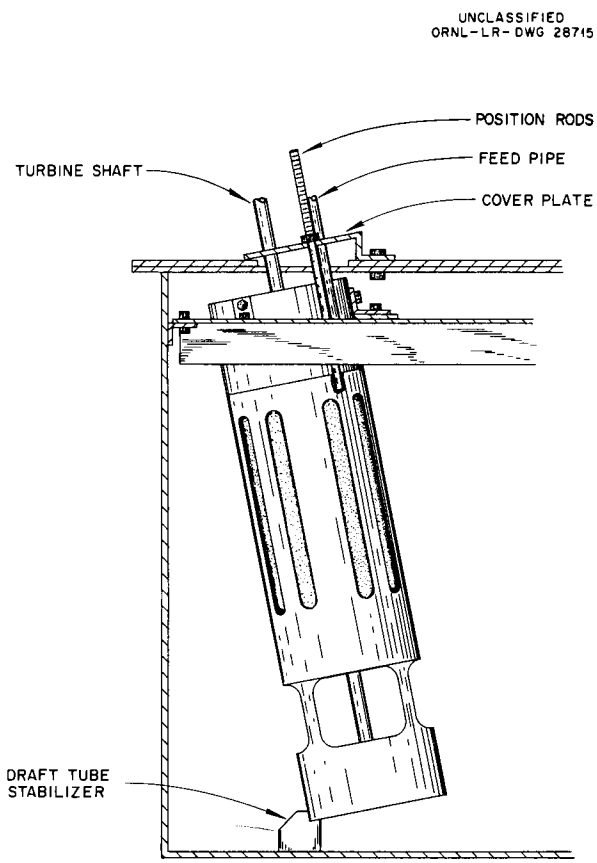

Fig. 19.8. Draft-Tube Agitator Installed in Pilot Plant Precipitator.

ThO_2 prepared from material processed in this way had small mean particle diameters (>0.5 μ) as compared with ThO_2 prepared from material processed at room temperature without methyl alcohol. Subsequent tests showed that the low-temperature alcohol alters, but does not eliminate, digestion effects.

The behavior upon digestion of precipitated $Th(C_2O_4)_2$ was greatly modified by a nitric-acid-extractable material present on new, unregenerated Dowex-3 anion exchange resin. Oxalate precipitated from $Th(NO_3)_4$ previously equilibrated with the resin was initially a fine, almost colloidal, precipitate which changed upon 1 to 2 hr of digestion into very uniform and perfect 2- to 5-μ cubical crystals. Addition of 0.64 *M* urea to non-resin-treated aqueous thorium nitrate gave similar cubical crystals, 3.0 μ mean size, after 2 to 5 hr digestion. The reagents used in the precipitation with urea were 1 *M* oxalic acid, 0.08 *M* $Th(NO_3)_4$, and 4 *M* excess HNO_3; these were added to the vortex cavity mixer at room temperature. The effects of other amino compounds, such as aniline, ethylenediamine, and propylenediamine, on oxalate particle shape and on the oxide products prepared by thermal decomposition of the oxalate are being investigated.

Table 19.11. Effect of Thorium Oxalate Recirculation Rate on Oxide Particle Size

Room temperature; oxide products fired at 800°C

Recirculation Rate	Geometric Mean Particle Size, d_g (μ)	
	4-min Mixing	6-min Mixing
Slow	0.99	0.99
Medium	0.91	1.42
Fast	1.30	2.48

19.9.3 Thorium Oxide Classification

The performance of hydroclones for the classification of thorium oxide was evaluated by tests with both single 0.40-in.-dia hydroclones and three-stage cascades of Dorr TM units (thirty-two 0.40-in.-dia hydroclones in parallel per stage). Results with single hydroclones (15 psi pressure drop, 70 vol % of the feed to the overflow) showed that dispersing agents were not necessary to obtain classification (Fig. 19.9). The curve for particle size vs separation (Fig. 19.10) has the shape predictable from hydroclone theory.

Based on the present scale and requirements for thorium oxide production, a cascade somewhat analogous to a batch rectification column was designed as the optimum hydroclone classification system. The equipment arrangement (Fig. 19.11) has the advantages of simple control, the ability to obtain a sequence of product fractions, and operating flexibility. The performance predicted for this system is presented as a C_w/C_p concentration ratio vs particle-size curve in Fig. 19.12. Capacity would be from 0 to 1 kg of ThO_2 per min, depending on the centrifuge capacity.

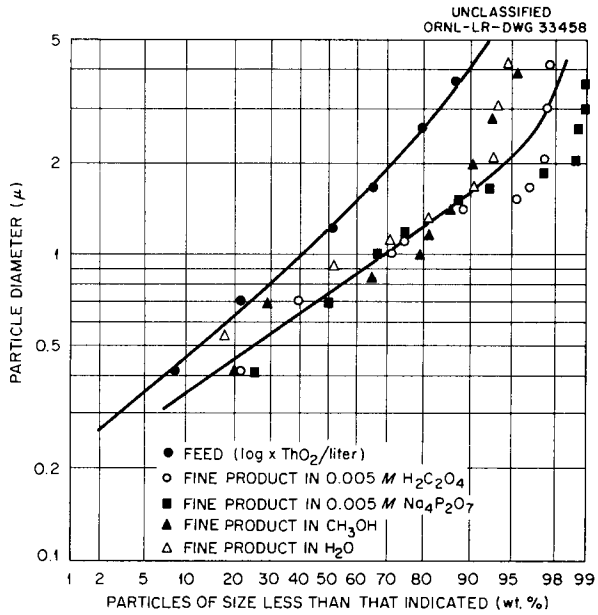

Fig. 19.9. Single-Hydroclone Classification of ThO_2.

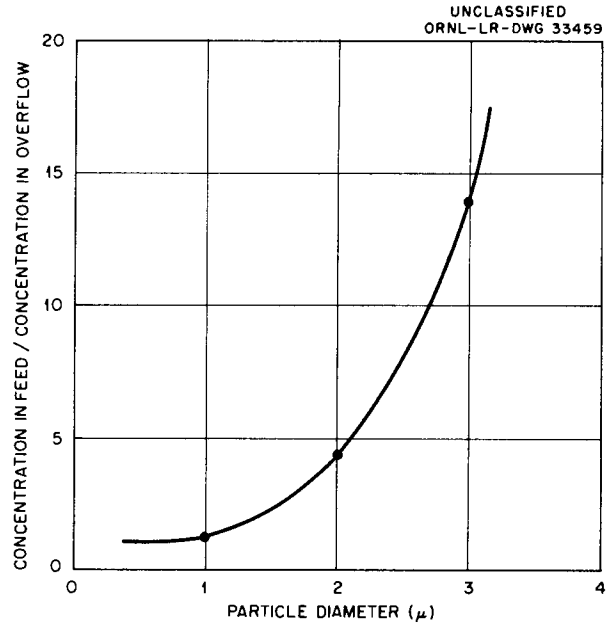

Fig. 19.10. Hydroclone Separation Factor vs Particle Diameter for ThO_2 Slurry; Single Hydroclone.

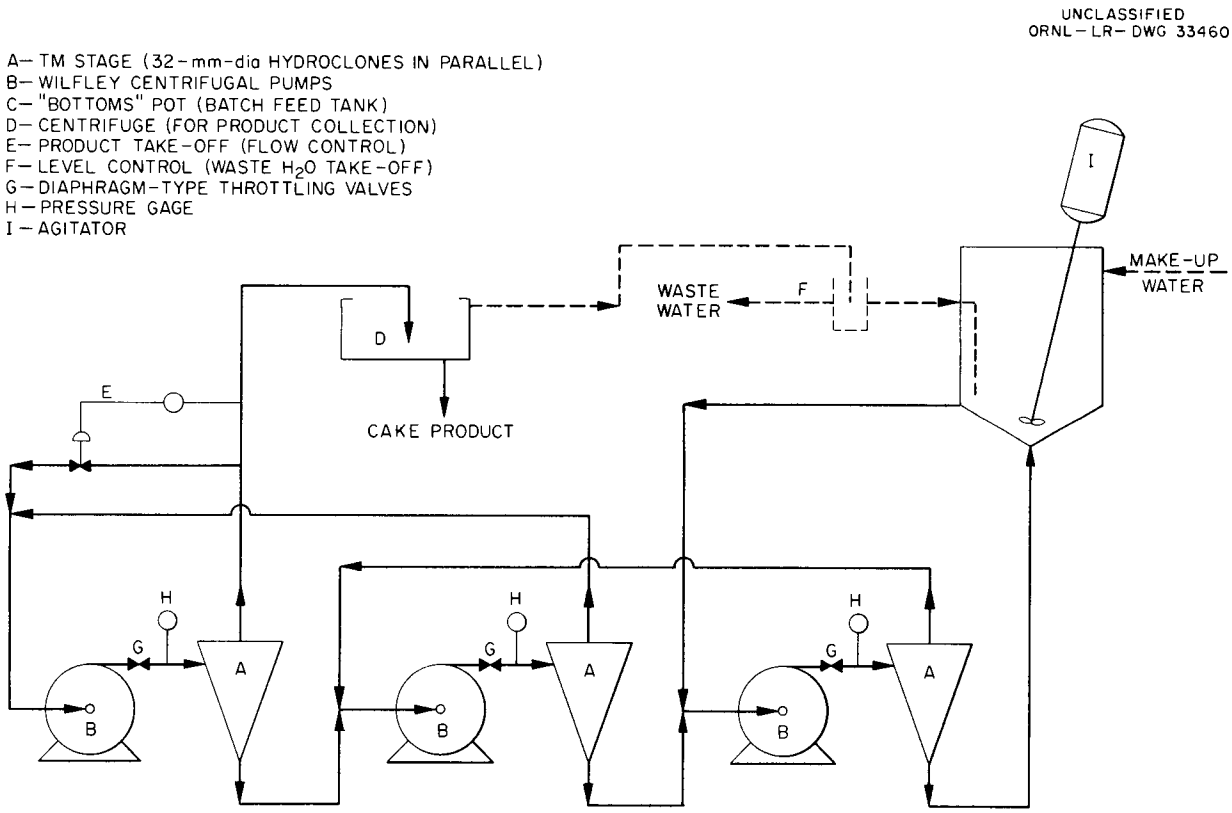

Fig. 19.11. Simple Three-Stage Hydroclone Classification System.

A Sharples Super Classifier was tested for removing oversize particles from two lots of 1600°C-fired, micropulverized thorium oxide.[8] During an initial pass, feed of about 7 μ mean diameter was classified to give a 2.3-μ-mean-diameter product stream essentially free of material over 8 μ (Fig. 19.13). These size analyses were obtained on a Sharples Micromerograph; the apparent Stokes diameters reported from neutron activation analyses were consistently about two-thirds of the Micromerograph values.

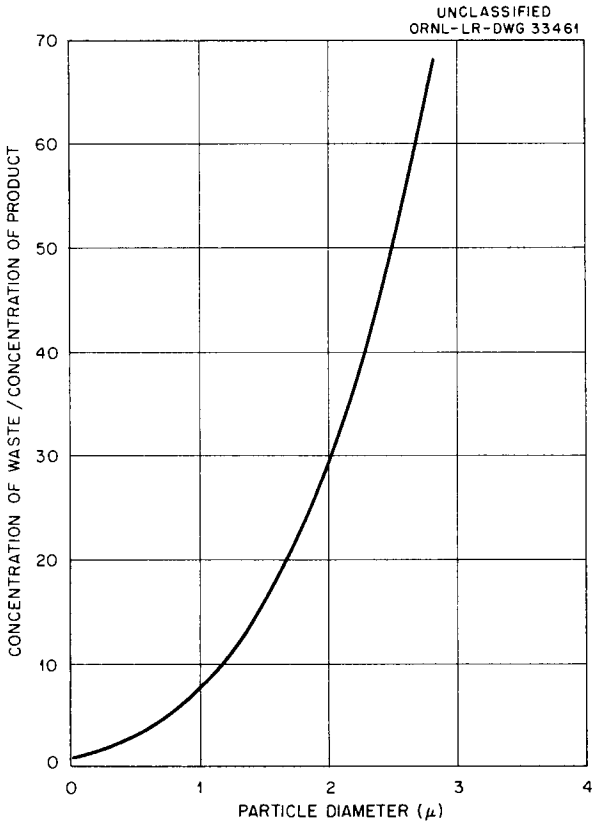

Fig. 19.12. Typical Separation Curve for ThO_2 with TM-3 Hydroclone Cascade.

19.9.4 Thorium Oxide Slurry Concentration

A Sharples P-4 Super-D-Canter was used for the continuous concentration and discharge of slurries, 1.2 μ average particle size, containing 45 to 90 g of ThO_2 per liter. For feed rates of 375 to 2000 cc/min, losses of thorium oxide to the supernatant were 0.11 to 1.1% of the feed (Table 19.12). The

[8] Machine was operated by members of the Oak Ridge Gaseous Diffusion Plant Technical Division.

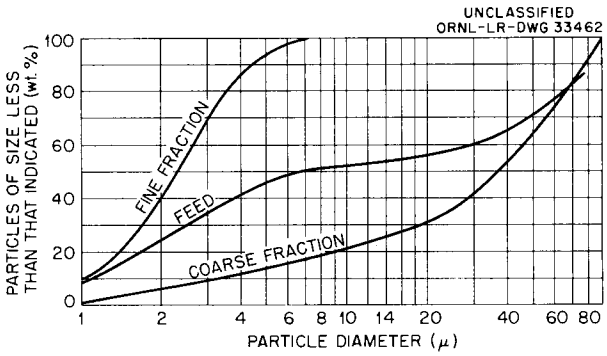

Fig. 19.13. Particle Size Distribution of Thorium Oxide from Sharples Super Classifier.

Table 19.12. Sharples P-4 Super-D-Canter Thorium Oxide Centrifugation Test

Super-D-Canter speed: 6000 rpm
Centrifugal force: 2100*G*
Solids in underflow stream: about 84%

Feed Stream			Overflow Stream			
Rate (ml/min)	Solids Concentration (g/liter)	Mean Particle Size (μ)	Solids Concentration (g/liter)	Mean Particle Size (μ)	Appearance	Solids Removed (%)
300	16.0	1.2	0.039		Slightly hazy	99.76
820	89.6	1.2	0.132	0.7	Hazy	99.85
2000	47.8	1.3	0.523	0.6	Milky	98.91
1460	89.6	1.3	0.396	0.6	Milky	99.56
375	44.9	1.2	0.050		Slightly hazy	99.89

thorium oxide was discharged as an 84% solids cake.

19.9.5 Flame Calcination

Experiments on the flame firing of thoria slurries in methanol were continued in a reflected-flame apparatus. The reflector was built by drilling a 1-in.-dia hole lengthwise through a 2.5 × 2.5 × 9 in. graphite block. The reflector was then mounted in magnesia fire brick so that it would exhaust directly into the intake of the spray cooling system. A new type of tubular torch was built that was capable of furnishing a fully carbureted alcohol-oxygen-acetylene gaseous mixture to the intake of the reflector. Operation of the torch and feeding system was uneventful throughout the feeding of 1 lb of material, with the exception of a few leaks in the feeding system. The service life of the graphite reflector was about 2 hr, and heat losses from the uninsulated ends of the reflector block were high. Reflector temperatures ranged from 1300°C at the exposed ends to >1600°C in the insulated center section. Exhaust gases from the reflector were above 1750°C, which is the limit of available thermocouples.

The results obtained in run 14 show an improvement over those from the most nearly comparable previous run (Fig. 19.14). Surface areas were smaller: 2.3 to 2.7 m^2/g as compared with 2.9 to 3.1 m^2/g. The dispersion of the feed material was considerably improved, as indicated by the comparative increase of the particle sizes in the spray cooler. The spray-cooler product from run 9 increased from 1.5 μ average particle size in the feed to 12 μ in the product from the spray cooler. The product of the spray cooler collected in run 14 increased from 0.86 to 1.6 μ.

Runs 19–24 demonstrated the reproducibility of results: runs 23 and 24 with ThO_2, runs 20 and 21 with $Th(C_2O_4)_2$, and run 19 with a ZrO_2 reflector (Table 19.13). An electron micrograph of product from run 19 with a ZrO_2 reflector (Fig. 19.15) shows a change in particle shape; particle shapes had not previously changed during calcination.

19.10 THORIUM OXIDE PRODUCTION

Thorium oxide production was discontinued in March for about six weeks to permit modifications for improved process ventilation, since there was evidence that some operating personnel had breathed or ingested significant quantities of thoria. Modifications consisted in installing glove-box hoods over each piece of equipment

Table 19.13. Flame-Calcination Experiments; Summary of Data from Recent Tests

All measurements at a specific gravity of 2.0

Run No.	Reflector Material	Feed Material		Product Material		
		Description	Average Particle Diameter (μ)	Average Particle Diameter (μ)	Surface Area (m^2/g)	Yield Stress (lb/ft^2)
19	ZrO_2	ThO_2 LO-43	0.86	2.4 2.6	1.2 1.4	0 0
20	Graphite	Thorium oxalate	1.4	1.6	2.5*	
21	Graphite	Thorium oxalate	1.4	1.8	5.5	0.20
23	Graphite	ThO_2 LO-43	0.86	1.1	2.5	0.25
24	Graphite	ThO_2 LO-43	0.86	1.15	2.4	0.27
Pilot-plant product		LO-43	0.86	1.6	1.6	0.25–0.35

*Residual thorium oxalate in product <0.4%.

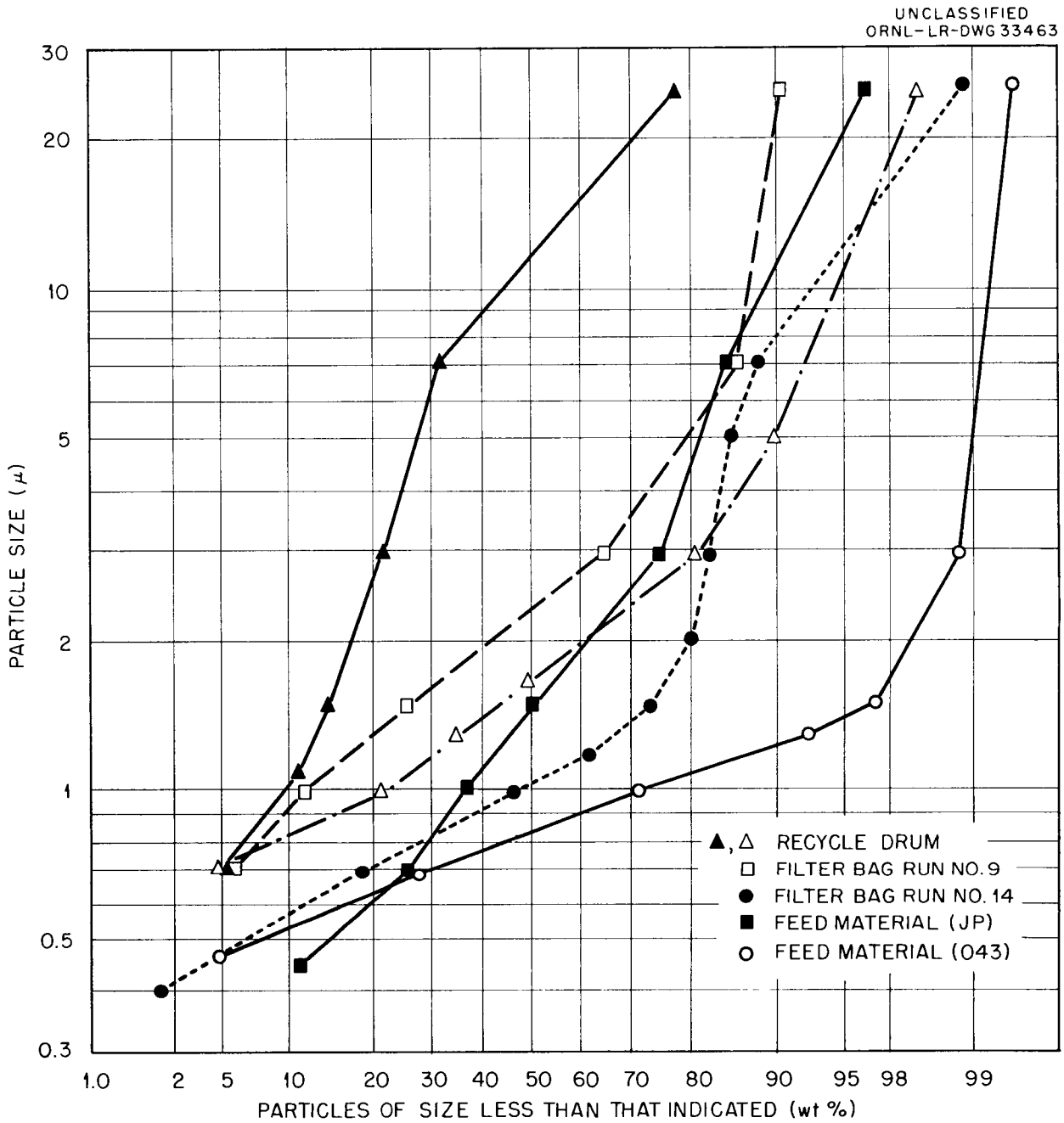

Fig. 19.14. Flame Calcination: Comparison of Particle Size Distribution Data from Runs 9 and 14.

and in providing greater ventilation. Operations since the modifications have been accomplished without indication of significant internal exposure. The new bottom-load gas-fired furnace (vended by Ohio Kilns, Inc.) and the classified-product dewatering centrifuge (vended by American Tool & Machine Company) were received and installed. The furnace was fired and "baked-out" and will be put into operation on receipt of the crucibles and firing-cycle programmer. The centrifuge was tested and shown to be suitable for product dewatering and for oxalate filtration and washing. The classification system was modified to permit larger-particle product fractions. The multistage

hydroclone system was installed and will be tested for classification. Maintenance items included replacement of the filter cloth twice and the electric furnace heating elements and thermocouples.

Prior to suspending operations, eight precipitations were made to prepare quantities of standard and special oxides. Following the modifications, 16 precipitations were made. The special oxides were prepared by varying solution concentrations, precipitation temperatures, digestion time and temperatures, and the percentage opening of the draft tube. About 5560 lb of 650°C-calcined oxide was prepared from the oxalate, and an additional 2535 lb of 650°C-recalcined oxide was prepared from classified product. Totals of 4025 lb of 1600°C-calcined oxide and 190 lb of 1400°C-calcined oxide were prepared in two gas-fired furnaces. Of the 4025 lb of oxide, 2915 lb was classified for use in slurry engineering studies.

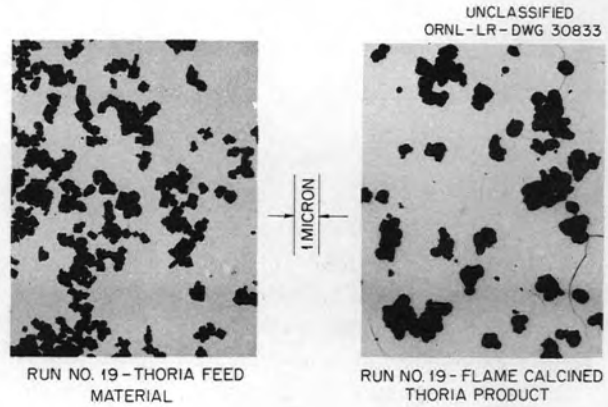

Fig. 19.15. Flame-Calcination Experiments; Effect of Passing Thoria Through a Zirconia-Reflected Flame.

20. IN-PILE SLURRY LOOP

W. E. Unger

T. A. Arehart
J. W. Brown, Jr.
R. S. Culver
L. J. King
B. B. Klima
W. F. Schaffer, Jr.
L. B. Shappert
J. W. Snider

The in-pile slurry loop program is a joint operation between the PAR Project and ORNL to obtain information on the performance of circulating slurries exposed to high neutron flux.

Radiation exposure of personnel during maintenance will be lessened by recent design changes. The location of equipment in the auxiliary cubicles has been rearranged and the design of the cubicle closures altered to ensure ready access to equipment components likely to require maintenance. Where possible, valves have been grouped into assemblies. An assembly, fitted with disconnects, is to be replaced as a unit if one of the valves fails. Other valves, which must be positioned close to the loop and cannot be grouped into assemblies, will be mounted integrally with the loop package and will be replaced, in effect, each time the loop is replaced.

After the completion of an irradiated slurry run, the loop will be dismantled by dismembering the various components by sawing and cutting in the segmenting facility. In order to minimize contamination of the cell and the installed equipment, the removal of all slurry from the loop package is extremely desirable, if not mandatory. The removal of slurry by displacement washings, while not completely unacceptable, does not reduce the slurry to the minimum level desired. Repeated batch rinses (~11 loop volume rinses) of the slurry mockup loop at Westinghouse removed only 90% of the slurry.

A continuous removal, by adding water to the loop and discharging slurry to a waste tank with the circulating pump operating, is somewhat more effective. However, in both cases, the amount of rinse water required would create a serious and expensive waste disposal problem. The slurry disposal and loop cleanup system currently planned employs a hydroclone to concentrate the slurry in a removal carrier. The hydroclone overflow stream is returned to the loop as a rinse.

Recent tests indicated that more than 99% of the slurry can be removed into a receiver with a volume equal to that of the loop if the loop circulating pump is operable for keeping the loop slurry in suspension (Table 20.1). Tests were run on a simulated system at room temperature. An agitated beaker of slurry provided the feed to, and continuously received the overflow from, the hydroclone. The rate of thorium oxide removal from the beaker to the hydroclone overflow receiver was a function of the hydroclone flow capacity, its efficiency, and the induced-underflow rate.

The current flowsheet employs a hydroclone designed integral with the slurry removal carrier and utilizes an auxiliary canned-motor pump to feed

Table 20.1. Tests of a Hydroclone for ThO_2 Slurry Collection

Hydroclone: 0.40 in. in diameter
$P_f - P_0$: 44 ft
Feed flow: 1.7 liters/min

Run No.	ThO_2 in Underflow Pot (% of total)	Underflow-Pot Geometry	Ratio of Underflow-Pot Volume to Loop Volume	Loop Volume (liters)
2	99.87	6 in. × 8 in.	4.67	3.000
3	99.20	3 in. × 12 in.	0.954	1.630
4	99.30	3 in. × 18 in.	0.952	3.224
5	98.10	4 liter flask	0.951	4.410

slurry from a bypass stream on the loop to the hydroclone. Cleanup of the loop to better than 99% is expected in approximately 4 hr of operation. The present system, as well as the alternate systems previously mentioned, unfortunately must depend upon continued operation of the pump in the main circulating loop to maintain the slurry in a suspended condition. The addition of lines and valves to the first loop package is impractical, since it is in the final stages of assembly; however, future loops will incorporate a special line for flushing so that the loop may be unloaded without dependence upon the main loop pump.

Standard high-pressure valves of the type used on in-pile solution loops have been modified in an effort to attain a reasonable longevity and satisfactory leak-tightness in slurry service. Such valves fitted with gold seats and 18% nickel–gold alloy seats have shown promising results in limited tests (Table 20.2). Similarly modified valves have been installed on loops at Y-12 for extended-period use tests.

The in-pile slurry loop experiment has been tentatively approved by the Experiment Review Committee for safety of operation. Only minor points remain to be cleared for final approval.

The in-pile loop, to be finally assembled at Westinghouse, is scheduled for a 500-hr slurry demonstration run in September, with ORNL operating personnel participating as part of a training program. The loop will then be shipped to ORNL for attachment of the vapor container. The assembled vapor container has already been trial-inserted in the south facility plug of the ORR to confirm an easy fit (see Figs. 20.1 and 20.2). The auxiliary equipment will be shipped from

Table 20.2. Results of Tests on Autoclave Valves with Gold Seats, Assembled at ORNL

Valve Size	Valve Seat	Valve Packing	Operation*
$\frac{3}{8}$ in., small body	Pure gold	Glass-Teflon, 12-ft-lb torque	300 operations in air by ORNL with no leaks 32 operations in ~525° F slurry; no leak around seat but packing leaked 120 operations in ~525° F ThO_2 slurry; seat and packing leaked
$\frac{9}{16}$ in.	Pure gold	Cu-graphite, 28-ft-lb torque	Operation in air by ORNL with no leaks 20 additional operations in ~525° F slurry; valve still good with seat leakage only 0.42×10^{-6} cc/sec, packing leakage only 0.28×10^{-6} cc/sec 120 additional operations in ~525° F slurry; seat and packing leaked
$\frac{3}{8}$ in.	18% Ni, 72% Au	Teflon	Operation in air by ORNL with no leaks 20 operations in air with no leaks 120 additional operations in ~525° F slurry with no leaks
$\frac{9}{16}$ in., large body	18% Ni, 72% Au	One Teflon washer; one gold washer	Operation in air by ORNL with no leaks 20 operations in air with no leaks 120 additional operations in ~525° F slurry with no leaks

*Leaks detected by helium leak detector. When leakage occurred but a leak rate is not specified, the leakage rate was beyond the range of leak detection.

Westinghouse in October and installed in the shielded cubicles by January, making the scheduled startup in the reactor about March 1959.

The over-all design is approximately 77% complete, the installation of the experiment in the ORR is approximately 27% complete, and the procurement and fabrication of the carriers and handling tools are approximately 57% complete.

The segmenting facility, a conversion of the shielded cells in Building 3026 to a remote-handling facility for segmenting and dismantling irradiated loops, was begun on April 21, 1958, by a prime contractor selected by the Commission. It is estimated that the facility will be ready to receive an irradiated loop for dismantling in April 1959.

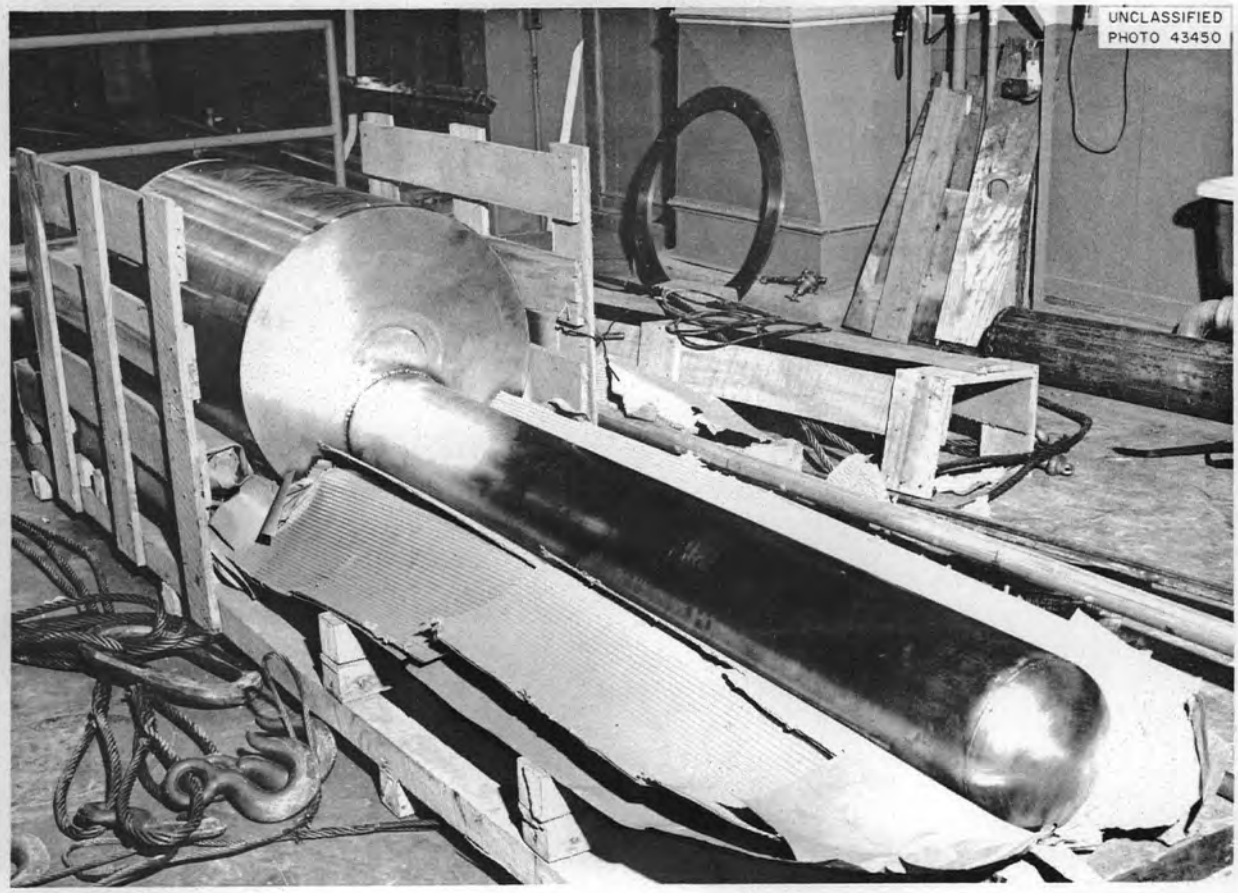

Fig. 20.1. Exterior View of Vapor Container as Received from Process Equipment Company, Tipp City, Ohio.

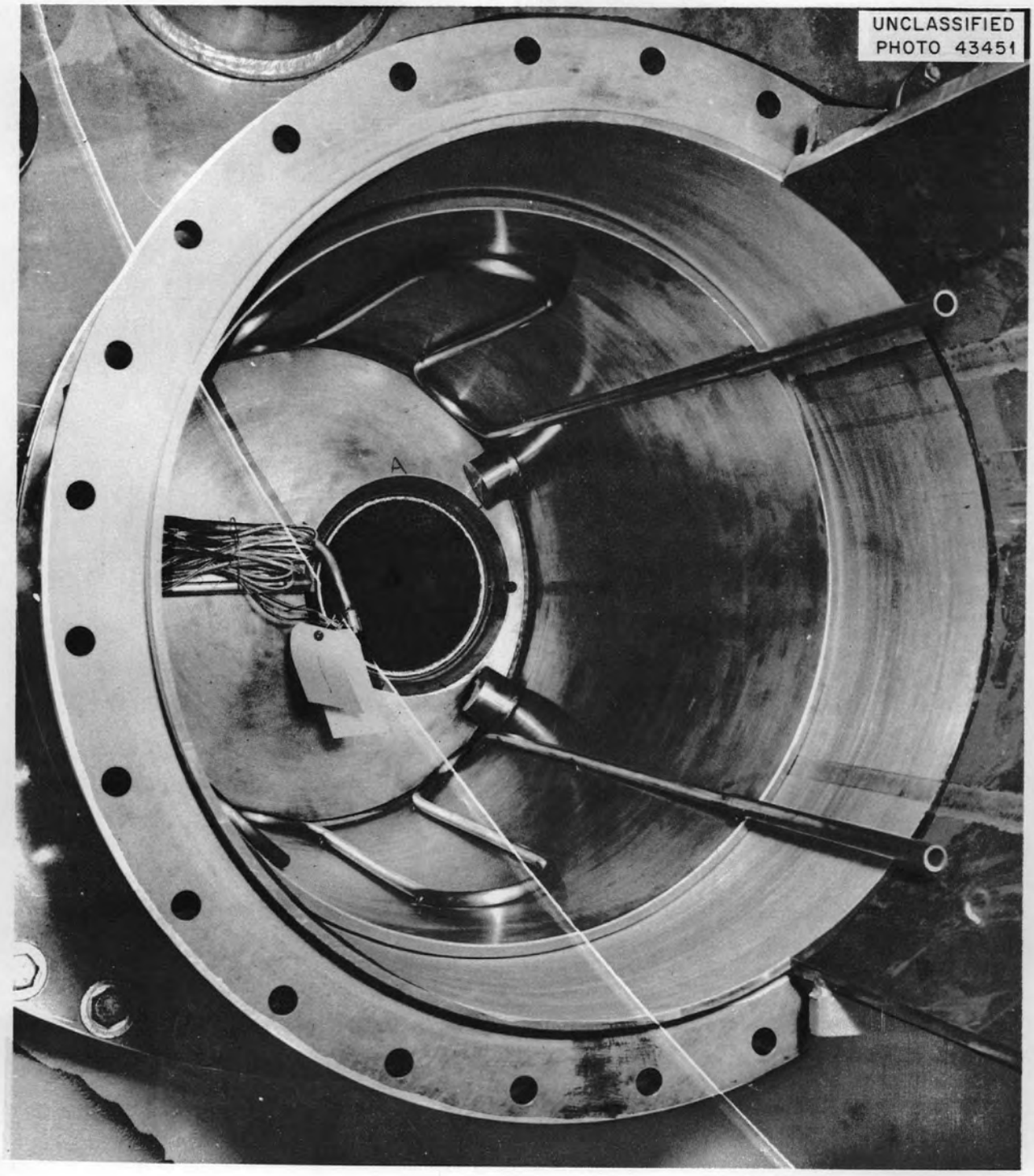

Fig. 20.2. Interior View of Vapor Container Inserted in HS-1 Facility of the ORR.

Part VI

SUPPORTING CHEMICAL RESEARCH

E. H. Taylor

21. AQUEOUS SYSTEMS AT ELEVATED TEMPERATURES

W. L. Marshall

J. S. Gill
G. M. Hebert
E. V. Jones
R. Slusher

21.1 CALCULATIONS OF SOLUBILITY IN MULTICOMPONENT SYSTEMS FROM SOLUBILITIES IN SIMPLER SYSTEMS

Preliminary calculations were carried out for the solubility of antlerite ($3CuO \cdot SO_3 \cdot 2H_2O$) in the system UO_3-CuO-SO_3-H_2O at 290°C by using solubility data from simpler related systems. The particular system was chosen for evaluation since (1) phase-equilibrium data were available[1] at 285–355°C for the system, (2) solubility data were available[2] for the system UO_3-SO_3-H_2O at 290°C, and (3) experimental solubility data for CuO-SO_3-H_2O at lower temperatures[3] could be extrapolated to 290°C.

The basic assumptions in the calculation procedure were: (1) the solvating medium is SO_3-H_2O; (2) if the solid phase is an oxide, hydroxide, oxysulfate, or sulfate at equilibrium with the solution, then the solvent, SO_3-H_2O, is saturated with respect to *all* cationic, anionic, and neutral sulfate species in solution, including the solid-phase component; and (3) for each soluble species an amount of sulfate is removed from effective participation in solvating other species. The last assumption implies that complexes with sulfate are the predominant species. In addition to these three assumptions, solubilities for the two separate three-component systems are compared at the *same* total SO_3 concentration as would exist in the four-component system. Therefore, in comparing solubility relationships in the four-component system at constant temperature with those in separate related systems at the same temperature, the over-all ionic strength and concentration of SO_3 in the "solvent," SO_3-H_2O, are constant before being saturated by other species. Admittedly, these assumptions are rather simplified and can be mutally inconsistent since the ionic strengths would be reduced by formation of neutral sulfate complexes and would be a function of the concentrations of ionic species in the separate and combined systems. There was no need to consider values for activities of the individual species without accurate knowledge of the extent of complexing and without rather accurate solubility data for all three systems for comparison. However, agreement of calculated solubilities with experimental data was obtained by the use of the above assumptions.

In order to calculate the solubility of antlerite in the *four*-component system, the respective solubility curves were drawn for antlerite and UO_3 at 290°C in their respective three-component systems as log total m_{SO_3} in solution vs the saturation mole ratio, metal oxide/SO_3. Each saturation ratio was taken at the equivalent total SO_3 concentration for the four-component system composition under consideration. Therefore, given a total SO_3 and UO_3 concentration, the amount of SO_3 necessary to "solvate" UO_3 was determined, after which the remaining SO_3 was equated to solvate a saturating "equivalency" of CuO. This saturating amount was determined from the solubility curve for antlerite in the system CuO-SO_3-H_2O.

A comparison between the calculated and experimental data at 290°C is given in Table 21.1 and indicates rather consistent agreement between the two sets of data. The large *percentage* deviation at low concentrations either can be real or can be due to the rather constant absolute difference (−0.01 to −0.03 m units) producing a greater difference on a percentage basis. The difference in absolute units between the calculated and experimental solubility values is approximately the same over the entire concentration range.

Apparently, by making use of some rather simplified assumptions, solubilities in multicomponent systems were determined from solubilities in simpler three-component systems. However, there are many problems to be solved before a clear picture can be forthcoming on the solubility

[1] W. L. Marshall *et al.*, *HRP Quar. Prog. Rep. Oct. 31, 1957*, ORNL-2432, p 171.

[2] W. L. Marshall, *Anal. Chem.* 27, 1923 (1955).

[3] E. Posnjak and G. Tunell, *Amer. J. Sci.* [5]18, 1 (1929).

Table 21.1. Comparison of Calculated and Experimental Solubilities of Antlerite ($3CuO \cdot SO_3 \cdot 2H_2O$) in the System UO_3-CuO-SO_3-H_2O (290°C)

Molality SO_3	Molality UO_3	Molal Solubility of Antlerite		Absolute Difference	Per Cent Deviation
		Experimental	Calculated		
1.626	0.820	0.806	0.785	−0.02	−3
1.557	0.359	1.058	1.029	−0.03	−3
1.487	0.102	1.145	1.124	−0.02	−2
1.388	0.135	1.029	1.023	−0.01	−1
1.217	0.167	0.854	0.855	0	0
1.181	0.651	0.530	0.515	−0.02	−3
1.002	0.172	0.668	0.663	−0.01	−1
0.886	0.511	0.375	0.352	−0.02	−6
0.882	0.259	0.544	0.508	−0.04	−6
0.763	0.157	0.481	0.469	−0.01	−2
0.655	0.389	0.266	0.242	−0.02	−9
0.509	0.183	0.280	0.250	−0.03	−11
0.461	0.278	0.183	0.157	−0.03	−14
0.444	0.119	0.253	0.237	−0.02	−6
0.285	0.177	0.108	0.0865	−0.02	−2
0.278	0.0869	0.146	0.130	−0.02	−11
0.267	0.116	0.127	0.107	−0.02	−16
0.164	0.0566	0.0811	0.0672	−0.01	−17
0.137	0.0852	0.0521	0.0349	−0.01	−33
0.104	0.0561	0.0386	0.0294	−0.01	−24
0.0750	0.0278	0.0351	0.0250	−0.01	−29

behavior in multicomponent systems, in our case, at high temperature. Several rather formidable questions to be considered are (1) which solid (or solids at an invariant point) will be the saturating *solid* phase, (2) what are the conditions for formation of *double* salts as a saturating solid, and (3) how does the existence of ionic species in solution together with nonionic species complicate the solubility characteristics of any one species?

21.2 SOLUBILITY EQUILIBRIUM IN THE SYSTEM NiO-SO_3-H_2O AT HIGH TEMPERATURE

The investigation of the NiO-SO_3-H_2O system at high temperature in the absence of other components was initiated in view of (1) the apparent complexity of multicomponent reactor fuel systems with regard to phase stability and interpretation and (2) the preliminary success in calculating solubilities in a four-component system from data on two three-component systems (see Sec 21.1). In order to have a complete picture of the general behavior of this system, studies were carried out from 150 to 300°C and from 10^{-4} to 1 *m* total SO_3. These data and their interpretation are to be considered along with those for the system UO_3-SO_3-H_2O and with those to be obtained for the system CuO-SO_3-H_2O over the same concentration and temperature ranges. An attempt will be made to correlate phase-equilibrium data for a multicomponent system, NiO-CuO-UO_3-SO_3-H_2O, with solubilities calculated from three-component systems alone.

Experimental procedures have been discussed in some detail in previous HRP Quarterly Reports. The experimental results for phase equilibria in the system NiO-SO_3-H_2O are given in Figs. 21.1 and 21.2. These results at the present time represent our best interpretation of the system. In studying a system over a wide concentration range, it is difficult to choose any one type of graphical presentation for the best description.

The log-log plot, total log m_{NiO} vs total log m_{SO_3} (Fig. 21.1), covers the widest range and shows the general behavior of the system from 150 to 300°C. However, this type of plot de-emphasizes both the accuracy of the data and small changes in curvature,

$$\frac{d}{dm_{SO_3}}\left(\frac{dm_{NiO}}{dm_{SO_3}}\right).$$

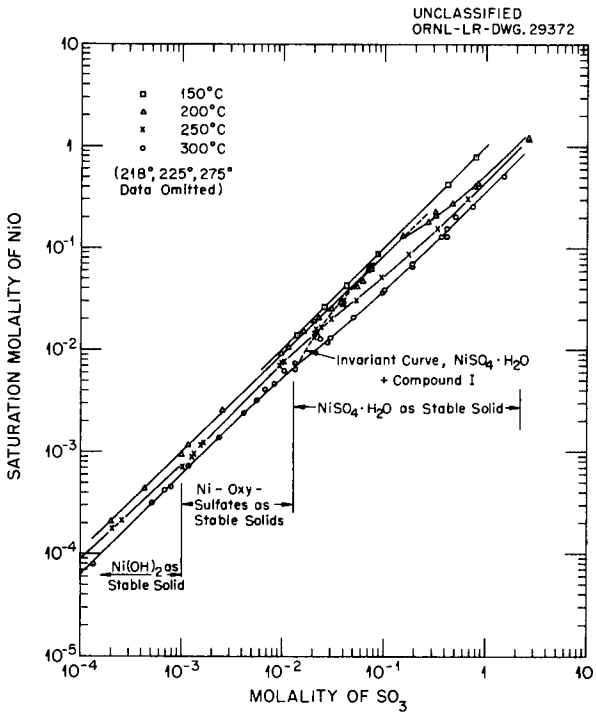

Fig. 21.1. The System $NiO\text{-}SO_3\text{-}H_2O$, 150–300°C; Log-Log Plot.

Therefore, for working curves, in order to emphasize this latter curvature factor, plots were made of log m_{SO_3}', where m_{SO_3}' = total m_{SO_3} in the solution, vs the "saturation mole ratio," that is, the number of moles of NiO which will dissolve per mole of total m_{SO_3} and thus saturate the resultant solution. In this type of graph minor curvature is emphasized, and the degree of precision of the data can be readily observed (Fig. 21.2).

The regions of stability for the various solids are defined in Figs. 21.1 and 21.2. Solid phases of the same structure were identified by means of x-ray diffraction pictures by R. L. Sherman of the Analytical Chemistry Division. Upon examination of Fig. 21.2 considerable disagreement and overlap of solid phases are found as defined by x-ray analysis. At present, there is no good explanation for these discrepancies. Since the solids were obtained after the solid and solution mixtures were quenched to room temperature and opened, there is a possibility that the solid phases could have changed composition or character upon cooling. Assuming that this change did *not* occur, at the higher concentrations, the stable solid is $NiSO_4 \cdot H_2O$. The gram amounts of solid were chosen for each run so that the relative change in the mole ratio in the solid phase would be small after attainment of equilibrium. Accordingly, the initial starting ratio of the solid could be adjusted to represent an approximate total ratio in a solid phase after equilibrium was attained. An examination of the relative solution composition groupings, presumably at or near invariant points with respect to the initial solid-phase compositions would favor $\frac{1}{2}Ni(OH)_2 \cdot NiSO_4$ hydrate for compound I and $Ni(OH)_2 \cdot NiSO_4$ hydrate for compound II. The $Ni(OH)_2$ has been identified at lower SO_3 concentrations by x-ray diffraction. A compound III seems to be existent also in the lower concentration ranges, as well as a compound IV in the 200°C range. Apparently, excellent analytical results were obtained for the one run at 150°C, although the exact nature of the solid phases is in doubt. The behavior of nickel in this system is similar to that of some of the other transition metals. Certainly the results presented here for low concentrations are far from complete with respect to the solid phases.

21.2.1 $NiSO_4 \cdot H_2O$ Solid and Its Region of Stability

At first glance, Fig. 21.2 shows a striking curvature in the solubility curve at constant temperature for $NiSO_4 \cdot H_2O$ in $SO_3\text{-}H_2O$ solutions. However, if these data are converted to m_{NiSO_4} and $m_{H_2SO_4}$ and if the solubility of $NiSO_4$ is plotted as a function of $m_{H_2SO_4}$ (Fig. 21.3), an approximate linear relationship is observed, which line can be extrapolated to zero molality H_2SO_4. From the slope at a particular temperature, a value for this hypothetical solubility was derived from

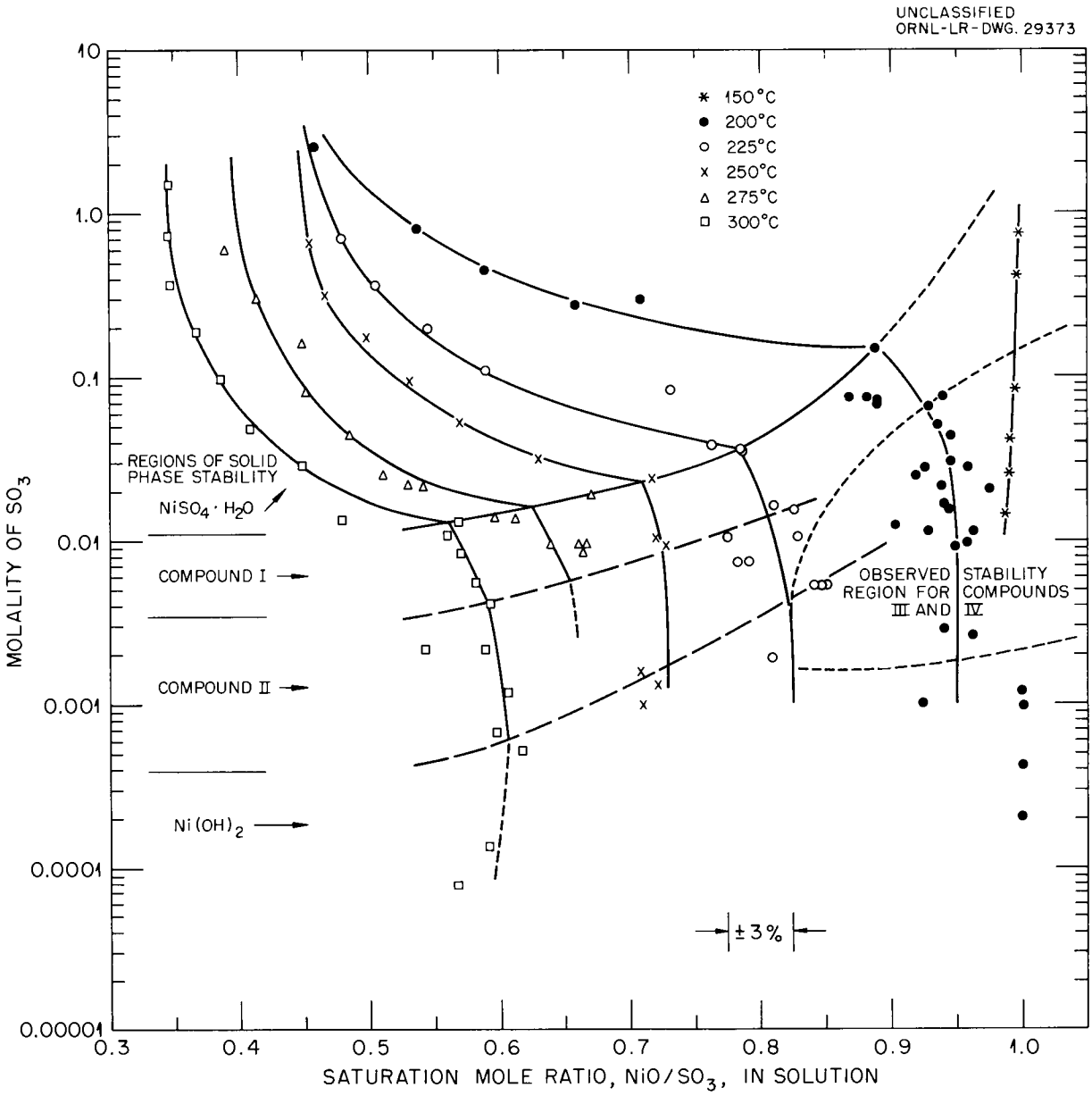

Fig. 21.2. The System $NiO\text{-}SO_3\text{-}H_2O$, 150–300°C; Log–Mole-Ratio Plot.

the individual data by means of the relation,

$$x = m_{NiSO_4} - k m_{H_2SO_4} ,$$

where

x = soly. $NiSO_4$ in H_2O,

m_{NiSO_4} = soly. of $NiSO_4 \cdot H_2O$ in H_2SO_4 at $m_{H_2SO_4}$,

$m_{H_2SO_4}$ = m concentration of H_2SO_4,

k = linear slope, $\Delta m_{NiSO_4} / \Delta m_{H_2SO_4}$.

The hypothetical solubilities for $NiSO_4 \cdot H_2O$ in H_2O alone were determined. These solubilities are never achieved, however, owing to the conversion of the solid phase to the hydroxy-sulfates and hydroxides at low concentrations of H_2SO_4.

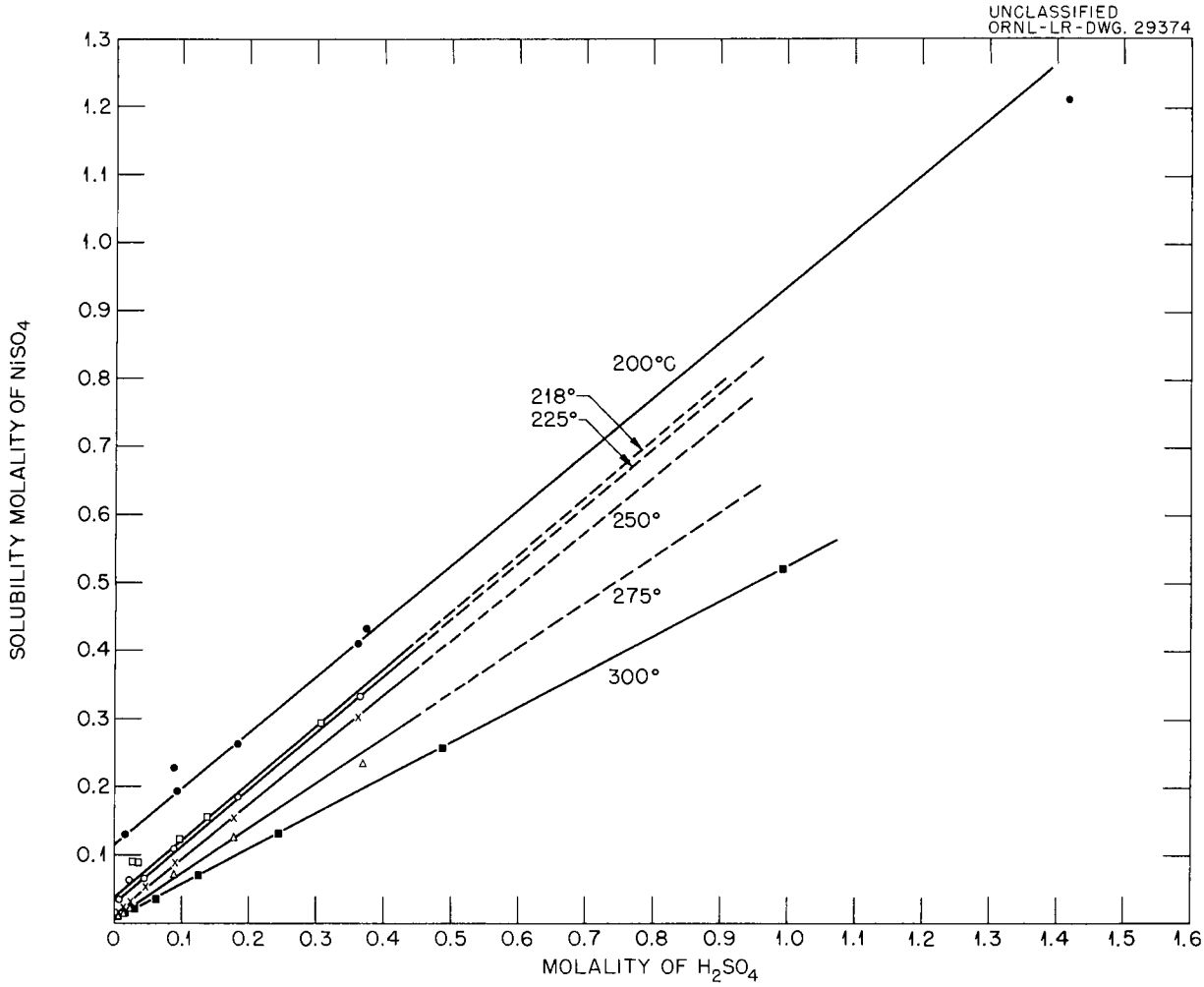

Fig. 21.3. The Solubility of $NiSO_4$ in H_2SO_4-H_2O, 150–300°C.

Upon examination of Fig. 21.3 it is apparent that the slopes, that is, $\Delta m_{NiSO_4}/\Delta m_{H_2SO_4}$ for 200, 218, 225, and 250°C have nearly the same value, which is approximately 0.8. This value might indicate a complex of the type $Ni(HSO_4)_2$ or Ni^{++} and HSO_4^- ions in solution. For 100% formation, either of the complex or ions, $\Delta m_{NiSO_4}/\Delta m_{H_2SO_4} = 1$. At 300°C this slope equals 0.5, which might indicate a complex in solution of a type $Ni(HSO_4)_2 \cdot H_2SO_4$. Considering the apparent linearity of the data at any one temperature, the formation of undissociated complexes of the above nature is certainly suggested.

21.3 MEASUREMENT OF AQUEOUS VAPOR PRESSURE AT ELEVATED TEMPERATURE AND PRESSURE

The program of vapor pressure measurement of aqueous systems at elevated temperature[4,5] has been resumed. The current goal of this investigation is to attain a method for measuring absolute vapor pressures of aqueous solutions to a high

[4] H. O. Day, Jr., and C. H. Secoy, *Chem. Semiann. Prog. Rep. Dec. 20, 1953*, ORNL-1674, p 98.

[5] H. O. Day, Jr., *HRP Quar. Prog. Rep. March 31, 1953*, ORNL-1554, p 109.

degree of precision and accuracy to temperatures approaching the critical temperature of water. The satisfactory development of a method will supplement the isopiestic apparatus developed in the Chemistry Division for studies of aqueous solutions at elevated temperature.[6] If very accurate pressures for *any* solutions were indeed known at elevated temperature, the isopiestic method could make use of these data to determine absolute values of pressure. Water vapor pressure cannot be equated with solution vapor pressure in the present isopiestic unit since there would be no difference in temperature between water and the solutions under study.

The use of a differential manometer for measurement is being investigated. This approach seems a logical one since the ultimate pressures to be encountered are of the order of 200 atm near the critical point of water. The use of an *absolute*-pressure measuring device such as a Michels pressure balance in addition to the necessity of ultimate precision of temperature control and accuracy of temperature measurement would appear to be a rather formidable approach. As a first consideration the vapor pressure of water has been balanced against the vapor pressure of a known solution at the same elevated temperature. A mercury differential manometer at room temperature has been used to make the balance and to measure the difference in pressure. Another approach currently being investigated is the use of a strain gage for the measurement of difference in pressure between the two vessels containing water and solution, respectively. By using a differential rather than an absolute method of measurement, knowledge and control of temperature to a high degree of precision and accuracy is less important; however, the temperature gradient between the two vessels must be negligible in relation to the temperature coefficient of pressure.

[6] B. A. Soldano, R. J. Fox, and R. W. Stoughton, *Chem. Ann. Prog. Rep. June 20, 1957*, ORNL-2386, p 74.

21.4 EQUILIBRIUM COMPOSITIONS OF THE LIGHT AND HEAVY LIQUID PHASES IN THE SYSTEM UO_3-SO_3-H_2O

Measurements are being made of the equilibrium compositions of the light and heavy liquid phases in the systems UO_3-SO_3-H_2O and UO_3-SO_3-D_2O. The technique involves the equilibration of the two phases at temperature in a sealed glass tube, freezing the contents of the tube before intermixing of the two phases can occur, and subsequent analyses of both phases for UO_3 and SO_3. With stoichiometric UO_2SO_4 from 0.8 to 2 *m* in the H_2O system, preliminary experiments at 300°C indicate the light-phase composition to be in the range of 0.38 *m* uranium with approximately 8 mole % excess free acid. The heavy-phase composition is approximately 4.9 *m* uranium with a 2 mole % deficiency in free acid.

22. REACTIONS IN AQUEOUS SOLUTIONS

H. F. McDuffie L. O. Gilpatrick

22.1 PEROXIDE DECOMPOSITION IN URANYL SULFATE SOLUTIONS

During the past two quarters the study of the decomposition of peroxide in aqueous reactor fuel solutions was resumed. A previous study[1] just prior to the operation of HRE-1 established the kinetics of peroxide decomposition in light-water solutions at temperatures up to 100°C. The rate of decomposition was found to be first order with respect to peroxide concentration, the activation energy was found to be around 25 kilogram calories, and catalysts (notably a combination of cupric and ferrous ions) were found to increase the decomposition rate. These findings enabled limits to be set for low-temperature reactor operating conditions which would avoid uranium peroxide precipitation. An extension of the early study demonstrated that uranium peroxide and hydrogen peroxide, present in equilibrium when peroxide is added to uranyl solutions, are simultaneously decomposed although at different rates.[2] In typical reactor fuel solutions most of the decomposition occurs via uranium peroxide.

22.1.1 Effect of Solvent Isotopic Composition on Temperature Dependence of Peroxide Decomposition

The use of heavy water in the HRT fuel solution suggested that the decomposition rates in heavy-water solutions be studied at temperatures below 100°C for comparison with the previously obtained results with light-water solutions. The apparatus and techniques used were essentially those already reported,[1] with slight modifications such as the use of a magnetic stirrer and a butyl phthalate constant-temperature bath. It will be recalled that the decomposition of peroxide can be followed either by titration of solution samples or by measurement of the change in conductance (as hydrogen ions are replaced by regenerated uranyl ions). Both of these methods were used; the conductance method is preferred, but the chemical method is used when the acidity of the solution is so high that the conductance change is inconveniently small.

Peroxide decomposition rates were determined at 50, 70, and 90°C in a solution which had been prepared to simulate the HRT fuel.[3] Figure 22.1 shows the effect of temperature compared

[1] M. D. Silverman, G. M. Watson, and H. F. McDuffie, *The Radiation Chemistry of Aqueous Reactor Solutions. II. The Decomposition of Hydrogen Peroxide in Aqueous Homogeneous Reactor Systems*, ORNL CF-53-4-294 (May 19, 1953); *Ind. Eng. Chem.* 48, 1238 (1956).

[2] M. D. Silverman and C. H. Secoy, *Chem. Semiann. Prog. Rep. June 20, 1953*, ORNL-1587, p 106–8.

[3] H. F. McDuffie and H. H. Stone, *HRP Quar. Prog. Rep. Jan. 31, 1958*, ORNL-2493, p 181. The solution was identified as solution S.

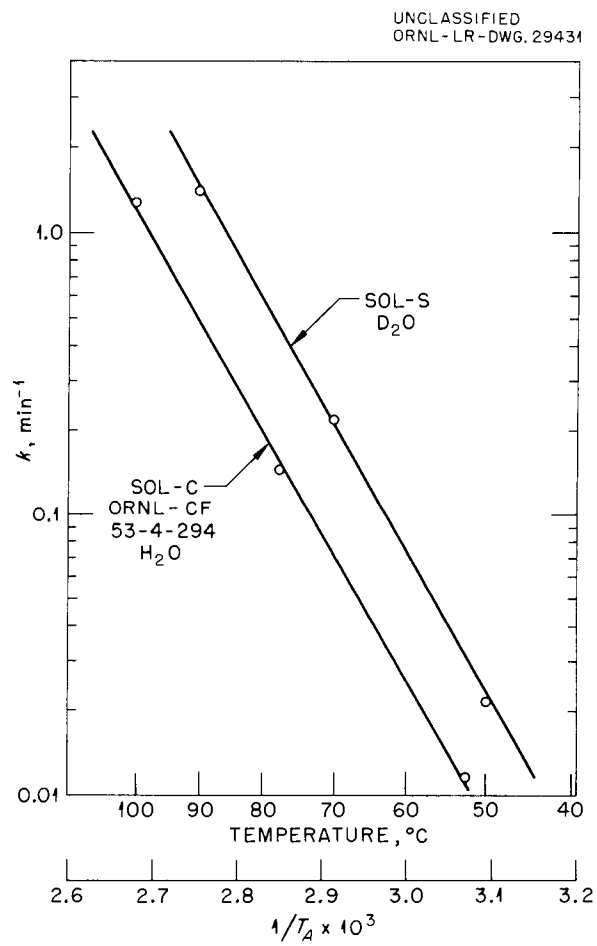

Fig. 22.1. Temperature Dependence of Peroxide Decomposition.

with the previously determined[1] effect of temperature upon the light-water simulated (U^{238}) fuel solution from HRE-1. The slopes of the two lines are not significantly different, and it therefore appears that the temperature dependence of peroxide decomposition has not been affected by the change from the light-water to the heavy-water system.

22.1.2 Effect of Solvent Isotopic Composition on Decomposition Rates

Although the temperature dependence for the heavy-water solution was not significantly different from that previously observed for light-water solutions, the actual decomposition rates in the heavy-water solution at a given temperature were much greater than the rates in the light-water solution. The difference seemed greater than could be accounted for by the known amounts of catalytically active material (0.001 *M* copper) present in the heavy-water solution. The presence of isotope effects or impurities in the heavy water was therefore suspected. (In preparing the actual HRT fuel solution and the simulated HRT solution used above, heavy water was used as received without any purification.) Because of this unexplained difference between the rates, although measured at different times, it was considered desirable to make a direct comparison between the decomposition rates in light- and heavy-water solutions in the same apparatus, by the same person, and with, as far as possible, the same impurities. In order to avoid solution contamination and loss through sampling and evaporation, it was decided to use the conductance technique for determining the rates; this, in turn, necessitated the use of unacidified uranyl sulfate as the solute. In order to minimize and standardize the effects due to impurities introduced with the solute, test solutions were prepared by diluting equal small volumes (3.66 ml) of a concentrated stock solution of uranyl sulfate in light water to a total volume of 200 ml with water of the desired isotopic composition. (Peroxide is commonly injected with a micropipette at the start of a run. The amount used is 50 to 100 mm^3 of a freshly prepared 1.0 *M* solution in H_2O. The isotopic dilution from this volume is considered insignificant, and the rapid exchange of the added hydrogen with the hydrogen or deuterium of the water via ionization of the peroxide is considered to make it unnecessary to prepare D_2O_2 for tests in heavy-water solutions.) The results of the direct-comparison tests conducted at 60°C confirmed the previously found effect; there was a substantial and fairly regular increase in the decomposition rate as the percentage of heavy water was increased. Purification of the heavy water by fractional distillation through a short column packed with glass helices, with rejection of the first 10% and the last 33% of the distillate, lowered the decomposition rate in solutions prepared from this purified heavy water to a value 13% higher than the rate in light-water solutions. Tests on light-water solutions prepared from light water which had been purified in several ways did not change the light-water rates significantly.

From the point of view of practical reactor operation the difference in rates is not significant; the direction and magnitude of the isotope effect are consistent, however, with the concept of an acid-catalyzed reaction.[4,5] The significance of this with respect to the mechanism of the reaction is being explored further.

22.1.3 Effect of Copper and Iron Salts upon Decomposition Rate and Dependence

For proper development of aqueous homogeneous reactor technology it is important to know whether limitations on the stability of the fuel solution are imposed by precipitation of uranium peroxide at elevated temperature. Rates of peroxide formation can be estimated from the reactor power level. Rates of peroxide decomposition must be measured directly at elevated temperatures or inferred from extrapolation procedures based on low-temperature data. From these rates (formation and decomposition) the steady-state concentrations may be calculated.

The previous study[1] included an investigation of the temperature dependence of peroxide decomposition only for solutions to which decomposition catalysts had not been added or for solutions in which any catalytic iron (from corrosion) had become "aged" through recirculation through the reactor at elevated temperatures. Solutions containing very effective decomposition catalysts were studied only at 100°C.

[4] K. F. Bonhoeffer and O. Reitz, *Z. physik. Chem. (Frankfort)* **179A**, 135 (1937).

[5] K. F. Bonhoeffer, *Z. Elektrochem.* 40, 469 (1934).

Since the action of a catalyst is frequently considered to involve a lowering of the activation energy for the reaction, it was of interest to learn how the copper and iron catalysts affected the temperature dependence of peroxide decomposition. If the temperature dependence were very substantially lowered, extrapolation to elevated temperatures would give low decomposition rates at elevated temperatures; this would limit the acceptable reactor power density.

(a) Effect of Copper. – In the previous study[1] the addition of cupric copper up to a concentration of 0.0125 *M* increased the decomposition rate at 100°C. In the present study the effect of copper concentration has been studied at temperatures of 60–95°C. Figure 22.2 shows a normalized plot of relative catalytic decomposition rate vs copper concentration for the various temperatures. The

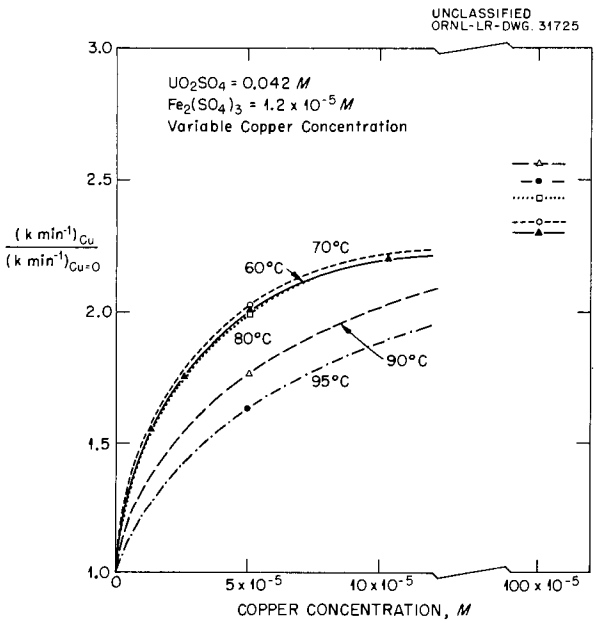

Fig. 22.2. Effect of Copper Concentration on Peroxide Decomposition.

relationships shown in the figure suggest that the maximum percentage increase in rate, relative to the rate with no copper, is approximately the same at each temperature, but the amount of copper required to produce this maximum increase in rate is greater at higher temperatures. Thus the apparent activation energies for the solutions containing no copper or a relatively high concentration of copper, 10^{-3} *M*, are indistinguishable as illustrated by Fig. 22.3, while the apparent activation energy for the solution containing an intermediate amount of copper is somewhat lower. These data do not support the hypothesis that the copper is acting as a catalyst by reducing the activation energy for a reaction.

It may be speculated that the copper is potentiating the small amount of iron present in the solution; at higher temperatures the hydrolysis of iron becomes more pronounced, with more copper required to keep all the iron in an active condition. This speculation suggests that the decomposition effectiveness of copper alone, reported to be poor but present in the previous study,[1] might be lower (or even absent entirely) if all traces of iron were excluded from the solution. It is also possible that the previously reported aging of iron in uranyl sulfate solutions (so that, after 20 hr at 100°C, the activity was reduced to the same low value regardless of the original iron concentration) might be prevented or altered by the presence of sufficient copper. Experiments are being arranged to test both these points.

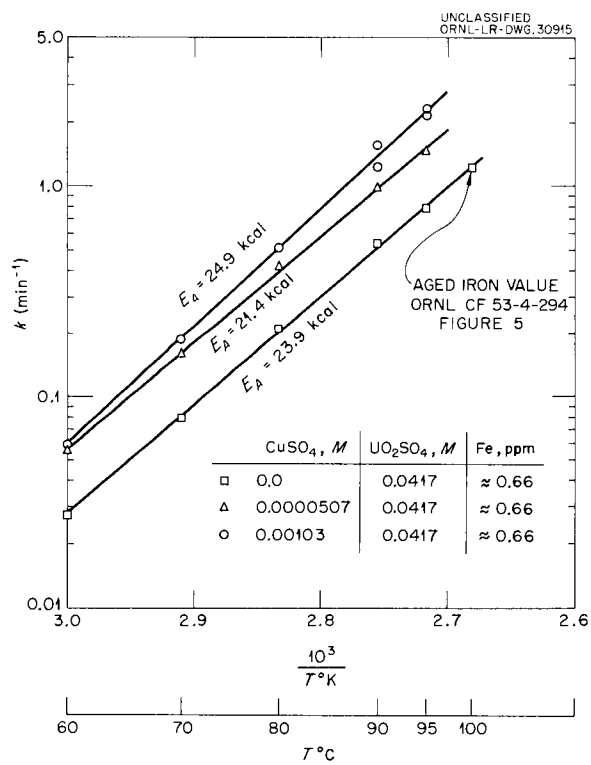

Fig. 22.3. Effect of Copper Concentration on Temperature Dependence of Peroxide Decomposition.

(b) Effect of Iron. – The effect of temperature upon the iron-catalyzed peroxide decomposition rate is being determined. Figure 22.4 shows the temperature dependence for uranyl sulfate solutions containing two different concentrations of iron; the lower concentration (1.2×10^{-5} *M*) represents the amount of iron adventitiously present in the particular stock solution being used; the higher concentration represents the addition of an equal amount of iron to double the iron concentration. The activation energy is apparently unchanged by doubling the iron, and the rates at 100°C are about the same as that previously reported for aged iron. However, there was no indication of any aging throughout the course of the experiments over the temperature range of 60–100°C; solutions were frequently left overnight or longer at the reaction temperature without changing the reaction rate, and retests at a given temperature after tests at higher temperatures gave the same results as before. If aging of the solution occurred so quickly that it was not detectable by the time of our first experiments at any given temperature, it would be expected that both solutions would age to the same rate constant. Since this was not the case and since the higher concentration solution preserved a 35% rate advantage over the whole temperature range, further studies of the aging phenomenon are in order. As mentioned above, the effect is being studied in connection with the effect of copper.

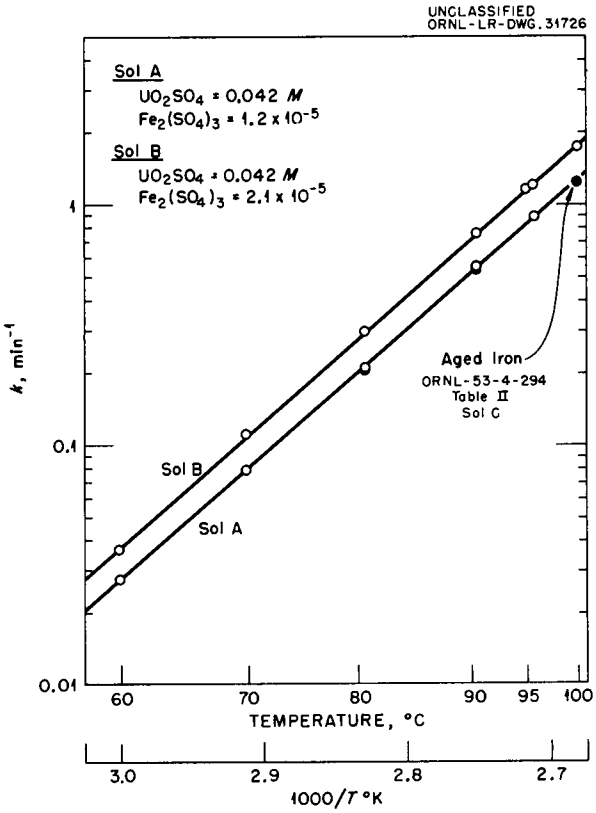

Fig. 22.4. Effect of Iron on Peroxide Decomposition; Arrhenius Plot.

23. THORIUM OXIDE SYSTEMS

F. H. Sweeton

23.1 pH OF THORIUM OXIDE SLURRIES

The measurement of the pH of thorium oxide slurries is important because the pH is known to affect the surface voltage of the individual ThO_2 particles and thus the repulsive forces between the particles. However, it is also known that the normal direct techniques for measuring pH are not suitable for use with slurries, because suspensions often affect the operation of the calomel electrode and have been known to cause errors as large as 2.0 pH units.[1] Therefore a method of measuring pH which does not require that the slurry come into direct contact with the calomel electrode should be useful in the ThO_2 slurry program. The work to be described was undertaken to develop such a method and test it on ThO_2 slurries containing varying amounts of HNO_3, an acid chosen because it is monovalent and forms a soluble salt with thorium.

Of the several attempts made to find a suitable method, two involved putting the calomel electrode into the supernatant resulting from the solid settling out of the slurry by either gravitational or centrifugal forces, but the settling rates achieved were too low. Another method consisted of placing the calomel electrode in a solution separated from the slurry by a membrane, the solution being the supernatant of a special slurry made up of only large fast-settling particles. This approach was discarded both because of the tediousness of eliminating the liquid-junction error across the membrane and because of the erratic readings often obtained. The last method, described below, was similar except that the solution in contact with the calomel electrode was a filtrate of the slurry being tested, thus giving no junction potential at the membrane.

The experimental equipment was designed to keep the ThO_2 from coming in contact with atmospheric CO_2, because it has been shown that CO_2 is absorbed and held strongly on ThO_2 surfaces.[2] Figure 23.1 shows the apparatus used to determine the slurry pH as a function of added nitric acid. The cell holding the slurry was constructed of a 55-ml Pyrex weighing bottle with interchangeable ground joints. The filter, about 1 cm in diameter, was constructed of a sintered glass disk with a flat outer face. A VF Millipore filter,[3] having 100 ± 20 Å pores, was held tight against the disk by cement applied around the edge. The opening in the top of the slurry cell was used for admitting H_2O and HNO_3 solution. The bypass served to let filtrate back into the slurry when it was desired to flush the tubing without depleting the volume of slurry at the same time.

Measurements were made with a model M Beckman pH meter and regular Beckman glass and calomel electrodes, which were standardized with commercial buffer solutions having pH's of 4.0, 6.4, and 10.0.

[1] J. T. G. Overbeek, vol I, p 184–87 in *Colloid Science* (ed. by H. R. Kruyt), Elsevier, New York, 1952.

[2] C. H. Pitt and M. E. Wadsworth, *Carbon Dioxide Adsorption on Thoria*, Technical Report No. I, Univ. of Utah, UCNC subcontract (Feb. 15, 1958).

[3] Manufactured by the Millipore Filter Corp., Watertown, Mass.

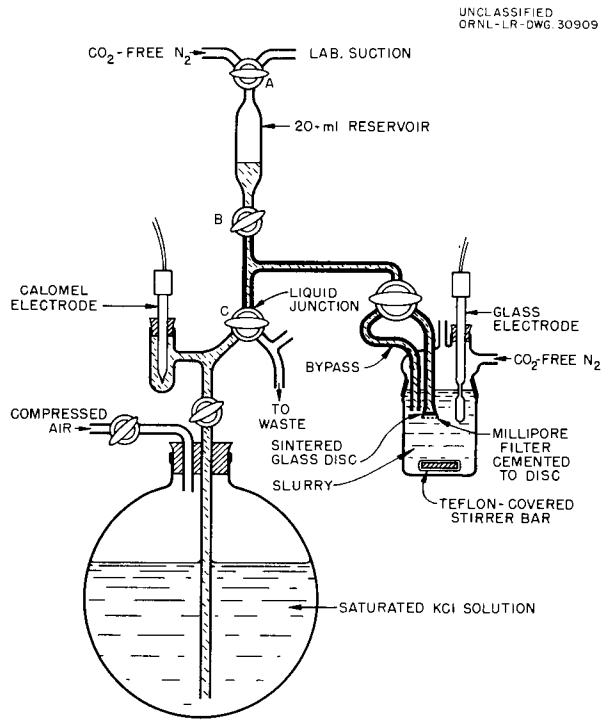

Fig. 23.1. Apparatus for Determining pH of Slurries.

The ThO_2 used had been prepared by the Chemical Technology Division and is known as D-16 material. It had been originally calcined at a maximum temperature of 650°C and had been shown by N_2 adsorption data to have a specific surface area of 37.6 m^2/g. Before use, this material was outgassed for several hours at 600°C under an absolute pressure of approximately 0.1 mm Hg. Such treatment has been found to reduce the CO_2 concentration to approximately 0.1%, which is about 0.6 μmole per square meter of surface. The water used to make up the first two slurries was prepared by aerating regular laboratory distilled water; that for the other two runs had been redistilled and gave pH readings between 6.3 and 7.4.

A weighed sample of dry ThO_2 (3.6–12.0 g) in a weighing bottle was transferred to the slurry cell of the titration apparatus and water was added. After stirring, filtrate was pulled through the filter up into the reservoir by applying laboratory suction (~ 1 atm) through stopcock A. The filtering speed varied between 0.05 and 0.5 ml/min for these tests. Then some filtrate was allowed to flow down through stopcock C to waste. After pushing saturated KCl solution to waste through the same stopcock and thereby filling the bore, the stopcock was turned to establish a sharp liquid junction between the saturated KCl solution and the filtrate. Then the pH reading was followed over a period of time varying between 10 and 60 min to check for drift. During runs 8 and 9 in particular, this procedure was normally repeated several times to check the consistency of the readings. Enough acid was then added to lower the reading by about 1.0 pH unit. This procedure was repeated until a pH reading of about 5 had been obtained.

Figure 23.2 gives a plot of the data obtained in four runs. The indicated surface concentration is calculated on the assumption that all of the added HNO_3 was absorbed on the surface. The square-root function is used for plotting merely because it results in an approximately straight line. The vertical bars through the points correspond to ±0.10 pH unit. The total spread among the different runs at any particular part of the graph amounts at most to about 0.7 pH unit. However, it can be seen that an appreciable part of this is contributed by run 1 and the first point of run 2. The rest of the points disagree by a maximum of about 0.4 unit. Furthermore, it can be seen that

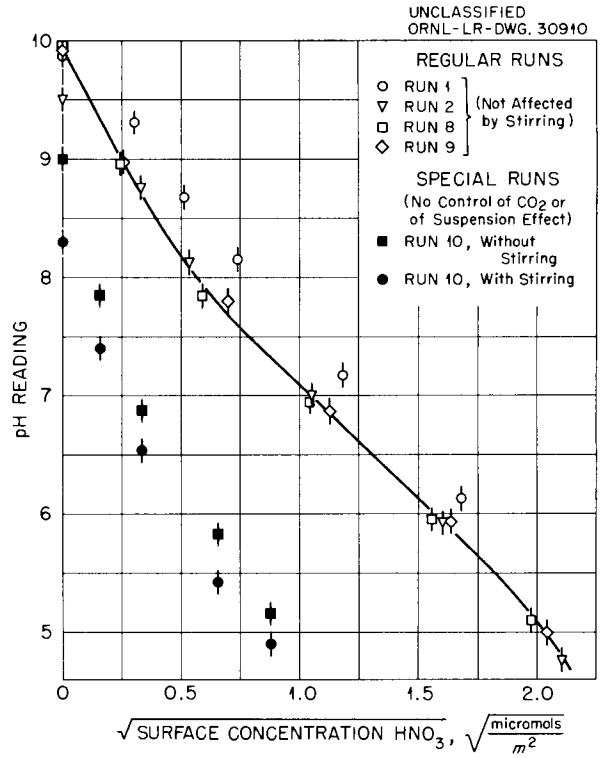

Fig. 23.2. Adsorption of Nitric Acid by Thorium Oxide Slurry.

the last two runs differ by hardly more than 0.20 unit.

Run 10, the data for which are also included in the figure, was made to determine qualitatively the combined effect of not excluding CO_2 and of not eliminating the suspension effect. In this run the calomel, as well as the glass electrode, was immersed in a slurry that was similar to slurries used in previous runs except that the ThO_2 had not been degassed. No attempt was made in run 10 to exclude atmospheric CO_2. Stirring, which had not affected the previous readings significantly, in this case had an appreciable effect, as can be seen on the graph.

In addition to showing the reproducibility that has been achieved in measuring pH by this method, the data are also of direct interest. If it is assumed that all of the added HNO_3 is absorbed on the ThO_2 surface and also that at saturation two nitrate ions are held by an area equal to one side of a unit cell of the solid, then adsorption at pH 5, for instance, corresponds to about 40% coverage of the ThO_2 surface.

It appears that the described method of measuring the pH of ThO_2 slurries improves the precision of the determination and thereby better defines the value of a parameter that is very important in the characterization of such slurries.

23.2 EFFECT OF pH ON SLURRY PROPERTIES

In the course of developing a method of pH measurement, it was noted that ThO_2 slurries containing added HNO_3 tended toward a high degree of peptization. One such peptized slurry sample was made from micropulverized ACDC-13 ThO_2 which had been degassed as described above and which had a specific surface area of 17.7 m^2/g before micropulverizing. This slurry contained approximately 30 μmoles of HNO_3 per gram of ThO_2, and according to the data in Fig. 23.2 must have had a pH of approximately 6.5. When stored in a desiccator to protect it from thermal cycling and from contamination by CO_2, it had settled enough after 2½ weeks to leave a ⅜-in. clear zone. After 10½ months there was a 3-in. clear zone and a ¼-in. opalescent zone over the settled bed. At the end of this time, careful tilting of the container resulted in the settled bed moving to a new rest position in a matter of less than 30 min. This showed that the settled bed of this acidified slurry was a Newtonian fluid after having been undisturbed for nearly a year.

Another sample of slurry (the product of run 2) was sealed in a 4-in. ampoule after enough acid had been added during mild stirring to reduce its pH to approximately 4.3 (5 μmoles of HNO_3 per square meter of ThO_2, or 200 μmoles/g). After standing undisturbed for three months, the sample is a transparent blue at the top and white in the bottom half, with a smooth transition between these regions. This is significant because it indicates that some of the particles are very fine (in the order of 0.01 μ) and raises the question of whether these fines were present when the material was originally prepared, or were formed later either by the mechanical comminution of mild stirring or by the attack of the acid on the relic structure.

24. HEAVY-ELEMENT AND FISSION-PRODUCT CHEMISTRY

R. W. Stoughton

J. Halperin J. H. Oliver[1]

W. C. Waggener

24.1 QUANTITATIVE SPECTROMETRY OF AQUEOUS NEPTUNIUM IONS AT ELEVATED TEMPERATURES AND PRESSURES

The equipment for quantitative spectrometry of aqueous neptunium ions at elevated temperatures and pressures has been briefly described previously.[2] It consists of an adaptation of a Cary model 14M recording spectrophotometer for measurements of liquid-phase spectra above the normal boiling point. The sample cell and reservoir assembly have a working range of 0 to 250°C and 0 to 1000 psi. The sample cell at any operating temperature and pressure is measured optically against a geometrically similar solvent cell which is thermostated at 25°C. The stability and reproducibility of measurements over the entire design range are comparable to those at room temperature.

The fate of the neptunyl ion in a nitric acid solution [7.43×10^{-4} *M* $RbNp^{237}O_2(NO_3)_3$ in 0.1 *M* DNO_3–D_2O at 250°C][3,4] has been followed spectrophotometrically from 0.6 to 1.3 μ for a period of 45 hr and a temperature range from 4.5 to 252°C. Deuterated solutions were used to decrease both the absorbance and the effect of temperature upon the absorbance of the solvent.[2,5] The sample solution was saturated with ozone and then degassed immediately before introduction into the titanium cell and reservoir assembly, which had been pretreated previously at 250°C with 1 *M* HNO_3.

In this first experiment Np(VI) was found to be reduced irreversibly and quantitatively to Np(V). The course of the experiment is illustrated in the graph and table of Fig. 24.1. The transfer of the sample to the degassing chamber and burette assembly and the subsequent degassing were carried out with special care to reduce the chance of alpha contamination. For this reason, the solution was not scanned until 6.9 hr after preparation, that is, after the dissolution of the single crystal of $RbNpO_2(NO_3)_3$ in the ozone-saturated solvent solution. At that time about 9% of the Np(VI) had been reduced to Np(V). Further spectral scans as a function of time indicated that reduction of the sample in the cell at 25°C was proceeding at the rate of roughly 0.2%/hr. The data of curve A, Fig. 24.1, indicate that at 21.7 hr 13% of the neptunium was present as Np(V).

Immediately after scan A, the temperature of the sample cell was reduced to near the freezing point of the solution. Scan B was run at 4.5°C, and then the sample cell was heated slowly (<1°C/min) to 252°C. Scan C, made at 110°C, indicates the increasing rate of the reduction with rising temperature. Scan D was made at the peak temperature of the run with the cell at 252°C.

To preclude bubble formation in the optical path, the reservoir was operated at temperatures a few degrees above the cell. For example, while the cell was at 252°C the reservoir, with an imposed temperature gradient over its length, was automatically controlled, its four thermocouples (located from bottom to top) reading 261, 263, 259, and 259°C, respectively. The reservoir pressure reading of 700 psia corresponds to a saturated D_2O vapor temperature of between 261 and 262°C, indicating good agreement between the reservoir temperature and pressure measurements.

No measurable change was noted in the spectrum of the sample (represented by curve D in Fig. 24.1) over a period of more than 3 hr at 251 to 252°C.

Chart scan E was made at the end of the run, with the sample cell again at room temperature. In regions of the spectrum where neither Np(VI) nor Np(V) ion absorbs measurably (e.g., around 0.85, 1.05, and 1.3 μ), the match of curves A and E is excellent.

---

[1] Analytical Chemistry Division.

[2] W. C. Waggener and R. W. Stoughton, *Chem. Ann. Prog. Rep. June 20, 1957*, ORNL-2386, p 64–67.

[3] The $RbNp^{237}O_2(NO_3)_3$ in the form of a single crystal was provided by P. M. Lantz and G. W. Parker of the Chemistry Division.

[4] The stock solution of DNO_3 was prepared by B. M. Benjamin of the Chemistry Division.

[5] W. C. Waggener, *J. Phys. Chem.* 62, 382 (1958); *Anal. Chem.* (to be published).

UNCLASSIFIED
ORNL-LR-DWG 26451A

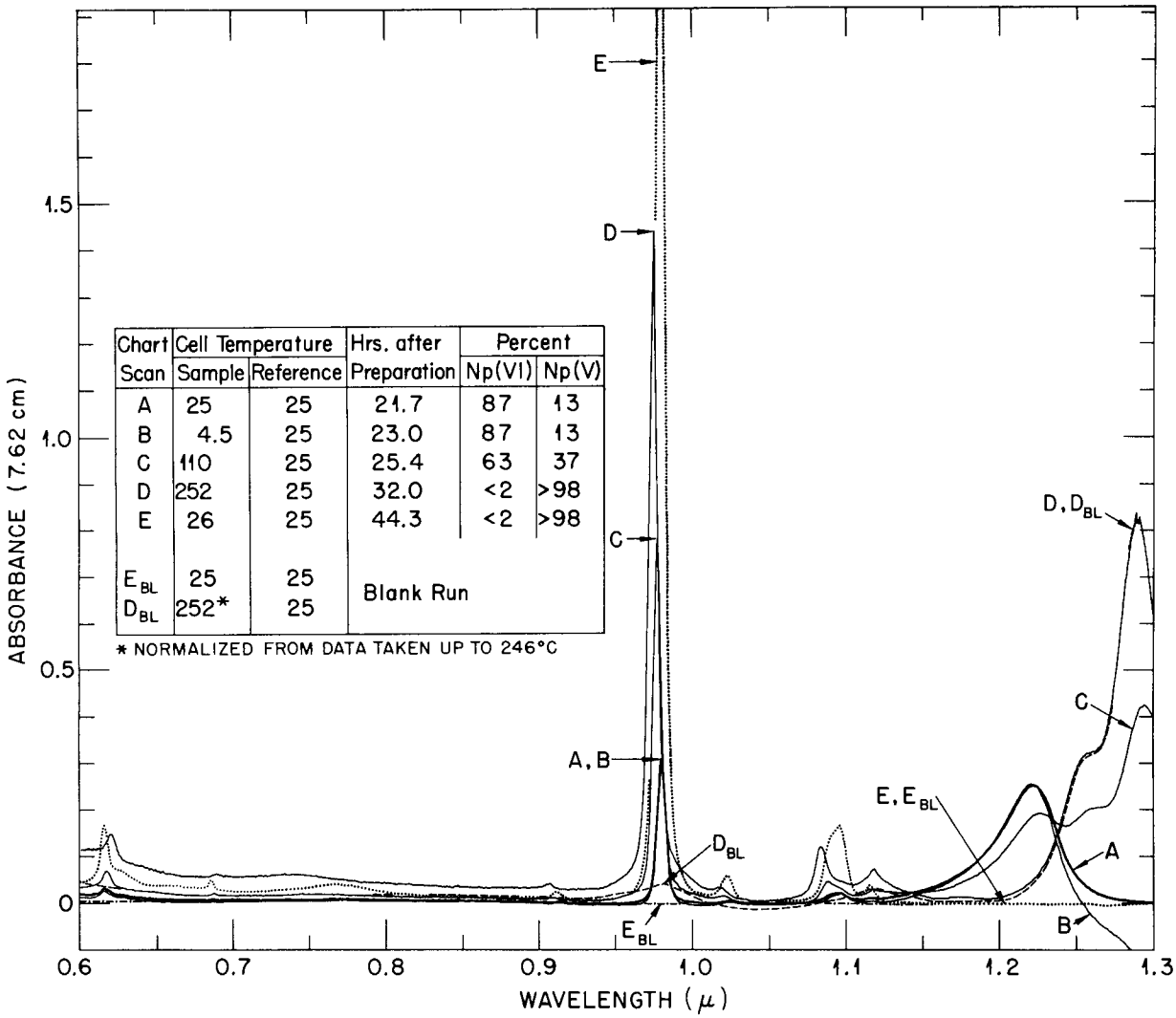

Chart Scan	Cell Temperature Sample	Cell Temperature Reference	Hrs. after Preparation	Percent Np(VI)	Percent Np(V)
A	25	25	21.7	87	13
B	4.5	25	23.0	87	13
C	110	25	25.4	63	37
D	252	25	32.0	<2	>98
E	26	25	44.3	<2	>98
E_{BL}	25	25	Blank Run		
D_{BL}	252*	25			

* NORMALIZED FROM DATA TAKEN UP TO 246°C

Fig. 24.1. Absorbance of a 7.43×10^{-4} *M* Sample of $RbNpO_2(NO_3)_3$ in 0.1 *M* DNO_3–D_2O as a Function of Time and Temperature.

All curves in Fig. 24.1 were traced directly from the strip-chart records. Curves E_{BL} and D_{BL} represent chart scans made at 25 and 252°C, respectively, during a blank run with the solvent solution in both sample and reference cells. The effect of differential-temperature absorbance of the solvent may be noted in curves B, C, D, and D_{BL}. Below 1.2 μ it introduces a minor correction, but above 1.2 μ the effect becomes large enough to complicate seriously the measurements of Np spectra.

The experiment was completed and the sample removed without alpha contamination being found exterior to the sample space. Good decontamination of the sample space was achieved by very slowly flushing with 1 *M* HNO_3 until the effluent contained less than 10^{-3} μg Np^{237} per 100 ml.

24.2 RADIONUCLIDES FORMED IN THE HRT

During HRT runs 13 and 14, a number of samples were withdrawn for the analysis of certain radionuclides.[6] These nuclides included 12 fission

[6]The radiochemical analyses were carried out by E. I. Wyatt, S. A. Reynolds, and co-workers. The chemical analyses were performed by U. Koskela and associates.

products: Y^{91}, Ce^{144}, Nd^{147}, Sr^{89}, Ba^{140}, $Cs^{136,137}$, Zr^{95}, Mo^{99}, Ru^{103}, I^{131}, Te^{132} and the isotopes Np^{239}, U^{237}, S^{35}, Cu^{64}, and P^{32}. The concentration of each fission product was compared with that calculated to be present if it were completely soluble in solution, that is, assuming none had precipitated or been deposited from the solution. These calculated concentrations of each fission product were computed from the power history of the reactor. The elapsed time of the run was divided into sufficiently short intervals to permit an accurate computation for each interval, allowing for the many variations of pile power that took place; then a numerical summation was made of growth and decays for each interval.

Each analysis could thus be expressed in terms of the ratio of the experimental to calculated concentrations, R(exp/calc). Since the isotopes of cesium have given evidence of being most likely to remain dissolved in the solution, all the R(exp/calc) for the fission products were normalized relative to the solubility of Cs^{137} taken as 100%. Thus R(exp/calc) values for the fission products depend on the experimental ratio of the fission product to Cs^{137} concentration (which involves the measurement of the absolute disintegration rate of the samples), the values of the fission yields, and a function of the power history of the reactor. The calculations involving Np^{239} and U^{237} involve identical considerations with the additional dependence upon the mass analysis of the uranium and effective neutron capture cross sections of U^{238} and U^{236}, respectively. Conversely, if the U^{237} and Np^{239} are assumed to be soluble, their effective cross sections may be computed. The calculations for S^{35}, P^{32}, and Cu^{64} depend additionally upon the chemical analyses of sulfur, copper, and uranium as well as all the pertinent effective cross sections. The effective cross section as used here is defined[7] as

$$\sigma_{eff} \equiv \frac{\text{reaction rate/atom}}{\text{"thermal flux"}} ,$$

and refers to the average over the reactor. The "thermal flux" refers to that flux measured by a $(1/v)$ absorber for subcadmium neutrons using the 2200 m/s cross section of the absorber. Furthermore, superimposed upon the various analytical uncertainties are uncertainties that originate in the complexity of the reactor system (e.g., high- and low-pressure systems at different concentrations and their rates of mixing) and the uncertainties inherent in the sampling process.

The results of the fission-product analyses are in substantial agreement with those found in the in-pile loops.[8] The essentially "soluble" fission products include examples of the alkaline and the rare earths. ("Solubility" is used here as an apparent solubility regardless of the mechanism of removal from solution, e.g., adsorption or co-precipitation.) At least initially they exhibit high "solubility"; however, barium shows evidence of exceeding its solubility product after a short time of operation. Strontium is expected to behave similarly but to saturate after a longer period of time; however, the experimental evidence in these runs is not so clear on this point. The isotopes Y^{91}, Ce^{144}, and Nd^{147} appear to be appreciably and almost equally "soluble" within the uncertainties of the experiment. It is not clear why their R(exp/calc) is different from 100% and whether this difference is significant. In the in-pile loop experiments cerium and yttrium exhibited 100% relative solubilities; analyses were not carried out in this case for neodymium.

On the basis of an independent fission yield of $Cs^{136} = 6 \times 10^{-3}\%$, the R(exp/calc) for Cs^{136} ranged from about 50 to 75%. Since the Cs^{136} is expected to show identical chemical behavior to Cs^{137}, this suggests that the average fission yield of Cs^{136} under these conditions is about $4 \times 10^{-3}\%$. The mass-137 chain was expected to be depleted if the 3.8-min Xe^{137} precursor to Cs^{137} were lost from the system through the purging action of hydrogen and oxygen gas. However, R(exp/calc) for Cs^{136} (which is formed only directly in fission) is less than that for Cs^{137}. Furthermore, the relative concentration of Cs^{137} is high compared with that of the other radionuclides; thus it appears that mass-137 chain losses are probably small.

The more readily hydrolyzable fission products Zr, Ru, Mo, and Te were found to be the least

[7] J. Halperin and R. W. Stoughton, *Proc. 2d Intern. Conf. Peaceful Uses Atomic Energy, Geneva, 1958*, paper 1072 (to be published).

[8] J. Halperin, J. O. Oliver, and R. W. Stoughton, *Chem. Ann. Prog. Rep. June 20, 1957*, ORNL-2386, p 12.

"soluble," ranging in values of R(exp/calc) from a fraction of 1% to a few per cent. Of these, the molybdenum was most soluble (as high as 10%) as in the in-pile loop. Since iodine was chemically removed from the solution with metallic silver, the relative iodine concentration was appreciably lower in the HRT [R(exp/calc) $\cong$ 3%] than in the in-pile loop, where R(exp/calc) was variable, ranging from about 10 to 50%.

With the assumption that both U^{237} and Np^{239} may be considered completely "soluble," an effective cross section of about 26 barns is measured for U^{238} and about 35 barns for U^{236}. These cross-section values are consistent with each other in that they both yield a ratio of the average of the resonance to thermal flux, ϕ_r/ϕ_{th}, of about $1/12$, where

$$\frac{\phi_r}{\phi_{th}} = \frac{\sigma_{eff} - \sigma_{th}}{S\sigma\, d(\ln E)} .$$

This value of $\phi_r/\phi_{th} = 1/12$ is approximately equal to that observed in fuel elements of the MTR.[9] It is of interest to note that there exists a discrepancy between the value of the effective cross section of U^{238} found in the HRT and in the in-pile loop tests. In the latter experiments, cross-section values about a factor of 2 higher than the present value were observed.[8]

The values of R(exp/calc) for S^{35} suggest that the effective cross section may be about 50% greater than the 0.26 barn taken for the thermal cross section. The values for Cu^{67} suggest a cross section somewhat lower than the 4.1-barn thermal value. However, the uncertainties in the data for both S^{35} and Cu^{64} are sufficiently large to prevent definite conclusions.

If P^{32} produced from the (n,p) reaction upon S^{32} remained in solution, it would be possible to estimate the fast flux. The threshold for the reaction is about 1.0 Mev, although the effective threshold is about 3.5 Mev and an average cross section of 0.3 barn for the reaction has been reported.[10,11] However, the "solubility" of P^{32} is erratic and low, making the method inapplicable. The data for P^{32} in Table 24.1 are based upon an average of the fast (>3.5 Mev) to thermal flux ratio of 0.1. This ratio has been measured[12] in an LITR fuel element as lying between 0.1 and 0.15.

The results of HRT runs 13 and 14 are summarized in Table 24.1. The first column lists the nuclides, and the second column their half-lives. The third column lists the fission yields for the fission products and the effective cross sections assumed for the other nuclides based upon their being completely "soluble". The next eight columns list the values of R(exp/calc) found in the various samples of runs 13 and 14. Each column lists the sample number and the megawatt-hours of reactor power that the sample had accumulated. It should be noted that the last sample listed for both run 13 and run 14 are for samplings of the low-pressure system, whereas the others are for the high-pressure system. The power history of the fuel solution in run 13 was more complex than that of run 14, and some of the analyses are thought to be less precise in run 13. The data in run 14 are therefore probably more reliable.

[9] J. Halperin, J. O. Blomeke, and D. A. Mrkvicka, *Nuclear Sci. and Eng.* 3, 395 (1958).

[10] D. J. Hughes, *Pile Neutron Research*, p 100, Addison-Wesley, Cambridge, Mass., 1953.

[11] P. M. Uthe, Jr., WADC-TR-57-3, p 15 (1957).

[12] G. Leddicotte, private communication, 1958.

Table 24.1. Radionuclides Formed in the HRT

Nuclide	$T_{1/2}$	Fission Yield (%) or σ_{eff}**	R(exp/calc) (%)							
			Run No. 13				Run No. 14			
			Sample H-22, 2.62 Mwhr	Sample H-39, 13.8 Mwhr	Sample H-71, 36.1 Mwhr	Sample L-81, 36.4 Mwhr	Sample H-103, 21.4 Mwhr	Sample H-126, 55.8 Mwhr	Sample H-174, 134.8 Mwhr	Sample L-208, 277.9 Mwhr
Cs^{137}*	30 yr	6.0	100	100	100	100	100	100	100	100
Cs^{136}	13.0 d	0.006	72	77	73	65	56	49	49	250
Sr^{89}	51.0 d	4.8	80	96	79	65	108	90	88	87
Ba^{140}	12.8 d	6.4	34	66	53	13	27	19	17	2.7
Y^{91}	58.0 d	5.8	84	78	82	60	90	92	75	85
Ce^{144}	290 d	5.7	71	48	51	38	119	108	76	79
Nd^{147}	11.3 d	2.4	82	48	49	36	75	71	63	80
I^{131}	8.05 d	2.9	6.4	3.7	2.5	1.8	4.0	3.3	4.0	0.11
Zr^{95}	63.3 d	6.3	5.8	0.94	1.0	0.26	2.8	1.2	0.69	0.36
Ru^{103}	41.0 d	3.0	0.91	0.41	0.51	0.15	0.51	0.25	0.33	0.74
Mo^{99}	67.0 hr	6.1	1.1	0.21	4.8	3.0	9.6	5.8	5.0	0.25
Te^{132}	77.7 hr	4.3	0.32	0.032	1.5	0.85	2.5	1.8	0.96	0.18
U^{237}	6.75 d	35 barns	123	102	110	103	105	98	96	112
Np^{239}	56 hr	26 barns	12	19	77	97	99	106	96	103
S^{35}	87.1 d	0.26 barn	400	170	260	110	160	140	160	140
Cu^{64}	12.8 hr	4.1 barns	49	52	195		140	81	89	80
P^{32}***	14.3 d	0.3 barn	29	20	47	12	6	5	7	2

*Normalized to R(exp/calc) = 100%.

**Effective cross section for formation assuming complete "solubility."

***Based upon "fast" to thermal flux ratio = 0.1, and cross section for >3.5-Mev neutrons equal to 0.3 barn.

Part VII

ANALYTICAL CHEMISTRY

M. T. Kelley

25. ANALYTICAL CHEMISTRY

O. Menis U. Koskela

J. E. Attrill
C. P. Baker
R. G. Ball
C. M. Boyd
R. E. Corcoran
S. R. Dinsmore
L. G. Farrar
G. Goldstein
B. B. Hobbs
A. D. Horton
H. P. House
D. L. Manning
J. L. Mottern
R. H. Powell
T. C. Rains
I. B. Rubin
W. D. Shults, II
P. F. Thomason

25.1 ANALYSIS OF THORIUM OXIDE

25.1.1 Determination of Thorium

A radiofrequency oscillator[1] operating at 250 Mc/sec was utilized in ascertaining the end-point in the direct titration of thorium in concentrations of approximately 3 mg/ml with either oxalic acid or ethylenediaminetetraacetic acid (EDTA). In using the latter as the titrant, the end-point is established by plotting the volume of titrant vs either the oscillator-grid current or the potential drop through a load resistor, followed by extrapolation of the two straight-line portions of the graph to the point of intersection. With oxalic acid as the titrant, however, two end-points were observed, either of which, preferably the latter owing to the increased precision engendered by the larger volume of titrant, may be used. It has been postulated from these observations that the following stepwise reactions are involved in the titration of thorium with oxalic acid:

$$Th^{4+} + H_2C_2O_4 \longrightarrow Th(C_2O_4)^{++} + 2H^+ \text{ (first end-point)}$$

$$Th(C_2O_4)^{++} + H_2C_2O_4 \longrightarrow \underline{Th(C_2O_4)_2} + 2H^+ \text{ (second end-point)}$$

The coefficient of variation of this method, with either titrant, was found to be of the order of 0.7%, with every indication that the ultimate precision may be of the order of 0.2%. This degree of precision is comparable with that ordinarily associated with gravimetric methods, but, since the radiofrequency method is less susceptible to interferences from impurities, it can be applied with considerably greater dispatch in the determination of thorium.

[1] R. W. Stelzner and M. T. Kelley, *Radio-Frequency Oscillators for Determination of Alkali*, ORNL-1742 (June 9, 1955).

25.1.2 Estimation of Zirconium

A method was developed for the determination of microgram amounts of zirconium in slurries of thorium oxide in order to secure information for evaluating the corrosion rate of the Zircaloy components of test loops. Zirconium is separated from thorium and minor components by extraction from an acidic solution into a solution of thenoyltrifluoroacetone (TTA) in hexone, followed by back-washing the organic phase with 10 *M* hydrochloric acid. After removal of the organic material by evaporation and oxidation, the residual zirconium is reacted with quercetin and is then determined photometrically in a mixture of hydrochloric acid and ethanol by measuring the absorbency of the quercetin-zirconium complex at 420 mμ, or, for extremely low concentrations of zirconium, the fluorescence intensity of a morin-zirconium complex is evaluated at 440 mμ. Concentrations as low as 1 ppm of zirconium can be determined. Over the range of 1 to 10 ppm the coefficient of variation is of the order of 3%.

25.1.3 Determination of Titanium in Thorium Oxide

The colorimetric method for the determination of titanium, by Menis *et al.*,[2] based on the use of disodium-4,5-hydroxy-*m*-benzenedisulfonate (Tiron) as the chromogenic reagent, has been modified for the purpose of eliminating the interferences of chromium(VI), uranium, and molybdenum(VI) which are often encountered in slurries of thorium oxide.

Chromium(VI) can be readily separated from titanium by extraction from 1 to 3 *M* HCl with hexone,[3] but, in the presence of thorium, a portion

[2] O. Menis *et al.*, *HRP Quar. Prog. Rep. Jan. 31, 1958*, ORNL-2493, p 187.

[3] A. E. Weinhardt and A. N. Hixson, *Ind. Eng. Chem.* 43, 1676 (1951).

of the chromium is reduced to Cr(III) and escapes extraction. In this case, however, chromium can be eliminated by resorting to the volatilization as chromyl chloride.[4] If less than 100 μg of chromium is present in solution, reduction to Cr(III) is sufficient to prevent its interference.

Molybdenum, which interferes in concentrations as low as 0.08 μg/ml, can be removed either in the presence or absence of thorium by extracting it three times from 6 to 7 *M* HCl with hexone.[5] Traces of residual molybdenum can be masked with thioglycolic acid, but the inhibiting effect of this acid on the formation of the complex must be eliminated by heating the solution at 100°C for 10 min.

If uranium as well as molybdenum is present, a single hexone extraction is made to remove essentially 90% of the molybdenum, after which the raffinate is made 6 *M* with HCl and passed through a column of Dowex-1 exchange resin in order to separate the uranium and residual molybdenum from titanium. The coefficient of variation of this procedure, for concentrations of titanium in the range of 2 to 10 ppm in slurries of ThO_2, was found to be of the order of 10%. The bias is of the order of +2%.

25.1.4 Flame Photometric Determination of Aluminum

A modified form of a method previously reported by Menis *et al.*[6] for the flame-photometric determination of aluminum was of necessity modified further because of the presence of fluoride. The method originally involved the prior extraction of thorium from an acetate solution at a pH of 1 to 1.5 with a mixture of TTA and chloroform, followed by the extraction of aluminum, after adjustment of the aqueous phase to a pH of 6, with a mixture of TTA and hexone. A much simpler procedure has now been devised whereby the interference of fluoride is overcome and the prior extraction of thorium is rendered unnecessary. In this new procedure, the thorium solution is saturated with ammonium carbonate which reacts with thorium to form a soluble complex, after which the aluminum is extracted with a 0.2% solution of 8-quinolinol in hexone. If iron is present, its interference is minimized by the addition of thioglycolic acid to the carbonate solution prior to the extraction of the aluminum. The aluminum in the hexone extract may be determined either flame photometrically by measuring the emission at 484 mμ or fluorometrically. Both methods have been used in the determination of aluminum in a series of slurries of thorium oxide. At a concentration level of 20 ppm, the difference in aluminum content by the two methods was found to be less than 5 ppm.

25.1.5 Separation of Fluoride and Chloride from ThO_2 by Fusion-Pyrolysis

The fusion-pyrolysis method of Powell and Menis[7] was modified and was applied to the separation of occluded or otherwise nonleachable (by HNO_3) chloride and fluoride from high-fired (1600°C) ThO_2. For the liberation of fluoride, the original method was modified by the substitution of a silica boat for the nickel boat and of $NaBiO_3$ as the flux instead of Na_2WO_4. With the bismuthate flux, which has a very low fluoride content, 2 μg per 8-g charge of flux, the pyrolysis is carried out at 1000°C. Commercially available bismuthate is not, however, suitable for the pyrolytic separation of chloride because of its high chloride content. For chloride removal and determination, experimental work with heteropoly vanadium, molybdenum, and other compounds (reagent grades) has revealed that the compound $Na_2Mo_3O_{10}$ has a sufficiently low chloride content and, consequently, is now the preferred flux material for this pyrolysis. By using this particular compound, the pyrolytic separation can be made at temperatures as low as 700°C on samples with chloride concentrations as low as 2 ppm on test portions containing as much as 5 to 10 g of ThO_2. The effectiveness of this procedure has been demonstrated experimentally by the separation and determination of chloride, when present in ThO_2, as AgCl. At the present time, the experimental work gives indication that the molybdate

[4] W. F. Hillebrand and G. E. F. Lundell, *Applied Inorganic Analysis*, 2d ed., p 526, New York, 1953.

[5] I. Nelidow and R. M. Diamond, *J. Phys. Chem.* 59, 710 (1955).

[6] O. Menis *et al.*, *HRP Quar. Prog. Rep. July 31, 1957*, ORNL-2379, p 171.

[7] R. H. Powell and O. Menis, *Separation of Fluoride from Refractory Materials by Fusion-Pyrolysis*, ORNL-2512 (April 28, 1958).

flux is not suitable for the fusion pyrolysis of fluoride, in which case a separate pyrolytic determination is made by using the bismuthate flux.

25.1.6 Thermogravimetric Analysis of Thorium Compounds

The thermogravimetric analysis of various compounds used in the production of thorium oxide, such as thorium nitrate and oxalate, was instituted and is now being conducted at an accelerated pace. In this work, an attempt is being made to evaluate the effect of certain additives on the magnitude and rate of changes in the weight of thorium oxide as functions of temperature. The Stanton thermo-balance, which has a sensitivity of 1 mg over its entire temperature range up to 1000°C, is being used in this study.

25.1.7 The Effect of Acetic Acid on the Extractability of Thorium with Thenoyltrifluoroacetone (TTA) in Carbon Tetrachloride

The extractability of thorium by thenoyltrifluoroacetone (TTA), dissolved in carbon tetrachloride, is enhanced by the addition of acetic acid to the aqueous phase (0.1 *M* $HClO_4$). Since this effect may be useful in the control of extraction conditions whereby thorium may be effectively separated from other elements, a detailed study was made of the effect of the acetic acid concentration on the extractability of thorium with particular emphasis on the predominant complexing reactions as functions of acetate concentration. The reactions which can be postulated from this experimental work are listed in Table 25.1.

In case 1, in the absence of acetate, the distribution ratio, E_a^0, is proportional to the fourth power of the TTA concentration and inversely proportional to the fourth power of the H-ion concentration of the aqueous phase. This is in agreement with the findings of Day *et al.*[8] When the aqueous phase is 1 *M* in acetic acid (case 2), an additional reaction is postulated whereby an adduct of Th-TTA-HAc is formed, which accounts for an increase in the extractability of thorium. With acetic acid in somewhat higher concentration, 3.5 *M* (case 3), the distribution ratio is inversely proportional to the third rather than the fourth power of the H-ion concentration in the aqueous phase. This is interpreted as evidence that $ThAc^{+++}$ is first formed and that this species rather than Th^{4+} then reacts with TTA to form the adduct which is extracted. In the presence of acetic acid in high concentration, 5.5 *M* (case 4), the thorium-TTA chelate apparently coordinates with two molecules of acetic acid, so that an additional species, $Th(T)_4 \cdot 2HAc$, becomes available for extraction and the distribution ratio increases. In this case the distribution ratio is also inversely proportional to the third power of the H-ion concentration; therefore it may be postulated that the principal species which remains in the aqueous phase is still $ThAc^{+++}$.

[8] R. A. Day, Jr., and R. W. Stoughton, *Chemistry of Thorium in Aqueous Solutions. I. Some Organic and Inorganic Complexes*, ORNL-468 (Jan. 5, 1950).

Table 25.1. Predominant Complexing Reactions of Thorium with Acid Form of TTA as Functions of Acetate Concentration

Case	Acetate Concentration (*M*)	Predominant Reactions of Th with HT (Acid Form of TTA)
1	None	$Th^{4+} + 4HT \longrightarrow Th(T)_4 + 4H^+$
2	1	$Th^{4+} + 4HT + HAc \longrightarrow Th(T)_4\,HAc + 4H^+$
3	3.5	$Th^{4+} + HAc \longrightarrow ThAc^{+++} + H^+$
		and $ThAc^{+++} + 4HT \longrightarrow Th(T)_4 \cdot HAc + 3H^+$
4	5.5	$ThAc^{+++} + 4HT + HAc \longrightarrow Th(T)_4 \cdot 2HAc + 3H^+$

25.2 ANALYSIS OF URANYL SULFATE SOLUTIONS

25.2.1 Polarographic Determination of Mercury and Copper

A polarographic method has been applied to the simultaneous determination of mercury and copper in solutions of uranyl sulfate. The reduction waves of these two elements coalesce unless a suitable complexing agent is added to the supporting electrolyte. It was established that if 0.9 *M* NaCl at pH 9, which contains 0.25 *M* of either of the two complexing agents, ethylenediaminetetraacetate (EDTA)[9] or nitrilotriacetate (NTA), is used as the supporting electrolyte, the half-wave potentials, vs the SCE, of mercury and copper are −0.1 and −0.5 v, respectively. The reduction waves of the two elements may, therefore, be readily resolved, and concentrations of each element as low as 4 μg/ml can be estimated with a coefficient of variation of 4%. In these media, Fe(III) interferes with the determination of mercury; however, this interference can be eliminated by the use of a mixture of sodium citrate and ammonium carbonate as the complexing agent. In the NaCl-citrate-carbonate medium, $E_{1/2}$, vs the SCE, of mercury is −0.06 v, while that of iron is −0.55 v. As much as 300 μg of Fe(III) per milliliter can be tolerated. Copper exhibits two reduction waves in this medium, Cu(II)-Cu(I) at −0.21 v and Cu(I)-Cu at −0.41 v vs the SCE. Iron(III) interferes with the latter reduction wave, but in this case the wave at −0.21 v can be utilized for the estimation of copper. However, for the estimation of copper in low concentrations (∼20 μg/ml), a supporting electrolyte containing either EDTA or NTA is to be preferred because the sensitivity is about twice as great as in the citrate-carbonate medium. Uranium does not interfere in any of the media tested since it is not reduced within the range of potentials investigated.

25.2.2 Determination of Iron

An extraction procedure has been made applicable to the separation of iron from copper in uranyl sulfate solutions prior to the spectrophotometric determination of the iron by the α,α′-bipyridyl method. In this method, internal electrolysis is avoided as a means of removal of copper, a procedure which often leads to uncertain or erratic results. This procedure involves the extraction of iron from 6 *M* HCl with hexone[10] after which it is re-extracted from the organic phase with an aqueous acetate-buffered solution of hydroxylamine hydrochloride containing α,α′-bipyridyl. The interferences of uranium and copper are thus effectively eliminated. The absorbancy of the iron-bipyridyl complex is measured at 522 mμ. Alternatively, the iron in the organic phase may be estimated flame photometrically by measuring the radiant intensity of the flame at a wave length of 372 mμ. Over the range of 2 to 10 μg of iron per milliliter, the coefficient of variation of the extraction-colorimetric procedure is about 2%, whereas that of the flame-photometric method is of the order of 10%.

25.2.3 Coulometric Determination of Uranium in Synthetic Homogeneous Reactor Fuel

Synthetic HRT fuels were analyzed by the coulometric titration method with the Mark II controlled-potential coulometric titrator, both outside and inside a cell in the High-Radiation-Level Analytical Facility (HRLAF). The Mark II instrument was designed by Kelley *et al.*[11] and is a modified version of the titrator described by Booman *et al.*[12]

Three series of determinations were made in order to determine the precision obtainable in the remote facilities of the HRLAF. Determinations of uranium were made outside the HRLAF cell in order to provide a basis for comparing the results obtained from the use of the remote-control facilities.

The synthetic fuel solutions contained UO_2SO_4 (10.78 mg of U per ml) in 0.5 *N* H_2SO_4. The first series of titrations was made on 0.5-ml samples which were titrated outside of the cell. The coefficient of variation of this set was found to be 0.2%. The second series of titrations was made inside the HRLAF cell, by use of the remote pipetter and the master-slave manipulators. The

[9] A. D. Horton, P. F. Thomason, and M. T. Kelley, *Anal. Chem.* **29**, 388 (1957).

[10] H. Specker and W. Doll, *Z. anal. Chem.* **152**, 178 (1956).

[11] M. T. Kelley, H. C. Jones, and D. J. Fisher, "Electronic Controlled-Potential Coulometric Titrator," *Anal. Chem.* (in press).

[12] G. L. Booman, *Anal. Chem.* **29**, 213 (1957).

coefficient of variation for this group was found to be 0.4%. In the third set of determinations the remote facilities were used in a simulated removal of certain fission products which are known to interfere with the determination of uranium. The solvent extraction procedure developed by Farrar *et al.*[13] was followed for this simulated removal of fission products. Although no fission products were present, all steps necessary for the removal of these products were carried out. Briefly, these steps were as follows:

1. The sample was extracted for 10 min with chloroform saturated with α-benzoin oxime.
2. The aqueous phase was washed for 5 min with chloroform.
3. The electrolyte (aqueous phase) was sparged with argon for 5 min before the addition of the mercury-pool cathode.
4. The solution was titrated in the normal manner.

In this series of tests, the coefficient of variation was found to be 0.3%. This work demonstrated that the controlled-potential coulometric titration method is superior in precision to a redox titration method; furthermore, interferences in the titration of uranium can be eliminated more easily. By this method, manipulations inside the cell are also held to a minimum. This method is now being used on a routine basis for the analysis of HRT fuel.

25.2.4 Coulometric Determination of Nickel in Homogeneous Reactor Fuel

The procedure[13] for determining copper and uranium by the use of the controlled-potential coulometric titrator has been extended to the determination of nickel in HRT fuel. Nickel is determined coulometrically by electrolyzing it in an ammoniacal solution at a potential of −1.2 v vs the Ag-AgCl reference electrode after copper and uranium have been estimated. Copper is determined first by electrolyzing at zero potential and measuring the integrated current necessary to remove all the copper. Following this step, the potential is adjusted to −0.3 v and the solution is electrolyzed until the background current is 0.05 ma, which value indicates that all the U(VI) has been reduced to U(IV). The integrated current for this second stage of the electrolysis is a measure of the uranium content. At this point, the solution is made alkaline with NH_4OH, degassed with nitrogen, then pretitrated at a potential of −0.8 v. The potential is then adjusted to −1.2 v, and the solution is electrolyzed until the background current is 0.05 ma. The integrated current for this third stage is a measure of the nickel present in the sample.

In testing this procedure on synthetic samples, it has been observed that the method is negatively biased, for the determination of nickel, to the extent of about 5%. The bias appears to be due to the occlusion of some nickel on the precipitate of uranous hydroxide which is formed when NH_4OH is added to the solution. The coefficient of variation for samples containing 25 μg of nickel was 2.5% and for samples containing 50 μg or more of nickel, 1%. By this method, which was developed to supplement rather than replace the polarographic method now in use, it will be possible to determine these three elements in a single aliquot of highly radioactive solutions of HRT fuel.

25.3 CHEMICAL ANALYSES INCIDENT TO REACTOR OPERATIONS

Late in 1957 the Reactor Analysis Laboratory of the High-Radiation-Level Analytical Facility (HRLAF) took over the operation of opening bombs which contained samples of ThO_2 slurry from the Chemical Technology Division. This operation has proceeded without difficulty.

The following is an account of the analytical services incident to the operation of the HRT. Analyses for critical run 12 were performed outside the remote facilities, but for power runs 13 and 14, full use was made of the HRLAF. A sudden increase in nickel concentration during run 13 necessitated a careful re-evaluation of the precision and accuracy of the methods. The spectrochemical group assisted in this work in establishing the nickel content of this run. No real difficulties were encountered during run 14, but just prior to termination of the run, the activity level of fuel samples which glowed in the dark was found to be greater than 100 r at 5 ft. With the samples adjacent to the zinc bromide window, readings of about 2 mr were obtained outside the cell.

The methods used in these analyses were essentially as described in the ORNL Master Analytical Manual. To minimize the possibility of

[13] L. G. Farrar, M. T. Kelley, and P. F. Thomason, *Anal. Chem.* 30, 1511 (Sept. 1958).

personnel exposure, however, the new coulometric titration method for uranium and copper described in Sec 25.2.4 was put into service shortly before run 14 was terminated. More recently, analyses have been made as required in connection with HRT run 16. Polarographic methods described in the ORNL Master Analytical Manual were used for the determination of nickel and also for copper until the activity level rose to more than 100 r per sample. Uranium was determined by four different methods. Initially, a fluorometric method was used, but as the uranium concentration was increased, a colorimetric thiocyanate method was added. Later the potentiometric ceric sulfate method was adopted. Up to this point (end of run 14), samples were prepared in a hot cell, but the final determinations were made outside the cell. When the activity level rose to more than 100 r per sample, the coulometric titration method,[13] referred to above, was introduced for determining both copper and uranium. Remote-handling techniques were used altogether in making these analyses. Sulfate was titrated photometrically with $Ba(ClO_4)_2$ (refs 14 and 15) after it had been separated by an ion-exchange method. It was discovered that at high radiation levels the resin has a limited lifetime; as a consequence, new columns are now prepared once a day, or more frequently if many samples are processed. Microelectrodes were used to determine the apparent pH. Since no deuterated buffer solutions were available, it was not possible to determine the true pD; however, correction factors were available for application in estimating this value.[16] Free acid was determined potentiometrically,[17] by using a combination of glass and calomel electrodes. Some of the results appeared to be rather high, owing possibly to the effects of intense radiation on the electrodes.

[14] F. J. Miller and P. F. Thomason, *Automatic Photometric Titration of Sulfate*, ORNL-2040 (Feb. 29, 1956).

[15] J. L. Mottern and C. P. Baker, *Anal. Chem. Semiann. Prog. Rep. April 20, 1956*, ORNL-2070, p 31.

[16] R. B. Fischer and R. A. Potter, *Standardization of the pD Scale*, MDDC-715 (Sept. 12, 1945).

[17] J. L. Mottern, *Anal. Chem. Ann. Prog. Rep. Dec. 31, 1957*, ORNL-2453, p 56.

OAK RIDGNATIONAL LABORATORY
HOMOGENEIS REACTOR PROJECT

AUGUST 1, 1958

PROJECT DIRECTOR
R. B. ..S — O

OCIATE PROJECT DIRECTOR
C. E. ..ES* — D
..UNNELS, SEC. — REE

TECHNICAL ASSISTANT
F. KERTESZ — REE

PROJECT EDITOR
W. D. REEL — TI

DESIGN AND ENGINEERING
R. N. LYON, ASSISTANT DIRECTOR — REE
T. S. CARLSMITH,* SEC. — REE

DESIGN
W. R. GALL, SECTION CHIEF — REE
M. I. LUNDIN, ASSISTANT SECTION CHIEF — REE

SPECIAL PROBLEMS
C. L. SEGASER — REE

MECHANICAL DESIGN, SPECIFICATIONS AND DRAFTING
F. C. ZAPP, GROUP LEADER — REE
C. A. BURCHSTED — REE
C. W. COLLINS — REE
J. E. JONES — REE
W. ROBINSON — REE
H. H. BRADFORD — REE
R. L. CAUBLE — REE
C. W. DAY — REE
J. P. DILORENZO — REE
F. GUINNESS — REE
T. E. HAYNES — REE
A. R. KERR — REE
W. B. KRICK — REE
A. S. LUDLOW — REE
C. A. ROBERTS — REE
R. D. SATTERFIELD — REE
R. H. SIGLER — REE
W. G. STERLING — REE

SITE AND STRUCTURES
J. N. ROBINSON — REE

J. R. MCWHERTER, ASSISTANT SECTION CHIEF — REE

PROCESS DESIGN
R. C. ROBERTSON, GROUP LEADER — REE
J. C. BOLGER — REE
E. H. GIFT — REE
L. A. HAACK — REE
N. HILVETY — REE
H. A. MCLAIN — REE

REACTOR LAYOUT AND COMPONENT DESIGN
R. H. CHAPMAN, GROUP LEADER — REE
C. J. CLAFFEY — REE
R. E. SCHAPPEL — REE
O. W. VROOM — REE

COMPONENT DEVELOPMENT
I. SPIEWAK, SECTION CHIEF — REE

HEAT EXCHANGERS AND MECHANICAL ENGINEERING PROBLEMS
J. S. CULVER, GROUP LEADER — REE
B. D. DRAPER — TVA
P. P. HOLZ — REE
I. K. NAMBA — REE
H. C. ROLLER — REE
T. L. CASTILE — REE
C. JONES — REE

CIRCULATING PUMPS
C. H. GABBARD, GROUP LEADER — REE
T. G. CHAPMAN — REE
J. C. MOYERS — REE
H. R. PAYNE — REE
C. C. HURTT — REE
R. J. LOCKETT — REE

FEED PUMPS AND VALVES
E. C. HISE, GROUP LEADER — REE
R. BLUMBERG — REE
J. P. HURST — REE
G. A. WINDLE — REE

CORE AND BLANKET AND CHEMICAL ENGINEERING PROBLEMS
C. G. LAWSON, GROUP LEADER — REE
D. M. EISSENBERG — REE
B. A. HANNAFORD — REE
J. K. HAYES — COMBUSTION
J. E. MOTT — REE
D. L. SNYDER — REE
A. B. DAFFRON — REE
H. GOODMAN — REE
S. R. WEST — REE
B. J. YOUNG — REE

SYSTEMS DEVELOPMENT
R. B. KORSMEYER, SECTION CHIEF — REE
F. N. PEEBLES, ASSISTANT SECTION CHIEF — REE

SLURRY SYSTEMS DEVELOPMENT I
R. VAN WINKLE, GROUP LEADER — REE
R. B. GALLAMER — REE
C. H. GIBSON — REE
R. H. NIMMO — REE
H. B. PIPER — REE
C. M. FITZPATRICK — REE
W. M. PARKS — REE

SLURRY SYSTEMS DEVELOPMENT II
L. F. PARSLY, GROUP LEADER — REE
R. J. KEDL — REE
M. RICHARDSON — REE
R. E. CARNES — REE

HRT CORE MOCKUP
P. H. HARLEY, GROUP LEADER — REE
D. E. WILLIS — REE
L. E. PENTON — REE
T. R. WILSON — REE

OPERATIONS
A. N. SMITH, GROUP LEADER — REE
T. L. BOSWELL — REE
B. R. CHILCOAT — REE
J. T. DICKIE — REE
C. A. GIFFORD — REE
C. A. MCLAUGHLIN — REE
H. G. MOORE — REE
R. E. POTTER — REE
D. M. WALLACE — REE

INSTRUMENTATION AND CONTROLS
D. S. TOOMB, SECTION CHIEF — I&C

REACTOR I&C SYSTEM DESIGN
J. R. BROWN, GROUP LEADER — I&C
J. A. RUSSELL — I&C
R. W. BORGERS — I&C

HRP SUPPORTING SERVICES
O. G. DAVIS, GROUP LEADER — I&C
S. J. BALL — I&C
G. W. GREENE — I&C
P. G. HERNDON — I&C
H. D. WILLIS — I&C
R. M. BURNETT — I&C
M. A. MEACHAM — I&C
P. E. SMITH — I&C

VALVES AND ACTUATORS
A. M. BILLINGS, GROUP LEADER — I&C
E. H. BELL — I&C
B. J. JONES — I&C
P. F. HURAY — I&C

INSTRUMENT DEVELOPMENT
R. L. MOORE, GROUP LEADER — I&C
J. L. REDFORD — I&C
T. M. CATE — I&C

RESEARCH AND ANALYSIS
P. R. KASTEN, SECTION CHIEF — REE

REACTOR ANALYSIS
M. W. ROSENTHAL, GROUP LEADER — REE
S. JAYE — REE
B. E. PRINCE — REE

REACTOR PHYSICS
M. TOBIAS, GROUP LEADER — REE
R. CHALKLEY — REE
C. W. NESTOR, JR. — REE

PROGRAMING
T. B. FOWLER — REE
M. P. LIETZKE — REE

TRANSPORT PROPERTIES OF SLURRIES
D. G. THOMAS, GROUP LEADER — REE
L. L. BENNETT — REE
P. H. HAYES — REE
R. M. SUMMERS — REE

PHYSICAL CHEMISTRY OF SLURRIES
C. S. MORGAN, GROUP LEADER — REE
B. G. SUTTON — REE

FLUID FLOW AND HEAT TRANSFER
H. C. CLAIBORNE, GROUP LEADER — REE
H. A. MACCOLL — REE

STRESS ANALYSIS AND CLOSURE RESEARCH
R. D. CHEVERTON, GROUP LEADER — REE
T. H. MAINEY — REE
E. VOLK — COMBUSTION

REACTOR MATERIALS RESEARCH
E. G. BOHLMANN, ASSISTANT DIRECTOR
T. S. CARLSMITH,* SEC
R. R. HOWELL
S. J. LIDE
R. E. WACKER, RECORDS

SOLUTIONS
J. C. GRIESS, ASSISTANT SECTION — REE

LOOPS
R. S. GREELEY, GROUP LEADER — REE
S. R. BUXTON — REE
E. S. SNAVELY — REE
J. E. JACKSON — REE
W. H. HINDS — REE

LABORATORY STUDIES
J. L. ENGLISH, GROUP LEADER — REE
D. N. HESS — REE
P. D. NEUMANN — REE
L. L. FAIRCHILD — REE
H. L. BARKER — REE
F. B. DAVIS — REE
B. L. JOHNSON — REE
H. R. TINCH — REE
J. L. UNDERWOOD — REE

SLURRIES
E. L. COMPERE, ASSISTANT SECTION CHIEF — REE

LOOPS
S. A. REED, GROUP LEADER, OUT-OF-PILE STUDIES — REE
H. F. HENDERSON — REE
F. E. MCDANIEL — REE

TOROIDS
L. RICE — REE
R. F. BENSON — REE
B. H. PARKS — REE
G. G. WARNER — REE

IN-PILE BOMBS
L. F. WOO — REE

ENGINEERING
H. C. SAVAGE, ASSISTANT SECTION CHIEF — REE

SOLUTIONS
S. E. BOLT, GROUP LEADER — REE
A. J. SHOR — REE
W. C. ULRICH — REE

IN-PILE MOCKUPS
J. R. HART, LEADER — REE
C. H. BURBAGE — REE
R. W. RAY — REE
T. F. RAYBURN — REE
D. G. PFACH — REE

100A LOOP OPERATIONS
J. F. WINESETTE* — REE
C. M. BURCHELL — REE
C. L. FRANCIS — REE
J. B. FRENCH — REE
J. W. GOOCH — REE
W. H. WAGNER — REE

SLURRIES
D. T. JONES, GROUP LEADER — REE
J. M. BAKER — REE
D. W. HUBBARD — REE

IN-PILE SLURRY
H. C. HOOVER — REE

100A LOOP OPERATIONS
J. F. WINESETTE* — REE
L. L. ALLEN — REE
C. R. BENSON — REE
D. G. GATES — REE
G. A. MOORE — REE
L. G. PHELPS — REE
A. E. PUGH — REE

IN-PILE OPERATIONS
R. A. LORENZ, GROUP LEADER — REE
V. A. DECARLO — REE
V. R. BULLINGTON — REE
W. E. TEICHERT, A SHIFT LEADER — REE
J. W. MOSIER — REE
C. E. ROBERTS — REE
E. H. QUINN, B SHIFT LEADER — REE
J. P. GORDON — REE
A. L. SUTTON, C SHIFT LEADER — REE
R. A. JONES — REE
R. W. WALLER — REE
J. W. MYERS, D SHIFT LEADER — REE
R. G. ROSS — REE
D. M. SMITH — REE

RADIATION
G. H. S, SECTION CHIEF — REE

IN-PILE LOOPS
M. D. ERMAN, GROUP LEADER — C
J. E. R — REE
S. N. ILER — REE
W. C. — C

IN-PILE BOMBS
R. J. S, GROUP LEADER — C
F. A. K — REE
K. S. KEN — C
RUTHERFORD — REE

SUPPORTING RESEARCH
A. L. ARELLA — C
J. C. TER — REE

REMOTE EVALUATION
A. R. N — REE
MCCOLLUM, SHIFT LEADER — REE
SCHILL — REE
SMITH, JR. — REE
THOMPSON — REE

METALLURGY
G. M. MSON, SECTION CHIEF — M

METALLURGICAL RESEARCH
M. L. CLESIMER, LEADER — M
S. G. SON — M
P. L. FENHOUSE — M
R. L. PHENSON — M
JONES — M
NELSON — M
WOODHOUSE — M

METALLURGICAL ENGINEERING *
E. S. SAR, LEADER — M
F. W. IKE — M
W. J. HARD — M
J. J. SLINGER — M
J. K. TE — M
C. H. TKE — M
S. SMITH — M
WHEELER — M

METALLOGRAPHY
R. S. XUSE,** LEADER — M
T. M. ILEY, JR. — M
BOYD — M
DAY** — M
FITZGERALD — M
HENSON** — M
SHRADER** — M
ZACHARY — M

RADIATION DAMAGE
R. G. RGREN — SS
J. C. SON** — SS
B. GRIZZEL — SS

SUBCONTRACTS
FRANKLIN UNIVERSITY
RICE INSTITUTE
STANFORD RESEARCH INSTITUTE
SYRACUSE UNIVERSITY
TULANE UNIVERSITY
UNIVERSITY OF UTAH

INDUSTRIAL PARTICIPATION
COMUSTION ENGINEERING, INC.
TENESSEE VALLEY AUTHORITY
PUERTO RICO WATER RESOURCES AUTHORITY

CHEMICAL TECHNOLOGY
D. E. FERGUSON,* PROGRAM LEADER — CT
I. LOOPE, SEC. — CT

CHEMICAL DEVELOPMENT
D. E. FERGUSON,* SECTION CHIEF — CT

BLANKET PROCESSING
R. E. LEUZE, GROUP LEADER — CT
J. M. CHILTON — CT
R. L. HICKEY — CT

CORE PROCESSING
R. A. MCNEES, GROUP LEADER — CT
M. H. LLOYD — CT
S. PETERSON — CT
W. B. HOWERTON — CT

THORIUM BLANKET STUDIES
J. P. MCBRIDE, GROUP LEADER — CT
R. L. PEARSON, PROBLEM LEADER, OXIDE PREPARATION — CT
A. T. KLEINSTEUBER — CT
C. E. SCHILLING — CT
C. W. GREENE — CT
W. L. PATTISON — CT
N. A. KROHN, PROBLEM LEADER, IRRADIATION STUDIES — CT
K. H. MCCORKLE — CT
L. E. MORSE — CT
P. P. HAYDON — CT
H. F. SOARD — CT

DESIGN
W. E. UNGER, ASSISTANT SECTION CHIEF — CT

TiO_2 DEVELOPMENT DESIGN
J. C. SUDDATH — CT

HRP-CP DESIGN SUPPORT
H. O. WEEREN — CT
F. J. FRITZ — CT
F. C. MCCULLOUGH — CT

LOOP FACILITIES DESIGN
T. A. ARKHART — CT
R. A. CULVER — CT
B. B. KLIMA — CT
W. F. SCHAFFER — CT

INSTRUMENTATION
C. S. LISSER — CT

DRAFTING
E. E. BRIDGES** — E&M
J. D. CUPP** — E&M
J. W. DAY — E&M
H. W. FALLON** — E&M
L. C. HUBBARD — E&M
J. H. MANNEY** — E&M
J. D. PHILLIPS** — E&M
F. L. PEISHEL** — E&M
K. F. STOCKSBURY** — CT
J. H. THOMPSON — E&M
J. N. WHEELER** — E&M

PILOT PLANT
R. B. LINDAUER,** SECTION CHIEF — CT

IN-PILE LOOP OPERATIONS
W. D. BURCH,* GROUP LEADER — CT
J. W. BROWN — CT
L. J. KING — CT
L. B. SHAPPERT — CT

SLURRY PREPARATION
E. M. SHANK, PROBLEM LEADER — CT
C. V. ELLISON — CT
W. M. WOODS — CT

UNIT OPERATIONS
P. A. HAAS, GROUP LEADER — CT

SLURRY PREPARATION DEVELOPMENT
C. C. HAWS, JR. — CT
K. O. JOHNSSON — CT
R. O. ARTHUR — CT
V. L. FOWLER — CT
D. A. MCWHIRTER — CT

COMPONENT DEVELOPMENT STUDIES
J. W. SNIDER — CT
E. L. YOUNGBLOOD — CT
R. C. EARLY — CT
F. N. MCLAIN — CT

CHEMICAL RESEARCH
E. H. TAYLOR,** DIRECTOR — C
H. A. STEINKE, SEC. — C

FUEL SOLUTION CHEMISTRY
H. F. MCDUFFIE, GROUP LEADER — C
W. L. MARSHALL, GROUP LEADER — C
J. S. GILL — C
L. O. GILPATRICK — C
G. M. HEBERT — C
R. SLUSHER — C
H. H. STONE — C
F. H. SWEETON — C

RADIATION CHEMISTRY
C. J. HOCHANADEL,** GROUP LEADER — C
J. W. BOYLE** — C
H. A. MAHLMAN** — C

HEAVY ELEMENT CHEMISTRY
R. W. STOUGHTON,** GROUP LEADER — C
J. HALPERIN** — C
M. H. LIETZKE** — C
W. C. WAGGENER** — C

INORGANIC SOLUTION CHEMISTRY
K. A. KRAUS,** GROUP LEADER — C
H. O. PHILLIPS** — C

ANALYTICAL CHEMISTRY
MYRON T. KELLEY,** DIRECTOR
C. D. SUSANO,** ASSOCIATE DIRECTOR
K. A. ODOM, SEC. — AC

CORROSION ANALYTICAL LABORATORY
O. MENIS,* SECTION CHIEF — AC
H. P. HOUSE, ASSISTANT SECTION CHIEF — AC

RESEARCH
O. MENIS,* GROUP LEADER — AC
C. M. BOYD — AC
R. H. POWELL — AC
D. L. MANNING, GROUP LEADER — AC
R. G. BALL — AC
G. GOLDSTEIN — AC
T. C. RAINS, GROUP LEADER — AC
I. B. RUBIN — AC

SERVICE
C. K. TALBOTT, GROUP LEADER — AC
D. E. CARPENTER — AC
N. M. FERGUSON — AC
F. L. LAYTON — AC
T. P. BACON — AC
W. D. CLAPP, JR. — AC
C. A. CLARK — AC
P. S. GOODWIN — AC
B. D. HICKS — AC
A. H. MATTHEWS — AC
T. O. MILLER — AC
V. S. NORMAN — AC
E. ONKST — AC
C. M. WILSON — AC

HRT AND IN-PILE LOOP ANALYSIS
U. KOSKELA, SUPERVISOR — AC
L. G. FARRAR, ASSISTANT SUPERVISOR — AC
J. E. ATTRILL — AC
C. P. BAKER — AC
R. E. CORCORAN — AC
S. R. DINMORE — AC
J. L. MOTTERN — AC
G. M. CAMPBELL — AC
G. I. GAULT — AC
F. K. HEACKER — AC
M. H. MCCORQUODALE — AC
J. L. SHARP — AC
J. SLESSINGER — AC
W. R. WARREN — AC
H. L. WEBB — AC
H. L. WHITTINGTON — AC

RADIOCHEMICAL ANALYSES
E. I. WYATT** — AC

HRT DEVELOPMENT
P. F. THOMASON,** GROUP LEADER — AC
R. E. BIGGERS** — AC
F. J. MILLER** — AC
S. A. REYNOLDS,** GROUP LEADER — AC
J. S. ELDRIDGE** — AC
T. H. HANDLEY** — AC
W. S. LYON** — AC

HIGH RADIATION LABORATORY
J. E. MORTON** — AC

HOMOGENEOUS REACTOR TEST
S. E. BEALL, PROJECT ENGINEER — REE
B. FUBANK, SEC. — REE
M. SWANK, SEC. — CT

REACTOR PLANNING
S. I. KAPLAN, GROUP LEADER — REE
J. R. BUCHANAN — CT

PLANT OPERATIONS
J. W. HILL, JR., CHIEF — REE
N. C. BRADLEY — CT
D. SCOTT, JR. — REE
D. W. LEIGH — REE
J. R. ENGEL, SUPERVISOR — CT
R. J. HARVEY — REE
H. D. CURTIS — REE
D. T. GODWIN — REE
T. W. HODGE — REE
A. L. JOHNSON — REE
L. P. PUGH — REE
J. D. FLYNN, SUPERVISOR — REE
H. F. BAUMAN — CT
J. D. BARNES — REE
E. D. BOLLING — REE
W. T. BOSTIC — CT
E. W. BROWN — CT
T. G. HILL — REE
J. O. KOLB, SUPERVISOR — REE
D. F. FRECH — REE
J. E. EVE — REE
R. J. SHANNON — CT
L. J. SHERSKY — CT
J. E. WOLFE — REE
R. H. GUYMON, SUPERVISOR — CT
D. F. BRULEY — CT
H. L. BROWN — REE
F. L. ROUSER — REE
R. SMITH, JR. — REE
J. L. STEPP — REE

REACTOR MATERIALS AND CHEMISTRY
D. M. RICHARDSON, GROUP LEADER — REE
J. E. SUTHERLAND — REE
J. D. JONES — REE

CHEMICAL PLANT
W. D. BURCH,* GROUP LEADER — CT
R. H. WINGET — CT
O. O. YARBRO — CT
W. A. LINDSEY — CT

REACTOR ANALYSIS
P. H. HAUBENREICH, GROUP LEADER — REE
J. HERNANDEZ — PUERTO RICO WATER RESOURCES AUTHORITY
J. A. WATTS — REE

MAINTENANCE PLANNING
W. TERRY, SUPERVISOR — REE
G. H. JOHNSON — REE

INSTRUMENTATION
K. W. WEST, GROUP LEADER — I&C
J. A. RUSSELL — I&C

AC ANALYTICAL CHEMISTRY DIVISION
C CHEMISTRY DIVISION
CT CHEMICAL TECHNOLOGY DIVISION
D DIRECTOR'S DIVISION
E&M ENGINEERING AND MECHANICAL DIVISION
I&C INSTRUMENTATION AND CONTROLS DIVISION
M METALLURGY DIVISION
REE REACTOR EXPERIMENTAL ENGINEERING DIVISION
SS SOLID STATE DIVISION
TI TECHNICAL INFORMATION DIVISION
* DUAL CAPACITY
** PART TIME ON PROJECT

PERSONNEL SUMMARY

	FULL TIME	PART TIME	INDUSTRIAL PARTICIPATION	TOTAL
ADMINISTRATION	7	4		11
ANALYTICAL CHEMISTRY	39	9		48
CHEMICAL RESEARCH	8	9		17
CHEMICAL TECHNOLOGY	47	9		56
DESIGN AND ENGINEERING	123		3	126
HOMOGENEOUS REACTOR TEST	45		1	46
REACTOR MATERIALS RESEARCH	101	5		106
TOTAL	370	36	4	410

INTERNAL DISTRIBUTION

1. C. E. Center
2. Biology Library
3. Health Physics Library
4. Metallurgy Library
5-6. Reactor Experimental Engineering Library
7-9. Central Research Library
10-14. Laboratory Records Department
15. Laboratory Records, ORNL R.C.
16. G. M. Adamson
17. T. A. Arehart
18. A. L. Bacarella
19. J. E. Baker
20. R. G. Ball
21. S. J. Ball
22. R. D. Baybarz
23. S. E. Beall
24. L. L. Bennett
25. R. G. Berggren
26. G. B. Berry
27. R. E. Biggers
28. A. M. Billings
29. D. S. Billington
30. E. P. Blizard
31. R. Blumberg
32. E. G. Bohlmann
33. S. E. Bolt
34. C. J. Borkowski
35. B. F. Bottenfield
36. G. E. Boyd
37. J. C. Bresee
38. N. A. Brown
39. F. R. Bruce
40. J. R. Buchanan
41. W. D. Burch
42. C. A. Burchsted
43. S. R. Buxton
44. A. D. Callihan
45. T. A. Carlson
46. W. L. Carter
47. G. H. Cartledge
48. R. H. Chapman
49. R. A. Charpie
50. R. D. Cheverton
51. J. M. Chilton
52. C. J. Claffey
53. H. C. Claiborne
54. W. E. Clark
55. S. D. Clinton
56. T. E. Cole
57. C. W. Collins
58. E. L. Compere
59. R. S. Crouse
60. F. L. Culler
61. J. S. Culver
62. D. G. Davis
63. R. J. Davis
64. V. A. DeCarlo
65. B. D. Draper
66. J. S. Drury
67. W. K. Eister
68. L. B. Emlet (K-25)
69. J. L. English
70. D. E. Ferguson
71. J. D. Flynn
72. D. F. Frech
73. J. H. Frye, Jr.
74. C. H. Gabbard
75. J. L. Gabbard
76. W. R. Gall
77. R. B. Gallaher
78. C. H. Gibson
79. E. H. Gift
80. H. E. Goeller
81. R. S. Greeley
82. A. T. Gresky
83. J. C. Griess
84. W. R. Grimes
85. E. Guth
86. R. H. Guymon
87. L. A. Haack
88. P. A. Haas
89. J. Halperin
90. B. A. Hannaford
91. P. H. Harley
92. R. J. Harvey
93. P. N. Haubenreich
94. D. N. Hess
95. J. W. Hill
96. E. C. Hise
97. A. Hollaender
98. P. P. Holz
99. H. P. House
100. A. S. Householder

101. S. Jaye
102. G. H. Jenks
103. D. T. Jones
104. E. V. Jones
105. K. O. Johnsson
106. W. H. Jordan
107. S. I. Kaplan
108. P. R. Kasten
109. C. P. Keim
110. M. T. Kelley
111. F. Kertesz
112. S. S. Kirslis
113. J. O. Kolb
114. R. B. Korsmeyer
115. U. Koskela
116. K. A. Kraus
117. N. A. Krohn
118. J. A. Lane
119. C. G. Lawson
120. R. E. Leuze
121. S. C. Lind
122. R. B. Lindauer
123. C. S. Lisser
124. R. S. Livingston
125. M. H. Lloyd
126. R. A. Lorenz
127. M. I. Lundin
128. R. N. Lyon
129. J. L. Marsh (C&CC, South Charleston)
130. W. L. Marshall
131. J. P. McBride
132. F. C. McCullough
133. H. F. McDuffie
134. H. A. McLain
135. R. A. McNees
136. J. R. McWherter
137. O. Menis
138. E. C. Miller
139. C. S. Morgan
140. K. Z. Morgan
141. L. E. Morse
142. J. P. Murray (Y-12)
143. I. K. Namba
144. M. L. Nelson
145. P. D. Neumann
146. R. H. Nimmo
147. A. R. Olsen
148. L. F. Parsly
149. R. L. Pearson
150. F. N. Peebles
151. Sigfred Peterson
152. H. O. Phillips
153. M. L. Picklesimer
154. R. M. Pierce
155. R. H. Powell
156. B. E. Prince
157. J. J. Prislinger
158. L. R. Quarles
159. S. A. Reed
160. W. D. Reel
161. P. M. Reyling
162. S. A. Reynolds
163. L. Rice
164. D. M. Richardson
165. A. E. Richt
166. G. W. Rivenbark
167. R. C. Robertson
168. W. Robinson
169. H. C. Roller
170. A. M. Rom
171. M. W. Rosenthal
172. H. C. Savage
173. W. F. Schaeffer
174. C. E. Schilling
175. H. E. Seagren
176. H. K. Search
177. C. H. Secoy
178. C. L. Segaser
179. E. M. Shank
180. E. D. Shipley
181. M. D. Silverman
182. M. J. Skinner
183. A. N. Smith
184. E. S. Snavely, Jr.
185. A. H. Snell
186. J. W. Snider
187. D. L. Snyder
188. I. Spiewak
189. H. H. Stone
190. R. W. Stoughton
191. C. D. Susano
192. J. E. Sutherland
193. J. A. Swartout
194. E. H. Taylor
195. W. Terry
196. D. G. Thomas
197. P. F. Thomason
198. M. Tobias
199. D. S. Toomb
200. W. E. Unger
201. W. C. Ulrich
202. R. Van Winkle
203. D. W. Vroom
204. R. E. Wacker

205. F. J. Walter
206. K. S. Warren
207. B. Weaver
208. H. O. Weeren
209. A. M. Weinberg
210. S. H. Wheeler
211. J. K. White
212. E. P. Wigner (consultant)
213. H. D. Wills
214. G. C. Williams
215. J. C. Wilson
216. R. H. Winget
217. C. E. Winters
218. L. F. Woo
219. W. C. Yee
220. F. C. Zapp
221. ORNL – Y-12 Technical Library Document Reference Section
222. HRP Director's Office, Y-12

EXTERNAL DISTRIBUTION

223. E. B. Christiansen, Department of Chemical Engineering, University of Utah
224. F. C. Moesel, AEC, Washington
225. Houdry Corporation (Attn: G. A. Mills)
226. Division of Research and Development, AEC, ORO
227-233. TISE for P.A.R.P.
234-821. Given distribution as shown in TID-4500 (14th ed.) under Reactors–Power category (75 copies – OTS)

Reports previously issued in this series are as follows:

ORNL-527	Date Issued, December 28, 1949
ORNL-630	Period Ending February 28, 1950
ORNL-730	Feasibility Report – Date Issued, July 6, 1950
ORNL-826	Period Ending August 31, 1950
ORNL-925	Period Ending November 30, 1950
ORNL-990	Period Ending February 28, 1951
ORNL-1057	Period Ending May 15, 1951
ORNL-1121	Period Ending August 15, 1951
ORNL-1221	Period Ending November 15, 1951
ORNL-1280	Period Ending March 15, 1952
ORNL-1318	Period Ending July 1, 1952
ORNL-1424	Period Ending October 1, 1952
ORNL-1478	Period Ending January 1, 1953
ORNL-1554	Period Ending March 31, 1953
ORNL-1605	Period Ending July 31, 1953
ORNL-1658	Period Ending October 31, 1953
ORNL-1678	Period Ending January 31, 1954
ORNL-1753	Period Ending April 30, 1954
ORNL-1772	Period Ending July 31, 1954
ORNL-1813	Period Ending October 31, 1954
ORNL-1853	Period Ending January 31, 1955
ORNL-1895	Period Ending April 30, 1955
ORNL-1943	Period Ending July 31, 1955
ORNL-2004	Period Ending October 31, 1955
ORNL-2057	Period Ending January 31, 1956
ORNL-2096	Period Ending April 30, 1956
ORNL-2148	Period Ending July 31, 1956
ORNL-2222	Period Ending October 31, 1956
ORNL-2272	Period Ending January 31, 1957
ORNL-2331	Period Ending April 30, 1957
ORNL-2379	Period Ending July 31, 1957
ORNL-2432	Period Ending October 31, 1957
ORNL-2493	Period Ending January 31, 1958